POWER MANAGEMENT AND FREQUENCY REGULATION FOR MICROGRID AND SMART GRID: A REAL-TIME DEMAND RESPONSE APPROACH

by

Seyyed Ali Pourmousavi Kani

A dissertation submitted in partial fulfillment
of the requirements for the degree

of

Doctor of Philosophy

in

Engineering

MONTANA STATE UNIVERSITY
Bozeman, Montana

July 2014

©COPYRIGHT

by

Seyyed Ali Pourmousavi Kani

2014

All Rights Reserved

DEDICATION

To my wife, Atefeh
for her love, patience and support

and to my parents and sisters,
who always believed in me

تقدیم به وجود مهربان همسرم، عاطفه
و به پدر، مادر و خواهران نازنینم

ACKNOWLEDGEMENTS

I would like to extend my sincerest thanks to my committee members, Drs. Hashem Nehrir, Robert Gunderson, Don Hammerstrom, Rob Maher, Dan Trudnowski, especially and foremost to Dr. Hashem Nehrir for his unparalleled support, encouragement, and outstanding mentorship throughout my PhD education. Also, I would like to thank all of my professors in the Electrical and Computer Engineering (ECE) department at MSU, Drs. Bob Gunderson, Hongwei Gao, and Steve Shaw for their dedication and excellent professorship. Further, I would like to thank U.S. Department of Energy, Pacific Northwest National Lab (PNNL), and NEC Laboratories America Ltd. (NECLA) for their financial support in the last five years. Over the course of my PhD education, I had privilege to work with so many brilliant minds, hardworking scientists and students, and great personalities: Drs. Caisheng Wang (Wayne State University), Christopher M. Colson (Western Area Power Administration), and Ratnesh K. Sharma and B. Asghari (NECLA); and former and current MS students at MSU: Ms. Stasha N. Patrick, and gentlemen Jonathan D. Wilson, Andrew S. Cifala, Aric J. Litchy, Colin Young, and Kevin Marchese. Last but not least, thanks to every technical support and staff member at the ECE department for their assistance and kindness.

TABLE OF CONTENTS

1. INTRODUCTION 1

Background 3
Existing Power Grid vs. Smart Grid 6
Definition and Features of the Smart Grid 6
Power System Infrastructure 10
Current Power System. 10
Smart Grid. 13
Deregulated Electricity Market 19
Current Power System. 19
Smart Grid. 21
Reliability 22
Current Power System. 22
Smart Grid. 23
National Economy and Global Competitiveness 25
Current Situation. 25
Smart Grid. 26
National Security 27
Current Power System. 27
Smart Grid. 28
Load Demand 30
Current Power System. 30
Smart Grid. 32
Efficiency 36
Current Power System. 36
Smart Grid. 38
Affordability 40
Current Power System. 40
Smart Grid. 43
Environment and Climate Change 44
Current Power System. 44
Smart Grid. 46
Smart Grid Challenges 47
Renewable Electricity Production 47
Overvoltage. 48
Safety and Protection. 48
Power Quality. 49
Operating Reserve. 50
Overloaded Transmission Lines. 52
Transmission System Planning. 55

TABLE OF CONTENTS - CONTINUED

Energy Consumption Reduction 56
Base-Load Power Plants. 56
Power Quality. 56
Electricity Market 57
Wind and Solar PV Generation 58
Solutions to the Challenges in the Smart Grid 66
Classical Solutions 66
Technology for Increasing Transport Capacity 68
High-Voltage Direct Current (HVDC) and Flexible AC Transmission Systems (FACTS). 68
Dynamic Line Rating 72
Risk-Based Operation 73
Large-Scale Storage 74
Protection Practices 76
Voltage Control Techniques 77
MGs 79
Renewable Energies. 81
Storage Devices. 82
Power Quality. 83
Energy Efficiency. 84
Demand Response. 84
Self-Healing. 85
Electricity Market 86
Frequency and Voltage Stabilization within MGs 87
Real-Time Power Management of MGs 91
Organization of the Dissertation 95
References Cited 98

2. IMPACT OF HIGH PENETRATION OF PV GENERATION ON FREQUENCY AND VOLTAGE IN A DISTRIBUTION FEEDER 110

Contribution of Authors and Co-Authors 110
Manuscript Information Page 111
Abstract 112
Introduction 112
System Studied 115
Simplified Grid Model (SGM) 117
Feeder Configured MG 119
Simulation Results 122
15% PV Penetration 123
CASE I: 15% Concentrated PV Generation. 124
CASE II: 15% Distributed PV Generation. 127

TABLE OF CONTENTS - CONTINUED

30% PV Penetration 129
CASE III: 30% Concentrated PV Generation. 130
CASE IV: 30% Distributed PV Generation. 133
Conclusions 135
Acknowledgement 136
References Cited 137

3. REAL-TIME CENTRAL DEMAND RESPONSE FOR PRIMARY FREQUENCY REGULATION IN MICROGRIDS 139

Contribution of Authors and Co-Authors 139
Manuscript Information Page 140
Introduction 141
The Proposed DR Strategy 142
Adaptive Hill Climbing 143
Step-by-Step Control 144
Study System 144
Simulation Results 145
Scenario I: Light Loading – Decrease in Load (NO WIND) 145
Scenario II: Heavy Loading – Increase in Load (NO WIND) 146
Scenario III: Excess Wind Power Generation 147
Scenario IV: Unexpected Shortage in Wind Power Generation 147
Discussion 147
Conclusions 148
References Cited 148

4. THE APPLICATION OF DEMAND RESPONSE FOR FREQUENCY REGULATION IN AN ISLANDED MICROGRID WITH HIGH PENETRATION OF RENEWABLE GENERATION 150

Contribution of Authors and Co-Authors 150
Manuscript Information Page 151
Abstract 152
Introduction 152
The Proposed Control Strategy 154
System Studied 157
Simulation Results 160
System Performance Using Load Step Change 160
Impact of the PV Farm 163
Conclusion 167
Acknowledgement 167
References Cited 168

TABLE OF CONTENTS - CONTINUED

5. REAL-TIME OPTIMAL DEMAND RESPONSE FOR FREQUENCY REGULATION IN SMART MICROGRID ENVIRONMENT 170

Contribution of Authors and Co-Authors 170
Manuscript Information Page 171
Abstract 172
Introduction 172
Economic Model of DR in PJM Electricity Market 174
Proposed Optimal DR Strategy 176
Simplex Method 179
System of Study 180
Simulation Studies 182
Scenario I 184
Scenario II 186
Conclusion 188
Acknowledgement 188
References Cited 189

6. INTRODUCING DYNAMIC DEMAND RESPONSE IN THE LFC MODEL 192

Contribution of Authors and Co-Authors 192
Manuscript Information Page 193
Introduction 194
Problem Formulation for Single-Area Power System 195
State-Space Dynamic Model for LFC-DR 195
Padé Approximation 196
Analytical Evaluation of the Model 196
Steady-State Error Evaluation 197
Sensitivity Analysis for the Feedback System with and without DR 198
Stability Analysis of the Closed-Loop Systems 199
General Approach for Controller Design for the LFC-DR Model 200
Simulation Results for Single-Area Power System 201
Discussion and Future Work 202
Conclusions 203
Acknowledgement 203
References Cited 203

TABLE OF CONTENTS - CONTINUED

7. LFC-DR MODEL EXPANSION TO MULTI-AREA POWER SYSTEMS 205

Contribution of Authors and Co-Authors 205
Manuscript Information Page 206
Abstract 207
Introduction 207
Formulation Expansion to Multi-Area Power System with Multiple Gencos and Lagcos 209
Simulation Results for Multi-Area Power System with Single Genco and Lagco 216
Deviation in ACE, Frequency, and Tie-Line Power 218
The Impact of Latency on Dynamic Response 220
Simulation Results for Multi-Area Power System with Multiple Gencos and Lagcos 220
Conclusion 223
Acknowledgement 224
References Cited 225

8. REAL-TIME DEMAND RESPONSE THROUGH AGGREGATE ELECTRIC WATER HEATERS FOR LOAD SHIFTING AND BALANCING INTERMITTENT WIND GENERATION 227

Contribution of Authors and Co-Authors 227
Manuscript Information Page 228
Introduction 229
Problem Formulation 230
Individual EWH Model 230
Aggregated EWH Model 231
EWHs Thermostat Setpoint Control 231
Control Based on Desired Balancing (INC/DEC) Reserve Signal 231
Calculation of Required Number of EWHs for DR Based on the INC/DEC Signal 232
Simulation Setup and Configurations 233
Simulation Results and Discussion 234
Simulation Results for CASE3 234
Comparison of the Different Control Strategies 235
Discussion and Conclusion 237
References Cited 239

TABLE OF CONTENTS - CONTINUED

9. OWNERSHIP COST CALCULATION FOR DISTRIBUTED ENERGY RESOURCES USING UNCERTAINTY AND RISK ANALYSES 239

Contribution of Authors and Co-Authors 239
Manuscript Information Page 240
Abstract 241
Introduction 241
Problem Statement 244
The Proposed General Framework for Ownership Cost Calculation 245
Approach I (Base-case): No Replacement Cost 247
Approach II: No Replacement Cost and Effective Annual Interest Rate 249
Approach III: Cost Calculations Considering Replacement Cost 249
Approach III.A-EUAC with Replacement. 250
Approach III.B-Depreciation with Replacement. 250
Uncertainty and Risk Analysis 251
Simulation Studies and Results 254
Verification Study 255
Uncertainty and Risk Analyses 256
Appropriate DPDF for DiG Useful Lifetime. 257
Appropriate DPDF for DiG Annual Operation Hours. 258
Ownership Cost Formulation for Batteries 263
Conclusion 265
Acknowledgement 265
References Cited 267

10. A FRAMEWORK FOR REAL-TIME POWER MANAGEMENT OF A GRID-TIED MICROGRID TO EXTEND BATTERY LIFETIME AND REDUCE COST OF ENERGY 270

Contribution of Authors and Co-Authors 270
Manuscript Information Page 271
Abstract 272
Nomenclature 273
Introduction 274
The Proposed Real-Time Power Management Framework 276
Battery Lifetime Estimator, BLE 280
Calculation of Cost of Energy from Battery (CEB) 283
Simulation Results 284
Results of Curve Fitting and Interpolation 285

TABLE OF CONTENTS - CONTINUED

BLE and CEB Test....287
The Proposed Management Framework....291
Conclusion....297
References Cited....298

11. REAL-TIME ENERGY MANAGEMENT OF A STAND-ALONE HYBRID WIND-MICROTURBINE ENERGY SYSTEM USING PARTICLE SWARM OPTIMIZATION....300

Contribution of Authors and Co-Authors....300
Manuscript Information Page....301
Introduction....301
Formulation of the Optimization Problem....302
MT Cost Function and Constraints....302
WECS Cost Function and Constraints....303
Proposed Real-Time EMS....303
Particle Swarm Optimization....304
PSO-Based Energy Management....305
Simulation Results....306
Discussion....308
Conclusions....308
Acknowledgement....308
References Cited....309

12. MULTI-TIMESCALE POWER MANAGEMENT FOR ISLANDED MICROGRIDS INCLUDING STORAGE AND DEMAND RESPONSE....311

Contribution of Authors and Co-Authors....311
Manuscript Information Page....312
Abstract....313
Introduction....314
MG Design and Modeling....316
MG Design....316
MG Dynamic Model....317
PV Model.....317
DiG Model.....318
Battery Model.....322
EWH Model.....323
The Proposed Power Management Algorithm....325
RULE I (Right Column in Figure 12.5)....328
RULE II (Middle Column in Figure 12.5)....330
RULE III (Left Column in Figure 12.5)....330

TABLE OF CONTENTS - CONTINUED

Simulation Results and Discussion 332
Solar PV Panel 335
DiG 336
Battery 336
MG Emission 339
Total Undelivered Load 340
Total MG Operational Cost 340
Conclusion 341
Acknowledgement 342
References Cited 343

13. CONCLUSIONS 347

REFERENCES CITED 352

APPENDICES 390

APPENDIX A Simulation Diagrams of the Feeder-Configured MG 391
APPENDIX B Sub-Matrices for the LFC-DR Model Developed for Multi-Area Power System with Multiple Gencos and Lagcos 394
APPENDIX C Battery Life Estimation and Operational Cost Calculation GUI 398
APPENDIX D Multi-Timescale Power Management GUIs 400
APPENDIX E Input Descriptions, Algorithms, and Pseudo-Codes 403
APPENDIX F Author Peer-Reviewed Publications 409

LIST OF TABLES

Table Page

1.1. Different shunt connected FACTS controllers [1.61]. 70

1.2. Different series connected FACTS controllers [1.61]. 71

1.3. Different two-port FACTS controllers [1.61]. 72

1.4. Comparison of different storage technologies [1.64]. 75

1.5. Different objectives and constraints for MGs' operation [1.84], [1.125]. 93

2.1. The SGMs parameters. 124

2.2. System frequency statistics for both SGM1 and SGM2 in CASE I. 126

2.3. System frequency statistics for both SGM1 and SGM2 in CASE II. 128

2.4. System frequency statistics for both SGM1 and SGM2 in CASE III. 131

2.5. System frequency statistics for both SGM1 and SGM2 in CASE IV. 133

3.1. DG parameters 149

4.1. System frequency statistics for the three control methods in 9000 sec simulation for 25% PV penetration. 165

5.1. The DiG parameters. 181

5.2. G&T prices for different zones. 182

6.1. *Padé* approximations feed-forward and feedback values for signal flow graph 198

6.2. Power system parameters for the simulation study 201

6.3. Phase and gain margins for the open-loop transfer function associated with each closed-loop 202

6.4. Power system parameters for the simulation study 204

LIST OF TABLES - CONTINUED

Table Page

7.1. Three-area power system parameters for the simulation study [7.2].....218

7.2. Three-area power system with three Gencos and Lagcos for the simulation study [7.2].....221

8.1. Parameters of 1000 EWHs in the aggregated model 233

8.2. Parameters that are the same for all EWHs throughout the duration of the simulation.....233

8.3. Base rate for electricity energy consumed in ToU pricing scheme for Pacific Power.....235

8.4. ToU electricity rate adjustments in residential sector (rate schedule 4) for Pacific Power 235

8.5. Brief description of all four different cases.....236

8.6. Brief description of all six different goals.....236

8.7. The one-week energy consumption of the EWHs during off-peak and on-peak periods for different CASEs 238

9.1. Ownership cost calculation data. 256

9.2. MG design specifications obtained from HOMER®.....258

9.3. Ownership cost calculation fata for the DiG. 262

10.1. Amperes on Discharge table for Intensium Flex High Energy Li-Ion battery, SAFT Company. 285

10.2. The arbitrary discharge pattern created for a day. 288

10.3. Intensium Flex High Energy Lithium-Ion battery specification. 293

10.4. Cost of electricity from the grid. 293

10.5. Controlled power cost in each case and percentage of savings. 295

11.1. Computation time for different optimization techniques 311

LIST OF TABLES - CONTINUED

Table Page

12.1. Actual fuel consumption for the DiG studied [12.19]. 319

12.2. Curve-fitted coefficients of the functions for emission production. 322

12.3. Simulation results of the MG operation for the three PMAs for 24 hours. 335

12.4. Reduction in CO_2 and non-CO_2 emissions in the *DR.A* and *DR.B* PMAs. 340

LIST OF FIGURES

Figure Page

1.1. North American electrical grid interconnections, including the 10 North American Electric Reliability Corporation (NERC) regional reliability councils [1.3]. 1

1.2. Different features envisioned for the smart grid. 8

1.3. Installed generation capacity annual growth vs. load demand annual growth [1.8], [1.9]. 11

1.4. Decrease in transmission investment in U.S. (billion US$) [1.4]. 11

1.5. Utilities construction and depreciation expenditures from 1960 to 2000 [1.6]. 12

1.6. R&D investments as percentage of revenue [1.4]. 13

1.7. Renewable Energy Portfolio (RPS) standard policies [1.14]. 15

1.8. Added and projected additions to power plant capacity from 1985-2040 [1.16]. 16

1.9. Levelized electricity costs for new power plants, 2020 and 2040 estimation (2011 cents per kWh) [1.15]. 17

1.10. Actual and planned transmission investment by shareholder-owned electric utilities (2001-2015) [1.17]. 19

1.11. Increasing frequency and size of U.S. power outages 100 MW or more (1991-1995 vs. 1996-2000), affecting 50,000 or more consumers per event [1.6]. 23

1.12. Electricity retail sales to all sector from 1949-2011 and 5-year growth in demand, power plants direct use is not considered [1.9]. 31

1.13. U.S. electricity demand growth, 1950-2040 [1.15]. 31

1.14. Results of load demand management for all sectors in terms of energy savings, actual peak load reduction, and potential peak load reduction [1.16]. 34

LIST OF FIGURES - CONTINUED

Figure Page

1.15. Non-coincident peak load, by North American Electric Reliability Corporation Assessment Area, 1990-2011 (actual), and 2012-2016 (projected) [1.26].....35

1.16. T&D losses as a percentage and its cost estimation based on averaged electricity retail price [1.9], [1.29], [1.30].....37

1.17. Average retail price of electricity to ultimate customers by sectors, 2003-2013 [1.16]. 41

1.18. Electric net summer capacity for fossil fuels power plants (i.e., coal, petroleum, natural gas, and other gases) for 1949-2011 [1.33].....45

1.19. Emissions from energy consumption for electricity generation and useful thermal output (Millions Metric Tons of Gas) 1989-2010 [1.34].....45

1.20. Electricity generation by fuel, 1990-2040 [1.35].....47

1.21. Total estimated technical potential for urban utility-scale PV in the U.S. [1.43]. 53

1.22. Total estimated technical potential of roof-top PV in the U.S. [1.43].....54

1.23. Total estimated technical potential for onshore wind power in the U.S. [1.43].....54

1.24. Total estimated technical potential for offshore wind power in the U.S. [1.43]. 55

1.25. Renewable electricity generation capacity by energy source, including end-use capacity, 2011-2040 [1.16].....59

1.26. Monthly average wind energy production from Lake Benton, Minnesota, USA [1.48].....60

1.27. 2010 average hourly wind power profiles by month from Lake Benton, Minnesota, USA [1.48]. 61

LIST OF FIGURES - CONTINUED

Figure Page

1.28. Monthly average global irradiation data for Ashland, OR, 2009-2012 [1.49]. 62

1.29. 5-minute interval solar irradiation data for the first day of January 2012 in Ashland, OR [1.49]. 63

1.30. Generated power from 15 kW solar PV array tilted 15º South- January 01, 2010 in Ashland, OR, USA [1.49]. 63

1.31. Classification of DR programs [1.105]. 90

2.1. Configuration of the generic feeder (a) with concentrated PV generation, and (b) distributed PV generation. 114

2.2. Components of the proposed SGM. 117

2.3. Speed governor of the proposed SGM. 118

2.4. Actual data for (a) solar insolation and (b) air temperature used in the simulations. 123

2.5. Simulation results for (a) system frequency and voltages of nodes (b) B9, (c) B15, and (d) B17 for both models of the grid. 125

2.6. (a) SGMs output mechanical power for 15% concentrated PV generation and total PV generation, and (b) zoomed-in output mechanical power of the SGMs. 127

2.7. Simulation results for (a) system frequency and voltages of nodes (b) B9, (c) B15, and (d) B17 for both models of the grid. 128

2.8. (a) SGMs output mechanical power for 15% distributed PV generation and total PV generation, and (b) zoomed-in output mechanical power of the SGMs. 130

2.9. Simulation results for (a) system frequency and voltages of nodes (b) B9, (c) B15, and (d) B17 for both models of the grid. 131

LIST OF FIGURES - CONTINUED

Figure Page

2.10. (a) SGMs output mechanical power for 30% concentrated PV generation and total PV generation, and (b) zoomed-in output mechanical power of the SGMs. 132

2.11. Simulation results for (a) system frequency and voltages of nodes (b) B9, (c) B15, and (d) B17 for both models of the grid. 134

2.12. (a) SGMs output mechanical power for 30% distributed PV generation and total PV generation, and (b) zoomed-in output mechanical power of the SGMs. 135

3.1. The scheduling process of the central DR strategy....143

3.2. Concept of the proposed control strategy....144

3.3. Decision tree for determining the MODE of operation 144

3.4. The flowchart of the AHC control....144

3.5. Modified IEEE 13-bus standard distribution system schematic diagram 145

3.6. Schematic of modeling of the active variable load....146

3.7. The technical characteristic of the load in the test system 146

3.8. Frequency, voltage, and total load demand: Light loading with no wind power generation. (a) System frequency, (b) Zoomed-in system frequency, (c) Voltage at the 69 kV bus. (d) Total load demand 147

3.9. Frequency, voltage, and total load demand: Heavy loading with no wind power generation. (a) System frequency, (b) Zoomed-in system frequency, (c) Voltage at the 69 kV bus. (d) Total load demand 147

3.10. Frequency, voltage, and total load demand: Excess wind power generation. (a) System frequency, (b) Zoomed-in system frequency, (c) Voltage at the 69 kV bus. (d) Total load demand....148

LIST OF FIGURES - CONTINUED

Figure Page

3.11. Frequency, voltage, and total load demand:
Unexpected shortage in wind power generation.
(a) System frequency, (b) Zoomed-in system frequency,
(c) Voltage at the 69 kV bus. (d) Total load demand 149

3.12. System frequency with different latencies,
light loading comprehensive controller case.....149

4.1. The proposed SGM with governor droop control and AGC.....155

4.2. Block diagram of the proposed DR controller. 156

4.3. Schematic of the MG-configured distribution feeder.....159

4.4. PV power generation in Oahu, Hawaii, U.S.....159

4.5. Load step change with variable integrator gain.....161

4.6. Load step change with variable responsive load. 162

4.7. Load step change with different DR latencies.....163

4.8. System frequency response with (a) 15%,
(b) 25% PV penetration. 164

4.9. System frequency response with variable
responsive load with 25% of PV penetration.....165

4.10. (a) System frequency response with
25% PV penetration, (b) zoomed-in view.....166

5.1. Schematic diagram of the proposed optimal DR strategy.....177

5.2. Modified IEEE 13-bus standard
distribution system schematic diagram.....183

5.3. System frequency in Scenario I.....185

5.4. Total responsive load changes in Scenario I. 185

5.5. System frequency in Scenario II.....187

5.6. Total responsive load changes in Scenario II.....187

LIST OF FIGURES - CONTINUED

Figure Page

6.1. Block-diagram representation of a single-area power system model 197

6.2. Different order of *Padé* approximation for pure time delay 198

6.3. Signal flow graph of the single-area power system model with 5th-order *Padé* approximation.....198

6.4. Modified power system model with integral controller for DR and supplementary control loop.....200

6.5. Closed-loop system w.r.t. the open-loop system sensitivity values of a simulation study for LFC with and without DR 201

6.6. Closed-loop system w.r.t. α sensitivity values for the LFC-DR model, α=0.1 and α=0.8 201

6.7. Bode plot of the closed-loop systems for stability analysis, (a) magnitude, and (b) phase 202

6.8. Frequency deviation for conventional LFC and LFC-DR models 203

6.9. Steady-state values of the control inputs for the LFC-DR model 203

6.10. Controller performance for different order of *Padé* approximation.....204

6.11. Impact of different unified inputs on the performance of the LFC-DR model.....204

6.12. Impact of latency on the performance of the LFC-DR model.....204

6.13. Impact of DR latency on the performance of a slower single-area power system.....204

7.1. Multi-area power system with multiple Gencos and Lagcos. 210

7.2. Block-diagram representation of area *i* of a general multi-area power system with multiple Gencos and Lagcos in each area. 211

LIST OF FIGURES - CONTINUED

Figure Page

7.3. ACE, Frequency deviation, and total tie-line power in different areas for different α, multi-area power system with single Genco and Lagco. 217

7.4. The impact of communication latency on, (a) frequency deviation, and (b) total tie-line power deviation in area 1. 219

7.5. ACE, Frequency deviation, and total tie-line power in different areas for different α, multi-area power system with multiple Gencos and Lagcos. 222

8.1. Total power demand and EWH demand of an average house 233

8.2. Response of a single EWH with a 50-gallon hot water tank....233

8.3. Outgoing water temperature of 1000 EWHs, CASE3 237

8.4. Total power demand of 1000 EWHs, Wednesday, CASE3....237

8.5. Total EWHs demand for the one-week of simulation 237

8.6. Balancing reserve (INC/DEC signals) desired and created, Saturday, CASE3 237

8.7. PDF for absolute error between balancing reserve desired and created, CASE2....238

8.8. Total demand during on-peak hours for different CASEs 238

8.9. Maximum total EWHs' power demand for different CASEs 238

8.10. Total weekly energy demand for different CASEs....239

8.11. Average weekly cost per EWH for different CASEs....239

9.1. Overview of the operational cost calculation model adapted for this chapter....245

9.2. Accumulative payment of the DiG ownership cost for different approaches and their corresponding error in comparison with Approach I....256

LIST OF FIGURES - CONTINUED

Figure Page

9.3. PDF for DiG useful lifetime created by Hypergeometric DPDF. 258

9.4. PDF for DiG annual operation hours created by Extreme Value DPDF. 260

9.5. Hourly cost for the DiG with different outcomes generated for the two uncertain parameters for (a) Approach I (base-case), (b) Approach III.A, and (c) Approach III.B.....261

10.1. Block-diagram of the proposed management framework. 278

10.2. Schematic diagram for the proposed PM strategy. 279

10.3. BLE model represented in a block-diagram. 283

10.4. Cycle life vs. DoD for Intensium Flex High Energy Li-Ion battery, SAFT Company. 285

10.5. Curve fitting results for two different methods. 286

10.6. Actual capacity of the battery at different discharge rates. 287

10.7. The BLE calculations for different current magnitudes, obtained from the curve fitting using NLLS and PSO methods. 289

10.8. The CEB for different discharge current magnitudes, obtained from the curve fitting results using NLLS and PSO methods. 290

10.9. The BLE values for different time duration studies, obtained using NLLS and PSO curve fitting methods. 290

10.10. The calculated CEB for different discharging time durations obtained using NLLS and PSO curve fitting methods. 291

10.11. Battery life estimation for CASES I and II for a year of simulation. 294

10.12. The CEB per kWh in both CASEs for a year of simulation. 295

LIST OF FIGURES - CONTINUED

Figure Page

10.13. Accumulative cost of energy extracted from battery for both CASEs for a year of simulation. 296

11.1. Configuration of the proposed system 305

11.2. Proposed energy management strategies for the WECS-MT-ES-EWH system....306

11.3. (a) Three fundamental elements the particle position updating, (b) Graph of influence of a swarm of N particles in circular form with three informants for each particle 308

11.4. Flowchart for the proposed PSO algorithm....309

11.5. Hourly average demand of 120 typical residences in the Pacific Northwest area 309

11.6. Actual corrected wind speed data for Deer Lodge, MT on March 12, 2007, corrected to hub height of 40 m....310

11.7. Wind power output for different management algorithm and optimization 310

11.8. MTG output power for different management algorithms and optimization methods....310

11.9. SOC of battery for different algorithms and optimization methods....310

11.10. Battery power for different power management algorithms in a day....311

11.11. Auxiliary water heater power for a day in the proposed energy management strategy 311

12.1. Schematic diagram of the MG configuration. 317

12.2. The overall efficiency of the DiG based on input and output energy.....322

LIST OF FIGURES - CONTINUED

Figure Page

12.3. Classification and operational framework for battery SOC limits [12.30].....323

12.4. Flowchart diagram of the MG simulation environment developed for this study.....324

12.5. Schematic diagram for the proposed multi timescale rule-based power management algorithm.....327

12.6. Minute-by-minute active non-EWH load demand (winter weekday) for 100 houses [12.13].....333

12.7. Hot water consumption for 100 houses in the MG, winter weekday.....333

12.8. Temperature and solar irradiation for a non-cloudy weekday in the winter [12.9].....334

12.9. Battery SOC for the proposed management systems, with and without DR.....338

12.10. The hot water temperature for all household in (a) DR.A, and (b) DR.B PMAs.....339

GLOSSARY

Ancillary services (AS): this term, sometimes called frequency and voltage AS, is defined as any action taken by the utilities in order to maintain the frequency and voltage of the delivered power at the pre-defined standard range.

Automatic generation control (AGC): it is a significant and important control process that operates constantly to balance generation and demand in power systems at a minimum cost, and is responsible for frequency control and power interchange, as well as economic dispatch.

Capacity credit: it is the level of conventional generation that can be replaced with wind generation.

Capacity factor: it is the ratio of a power generation resource's actual output over a period of time, to its potential output.

Demand response (DR): this term has been defined by the U.S. DOE as any changes in electric usage by the end-use customers from their normal consumption patterns in response to change in the price of electricity over time, or to incentive payments designed to induce lower electricity use at times of high wholesale market prices or when system reliability is jeopardized.

Demand side management (DSM): this term is used to describe the actions of a utility, beyond the customer's meter, with the objective of altering the end-use of electricity, whether it be to increase demand, decrease it, shift it between high and low peak periods, or manage it when there are intermittent load demands, in the overall interests of reducing utility costs. In other words, DSM is improving the efficiency of various end-uses through better housekeeping correcting energy leakages, system conversion losses, etc., developing and promoting energy efficient technologies, and demand management through adopting soft options like higher prices during peak hours, concessional rates during off-peak hours seasonal tariffs, interruptible tariffs, etc.

Direct load control (DLC): any direct actions on the customers' loads that can interrupt load for a certain period of time by consumer premises.

Dispatchability: it refers to sources of electricity that can be dispatched at the request of power grid operators; that is, generating plants that can be turned on or off, or can adjust their power output on demand.

Distributed energy resource (DER): small-scale power generation technologies (typically in the range of 1 kW to 10,000 kW) used to provide an alternative to or an enhancement of the traditional electric power system.

GLOSSARY - CONTINUED

Federal energy regulatory commission (FERC): the U.S. federal agency with jurisdiction over interstate electricity sales, wholesale electric rates, hydroelectric licensing, natural gas pricing, and oil pipeline rates.

Intermittency: it means a power resource is unintentionally stopped or unavailable, and is frequently used as variability.

Load Factor: it is the ratio of the average or actual amount of load and the maximum possible over a day.

Load frequency control (LFC): this term relates generation control to power system frequency regulation as a supplementary frequency control and is a major function of AGC [52]. The LFC model is referred to as the small-signal stability model of the power system at transmission level which has been widely used for controller design and stability analysis in the power systems.

Microgrid (MG): a MG is a regionally limited energy system of distributed energy resources, consumers and optionally storage which is designed to work in both grid-tied and islanded modes. MG is known as an important technology to ascertain the smart grid goals.

Monthly peak hour demand: maximum load during an integrated specified hour of time for the month of greatest electrical generation during the winter season (December-February) and summer season (June-September), respectively. Or, for each of the twelve calendar months.

North American electric reliability corporation (NERC): a not-for-profit international regulatory authority whose mission is to ensure the reliability of the bulk power system in North America.

Net energy for load: net generation of main generating units that are system-owned or system-operated, plus energy receipts minus energy deliveries.

Net internal demand: represents the system demand that is planned for by the electric power industry's reliability authority.

On-peak hours: it is the period of time when load demand is relatively high which varies geographically, seasonally, monthly, and based on workdays and weekends.

Peak load: maximum load during a specified period of time.

GLOSSARY - CONTINUED

Planned (net) capacity resources: it represents existing net generator capacity plus the addition and subtraction of capacity that either enters or leaves the region via purchases, sales, ownership, or entitlements.

Power system stability: it is the ability of an electric power system, for a given initial operating condition, to regain a state of operating equilibrium after being subjected to a physical disturbance.

Regulation services: it corrects short-term changes in generation and demand which affect the stability of the power system.

Smart grid: it is defined as a smarter grid with less centralized and more customer-interactive capabilities, enabling new products such as nationwide use of plug-in hybrid electric vehicle, allowing seamless integration of RES such as wind and PV, ushering in a new era of consumer choice and response, exploiting the use of green building standards, and making large-scale energy storage a reality.

Variability: it means a power source may exhibit undesired or uncontrolled changes in output.

ABSTRACT

Future power systems (known as smart grid) will experience a high penetration level of variable distributed energy resources to bring abundant, affordable, clean, efficient, and reliable electric power to all consumers. However, it might suffer from the uncertain and variable nature of these generations in terms of reliability and especially providing required balancing reserves. In the current power system structure, balancing reserves (provided by spinning and non-spinning power generation units) usually are provided by conventional fossil-fueled power plants. However, such power plants are not the favorite option for the smart grid because of their low efficiency, high amount of emissions, and expensive capital investments on transmission and distribution facilities, to name a few. Providing regulation services in the presence of variable distributed energy resources would be even more difficult for islanded microgrids.

The impact and effectiveness of demand response are still not clear at the distribution and transmission levels. In other words, there is no solid research reported in the literature on the evaluation of the impact of DR on power system dynamic performance. In order to address these issues, a real-time demand response approach along with real-time power management (specifically for microgrids) is proposed in this research. The real-time demand response solution is utilized at the transmission (through load-frequency control model) and distribution level (both in the islanded and grid-tied modes) to provide effective and fast regulation services for the stable operation of the power system. Then, multiple real-time power management algorithms for grid-tied and islanded microgrids are proposed to economically and effectively operate microgrids. Extensive dynamic modeling of generation, storage, and load as well as different controller design are considered and developed throughout this research to provide appropriate models and simulation environment to evaluate the effectiveness of the proposed methodologies.

Simulation results revealed the effectiveness of the proposed methods in providing balancing reserves and microgrids' economic and stable operation. The proposed tools and approaches can significantly enhance the application of microgrids and demand response in the smart grid era. They will also help to increase the penetration level of variable distributed generation resources in the smart grid.

CHAPTER 1

INTRODUCTION

It has been over 120 years since the first full AC power system was demonstrated in Great Barrington, Massachusetts in 1886 by William Stanley [1.1]. Since then, electricity has become the number one source of energy for industry, commercial, and residential applications, and recently has been used extensively for transportation. The increase in consumption essentially resulted in larger power system with more complexity in terms of generation, consumption, observation, and control. Today, the North American power system is the largest man-made machine on earth with four interconnections that include 10 regions in U.S. and Canada, as shown in Figure 1.1. This large infrastructure has served the two countries for over 120 years and has been considered as the most "supreme engineering achievement of the 20th century" [1.2].

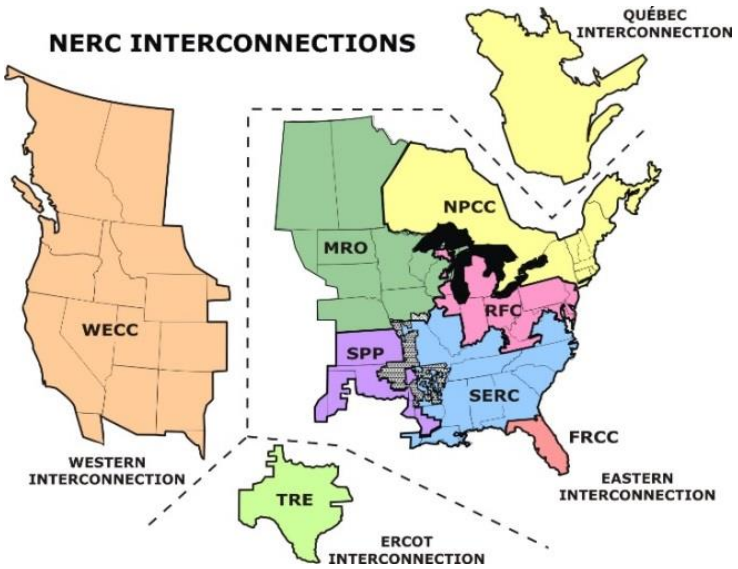


Figure 1.1. North American electrical grid interconnections, including the 10 North American Electric Reliability Corporation (NERC) regional reliability councils [1.3].

In the past century, electricity has steadily evolved from a scientific curiosity to a luxury of the wealthy, and now to a modern necessity. In today's culture, electricity is a vital part of functioning of a society. It is the primary source of energy for the most end-use applications outside of transportation and heating. Electricity is essential for economic prosperity, national security, and public health and safety. However, one only needs to consider the consequences of a relatively short power outage, which can result in billions of dollars of loss. This is how power-dependent our society has become and how vulnerable the current electrical system is.

In 1940, 10% of energy consumption in America was used to produce electricity and this fraction reached 25% in 1970. Today, more than 40% of the energy produced is used to generate electricity [1.2]. The current design, which has evolved around the original electrical system, no longer can effectively and efficiently sustain the modern electrical demand in modern societies. This requires necessary action to modernize our current power system to address the needs of the future generations. This mission has been formulated as the "smart grid" concept: it applies technologies, tools, and techniques available and under development to make the grid more efficient, accessible, affordable and reliable [1.2], [1.4].

This chapter attempts to broadly explain the status of the current power system and to introduce new technologies to overcome the existing problems and build a smart grid. The necessity of smart grid, the technology and ideas which drive smart grid development and implementation, alternative solutions to the smart grid and their pros and cons, and the state-of-art of the technologies will be explained in depth in this

chapter. The focus of this dissertation, its merits and contributions to the smart grid, are presented in the flowing chapters.

Background

In the early days of power system development, there was only small, autonomous (or islanded) grids electrifying a small area for mostly residential applications. However, increasing load demand, new electrical gadgets, and industrial applications of electricity over the past century drove the local grids to grow in size and complexity. Eventually, interconnection of the small autonomous grids was unavoidable for economic and reliability reasons. By the 1960s, the electric grids in developed countries had become very large, mature and highly interconnected, with thousands of central generation power stations delivering power to major load centers via high capacity power lines (i.e., transmission system). Then, the transmission systems were branched out and divided to provide power to smaller industrial and residential customers over the entire supply area. Consequently, the topology of the 1960s grid was an outcome of the strong economic growth of the United States and Canada at the time. Large coal-, gas- and oil-fired power stations in the 1-3 GW scale were built. These power stations were mostly, localized strategically close to the fossil fuel reserves. The very polluting fossil fuel-fired power stations were located, as far as economically and technically possible, far from population centers. Hydro-electric dams were developed in mountainous areas, and nuclear power plants were built near water reserves for cooling purposes. By the late 1960s, the electricity grid reached the majority of the population in the developed countries.

Currently, the North American power system consists of more than 9,200 electric generating units with more than 1,000,000 MW of generating capacity. The system is connected to more than 300,000 and 1,000,000 miles of transmission and distribution lines, respectively [1.4], [1.5]. Approximately, 120,000 people are directly employed at the generation level, while over 15,000 and 400,000 people are currently working in transmission and distribution sectors, respectively [1.5]. In 2000, the North American transmission and distribution system were valued at US$358 billion, and the whole system was estimated to be worth over US$ 800 billion [1.6]. This is an infrastructure that not only drives economic and technology innovation for the future but also employs hundreds of thousands of people directly.

Generally speaking, the existing power system infrastructure has almost perfectly served the U.S. and Canada for over 100 years. Its development has initiated many critical technology and scientific achievements world-wide. Today, all economic and social progress relies on a trustworthy and efficient energy infrastructure; examples include secure and reliable banking and finance services that completely depend on the electricity availability, cable and wireless telecommunications, and transportation systems such as military and commercial aircraft or land and sea vessels, which rely on robust communication links and reliable electricity networks [1.6]. Briefly speaking, the smart grid is more than just an electric power grid, it is evolving to be an infrastructure that links telecommunication, transportation, electric generation with oil, water and gas, and more.

Within this paradigm, customer reliability expectations have grown with the

advancement of a persistently digital world that has evolved in vehicles, homes, offices, and industrial facilities. This demand has drastically increased grid congestion and power flow problems throughout the power system. While a secure and robust operation of these systems is critical, a large interconnected power system, like what exists currently, makes the whole world more vulnerable to local disruptions that can be presented by physical failure, natural disasters, intentional attack, or human error. Clearly the power system built in the 1960s cannot suitably provide for our future needs. The aging electro-mechanical grid cannot keep pace with innovations in the digital information and telecommunications network where power outages and power quality disturbances cost the economy billions of dollars each year. In other words, a new paradigm shift requires drastic advances in the grid structures, generation resources, standards, policies, and approaches in planning and operations.

To address this paradigm shift in the power system, 65 senior executives representing the electric utility industry, equipment manufacturers, information technology providers, federal and state government agencies, interest groups, universities, and national laboratories met on April 2-3, 2003 to discuss the future of North America's electric system [1.2]. The intent of this committee was to classify a national vision of the future electric system including generation, transmission, distribution, storage, and customers. The final vision articulated at that meeting is briefed as follows [1.2]:

"***Grid 2030*** *energizes a competitive North American marketplace for electricity. It connects everyone to abundant, affordable, clean, efficient, and reliable electric power*

anytime, anywhere. It provides the best and most secure electric services available in the world."

This was the start of a nation-wide effort to modernize power system to support national economy and security in the future; this is what has become known as the "smart grid".

Existing Power Grid vs. Smart Grid

To understand the significance of the smart grid, and the solutions it will offer to existing problems within the power system, a comparative study is presented in this section. At the beginning, a brief sub-section is devoted to define the smart grid and its features. Then, the existing problems in the power system are analyzed and presented with solutions offered by the smart grid.

Definition and Features of the Smart Grid

Although revolutionizing of the north American power system was announced publically in 2003 by U.S. DOE [1.2], the "smart grid" term was emerged in 2005. However, its real origin goes back to 1998, published in an article in the IEEE Power and Energy Magazine [1.7]. Since then, many definitions of smart grid have been given in different literature and scientific groups. The comprehensive definition of the smart grid is defined as a smarter grid with less centralized and more customer-interactive capabilities, enabling new products such as nationwide use of plug-in hybrid electric vehicle (HEV), allowing seamless integration of renewable energy sources (RES) such as wind and PV, steering in a new era of consumer choice and response, exploiting the use

of green building standards, and making large-scale energy storage a reality [1.4]. Unlike today's grid, the smart grid will enable bidirectional flow of energy and uses two-way communication and control capabilities that will lead to a collection of new functionalities and applications. Additionally, customers will be actively involved in both the power generation and consumption, where they can produce power and sell it to the upper grid. Emerging storage technologies such as high-speed flywheel, supercapacitor, superconducting magnetic energy storage (SMES), Sodium-Sulfur (NaS) and flow batteries, and compressed air energy storage (CAES) will be widely applied to provide high quality power to every single customer. In general, reliability in the smart grid era will be ensured to degrees not possible in the past. In addition, cost of electricity is projected to be affordable and relatively cheap. Industries actively working on different smart grid technologies (such as renewable generation and storage devices, metering infrastructure, cyber security and large-scale data analysis, fast and reliable communications, etc.) will enhance all markets worldwide and convey a new level of global competitiveness. The potential for high penetration of renewable energies, in addition to increased efficiency from traditional power plants, will decrease the carbon footprint significantly. Moreover, the smart grid is envisioned as a resilient energy infrastructure against any physical and/or cyber-attack and natural disasters. This is projected to happen through more decentralized generation, advanced secure communication medium and protocols, real-time diagnosis and prognosis algorithms, and fast switching devices. Information technologies, new materials and high temperature superconductors, large-scale electricity storage, advanced power electronics, distributed

energy technologies, and advanced control methods to monitor essential components enabling rapid diagnosis, and precise solutions are considered to be other technologies that will drive the smart grid [1.2]. The main features of the smart grid are summarized in Figure 1.2.

Although each feature proposed for the smart grid addresses at least one issue related to the existing power system, some of these goals are conflicting and competing with each other. As an example, increasing the generation capacity by adding large-scale renewable generation units needs new transmission infrastructure because appropriate locations for renewables exploitation are usually far away from load centers. This will raise the required capital investment and result in cost of electricity increase for the customers. It will also increase the power losses which consequently decreases the energy efficiency.

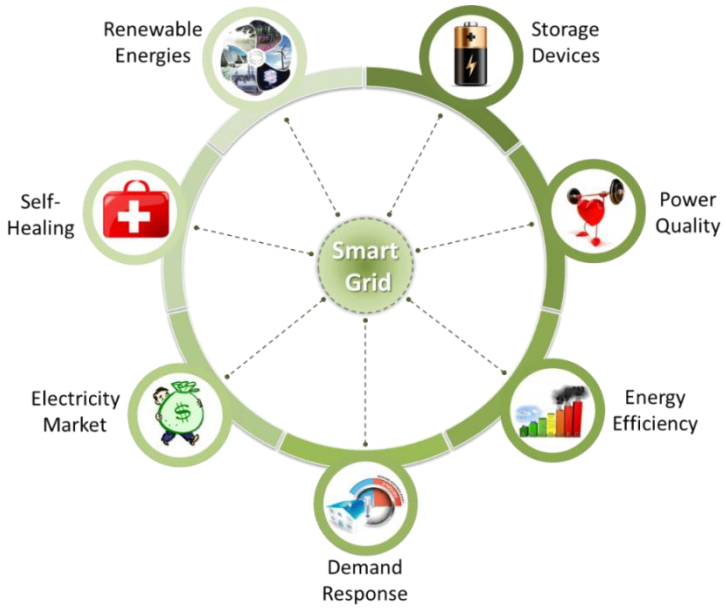


Figure 1.2. Different features envisioned for the smart grid.

The need to move from centralized power system to more decentralized power system structure in the smart grid era for improved system resiliency and self-healing, to achieve seamless integration of renewables in power systems, power quality, and demand response (DR) pushed the researchers and developers to find solutions in small-scale power system within the bulky system. This bridging technology is called microgrid (MG) and is expected to be a driving technology for broadening the smart grid implementation and acceptance in the future power system. A MG is a regionally limited energy system consisting of distributed energy resources (DERs), consumers, and optionally storage, controlled to maintain high quality, sustainable, and reliable electricity economically in grid-connected and/or off-grid (islanded) mode. Different features of the smart grid, shown in Figure 1.2 will also be considered in the MG design and implementation. MGs are excellent enhancement for the facilities with critical loads such as hospitals and military bases. Additionally, they offer economic benefits including revenues for the sale of energy and ancillary services, lowering of the demand charges, and load shifting from peak demand periods to lower usage periods. Also, it is expected that the MGs will be capable of accommodating significant amount of variable RES generations.

Despite the benefits mentioned for the smart grid and MGs, there are several issues related to real-world implementation and controls which have to be addressed prior their vast utilization. These challenges will be discussed in details in the next sections. In the following sub-section, the existing power system issues and challenges will be reviewed and the solutions offered by the smart grid are presented.

Power System Infrastructure

The power system infrastructure is the most visible part of the larger and growing U.S. energy crisis, which is the result of insufficient investments in the past several decades. The power system infrastructure can be structurally divided in three different levels: 1) generation, 2) transmission, and 3) distribution. In this section, the existing power system infrastructure will be compared with the one envisioned for the smart grid.

Current Power System. In the vertically-designed power system of 1960s, the different levels work in series to deliver generated power to the individual customers (residential, commercial, and industrial). One major problem with this system is if one of the levels fails for some reason (such as component failure, terrorist attacks, vandalism, etc.), wide-area power outage can occur. Further, the infrastructure in the three levels is so old that their efficiency is very low.

Regarding the generation infrastructure in the existing power system, the average power station was built in 1960s [1.4]. Since then, generation capacity has relatively decreased while the load demand has consistently increased. As sown in Figure 1.3, only in 1986 and 1992 the installed generation capacity exceeded the load demand growth. This shows a chronic underinvestment at the generation level. It also implies that the majority of existing installed capacity operates with outdated technology. Inefficiency, undesirable emissions, higher cost of production, and unexpected outages are a few of the major issues related to the old generation infrastructure.

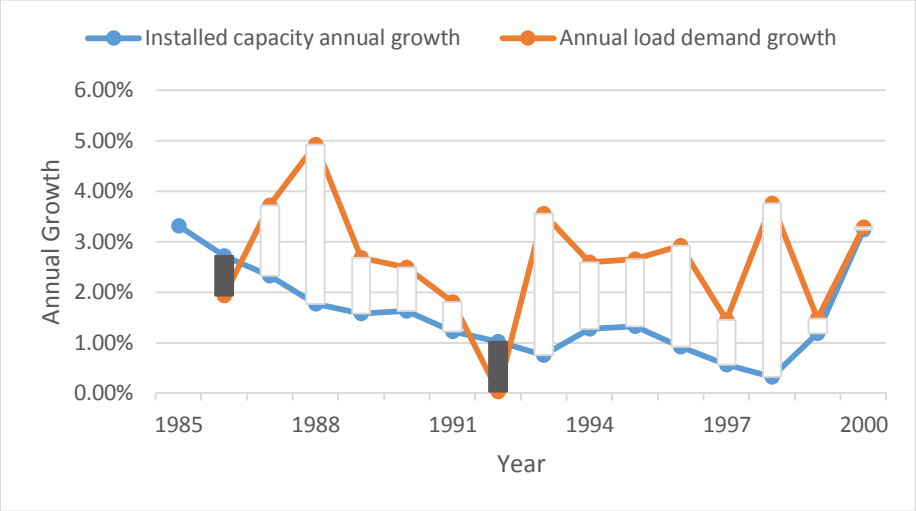


Figure 1.3. Installed generation capacity annual growth vs. load demand annual growth [1.8], [1.9].

Similar to generation, the transmission and distribution infrastructure are also suffering from underinvestment in facilities over the last 40 years. As an example, only 668 additional miles of interstate transmission line have been built during 2000 to 2005 [1.4]. Since 1982, growth in peak demand has exceeded transmission expansion by almost 25% every year [1.4].

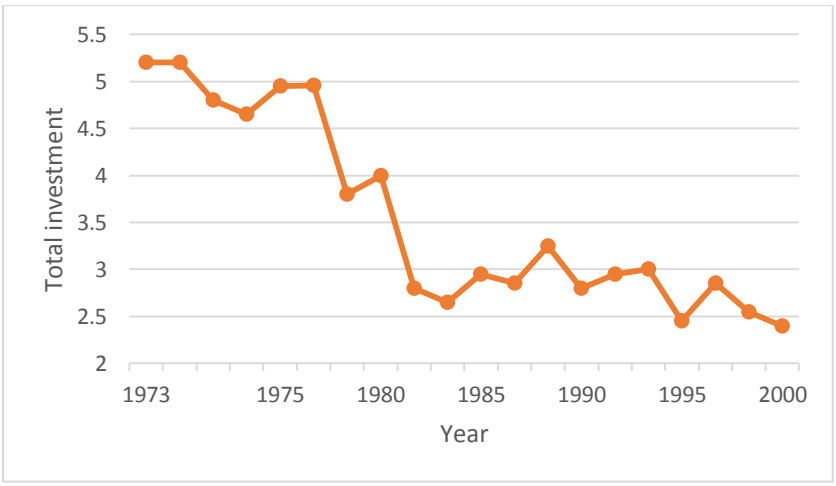


Figure 1.4. Decrease in transmission investment in U.S. (billion US$) [1.4].

The decreasing trend in transmission investment is obvious in Figure 1.4, between 1970 and 2000. As a result, most of the transmission lines are experiencing congestion which further decreases system reliability and efficiency, and increases operational cost.

In a study performed at EPRI [1.6], the infrastructure depreciation rate exceeded utility construction expenditures from 1995 to 2004 (Figure 1.5). Also, as shown in Figure 1.6, research and development (R&D) expenditure among power system utilities is less than 2%, which is the smallest investment compared to other industries. As a result, the network has become progressively stressed, where the carrying capacity or safety margin to support expected and unexpected demand is in question. In addition, the complex systems of generation and transmission used to relieve the stress or to clear disturbances during periods of peak demand are in a critical condition [1.6]. This can result in a huge crisis for the power system infrastructure because of the amount of required capital investment from utilities in the near future.

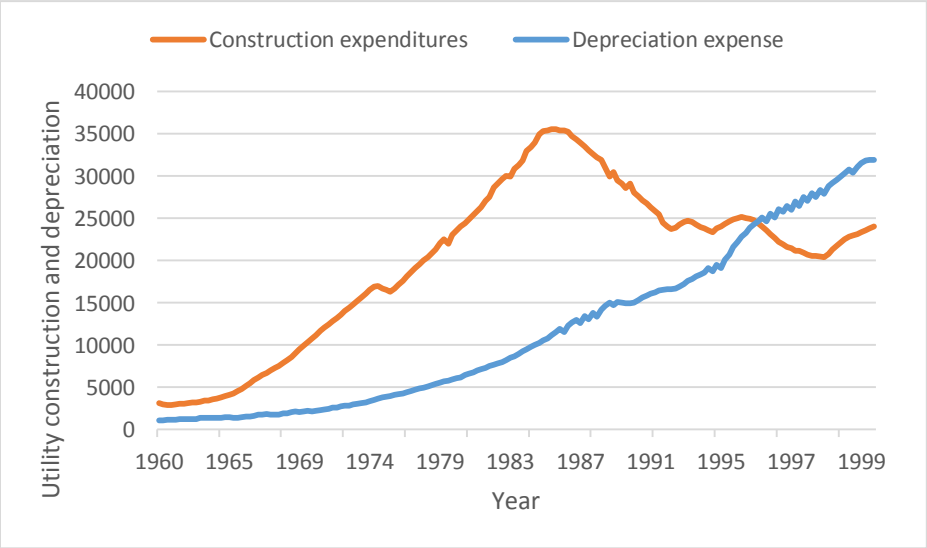


Figure 1.5. Utilities construction and depreciation expenditures from 1960 to 2000 [1.6].

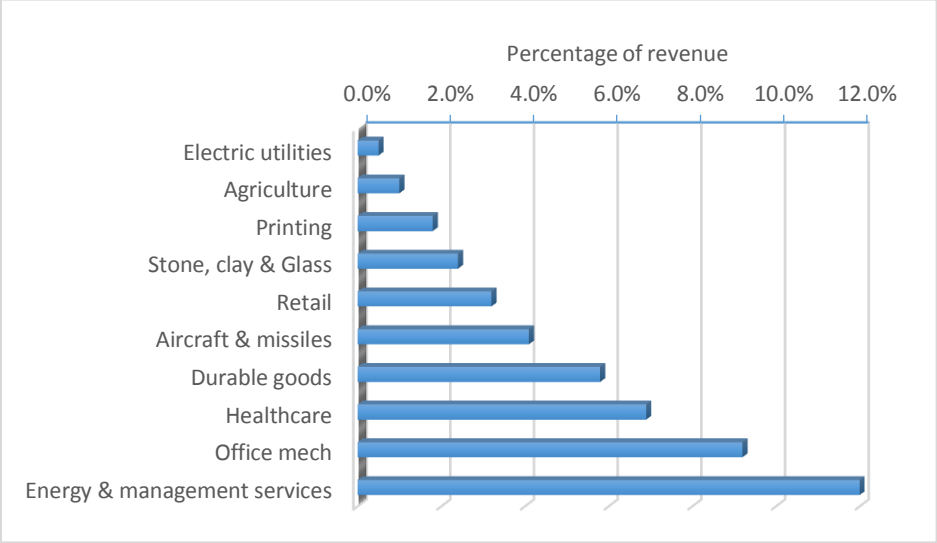


Figure 1.6. R&D investments as percentage of revenue [1.4].

The existing distribution system infrastructure is so obsolete that the only way a utility knows about an outage in many areas of the country is only by customers' call [1.4]. It is obvious that because of chronic underinvestment in power system infrastructure, lack of R&D investment, old technologies at different levels, and load demand increase, the integrity of the power system is in a great danger. This way, the distribution system cannot meet the expectations of the consumers in the future. It certainly needs renovation to keep up with changes in consumption and new capabilities required for the future society. So, broadly, the present power system needs major renovation to be able to handle the features of the smart grid.

Smart Grid. Renovating the existing power system infrastructure is one of the major missions of the smart grid effort. A wide range of technologies, such as advanced metering infrastructure (AMI), RES, storage devices, DR, and wide-area communications are foreseen to be applied in the smart grid to increase its visibility, generation diversity,

affordability, cleanness and higher efficiency. Additionally, a complex interaction of devices is expected in the smart grid era, which needs distributed intelligence and smart control through complex real-time power management algorithms for its safe and economical operation. Furthermore, a revolution in the regulatory framework governing power system markets, both at the federal and state levels, is also necessary for the smart grid technology to loosen regulations and unleash competition in the power system [1.2].

The generation infrastructure is one of the first targets in the smart grid effort. Since load demand growth has been far ahead of the added generation capacity for so many years, as shown in Figure 1.3, incentives are necessary to encourage utilities to install new generation capacity. But this effort is not only limited to the utilities. In fact, each consumer in the smart grid is assumed to be a producer simultaneously, called prosumer [1.10]. In other words, consumers will be encouraged to install residential DERs (such as solar photovoltaic (PV) panels) and small-scale storage devices to produce a part of their electricity on their own. This way, the customers may also be able to support the grid in peak hours by selling their excess generated power to the utilities as ancillary services. Technically, this is possible by using modern power electronic interfaces (PEIs) with more efficient and lighter PV modules.

In terms of financial motivations, several subsidiary programs are offered at the federal and state governments in the U.S. Currently, a federal tax credit of 30% is offered to the residential and businesses who install PV [1.11]. As an example of such programs at the state level, Burbank Water & Power in California provided a rebate program for commercial and multi-family residential to return $15,000-$30,000 to customers who

installed DERs, such as solar PV panels or wind turbine [1.12]. Implementation of such programs resulted in over 186 MW of solar PV installation in the residential sector by the third quarter of 2013 [1.13].

In the utility scale, most states have passed their own renewable energy portfolio (Figure 1.7). This is a part of the smart grid effort to keep up with the load demand growth. These policies help to diversify primary energy resources for electricity generation and shift from fossil fuels such as oil, coal and natural gas to abundant, free, and clean energy sources such as wind and solar power. As a result of such programs, the amount of renewable generation has increased in the power system (Figure 1.8). As shown in Figure 1.7, a significant share of generation is projected to be from renewable resources by 2040.

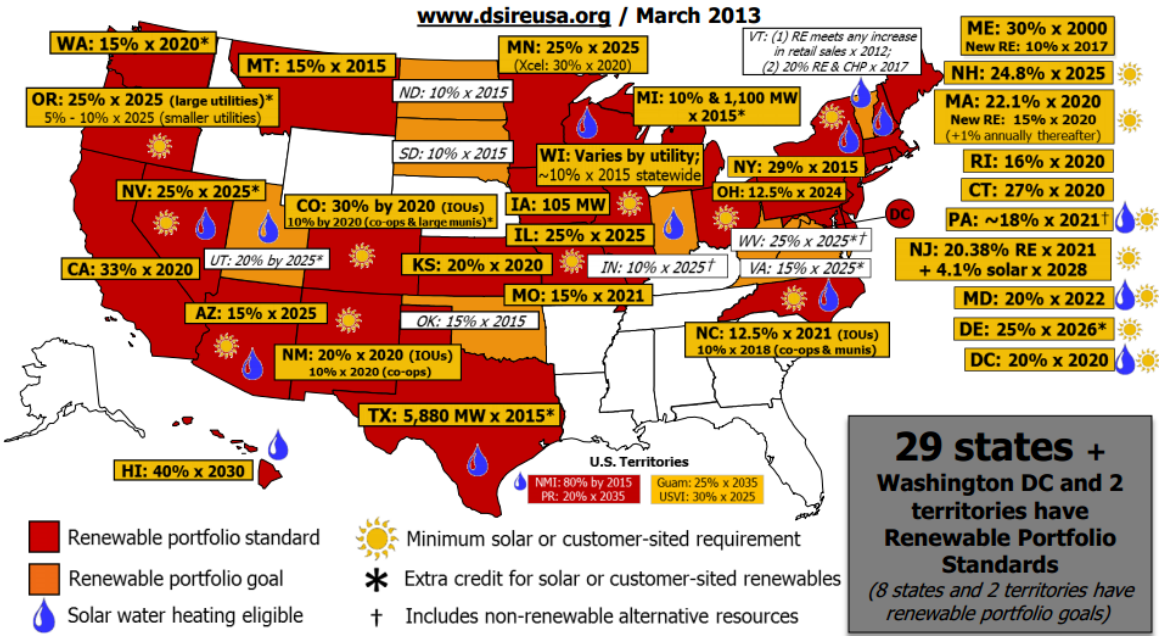


Figure 1.7. Renewable Energy Portfolio (RPS) standard policies [1.14].

As an example in the third quarter of 2013, 930 MW of new PV capacity was

installed in the U.S., and the state of California was ranked first with 455 MW capacity [1.13]. In general the generation infrastructure is being renovated with not only added capacity, but also with larger amount of renewable generation. The centralized structured power system is gradually being replaced with customer oriented generation in smaller scales that are closer to the consumers.

Technology selections for new generation capacity are based mainly on capital, operating, and transmission costs [1.15]. Coal, nuclear, and wind plants are capital-intensive (Figure 1.9). The capital cost of each technology depend on factors such as equipment costs, interest rates, and cost recovery periods, which are different from one technology to another.

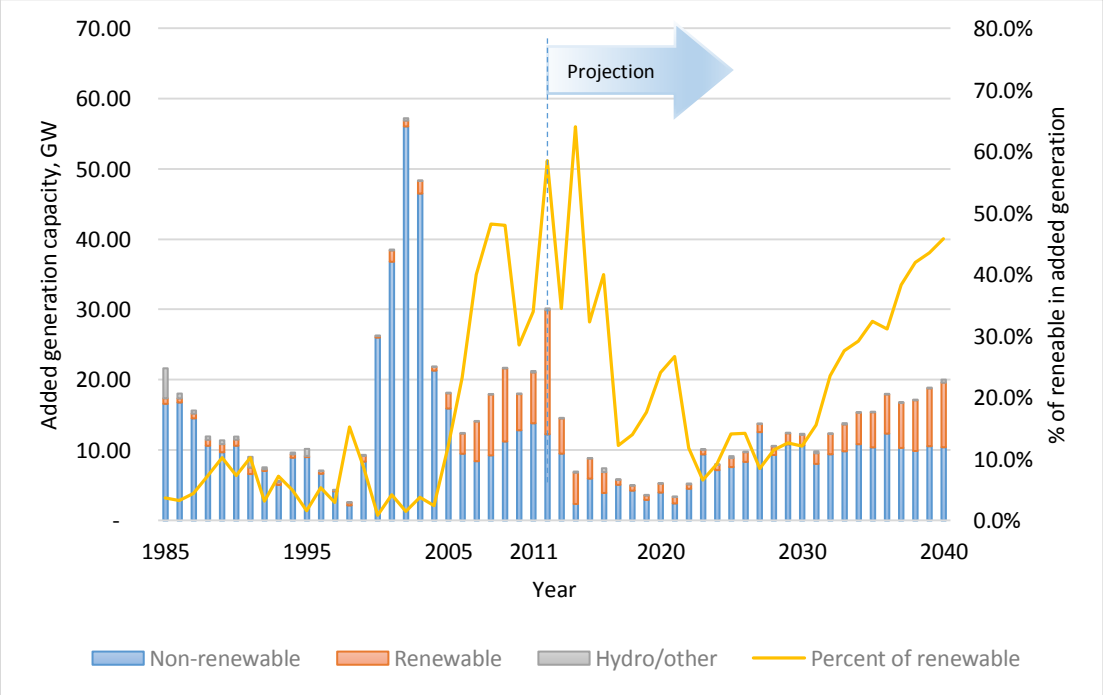


Figure 1.8. Added and projected additions to power plant capacity from 1985-2040 [1.16].

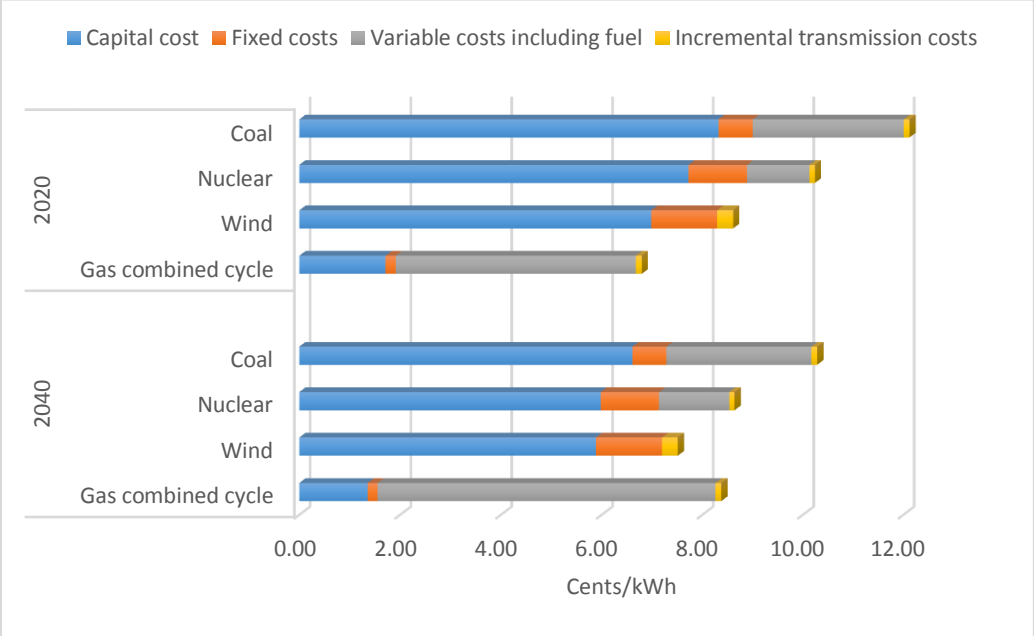


Figure 1.9. Levelized electricity costs for new power plants, 2020 and 2040 estimation (2011 cents per kWh) [1.15].

Operational expenses (such as fuel cost) make up most of the costs for natural gas plants. Fuel costs vary with operating efficiency, fuel price, and transportation costs. Figure 1.9 shows that wind generation is cheaper than coal and nuclear power plants, which raises lots of hopes when considering potential technologies for the smart grid.

Renovating and investment on transmission and distribution infrastructure along with new operational practices and methodologies are absolutely required for safe and economic operation of the future power system. However, it is becoming increasingly difficult to site new conventional overhead transmission lines, particularly in urban and suburban areas experiencing the greatest load growth. In order to resolve this dilemma, power electronic developments are required to allow more power flow through existing transmission assets. In addition, developing low impact transmission lines, such as

advanced conductors made from new composite materials and high temperature superconducting materials, is crucial for respectful land use concerns [1.2]. Moreover, transforming the centralized power system structure to a more decentralized structure (by employing more DERs generation in residential and commercial sectors) will help to reduce the congestion on the transmission and distribution systems and postpone the need for new transmission and distribution infrastructure.

As a result of the need for new transmission systems, more utilities have plans for new transmission infrastructure. Construction of new transmission lines in recent years has slightly increased. For example, Edison Energy Institute (EEI) members' year-over-year transmission investment has nearly doubled from $5.8 billion in 2001 to $11.1 billion in 2011 (real $2011) [1.17]. This can be clearly seen in Figure 1.10.

A new revolution for the distribution system is required in the smart grid era. In order to link the information technology revolution to that of the power system, AMIs are expected to be implemented at every level from individual customers to each of the components in the distribution network (transformers, capacitor banks and voltage regulators). The AMIs installed at each consumers' building will reform the existing practices of load and generation balancing in the power system. Additionally, a protection concept in the distribution level will be added to make the reverse power flow possible by new relay coordinating algorithms and protection philosophies. Moreover, the concept of MG, as the most important driving technologies of the smart grid, will transform the role of distribution system for ancillary services (AS) providers and power system operators in the smart grid era.

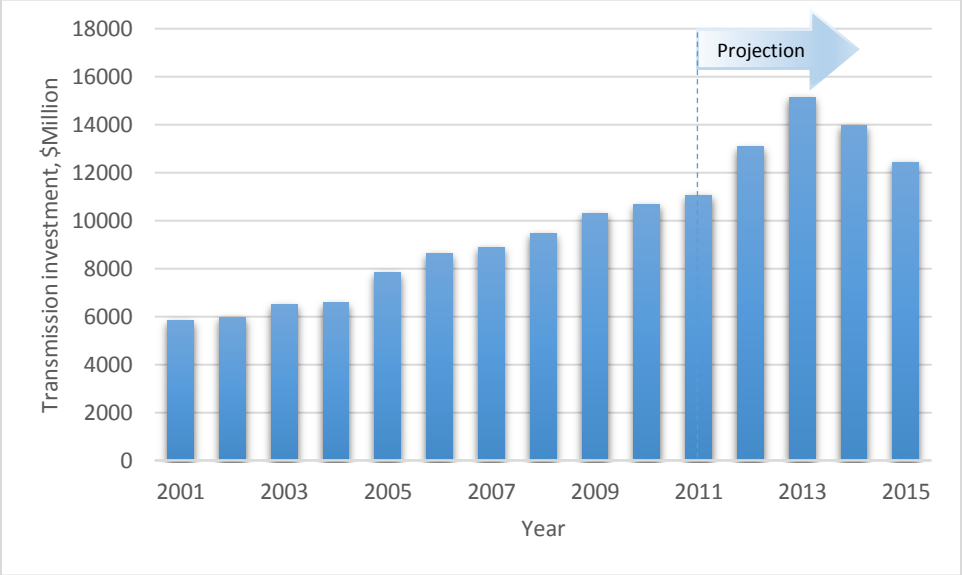


Figure 1.10. Actual and planned transmission investment by shareholder-owned electric utilities (2001-2015) [1.17].

Deregulated Electricity Market

Although complete deregulation of the electric industry is not a realistic goal [1.2], restructuring of regulations to open more sections of the industry to competitive market is possible with increasing benefits to the customers. Because of the importance of deregulation in power industry, this section makes an attempt to reveal current problems with deregulation in U.S. power industry and to show the impact of the smart grid on this particular matter.

Current Power System. As mentioned earlier, the existing power system is structured centrally where electric utility companies (known as utilities) have been mostly owned by private sector, vertically integrated, and locally regulated. In this configuration, separate utilities were responsible for operating the power system, each of which is independent in its own control area and regulated by local legislators. Therefore,

utilities were supposed to transmit power from generation to load centers reliably and economically as a non-competitive, regulated monopoly. The emphasis was on the reliability and security at the expense of economy [1.6]. Additionally, there were national regulations in the areas of safety, pollution, and network reliability; these regulations have constrained utilities' operation to some degree. Power system restructuring and deregulation in U.S. started in 1992 with the National Energy Policy Act (NEPA) bill [1.2], [1.18]. This law permitted individual power producers to compete for the sale of electricity to utilities in an open electricity market. As a result, multiple energy producers have been created that must share the same regulated energy delivery network. Conventionally, new delivery capacity would be added to handle load increases through long-term planning, however, because of the difficulty in obtaining permits after deregulation and the uncertainty about achieving an adequate rate of return on investment, the annual addition to the transmission infrastructure fell behind the total load demand increase (Figure 1.3 and Figure 1.4).

Another concern related to the power system deregulation is whether there is a unifying approach for the simulation, analysis, and optimization of time-critical operations. This applies to both financial transactions and actual system control, in this multi-scale, multi-component, and distributed systems. Furthermore, mathematical models of inter-operating networks are either imprecise or may not even exist, and existing, classical methods are either unavailable or are not sufficiently powerful [1.6]. Therefore, optimal power system operation will be a necessary but complicated task in the deregulated power system without appropriate tools and mechanisms.

Smart Grid. Restructuring of the electricity industry in U.S. has been a difficult task over the past several years for a variety of reasons, but most significantly the degree of inter-governmental cooperation [1.2]. In this uncertain situation, investors are always worried about cost recovery and future rates of return; this may account for the underinvestment in power system infrastructure, for independent power producers, power marketing entities, and investor-owned utilities. As a result, electricity restructuring is considered as the most significant public policy drivers [1.2] and will be continued in the smart grid.

Electricity restructuring can also drive some other features of smart grid. Because the core idea of power system deregulation is to make utilities compete against each other, they will be indirectly obligated to develop new products, such as new home energy management systems, or integration of renewable energy systems [1.6]. In terms of renewable energy, deregulated markets create an environment, where each customer can show preference for renewable energy. In other words, customers will be aware of the source of electricity they purchase [1.19]. In addition, generation and transmission capacities will be increased by the utilities in order to increase their revenue.

To enhance competition in the smart grid era, a modern electricity market, applicable for the complex structure of the smart grid, is essential and is expected as a part of the smart grid program. This goal is reflected in the EPRI's electricity technology roadmap [1.2], [1.20], which can facilitate the implementation of deregulated electricity market involving customers, small electricity retailers, and producers. In addition to required regulations and policies for a successful power system deregulation program,

new simulation and planning algorithms must be developed.

Reliability

Reliable delivery of electricity is critical in our daily lives. In this section, the existing power system will be compared with the smart grid in terms of reliability.

Current Power System. The existing power system is said to be 99.97% reliable. However, power outages and interruptions cost the United States US$150 billion each year; this breaks down to about US$500 per year for every individual [1.2], [1.4]. A comprehensive list of major power outages in U.S. until 2003 is given in [1.6].

Power outages and interruptions also impose huge expenses for businesses. American businesses alone have an estimated US$100 billion in losses each year due to power outages [1.4]. For example, in 2000, the one-hour outage that hit the Chicago Board of Trade resulted in an estimated US$20 trillion in trades delayed [1.4]; Sun Microsystems estimates that a blackout costs its' company US$1 million every minute, and the Northeast blackout of 2003 resulted in a US$6 billion economic loss to the region [1.4].

In the last 40 years, five massive blackouts have occurred in U.S.; alarmingly three of them have occurred in the past nine years [1.4]. The average outage affected 15% more customers from 1996 to 2000 compared to the similar events from 1991 to 1995 (average size per event was 409,854 customers affected in the second half of the decade versus 355,204 in the first half), as shown in Figure 1.11.

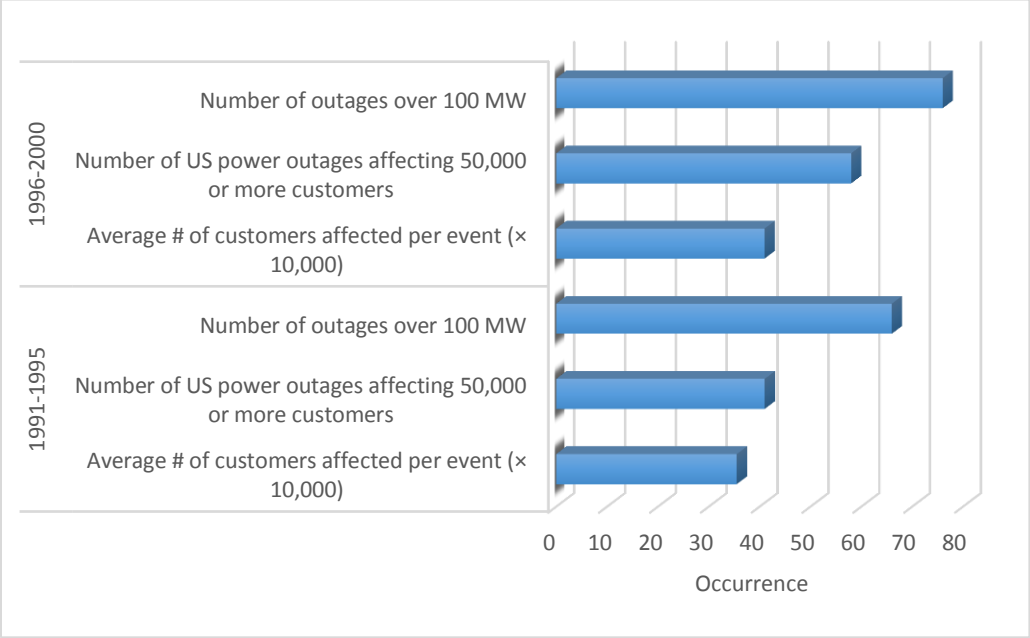


Figure 1.11. Increasing frequency and size of U.S. power outages 100 MW or more (1991-1995 vs. 1996-2000), affecting 50,000 or more consumers per event [1.6].

Further, the average undelivered load caused by an outage increased by 34%, from 798 MW between 1991 to 1995 to 1,067 MW between 1996 to 2000 [1.6]. The primary causes of the most of the outage events were slow response time of the existing mechanical switches, lack of real-time automated analysis of the system, weak observations of the power system, and lack of situational awareness on the side of the grid operators [1.6]. Other potential factors include the chronic underinvestment in generation and transmission infrastructure, as well as the poor visibility of the current power system components with lack of fast analyzing and restoration algorithms for bulk power system operation.

Smart Grid. It is clear that reducing the size and number of power outages will save huge expenses for utilities and customers. Several technologies are considered for

the smart grid to elevate the reliability of the power system. One major problem with the current power system is the lack of effective system monitoring. This problem will not exist in the smart grid where all individual customers and power system components will be monitored in real-time through AMIs. In addition, developing fast restoration algorithms to diagnose problems and find the best solutions can guarantee that the cascading blackouts will never happen. In terms of power systems' unreliable structure, new generation and transmission systems will be added with higher efficiency to reduce the congestion on the system. Transforming the power system from a centrally structured to more distributed topology will also increase the reliability of power system since power delivery is less dependent on the transmission and distribution infrastructure and more close to the load centers. Therefore, DERs application for small customers is a key to achieve higher reliability in the smart grid.

MG will be a key driving technology in the smart grid. MG, a regional group of generation, storage, demand, and distribution system, can work in grid-tied or islanded modes. This way, the current extra-large power system can be divided into many MGs which can work independently as well as in cooperation with other MGs and upper grids, and will substantially reduce the probability of a cascading failure to the whole power system, and large blackouts will not exist; power outages and failures will be confined to the small region of the MG. Additional technology adaptations for MGs (such as storage devices and power electronics) will enhance the power quality in terms of frequency, voltage, and harmonics to the consumers.

EIA determines power system reliability by peak load, monthly peak hour

demand, net energy for load, planned capacity resources demand, and planned capacity resources [1.21]. Considering these criteria, the projection of power system reliability for the next 10 years is given in [1.19]. According to the results of this study, it is recommended by the NERC that the bulk power system will require new operational tools and procedures for careful consideration, preparation, and planning. This is exactly aligned with the features included in the smart grid roadmap.

National Economy and Global Competitiveness

The impact of the power system reliability and outages on the national economy was discussed thoroughly in the previous section. The power system also encompasses a big industry that employ millions of people directly (about 550,000 [1.5]) and indirectly, which indicates its critical role in the national economy. Further, innovation in new technologies and products extend progress in the power system to global markets. In this section, a general overview will be given about global market for power generation resources and successful companies around the globe. Then, the role of the smart grid program to increase competitiveness of American companies in the global market will be explained.

Current Situation. In 2012, a report was published on the global status of renewable energy generations around the globe revealing the market share for different companies [1.22]. In solar operating capacity, the U.S. was ranked 5th with 5.7% of total solar PV capacity installed around the globe. Germany was the first country with 35.6% of the share. As a result, American solar PV manufacturers (namely First Solar and

SunPower) had only 8.5% of the total market share in 2011. Chinese companies with 30% of the total market share were in the first rank. In terms of wind power capacity, the U.S. with 6.8% added capacity in 2011 was in the 2nd place after China. Additionally, U.S. had the 2nd rank in the total wind power capacity installed around the globe. With this large amount of wind power capacity, American companies (namely GE Wind) had only 8.8% of the total market share, while Chinese companies hold 26.7% of the total market share. Clearly the global share of American companies in renewable energy is much less than that installed (i.e., wind and solar PV) in the country. This shows that foreign companies are providing a large percentage of technologies and products in the U.S., but not American companies and subsequently missing opportunities to benefit from the global market. One reason for this phenomenon is the fact that American companies and utilities do not invest enough money for R&D, as was shown in Figure 1.6.

Smart Grid. With governmental regulated renewable generation utilization within the power system, and the future plans shown in Figure 1.7 and Figure 1.8, more stakeholders and investors will be motivated to spend more money for R&D. At the same time, larger penetration of renewable generations in the power system will make larger revenue for the existing companies to increase R&D expenditure to achieve a larger share in the global markets. In addition, subsidies and new policies are strongly motivating individual customers to invest their money into the renewable generation by purchasing these products. This will extend the national market for these companies, which can result in better products and more innovations. Additionally, more labors and experts will

be employed in the electricity sector in the future. This can drive the economy and bring prosperous lives for more Americans in short- and long-term.

National Security

As explained earlier, electric power systems establish the fundamental infrastructure of modern society. However, a successful rebellious effort to interrupt electricity supplies could have overwhelming impacts on the national security, the economy, and the lives of every citizen. This section tries to explain current power system issues regarding national security. Following that, the role of the smart grid will be discussed to resolve those issues for resilient and secure power system of the future.

Current Power System. The existing power system consists of widely dispersed assets that can never be absolutely protected against a determined attack. In other words, the grid's centralized structure leaves the power system open to any attack. In response to the September 11th 2001 attacks, EPRI assessment highlights three different kinds of potential threats to the U.S. electricity infrastructure [1.6], [1.23]: 1) Attacks upon the power system where the electricity infrastructure itself is the primary target, 2) Attacks by the power system where the ultimate target is the population by using parts of the electricity infrastructure as a weapon, and 3) Attacks through the power system where the target is the civil infrastructure. These are all possible based on the current topology of the power system and the poor visibility of the system itself. In addition, there are legitimate concerns and challenges with power outages regarding national security. When the blackout of 2003 occurred, the largest in U.S. history, many people stuck in the dark

imagined another terrorist attack. The linkages of various grid components can be exemplified as domino effect, where sequences of failures could interrupt the whole nation's banking, communications, traffic, and security systems.

Todays, most of utilities own and operate at least parts of their telecommunications systems which often are based on fiber optic or microwave links connecting major substations with branches to smaller sites. However, as is true for other critical infrastructures, increased utilization of electronic automation raises significant concerns and challenges towards capability of operational security. In addition, reducing physical labors and personnel at remote areas can increase the vulnerability of the system to contentious threats. Even more concerns can be expected for interconnecting automation and control systems to public data networks (such as Internet). This way, the infrastructure will be accessible to individuals and organizations from any location around the globe using an inexpensive computer and communication link. Furthermore, use of interconnected electronic systems for metering, scheduling, trading or e-commerce imposes many financial risks linked with communication failures.

Moreover, a power system, densely dependent on fossil fuel power plants will be a threat to the national security. Imported fuel can always be threatened by any changes in political relation with exporting countries. Oil embargo of 1973 is a good example of such condition, which started by the members of Organization of Arab Petroleum Exporting Countries (OAPEC) [1.24]. So, the strong link between electricity and national security can be clearly realized from the facts given above.

Smart Grid. In fact, smart grid program necessitates advanced automated

decision making and algorithms for power system operation instead of human operations. Additionally, it emphasizes on a high visibility of the power system which only can be achieved through more measurement units and communication links. This essentially increases the size of the information even for the ordinary customers, which means easier access for ordinary people to reach out to the power system through their AMIs and phasor measurement units (PMUs). Despite the increased security risks in the smart grid era, standard communication protocols and integration techniques must be employed in the power system to avoid such threats. In order to overcome these issues, the smart grid features a secure communication infrastructure with the highest level of security. Because of this motivation, interdisciplinary research groups from communication engineers to computer scientists are cooperating together to find appropriate solutions.

Although a highly secure communication infrastructure in the smart grid can be achieved, the most important role of the smart grid for a more secure power system can be found in the MG technology. Basically, MGs transform power system topology from central to more dispersed and distributed configuration. This way, any possible attack to the infrastructure has less impact on the large number of individual customers. In addition, critical customers can have their own MG, which can survive even after a serious attack and can continue its service. Another advantage of the MGs for national security is the fact that these facilities are smaller in size (compared to the large central steam or nuclear power plants). The smart grid includes numerous small smart MGs, in which any cyber-attack will be only limited to a certain number of regional MGs, not the whole grid. Self-healing algorithms and fast switches will disconnect the attacked MG

from the rest of the power system. In other words, MGs in the smart grid era will be capable of self-containing attacks and failures to prevent cascading failures and large blackouts in the power system.

Load Demand

Power systems safe operation heavily relies on the balance of generation and demand at every instant. Therefore, study of load demand variations and its characteristics over time is critical. In this section, the current situation of load demand will be discussed. Then, the role of the smart grid program will be explained in terms of load demand and customers' rights.

Current Power System. As mentioned earlier, power system infrastructure experienced chronic underinvestment in the last several decades. On the other hand, load demand has increased by almost 30% during 1988 to 1998 [1.4]. This essentially means that load increased while generation and transmission assets were not increased as much. The increase in load demand occurred for several reasons: population growth, new electronic devices such as PCs, the digital revolution which added millions of new gadgets to the power system, more HVAC systems, and an extension of the power system to remote areas. The growth in electricity consumption is being, counterbalanced by efficiency improvements in new appliances and by investments on energy-efficient equipment (Figure 1.12 and Figure 1.13). As shown in Figure 1.13, demand is projected to increase about 28% from 2011 to 2040 (approximately 0.9% each year). This significant increase necessitates building new generation, transmission, and distribution

infrastructures other than renewing the obsolete components.

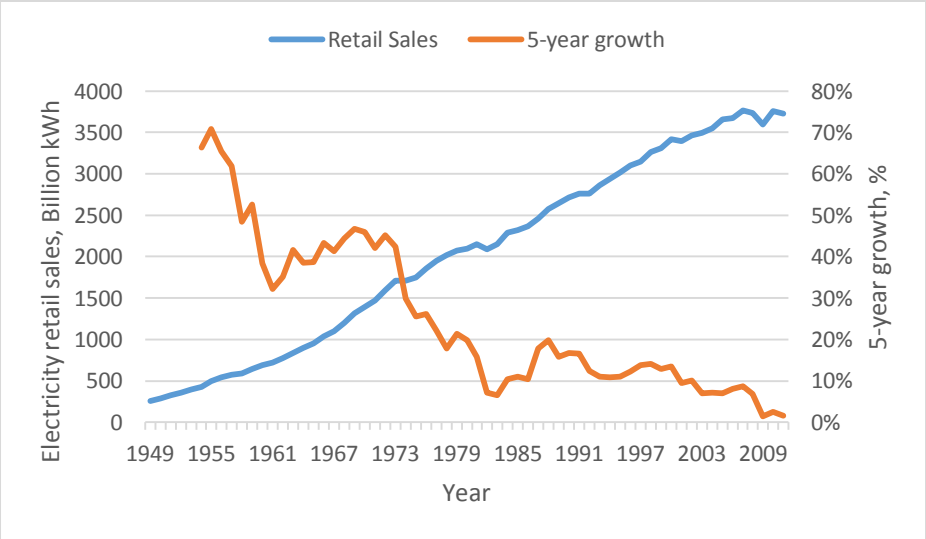


Figure 1.12. Electricity retail sales to all sector from 1949-2011 and 5-year growth in demand, power plants direct use is not considered [1.9].

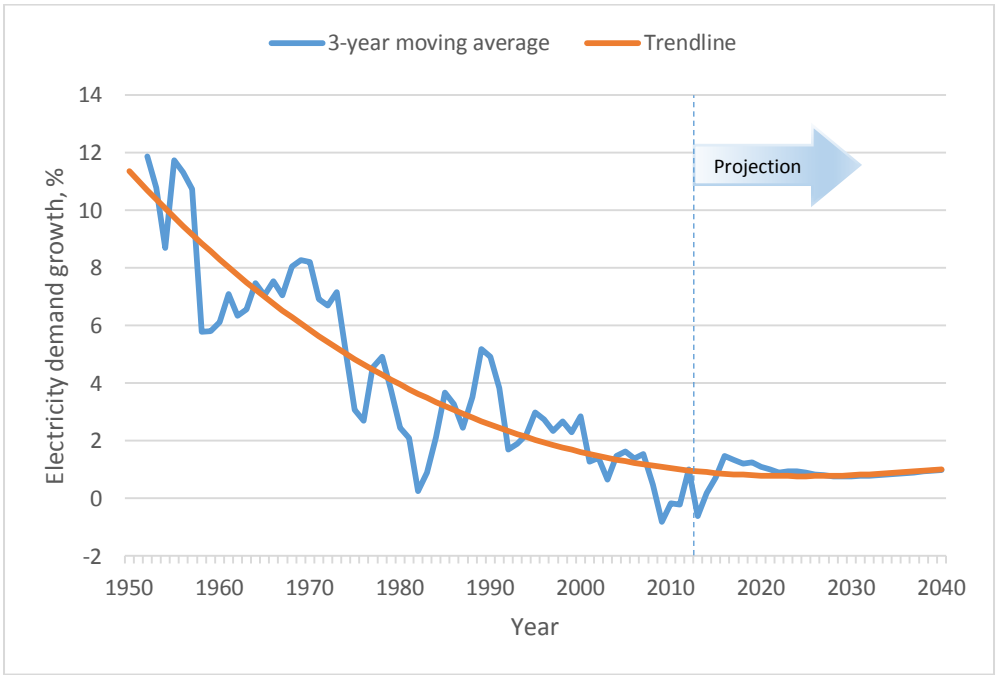


Figure 1.13. U.S. electricity demand growth, 1950-2040 [1.15].

The consequences of not keeping up with demand could be serious, and could have the potential of causing rolling blackouts. This essentially implies that utilities should actively invest in capital expenses to build new infrastructures in the near future. In addition, building new electricity infrastructure requires significant amount of time which obligates long-term planning based on demand projections and other technical constraints.

Another problem with the existing power structure is the fact that customers do not have different options to purchase their power. The availability of such capability in the power system will increase competitiveness among the different generators and utilities to produce high quality power with the minimum cost. Moreover, customers are passive in the existing power system regarding their power consumption. They consume electricity without noticing the cost of their consumption at the time of usage. However, having the information about electricity price, some customers may postpone their consumption from high-price hours (i.e., during peak demand hours) to the time when electricity is cheaper (i.e., during off-peak hours). This can result in shifting electricity demand from peak hours to off-peak hours, which helps to flatten the load profile and increases the load factor in the system.

Smart Grid. Although renovating and adding new generation and transmission systems is one possible solution to keep up with increasing load demand, this is not the sole solution proposed by the smart grid program. Demand side management (DSM) (i.e., modification of consumer demand through various methods such as financial incentives) is a very powerful approach in the smart grid era for balancing generation and demand.

DSM includes a broad set of actions on the consumer and utility sides and includes everything from installing energy-efficient appliances and switching off unused lights, to adding local off-grid generation abilities, to implementing a complicated electricity pricing system in which rates vary based on time-of-day and aggregate power usage intensity [1.25]. Based on the U.S. DOE report [1.2], economic benefits from DSM in the U.S. can range from about US$80M to about US$800M annually, in addition to another US$85M to more than US$300M annually through emergency DR.

The national average load factor (which is a measure on actual physical facilities utilization) is about 55% [1.2]. DSM can be very helpful to increase load factor by reducing consumption during peak hours, which can increase efficiency of the power system and reduce operational cost. Furthermore, a wide variety of information technology is expected to be utilized in the smart grid that can transform the electric distribution business to a new model. For instance, different direct and indirect DSM programs based on AMIs secure communication links, and fast computation methods can be applied to effectively monitor and influence each customer's usage, in real-time. In this way, load demand can be controlled, in addition to the traditional generation control, by utilities which can result too many technical and economic benefits for both system operators and customers. Mechanisms to reduce peak demand include time-of-use pricing, load management devices such as "smart" thermostats, load-shifting technologies such as energy storage, and peak-eliminating techniques such as distributed generation and thermally activated heating, cooling, and humidity control devices [1.2].

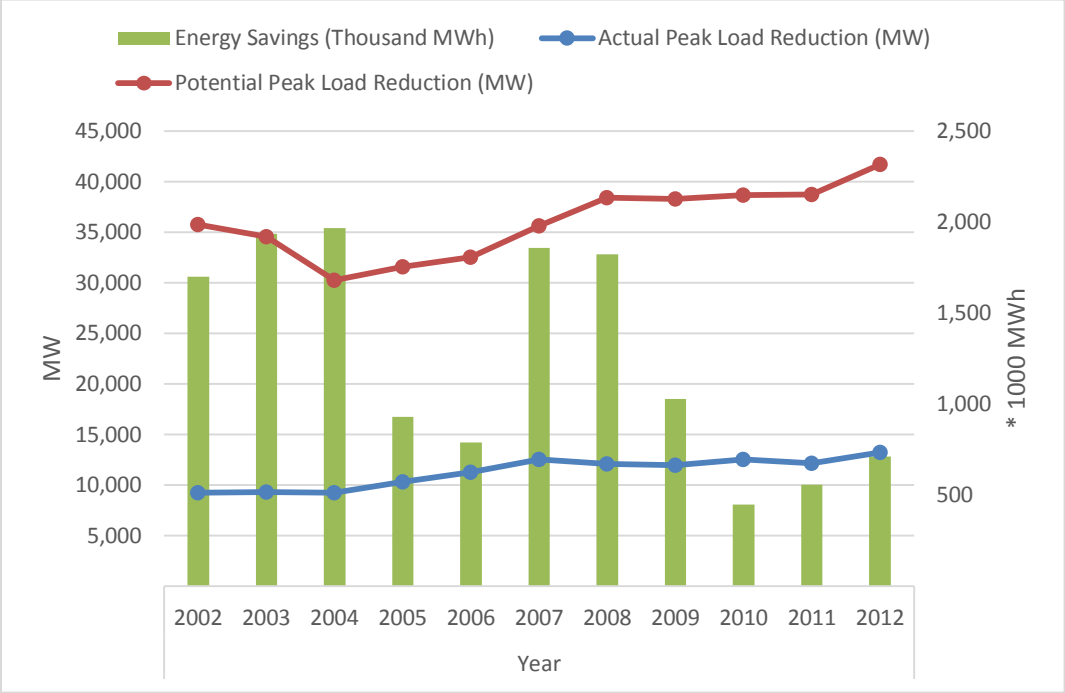


Figure 1.14. Results of load demand management for all sectors in terms of energy savings, actual peak load reduction, and potential peak load reduction [1.16].

Results of the different DSM programs in U.S. from 2002 to 2012 are shown in Figure 1.14. It can be seen that there is still a huge potential for DSM in the power system operation which can be exploited. Energy saving is also significant considering the fact that DSM programs are relatively new and many customers are not effectively familiar with the idea yet.

Figure 1.15 shows the results of DSM programs on the actual peak power for summer and winter from 1990 to 2011 and the projection for 2012 to 2016. After almost a steady increase in peak demand during 1990 to 2002, peak power decreased significantly during 2006 to 2009 despite the steady increase in total power demand, shown in Figure 1.12.

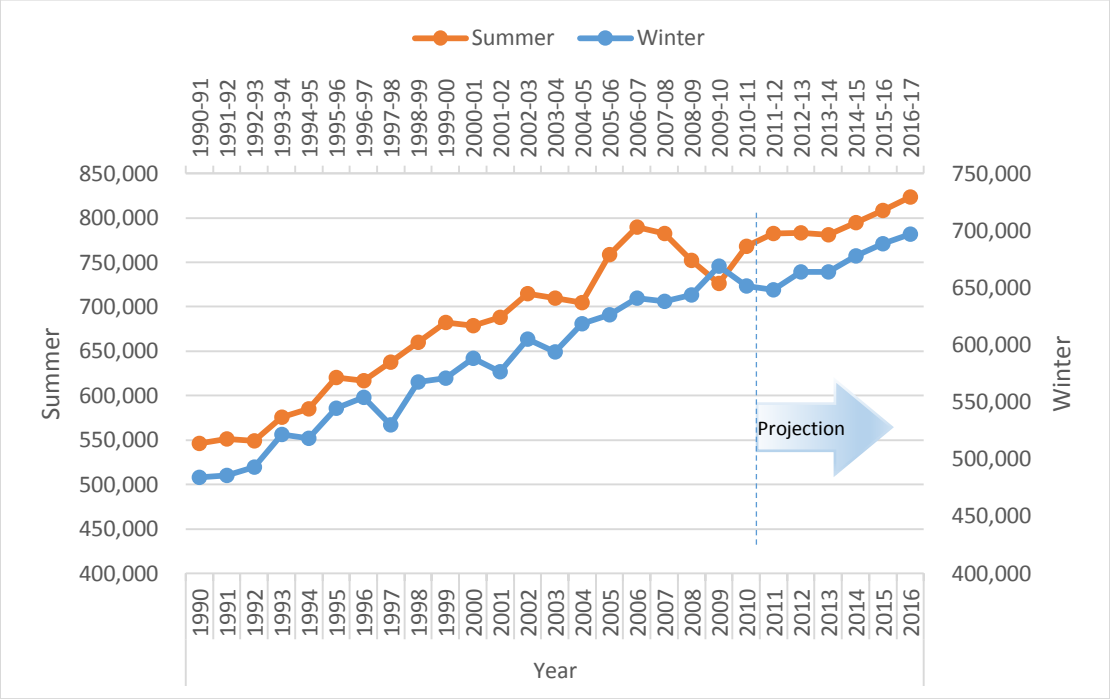


Figure 1.15. Non-coincident peak load, by North American Electric Reliability Corporation Assessment Area, 1990-2011 (actual), and 2012-2016 (projected) [1.26].

The projection for 2012-2016, shown in Figure 1.15, shows a steady increase with a relatively small slope. Nevertheless, utilities strive on cooperation from consumers to participate in different DSM programs. It necessitates educating consumers and developing new algorithms to automatically control their appliances, i.e. direct load control (DLC). DLC as one of the major categories of the DSM programs requires AMI and fast communication links to/from individual customers' devices and very fast algorithms to generate appropriate commands considering customers' welfare. Recently, many research groups have made efforts in this area to develop real-time central or distributed DLC algorithms. Since real-time DR is one of the two focus areas of this dissertation, this part will be discussed in details in later sections of this chapter.

Efficiency

Efficiency of any infrastructure (such as power systems) is an important factor in any engineering analysis. Essentially, efficiency directly affects many other parameters in a power system, which is related to the operational cost and reliability of the power system. Based on a report by the U.S. DOE, improving energy efficiency could reduce national energy use by 10% or more in 2010, and as much as 20% in 2020 with economic benefits for consumers and businesses [1.27]. Also, it is estimated that if the grid was just 5% more efficient, the energy savings would equate to permanently eliminating the fuel and greenhouse gas emissions from 53 million cars [1.4]. In this section, the current situation of North American power system regarding efficiency is presented. Then, features of the smart grid which will help to increase efficiency are explained.

Current Power System. It is obvious that increasing efficiency can save a lot of money from customers' monthly bill. Efficiency of the power system should be measured on four infrastructures: 1) generation, 2) transmission, 3) distribution, and 4) electrical appliances and devices. Regarding generation infrastructure, more than 81.4% of U.S. electricity nameplate capacity belongs to thermal power plants (including coal, nuclear, and natural gas) [1.28]. Unfortunately, the majority of the generation capacity is 30 or more years old and their average thermal efficiency is around 33% [1.2]. Since 1960s, efficiency has not changed considerably because of slow turnover of the capital stock and the innate inefficiency of central power generation that cannot recycle heat [1.2]. The supercritical coal power plants may increase efficiency to mid-40, and the latest coal technology, known as integrated gasification combined cycle or IGCC, is capable of

efficiency above 60%. The most efficient gas-fired generators achieve a similar level of efficiency [1.27]. This is while the average efficiency of about 5,600 distributed energy facilities with combine heat and power (CHP) generation is between 65% and 90%. Unfortunately, these type of distributed energy facilities only accounted for about 6% of U.S. power capacity in 2001 [1.2]. Therefore, there is incredible economic and ecological incentive to improve the efficiency of power generation so that more of the energy content of the input fuel can be turned out to electricity.

A similar situation can be seen in the transmission infrastructure because of chronic underinvestment over the last 25 years [1.2]. The result is grid congestion, which can increase the line losses. Transmission and distribution (T&D) losses are related to the loading of the system. T&D losses in the U.S. and its corresponding cost are shown in Figure 1.16. It can be seen that the cost of losses was continuously increasing until 2008.

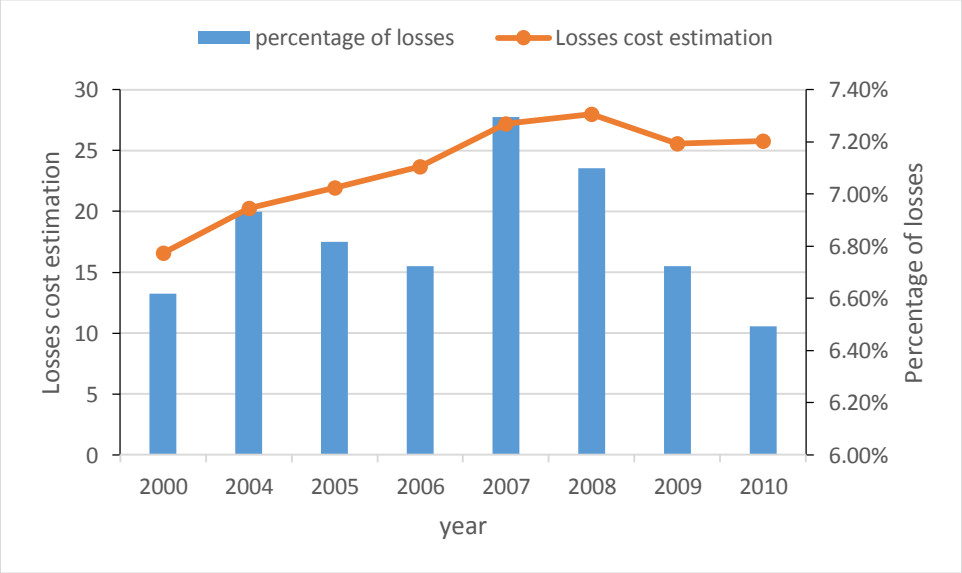


Figure 1.16. T&D losses as a percentage and its cost estimation based on averaged electricity retail price [1.9], [1.29], [1.30].

Another side of the efficiency in power systems is consumers' appliances. For so many years, efficiency was not a primary concern for companies and developers because of cheap primary energy resources such as fossil fuels. As a result, many old appliances are inefficient and waste energy. If every American household replaces just one incandescent bulb with a compact fluorescent bulb, the country would conserve enough energy to light 3 million homes and save more than US$600 million annually [1.4]. This shows the existing potential to decrease unnecessary consumption from the customers' side. In a larger scale, the national average load factor is estimated to be about 55% [1.2], which means that electric system assets are used about half of the time. Moreover, it shows that there is an enormous pressure on the assets during on-peak hours which increase power losses in T&D systems and results in a less efficient power system.

Smart Grid. As mentioned earlier, smart grid targets the generation infrastructure for renovation and diversification as one of its primary goals. Modern technologies will be utilized in the old and the newly added generation units to increase their efficiency. CHP technology in the thermal units is one promising candidate to raise the efficiency of the generation units. In addition, transforming power system structure from a central to more distributed system will also increase power system efficiency since less T&D will be involved in the process of generation and consumption. As a result, typical power losses (6%-8%) through the T&D systems can possibly decline. The utilization of advanced materials such as high temperature superconductors are also expected to be deployed in phase III in the smart grid program by 2030 [1.2]; this technology will also considerably increase the efficiency of the power system.

At the distribution level, there is a huge potential to increase efficiency. As an example, there are over 40 million distribution transformers in service today in the U.S., which are among the most standardized electrical component. Therefore, they can be a prime target for improvements. A new efficiency standard for distribution transformers is under development in efforts to force utilities to increase their efficiency by 4% over current models [1.6]. One can imagine the impacts of this incremental gain across the thousands of distribution transformers under operation.In terms of demand and customers, several features of the smart grid program can help to increase the overall efficiency of the power system. Grid-Friendly Appliance Controller (GFAC) is one the programs of the smart grid to increase the smartness of the electrical appliances [1.2]. The GFAC, which is very small in size, is capable of monitoring line frequency to change consumption pattern on a case by case basis. The controller has been successfully installed on refrigerators, air conditioner, water heaters, and different other household appliances. It has been shown that the devices with the GFAC can support the grid during peak hours by turning the devices off. This essentially results in less congestion in the T&D systems during on-peak hours. Amongst the different electrical devices, industrial motors are known to be the single largest consumer of electric power [1.27]. It is approximated that 65% of industrial power is used in motors of different sizes, most of which run at full speed even if they don't need to [1.27]. Developing and implementation of variable speed drives based on advanced power electronics can change the motor's speed to meet the requirements at any given moment. The resulting energy savings can be immense since reduction in consumption is estimated to be about 60% [1.27].

Informing people about their consumption is another way to help both customers and utilities to control power consumption. As an example, the last several years have seen ads and commercials to encourage people to use compact fluorescent light bulbs instead of old incandescent bulbs with longer lifetime, same amount of light, and less electricity consumption. In-Home Displays (IHD) is another way to involve customers in the power system operation. During on-peak hours when electricity price is higher than usual, IHD informs occupants of the real-time price of electricity. Therefore, it is expected to see many residential customers postpone their unnecessary consumption (such as laundry) to some other time of day when electricity prices are lower. This helps to shift power consumption from on-peak to off-peak periods which further alleviate the congestion on the power system and increase efficiency.

Affordability

Since electricity is an essential part of modern life and an indicator of prosperity, health and safety, it should be affordable and accessible for all citizens to create the same opportunity. In this section, a general overview of the affordability of the electricity in the existing power system is given first. Then, specific features of smart grid will be reviewed which can help to overcome this issue.

Current Power System. Based on a survey carried out at NERC, 65% of the customers' monthly bill involves the expenses at the generation level, while another 5% and 30% comes from T&D operational cost, respectively [1.5]. This shows that any increase in losses and inefficiency of the power system will be reflected in the customers'

bill. In other words, the invisible costs associated with an under-performing grid are paid by every citizen. Based on Figure 1.16, the cost of losses has increased from 2000 to 2008 continuously. This implies a higher cost of electricity for the customers as well, which is shown in Figure 1.17. It can be seen that the average retail price of electricity for all sectors constantly increased until 2008, when the electricity price started to decline for commercial and transportation sectors. However, the trend for the retail price of electricity in the residential sector shows a steady rise between 2003 and 2013. As a result of the price increase, it can be concluded that some low income families are not able to afford the expensive electricity, where they will be forced to curtail their consumption by lowering their standard of living.

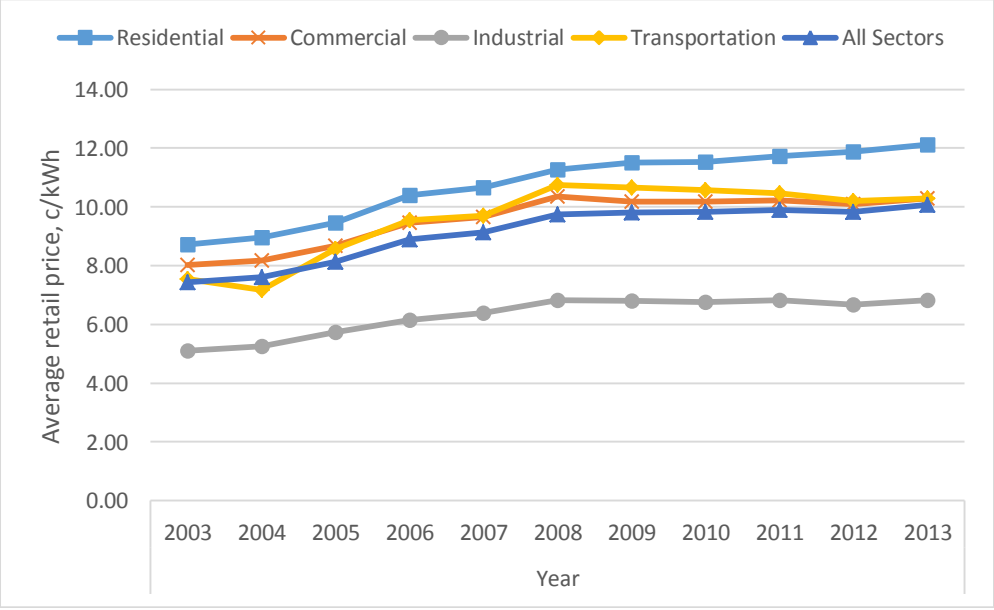


Figure 1.17. Average retail price of electricity to ultimate customers by sectors, 2003-2013 [1.16].

In addition to the infrastructure charges, congestion charges represent another

significant cost in the customers' bill. Congestion occurs when the scheduled or actual power flows are confined either by physical capacity constraints on a particular device or by operational safety constraints designed to preserve grid reliability. In this situation, the system operator must locate an alternative power source to meet the load demand in real-time. As a result, often the alternative generator will be less economical (because it is not the primary source that has been selected through optimal power flow approaches), and less efficient from a market viewpoint.

The California Independent System Operator (CAISO) reported congestion costs of US$1.1 billion in 2004, US$670 million in 2005, and US$476 million in 2006 [1.27]. Similarly, the PJM interconnection, which serves the largest area among all regional transmission organization in the U.S., reported congestion costs of US$750 million in 2004, US$2 billion in 2005, and US$1.6 billion in 2006. Additionally, the PJM indicates that since 2002, congestion costs have formed 7-10% of its annual total billings [1.27]. These numbers and the trend in the last several years clearly project a consistent increase in the price of electricity for utilities and consequently customers, if current power system remains the same. Moreover, the impact of congestion is not only limited to the cost associated with employing less economical generation. Often the situation requires grid operators to curtail service to consumers in some areas to protect the integrity of the grid as a whole, which is called transmission loading relief (TLR) action. The number of TLR actions have increased significantly in recent years, up nearly 150% only in 2001-2005 period [1.27]. The calculations also demonstrate that CAISO has collected US$299 Million over the period April 1998 – Sept. 2000 for TLR. For the year before (Oct. 99 –

Sept. 2000), the congestion rent was US$222 Million [1.31]. It can be easily seen that the congestion rents have constantly increased. This also results in higher price of electricity for the customers.

Greater demand for energy in the future will put pressure on the availability and cost of all natural resources as primary sources of energy. This can potentially increase the cost of the primary fossil-fuel sources in the future. Growing fuel costs have become more critical to the utilities' with expiring long-term coal contracts, which certainly increase the cost of electricity production in the future. This also results in higher electricity prices for the consumers.

Smart Grid. Renovating the power system infrastructure is one of the features of the smart grid program toward producing affordable electricity for anyone anywhere. As it is shown in Figure 1.9, levelized cost of wind power is less than nuclear and coal power plants. Increasing wind power generation in the power system, as shown in Figure 1.8, will decrease the cost of generation for the utilities, which will further decrease retail costs. Also, increasing T&D efficiency will help to decrease the retail price for the ultimate customers. T&D new infrastructure will also help to decrease the retail price of electricity by reducing the congestion on the transmission system which costs system operators a fortune right now.

MG technology is the most important feature of the smart grid to bring the cost of electricity down for the customers. Installing new power generation close to the consumption through DERs will provide relief and consequently congestion on the transmission system. This will directly decrease the cost of operation and retail price of

electricity for the consumers. On the other hand, each customer can have its own generation (such as solar PV) to cover a part of their consumption. Since these technologies are subsidized by the federal and state governments in most part of the country, and considering the fact that solar PV systems have almost zero operation and maintenance (O&M) cost [1.32], renewable generation will be very cheap. IHD devices and smart appliances can also decrease the cost of energy consumption for the customers by shifting their power consumption from on-peak hours to the off-peak hours. Also, making appliances more efficient can help to reduce total energy consumption.

Environment and Climate Change

From food safety to personal health, a compromised environment threatens us all. Unfortunately, U.S. produces 25% of the global greenhouse gases while it only accounts for 4% of the world's population [1.4]. In this section, the current power system will be reviewed first regarding environment and climate change. Then, the role of the smart grid will be presented to reveal its impact to loosen the environmental concerns.

Current Power System. Most electricity is still produced by fossil–fuel-based power plants in the U.S., which are major contributors to global warming Figure 1.18 shows that more than 70% of the total summer generating capacity belongs to the fossil-fuel power plants. This trend started to decrease in early 1980s and picked up again in 2000s with new technology from natural gas power plants that generate less emission.

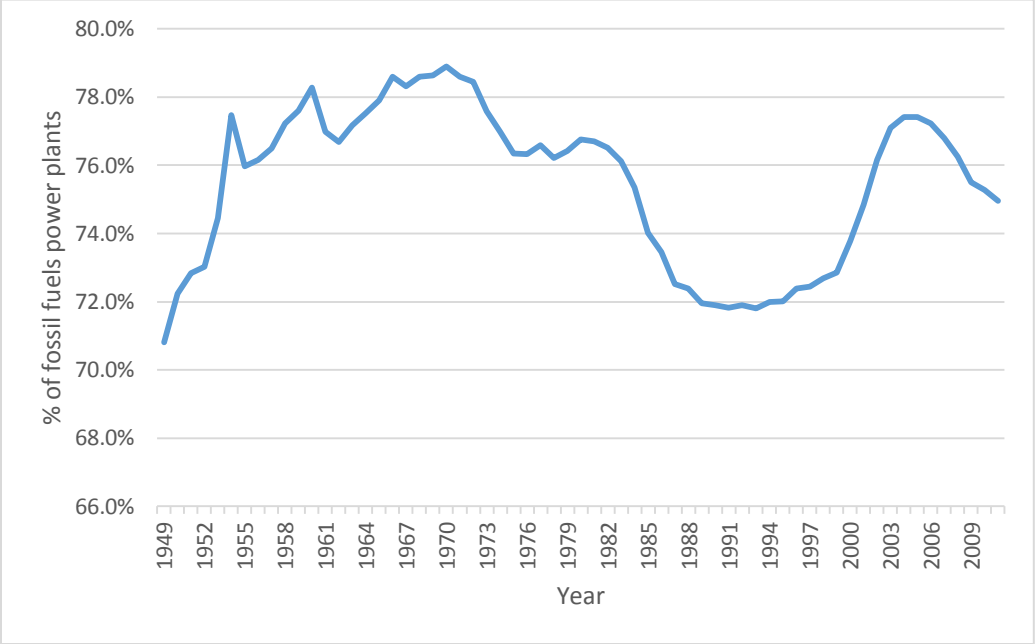


Figure 1.18. Electric net summer capacity for fossil fuels power plants (i.e., coal, petroleum, natural gas, and other gases) for 1949-2011 [1.33].

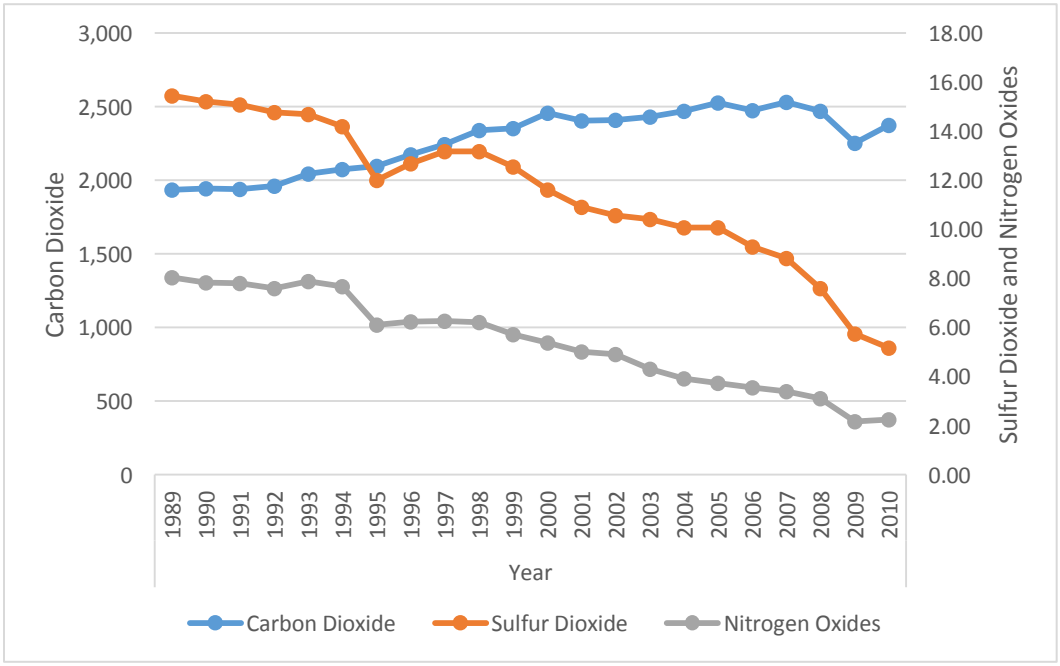


Figure 1.19. Emissions from energy consumption for electricity generation and useful thermal output (Millions Metric Tons of Gas) 1989-2010 [1.34].

The emission production from fossil-fuel power plants are shown in Figure 1.19. The values are for traditional fossil-fuel-based power plants including coal, natural gas, and petroleum burners. Emissions from geo-thermal and non-biomass wastes power plants are not shown in this figure, where their emissions are relatively low

Carbon dioxide production did not change considerably in the last several years (Figure 1.19); however, sulfur dioxide and nitrogen oxides have decreased significantly, and this trend is still decreasing. The reason for this might be the new technology utilized in the new fossil-fuel-based power plants and modern technologies applied to purify the fuels at the refineries.

Smart Grid. To reduce carbon footprint and stake a claim to global environmental leadership, clean, renewable sources of energy like solar, wind and geothermal must be integrated. As a part of smart grid program, renewable generation installations in the U.S. (excluding hydropower) have more than tripled since 2000 (Figure 1.8) and reached to 53 GW in 2009 (14% per year from 2000-2009) [1.28]. Wind and PV are the fastest growing renewable energy sectors with 39% and 52% increase in installed capacity in 2009 [1.28].

Although these numbers are promising for the future power system, renewables only comprise 4.7% of the installed capacity and 3.6% of the total generation [1.28]. Therefore, increasing renewable generation on the power system will definitely help to reduce the emission footprint in the U.S. The projection of renewables' share in total generation up to 2040 is given in Figure 1.20. It shows a 4% and 5% increase for renewable and natural gas, respectively, which will decrease emissions in the future.

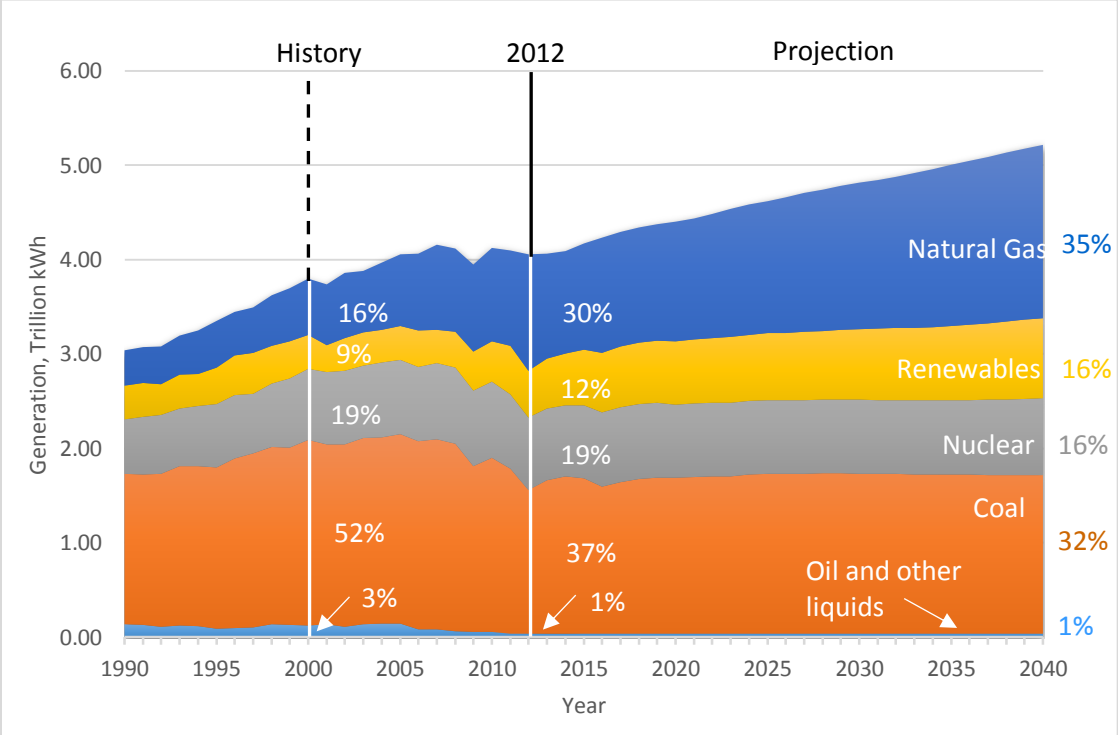


Figure 1.20. Electricity generation by fuel, 1990-2040 [1.35].

Smart Grid Challenges

In the previous section, problems with the existing power system were described and paralleled with potentials solutions provided by the smart grid. However, smart grid implementation bumps in to several technical issues which have to be resolved for actual technology implementation. In this section, challenges related to the smart grid implementation will be reviewed.

Renewable Electricity Production

Large RES integration in the grid is one of the major features of the smart grid. Almost every state has a renewable energy portfolio which will increase the RES penetration to the power system in the near future (Figure 1.7). A too large penetration of

RES in the power grid introduces new technical challenges for many network operators at distribution as well as at transmission level. Reliability and quality of supply are two primary challenges with integration of large RES in the power grid as a whole, as well as in islanded MGs. Even for small amount of RES, negative impacts exist, but it is not a concern as long as the performance of the electricity network remains within the standard limits. For example, connecting limited number of RES to the distribution network can provide a part of the load locally, reducing peak load demand and power losses for the upper grid and improving the voltage profile.

The different impacts of RES integration is evaluated in different textbooks in details [1.36]-[1.41]. In the following subsections, a brief review is given regarding the negative impacts of the RES on the power system.

Overvoltage. Injecting active power in a medium- or low-voltage network may result in an overvoltage. This is more often for rural networks where the maximum voltage during a day is close to the standard upper limit even without RES [1.41]. As a result, integration of small amount of RES (such as wind or solar PV) can result in unacceptable overvoltages. It has been reported that overvoltages significantly reduced the lifetime of incandescent lamps and resulted in disconnection of solar PV by overvoltage protection relays [1.41].

Safety and Protection. During an uncontrolled islanding operation, due to a fault or maintenance, DER will continue to provide the local load demand. This can be very dangerous to the other network components and to maintenance personnel. Notice that

this phenomenon is different from island operation of MGs (or controlled islanding operation) where a MG with its own load, generation, and storage operates independently from the upper grid. Additionally, large RES generation jeopardizes protection coordination where an incorrect trip or fail-to-trip may happen. The fail-to-trip events can damage other components in the network.

Power Quality. RES are connected to the grid or islanded network through PEI with appropriate controls. As it is common with PEI in any applications, the amount of harmonics are usually higher than pre-defined limits which can be dangerous not only for the local consumers and components, but also for the major grid in the grid-tied applications. Note that the actual harmonic levels from DERs are much smaller than the harmonic levels in typical low-voltage equipment such as new TV sets and computers. However, these PEIs inject even harmonics, inter-harmonics (i.e., frequency components that are not an integer of the fundamental frequency), and high-frequency harmonics (i.e., harmonics in the range of 2 to 150 kHz), in addition to the normal harmonics [1.42]. High-frequency components with large magnitudes can be very dangerous for the grid components such as transformers. Additionally, installation of capacitor bank and underground cables is more common with increasing DER integration in the power system, which can result in harmonic resonances (i.e., high levels of harmonic voltage and current) [1.42]. These new efficient technologies are adapted or undergoing to be adapted in the appliances. Although these technologies increase the overall efficiency of the power system, some of the technologies contribute to the harmonics generated by the load. As an example, due to increase in the efficiency of lightning, new efficient lamps

are utilized instead of incandescent lamps which can increase the efficiency up to 90% [1.40]. However, power converters are the core of operation in these lamps which inject lots of harmonics to the power system. This can endanger the voltage quality experienced by other users in the network and can result in shorter lifetimes for grid components. Additionally, utilizing new lamps increases the required reactive power at the distribution network [1.40].

Operating Reserve. Connecting the RES at the transmission level increases the complexity of control and operation of the power system. In one case, large penetration of RES may result in overload or insufficient operating reserve because of inherent variability in the RES generation. This occurs as a result of the conventional power system operation practice where generation always follows the load demand with specific amount of generating capacity reserve at each time instance. The worst-case scenario is when the maximum production happens with minimum consumption. The RES generation is inherently variable which cannot be predicted nor controlled effectively. The variable and uncertain nature of RES generation adds a significant uncertainty to the power system operation along with the uncertainty of load demand and components failure. These new sources of uncertainty on the generation side can jeopardize power system stability which requires larger operational margins. This essentially means that new spinning and non-spinning reserves (which mostly are fossil-fuel units) are required. Although RES generation forecasting has attracted lots of attention in the last decade, the accuracy of the proposed methods is still far from the safe margins. As an example, the production errors for wind-power production in North-Eastern Germany (a 300 by 450

km area where maximum production was around 8000 MW in 2009) is compiled and analyzed in [1.41]. It has been observed that there was a probability of 3% for 1,000 MW error in prediction; while the probability of more than 2,000 MW (which is about 25% of the maximum production) error was about 0.3% (equal to 26 hours each year.) This is a critical challenge for the system operator in day-ahead and hourly planning which necessitates larger operational reserve. The replacement of thermal generating units by renewable sources introduces a challenge for power systems operation. The reason is that large production units (thermal and hydro) not only produce electrical energy but also help to maintain power systems stability. Using existing technology and operational tools, stable operation of the power system will not be possible without at least some of those large production units to provide AS to the grid. Some of the most important AS is given in the following:

- *Operational Reserve.* In this case, a part of the large production units' capacity is set in reserve to manage unexpected shortages, e.g., due to the loss of a large amount of production, the loss of an important transmission line, or large prediction errors.
- *Frequency control.* Many of the large production units are equipped with power-frequency control. This control system keeps the actual balance between production and consumption within the interconnected power system (called primary control) and within each control area (called secondary control). As a result, the control system maintains the frequency close to its nominal value of 60 Hz at different time interval.

- *Voltage control.* A separate control system maintains the voltage magnitude close to the standard value throughout the power system. Voltage and reactive power are closely linked in the same way that (active) power and frequency are linked. There should therefore be reserves in reactive power to allow voltage control in case something unexpected happens.
- *Short-circuit capacity.* Short-circuit capacity is a measure for the amplitude of the current during a fault in the transmission system. The magnitude of these currents can be very high and cause serious damage to equipment. Short-circuit capacity is also a measure of the strength of the electricity network and its ability to cope with changes in consumption [1.42]. Too low a value of short-circuit capacity will have a number of adverse consequences, like risks of incorrect operation of the protection, risk of system instability after a fault or the loss of a component, and insufficient voltage quality. The only source of short-circuit capacity at transmission level are the large conventional power stations.
- *Power System Stability.* The presence of large and stable production units in the transmission system makes the system more stable in most cases. Their contributions to the voltage and frequency control and to short-circuit capacity were already mentioned. Additionally, their contribution to the total inertia of the system is important to prevent frequency and angular instability. Large production units are also equipped with additional controllers (power system stabilizers) to damp local and inter-area power oscillations.

Overloaded Transmission Lines. Large RES units employed (or foreseen to be

employed) at the transmission level are often far away from populated areas. As it is shown in Figure 1.21, most of utility-scale solar PV sources in the U.S. are located in the south and southwest which may be more than the total consumption of that region. Almost similar pattern can also be recognized for roof-top PV panels in Figure 1.22. Since the excess generated power should be consumed somewhere, it has to be transmitted through transmission infrastructure to places with less solar PV generation, e.g., north and northwest. As a result, new transmission infrastructure is required to be built which increases the final cost of electricity production.

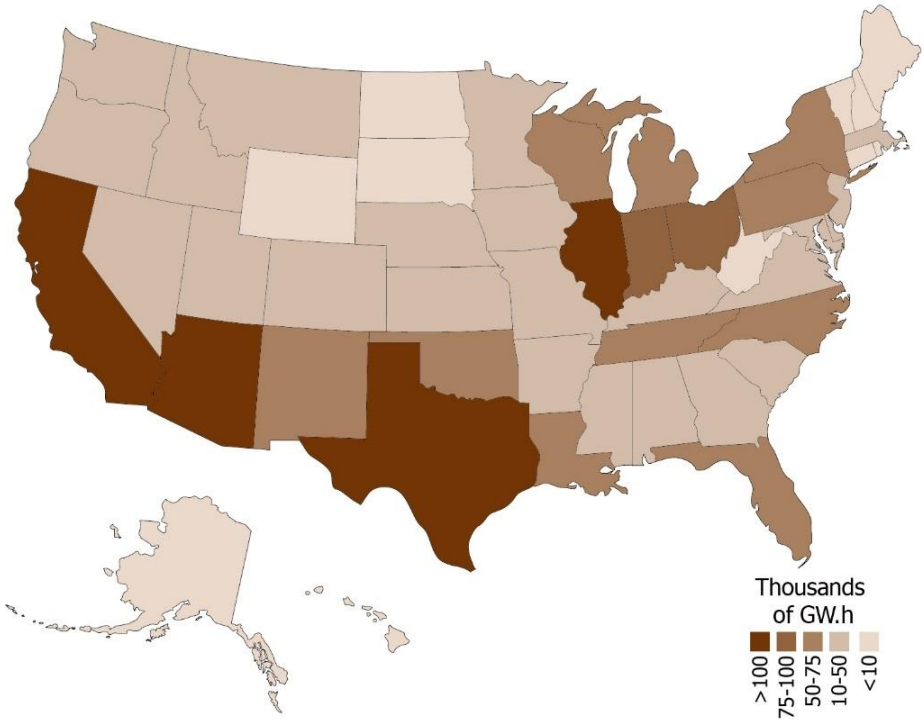


Figure 1.21. Total estimated technical potential for urban utility-scale PV in the U.S. [1.43].

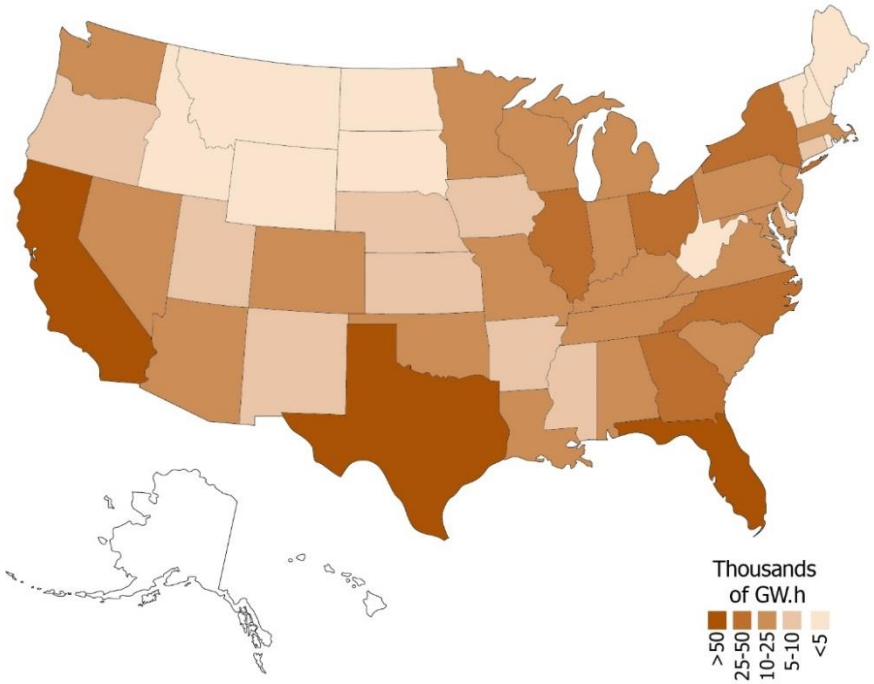


Figure 1.22. Total estimated technical potential of roof-top PV in the U.S. [1.43].

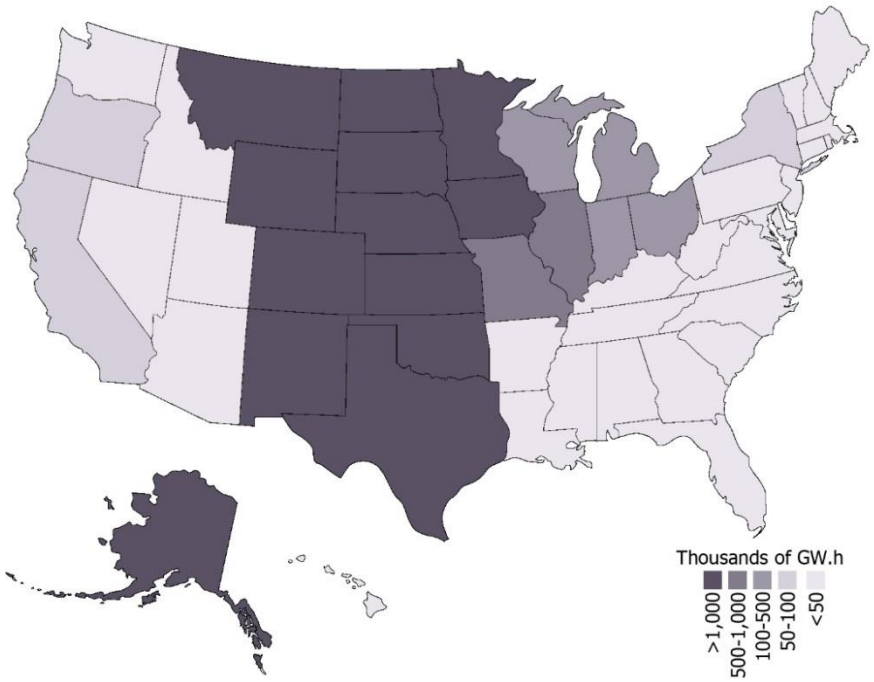


Figure 1.23. Total estimated technical potential for onshore wind power in the U.S. [1.43].

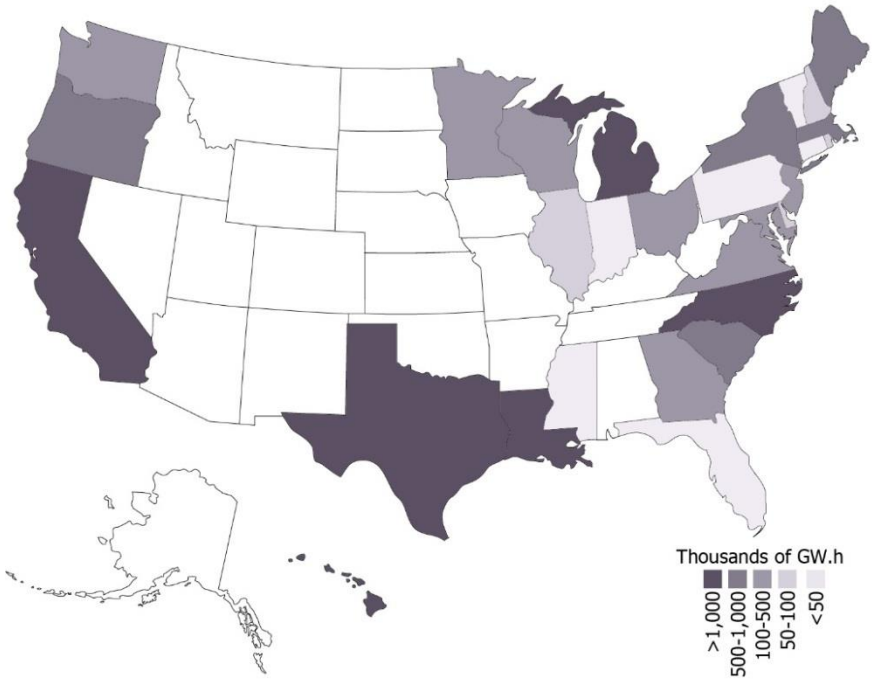


Figure 1.24. Total estimated technical potential for offshore wind power in the U.S. [1.43].

Additionally, increasing PV installation will increase power losses through transmission which results in lower efficiency. Similar pattern for onshore and offshore potential wind power generation can be seen in Figure 1.23 and Figure 1.24, respectively, where the distribution of potential resources are far from homogeneous.

Transmission System Planning. In order to add new transmission infrastructure, planning a few years ahead is required. In the existing power system, the required transport capacity from the transmission grid into a distribution network is calculated considering maximum load demand in the distribution network. The expected load demand growth for several years ahead, and the amount of reserve required to cope with the loss of important components are also required. However, with high penetration of

DER in the smart grid era, maximum production and variations should also be considered in the design algorithms. Therefore, the existing practice in designing will not support the new needs in the smart grid era.

Energy Consumption Reduction

Reducing energy consumption is one of the features of the smart grid which can happen by using appliances less often, by controlling their operation through DR, and by using higher efficiency appliances. Reduction in energy consumption can potentially decrease peak power demand and losses, which can result in stability improvement. However, reduction in the electricity consumption may cause challenges in the power system operation which are briefly described in the following sub-section:

Base-Load Power Plants. When the total reduction in consumption results in a large reduction of the minimum consumption, the scheduling of production units will need to be modified accordingly. In most countries, the so-called base-load production is running constantly for weeks or even months [1.41]. Base-load generation is relatively cheap production (such as nuclear and coal power plants) that takes a long time to start. The amount of base-load generation can obviously not be more than the minimum consumption. As a result, a large reduction in the minimum consumption necessitates less base-load production and that more expensive peak-load production would be required.

Power Quality. New efficient technologies have been adapted or are being adapted in the appliances. Although this adaptation would increase the overall efficiency of the power system, some of these technologies contribute to harmonics generated by the

load consumption. As an example, due to increase in efficiency of the lightning consumption, new efficient lamps are utilized instead of incandescent lamps which can increase the efficiency up to 90% [1.40]. However, power converters are the core of operation in these lamps which inject lots of harmonic to the power system and can degrade the voltage quality of the network and result in shorter lifetime of the grid components. Additionally, utilizing new lamps increases the required reactive power at the distribution network [1.40].

Electricity Market

Currently, the electricity market consists of a number of more or less separated markets, the wholesale market, the retail market and the balancing or real-time market are the ones that have the main impact on the grid [1.42]. In the existing power system structure, the retail market has much less impact on the grid operation compared to the other elements of the power system market. A retailer purchases electricity on the wholesale market and sells the electricity to its consumers. This way, if a consumer switches to another retailer, the transition does not affect power flows in the grid. However, the price elasticity of the consumption kicks in to the system operation with the retail market. Currently, the price elasticity is low since consumers are not exposed to the price variations in the wholesale market [1.42]. In the future power system, the retailers will offer hourly (real-time) prices to the consumers where their elasticity is unknown. Therefore, the difference between predicted and actual consumption is expected to become larger, particularly at the early stage of the smart grid implementation. As a result, large price variations in the balancing and real-time markets will be inevitable.

Thus, higher unpredictable power flows are expected which necessitates larger reserve margins for safe operation.

In the existing power system, the wholesale market does not have any impact on the distribution network. However, this pattern will change in the smart grid when large amounts of DER will participate in the wholesale market. Additionally, large availability of DR in the smart grid could result in unexpected changes in power flows through the distribution networks.

Wind and Solar PV Generation

In addition to the challenges explained in earlier sub-section for the RES integration to the power system, this section makes an attempt to explain the serious challenges in the smart grid regarding the variable generation nature of solar PV and wind. Focus will be on the negative impacts of these two RESs on the power system operation at the transmission and distribution level (i.e., for gird-tied and islanded MGs). As it is shown in Figure 1.20, about 12% of the electricity generation in 2012 came from renewable energies, and the share of the renewables is projected to increase to 16% in 2040. Here, wind and solar PV are the fastest growing renewables in the power system [1.16]. According to the 2012 U.S. Renewable Energy Data Book published by NREL [1.44], installed wind and solar PV capacity increased by nearly 28% and 83%, respectively, compared to 2011.

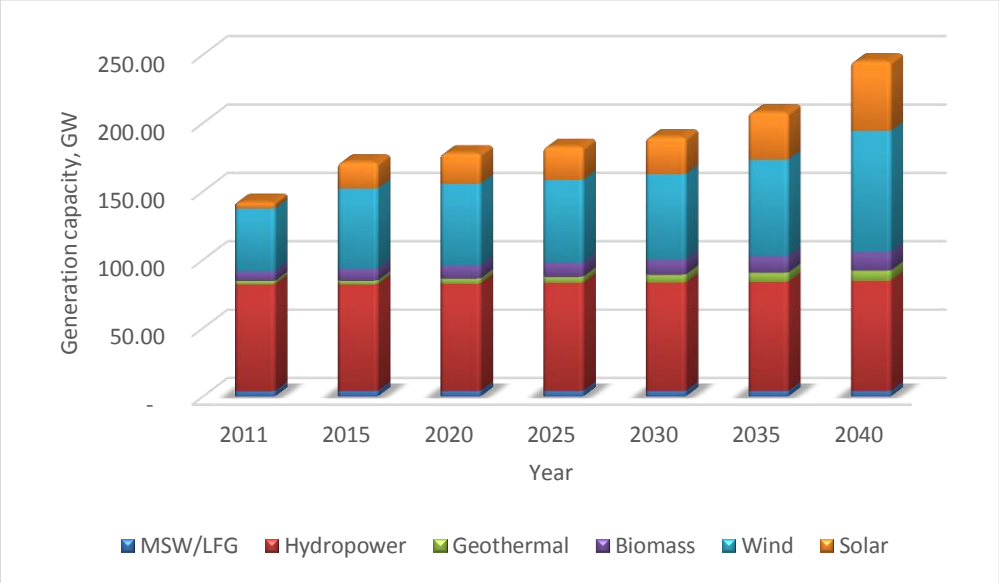


Figure 1.25. Renewable electricity generation capacity by energy source, including end-use capacity, 2011-2040 [1.16].

It also shows that wind energy accounted for about 75% of the new installed RES in 2012. The increase in wind and solar PV will continue for the years coming, as shown in Figure 1.25. Hydropower is reached to its maximum, and other renewables are less likely to be widely utilized in the power system in the near future.

Although wind and solar PV power are clean, abundant, domestically available, have the lowest price between renewables, and have the fastest growth in the U.S. [1.45], their large application in the power system introduces a lot of challenges which have to be studied. These challenges are briefly explained in the following, where focus is given to wind and solar PV generation characteristics and their corresponding challenges in the smart grid era.

Intermittency: Since blowing wind and its speed is a natural intermittent phenomenon, the output power generation of a single wind turbine is highly intermittent.

The inherent intermittency is a big challenge in the day-ahead planning and real-time control of a power system. Theoretical arguments often claim that wind farms spread over a geographically diverse area rarely stop producing power altogether, however this is in contradiction to the observed variability in total power output of wind turbines installed in Ireland and Denmark [1.46], for example. On the other hand, according to a study of wind in the U.S., ten or more widely separated wind farms connected through the grid could be relied upon for about 33 to 47% of their average output (15–20% of nominal capacity) as reliable [1.47]. Therefore, aggregating large wind farms in widely dispersed geographical areas may or may not reduce the intermittency in wind-generated power.

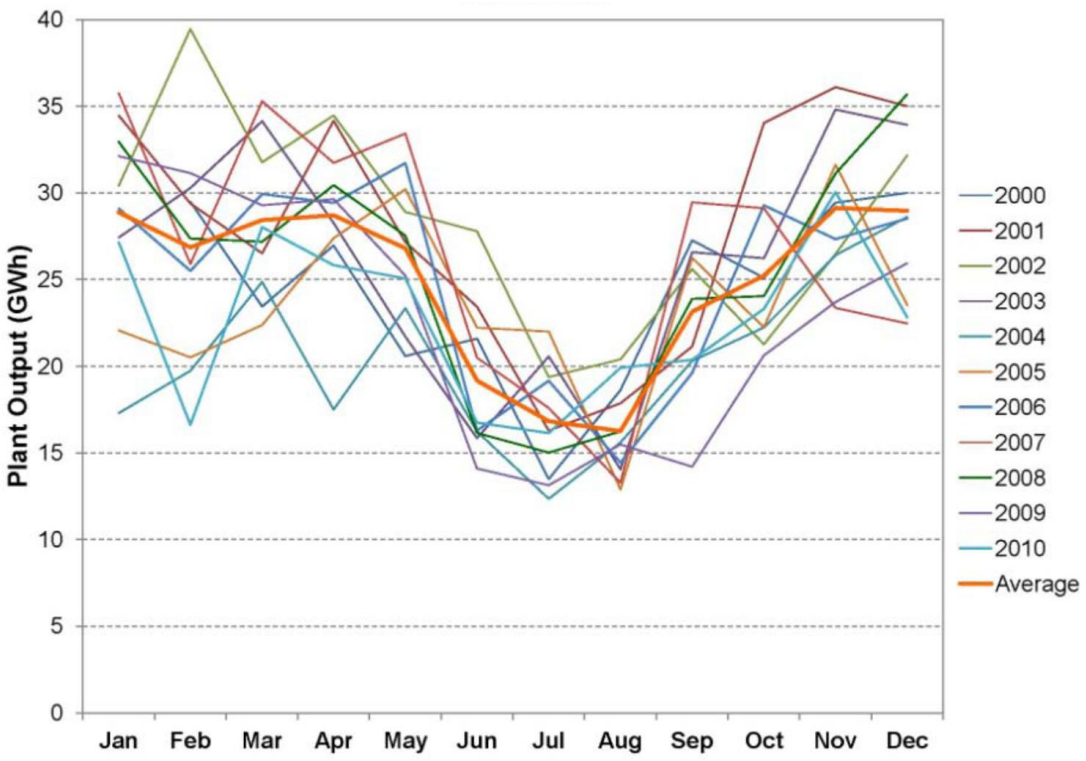


Figure 1.26. Monthly average wind energy production from Lake Benton, Minnesota, USA [1.48].

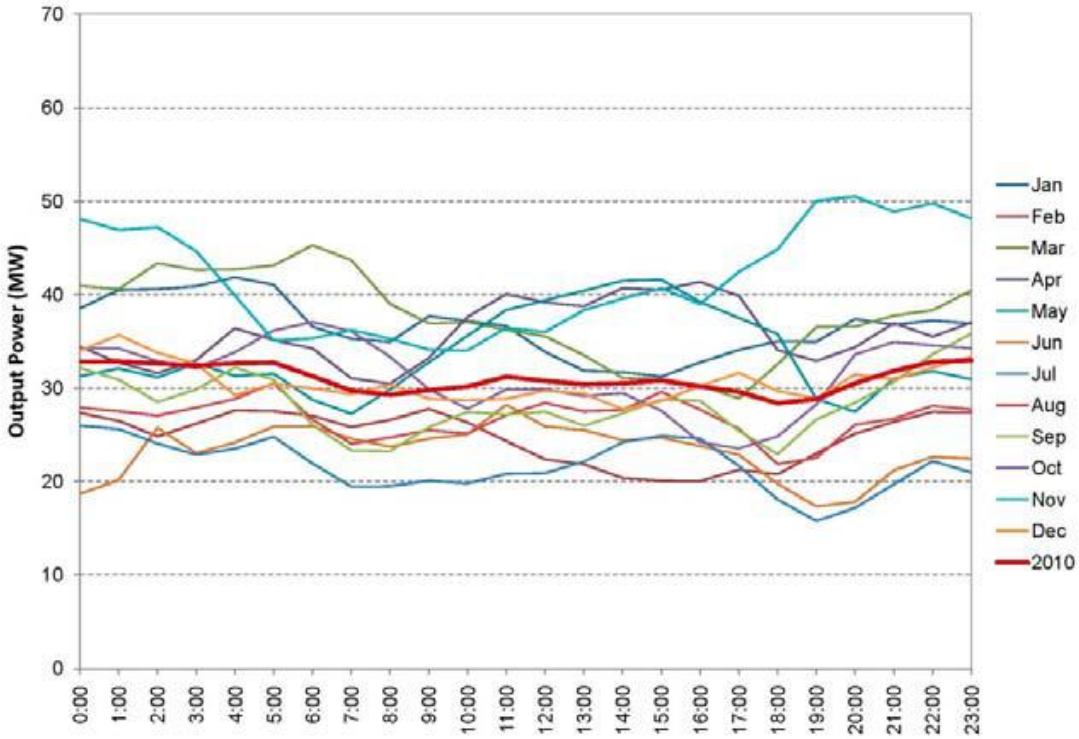


Figure 1.27. 2010 average hourly wind power profiles by month from Lake Benton, Minnesota, USA [1.48].

In order to show the variability in the wind power generation, monthly average wind power production from Lake Benton wind power provider (WPP) in Minnesota is shown in Figure 1.26. It can be seen that from one year to another for the same month, the average value is changed significantly. This fact makes the long-term planning very difficult for the power system operators. The variability of the wind-generated power is not limited to yearly, seasonal, monthly, or daily variations, short-term behavior of wind power is also unpredictable. It is more because of turbulence intensities which are directly related to the surface roughness of the ground [1.48]. The average monthly wind power production for Lake Benton, Minnesota is shown in Figure 1.27. It is obvious that from one hour to another, wind speed shows significant variations which make it difficult

to keep the demand and generation balanced in real-time.

Solar PV power has similar characteristics where its output power is highly variable and unpredictable. Seasonal and yearly variation of solar irradiation is shown for a measurement station in Ashland, OR, USA in Figure 1.28. Data are shown as daily average global irradiation based on kW.h/m^2/day. Variations from one year to another and from one season to another are obvious. The variability from one year to another for the same season and month may seem small, however this variability results in huge uncertainty in power system planning and operation when significant amount of solar PV is installed in the future power system. Variability in solar irradiation is not only limited to the seasonal and yearly variations, where minute-by-minute variation is normal in PV solar irradiation. Solar irradiation level for the same area measured in 5-minute intervals is shown in Figure 1.29. The variations in the solar irradiation are huge. Therefore, sufficient operational reserve is essential to compensate for the variations.

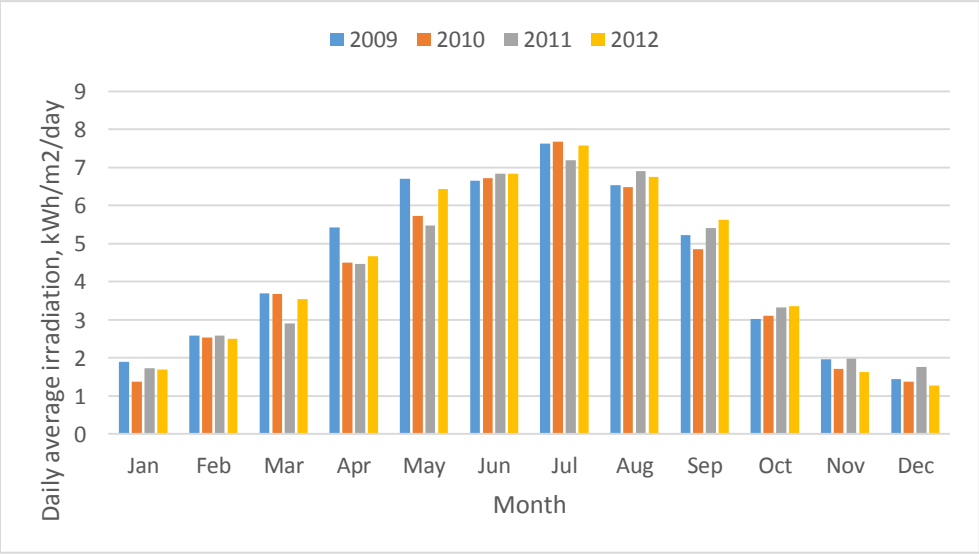


Figure 1.28. Monthly average global irradiation data for Ashland, OR, 2009-2012 [1.49].

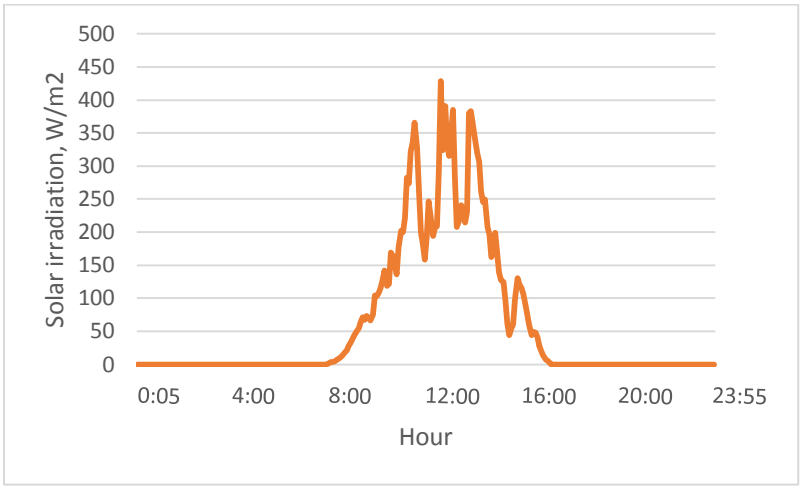


Figure 1.29. 5-minute interval solar irradiation data for the first day of January 2012 in Ashland, OR [1.49].

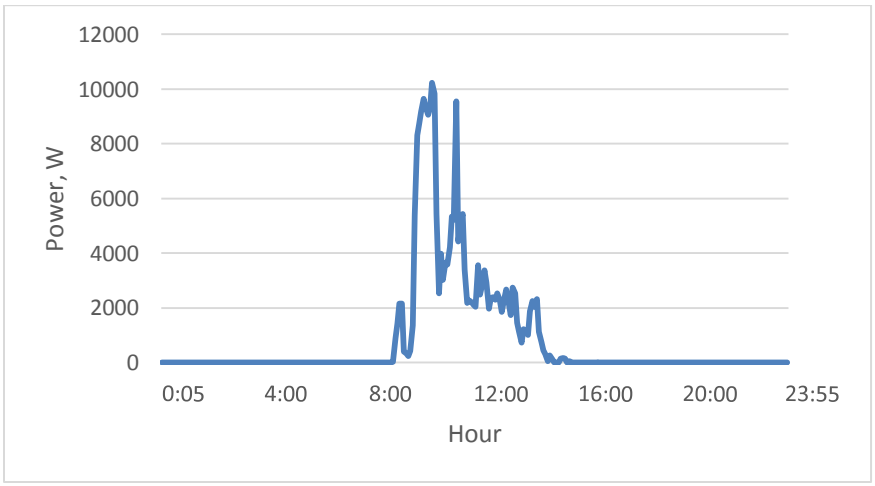


Figure 1.30. Generated power from 15 kW solar PV array tilted 15º South- January 01, 2010 in Ashland, OR, USA [1.49].

Temperature variation is another parameter affecting the output power of solar PV modules which increases the overall variations in the output power from a solar farm or single solar PV module. The combined effects of solar irradiation and ambient temperature variations on the generated power are depicted in Figure 1.30.

Capacity Factor: Wind power typically has a capacity factor of 20-40%. The

Danish wind farm Horns Rev II (the world's largest as of February 2014), inaugurated in September 2009 [1.50], comprising 91 Siemens SWT-2.3-93 wind turbines each of 2.3 MW with a nominal total capacity of 209.3 MW, has the best capacity factor of any offshore wind farm at 49.1%. The wind farm produced over 3,859 GWh in 2013 [1.51]. Since generator with high capacity factor (70% or more, such as nuclear power plants) are considered to supply base-load power [1.52], wind generation can be used for peak periods or whenever they are available. This would result in extra complexity in power system planning and real-time control.

Dispatchability: Wind power is not dispatchable because the amount of input energy to the wind turbine (i.e., wind) is not controllable. Therefore, traditional droop control (or other AS) cannot be expected from wind power plants when needed.

Capacity Credit: At low levels of penetration, the capacity credit of wind power is about the same as the capacity factor. However, when the penetration of wind power in the grid increases, the capacity credit percentage drops significantly. At a penetration of 20%, wind power plants capacity credit drops to about 10%. According to a detail study reported in [1.53], 10,000 MW of installed nameplate wind capacity is equivalent to approximately 2,000 MW of firm generation capacity. However, utilities are often reluctant to assign any capacity credit to wind power plants, largely because of the intermittent nature of the resource and the perceived difficulties in accurately forecasting wind power output [1.54].

Reliability: A wind farm is highly reliable (although highly intermittent). The total shut down of wind turbines is predictable via weather forecasting. The average

availability of a wind turbine is 98%, and when a turbine fails or is shut down for maintenance it only affects a small percentage of the output of a large wind farm. For example, the failure rates for wind turbines located in Northern Germany was 2.2% in 2001 [1.55]. In another study conducted for wind turbines failure in Sweden, Finland, and Germany for 500-1500 kW turbines from a variety of manufacturers between 2000 and 2004, the average number of failures per turbine per year was 0.402 [1.56]. In [1.57], it is demonstrated that a significant cross-correlation exists between the failure rate and the weather conditions; temperature and humidity were more significant than the wind speed. As a result, it can be concluded that wind turbine technology is very reliable itself.

In term of large implementation of wind and solar PV in power systems and their impacts on bulk power, a long-term reliability analysis is carried out for the next 10 years in [1.19]. In this report, six issues are identified that would be most impactful over the next 10 years. One of the issues is the risk of high level of variable generation for operation and planning of the power system. It is mentioned that significant changes are required in the traditional methods used for power system planning and operation to reliably integrate 46 GW of wind and solar in the next 10 years in the power system [1.19]. Otherwise, power system reliability will be negatively affected in the coming years with large penetration of renewables.

Correlation with Load Demand: Wind usually blows more at night when load demand is low. Therefore, it can be said that the wind power generation has a weak correlation with the load demand. In a study carried out on wind speed data of 66 onshore weather recording in the U.K. during 1970-2003 in [1.58], it is observed that the wind

power output in the U.K. has a weak, positive correlation to the current electricity demand patterns. Similar to the U.K., the profile of wind generation is inversely correlated with the load demand in ERCOT [1.59].

Solutions to the Challenges in the Smart Grid

Different solutions are proposed to resolve the issues related to the smart grid operation. Some of these methods are the extension of the classical solutions, while others are new ideas for the future relying on the new technology developments and improvements. In this section, different solutions are presented to resolve the challenges with the smart grid and MGs, however the focus will be on the MG and its real-time power management and DR.

Classical Solutions

These solutions include adding more transmission and distribution lines and cables, transformers and substations, and generation units for base-load and spinning reserve operation. These solutions are well-known and have been in practice for so many years. In the past, they have not only been the best technical solutions, but also the most cost-effective answer to the power system issues such as reliability, shortage in generation, efficiency, and load following strategies. At the distribution level, building new lines, replacing overhead lines with underground cables, and strengthening the existing feeders can resolve many problems such as voltage drops and rises, high power losses, high penetration of RESs by building dedicated feeders for wind and solar PV power installations which resolve the protection-coordination problem as well, reliability

and availability issues [1.41].

Building new transmission and distribution lines along with substations can increase the power transfer capability of the power system, reduces the overload in the power system, which consequently reduces the risk of overvoltage and over current. However, building the new infrastructure needs a huge amount of capital investments. For the transmission lines besides the cost factor, it is getting harder to find an appropriate path and permission from authorities to build new lines. This is a big problem particularly for the highly populated load demand centers which are imposing a large load growth to the network as well. Additionally, the required time to build a long transmission line is long and can only be foreseen as an option in long-term planning.

Although the utilization of cables instead of overhead lines increases the reliability of the distribution feeder in terms of vandalism, terrorist attack, and severe weather conditions, it has some negative impacts as well in terms of reliability and cost. Despite the overhead lines, failure rate of the underground cables is much rare [1.41]. However, once they fail, it will take longer time to fix. Therefore, a backup supply is absolutely needed to avoid long-term interruption. A backup supply and the cost of power interruption are the two factors which limit this option. Additionally, certain type of switchgear is required for underground cable which increases the cost of installation accordingly. These above facts make this option less attractive.

In order to resolve the protection-coordination issues in the presence of DER, directional protection with anti-islanding protection can be utilized at the distribution level [1.41]. However, directional protection needs voltage transformer which essentially

increases the cost of protection in distribution networks. On the other hand, although anti-islanding protection is relatively cheap [1.41], the risk of unnecessary trips increases with large amount of DER. As an example, during the two large disturbances in Europe in 2003 and 2006, most of the DER unnecessarily tripped only because of anti-islanding protection [1.41]. In areas with large penetration of roof-top PV panels, anti-islanding protection may trip on sunny days because of overvoltage [1.41].

Technology for Increasing Transport Capacity

As was explained in the last sub-section, building new transmission lines and substations are not a comprehensive answer to the problems in the smart grid, particularly for transporting large amount of RES generation to the load centers, as shown in Figure 1.22-Figure 1.25. However, based on the recent technology improvements in power electronics, methods are developed to limit the number of lines to be built and to increase the transport capacity of the existing transmission infrastructures. It has been shown in [1.60] that increased transport capacity can reduce the operational cost by 1.5 billion Euro each year, which is equal to 20 billion Euro saving in the investment costs. Additionally, it means that during the peak demand periods, it is more likely to have sufficient production capacity available which results in electricity price reduction for the customers. In the following sub-sections, different methods to increases transport capacity are explained briefly.

High-Voltage Direct Current (HVDC) and Flexible AC Transmission Systems (FACTS). HVDC transmission lines are the best choice for large power transportation in a long distance, where power flow can

be fully controlled independent of the power flows in other areas and transmission lines. Additionally, their losses per km are lower than the losses in AC transmission systems. Losses in DC transmission lines mainly come from the converter stations [1.41]. Recently, SVC-HVDC (voltage source converter-HVDC) links are developed which are capable of controlling reactive power as well as active power simultaneously [1.41]. As a result, an AC transmission system can be converted to a DC system only by adding converting stations at both ends of the line, which can increase transport capacity 2-3 times the AC system without any stability issues [1.41]. However, building new HVDC links is still an expensive option compared to the AC transmission systems. Also, there is a huge lack of experience among transmission system operators with the integration of DC lines into the AC system. This is the reason that HVDC links embedded in an AC system is less common. Furthermore, HVDC links with underground cables require much longer repair times compared to the overhead transmission lines [1.41]. Nowadays in North America, the majority of HVDC lines are utilized to connect different synchronous areas together. In Canada, there are several HVDC links to transport hydropower from the north to the load centers in the south [1.41]. As a result, technology improvement and more applicable control strategies and planning practices are required to be developed in order to increase the acceptance and usage of HVDC in power system. FACTS devices can also be used to increase the transport capacity of the existing transmission lines. FACTS devices can be classified into three categories, 1) shunt devices given in Table 1.1, and 2) series devices given in Table 1.2, and 3) Two-port (or combination of series-shunt) devices given in Table 1.3.

Table 1.1. Different shunt connected FACTS controllers [1.61].

FACTS device	Main Functionality	Secondary functionality
BESS Battery energy storage system	Load leveling	Voltage stabilizer, active filter, UPS
SSC Static synchronous compensator	Voltage control	VAR compensation, damping of oscillation, transient stability
SSG Static synchronous generator	Exchanging independently controllable real & reactive power with power system.	--
SVC Static VAR compensator	Voltage control	VAR compensation, steady state and dynamic stability
SVG Static VAR generator	Generating or absorbing reactive power	Steady state & dynamic stability (TCR and TSC in parallel)
SVS Static VAR systems	Stability limit extender at the midpoint of a long transmission line.	Voltage control
SMES Superconducting magnetic energy storage	Dynamical control of power flow in ac system	As SSC, the energy storage is superconducting reactor
TCBR Thyristor controlled braking resistor	Aiding to damp power flow oscillation and decrease risk of losing synchronism	--
TCR Thyristor controlled resistor	Continuous reactive power absorber	--
TSC Thyristor switched capacitor	Stepwise reactive power generator	--
TSR Thyristor switched reactor	Stepwise reactive power absorber	--
BVI (parallel connected) bootstrap variable inductance	Voltage stabilizer and/or load power factor corrector	--

Similar to HVDC, improvement and development of new control practices are required in the transmission system design and operation to improve their performance. Additionally, utilization of power electronic devices at various voltage levels can increase

current and voltage harmonics in the power system which decreases the power quality. As a result, FACTS devices have not been utilized widely in the power system at different voltage levels. Shunt devices control the reactive power flow and voltage magnitude in power system. Series FACTS devices can change the impedance of the transmission lines which can affect active power flow. This way, the active power flow can be limited in the weak part of the grid while increases the power flow from other stronger part of the grid [1.41].

Table 1.2. Different series connected FACTS controllers [1.61].

FACTS device	Main Functionality	Secondary functionality
SSSC Static synchronous series compensator	Controlling transmitted electric power by increasing or decreasing reactive voltage drop while expecting no SSR effect	Increase or decrease resistive voltage drop across the transmission line to enhance dynamic behavior
TCSC Thyristor controlled series capacitor	Capacitive reactance compensator in a continuous manner	--
TCSC' Thyristor controlled series compensator	Capacitive/inductive reactance compensator in a continuous manner	--
TCSR Thyristor controlled series reactor	Inductive reactance compensator in a continuous manner	--
TSSC Thyristor switched series capacitor	Capacitive reactance compensator in a stepwise manner	--
TSSC' Thyristor switched series compensation	Capacitive/inductive reactance compensator in a stepwise manner	--
TSSR Thyristor switched series reactor	Inductive reactance compensator in a stepwise manner	--
BVI (series connected) Bootstrap variable Inductance	Capacitive/inductive reactance compensator without SSR	Transient stability improvement, fault current limiter

Table 1.3. Different two-port FACTS controllers [1.61].

FACTS device	Main Functionality	Secondary functionality
IPC Interphase power controller	Independent active and reactive power controller	--
TCPST Thyristor controlled phase shift transformer	Power flow distribution and high speed variable phase angle control for transient and dynamic stability	--
UPFC Unified power flow controller	Terminal voltage control, phase angle regulation, series line compensation	VAR compensation

Dynamic Line Rating

Transmission line loading is limited to some certain degree because of instability in long lines and thermal limit in short and medium lines. For short-length overhead lines, the maximum loading can be adapted considering weather circumstances. For instance in a cold windy day, the line will be able to tolerate higher currents and consequently power transportation. The reason is the fact that the temperature rise in the conductors will be less and the problem with conductor sag is less likely to happen. Therefore, a dynamic line rating can be used instead of static limits which currently are being practiced in power system operation. The main application of the idea is related to the wind-power integration at substation level [1.62], [1.63]. At this voltage level, the thermal capacity of the lines determines the limits on the transport. This solution may resolve some of the issues related to large penetration of RES generation in the future power system at the transmission and distribution level in terms of power transport and the need for new infrastructure.

Although the principle of dynamic line rating is simple and straight-forward, its

wide application needs further inspections and investigation. Determining the actual limit on the line transport capability and the fact that who accepts the risk associated with this are two primary issues which should be addressed [1.41].

Risk-Based Operation

Traditionally, the large power system operation was based on the "(N-1) criterion" where the loss of any single component should not result in an interruption of any of the customers [1.41]. Additionally, power system should always perform under "secure operation." This way, system operator should get the system back to secure operation within a certain period of time, e.g., 15 minutes [1.41]. Despite successful practice with the above criterion for reliable power system operation, these operational practices are not effective anymore. The main reason is large penetration of variable RES generation in the power system which results in large and fast variation in the production. This is equivalent to a failure in a production unit or any other components causing outage of large generation unit. This phenomenon often happens in power systems with large penetration of variable RES. With risk-based scheduling of primary reserve, as a part of power-frequency control, total cost of maintaining the reserve plus the expected value costs of interruption will be minimized [1.41]. Therefore, a dynamic criterion for reliable operation of power system will be achieved which helps to increase the reliability of the system with backup reserve, considering variability of RES generation. However, there is always a risk that the transport capacity of the transmission infrastructure reduces to insufficient levels for all transactions resulting from electricity market. This way, the transactions should be limited which consequently increases the price of electricity either

at the day-ahead or balancing reserve markets [1.41]. The actual risk of risk-based operation is the regional or large-scale blackouts even though its probability is small [1.41]. Additionally, successful implementation of risk-based operation requires the definition of acceptable risk level which needs more research.

Large-Scale Storage

Large-scale storage is an old solution for the power system reliability and safe operation, which was not technologically available. Utilization of storage in the power system can flatten the load profile. It stores any excess power available during off-peak hours and delivers any amount required during on-peak hours. It also can significantly support large penetration of variable RES generation in power systems. This way, excess RES generation, e.g., in a wind farm, can be stored in the storage unit and the required amount delivered during the periods of low availability of variable RES generation, so that the output power of the wind farm can be levelized. Different factors should be considered in the storage sizing and scheduling including capital investment, operation and maintenance cost, physical sizes and weight, life expectancy, maximum charging/discharging rate, losses during charging/discharging, and the storage leakage in the idle mode. Different large-scale storage technologies are compared in Table 1.4.

Amongst different existing battery technologies, Li-Ion batteries have attracted a lot of attention in recent years. They have reasonable life cycles which make them suitable for daily applications, such as peak power period. They are still expensive with relatively small energy density. More improvement on this very technology is ongoing.

Table 1.4. Comparison of different storage technologies [1.64].

Technology	Capital cost		Efficiency	Life	Density	Rating
	$/kW	$/kWh	%	cycles	kWh/m^3	
NaS	1000-2000	200-1000	87	2000	200	10 MW, 10 hr
Flow Battery	700-2500	150-600	80	2000	25	1 MW, 6 hr
Li-Ion	700-1500	800-3000	95	4000	300	1 MW, 15 min
Ni-Cd	500-1500	800-1500	60-70	1500	50	5 MW, 10 min
Flywheel	4000-10000	1000-3000	93	20000	15	1 MW, 15 min
Electrochemical Capacitor	200-600	100-200	97	30000	20	1 MW, 5 sec
Compressed air	500-1000	30-100	75	10000	-	100 MW, 10 hr
Pumped hydro	600-1500	50-150	70-85	20000	-	1000 MW, 24 hr

Ni-Cd and NaS batteries have already been utilized in power applications in rural areas. As an example, Ni-Cd batteries have been in operation in Fairbanks, Alaska which is able to provide 26 MW for 15 minutes or 40 MW in 7 minutes [1.41]. First-generation compressed air technology is implemented in McIntosh, Alabama, U.S. and is currently operating. Additionally, DOE awarded the smart grid matching grants for the construction of 150 MW/10 hr and 300 MW/10 hr advanced second-generation compressed air storage [1.64]. A 1 MW/1.5 MWh lead-acid battery bank has been operating for 12 years at a remote island location in Metlakalta, Alaska [1.64].

Hydrogen storage is another storage technology which has been drawn lots of attention. Compared to pumped storage and batteries, hydrogen storage has a higher level of energy density [1.65]. Hydrogen can be generated by reforming natural gas with steam

or by the high-temperature and high-pressure electrolysis of water. Reforming natural gas for hydrogen production generates carbon dioxide as by-product which is not desirable [1.66]. Then, the hydrogen can be stored (either as compressed gas or in liquid form) and utilized as fuel in internal combustion engines or a fuel cell. The AC-to-DC efficiency of hydrogen storage has been shown to be in the order of 20 to 45% [1.65]. Besides their relatively low efficiency, fuel cells do not have a quick response to the transient variation of the load [1.67]. Other issues related to hydrogen production and storage can be summarized as follows [1.68], [1.69]:

- ✓ operation pressure and temperature,
- ✓ life span of the storage material and their stability,
- ✓ requirement for hydrogen purity imposed by the fuel cell technology,
- ✓ reversibility of hydrogen uptake and release,
- ✓ rate of refueling,
- ✓ hydrogen delivery pressure, overall safety, toxicity, and cost.

As a result, a lot of research is required to bring hydrogen storage to a level of practicality and cost effectiveness.

Protection Practices

As one of the major issues in the distribution networks of the future smart grid, new philosophies and practices are required for effective protection within large penetration of DER, particularly in the distribution networks [1.40]. Short-circuit contribution from DERs connected to the distribution feeders can result in unwanted trip of the protection devices. Additionally, DER reduce the short-circuit level which further

increases the chance of fail-to-trip conditions [1.40], [1.41]. Furthermore, the local protection of DER can fail to detect the fault in the distribution feeders, which can cause uncontrolled islanded situation [1.41]. Since the existing protection practices are usually based on local measurements, more advanced and effective protection schemes are necessary to be developed for the large application of DER in the distribution networks. New directional protections are under development where advanced signal processing tools are utilized to detect the direction of fault current which would solve the first two issues with DER in the distribution networks. The new approach does not need any communications [1.41]. Additionally, adaptive protection scheme is proposed in [1.70] where the protection decides locally; however, the threshold settings are calculated centrally based on power flow studies and operational information. In this scheme, communication links are required to update the setting thresholds every few months or years. In another adaptive protection scheme with less communications, protection devices make the decision locally with limited information from other protection devices. Several other advancements are reported in different literature for power system protection with large DER penetration, however much more research and developments are needed, particularly for the protection of transmission networks [1.41]. The required improvements are more towards making protection faster and more reliable for the smart grid with all DERs.

Voltage Control Techniques

Conventionally, voltage profile is always maintained within the pre-defined range using on-load tap changing transformers, off-load tap changing transformers, and by

limiting the length of cables and lines in the medium and low voltage networks. Utilization of series compensators, shunt reactors, condenser, capacitor banks and several FACTS devices are other approaches for voltage regulation both in the transmission and distribution systems. When DER added to the distribution networks, the behavior of the system can totally change. For instance, at the time of excess DER generation and low load demand, negative load can be realized which causes undesirable over-voltage at the point of connection. Similar issue can occur during low DER generation and peak load demand for under-voltage. One way to overcome this problem is to optimally size and allocate the DER in the distribution networks in order to reduce losses, voltage deviations, cost of operation and allocation, and to increase penetration of renewable generation. Different approaches are proposed for this purpose which has been reviewed in [1.71]. However, so many uncertainties and variations exist in the distribution network which reduces the effectiveness of these methods in real-time operation of the system to a minimum level. For real-time operation, several methods for voltage regulation are proposed in the presence of variable DER. These techniques are comprehensively reviewed and compared in [1.72], [1.73]. With DER equipped with power electronics interface, or in synchronous machines, it is possible to control the voltage level by setting the reactive power generation to some extent. In a simple scheme, a generator can absorb reactive power to compensate for the voltage rise. However, this scheme increases loading and losses in the network due to additional reactive power [1.41]. Additionally, DER can react to voltage changes much faster than the traditional voltage control techniques, such as tap changing transformers. This way, DER would inject higher

reactive power which may be exported to the transmission system as well. As a result, the coordination between the voltage control by the generator and other existing automatic control is essential in these schemes. As another proposed voltage control method for the distribution networks with high penetration of DERs, Volt-VAr control can be employed where a central controller calculates the optimal voltage settings for different existing control devices. An optimization is usually performed to calculate the operating point based on minimization of losses, considering technical limitation of the network and other components [1.41]. These types of schemes heavily rely on the availability of communication links and a central controller unit. The communication links are foreseen to be available in the smart grid era.

MGs

As it was mentioned in the earlier section, MGs are the driving technology and the bridging solution to the wide application and implementation of smart grid with all its features, particularly to achieve large utilization of RES [1.74]. A MG is a regionally limited energy system of DERs, consumers, and optionally storage and controllable loads, controlled to maintain high quality, sustainable, and reliable electricity economically in grid-connected or off-grid (islanded) mode, as well as in dual mode (i.e. by changing the grid connection status.) MGs can be categorized as utility-size, industrial-size and commercial-size, and remote MGs [1.75]. While remote MGs could be grid-connected or an island, or a part of a larger grid in a very remote area, the industrial and commercial MGs are those that belong to single customers such as an industrial plant, a government agency, or a shopping center. Application of RES and storage within

a MG can significantly reduce cost of electricity for the remote MGs' users as well as producing pollutions. In the industrial and commercial MGs, higher electricity availability can be recognized even during and shortly after severe weather conditions, which increases security and reliability of electricity. Utility-size MGs are under control and supervision of the system operator, where the users can contribute to their operation by their DER and/or controllable loads [1.41]. One of the biggest utility-size MG is the one developed by Energinet, the Danish transmission system operator [1.76]. The MG consists of 28000 customers, four CHP power plants, and 47 wind turbines. In U.S., CERTS MG testbed is designed to demonstrate conceptual and technical approaches for enabling the integration of multiple DER into an electric distribution system which are able to work autonomously or in grid-tied mode [1.77]. In terms of reliability, it has been shown by the Lawrence Berkeley National Lab (LBNL) that 80-90% of all grid failures started at the distribution level where MGs will play an important role [1.78]. Therefore, the application of MGs in the distribution networks can improve the overall reliability of the bulk power system.

The great feature of MGs in general is their ability to work in islanded mode (when they lose connections to the main grid). Controlling MG operation in islanded mode with large penetration of variable RES generation is a very difficult task for MG developers and researchers. As a result, many efforts from researchers and companies are put into the development of appropriate control schemes for the safe and secure operation of MGs, particularly in the islanded mode. Additionally, the utility-size MGs are desired to work in dual mode, where they are capable of operating in grid-tied and islanded mode

when it is needed. Therefore, islanding detection techniques play important role for such MGs. An extensive literature review on different islanding detection techniques are reviewed in [1.79]. Based on the definition of the MG and the different features envisioned for the smart grid in Figure 1.2, the role of MGs for wide acceptance and implementation of the smart grid can be realized. In the following sub-section, the role of MGs is reviewed for each feature.

Renewable Energies. DER at the low voltage level is most likely to have variable renewable generation. As a result, each consumer at the distribution level could be potentially a power generator that can participate in the power market through other mediums, such as aggregators. In the medium voltage MGs, a lot of incentive programs are designed to increase the generation from small green generation resources, such as wind. As a result, the inherent characteristics of MGs will result in increase of variable RES utilization in large quantities. Additionally, large integration of variable RES in smaller scale as in MGs will help developers and researchers to diagnose the potential issues. Then, it would be much easier to find solutions to the problems for large application of variable RES in larger power systems. This increase in RES integration requires structural and conceptual changes in the existing power system, as explained in details in earlier sections. However, MGs could be a medium to test and verify new structural and conceptual means for larger power systems Another useful characteristic of the MG for RES integration is the ability of MGs for islanding operation. This way, even if a large penetration of variable RES causes a blackout in that MG, the fault will be contained and other MGs will perform in completely healthy condition. Therefore, any

fault in one MG will be limited geographically and to a small amount of customers. As a result, the developers and system operators (such as utilities) will be more confident to employ large amount of variable RES. Large application of the renewable generation is aligned with other goals of the smart grid such as global competitiveness and millions of job opportunities.

Storage Devices. In the definition of MG, storage is considered to be optional. However, the safe and reliable operation of a MG (particularly in islanded mode) without storage devices is almost impossible especially in the case of large variable RES generation. This is because of the fact that the generation and demand always should be equal in a power system. With a large penetration of variable generation, it is always necessary to have storage device to act as a buffer between generation and demand. This way, when generation exceeds load demand, the excess available power will be stored in the storage devices. Alternatively, the storage device will provide required power when load demand exceeds the generation. The application of storage units within MGs can decrease the amount of spinning resources (such as diesel generator or microturbine) required, which consequently decreases the dependency on fossil fuels and amount of pollutions. Additionally, the penetration of variable RES within MGs can be increased with appropriate amount of storage, which is aligned with the smart grid goals. Different storage devices are required for reliable power delivery in MGs, particularly in the islanded operation mode. Fast storage devices with low energy capacity (such as super capacitors, flywheels, and SMES) are required to capture very fast changes in the output of RES, while slow storage devices with large energy capacity (such as different types of

batteries and fuel cells) are necessary to cover long-term needs for energy. Although implementing large-scale storage devices in the high voltage networks are expensive and less technically applicable because of relatively small energy capacity, they are relatively cheap and in the order of the needs within MG framework. Then, the hypothetical aggregation of the storage devices within all MGs in the same power system introduces a very large amount of storage which can be very useful for AS and voltage/frequency stabilization purposes. Similar to the renewable energies, the small-scale MGs will let the developers and researchers to diagnose any issues related to the application of storage devices. Then, it gives a chance to develop appropriate schemes and techniques to resolve the issues for large-scale applications of storage devices. Additionally, MGs provide an opportunity for new storage devices to be examined and verified for larger applications.

Power Quality. One of the features of the smart grid is to provide power for anyone anywhere with an appropriate level of power quality. However, large penetration of renewable generation and storage devices in the smart grid era introduces a new level of harmonics and essentially degrades power quality. Similar issues can also be realized in small-scale MGs, where a large share of the generation belongs to the electronically-interfaced power sources. As a result, it can be concluded that any improvement in the power quality of MGs impact the power quality of bulk power systems with large penetration of RES. In order to enhance the power quality of the electronically-interfaced DER, different methods are proposed such as optimization techniques, dynamic and static filters, controllers, FACTS devices, compensators, and storage devices, as reviewed extensively in [1.80], [1.81]. Additionally, it is argued in [1.82] that meeting the power

quality requirements by local provisions (available in MGs) may be more cost-effective than increasing quality of supply from upstream networks. Therefore, MGs can improve power quality with more cost-effective approaches.

Energy Efficiency. As the definition of a MG states, local generating units will be seamlessly connected to a power system. This essentially means that, with the application of MGs, the power system structure will be more decentralized in the smart grid era. This way, the generation will be closer to the load centers and large transmission lines will be avoided. As a result of this transition, the power losses through transmission lines and medium voltage networks will decrease significantly. Therefore, higher energy efficiency will be achieved by decentralized power system. It can then be concluded that the wide application of MGs will essentially result in higher efficiency of the power generation and transmission. Additionally, it is shown in several studies that MG technology provides an opportunity and a desirable infrastructure for improving efficiency of energy consumption in a building with appropriate generation sources and storage devices [1.83]-[1.85]. Furthermore, the application of CHP within MGs can improve system efficiency. As a result, less electricity will be drawn from the upper grid which results in higher efficiency of the transmission system.

Demand Response. DR as a part of DSM is a set of actions to defer or reduce the consumption without jeopardizing customers' welfare. Enabling active participation by electricity customers in DR has been identified by the U.S. DOE as an important feature of smart grid [1.2]. MGs might help the smart grid industry to achieve the dream of DR

as an active part of power system operation. In [1.86], it is shown that wide utilization of MGs for load management not only benefit the participating consumers, but also reduces the wholesale market price for other consumers. This fact is also proved through numerical simulation for PJM real-time balancing market [1.87]. It is also shown that the DR can provide highly elastic demand curve for wholesale electricity markets which is of a significant value in day-ahead markets [1.88]. DR is one of the main focuses of this dissertation and will be covered in more details later.

Self-Healing. Generally speaking, self-healing is defined as the capability of a system to automatically detect a fault of any kind and to recover to the normal operation as quickly as possible after removing the fault [1.89]. This capability will help the bulk power system to be more reliable and secure in terms of any kind of faults. A self-healing grid will be more stable and reliable. Three primary functions of a self-healing grid include: 1) real-time monitoring and reaction, which permits the power system to continuously tune itself to an optimal state; 2) anticipation (or prognosis), which empowers the system to automatically search the power system for potential issues in the future that could start larger disturbances; and 3) rapid isolation, which enables the larger system to isolate parts of the network that experience fault from the rest of the system, to avoid the spread of disruption and enable a more rapid restoration [1.90]. As a result of these functions, a self-healing smart grid system is able to reduce the number and size of power outages and minimize the time required to restore the faulty areas. Furthermore, the self-healing system would be capable of end-to-end resiliency, which means that it can detect and override human errors that sometimes can cause power outage as the one

in California in 2011 [1.90]. To transform the existing power system to a resilient self-healing smart grid, it is needed to improve the bulky power system to a smart grid which consists of numerous small-scale MGs. With MGs and their connections together, bulky power system will be divided into numerous small-scale MGs at the distribution and medium-voltage level. Each of the MGs can operate autonomously if needed, and they can share load and generation between each other based on technical and economic functionality. Additionally, inter-connecting lines between MGs will be supervised by intelligent diagnosing and prognosis algorithms with superfast solid-state switches. As a result, each MG will be able to react quickly to any unexpected changes or faults, where appropriate inter-connecting lines will be open to prevent cascading faults to other areas. This way, any fault within a MG will be limited to its customers, and not the whole power system which results in significant reliability improvement. A comprehensive literature review on this topic and a multi-agent based approach for MG power management is given in [1.91].

Electricity Market. Appropriate electricity market is an essential part of MGs, particularly in the medium-voltage networks [1.92]. In the smart grid era where numerous variable RES, storage devices, DR, and CHP units will be added to the power system, complexity will affect its reliable operation. This issue exists in smaller scale within MGs, particularly in the medium-voltage level. Effective policies and pricing schemes for the MGs can also affect the bulk power system in the smart grid era.

As it is comprehensively explained in earlier section and in [1.78], MGs are the most promising and important solution for successful implementation of smart grid.

However, several issues need to be addressed prior to the successful implementation of MGs. These issues can be divided into two categories: 1) economical, and 2) technical. The coverage of economic issues related to the successful implementation of MGs is out of the scope of this dissertation. A comprehensive review of the economic issues are given in [1.78], [1.92]. Most of the technical issues mentioned for the smart grid will exist for MGs as well. Such issues include power quality and reliability, transition from grid-tied to islanded mode, and integrating MGs in to the existing system with legacy equipment. A comprehensive review of the technical issues of MG implementation is given in[1.93], [1.94]. The focus of this dissertation is to propose appropriate solutions for two major problems in MG operation: 1) voltage and frequency stabilization in islanded mode, and 2) real-time power management in both islanded and grid-tied mode. In the following sub-sections, each of these issues will be reviewed and explained.

Frequency and Voltage Stabilization within MGs

A MG is a regionally limited energy system of DERs, consumers, and optionally storage, controlled to maintain high quality, sustainable, and reliable electricity economically in grid-connected or off-grid (islanded) mode, as well as in dual mode (i.e., by changing the grid connection status.) Depending on the type and depth of penetration of DER units, load characteristics, power quality constraints, and market participation strategies, the required control and operational strategies of a MG can be significantly, and even conceptually, different than those of the conventional power systems [1.95]. The control strategy of a MG is a new concept in the modern power system and a challenging task from generation-, storage- and demand perspective. This challenge is

will be more complicated when the MG operates in islanded mode, where providing power with standard quality (in voltage and frequency) is a difficult task for the MG operator/owner in the absence of traditional AS available from the grid. At the transmission level, a significant penetration of DER is desired. However, the uncertain and variable nature of RES can create problems for power systems in providing balancing reserves when RES penetration is high, e.g. exceeding 20% [1.96]. As RES penetration increases, the conventional solution is to increase the amount of available reserve [1.97]. Since spinning reserves are mostly provided by fossil fuel-based power plants, their operation is costly and results in increased release of undesired emissions. While it is necessary to account for the variability of RES-based generation with balancing reserves, it is also desirable to have the ability to store any excess available energy. To overcome these issues related to the application of DER, several solutions have been proposed, some of which have been implemented and some under experimental study. Amongst all, energy storage and DSM have been chosen as the most viable options in the smart grid era. Although short- and long-term energy storage units can play a major role in control and operation of a MG [1.64], [1.95], [1.98], storage devices (such as pump storage, thermal energy storage, hydrogen storage and batteries) have a small chance to be widely applied in the near future because they:

- ✓ are expensive to install and maintain,
- ✓ have low efficiency,
- ✓ may have certain geographical topology requirement, which is not available in most cases especially in the case of MGs in populated areas,

- ✓ may require expensive facilities, with certain conditions, such as temperature humidity control.

In comparison, DSM is considered as a viable solution, although it has its own shortcomings and challenges [1.25], [1.99]-[1.104]. Based on the U.S. DOE report [1.2], economic benefits from DSM in the USA can range from about $80M to about $800M annually, in addition to another $85M to more than $300M annually through emergency DR. Previous pilot studies have also shown that DSM is beneficial to both customers and utilities, particularly for peak load shifting and AS [1.99]-[1.109]. DSM is a very broad set of actions on the part of both consumers and utilities that includes everything from installing energy-efficient appliances and switching off unused lights, to adding local off-grid generation abilities, to implementing a complicated electricity pricing system in which rates vary based on time-of-day and aggregate power usage intensity [1.25]. Amongst different DSM strategies, DR is a popular subset of DSM programs which relies on a direct command signal and/or financial signals from the utilities for altering patterns of consumer electricity usage. Traditionally, DR referred to the changes in electricity usage by end-use customers from their normal consumption through DLC or interruptible/curtailable programs during peak hours [1.105]. Progress in communication protocols and technologies (such as Internet) has been extraordinary in the past decade, which provides inexpensive two-way communication with individual loads [1.110]. Therefore, a new way of thinking about DR is developed amongst power system researchers and operators, which results in the new definition of DR: “DR is redefined as the capability to aggregate and precisely control individual loads on command at all

time." [1.110] This definition is the core idea throughout this dissertation for utilization of DR for frequency and voltage stabilization. Different DR programs are classified in Figure 1.31. These programs are divided into two main categories: Incentive-Based Programs (IBP) and Price-Based Program (PBP).

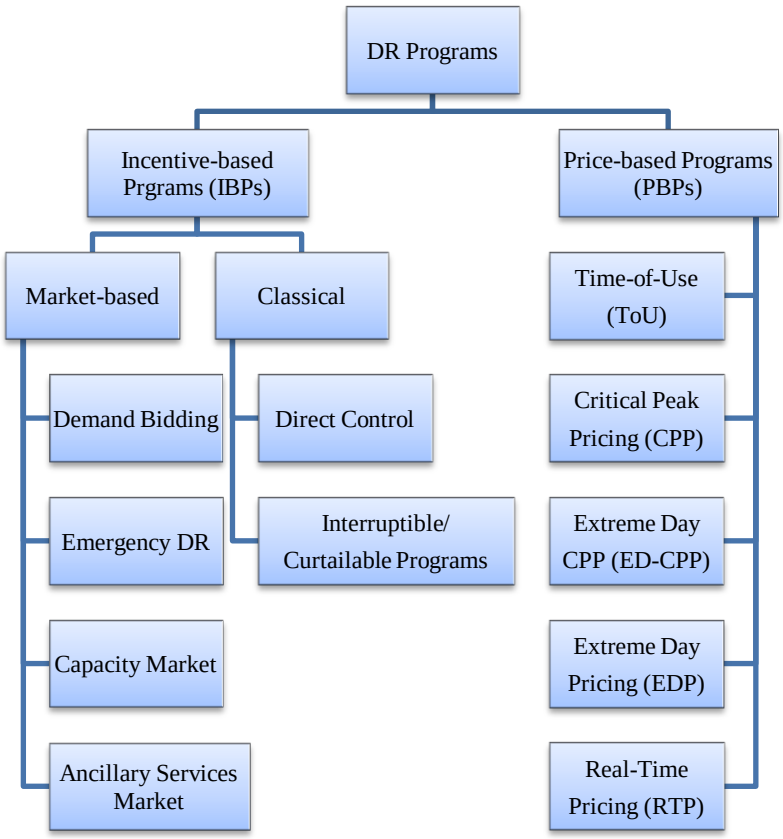


Figure 1.31. Classification of DR programs [1.105].

Regardless of the type of DR program, challenging and serious questions have to be answered for both researchers and system operators about the various impacts of DR on the economy, performance and operation of the power system and consumers, before taking any further steps. In many studies, researchers have tried to address the technical

and economic concerns and challenges on DR planning and modeling, e.g., [1.109], [1.111], [1.112], the economic costs/benefits analysis of DR for the utility and customers, e.g., [1.99]-[1.109], and the potential of DR for AS, e.g., [1.99], [1.113]-[1.124] at the distribution and transmission levels.

As a summary of the studies mentioned above, commonly anticipated and observed benefits of DR include:

- ✓ Lower risks of power interruptions from lower peak loads
- ✓ Improved operating conditions for utility firms from increased peak-time rates, reduced marginal costs of lower peak power quantities, and ability to postpone infrastructure investment
- ✓ Cost savings for end users from a combination of reduced off-peak tariffs and a greater awareness of one's level and pattern of power consumption
- ✓ Increased spread of energy-efficient appliances
- ✓ A general increase in responsibility and prudence with regard to electricity use.

Despite all the efforts that have been made so far, there is still a gap in research to clarify and quantify the impacts and potential of real-time DR on the performance of power systems and resolving related issues by proper management and control strategies for frequency regulation services, both at the distribution (in islanded MG without conventional AS) and transmission level (in load-frequency control (LFC) problem). These issues will be addressed in the first part of this dissertation.

Real-Time Power Management of MGs

Although the primary goal of any power system is to keep the load and generation balanced for safe operation, other objectives relevant to the features of smart grid should be considered in the operation of MGs. Since MGs are relatively expensive assets, it is always desirable to operate them with the minimum possible cost. Therefore, active and reactive power control within MGs (both in islanded and grid-tied operation) among different generation assets, storage devices, option of purchasing power form the upper grid in grid-tied mode, and the availability of DR resources seems to be essential. But MGs' control is not only limited to balancing generation and demand and cost-effective operation. Other realistic constraints and objectives which can be considered in a MG are given in Table 1.5. As a result, it can be concluded that the control philosophies and operational strategies of MGs are conceptually different from those in traditional power system. The main reasons for this are comprehensively reviewed in [1.95].

As it can be realized from Table 1.5, MGs substantially need power management architecture to achieve these goals simultaneously and quickly to keep up with variations in generation and demand. Satisfying different objectives within MGs infers multi-objective optimization problems, with several constraints, to be solved in real-time. In such problems, satisfaction of all objectives requires a combination of maximization and minimization simultaneously, while the optimal solution for one objective function may not necessarily be the optimal solution for other objectives. As a result, some of the objective functions may compete with each other for the optimal solution. This can make the optimization very difficult for real-time applications. To resolve this issue, a tradeoff between different objective functions should be made based on the requirement of the

MG at hand. This way, Pareto optimum can be reached, where the solution represents a state of satisfaction for one objective function which cannot be raised further without lowering another objective(s) satisfaction [1.84], [1.91], [1.125]. This shows the necessity of real-time power management systems for safe and reliable operation of MGs.

Table 1.5. Different objectives and constraints for MGs' operation [1.84], [1.125].

Objectives	Minimizing cost of operation and maintenance including all generation assets, storage devices, and DR resources
	Minimizing environmental impact (i.e., pollutions) in the presence of traditional generation sources
	Reducing losses in transmission and within MGs, providing VAR support
	Maximizing AS for the upper grid in grid-tied mode (i.e., maximizing MGs' profit)
	Scalability and plug-and-play operation
	Maximizing the total energy efficiency
	Maximizing load factor
Constraints	DERs availability, based on their generation prediction for variable RES
	Maintaining frequency and voltage standard levels
	Maintaining MGs stability and reserve margins for islanded operation
	Balancing active/reactive power generation and demand at all time

In general, real-time MG management is classified into energy and power management. Energy management algorithms deal with monitoring and operation of a complex system of electrical, thermal, and mechanical components with emphasis on desired longer term outcomes. The objective of power management is to affect the instantaneous operational conditions towards desired parameters, e.g. [1.126]-[1.133]. As a general viewpoint, both power and energy management refers to any control actions based on particular objectives in real-time (i.e., in the order of seconds to minutes). Here,

one might recognize the difference between day-ahead scheduling and economic demand and generation dispatch, which are performed off-line. MG management algorithms can be divided into centralized [1.126]-[1.131], and decentralized management architecture [1.132], [1.133]. Structurally, MGs can be operated in grid-tied [1.126], [1.129], [1.131]-[1.133]), islanded [1.127], [1.128], or both modes [1.130]. Each of the above modes has certain requirements to be fulfilled. A comprehensive literature review of specific requirements such as power management of MGs which include CHP and/or electric vehicle (EV) is given in [1.134], [1.135]. There are also numerous papers on the power electronic applications and appropriate controllers for MG safe operation, e.g. [1.136]-[1.141] to just name a few. A comprehensive literature review of the state-of-the-art of MGs is given in [1.91].

Real-time power management of MGs is an example of a complex automated decision-making framework which is faced with unique challenges in terms of required computational time and resources for real-world applications [1.125]. Multi-objective optimization existing in the MG management structure can be treated by two formal mathematical techniques to derive Pareto solutions. The first technique involves aggregating the various objective functions into a single objective function [1.125]. This technique is more suitable for gradient-based optimization techniques. It is relatively simple but requires the decision-maker to assign the relative weights of the constituent objective functions within the aggregation. The second broad category for addressing multiple objectives includes the class of intelligent methods [1.125]. The primary advantage of intelligent techniques is the fact that they can address many objectives

simultaneously with lower computational time, as shown in [1.127], [1.142]. As a result, in this dissertation, focus is also given to real-time power and energy management with heuristic optimization techniques compared to the results obtained from a well-known gradient-based technique, considering different generation and storage assets, and DR simultaneously. Both islanded and grid-tied operations are treated with emphasis on the islanded operation.

Organization of the Dissertation

This dissertation is organized in 12 chapters. A comprehensive introduction and the needs for this research are presented in Chapter 1. The rest of the dissertation is divided into three parts as follows:

Part I, including Chapters 2 to 5, is devoted to the applications of real-time DR and controller development for the islanded MGs. Specifically, Chapter 2 introduces a simulation framework to evaluate the impacts of high penetration of variable PV generation on the frequency and voltage of an islanded MG at the distribution level. Different simulation studies are designed and performed to thoroughly reveal the negative impacts of variable RES on the system operation parameters. In Chapter 3, a heuristic controller with minimum load manipulation is developed and utilized for IEEE 13-bus standard distribution system. The effectiveness of the proposed controller on the system frequency and voltage behavior is justified through different simulation studies. In Chapter 4, the proposed islanded MG is enhanced with the simplified grid model to include the automatic generation control in the analysis. Then, different simulation studies are carried out and the results are compared with those from real-time DR.

Chapter 5 presents an optimal real-time DR algorithm adapted for the application in the PJM regulation electricity market. An objective function with several technical constraints is solved using linear programming (LP) at each interval to find the best solution for regulation services in a test islanded MG.

Part II, which consists of Chapters 6 to 8, evaluates the application of real-time DR for system frequency control at the transmission level considering high penetration of variable RES, particularly wind generation. In Chapter 6, the well-known single-area LFC model is enhanced with real-time DR (called LFC-DR) control loop considering the DR communication delay. Different analytical studies are carried out to reveal the effectiveness of the enhancement. Finally, simulation studies are carried out for different single-area power system to show the impact of the proposed model. Then in Chapter 7, the proposed LFC-DR model is further developed for multi-area interconnected power systems with multiple generation companies (Gencos) and load aggregator companies (Lagcos). The analytical results and optimal controller design proposed for single-area power system in Chapter 6 is further extended for this purpose. Eventually, simulation studies are performed to reveal the effectiveness of the proposed model. Chapter 8 is devoted to the application of aggregated electric water heaters (EWHs) for transmission system for frequency regulation and shifting demand. Actual data for hot water demand and regulation services are utilized in several simulation studies. Different economical and technical analyses have been done to reveal the usefulness of the proposed DR approach.

In Part III, which includes Chapters 9 to 12, different real-time power

management algorithms (with and without DR) are developed for optimal and secure operation of grid-tied and islanded MGs. In Chapter 9, a general approach is proposed for ownership cost calculations of DERs. This is primarily useful for cost-effective power management algorithms. Then, Chapter 10 proposes a general power management framework for grid-tied MGs. Battery lifetime expansion and operational cost minimization are considered in the proposed approach. The performance of the proposed management algorithm is verified through different simulation studies. In Chapter 11, a real-time power management algorithm is introduced for an islanded MG considering battery and dump load operations. Particle swarm optimization (PSO) is utilized to find optimal solution in short intervals. Results of the heuristic optimization technique (i.e., PSO) are then compared with those from sequential quadratic programming (SQP) as a classical optimization technique. Finally, a multi-timescale power management algorithm considering dynamic model of generation, storage, and load is developed in Chapter 12. The optimality of the solutions is achieved and simultaneous generation, storage, and DR is included in the proposed algorithm. Different simulation studies revealed the effectiveness of the proposed approach.

Finally, the research and the results are concluded in Chapter 13.

References Cited

[1.1] Edison Tech. Center, "The history of alternating current: AC power history and timeline," Available online: http://edisontechcenter.org/AC-PowerHistory.html#early

[1.2] Office of Electric Transmission and Distribution, "Grid 2030: A national vision for electricity's second 100 years," U.S. Department of Energy, July 2030.

[1.3] North American Electric Reliability Corporation (NERC) Interconnections, Available online: http://www.nerc.com/AboutNERC/keyplayers/Pages/default.aspx

[1.4] U.S. Department of Energy, "The smart grid: An introduction. How a smarter grid works as an enabling engine for our economy, our environment and our future." Available online: http://energy.gov/oe/downloads/smart-grid-introduction-0

[1.5] J. Moura, "Assessment of the North American bulk power system: A reliability perspective on future needs and challenges," NERC Reliability Assessment Electricity Security Plan (ESAP) Workshop, Oct. 2013.

[1.6] M. Amin, "North American electricity infrastructure: system security, quality, reliability, availability, and efficiency challenges and their societal impacts," National Science Foundation (NSF) report on Continuing crises in national transmission infrastructure: impacts and options for modernization, Ch. 2, June 2004.

[1.7] K. Vu, M.M. Begouic, D. Novosel, "Grids get smart protection and control," *IEEE Comput. Appl. Power*, vol. 10, no. 4, pp. 40-44, Oct. 1997.

[1.8] Independent Statistics & Analysis, "International energy statistics," U.S. Energy Information Administration, Available online: http://www.eia.gov/cfapps/ipdbproject/iedindex3.cfm?tid=2&pid=2&aid=7&cid=US,&syid=1985&eyid=2011&unit=MK

[1.9] Independent Statistics & Analysis, "Annual energy review 2011," U.S. Energy Information Administration, Report NO: DOE/EIA-0384(2011), Sept. 2012.

[1.10] *Smart Grid Coordination Group – Sustainable Processes*, European Committee for Electrotechnical Standardization, pp. 84, Nov. 2012.

[1.11] Federal Incentives/Policies for Renewable Energy, "Residential renewable energy tax credit," Available online: http://www.dsireusa.org/library/includes/incentive2.cfm?Incentive_Code=US37F&State=federal&currentpageid=1&ee=0&re=1

[1.12] California Incentives/Policies for Renewable & Efficiency, "Burbank water &

power – green building incentive program," Available online: http://www.dsireusa.org/incentives/incentive.cfm?Incentive_Code=CA86F&re=0&ee=0

[1.13] Solar Energy Industries Association (SEIA), "Solar Industry Data in Q3 2013," Available online: http://www.seia.org/research-resources/solar-industry-data

[1.14] Renewable Portfolio Standard Policies, Database of State Incentives for Renewables & Efficiency, U.S. Department of Energy, March 2013, Available online: http://www.dsireusa.org/documents/summarymaps/RPS_map.pdf

[1.15] U.S. Energy Information Association (EIA), "Electricity market trends," Available online: http://www.eia.gov/forecasts/aeo/MT_electric.cfm

[1.16] Independent Statistics & Analysis, "Annual energy outlook 2013," U.S. Energy Information Administration, Dec. 2013, Available online: http://www.eia.gov/forecasts/aeo/MT_electric.cfm

[1.17] Edison Electric Institute (EEI), "Transmission investment: Adequate returns and regulatory certainty are key," June 2013.

[1.18] National Energy Policy Act of 1992, Available online: http://www.ferc.gov/legal/maj-ord-reg/epa.pdf

[1.19] North American Electric Reliability Corporation (NERC), "2013 long-term reliability assessment," Dec. 2013.

[1.20] The Electricity Technology Roadmap: Meeting the Critical Challenges of the 21st Century, 2003 Summary and Synthesis, EPRI, product no: 1010929, Available online: http://mydocs.epri.com/docs/CorporateDocuments/StrategicVision/Roadmap2003.pdf

[1.21] Independent Statistics & Analysis, "Electricity reliability data by NERC regions," U.S. Energy Information Administration, Available online: http://www.eia.gov/electricity/data/eia411/

[1.22] Renewables 2012 Global Status Report, Renewable Energy Policy Network for the 21st Century, Available online: http://www.ren21.net/Resources/Publications/REN21Publications/Renewables2012GlobalStatusReport.aspx

[1.23] EPRI 2001, *Electricity Infrastructure Security Assessment*, Vol. I-II, EPRI, Palo Alto, CA, Nov. and Dec. 2001.

[1.24] "OPEC Oil Embargo 1973–1974". U.S. Department of State, Office of the Historian, Available online: http://history.state.gov/milestones/1969-1976/oil-embargo

[1.25] J.H. Kim and A. Shcherbakova, "Common failures of demand response," *Energy*, vol. 36, no. 2, pp. 873–880, Feb. 2011.

[1.26] Independent Statistics & Analysis, "Electricity purchases, sales for resale, import/exports, reliability," U.S. Energy Information Administration, Dec. 2013, Available online: http://www.eia.gov/electricity/data/eia411/

[1.27] ABB Group. America, "Energy efficiency in the power grid," Published in 2007.

[1.28] Energy Efficiency & Renewable Energy, "2011 renewable energy data book," U.S. Department of Energy.

[1.29] U.S. Energy Information Administration, "State electricity profiles 2010," Report No DOE/EIA-0348(01)/2, Jan. 2012.

[1.30] Independent Statistics & Analysis, "Electric power monthly with data for December 2013," U.S. Energy Information Administration, Feb. 2014.

[1.31] Energy Laboratory, Massachusetts Institute of Technology, "Assessment of transmission congestion for major electricity market in the U.S.," Report NO: MIT EL 01-009 WP, Feb. 2001.

[1.32] S. Chakraborty and M.G. Simoes, "PV-microgrid operational cost minimization by neural forecasting and heuristic optimization," in *Proc*. IEEE Industry Applications Society Annual Meeting, Edmonton, Canada 2008, pp. 1–8.

[1.33] Annual Energy Outlook 2013, "Summary: Generating capacity," U.S. Energy Information Administration, Dec. 2013, Available online: http://www.eia.gov/totalenergy/data/annual/showtext.cfm?t=ptb0811a

[1.34] Annual Energy Outlook 2013, "Summary: Emissions from energy consumption for electricity generation," U.S. Energy Information Administration, Dec. 2013, Available online: http://www.eia.gov/totalenergy/data/annual/showtext.cfm?t=ptb1105a

[1.35] Independent Statistics and Analysis, "AEO2014 early release overview," U.S. Energy Information Administration, Dec. 2013, Available online: http://www.eia.gov/forecasts/aeo/er/early_elecgen.cfm?src=Renewable-b2

[1.36] N. Jenkins, et al., *Embedded Generation*, The Institution of Electrical Engineers, London, 2000.

[1.37] R.C. Dugan, et al., *Electric Power Systems Quality*, 2nd Ed., McGraw-Hill, 2003.

[1.38] T. Ackermann (editor), *Wind Power in Power Systems*, Wiley, 2005.

[1.39] B. Fox, et al., *Wind Power Integration - Connection and System Operational Aspects,* The Institution of Engineering and Technology, London, 2007.

[1.40] M.H.J. Bollen and F. Hassan, I*ntegration of Distributed Generation in Power Systems*, Wiley – IEEE Press, 2011.

[1.41] M.H.J. Bollen, *The Smart Grid: Adapting the Power System to New Challenges*, Morgan & Claopool Publishers, 2011.

[1.42] C.L. Wadhwa, *Electrical Power Systems*, New Age International Publishers, 2006, ch. 13.

[1.43] A. Lopez, et al., "U.S. renewable energy technical potentials: A GIS-based analysis," National Renewable Energy Laboratory, NREL/TP-6A20-51946, July 2012.

[1.44] Energy Efficiency & Renewable Energy, "2012 renewable energy data book," U.S. DOE, Available online: http://www.nrel.gov/news/press/2013/5302.html

[1.45] Office of Energy Efficiency & Renewable Energy, "Advantages and challenges of wind energy," U.S. DOE, Available online: http://energy.gov/eere/wind/advantages-and-challenges-wind-energy

[1.46] D.J.C. MacKay, *Sustainable Energy without Hot Air*, UIT Cambridge Ltd., 1st Ed., 2009, ch. 26.

[1.47] C.L. Archer and M.Z. Jacobson, "Supplying baseload power and reducing transmission requirements by interconnecting wind farms," *Journal of Applied Meteorology and Climatology* (American Meteorological Society), vol. 46, Issue. 11, pp. 1701–1717, Nov. 2007.

[1.48] Y.H. Wan, "Long-term wind power variability," National Renewable Energy Laboratory, NREL/TP-5500-53637, Jan. 2012.

[1.49] University of Oregon, Solar Radiation Monitoring Laboratory website. Available online: http://solardat.uoregon.edu/

[1.50] M. McDermott, "Denmark inaugurates world's largest offshore wind farm - 209 MW Horns Rev 2," Sept. 2009, Available online: http://www.treehugger.com/renewable-energy/denmark-inaugurates-worlds-largest-offshore-wind-farm-209-mw-horns-rev-2.html

[1.51] Energy Numbers, "Capacity factors at Danish offshore wind farms," March 2014, Available online: http://energynumbers.info/capacity-factors-at-danish-offshore-wind-farms

[1.52] Independent Statistics & Analysis, "What is a capacity factor?" U.S. Energy Information Administration, Available online: http://www.eia.gov/tools/faqs/faq.cfm?id=187&t=3

[1.53] D. Van Zandt, et al., "Ontario wind integration study: Final report to OPA, IESO, and CanWEA," GE Energy, Oct. 2006.

[1.54] M.R. Milligan, "Modeling utility-scale wind power plants Part 2: Capacity Credit," National Renewable Energy Laboratory, Technical Report NREL/TP-500-29701, March 2002.

[1.55] G.J.W. Van Bussel, and M.B. Zaaijer, "Reliability, availability and maintenance aspects of large-scale offshore wind farms," in *Proc.* 2001 European wind energy conference, Copenhagen, Denmark; 2011, pp. 557–60.

[1.56] J. Ribrant and L.M. Bertling, "Survey of failures in wind power systems with focus on Swedish wind power plants during 1997–2005," *IEEE Trans. Energy Convers.*, vol. 22, pp. 167–173, March 2007.

[1.57] P.J. Tavner, et al., "Influence of wind speed on wind turbine reliability," *Wind Engineering*, vol. 30, no. 1, pp. 55–72, Jan. 2006.

[1.58] G. Sinden, "Characteristics of the UK wind resource: Long-term patterns and relationship to electricity demand," *Energ. Policy*, vol. 35, no. 1, pp. 112–127, Jan. 2007.

[1.59] P. Brown, "U.S. renewable electricity: How does wind generation impact competitive power markets," CRS Report for U.S. Congress R42818, Congressional Research Service, Nov. 2012.

[1.60] D. Corbus, et al., "Up with wind - studying the integration and transmission of higher levels of wind power," *IEEE Power Energy Mag.*, vol. 7, no. 6, pp: 36–46, Nov/Dec. 2009.

[1.61] A.A. Edris, et al., "Proposed terms and definitions for flexible AC transmission system (FACTS)", *IEEE Trans. Power Del.*, vol. 12, no. 4, pp. 1848–1853, Oct. 1997.

[1.62] N. Etherden and M.H.J. Bollen, "Increasing the hosting capacity of distribution networks by curtailment of renewable energy resources", in *Proc.* IEEE Trondheim Power Tech, June 2011, pp. 1–7.

[1.63] A.K. Kazerooni, et al., "Dynamic thermal rating applications to facilitate wind energy integration", in *Proc.* IEEE Trondheim Power Tech, June 2011 pp. 1–7.

[1.64] D. Rastler, "Electricity energy storage technology options: A white paper primer

on applications, costs, and benefits," EPRI 1020676, Dec. 2010.

[1.65] U. Eberle, B. Muller, and R. von Helmolt, "Fuel cell electric vehicles and hydrogen infrastructure: Status 2012," *Energy & Environment Science*, vol. 5, no. 10, pp. 8780–8798, July 2012.

[1.66] P. Hoffmann, *Tomorrow's Energy: Hydrogen, Fuel Cells, and the Prospects for a Cleaner Planet*, MIT Press, 2002.

[1.67] C. Wang and M.H. Nehrir, "Fuel cells and load transients," *IEEE Power Energy Mag.*, vol. 5, no. 1, pp. 58–63, Jan/Feb 2007.

[1.68] Florida Solar Energy Center, "Hydrogen basics: Storage," Available online: http://www.fsec.ucf.edu/en/consumer/hydrogen/basics/storage.htm

[1.69] Hydrogen and Fuel Cells Program, "Hydrogen storage," U.S. Department of Energy, Available online: http://www.hydrogen.energy.gov/storage.html

[1.70] J.S. Thorp, et al., "Feasibility of adaptive protection and control", *IEEE Trans. Power Del.*, vol. 8, no. 3, pp. 975–983, July 1993.

[1.71] W.S. Tan, et al., "Optimal distributed renewable generation planning: A review of different approaches," *Renew. Sust. Energ. Rev.*, vol. 18, pp. 626–645, Feb. 2013.

[1.72] T. Xu and P. C. Taylor, "Voltage control techniques for electrical distribution networks including distributed generation," in *Proc.* 17th World Congress of the International Federation of Automatic Control, Seoul, South Korea, July 2008, pp. 11967–11971.

[1.73] T.J.T. Hashim, A. Mohamed, and H. Shareef, "A review on voltage control methods for active distribution networks," *PRZEGLĄD ELEKTROTECHNICZNY* (*Electrical Review*), vol. 88, no. 6, pp. 304–312, 2012.

[1.74] N. Hatziargyriou, "Microgrids - The key to unlock distributed energy resources?" *IEEE Power Energy Mag.*, vol. 6, no. 3, pp. 26–29, May/June 2008.

[1.75] J. Driesen and F. Katiraei, "Design for distributed energy resources", *IEEE Power Energy Mag.*, vol. 6, no. 3, pp. 30–39, May/June 2008.

[1.76] N. Martensen, P. Lund, and N. Mathew, "The cell controller pilot project: From surviving system black-out to market support," in *Proc.* 21st International Conference on Electricity Distribution (CIRED), Frankfurt, June 2011.

[1.77] *CERTS Microgrid Test Bed*, Dolan Technology Center, Available online:

http://certs.aeptechlab.com/

[1.78] P. Asmus, "Why microgrids are moving into the mainstream: Improving the efficiency of the larger power grid," *IEEE Electrific. Mag.*, vol. 2, no. 1, pp. 12–19, March 2014.

[1.79] A. Khamis, et al., "A review of islanding detection techniques for renewable distributed generation systems," *Renew. Sust. Energ. Rev.*, vol. 28, pp. 483–493, Dec. 2013.

[1.80] Z. Zeng, et al., "Topologies and control strategies of multi-functional grid-connected inverters for power quality enhancement: A comprehensive review," *Renew. Sust. Energ. Rev.*, vol. 24, pp. 223–270, Aug. 2013.

[1.81] C. Natesan, et al., "Survey on microgrid: Power quality improvement techniques," *ISRN Renewable Energy*, Hindawi Publishing Corporation, 2014, pp. 1–7.

[1.82] K. LaCommare and C. Marnay, "Microgrids and heterogeneous power quality and reliability," *International Journal of Distributed Energy Recourses*, vol. 4, no. 4, pp. 1–11, Oct. 2008.

[1.83] R. O'Neill, "Smart grids sound transmission investments," *IEEE Power Energy Mag.*, vol. 5, no. 5, pp. 104–102, Sep–Oct. 2007.

[1.84] C.M. Colson and M. H. Nehrir, "A review of challenges to real-time power management of microgrids," in *Proc*. IEEE PES General Meeting, Calgary, Canada, July 2009, pp. 1–8.

[1.85] X. Guan, Z. Xu, and Q-S. Jia, "Energy-efficient buildings facilitated by microgrid," *IEEE Trans. Smart Grid*, vol. 1, no. 3, pp. 243–252, Dec. 2010.

[1.86] R. Cowart, et al., "Efficient reliability: The critical role of demand-side resources in power systems and markets," The Regulatory Assistance Project prepared for The National Association of Regulatory Utility Commission, June 2001.

[1.87] S. A. Pourmousavi and M. H. Nehrir, "Real-time optimal demand response for frequency regulation in smart microgrid environment," in *Proc*. 11th IASTED International conference on Power and Energy Systems (EuroPES2012), Naples, Italy, June. 2012, pp. 194–200.

[1.88] J.D. Kueck, R.M. Staunton, and B.J. Kirby, "Microgrids and demand response," *Public Utility Fortnightly*, May 2003, pp. 55–58.

[1.89] M. Amin and B.F. Wollenberg, "Toward a smart grid: Power delivery for the 21st

century", *IEEE Power Energy Mag.*, vol. 3, no. 5, pg. 34–41, Sept/Oct 2005.

[1.90] M. Amin, "The self-healing grid: A concept two decades in the making," IEEE Smart Grid Technical Community, Available online: http://smartgrid.ieee.org/march-2013/813-the-self-healing-grid-a-concept-two-decades-in-the-making

[1.91] C.M. Colson, "Towards real-time power management of microgrids for power system integration: A decentralized multi-agent based approach," PhD Dissertation, Montana State University, Nov. 2012.

[1.92] C. Marnay, et al., "Policymaking for microgrids: Economic and regulatory issues of microgrid implementation," *IEEE Power Energy Mag.*, vol. 6, no. 3, pp. 66–77, May/June 2008.

[1.93] M.S. Mahmoud, S.A. Hussain, and M.A. Abido, "Modeling and control of microgrid: An overview," *Journal of Franklin Institute*, vol. 351, no. 5, pp. 2822–2859, May 2014.

[1.94] C.M. Colson and M. H. Nehrir, "A review of challenges to real-time power management of microgrids," in *Proc*. IEEE PES General Meeting, Calgary, Canada, July 2009, pp. 1–8.

[1.95] F. Katiraei, et al., "Microgrids management: Controls and operation aspects of microgrids," *IEEE Power Energy Mag.*, vol. 6, no. 3, pp. 54–65, May/June 2008.

[1.96] H. Holttinen, et al., "Design and operation of power systems with large amounts of wind power," *VTT Technical Research Centre of Finland*, Helsinki, Finland, Rep. 2493, 2009.

[1.97] R. Doherty and M. O'Malley, "A new approach to quantify reserve demand in systems with significant installed wind capacity," *IEEE Trans. Power Syst*., vol. 20, no. 2, pp. 587–595, May 2005.

[1.98] I. Gyuk, et al., "The United State of storage: Federal and state collaboration on electric energy storage," *IEEE Power Energy Mag.*, vol. 3, no. 2, pp. 31–39, March/April 2005.

[1.99] D. Westermann and A. John, "Demand matching wind power generation with wide-area measurement and demand-side management," *IEEE Trans. Energy Convers.*, vol. 22, no. 1, pp. 145–149, March 2007.

[1.100]A. Faruqui, S. Sergici, and A. Sharif, "The impact of informational feedback on energy consumption – A survey of the experimental evidence," *Energy*, vol. 35, no. 4, pp. 1598–1608, Apr. 2010.

[1.101]J.W. Zarnikau, “Demand participation in the restructured electric reliability council of Texas market,” *Energy*, vol. 35, no. 4, pp. 1535–1543, Apr. 2010.

[1.102]K. Herter and S. Wayland, “Residential response to critical-peak pricing of electricity: California evidence,” *Energy*, vol. 35, no. 4, pp. 1561–1567, Apr. 2010.

[1.103]J. Torriti, M.G. Hassan, and M. Leach, “Demand response experience in Europe: Policies, programs and implementation,” *Energy*, vol. 35, no. 4, pp. 1575–1583, Apr. 2010.

[1.104]J. Wang, et al., “Demand response in China,” *Energy*, vol. 35, no 4, pp. 1592–1597, Apr. 2010.

[1.105]M.H. Albadi and E.F. El-Saadany, “A summary of demand response in electricity markets,” *Electr. Pow. Syst. Res.*, vol. 78, no. 11, pp. 1989–1996, Nov. 2008.

[1.106]R. Walawalkar, et al., “An economic welfare analysis of demand response in the PJM electricity market,” *Energ. Policy*, vol. 36, no. 10, pp. 3692–3702, Oct. 2008.

[1.107]T.J. Park and S.H. Hong, “Experimental case study of a BACnet-based lighting control system,” *IEEE Trans. Autom. Sci. Eng.*, vol. 6, no. 2, pp. 322–333, Apr. 2009.

[1.108]M. Klobasa, “Analysis of demand response and wind integration in Germany's electricity market,” *IET Renew. Pow. Gen.*, vol. 4, no. 1, pp.55–63, Jan. 2010.

[1.109]H. Saele and O.S. Grande, “Demand response from household customers-Experiences from a pilot study in Norway”, *IEEE Trans. Smart Grid*, vol. 2, no. 1, pp. 102–109, Mar. 2011.

[1.110]A. Brooks, et al., “Demand dispatch: Using real-time control of demand to help balance generation and load,” *IEEE Power Energy Mag.*, vol. 8, no. 3, pp. 20–29, May/June 2010.

[1.111]J. Medina, N. Muller, and I. Roytelman, “Demand response and distribution grid operations: Opportunities and challenges,” *IEEE Trans. Smart Grid*, vol. 1, no. 2, pp. 193–198, Sept. 2010.

[1.112]A.J. Conejo, J.M. Morales, and L. Baringo, “Real-time demand response model,” *IEEE Trans. Smart Grid*, vol. 1, no. 3, pp. 236–242, Dec. 2010.

[1.113]D. Trudnowski, M. Donnelly, and E. Lightner, “Power-system frequency and stability control using decentralized intelligent loads,” in *Proc.* IEEE PES Conf. and Exhibition Transmission and Distribution, Dallas, TX, 2005, pp. 1453–1459.

[1.114]G.C. Heffner, C.A. Goldman, and M.M. Moezzi, “Innovative approaches to verifying demand response of water heater load control,” *IEEE Trans. on Power Delivery*, vol. 21, no. 1, pp. 388–397, Jan. 2006.

[1.115]J.A. Short, D.G. Infield, and L.L. Freris, “Stabilization of grid frequency through dynamic demand control,” *IEEE Trans. Power Syst.*, v. 22, no. 3, pp. 1284–1293, Aug. 2007.

[1.116]R. Jia, M.H, Nehrir, and D.A. Pierre, “Voltage control of aggregate electric water heater load for distribution system peak load shaving using field data,” in *Proc.* 39th North American Power Symposium (NAPS '07), Las Cruces, NM, 2007, pp. 492–497.

[1.117]J. Kondoh, N. Lu, and D.J. Hammerstrom, “An evaluation of the water heater load potential for providing regulation service,” *IEEE Trans. Power Syst.*, vol. 26, no. 3, pp. 1309–1316, Aug. 2011.

[1.118]A. Molina-Garcia, F. Bouffard, and D.S. Kirschen, “Decentralized demand-side contribution to primary frequency control,” *IEEE Trans. Power Syst.*, vol. 26, no. 1, pp. 411–419, Feb. 2011.

[1.119]D. Angeli and P.A. Kountouriotis, “A stochastic approach to dynamic-demand refrigerator control,” *IEEE Trans. Control Syst. Technol.*, vol. 20, no. 3, pp. 581–592, May 2012.

[1.120]S.A. Pourmousavi and M.H. Nehrir, “Demand response for smart microgrid: Initial results,” in *Proc.* IEEE PES Innovative Smart Grid Technologies (ISGT), Anahiem, CA, 2011, pp. 1–6.

[1.121]S.A. Pourmousavi, M.H. Nehrir, and C. Sastry, “Providing ancillary services through demand response with minimum load manipulation,” in *Proc.* North American Power Symposium (NAPS), Boston, MA, 2011, pp. 1–6.

[1.122]K.Y. Huang, H.C. Chin, and Y.C. Huang, “A model reference adaptive control strategy for interruptible load management,” *IEEE Trans. Power Syst.*, vol. 19, no. 1, pp. 683–689, Feb. 2004.

[1.123]F. De Ridder, M. Hommelberg, and E. Peeters, “Four potential business cases for demand side integration,” in *Proc.* 6th International Conference on the European Energy Market, 2009, pp. 1–6.

[1.124]N. Ruiz, I. Cobelo, and J. Oyarzabal, “A direct load control model for virtual power plant management,” *IEEE Trans. Power Syst.*, vol. 24, no. 2, pp. 959–966, May 2009.

[1.125]C.M. Colson, M.H. Nehrir, and S.A. Pourmousavi, “Towards real-time microgrid power management using computational intelligence methods,” in *Proc*. IEEE PES GM, Minneapolis, USA, July 2010, pp. 1–8.

[1.126]A.G. Tsikalakis and N.D. Hatziargyriou, “Centralized control for optimizing microgrids operation,” *IEEE Trans. Energy Convers*., vol. 23, no. 1, pp. 241–248, Feb. 2008.

[1.127]S.A. Pourmousavi, et al., "Real-time energy management of a stand-alone hybrid wind-microturbine energy system using particle swarm optimization," *IEEE Trans. Sustain. Energy*, vol. 1, no 3, pp. 193–201, Oct. 2010.

[1.128]F.A. Mohamed and H.N. Kovio, “Power management strategy for solving power dispatch problems in microGrid for residential applications,” in *Proc.* IEEE International Energy Conference and Exhibition, Manama, Bahrain 2010, pp. 746–751.

[1.129]Y. Riffonneau, et al., “Optimal power flow management for grid connected PV systems with batteries,” *IEEE Trans. Sustain. Energy*, vol. 2, no. 3, pp. 309–320, Feb. 2011.

[1.130]B. Belvedere, et al., “A microcontroller-based power management system for standalone microgrids with hybrid power supply,” *IEEE Trans. Smart Grid*, vol. 3, no. 3, pp. 422–431, May 2012.

[1.131]S.A. Pourmousavi, R.K. Sharma, and B. Asghari, "A framework for real-time power management of a grid-tied microgrid to extend battery lifetime and reduce cost of energy," in *Proc*. IEEE PES Innovative Smart Grid Technologies, Washington D.C., USA 2012, pp. 1–8.

[1.132]C.M. Colson and M.H. Nehrir, “Comprehensive real-time microgrid power management and control with distributed agents,” *IEEE Trans. Smart Grid*, vol. 4, no. 1, pp. 617–627, Jan. 2013.

[1.133]C. Colson, et al., “Improving sustainability of hybrid energy systems Part II: managing multiple objectives with a multi-agent system,” *IEEE Trans. Sustain. Energy*, vol. 5, no. 1, pp. 46–54, Jan. 2014.

[1.134]A. Dewan, et al., “Alternative power sources for remote sensors: A review,” *J. Power Sources*, vol. 245, pp. 129-143, Jan. 2014.

[1.135]M. Peng, L. Liu, and C. Jiang, “A review on the economic dispatch and risk management of the large-scale plug-in electric vehicles (PHEVs)-penetrated power systems,” *Renew. Sust. Energ. Rev*., vol. 16, no. 3, pp. 1508–1515, Apr. 2012.

[1.136]Y.W. Li and C. Kao, "An accurate power control strategy for power-electronics interfaced distributed generation units operating in a low-voltage multi-bus microgrid", *IEEE Trans. Power Electron*., vol. 24, no. 12, pp. 2977–2988, Dec. 2009.

[1.137]E. Serban and H. Serban, "A control strategy for a distributed power generation microgrid application with voltage- and current-controlled source converter", *IEEE Trans. Power Electron*., vol. 25, no. 12, pp. 2981–2992, May 2010.

[1.138]K. Jong-Yul, et al., "Cooperative control strategy of energy storage system and microsources for stabilizing the microgrid during islanded operation", *IEEE Trans. Power Electron*., vol. 25, no. 12, pp. 3037–3048, Sept. 2010.

[1.139]T. L. Vandoorn, et al., "A control strategy for islanded microgrids with DC-link voltage control", *IEEE Trans. Power Del*., vol. 26, no. 2, pp. 703–713, Jan. 2011.

[1.140]C. Cho, et al., "Active synchronizing control of a microgrid", *IEEE Trans. Power Electron*., vol. 26, no. 12, pp. 3707–3719, July 2011.

[1.141]S. Conti, et al., "Optimal dispatching of distributed generators and storage systems for MV islanded microgrids," *IEEE Trans. Power Del*., vol. 27, no. 3, pp. 1243–1251, May 2012.

[1.142]C.M. Fonseca and P.J. Fleming, "Multi-objective optimization and multiple constraint handling with evolutionary algorithms-Part I: a unified formulation," *IEEE Trans. on Systems, Man., and Cybernetics Part A: Systems and Humans*, vol. 28, no. 1, pp. 26–37, Jan. 1998.

CHAPTER 2

IMPACT OF HIGH PENETRATION OF PV GENERATION ON FREQUENCY AND VOLTAGE IN A DISTRIBUTION FEEDER

Contribution of Authors and Co-Authors

Manuscripts in Chapters 2 through 12

Author: S. A. Pourmousavi

Contributions: Developed the simplified grid model (SGM) for the simulation with all of its components conceptually and in MATLAB®/Simulink, designed different simulation setup including moving clouds, different type of SGM, and frequency/voltage figures.

Co-author: A. S. Cifala

Contributions: Prepared the actual PV irradiation and ambient temperature data, developed model of the distribution network in MATLAB®/Simulink.

Co-author: M. H. Nehrir

Contributions: Provided important insight and overview of the research, interpretation of the results, and aided in the preparation of the manuscript.

Manuscript Information Page

Seyyed Ali Pourmousavi Kani, Andrew S. Cifala, M. Hashem Nehrir

IEEE North American Power Symposium (NAPS), 2012

Status of the manuscript:
____ Prepared for submission to a peer-reviewed conference
____ Officially submitted to a peer-reviewed conference
____ Accepted by a peer-reviewed conference
_X_ Published in a peer-reviewed conference proceedings

Published by the Institute of Electrical and Electronics Engineering (IEEE)

IMPACT OF HIGH PENETRATION OF PV GENERATION ON FREQUENCY AND VOLTAGE IN A DISTRIBUTION FEEDER

The following work was presented at 2012 NAPS and is published in the conference proceedings

S.A. Pourmousavi, A.S. Cifala, and M.H. Nehrir

Department of Electrical and Computer Engineering, Montana State University, Bozeman, MT 59717

Abstract

This chapter presents an evaluation of the impact of various levels of PV power penetration in a distribution feeder connected to a simplified grid model (SGM). PV generation is implemented in second-by-second iterations with power output based on actual solar radiation and air temperature data. High penetration levels of intermittent PV generation (15% and 30%) are employed in a feeder-configured MG to evaluate grid frequency and voltage characteristics. In this study, only governor droop control is included in the proposed SGM without the secondary control action (known as load frequency control). Two different grid models (fast and slow grid), PV generation configurations (concentrated and distributed), and PV penetration levels (15% and 30%) are considered in the simulation studies. Simulation results indicate the impact of the aforementioned parameters on the system frequency and voltage. Results also reveal that distributed PVs in a wide geographical area with different weather regime have less impact on the frequency and voltage.

Introduction

The drive to provide more economical means of power production has resulted in

major technological advances toward the application of distributed generation (DG). In turn, the practicality of alternative energy system deployment has become much more apparent. One such rapidly developing technology is solar PV power generation. The evolution of distributed PV is made evident by the 878 MW increase in grid-connected PV capacity in the U.S. in 2010- nearly a 72% rise in capacity from 2009 [2.1]. However, the growing amount of penetration of DG (in particular intermittent renewable DGs, such as PV) can impact reliable operation of distribution system, to which they are connected [2.2].

The ability to balance generation and demand within a grid is imperative to maintaining electrical stability. At the distribution level, the impact of several highly variable sources such as PV can result in deviations in grid characteristics large enough to violate standard practices for implementation [2.3]. As the amount of grid-connected DG increases, grid operation and control becomes progressively more difficult and it may ultimately result in system failure. Consequently, dividing the main grid into smaller subsystems of MGs presents a much more manageable and controllable network. This allows for higher penetration of reliable power sources, such as PV, without requiring massive architectural reconstruction of the main grid [2.4]. Additionally, MGs provide greater system flexibility through the installation of inverter-interfaced inertia-less distributed generation systems (such as PV systems and fuel cells), as well as introducing adjustable base-load generators and energy storage systems to compensate for the variable generation that some renewable energy generation sources naturally exhibit [2.5], [2.6].

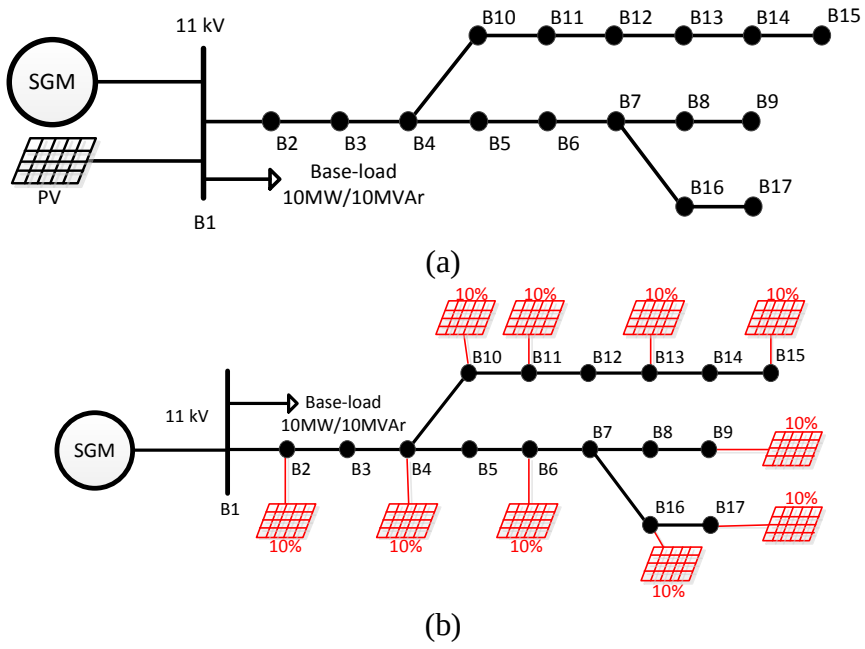


Figure 2.1. Configuration of the generic feeder (a) with concentrated PV generation, and (b) distributed PV generation.

In this chapter, a grid-tied distribution feeder with concentrated or distributed PV resembles a MG. Since higher penetration of renewable resources into the conventional grid is desired, evaluation of their variable generation on the system's frequency and voltage is necessary. In order to avoid complex modeling of the grid, a simplified grid model (SGM) is developed at the distribution level to resemble the behavior of the actual grid at that level. Only governor droop control is considered for the grid in this part of the research. No spinning reserve is included. The main purpose of this study is to investigate the actual impacts of large penetration of PVs in the order of seconds, whereas spinning reserves work in the order of minutes.

The distribution feeder as a part of the grid is connected to the SGM to show the effects of variable PV generation on the system frequency and voltage. Two different

SGMs (a slow and a fast response), and PV penetration values of 15% and 30% are studied. The PV generation is modeled as a PV farm and as distributed (customer owned) PV systems, as shown in Figure 2.1 (a), (b). The simulation diagram of the feeder-configured MG is shown in Figure A.1 in Appendix A.

Second-by-second solar insolation data is used to show the effects of abrupt variations in solar insolation. The SGM tries to adjust its output with variations in PV generation output to stabilize the system frequency and consequently voltage through its governor droop control. However, large penetration of PV generation causes the system frequency to fall out of the acceptable range most of the times. In a real system, LFC could compensate for some of the above frequency deviations. The addition of these features as well as load control (i.e., DR) for frequency stabilization is a part of the next chapter.

Simulation results show the significant impact of high PV penetration on the system frequency and consequently voltage; however, the impact is lower in the case of distributed PVs compared to concentrated PVs (solar farm) with the same penetration level. It has also been shown that a larger grid with slow-response generators experience larger variations in system frequency and voltage. All system models are developed and tested in MATLAB/Simulink® [2.7].

System Studied

The systems of study are modeled as grid-tied MGs with concentrated or distributed PV DGs, as shown in Figure 2.1 (a), (b). In both cases, the SGM with speed governor and exciter is utilized as presented in earlier section. The SGM is designed to

resemble the actual behavior of a grid at the distribution level. It includes governor droop control, but LFC is not considered. The main objective of this chapter is to show the impact of medium and high levels of PV generation on the system frequency and voltage where only governor droop control is available for frequency regulation.

The PV model obtained from [2.8] is used. The model incorporates a maximum power point tracking (MPPT) system consisting of 30 kW PV arrays with a buck-boost DC/DC converter and a DC/AC inverter. The PV output power is scaled to achieve the desired level of penetration based on the number of arrays in the system. The inputs to the PV system are solar insolation and air temperature, which are recorded in one-second and one-minute intervals, respectively. The data is obtained from the National Renewable Energy Laboratory (NREL) for Oahu, Hawaii Solar Measurement Grid [2.9]. This solar insolation data is especially attractive for this study since the one-second data gives more accurate representation of the variable nature of PV output power during sporadic clouding, thus providing a more realistic case. To expose the variability issues with PV generation, solar irradiation is represented for a sunny day with erratic clouding (June 18, 2010).

Penetration by renewables can be defined in a number of ways (i.e., percentage of energy supplied by renewables, rated renewable power generation in comparison to peak load, and renewable generation in comparison to system capacity) [2.10]. In this study, PV penetration is defined as the rated PV capacity in relation to total capacity of the grid. 15% and 30% PV penetration level is studied.

Simplified Grid Model (SGM)

In the majority of power system studies, the grid is modeled as an infinite bus, which can provide or absorb any amount of power requested by loads. However, this is unacceptable in reality and also for the sake of this study, where system frequency and voltage are investigated under transient and steady-state conditions. Computationally, it is not always feasible to use a detailed grid model, such as this study. Thus, a simplified grid model is required at the distribution level, which can be utilized for any frequency and voltage stabilization studies, DR studies and for evaluating the impact of renewable energy on the distribution grid. All the generators in the grid are modeled as a single generator with effective inertia of the grid, governor action, and load-frequency dependence [2.11], where the capacity of the grid model is the total capacity of the grid. The components of the proposed model are shown in Figure 2.2.

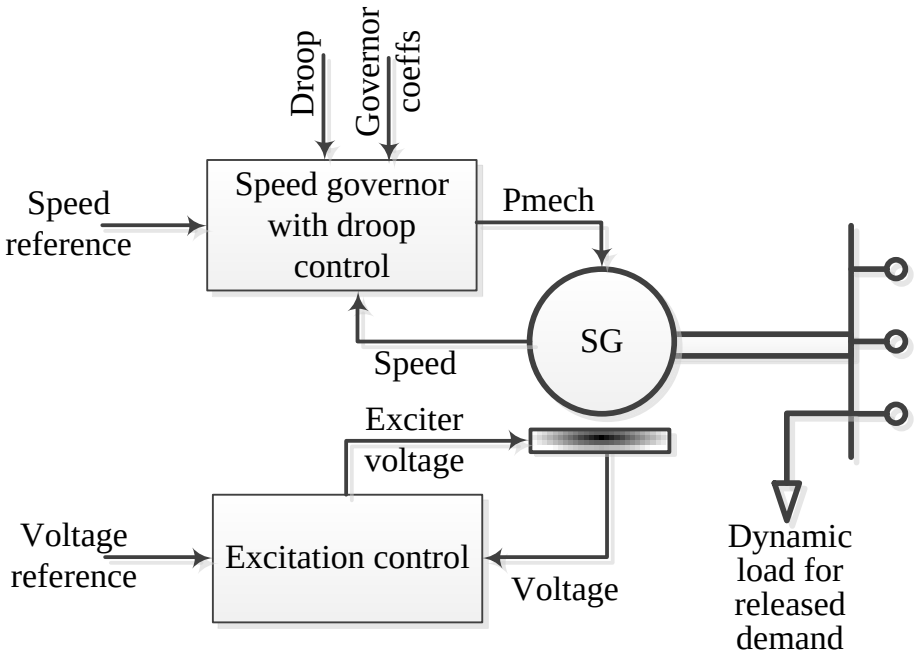


Figure 2.2. Components of the proposed SGM.

The proposed model includes a synchronous generator, speed governor, voltage controller (excitation system), and a dynamic load. It is equipped with a type AC4A exciter with transient gain reduction [2.11], [2.12]. This model includes the following characteristics of an actual grid:

- Governor droop characteristic can be applied to calculate the target mechanical power of the generator as follows [2.11], [2.13]:

$$P_{tar} = \left(\frac{f_{sp} - f_{act}}{R \times f_{nom}} \right) \ p.u. \tag{2.1}$$

where f_{sp} is the frequency setpoint, fact is the measured frequency, and f_{nom} is the nominal frequency, all in Hz. R is the droop value of the generator. Typically, speed governors are designed with 4%-20% “droop” characteristic [2.13]. For 4% droop value, the generator output will increase to 100% for a 4% drop in frequency.

- The speed governor and turbine model. This model, shown in Figure 2.3, is extracted from [2.12].

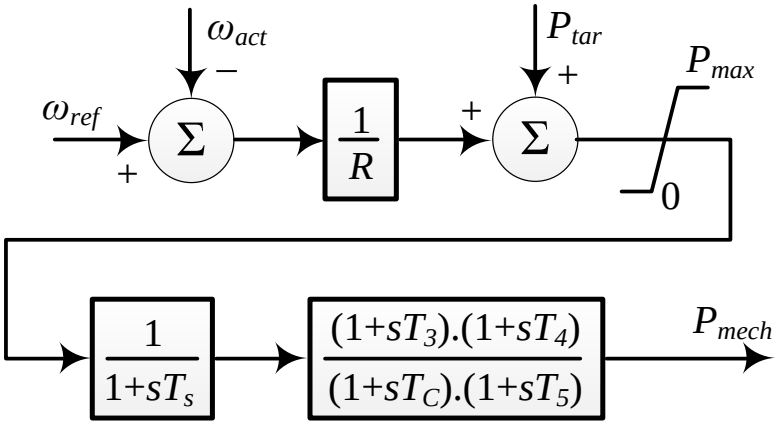


Figure 2.3. Speed governor of the proposed SGM.

In Figure 2.3, ω_{act} is the measured machine radian speed, ω_{ref} is the machine reference speed, P_{tar} is the reference target power, and P_{mech} is the mechanical power driving the generator, all in per unit. Also, T_s is the servo time constant, T_C is the high pressure (HP) turbine time constant, T_3 is the transient gain time constant, T_4 is the time constant to set HP ratio, and T_5 is the re-heater time constant, all in sec [2.12].

- Released demand consisting of the loads which have built-in frequency dependence. When the frequency drops, the power consumption of such loads will drop as well and vice versa. This effect can be modeled by a variable active load model defined by (2.2) [2.11], [2.13]:

$$P_R = D.P_L.\left(\frac{f_{act} - f_{nom}}{f_{nom}}\right) \ ,W \tag{2.2}$$

where D is the load-damping constant, and P_L is the total amount of active load, including the released demand.

- Inertia of an actual power system which typically varies between 2 and 8 sec [2.11], [2.13]. This effective inertia is used in the inertia of single synchronous generator.

- Total generation capacity of the grid can also be modeled as the capacity of a single large synchronous generator. The impedance of the single generator is tuned to result in the typical losses of the desired power system.

The simulation diagram of the SGM is shown in Figure A.2 of Appendix A.

Feeder-Configured MG

The system incorporates distributed aggregated loads in a grid-tied MG configured as a generic feeder, as shown in Figure 2.1 (a), (b). The parameters of the

lines and aggregated loads are obtained from a study on distribution system reconfiguration [2.14]. However, the grid in [2.14] is replaced by the proposed SGM in this chapter. In Figure 2.1 (a), the PV DG is implemented as a single concentrated source. This scenario represents a solar PV farm where all PV panels experience the same weather regime. The farm is sized to the desired level of penetration. The total load of the feeder is approximately 0.837 MW/0.626 MVAr for a total of approximately 1.06 MVA. The total resistive and reactive load for the top, middle, and bottom branches of the feeder are 0.256 MW/0.189 MVAr, 0.447 MW/0.352 MVAr, and 0.140 MW/0.085 MVAr, respectively. This feeder is considered as the added load to a grid with 10 MW/10 MVAr base-load. The released demand is implemented for the active base-load in the SGM. Simulations are performed with the concentrated PV system scaled to penetration levels of 15% and 30%, corresponding to 4.5 MW (150 30-kW arrays) and 9.0 MW (300 30-kW arrays), respectively.

To investigate the effect of the distributed PVs, an additional scenario is tested, where the PV arrays are distributed at arbitrary nodes within the feeder, as shown in Figure 2.1 (b). This scenario is intended to represent distributed PV throughout a community of loads. The total PV penetration capacity is distributed at 10 different nodes in the feeder, assumed to be in a large geographical area. It is also assumed that each PV station at each node is the aggregate of several distributed PV units in a geographical area with similar solar insolation and temperature regime. The total PV penetration capacity is the same as in the concentrated PV case. To emulate the moving clouds, insolation for each PV system is lagged for an arbitrarily chosen time of 500 seconds (just over eight

minutes). This delay represents a moving cloud in the area with several small PV generation units.

In power systems, a negative frequency deviation is an indication of excess load or lack of generation, while positive frequency deviation suggests a lack of demand or excess generation [2.12], [2.13], [2.15]. It is well known that mitigating the large deviations in frequency is crucial for restoring system stability; therefore, loads must be released or added according to the situational frequency in emergency circumstances. In North America, whenever a frequency error persists for a certain time (10 seconds for the east, 3 seconds for Texas, and 2 seconds for the west), a correction of ±0.02 Hz (0.033% of 60 Hz) is applied [2.15]. This corrective action starts with primary frequency regulation, and follows by secondary and tertiary frequency regulation, just in case. Since spinning reserves are expensive, and their use result in higher marginal cost of electricity, it is always desired to avoid purchasing spinning reserve for frequency regulation. Therefore, this study is undertaken to show the impact of high levels of PV generation with only governor droop control which finally translates to a need for a required amount of spinning reserve. In other words, larger frequency variations require more spinning reserve. As another possibility for providing AS in place of spinning reserve, DR is known as a promising technology in smart grid for frequency regulation [2.16], [2.17]. LFC could help partially reduce the frequency variations; however, because its response is not as fast as governor droop control, it is unlikely that the combination of governor droop control and LFC could reduce all the frequency variations [2.18]. We therefore investigate both the effect of LFC as well as DR for frequency regulation in the next

chapter.

Simulation Results

The systems described are simulated in MATLAB/Simulink® to evaluate their operational characteristics. The system is evaluated over a 9000-second (hrs: 12:36-15:06) portion of the day for the solar insolation and temperature curves shown in Figure 2.4 (a), (b). This time-span is chosen because of large fluctuations in insolation and therefore PV output power. The insolation data reaches near 1000 W/m^2 (standard maximum insolation) at its peak value. This helps maintain consistency in the rated peak power output of the PV system and, ultimately, accuracy when defining the level of penetration.

Multiple case studies are developed, including variations in the SGM characteristics, PV penetration level and configuration. The grid operation is evaluated through the different characteristics of the grid at the point of connection. Two different grid characteristics are examined in this chapter. The first grid model (SGM1) approximates a grid with slow response generators, such as the Western North American power grid with many hydro generators.

The governor droop for all of the generators in this power system is set to 20% [2.12]. The second one (SGM2) resembles a fast response grid with small-sized turbo or diesel generators, such as Lanai in Hawaii [2.19]. It consists of two isochronous 2.8 MVA diesel generators and two frequency-droop 1.2 MVA diesel generators with 4% droop [2.19]. The specifications of these two grids in SGM are shown in Table 2.1.

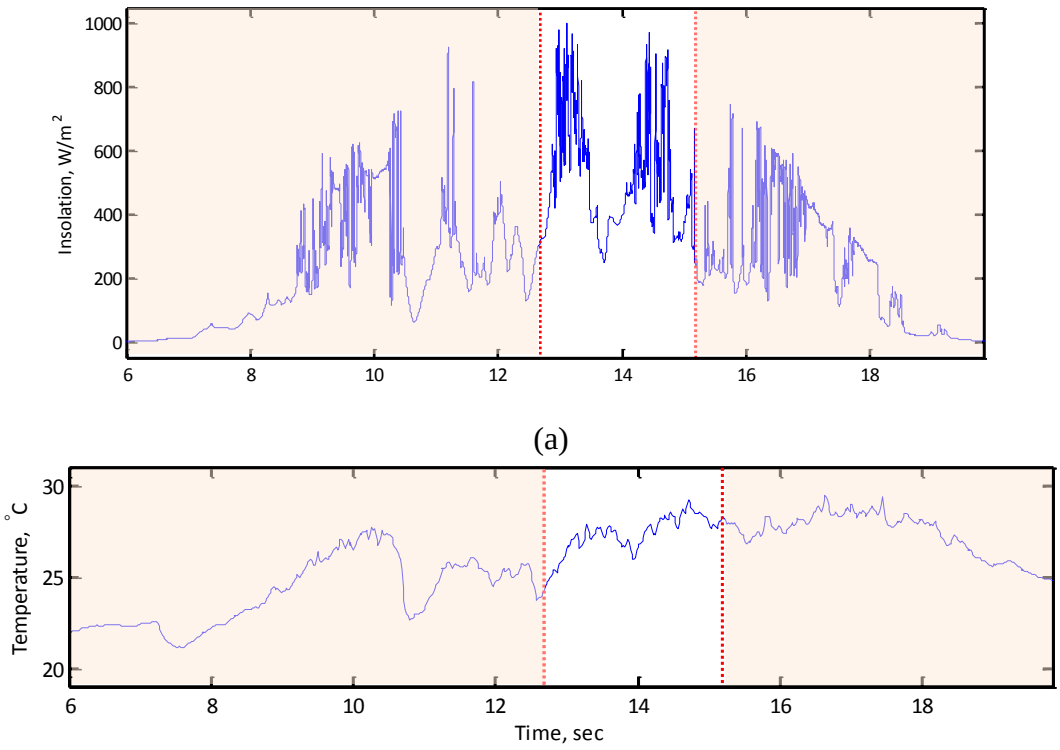


Figure 2.4. Actual data for (a) solar insolation and (b) air temperature used in the simulations.

For ease of comparison, the total capacity of the system for both SGMs is chosen to be 30 MVA. The base-load of the system is considered to be 10 MW/10MVAr, and the feeder load of 0.837 MW/0.626 MVAr is added to the base-load.

15% PV Penetration

In this case, the impact of 15% PV generation is evaluated on the performance of the system for the two grid models. Results for the concentrated and distributed PV generation are given. To evaluate the voltage at different nodes within the feeder, measurements are taken at nodes at the end of the feeders, nodes B9, B15, and B17 in Figure 2.1 (a), (b).

Table 2.1. The SGMs parameters.

	SGM1 (slow)	SGM2 (fast)
Synchronous Generator Parameters		
x_d (pu)	0.9	1.9
x'_d (pu)	0.27	0.27
T'_{d0} (sec)	9.0	6.0
x_q (pu)	0.6	1.6
x'_q (pu)	0.27	0.27
T'_{q0} (sec)	0.05	0.8
H (sec)	4.4	4.0
Governor Parameters		
Droop (pu)	0.2	0.04
P_{max} (pu)	1.0	1.0
T_s (sec)	0.4	0.04
T_c (sec)	75.0	0.2
T_3 (sec)	10.0	0.0
T_4 (sec)	2.4	1.5
T_5 (sec)	1.2	5.0
Exciter Parameters		
K_A	150	200
T_A (sec)	0.09	0.04
V_{max}, V_{min} (pu)	6.0/-3.0	6.0/-3.0

CASE I: 15% Concentrated PV Generation. This case shows the effect of concentrated PV generation on the feeder with aggregated loads. As seen in Figure 2.5 (a), the frequency is mostly outside the acceptable range (60±0.05 Hz), especially during the high PV generation hours. As it can be seen in Figure 2.5 (a), the frequency fluctuations are less in the case of SGM2 compared with those in the case of SGM1. This indicates that the performance of grid at the point of connection is an important factor for increasing the penetration level of PV generation. In other words, a slow-response power system has a major barrier for increased PV penetration level. For ease of comparison, Table 2.2 shows the frequency statistics for both the grid models.

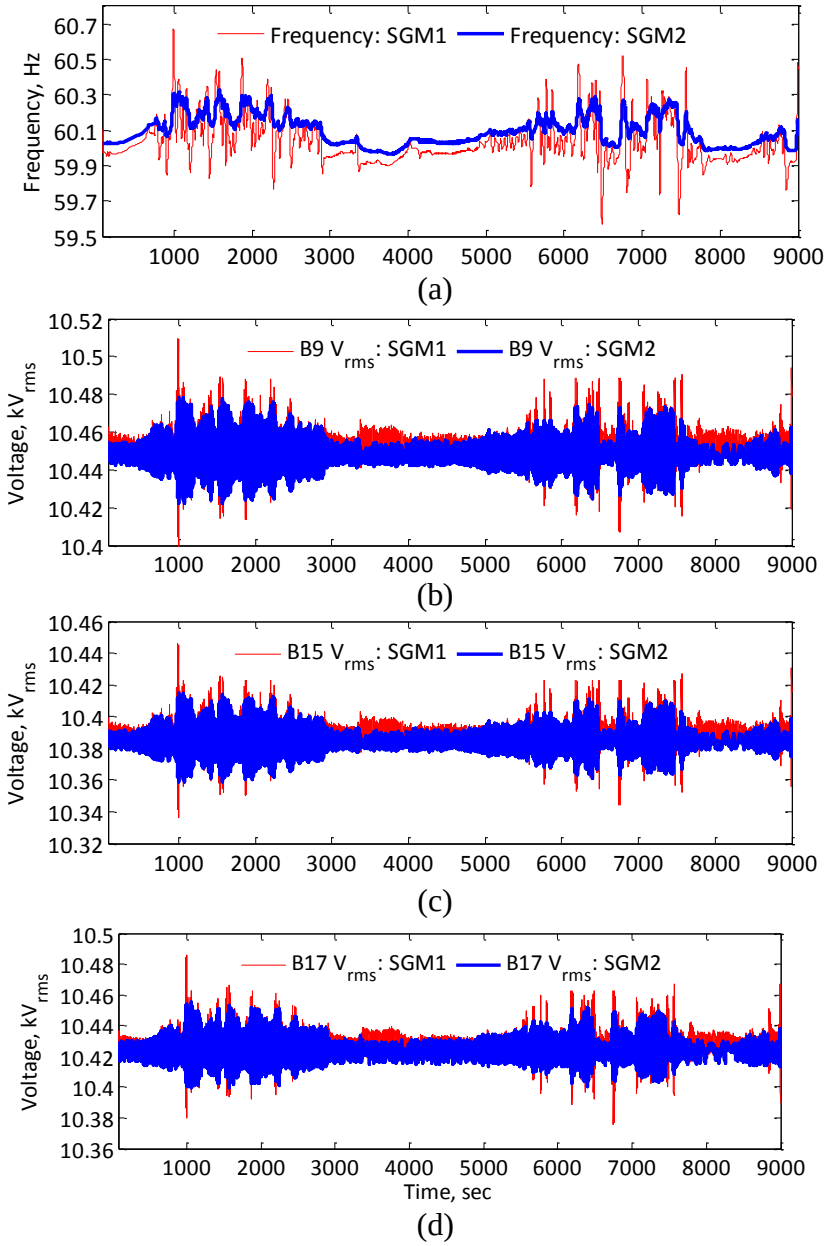


Figure 2.5. Simulation results for (a) system frequency and voltages of nodes (b) B9, (c) B15, and (d) B17 for both models of the grid.

The root mean square error (RMSE) in the Table 2.2 is calculated as follows:

$$RMSE = \sqrt{\sum_{i=1}^{n} \left(f_{act} - f_{nom} \right)^2 \Big/ n} \tag{2.3}$$

Table 2.2. System frequency statistics for both SGM1 and SGM2 in CASE I.

	Minimum frequency (Hz)	Maximum frequency (Hz)	Average frequency (Hz)	Standard deviation (Hz)	RMSE (Hz)
SGM1	59.57	60.67	60.03	0.128	0.133
SGM2	59.97	60.33	60.09	0.084	0.126

where n is the number of samples from simulations. It can be seen that the largest variations in the maximum and minimum frequency, standard deviation, and *RMSE* happen in the case of SGM1.

The voltage profiles at the feeder branches B9, B15, and B17 are shown in Figure 2.5 (b)-(d), respectively. In this case, the deviations in voltage are minimal and have no negative impact on the system performance. However, voltage variations are slightly more in the case of SGM1 compared to SGM2. The mechanical output power for both the grid models and the total PV generation are shown in Figure 2.6 (a). It can be seen that the variations in PV generation and mechanical output power from the SGMs are reversed. Although it seems that the output mechanical power for both SGMs is the same in Figure 2.6 (a), they show different transient behaviors with very similar performance, as shown in Figure 2.6 (b) (which shows the simulation results for 200 seconds). The similar performance is because the total generation and demand are almost the same in both cases. Since frequency is different in the two SGMs, the amount of frequency dependent load would be different, which finally causes slight difference in the output mechanical power of the two SGMs.

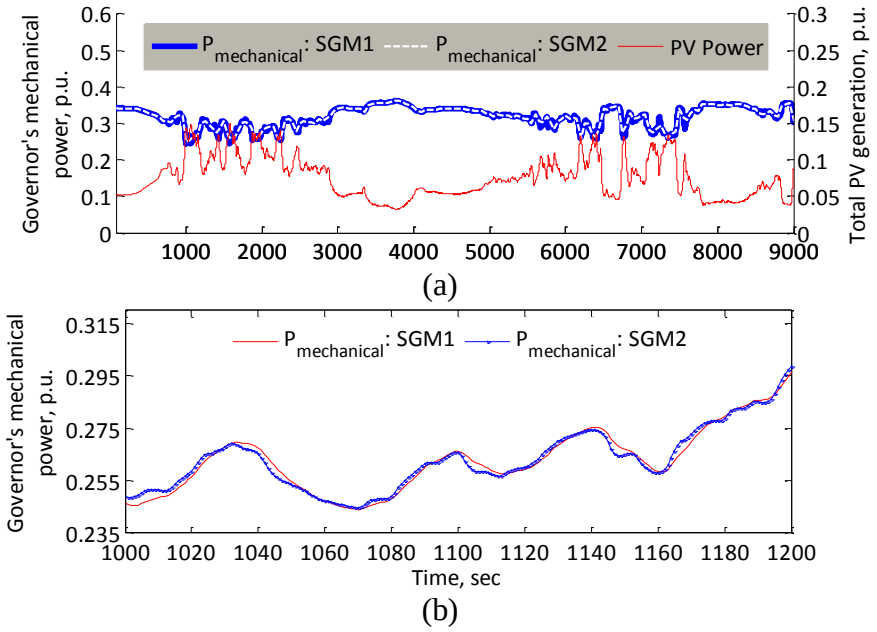


Figure 2.6. (a) SGMs output mechanical power for 15% concentrated PV generation and total PV generation, and (b) zoomed-in output mechanical power of the SGMs.

CASE II: 15% Distributed PV Generation. This case shows the effect of distributed PV generation on the feeder with aggregated loads. As seen in Figure 2.7 (a), the frequency is still out of the acceptable range; although the variations are much less compared to those of the concentrated PV generation. It basically shows that a higher level of penetration of PV generation is achievable if the generation is distributed in a large area with different weather regime. These variations are less in the case of SGM2 compared to those in SGM1 as a result of quick response of the speed governor in SGM2. Table 2.3 shows the frequency statistics for both the grid models. It can be seen that larger variations in frequency as well as standard deviation and *RMSE* happen in the case of the feeder with SGM1.

Table 2.3. System frequency statistics for both SGM1 and SGM2 in CASE II.

	Minimum frequency (Hz)	Maximum frequency (Hz)	Average frequency (Hz)	Standard deviation (Hz)	RMSE (Hz)
SGM1	59.93	60.14	60.05	0.043	0.064
SGM2	59.87	60.02	59.96	0.038	0.057

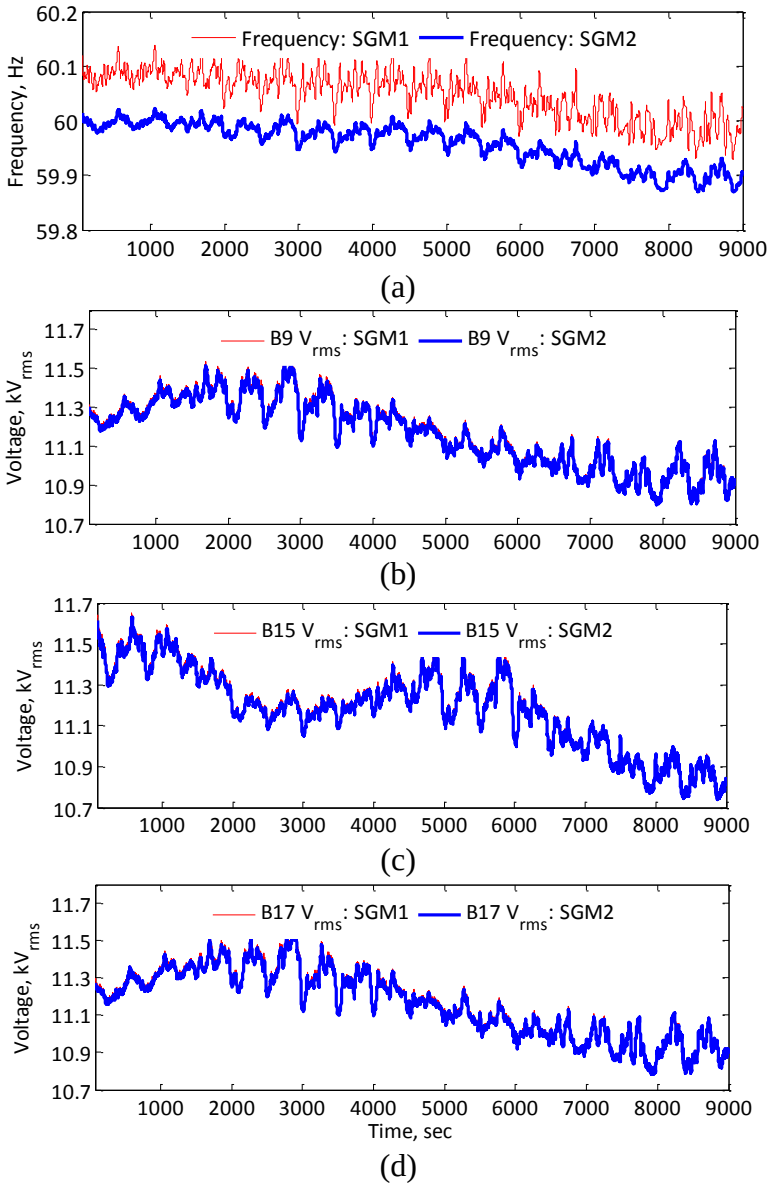


Figure 2.7. Simulation results for (a) system frequency and voltages of nodes (b) B9, (c) B15, and (d) B17 for both models of the grid.

The voltage profiles at nodes B9, B15, and B17 are shown in Figure 2.7 (b)-(d), respectively. Although the system frequency for distributed PV is reduced significantly compared to the concentrated PV generation case, the voltage deviations at the different nodes are considerably higher since the PV generation is distributed and is close to the load centers (consumers). As a result, the system power loss and distribution line loading are lower, and the node voltages (and also the voltage variations) are increased. This problem can be solved by installing smaller PV generation units at more distributed configuration. It can also be observed that there are no significant differences in the node voltages under the two SGMs.

The output mechanical power for both the grid models and the total PV generation are shown in Figure 2.8 (a). Again, it can be observed that the variations in the output mechanical power of SGMs are in such a way to compensate for the deficiency and excess of the PV generation. Figure 2.8 (b) shows the zoomed-in output mechanical power of both SGMs, which are almost the same. However, SGM1 has slower response due to its slower governor action.

30% PV Penetration

In this case, the impact of 30% PV penetration on the performance of the system for the two grid models is evaluated. The system frequency and node voltage variations for the concentrated and distributed PV generation are reported in the following two sub-sections.

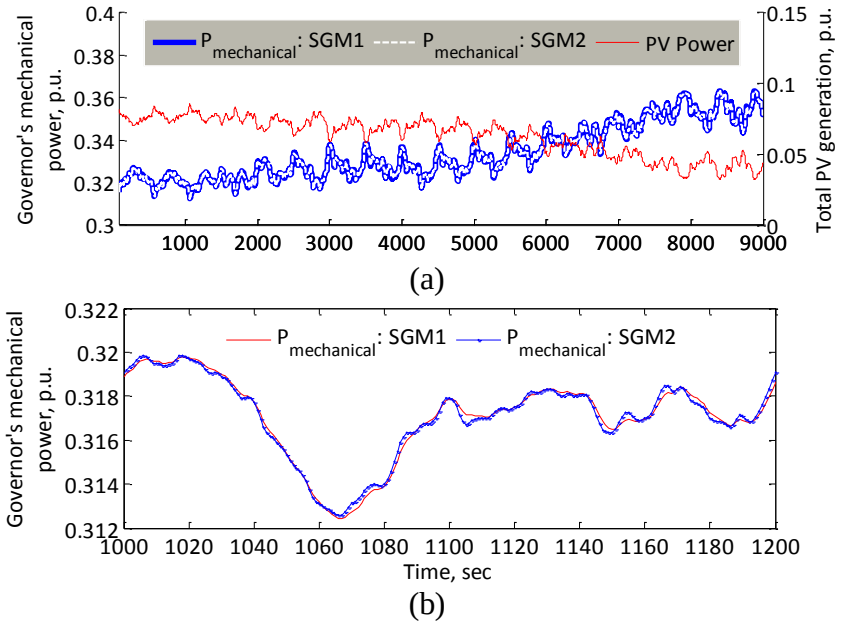


Figure 2.8. (a) SGMs output mechanical power for 15% distributed PV generation and total PV generation, and (b) zoomed-in output mechanical power of the SGMs.

CASE III: 30% Concentrated PV Generation. This case shows the impact of 30% penetration of concentrated PV generation (as in Figure 2.1 (a)) on the feeder with aggregated loads. As seen in Figure 2.9 (a), the frequency varies significantly and is mostly outside the acceptable limits, 60±0.05 Hz. Particularly, the 30% penetration of PV generation has corruptive effects for the slower response grid, SGM1. These variations are more than five times greater than they were in the previous study, with 15% PV penetration. Table 2.4 shows the frequency statistics for both SGMs. It can be seen that the system with SGM1 has a higher maximum frequency, lower minimum frequency, and higher standard deviation and RMSE.

The voltage profiles at nodes B9, B15, and B17 are shown in Figure 2.9 (b)-(d), respectively. These figures show unacceptable variations in the node voltages, which are the result of large frequency deviation, in particular when SGM1 is used.

Table 2.4. System frequency statistics for both SGM1 and SGM2 in CASE III.

	Minimum frequency (Hz)	Maximum frequency (Hz)	Average frequency (Hz)	Standard deviation (Hz)	RMSE (Hz)
SGM1	59.14	67.32	60.32	0.636	0.711
SGM2	60.06	60.79	60.32	0.167	0.361

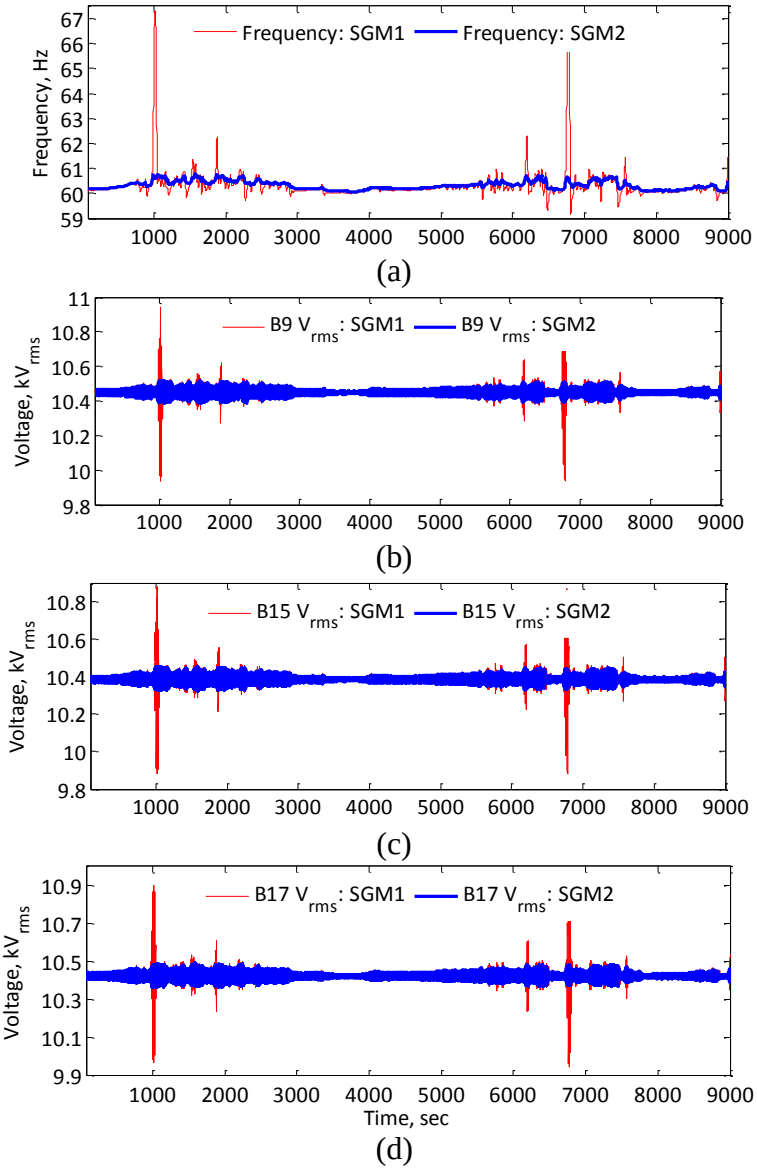


Figure 2.9. Simulation results for (a) system frequency and voltages of nodes (b) B9, (c) B15, and (d) B17 for both models of the grid.

The output mechanical power for both SGMs and the total PV generation are shown in Figure 2.10 (a). Similar pattern as in the case of 15% PV penetration exists for the output mechanical power in relation to the total PV generation can be observed, i.e. when PV generation is high, the output mechanical power of the SGMs are low and vice versa. Figure 2.10 (b) shows a part of the output mechanical power for better observation of the variations. The effect of large variations in the frequency on the frequency dependent loads is clear in the case of SGM1, as shown in the first 50 seconds in Figure 2.10 (b). It can be seen that the output mechanical power for the two SGMs are very close; however, they are different at the points when the frequency and voltage deviations in two SGMs are very different. As a consequence, these variations in mechanical power will result in load variations for both the frequency dependent and constant impedance loads.

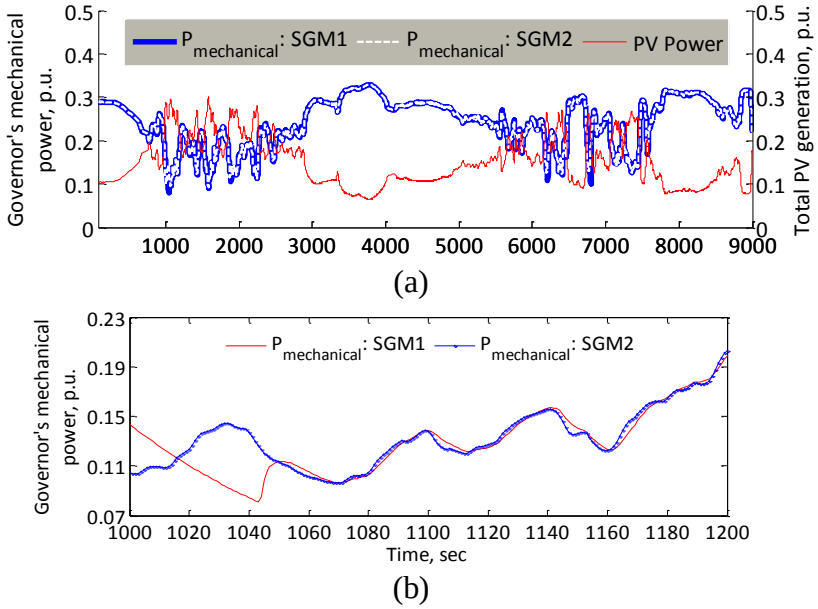


Figure 2.10. (a) SGMs output mechanical power for 30% concentrated PV generation and total PV generation, and (b) zoomed-in output mechanical power of the SGMs.

CASE IV: 30% Distributed PV Generation. This case shows the effect of 30% distributed PV generation on the feeder with aggregated loads. As seen in Figure 2.11 (a), the frequency variations are still out of the acceptable range; however, these variations are less than those with 30% concentrated PV for both SGMs, Figure 2.9 (a). The variations are smaller in the case of SGM2 due to its quicker response. Therefore, it can be concluded that proper distribution of PV generation in a wide geographical area could have a better effect on the existing system than concentrated PV generation (i.e., a PV solar farm). Table 2.5 shows the frequency statistics for both SGMs for the 30% distributed PV generation. It can be seen that larger maximum frequency, and larger standard deviation and RSME occur with the slow SGM (SGM1). The voltage profiles at nodes B9, B15, and B17 are shown in Figure 2.11 (b)-(d), respectively. Voltage deviations are beyond the acceptable range, which is primarily a result of large PV generation installed very close to the consumer loads. There is no significant difference between voltages at the two SGMs. The output mechanical power for both grid models and total distributed PV generation are shown in Figure 2.12 (a). Also, the zoomed-in mechanical power is depicted in Figure 2.12 (b) to show the difference in the transient response of the two SGMs.

Table 2.5. System frequency statistics for both SGM1 and SGM2 in CASE IV.

	Minimum frequency (Hz)	Maximum frequency (Hz)	Average frequency (Hz)	Standard deviation (Hz)	RMSE (Hz)
SGM1	59.84	60.26	60.08	0.086	0.116
SGM2	59.75	60.06	59.93	0.076	0.105

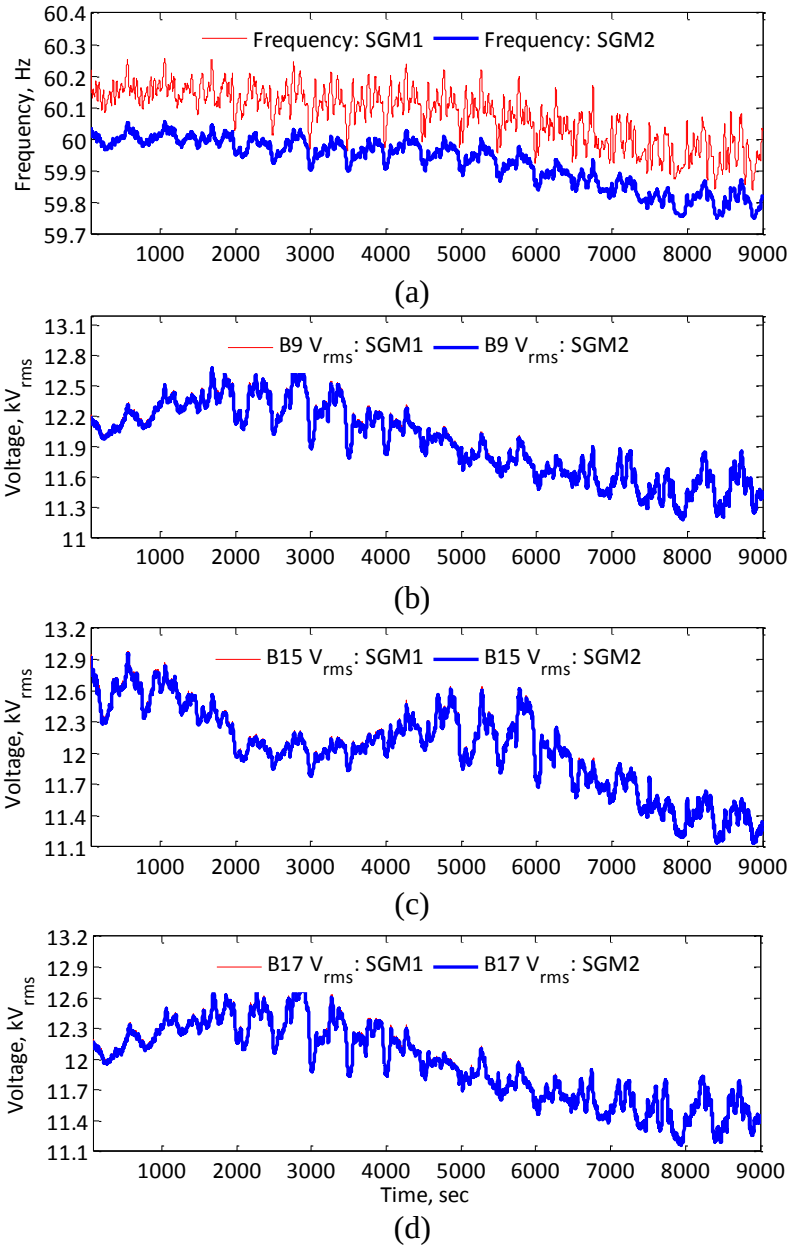


Figure 2.11. Simulation results for (a) system frequency and voltages of nodes (b) B9, (c) B15, and (d) B17 for both models of the grid.

The response is always faster in the case of SGM2 compared to the one in SGM1 as a result of faster governor action.

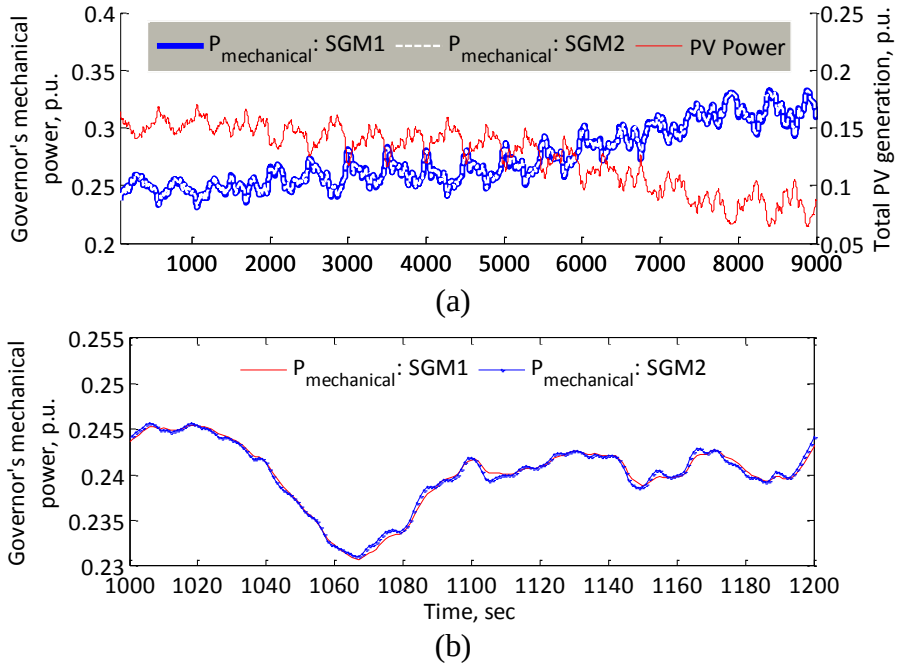


Figure 2.12. (a) SGMs output mechanical power for 30% distributed PV generation and total PV generation, and (b) zoomed-in output mechanical power of the SGMs.

Conclusions

This chapter presents the effect of high penetrations of solar PV generation on frequency and voltage in a distribution feeder configured as a grid-tied MG. Different PV penetration levels, grid characteristics at the point of connection, and PV configuration in the MG are considered in the chapter. A simplified grid model is presented to resemble the grid at the distribution level. Only governor droop control is considered in the SGM. Simulation results indicate that a higher level of PV penetration is achievable through small-sized distributed PV generation or a grid with faster response. A distributed PV in a large area with different weather regimes could also be beneficial to achieve higher levels of PV penetration.

It is also shown in this chapter that the corrective action of the governor droop

control of the SGMs is very limited in stabilizing the frequency and voltage in the distribution feeder. As a result, the SGM will be improved to include conventional AS as well as customer participation through an effective DR program for the stabilization of frequency and voltage under high penetration of solar PV generation in later chapter.

Acknowledgement

This work was in part supported by Pacific Northwest National Laboratory (PNNL), which is operated for the U.S. Department of Energy by Battelle under Contract DE-AC05-76RL01830, and by the DOE Award DE-FG02-11ER46817.

Reference Cited

[2.1] Solar Energy Industries Association, "U.S. Solar Market Insight (TM): 2010 Year in Review (Executive Summary)," 2010, Solar Energy Industries Association.

[2.2] T.S. Basso, "High-penetration, grid-connected Photovoltaic technology codes and standards," in *Proc.* 33rd IEEE Photovoltaic Specialists Conference, San Diego, USA, May 2008, pp. 1–6.

[2.3] IEEE STD 1547, *Standard for Interconnecting Distributed Resources with Electric Power Systems*, June 2003.

[2.4] P. Piagi and R. H. Lasseter, "Autonomous control of microgrids," in *Proc.* IEEE PES General Meeting, Montreal, CA, Jun. 2006, pp. 18–22.

[2.5] N. Hatziargyriou, "MICROGRIDS: Large scale integration of micro-generation to low voltage grids," EU Project No. ENK5-CT-2002-00610, Available online: http://www.microgrids.eu/micro2000/presentations/19.pdf

[2.6] P. Denholm and M. Hand, "Grid flexibility and storage required to achieve very high penetration of variable renewable electricity," *Energ. Policy*, vol. 39, no. 3, pp. 1817–1830, March 2011.

[2.7] MATLAB® SimPowerSystems Toolbox: Users' Guide, Available online: http://www.mathworks.com/help/releases/R13sp2/pdf_doc/physmod/powersys/powersys.pdf

[2.8] C. Wang, "Modeling and control of hybrid wind/Photovoltaic/fuel cell distributed generation systems," Ph.D. Dissertation, Montana State University, Bozeman, 2006.

[2.9] National Renewable Energy Laboratory (NREL), "NREL: MIDC/Oahu irradiance grid," Available online: http://www.nrel.gov/midc/oahu_archive/

[2.10] California Energy Commission's Intermittency Analysis Project Study, "Appendix B - Impact of intermittent generation on operation of California power grid," Available online: http://www.uwig.org/CEC-500-2007-081-apb.pdf

[2.11] P. Kundur, *Power System Stability and Control*, McGraw-Hill Inc., 1994, ch. 11.

[2.12] D. Trudnowski, M. Donnelly, and E. Lightner, "Power-system frequency and stability control using decentralized intelligent loads," in *Proc.* IEEE PES Conference and Exhibition Transmission and Distribution, Dallas, USA, May 2005, pp. 1453–1459.

[2.13] J.A. Short, D.G. Infield, and L.L. Freris, "Stabilization of grid frequency through

dynamic demand control," *IEEE Trans. on Power Syst*., vol. 22, no. 3, pp. 1284–1293, Aug. 2007.

[2.14] D. Das, "A fuzzy multiobjective approach for network reconfiguration of distribution systems," *IEEE Trans. Power Del*., vol. 21, no. 1, pp. 202–209, Jan. 2006.

[2.15] Y.G. Rebours, et al., "A survey of frequency and voltage control ancillary services—Part I: Technical features" , *IEEE Trans. Power Syst.*, vol. 22, no. 1, pp. 350–357, Feb. 2007.

[2.16] S.A. Pourmousavi and M.H. Nehrir, "Demand response for smart microgrid: Initial results," in *Proc*. 2nd IEEE PES Innovative Smart Grid Technologies Conference, Anaheim, USA, Jan. 2011, pp. 1–6.

[2.17] S.A. Pourmousavi, M.H. Nehrir, and C. Sastry, "Providing ancillary services through demand response with minimum load manipulation," in *Proc.* North American Power Symposium, Boston, USA, Aug. 2011, pp. 1–6.

[2.18] J.D. Glover, M.S. Sarma, and T.J. Overbye, *Power System Analysis and Design*, Stamford, CT, Cengage Learning, 2008, ch. 11.

[2.19] B.L. Schenkman, D.G. Wilson, and R.D. Robinett III, "Photovoltaic distributed generation for Lanai power grid real-time simulation and control integration scenario," in *Proc*. International Symposium on Power Electronics, Electrical Drives, Automation and Motion, Pisa, Italy, 2010, pp. 154–157.

CHAPTER 3

REAL-TIME CENTRAL DEMAND RESPONSE FOR PRIMARY FREQUENCY REGULATION IN MICROGRIDS

Contribution of Authors and Co-Authors

Manuscripts in Chapters 2 through 12

Author: S. A. Pourmousavi

Contributions: Designed and implemented a small-scale islanded MG at the distribution level by modifying original IEEE 13-bus standard distribution feeder in MATLAB®/Simulink, developed a generic controller based on adaptive hill climbing for frequency regulation for real-time DR with minimum manipulation, prepared all the simulation setup and results, manuscript and all figures.

Co-author: M. H. Nehrir

Contributions: Provided important insight and overview of the research, interpretation of the results, and aided in the preparation of the manuscript.

Manuscript Information Page

Seyyed Ali Pourmousavi Kani, M. Hashem Nehrir

IEEE Transactions on Smart Grid, 2012

Status of the manuscript:
____ Prepared for submission to a peer-reviewed journal
____ Officially submitted to a peer-reviewed journal
____ Accepted by a peer-reviewed journal
_X_ Published in a peer-reviewed journal

Published by the Institute of Electrical and Electronics Engineering (IEEE)

Real-Time Central Demand Response for Primary Frequency Regulation in Microgrids

S. Ali Pourmousavi, *Student Member, IEEE*, and M. Hashem Nehrir, *Fellow, IEEE*

***Abstract*—Providing ancillary services for future smart microgrid can be a challenging task because of lack of conventional automatic generation control (AGC) and spinning reserves, and expensive storage devices. In addition, strong motivation to increase the penetration of renewable energy in power systems, particularly at the distribution level, introduces new challenges for frequency and voltage regulation. Thus, increased attention has been focused on demand response (DR), especially in the smart grid environment, where two-way communication and customer participation are part of. This paper presents a comprehensive central DR algorithm for frequency regulation, while minimizing the amount of manipulated load, in a smart microgrid. Simulation studies have been carried out on an IEEE 13-bus standard distribution system operating as a microgrid with and without variable wind generation. Simulation results show that the proposed comprehensive DR control strategy provides frequency (and consequently voltage) regulation as well as minimizing the amount of manipulated responsive loads in the absence/presence of wind power generation.**

***Index Terms*—Adaptive hill climbing, ancillary service, demand response, microgrid, smart grid, step-by-step control.**

I. Introduction

DEMAND response (DR) offers a variety of financial and operational benefits for electricity customers, load-serving entities (whether integrated utilities or competitive retail providers), and grid operators [1]. In particular, DR can be an effective tool in providing balance between supply and demand in real-time. Traditionally, such services, known as ancillary services, are provided by utility-owned operating (spinning and nonspinning) reserves which are basically flexible capacity generators, available when needed, to maintain secure operation of power systems. From an economic perspective, these services and reserve power are costly and any method which manages to reduce the magnitude of these services, without sacrificing system stability, is of significant importance [1], [2].

Intermittent renewable power generation, such as wind and photovoltaic (PV), are projected to take a considerable share of future power generation, as distributed generation sources, installed at the distribution level. In order to compensate for the highly variable generation, more spinning and nonspinning reserve are necessary in the future which introduces new costs and more pollution, associated with the conventional power plants. These problems will increase in intensity and occurrence in the case of islanded microgrids, where no conventional ancillary services are technically available. Thus, more expensive storage devices will be necessary to provide reliable electricity to customers with acceptable quality. These challenges and uncertainties make DR a viable option-DR resources provide a reliable, low cost, environmentally-friendly alternative to conventional spinning reserves. DR can also provide ancillary services which grid operators-independent system operators (ISOs), regional transmission organizations (RTOs) or utilities-and other entities can use [2]. These entities can control customer controllable loads to shift or reduce their load profile or respond to excess or insufficient renewable generation.

Demand resources are specifically defined as a subset of nonspinning reserves and must be available within 10 min or shorter from the time they are called upon [2]. When the demand resources are controlled immediately upon the occurrence of disturbances, the strategy is often called direct load control (DLC). This capability can be technically and economically achieved through responsive electric devices such as electric water heaters (EWHs) equipped with hot water storage tank [3]–[5]. On the average, residential EWHs electricity consumption accounts for about 11% of the total electricity consumption and increases to over 30% during peak demand hours [4], [6]. Therefore, there is a considerable potential for EWHs to be effective in DR applications for providing ancillary services.

Although it may seem likely that the individual demand resources may have a high failure rate to curtail load on short notice, the aggregation of many small resources into one large resource makes it more probable that the assigned response will be achieved. This characteristic of demand resources potentially makes DR resources more reliable than conventional generation, where the failure of one generator to start can cause the loss of considerable spinning reserve capacity [1], [2].

Considerable attention has recently been given to DR for different purposes. The economic benefits of DR in the power market and the development of strategies to achieve such benefits are reported in [7]–[11]. DR has also been used for off-line planning and day-ahead scheduling, e.g., [12]–[18]. The availability of load as DR resource for reserve capacity (ancillary services market) has been investigated in [19]–[21]. However, these references do not examine the effect of DR on system frequency nor do they model the transmission or distribution grid.

Manuscript received July 17, 2011; revised December 02, 2011; accepted May 08, 2012. Date of publication June 22, 2012; date of current version December 28, 2012. This work was supported in part by Pacific Northwest National Laboratory (PNNL), which is operated for the U.S. Department of Energy by Battelle under Contract DE-AC05-76RL01830, and by the DOE Award DE-FG02-11ER46817. Paper no. TSG-00252-2011.

The authors are with the Electrical and Computer Engineering Department, Montana State University, Bozeman, MT 59717 USA (e-mail: s.pourmousavikani@msu.montana.edu; hnehrir@ece.montana.edu).

Color versions of one or more of the figures in this paper are available online at http://ieeexplore.ieee.org.

Digital Object Identifier 10.1109/TSG.2012.2201964

1949-3053/$31.00 © 2012 IEEE

A limited number of studies also address the effectiveness of decentralized dynamic demand control on stabilization of grid frequency, mainly at the transmission level [19], [22]–[25]. This paper presents a central DR strategy for primary frequency regulation in a microgrid at the distribution level, which is considered as a cornerstone of the future smart grid. The details of the proposed DR strategy are given below.

A comprehensive DR strategy has been designed by the authors to continuously balance generation and demand, using an adaptive hill climbing (AHC) strategy [26], which results in frequency regulation. The AHC control is then replaced with a step-by-step (SBS) controller to reduce the amount of manipulated load to a minimum at steady-state [26]. In these references, the designed strategies were tested on a very small (one-bus) system to show the proof of concept. The novelties and contributions of this paper (not reported in [26] and [27]) are as follows:

- The DR strategy is applied to a realistic (a standard IEEE 13-bus) distribution system operating as an independent microgrid, which shows the effect of DR on the system frequency, [10]. Because of high R/X ratio at the distribution level, the frequency regulation also results in voltage regulation.
- A decision tree is presented to accurately determine the operation MODE of the controller.
- The effectiveness of the DR strategy is evaluated under the presence of variable wind-generated power to show its ability for generation following to regulate the system frequency.
- The impact of communication delay (latency) in the performance of the DR strategy is evaluated.

Simulation results show the effectiveness of the DR approach in providing frequency (and consequently voltage) regulation in the presence and absence of wind power generation. The dynamic models of the islanded microgrid are developed in MATLAB/Simulink®.

The rest of the paper is organized as follows: Section II describes the proposed comprehensive DR strategy comprising of AHC and SBS controllers. System of study and simulation setup is explained in Section III. Simulation results for different scenarios with and without wind power generation are shown and discussed in Section IV. Section V presents a discussion about the latency and its impact on the results. Finally, conclusions of the study are given in Section VI.

II. The Proposed DR Strategy

In general a DR management involves four main participants: 1) the balancing authority, which includes the DR initiator and the entity having interest in this service, namely the utility. The central controller proposed in this paper is assumed to be owned by this balancing authority; 2) a DR aggregator (which integrates the individual DR resources); 3) the distribution utility (that operates the distribution feeders); and finally 4) the customers (energy consumers who participate in the DR program) [10]. Any DR scheduling process starts from the balancing authority, which determines and requests (announces) the volume of DR required at any given time [10]. This type of DR lies within the incentive-based program (IBP) of DR [28]. Although this structure can be used for all three frequency regulation services including the primary, secondary, and tertiary regulations, this paper only deals with the primary frequency control. In this process, active power of the generating units and the consumption of controllable loads are adjusted to quickly balance the load and generation and restore the frequency [29]. In this way, every balancing authority center needs a calculation center with a DR strategy to determine the amount of required DR to regulate the frequency based on the system frequency deviation. The focus of this paper is to solve this issue by introducing a comprehensive DR strategy, which is based on feedback of the frequency deviation, to regulate the system frequency in real time. This process is shown in Fig. 1

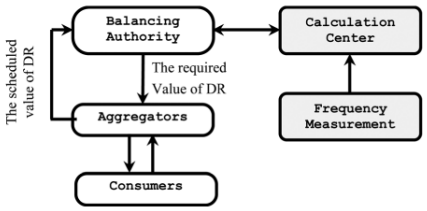


Fig. 1. The scheduling process of the central DR strategy.

The proposed DR strategy, referred to as central direct load control (CDLC), consists of three operation modes depending on the magnitude of the system frequency deviation ($\Delta \mathtt{f}$), as shown in Fig. 2. The figure shows a hypothetical curve of $\Delta \mathtt{f}$ vs. time, where three operation modes (0, 1, and 2) are shown as follows:

- MODE 0: Normal operation—no control needed.
- MODE 1: In this mode, $\Delta \mathtt{f}$ goes out of the desired range, and load control is applied to bring $\Delta \mathtt{f}$ within the range with maximum effort, as quickly as possible. The AHC control [26] is applied in this operation mode.
- MODE 2: In this mode, the frequency has returned to the normal range, and the SBS load manipulation strategy is used to minimize the amount of manipulated load [27]. We will call the combination of the above three steps "comprehensive control."

The conditions for the three operation modes discussed above are given in the decision tree shown in Fig. 3. In this figure, $\Delta \mathtt{f\_der}$ is the 1st-order derivative of frequency deviation with respect to time, `abs` is the absolute operator, and `AND/OR` are the logical and/or operators, respectively. The decision tree gives the required conditions which must be satisfied for the three operation modes. Checking the derivative of the system frequency deviation at every sample in MODEs 1 and 2 (to precisely determine the transition from one MODE to the other) is required to assure stable operation of the system. MODE 1 will begin once the system frequency deviation exceeds 0.05 Hz, if the system has previously been in MODE 0. MODE 1 will continue as long as $\Delta \mathtt{f\_der} \neq 0$. MODE 2 will take over the control of the system if the following three conditions hold true: 1) $\mathtt{abs}(\Delta \mathtt{f}) < 0.005$ Hz; 2) $\Delta \mathtt{f\_der} = 0$; and 3) the system has been in MODE 1 in the previous iteration. This mode of operation will remain active as long as $\Delta \mathtt{f\_der} \neq 0$ and

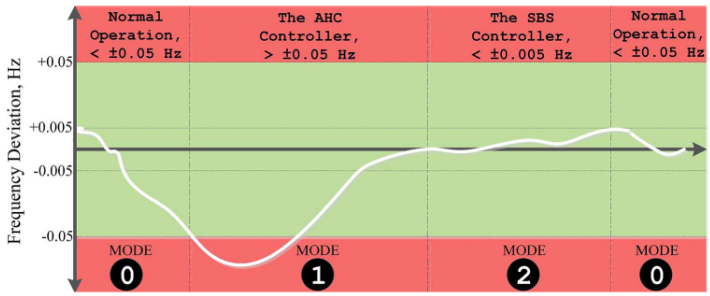


Fig. 2. Concept of the proposed control strategy.

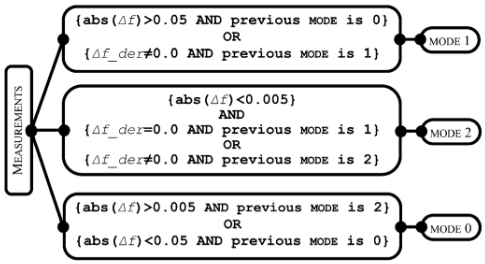


Fig. 3. Decision tree for determining the MODE of operation.

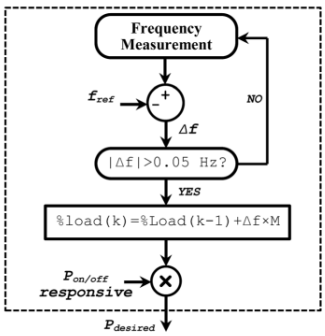


Fig. 4. The flowchart of the AHC control [26].

$\mathbf{abs}(\Delta \mathbf{f}) < 0.005$ Hz, if the system was in MODE 2 in the previous iteration. MODE 0 takes over if $\mathbf{abs}(\Delta \mathbf{f}) > 0.005$ and the system has been operating in MODE 2. This MODE will continue as long as $\mathbf{abs}(\Delta \mathbf{f}) < 0.05$ and the system was in MODE 0 in the previous iteration.

The 0.05 and 0.005 frequency deviations used in Fig. 3 are based on 60-Hz operation used in North America [29]. The AHC and SBS load control strategies used in operation modes 1 and 2, respectively, are explained in Sections II-A and II-B.

In North America, whenever a frequency error persists for a certain time (10 s for the east, 3 s for Texas, and 2 s for the west), a correction of ±0.02 Hz (0.033% of 60 Hz) is applied [30]. In this study, if frequency deviations reach 0.5 Hz, automatic load shedding or other control actions are used to restore system frequency. In addition, the time and magnitude effect is integrated in a desired dead-band of ±0.05 Hz (0.083% of 60 Hz) for this study. That is, when frequency deviation exceeds ±0.05 Hz under a disturbance (Fig. 2), the AHC controller will start operating to regulate the frequency by changing the amount of responsive loads. Once the AHC controller has brought the frequency within the ±0.005 Hz limit, the SBS controller becomes active to minimize the amount of manipulated load.

A. Adaptive Hill Climbing Control

The flowchart of the AHC controller (operating MODE 1) is shown in Fig. 4. The frequency, measured at the point of common coupling (PCC) of the microgrid, is the input variable to the controller. At each time step k, if the frequency deviation falls outside the dead-band (i.e., if $\mathbf{abs}(\Delta \mathbf{f}) > 0.05$ Hz), the percentage of the responsive load (that will turn on or off) is computed as follows:

$$\%Load(k) = \%Load(k-1) + \Delta f \times M \tag{1}$$

where $\%Load(k-1)$ is the percentage of manipulated load at time step $k-1$, and $\Delta \mathbf{f} \times \mathrm{M}$ is a perturbation parameter. M is a constant used to scale down the frequency deviation. In this study, after several simulation runs under different loading conditions, M was set to 0.1, which gave the most satisfactory result.

When the frequency is higher than acceptable ($\Delta \mathbf{f} > 0.05$), a percentage of the responsive loads (that are OFF) will turn ON, and when it is lower than acceptable ($\Delta \mathbf{f} < -0.05$), a percentage of the responsive loads (that are ON) will turn OFF. This procedure is adaptive since the amount of manipulated load is a function of the frequency deviation, which tends to reduce the deviation with maximum effort. More detail on the AHC algorithm is provided in [26].

The AHC controller acts faster than the speed governor of the diesel generator (DG) because of the rapid nature of control, since the power consumption status of controllable loads (such as EWHs and other resistive loads) can be changed instantaneously by the ON or OFF command signal they receive. This way, more responsive loads will be manipulated at the beginning of the disturbances (in an attempt to bring the frequency

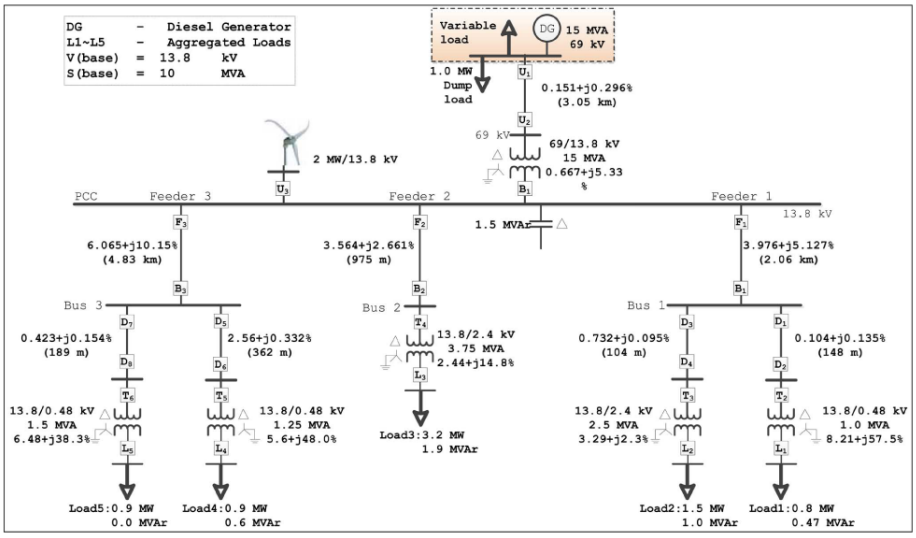


Fig. 5. Modified IEEE 13-bus standard distribution system schematic diagram.

within the desired limit as quickly as possible) than required at steady-state.

As a result, a higher percentage of the responsive loads are manipulated at steady-state, which maybe more than needed. Because of this, a SBS controller was designed, [27], to reduce the amount of manipulated loads to a minimum at steady-state. The operation of this controller is explained in the next subsection.

B. Step-by-Step Control

In order to assure that the minimum required amount of responsive load is activated (kept on or off) at steady-state, the SBS control (MODE 2), introduced in Fig. 2, is used. Once the frequency is stabilized by the AHC controller, the SBS controller will start operating to minimize the amount of manipulated responsive loads. In order to assure safe operation of the system, the SBS will act in a smaller dead-band ($\mathtt{abs}(\Delta \mathtt{f}) < 0.005$ Hz), as shown in Fig. 2. Using the SBS controller, the manipulated responsive load will be decreased by 5% at each 1-s time-step according to (2), until the frequency begins to go out of the desired dead-band.

$$\%Load(k) = 0.95 \times \%Load(k-1). \tag{2}$$

According to (2), the responsive load variation depends on its previous value. Therefore, the load control strategy begins with large variations in load which decrease with time. The SBS control strategy is therefore nonlinear with large load variations at the beginning and small ones at the end. As a result, the proposed control strategy minimizes the amount of responsive loads that need to be manipulated at steady-state to keep the system frequency within the desired range of ± 0.05 Hz. The advantage of the SBS strategy is that a lower percentage of responsive loads is manipulated at steady-state, which improves customers' quality of service (QoS). As a result of this improvement, a higher percentage of customer loads will be available for future control, if needed.

III. Study System

To verify the effectiveness of the comprehensive controller designed, it was applied to an IEEE standard 13-bus distribution network, [31] and [32], shown in Fig. 5. This feeder is assumed to be the distribution system company in the structure introduced in Section II, as shown in Fig. 1. However, to be able to observe the frequency behavior of the system as a microgrid, the utility source of the original model was replaced with a 15-MW DG and a variable load which can be adjusted to set the DG's operating point (e.g., to light or heavy loading). The DG is equipped with a speed governor and excitation system whose parameters are given in the Appendix. A 1-MW dump load is also added to the 69-kV bus. This load is only enabled in light loading conditions (in the no-control case) to prevent the frequency deviation from exceeding 0.5 Hz.

A 2-MW wind turbine (about 30% of the system load), shown in Fig. 5, is added to the system (at the PCC) in order to study the effect of the proposed comprehensive controller on a realistic distribution system with high penetration of wind power. To observe the system frequency deviation, the maximum mechanical torque of the DG has been limited to a certain point for each simulation case studied. The limit for each case is given in the simulation results.

The dynamic model for the diesel engine (with speed governor, excitation controller, and synchronous generator) is extracted from MATLAB/Simulink SimPowerSystems toolbox [33], which is based on IEEE standard 421.5 [34].

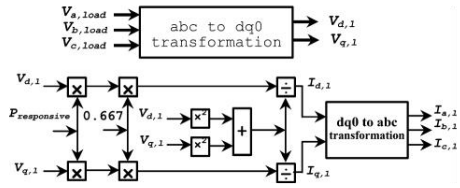


Fig. 6. Schematic of modeling of the active variable load.

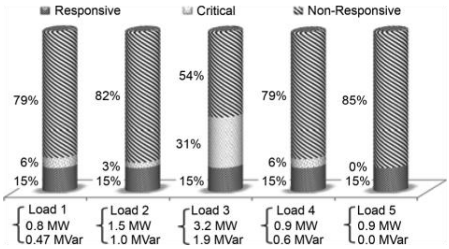


Fig. 7. The technical characteristic of the load in the test system.

It is desired to have a model of the load where active power (P) would explicitly vary during the simulation. Such a variable load has been modeled in the $d-q$ frame in terms of P and Q, given by (3), (4) and shown in the block-diagram of Fig. 6 [35].

$$i_d = \frac{2}{3}\cdot\frac{v_d}{v_d^2+v_q^2}\cdot P + \frac{2}{3}\cdot\frac{v_q}{v_d^2+v_q^2}\cdot Q \tag{3}$$

$$i_q = \frac{2}{3}\cdot\frac{v_q}{v_d^2+v_q^2}\cdot P - \frac{2}{3}\cdot\frac{v_d}{v_d^2+v_q^2}\cdot Q \tag{4}$$

where P and Q are the desired active and reactive power of the responsive load, respectively, and v_d , $v_q(i_d, i_q)$ are the load voltage (current) in the $d-q$ frame. To transform the values from the abc frame to the $d-q$ frame and vice versa, a phase locked-loop (PLL) is applied [35]. The voltage values in the $d-q$ frame are extracted from the actual voltage across the load through the "abc to $dq0$ transformation" block. The $d-$ and $q-$ axis currents are then calculated and transformed into the abc frame through the "$dq0$ to abc transformation" block.

Five aggregated loads ($L_1 - L_5$) are shown in Fig. 5, where each one represents a DR aggregator, as shown in Fig. 1. Each aggregated load is divided into three different types: responsive, critical, and nonresponsive. This categorization of the aggregated loads is shown in Fig. 7. The responsive loads are variable active loads, the amount of which is determined by the DR algorithm. The critical and nonresponsive loads are modeled as constant impedance loads. In this study, a central controller is responsible for frequency regulation. The controller can be considered as a utility owned control facility which has direct access to the individual responsive loads in the utility's distribution network through two-way communication (with a predefined latency), i.e., smart grid era.

IV. Simulation Results

In order to assess the effectiveness of the comprehensive controller (AHC + SBS) vs. the no-control and the AHC controller (alone) cases, several simulation experiments have been performed on the 13-bus distribution network, discussed in Sections IV-A through IV-D below. Each simulation has been carried out for the comprehensive controller, the AHC controller (alone), and the no-control case. No wind power is considered in subsections A and B to examine the impact of variations in load demand on the system frequency and voltage. Subsections C and D are devoted to assessing the impact of DR in the presence of variable wind power; load demand is kept constant in these cases.

A. Scenario I: Light Loading- Decrease in Load (NO WIND)

In this case, Load 5 (0.9 MW) is disconnected at $t = 7$ s, and as a result, the system frequency increases, resulting in $\Delta f > 0.05$ Hz. The lower setpoint of the DG torque is limited to 0.65 p.u. to prevent it from lowering the torque further to correct the frequency deviation under light loading. The light loading in conventional power system can be viewed as a condition where there are only base-load steam power plants available with limited capability for ramping up and down. In this situation, it is more convenient to add a dump load to the system instead of changing the output power of those power plants. This prevents mechanical and thermal stress on the generation units. In this study, a 1-MW dump load has been applied at the 69-kV bus to which the DG is connected (Fig. 5), to be activated once the frequency deviation exceeds 0.5 Hz, i.e., when the frequency cannot be stabilized through DR, or in the no-control case.

In Fig. 8 the frequency variation, voltage, and total power demand for the different DR approaches are compared with the no-control case. Fig. 8(a) and 8(b) show that both the DR approaches (AHC and comprehensive) bring the frequency to the desired range faster than the no-control case. The dump load is utilized to regulate the system frequency at around 7.8 s in the no-control case. This happens when the frequency deviation exceeds 0.5 Hz to stabilize the frequency. When the SBS controller is active, frequency fluctuation is more in the range of ± 0.005 Hz, which is safe for the system's operation. These variations are shown in the zoomed-in frequency variation, Fig. 8(b). This figure also shows the time at which the SBS controller lowers the amount of the manipulated load to a minimum, which occurs approximately at 19 s, when operation MODE 2 ends and the system will go to normal operation (MODE 0). As a result of frequency regulation, the system voltage is also stabilized faster, as shown in Fig. 8(c). Also, less voltage fluctuation is observed during the transient period, when the comprehensive controller and the AHC controller (alone) are applied. It is also noticed from this figure that the voltage remains in the acceptable range at the end of operation of the SBS controller at ($t \approx 19$ s).

Fig. 8(d) illustrates the total demand on the system for the different cases. It can be seen that in the comprehensive approach a smaller percentage of responsive load has been manipulated at steady-state compared to the AHC approach. Under the comprehensive control the total load demand at steady-state is 6.142 MW and 77.38% of the responsive load is manipulated, whereas for the AHC controller the total load at stead-state is 6.238 MW and 91.77% of the responsive load is manipulated. This difference between the manipulated loads in the two cases

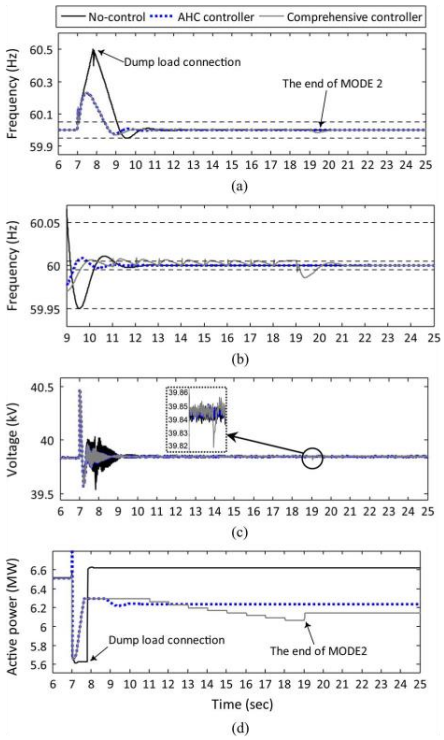


Fig. 8. Frequency, voltage, and total load demand: Light loading with no wind power generation. (a) System frequency. (b) Zoomed-in system frequency. (c) Voltage at the 69 kV bus. (d) Total load demand.

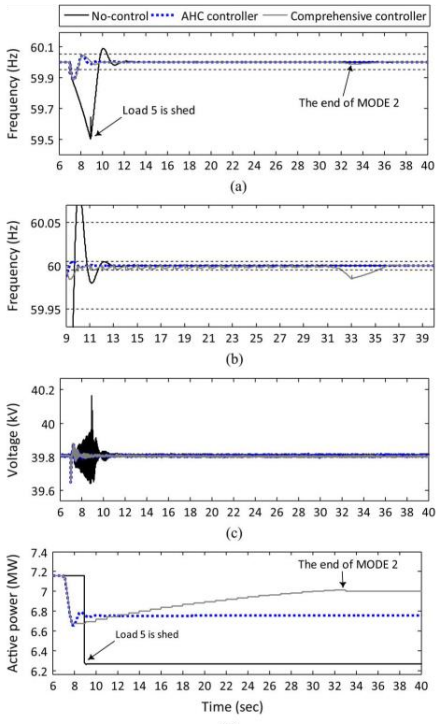


Fig. 9. Frequency, voltage, and total load demand: Heavy loading with no wind power generation. (a) System frequency. (b) Zoomed-in system frequency. (c) Voltage at 69 kV bus. (d) Total load demand.

corresponds to 14.39% savings when the comprehensive controller is used, which of course results in a higher customers' QoS.

Frequency regulation has been achieved in the no-control case with the aid of a 1-MW dump load, which is a waste of energy and not desirable. However, when the DR is applied, in addition to frequency and voltage regulation, it can also be effective in peak load shaving and load shifting.

B. Scenario II: Heavy Loading- Increase in Load (NO WIND)

In this case, a 0.6-MW load is added to the 69-kV bus at $t = 7$ s, resulting in a negative frequency deviation. The upper setpoint of the mechanical torque of the DG is limited to 0.96 p.u to prevent it from totally correcting the frequency deviation so that the effect of DR can be examined.

Fig. 9 shows the system frequency and voltage variations, and power demand under the different DR approaches and the no-control case. In the no-control case, as soon as the frequency deviation begins to exceed 0.5 Hz (Fig. 9(a)), it is brought back to within limits with unscheduled load shedding, which jeopardizes customers' QoS and is undesirable.

The frequency variation, given in Fig. 9(a) and 9(b), shows that both the AHC and comprehensive DR approaches bring the frequency to its desired range faster than the no-control case. As shown in Fig. 9(a), Load 5 on bus 3 (Fig. 5) is shed at around 8.7 s because the frequency deviation falls below -0.5 Hz. For safe operation in the no-control case, Load 4 has been considered as backup emergency to be disconnected from bus 3 whenever the frequency deviation falls below -0.8 Hz. This condition did not happen in this study.

In both the DR approaches, the frequency is stabilized through manipulating a small portion of the responsive loads—not by shedding the whole feeder, as in the no-control case. As shown in the zoomed-in Fig. 9(b), when the SBS controller is in operation, the system frequency fluctuation is more (in the range of ± 0.005 Hz) than when the AHC controller (alone) is operating. However, the fluctuations are small and the system is in the safe operation region. At around 33 s, the SBS controller minimizes the amount of responsive loads needed to stabilize the frequency. At this time, the system goes to the no-control MODE (MODE 0). As a result of frequency regulation, the voltage of the system is also stabilized, as shown in Fig. 9(c). No considerable voltage fluctuation is observed at the end of MODE 2, when the SBS controller ends. The reason is the adaptive nature of the SBS controller, according to (2),

which results in smaller step changes in the manipulated load at the end of MODE 2.

Fig. 9(d) shows the total demand on the system for the no-control case, the AHC (alone), and the comprehensive control. In each case, the amount of system load that remains active at steady-state to keep the system frequency at 60 Hz is shown. The amount of load that remains active in each case is as follows: 6.27 MW under no-control, 6.756 MW with the AHC (alone), and 7.002 MW with the comprehensive controller. The percentage of manipulated responsive load in the case of AHC and comprehensive controller are 52.07% and 20.30%, respectively. It is clear that a larger amount of load remains active under the comprehensive control approach. The difference between the percentages of manipulated load at steady-state for the comprehensive approach compared to the AHC approach is 31.77%, which again results in improved QoS for the customers.

C. Scenario III: Excess Wind Power Generation

In this case, a 2 MW wind turbine is connected to the network at the PCC, as shown in Fig. 5. The system frequency, voltage, and power demand are shown in Fig. 10. At $t = 7$ s, the wind power suddenly increases from 0.6 MW to 1.3 MW. In the no-control case, a 1-MW dump load is activated at the PCC (increasing the total system load to almost 7.5 MW) once the system frequency reaches 60.5 Hz at approximately $t = 8.3$ s [Fig. 10(a) and 10(b)]. As shown in Fig. 10(d), the total amount of load in the AHC and comprehensive cases at steady-state are: 7.037 MW and 6.778 MW, respectively. The percentages of manipulated responsive loads are 65.59% for the AHC and 33.04% for the comprehensive approach. This again shows the effectiveness of the comprehensive controller in manipulating (in this case activating) a smaller percentage of the responsive loads which translates to improved customers' QoS. In order to keep the system frequency at 60 Hz at steady-state, 32.55% of the responsive loads have been saved when the comprehensive controller is operating compared to when the AHC controller is applied.

Fig. 10(b) shows the zoomed-in frequency variation. In the case of comprehensive controller, the frequency varies within the acceptable range of 60 ± 0.005 Hz until around $t = 29$ s, when it tends to go outside the limit. At this time, the SBS controller has accomplished the minimization of the manipulated responsive loads (i.e., the end of MODE 2). As shown in Fig. 10(c), as a result of frequency stabilization the system voltage is also stabilized (in all cases).

D. Scenario IV: Unexpected Shortage in Wind Power Generation

In this scenario, the wind power generation suddenly decreases from 1.3 MW to 0.8 MW. In the no-control case, partial load shedding in load 5 (a noncritical load in Fig. 5) takes place as soon as the frequency falls to 59.5 Hz [Fig. 11(a), 11(d)]. Fig. 11(d) also shows the total system power demand when the AHC and comprehensive control are applied. It is clear from this figure that at steady-state, more loads are active when the comprehensive controller is operating as compared to when the AHC (alone) is applied. In each case the percentage of

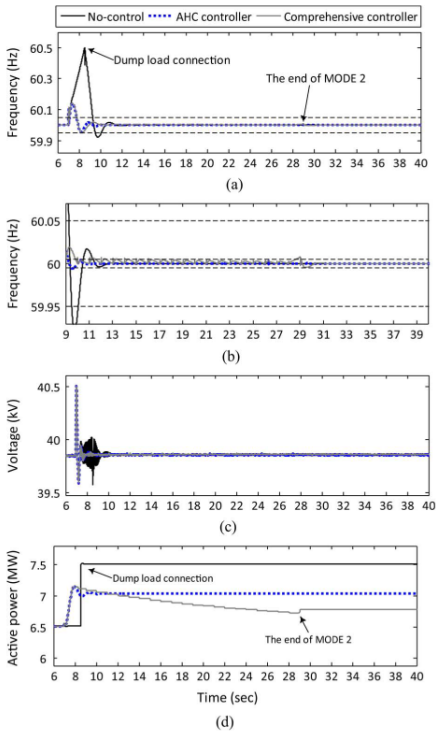


Fig. 10. Frequency, voltage, and total load demand: Excess wind power generation. (a) System frequency. (b) Zoomed-in system frequency. (c) Voltage at 69 kV bus. (d) Total load demand.

manipulated load is 44.63% for the AHC and 11.35% for the comprehensive approach. The difference results in a savings of 33.28% of the responsive loads in the comprehensive controller case compared to the AHC controller (alone), which again translates to improved customers' QoS.

Fig. 11(b) shows the zoomed-in frequency variation, and Fig. 11(c) shows the system voltage profile. It is clear from this figure that voltage stabilizes faster when the AHC and comprehensive controller are operating.

V. Discussion

In an actual system, there are two possibilities of delay in the operation of the system; one is related to the dynamic response of the loads and the other related to the delay in communication. Both delays should be considered in the DR control algorithms to prevent unnecessary switching of the responsive loads. Purely resistive loads (such as EWHs), considered in our study, respond instantly to the variations in their input voltage. Therefore, it can be assumed that there is no delay in their response to the changes in the input signal [4]. However, communication delay, often referred to as latency, should be considered. Latency is the length of time from when a request is made by a control entity to when the electrical device receives the request

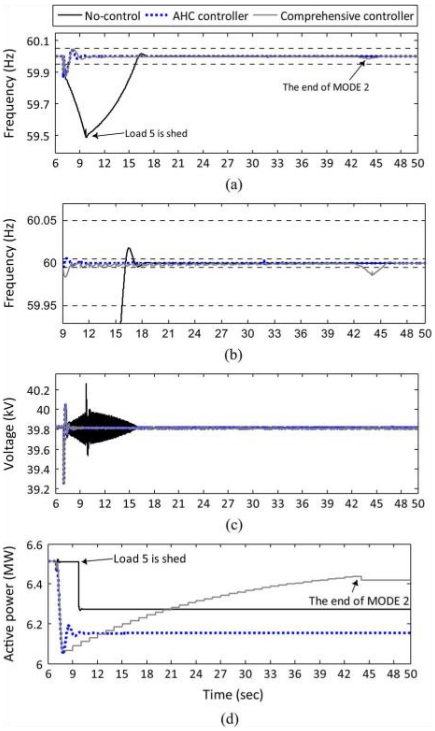


Fig. 11. Frequency, voltage, and total load demand: Unexpected shortage in wind power generation. (a) System frequency. (b) Zoomed-in system frequency. (c) Voltage at 69 kV bus. (d) Total load demand.

and acts on it. With the existing internet infrastructure, latencies of around 500 ms are achievable [9]. We have evaluated the impact of different latencies (between 20 ms and 500 ms) on the performance of the comprehensive controller. Fig. 12 shows the frequency variation with different latencies under light loading. It is clear from this figure that the controller is able to regulate the frequency successfully for latencies of up to 300 ms. At the latency of 500 ms, the system frequency is unstable.

In all the simulation studies reported earlier, a wireless network with a latency of 20 ms is assumed as the communication protocol between the control entities and loads.

In addition to the technical feasibility of the DR reported in this paper, a detailed cost-benefit analysis of the DR is also necessary to truly justify its deployment in the smart grid era. We have ongoing work on this topic, which will be reported in a follow-on paper.

VI. Conclusions

This paper presents a comprehensive DR strategy for frequency regulation in a microgrid with and without wind power generation. It has been shown through different scenarios that

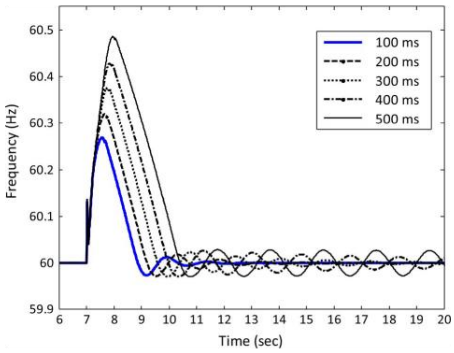


Fig. 12. System frequency with different latencies, light loading with comprehensive controller case.

the proposed DR strategy is able to regulate the system frequency and voltage in a microgrid by:

1. The application of the AHC controller to reduce the frequency deviation after a sudden disturbance with maximum effort.
2. Minimizing the amount of manipulated responsive loads needed to keep the frequency within the desired range at steady-state, which improves customers' QoS.

The central DR strategy is based on communication between the utility control center and the responsive loads and has been shown to be stable up to a latency of 300 ms.

Appendix

The DG specifications are given in Table I [33].

TABLE I
DG Parameters

Synchronous generator parameters	
Nominal power	15 MVA
Line-to-line voltage	69 kV
Nominal frequency	60 Hz
d-axis reactance (X_d, $X_{d'}$, $X_{d''}$)	1.305, 0.296, 0.252 p.u.
q-axis reactance (X_q, $X_{q'}$, $X_{q''}$)	0.474, 0.243, 0.18 p.u.
Inertia coefficient	2.2 sec
Governor and Diesel Engine parameters	
Regulator gain	40
Regulator time constants (T_1, T_2, T_3)	0.01, 0.02, 0.2 sec
Engine time delay	0.14 sec
Excitation controller parameters	
Regulator gain	200
Regulator time constants	0.02 sec
Damping filter gain and time constant	0.001, 0.1 sec

References

[1] "Benefits of demand response in electricity markets and recommendations for achieving them: A report to U.S. Congress," U.S. Dept. Energy, 2006 [Online]. Available: http://eetd.lbl.gov/ea/ems/reports/congress-1252d.pdf

[2] Assessment of demand response and advanced metering: A report to U.S. Congress," Federal Energy Regulatory Commission, 2008 [Online]. Available: http://www.ferc.gov/legal/staff-reports/demand-response.pdf

[3] G. C. Heffner, C. A. Goldman, and M. M. Moezzi, "Innovative approaches to verifying demand response of water heater load control," *IEEE Trans. Power Del.*, vol. 21, no. 1, pp. 388–397, 2006.

[4] R. Jia, M. H. Nehrir, and D. A. Pierre, "Voltage control of aggregate electric water heater load for distribution system peak load shaving using field data," in *Proc. 39th North Amer. Power Symp. (NAPS)*, 2007, pp. 492–497.

[5] J. Kondoh, N. Lu, and D. J. Hammerstrom, "An evaluation of the water heater load potential for providing regulation service," *IEEE Trans. Power Syst.*, vol. 26, no. 3, pp. 1309–1316, 2011.

[6] N. Lu and S. Katipamula, "Control strategies of thermostatically controlled appliances in a competitive electricity market," in *Proc. Power Eng. Soc. Gen. Meet.*, 2005, vol. 1, pp. 202–207.

[7] R. Walawalkar, S. Blumsack, J. Apt, and S. Fernands, "An economic welfare analysis of demand response in the PJM electricity market," *Energy Policy*, vol. 36, no. 10, pp. 3692–3702, 2008.

[8] M. Klobasa, "Analysis of demand response and wind integration in Germany's electricity market," *IET Renew. Power Gener.*, vol. 4, no. 1, pp. 55–63, 2010.

[9] A. Brooks, E. Lu, D. Reicher, C. Spirakis, and B. Weihl, "Demand dispatch: Using real-time control of demand to help balance generation and load," *IEEE Power Energy Mag.*, vol. 8, no. 3, pp. 20–29, 2010.

[10] J. Medina, N. Muller, and I. Roytelman, "Demand response and distribution grid operations: Opportunities and challenges," *IEEE Trans. Smart Grid*, vol. 1, no. 2, pp. 193–198, 2010.

[11] H. Saele and O. S. Grande, "Demand response from household customers: Experiences from a pilot study in norway," *IEEE Trans. Smart Grid*, vol. 2, no. 1, pp. 102–109, 2011.

[12] N. Ruiz, I. Cobelo, and J. Oyarzaabal, "A direct load control model for virtual power plant management," *IEEE Trans. Power Syst.*, vol. 24, no. 2, pp. 959–966, 2009.

[13] A. J. Conejo, J. M. Morales, and L. Baringo, "Real-time demand response model," *IEEE Trans. Smart Grid*, vol. 1, no. 3, pp. 236–242, 2010.

[14] D. T. Nguyen, M. Negnevitsky, and M. de Groot, "Pool-based demand response exchange-concept and modeling," *IEEE Trans. Power Syst.*, vol. 26, no. 3, pp. 1677–1685, 2011.

[15] P. Faria, Z. Vale, J. Soares, and J. Ferreira, "Demand response management in power systems using a particle swarm optimization approach," *IEEE Intell. Syst.*, 2011.

[16] M. Parvania and M. Fotuhi-Firuzabad, "Integrating load reduction into wholesale energy market with application to wind power integration," *IEEE Syst. J.*, vol. 6, no. 1, pp. 35–45, 2012.

[17] K. Dietrich, J. M. Latorre, L. Olmos, and A. Ramos, "Demand response in an isolated system with high wind integration," *IEEE Trans. Power Syst.*, vol. 27, no. 1, pp. 20–29, 2012.

[18] M. Rastegar, M. Fotuhi-Firuzabad, and F. Aminifar, "Load commitment in a smart home," *J. Appl. Energy*, 2012.

[19] N. Navid-Azarbaijani and M. H. Banakar, "Realizing load reduction functions by aperiodic switching of load groups," *IEEE Trans. Power Syst.*, vol. 11, no. 2, pp. 721–727, 1996.

[20] K. Y. Huang, H. C. Chin, and Y. C. Huang, "A model reference adaptive control strategy for interruptible load management," *IEEE Trans. Power Syst.*, vol. 19, no. 1, pp. 683–689, 2004.

[21] D. Westermann and A. John, "Demand matching wind power generation with wide-area measurement and demand-side management," *IEEE Trans. Energy Convers.*, vol. 22, no. 1, pp. 145–149, 2007.

[22] D. Trudnowski, M. Donnelly, and E. Lightner, "Power-system frequency and stability control using decentralized intelligent loads," in *Proc., IEEE PES Conf. Exhib. Transm. Distrib.*, 2005, pp. 1453–1459.

[23] J. A. Short, D. G. Infield, and L. L. Freris, "Stabilization of grid frequency through dynamic demand control," *IEEE Trans. Power Syst.*, vol. 22, no. 3, pp. 1284–1293, 2007.

[24] A. Molina-García, F. Bouffard, and D. S. Kirschen, "Decentralized demand-side contribution to primary frequency control," *IEEE Trans. Power Syst.*, vol. 26, no. 1, pp. 411–419, 2011.

[25] D. Angeli and P.-A. Kountouriotis, "A stochastic approach to dynamic-demand refrigerator control," *IEEE Trans. Control Syst. Technol.*, vol. 20, no. 3, pp. 581–592, May 2012.

[26] S. A. Pourmousavi and M. H. Nehrir, "Demand response for smart microgrid: initial results," *Proc. 2nd IEEE PES Innov. Smart Grid Technol. (ISGT)*, pp. 1–6, 2011.

[27] S. A. Pourmousavi, M. H. Nehrir, and C. Sastry, "Providing ancillary services through demand response with minimum load manipulation," in *Proc. North Amer. Power Symp. (NAPS)*, 2011, pp. 1–6.

[28] M. H. Albadi and E. F. El-Saadany, "A summary of demand response in electricity markets," *Electr. Power Syst. Res.*, vol. 78, no. 11, pp. 1989–1996, 2008.

[29] Y. G. Rebours, D. S. Kirschen, M. Trotignon, and S. Rossignol, "A survey of frequency and voltage control ancillary services-part I: technical features," *IEEE Trans. Power Syst.*, vol. 22, no. 1, pp. 350–357, 2007.

[30] *Time Error Correction*, Std. BAL-004-0, North American Electric Reliability Corporation, Apr. 2005 [Online]. Available: http://www.nerc.com/files/BAL-004-0.pdf

[31] F. Katiraei, M. R. Iravani, and P. W. Lehn, "Micro-grid autonomous operation during and subsequent to islanding process," *IEEE Trans. Power Del.*, vol. 20, no. 1, pp. 248–257, 2005.

[32] V. Menon and M. H. Nehrir, "A hybrid islanding detection technique using voltage unbalance and frequency set point," *IEEE Trans. Power Syst.*, vol. 22, no. 1, pp. 442–448, 2007.

[33] MATLAB/Simulink SimPowerSystems Documentation [Online]. Available: http://www.mathworks.com/

[34] *IEEE Recommended Practice for Excitation System Models for Power System Stability Studies*, 421.5, 2005.

[35] A. Yazdani and R. Iravani, *Voltage-Sourced Converters in Power Systems: Modeling, Control, and Applications*. Hoboken, NJ: Wiley, 2010, ch. 4.



S. Ali Pourmousavi (S'07) received the B.S. degree with honors from University of Mazandaran, Iran in 2005 and the M.S. degree with honors from Amirkabir University of Technology (Tehran Polytechnic), Iran in 2008, all in electrical engineering. He is currently working toward the Ph.D. degree in the Electrical and Computer Engineering (ECE) Department at Montana State University, Bozeman.

His research interests include energy management of hybrid power generation systems, load control and demand response, and wind speed and power forecasting.



M. Hashem Nehrir (S'68–M'71–SM'89–F'10) received the B.S., M.S., and Ph.D. degrees from Oregon State University, Corvallis, in 1969, 1971, and 1978, respectively, all in electrical engineering.

He was with the Electrical Engineering Department, Shiraz University, Iran, from 1971 to 1986. Since 1987, he has been on the faculty of the Electrical and Computer Engineering Department, Montana State University, Bozeman, where he is a Professor. His research interests include modeling and control of power systems, alternative energy power generation systems, and application of intelligent controls to power systems. He is the author of three textbooks and an author or coauthor of numerous technical papers.

CHAPTER 4

THE APPLICATION OF DEMAND RESPONSE FOR FREQUENCY REGULATION IN AN ISLANDED MICROGRID WITH HIGH PENETRATION OF RENEWABLE GENERATION

Contribution of Authors and Co-Authors

Manuscripts in Chapters 2 through 12

Author: Kevin Marchese

Contributions: Implemented a small-scale islanded MG at the distribution level for a typical distribution feeder in MATLAB®/Simulink, prepared actual solar irradiation and ambient temperature data for simulations, and wrote the first draft of the paper with all figures.

Co-author: S. A. Pourmousavi

Contributions: Developed and designed the simplified grid model (SGM) with automatic generation control (AGC), developed a generic controller based on adaptive hill climbing (AHC) for frequency regulation for real-time DR with minimum manipulation, and redesigned all the simulation setup and repeated simulation, finalized manuscript and re-plotted all the figures.

Co-author: M. H. Nehrir

Contributions: Provided important insight and overview of the research, interpretation of the results, and aided in the preparation of the manuscript.

Manuscript Information Page

Kevin Marchese, Seyyed Ali Pourmousavi Kani, M. Hashem Nehrir

IEEE North American Power Symposium (NAPS), 2013

Status of the manuscript:
____ Prepared for submission to a peer-reviewed conference
____ Officially submitted to a peer-reviewed conference
____ Accepted by a peer-reviewed conference
_X_ Published in a peer-reviewed conference proceedings

Published by the Institute of Electrical and Electronics Engineering (IEEE)

THE APPLICATION OF DEMAND RESPONSE FOR FREQUENCY REGULATION IN AN ISLANDED MICROGRID WITH HIGH PENETRATION OF RENEWABLE GENERATION

The following work was presented at the 2013 NAPS and is published in the conference proceedings

Kevin Marchese, S.A. Pourmousavi, and M.H. Nehrir

Department of Electrical and Computer Engineering, Montana State University, Bozeman, MT 59717

Abstract

Increasing the penetration of variable generation sources, such as wind and solar, potentially threatens the stability of the power systems. Past studies have shown that 15-20% renewable penetration is the largest amount the power systems can handle using conventional control. To overcome the challenge that variable renewable generation presents, this chapter proposes that real-time DR be used for AS. The impact of varying the amount of DR on the performance of a MG-configured distribution feeder is evaluated in this chapter. Simulation results have shown that a proper amount of DR resources can help to achieve higher penetrations of renewable generation while maintaining the desired system frequency.

Introduction

As a feature of the smart grid, variable renewable generation is projected to achieve a high penetration in the future power system. Many countries have stated goals to increase the amount of renewable energy penetration considerably in years to come. Past studies have revealed that renewable energy penetration greater than 20% will

potentially result in grid instability when using conventional control techniques, such as governor droop control and AGC [4.1], [4.2]. In order to overcome this challenge, more AS are needed, specifically during peak hours. Recently, studies have focused on using DR as an AS provider [4.3]. Many aspects of DR have been researched, such as DR markets and cost/benefit analysis [4.4] and DR modeling [4.5]-[4.7] and aggregation [4.8]. This chapter is a continuation of the study in Chapter 2, where DR is applied to stabilize the frequency of a MG-configured distribution feeder.

DR is fundamentally achieved by varying the load so that the power consumed matches the power generated; therefore, the grid frequency will always operate at its reference value. The traditional way to maintain a balance between load and generation is to vary generation to meet demand (i.e., load following). The distinct difference when using LFC through DR is that the load is varied to meet the available generation (i.e., generation following).

Past studies have shown that loads, such as EWHs, can be controlled to smooth out the demand curve while maintaining customer comfort [4.8]-[4.10]. EWHs make up 11% of residential loads and can increase to 30% during peak hours [4.11]. Therefore, the control of aggregated EWHs can be a viable option for DR. In this chapter, no individual load is considered as a responsive load (DR resource). The generic load used can consist of EWHs, HVAC, or other thermostatically controlled appliance (TCA).

In this chapter, the SGM proposed in Chapter 2 will be further modified to include AGC. For this study, adequate frequency regulation is defined as maintaining a grid frequency within 60±0.05 Hz, which is the Federal Energy Regulatory Commission

(FERC) standard. An adaptive hill climbing (AHC) control technique has been shown to control fluctuations in grid frequency and will be used during this chapter to implement DR [4.3]. Then various methods to control frequency, including, governor droop control, governor droop control with AGC, and governor droop control with DR will be examined. The objective here is to show the effectiveness of DR to provide AS in an islanded MG setting in comparison to traditional AS (governor droop control and AGC). In addition, various latencies will be studied to analyze the effect of communication delay on the performance of DR. Also, slow and fast AGC will be examined. Simulation results have shown that DR with governor droop control can yield adequate frequency stabilization in the MG-configured distribution feeder.

The Proposed Control Strategy

The need to balance generation and demand at all times through control action is a necessary process for a power system. Any load or generation variation can cause a mismatch between the two and result in unwanted frequency deviation. The traditional frequency correction action includes generator inertia (as an unintentional control), frequency droop control (known as primary control), and AGC (known as secondary control). In this chapter, all three of these control actions are modeled. The primary frequency correction comes from those generators that are outfitted with governor droop controllers where droop can vary from 4%-20%, shown in Figure 4.1. A generator outfitted with a 4% droop means that a 4% drop in frequency would result in a 100% increase in that generators output. Figure 4.1 shows the block diagram of a synchronous generator (SG) with droop and excitation control. The constant K_i shown in the figure is

the integral control constant of the secondary frequency control (AGC), which is set to zero when only droop control is active. We used the combination of the SG, droop control, AGC, and excitation control, shown in Figure 4.1, as a SGM to show frequency variation in the distribution system studied.

The required reserves for AGC are usually provided by fossil-fuel based power plants as either spinning or non-spinning reserve, which are normally not available for islanded MGs. In this chapter, the impact of AGC is presented by an equivalent model of all available traditional regulation providers by a single generator (Figure 4.1 when droop value is zero) with an integral controller (K_i), shown in Figure 4.1. The speed of the AGC controller can be increased by increasing the integrator coefficient, K_i. In addition, the capacity of the generator can be changed to represent available regulation services in the MG.

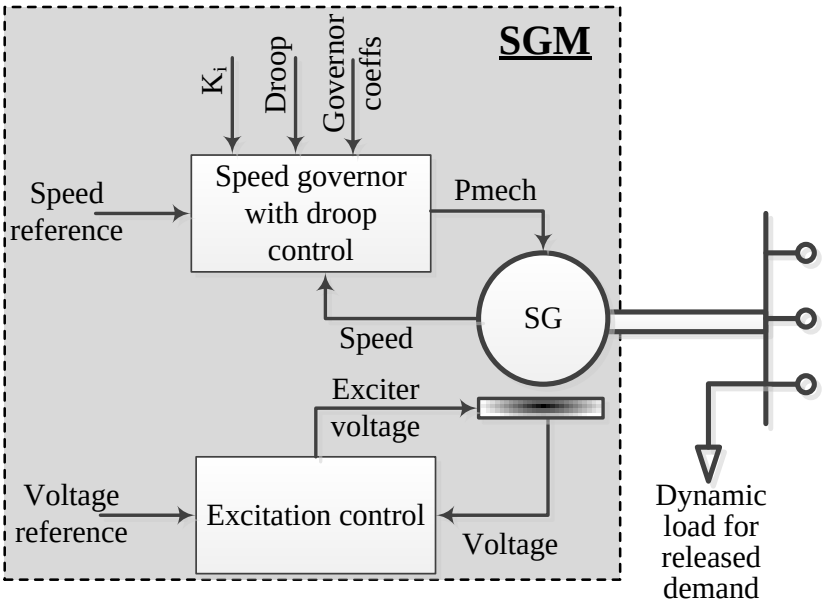


Figure 4.1. The proposed SGM with governor droop control and AGC.

Since AGC is not commonly available for MGs, as a viable alternative, DR is proposed in this study to replace the AGC controller (Figure 4.2). The DR strategy in this chapter includes an AHC technique, introduced in [4.3] and in Chapter 3. In order to obtain the percent frequency variation $L(t)$ at each step, the system frequency is measured and compared to a reference frequency (60Hz) in order to generate the frequency error (Δf). This frequency error (Δf) is then multiplied by a gain term, M, which is finally added to the percent frequency variation at the previous time step, $L(t\text{-}1)$, as follows.

$$L(t) = L(t-1) + M \times \Delta f \tag{4.1}$$

Increasing the gain leads (M) to faster response but introduces a larger overshoot. It is important to avoid ringing in power system control so that the generators are not oscillating, which puts undue torque and stress on the machines and can decrease their serviceable lifetime. It was determined that for the system under study, the best response was achieved by setting the gain, M, to 2.5.

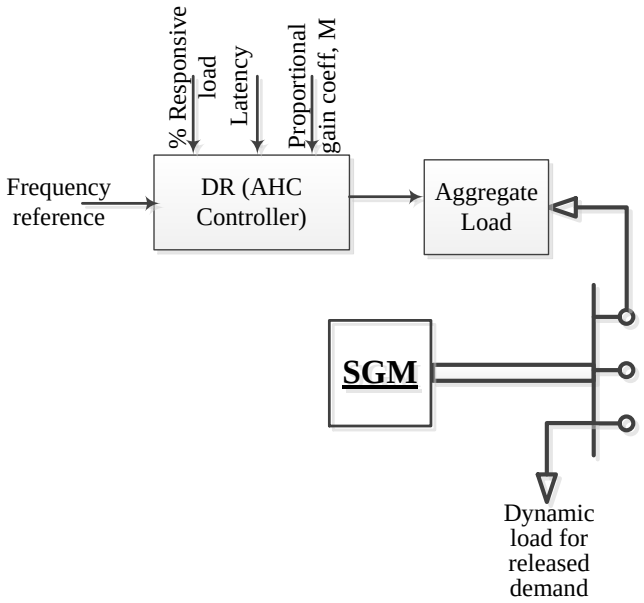


Figure 4.2. Block diagram of the proposed DR controller.

The percent frequency error, $L(t)$, represents the percentage of load that needs to be manipulated. If $L(t)$ is positive then frequency is rising and load must be increased, whereas if $L(t)$ is negative, the frequency is dropping and load needs to be curtailed. The AHC controller attempts to always achieve $\Delta f = 0$ by continuously changing the value of df/dt and move it toward zero. This is similar to the maximum power point tracking (MPPT) method for PV cells, which attempts to make $dP/dV = 0$ [4.12].

Latency delay was also considered for the DR control strategy. Previous studies have shown that a latency of 20 to 50 seconds can be associated with traditional AGC control [4.13]. This latency is due to communication delay and mechanical processes that must take place, such as opening or closing steam valves. It can take on the order of 30 minutes to an hour for the frequency to settle back to its reference frequency after a disturbance occurs [4.14]. Therefore, a latency period of approximately 30 minutes is used in this chapter to model the current response time of AGC control. However, a MG operating as a small-scale regional power system will experience much faster two-way communication (smaller latency period on the order of several hundred msec). According to the study reported in [4.15], latency of 500 msec or less is achievable with current Internet infrastructure. Furthermore, wireless communication can achieve much smaller latency periods. In this chapter, latencies of 100 msec and 500 msec were used for implementing DR.

System Studied

The system studied during this chapter resembles an islanded MG. MGs can function without assistance from the main grid and operate in islanded mode. The MG

includes distributed generators that may be controlled from a central location. The control may also be decentralized using distributed agents [4.16], [4.17]. A MG may not have the benefit of AS, such as governor droop and AGC control, to regulate frequency. Therefore, another means of control such as DR must be used.

Long-term dynamic simulation in MATLAB®/Simulink is very slow, so that modeling an entire distribution feeder was not possible in this study. To solve this problem, only a part of the feeder is modeled in detail and the rest of it is modeled by equivalent generation sources (SGM) and aggregated load. The SGM includes a 17 MVA generator with governor droop control and excitation control. The SGM with governor droop control is complemented with the proposed AGC, discussed in earlier section and in Chapter 3. This system also includes a 7.5 MW of concentrated PV farm, 13 MW/9.75 MVAr base load, and a distribution feeder, shown in Figure 4.3. The distribution feeder shown in Figure 4.3 is approximately 0.837MW/0.626MVAr (1.06 MVA). Although AGC is used in large-scale power systems, we have modeled the AGC in the SGM to show its impact on the system frequency behavior. Although energy storage is foreseen as a part of a MG, it is not the primary concern of this chapter, as the focus is to regulate system frequency with DR, and therefore is not included in the MG. Only responsive loads, such as EWHs and HVAC, become virtual energy storage (buffer) for the power system, which allows them to provide negative and positive reserve. When generation exceeds load, EWHs can be turned ON to absorb the excess power, which is stored as heat in the hot water tanks. Then during periods of peak demand the stored energy in the hot water tanks can be released [4.8]-[4.10].

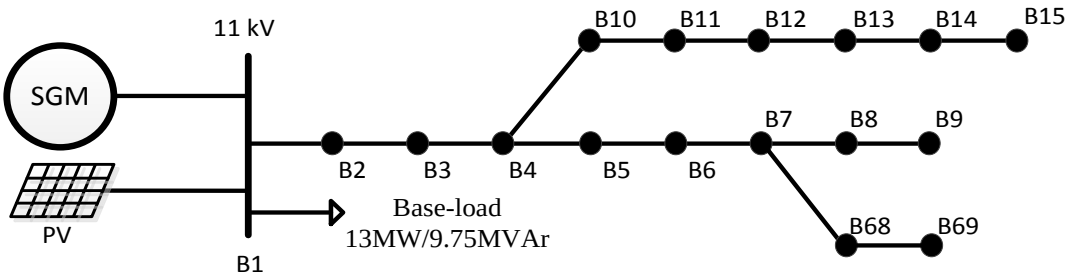


Figure 4.3. Schematic of the MG-configured distribution feeder.

For this study, the PV penetration was set to a maximum of 25% meaning that 25% of the total generation capacity available is from PV. The system studied has been previously used in [4.1] without AGC. The solar data for this study was obtained from the National Renewable Energy Laboratory (NREL) for a site in Oahu, Hawaii, U.S. on June 18, 2010. The solar irradiation and the temperature data for the hours 12:36–15:06 were used to obtain the output of the PV farm, shown in Figure 4.4. The PV output power data was reported in one second intervals and was input directly into the simulation.

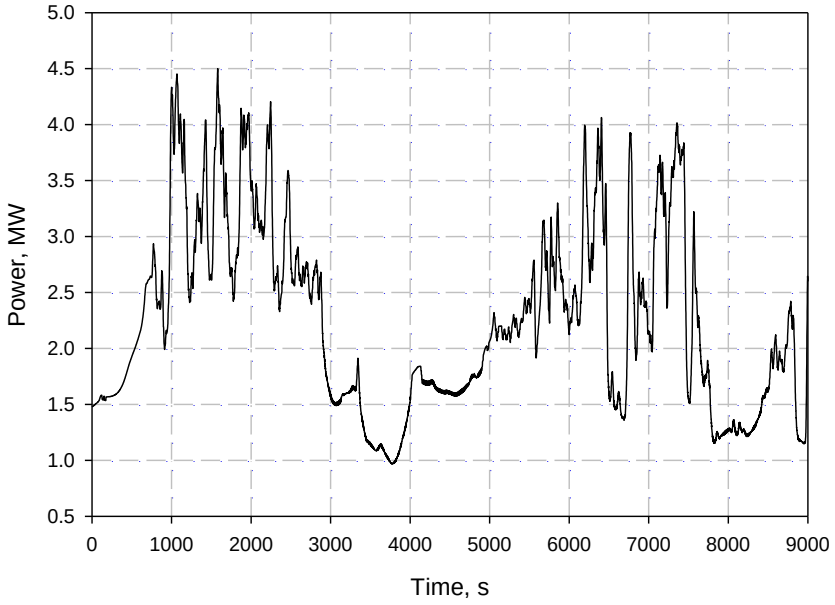


Figure 4.4. PV power generation in Oahu, Hawaii, U.S.

Simulation Results

The system introduced in earlier section is implemented in MATLAB®/Simulink. The first part of the simulation is for proof of concept and includes the proposed model and controllers without the feeder model. In this section, the impact of the proposed DR strategy with different latencies is compared with traditional AGC control. The second part of this section, is devoted to the MG system including the feeder. For these simulations, variable PV generation is also added and the simulations are carried out for 2.5 hours.

System Performance Using Load Step Change

In this section, several simulations are carried out to reveal the different features of DR application for frequency stabilization compared to the conventional AGC. For these simulations, the feeder and variable solar power are eliminated. The load was 10MW for the first 60 seconds, at which point the load was instantly increased by 20% to 12MW. The integral gain, K_i, for the AGC control and the proportional gain, M, for the AHC controller are determined throughout these simulations. These simulations also prove the hypothesis that applying DR through an AHC controller outperforms the conventional frequency regulation using governor droop control with AGC.

For conventional power systems, AGC is known as slow control which takes place in several minutes to bring the frequency back to 60Hz. In the first simulation study, the AGC responses with different speeds (gains) are compared with responses of the governor droop control and the DR with 25% of available responsive loads, shown in Figure 4.5.

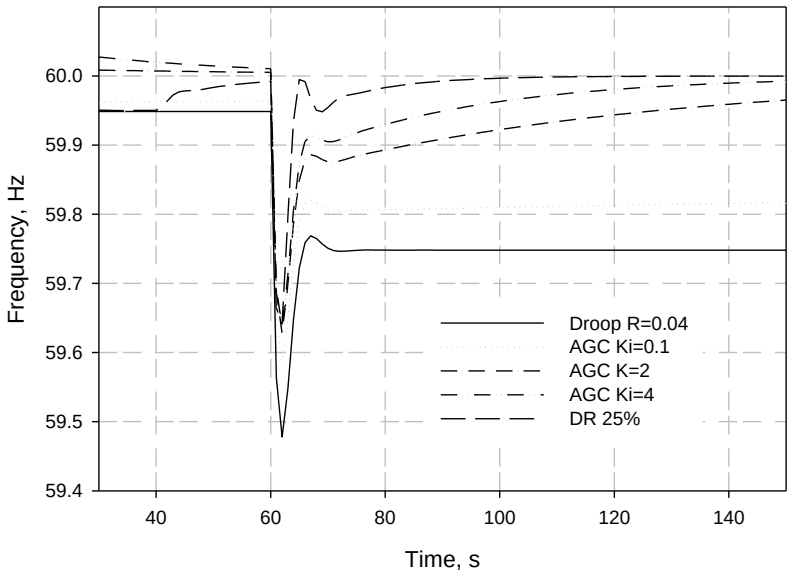


Figure 4.5. Load step change with variable integrator gain.

It can be seen in Figure 4.5 that the droop control response has a large steady-state error and does not bring the frequency to the acceptable range. Further, the frequency regulation performance with DR outperforms the conventional AGC, even the fastest AGC with K_i=4. Since the system under study is a small islanded power system, the AGC control is assumed to be fast. However, the objective of this figure is to show that LFC using DR is still faster than the fastest AGC control.

Figure 4.6 shows the impact that varying the amount of responsive load has on the system frequency. As it can be seen from this figure, 15% of responsive load is not enough for adequate frequency regulation. More responsive load should participate in DR to bring the frequency back to its nominal value. Once available DR is increased to 25%, the system frequency is stabilized and zero steady-state error is achieved. Frequency stabilization is achieved faster with 50% DR (compared to 25% of DR), but a frequency overshoot is observed. The overshoot, increases as the percentage of responsive load

available increases. The controller switches the status of a greater number of devices than necessary to quickly react to a frequency deviation, which can result in nuisance curtailment. A past study has shown that a step-by-step controller can be used to correct this problem [4.17]. The system frequency behavior was also evaluated under different communication latencies to ensure that the system frequency remains stable under such latencies. Figure 4.7 shows the impact that different latencies associated with DR have on system frequency, where 25% of responsive loads are available. As it can be seen from Figure 4.7, larger latencies result in oscillations in the system frequency since it takes longer for the central controller commands to be received by the loads. However, the system frequency is stabilized for latencies of up to 2 sec, which is well within the range of typical communication delays. According to [4.15], communication with 500 msec delay is achievable by the Internet today, and with that delay, the system frequency behavior is well within the acceptable range.

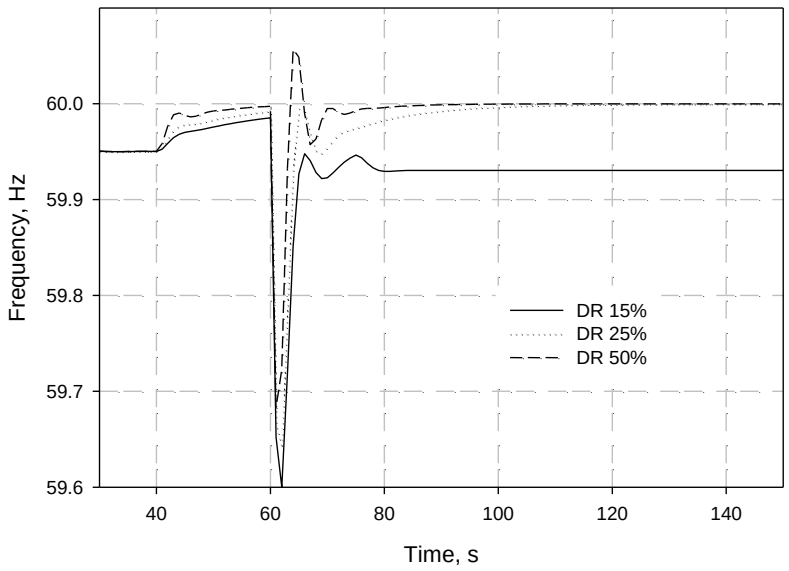


Figure 4.6. Load step change with variable responsive load.

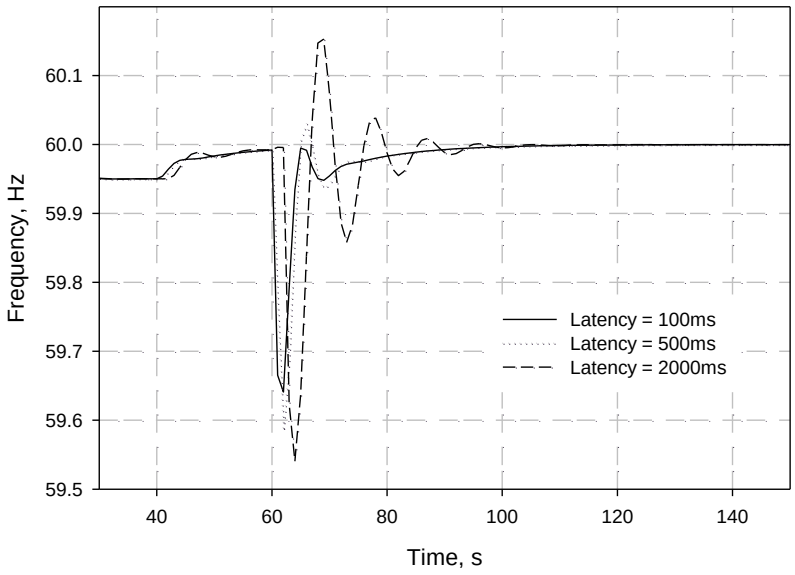
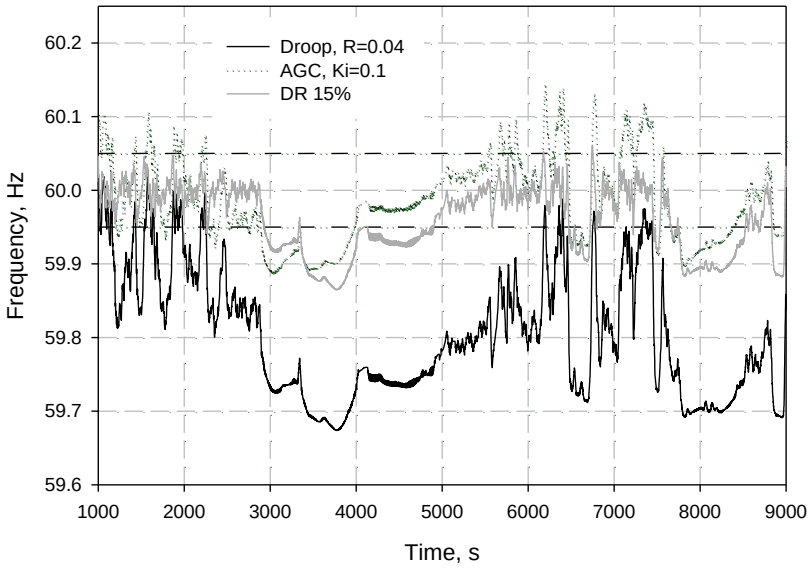


Figure 4.7. Load step change with different DR latencies.

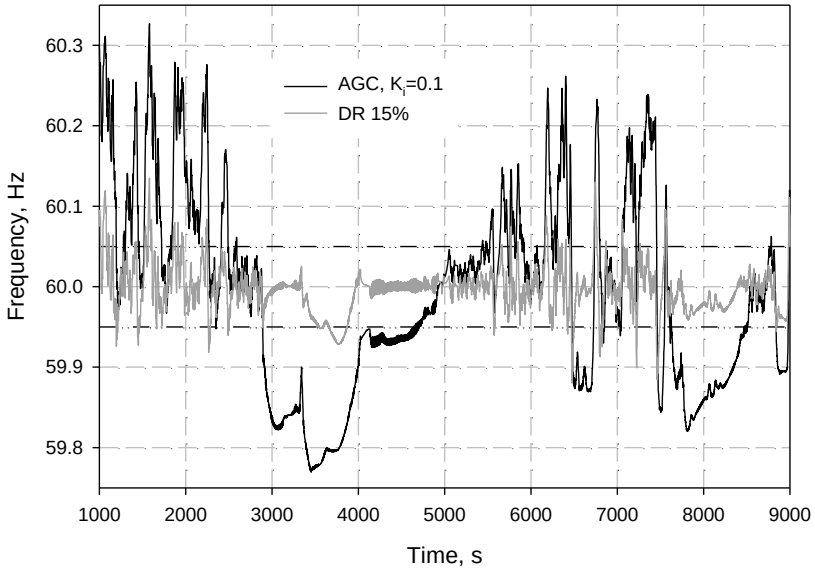
Impact of the PV Farm

In these simulations, the output power of the PV farm was added into the system and the simulations were carried out for 2.5 hours. 15% and 25% PV penetration is considered to show the effectiveness of DR in providing frequency regulation for a generic distribution feeder. All other parameters and coefficients are the same as those in the earlier sub-section except the parameters whose variability is being analyzed. For all simulations, the AGC integral gain, K_i, is 0.1, which stabilizes system frequency in approximately 30 minutes.

Figure 4.8 shows the frequency response with the three different control strategies discussed above for 15% and 25% of PV penetration. Figure 4.8 (a) shows the system frequency behavior with droop control, AGC, and DR with PV penetration of 15%. It is clear from the figure that the droop control is not capable of bringing the frequency to the acceptable range.



(a)



(b)

Figure 4.8. System frequency response with (a) 15%, (b) 25% PV penetration.

Although the DR performance is better than AGC, both methods are not able to keep the frequency in the desired range, as shown in Figure 4.8 (a). However, the DR control performance is superior in the case of 25% PV penetration, Figure 4.8 (b).

Figure 4.9 shows the impact of 15% and 25% responsive load on the system

frequency. The PV penetration is 25% in both cases. It is clear that when 25% responsive load is available for DR, the frequency deviations are within the acceptable range most of the time. Therefore, an increase in the amount of responsive load results in significant decrease in the frequency fluctuations magnitude. In addition, the average, standard deviation, and root mean square error (RMSE) of frequency deviation are better with 25% DR as compared with 15% available DR, as shown in Table 4.1.

Table 4.1. System frequency statistics for the three control methods in 9000 sec simulation for 25% PV penetration.

	Minimum Frequency (Hz)	Maximum Frequency (Hz)	Average Frequency (Hz)	Standard Deviation (Hz)	RMSE (Hz)
Governor	59.74	60.33	59.95	0.140	0.149
DR-15%	59.88	60.13	59.99	0.030	0.030
DR-25%	59.91	60.09	60.00	0.017	0.017
AGC	59.77	60.32	59.99	0.120	0.121

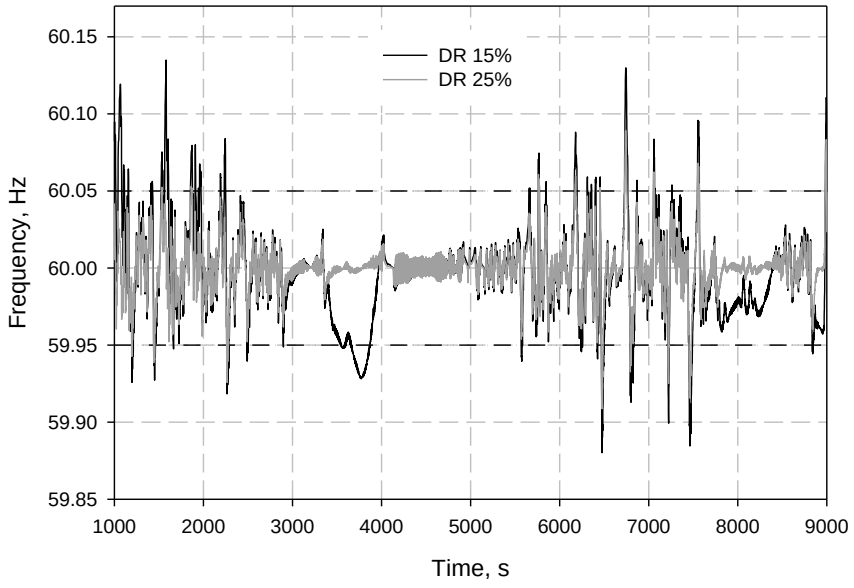
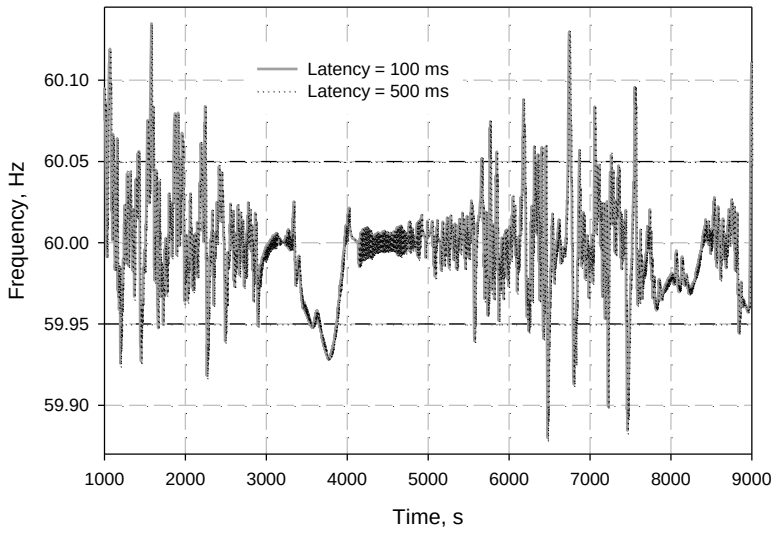
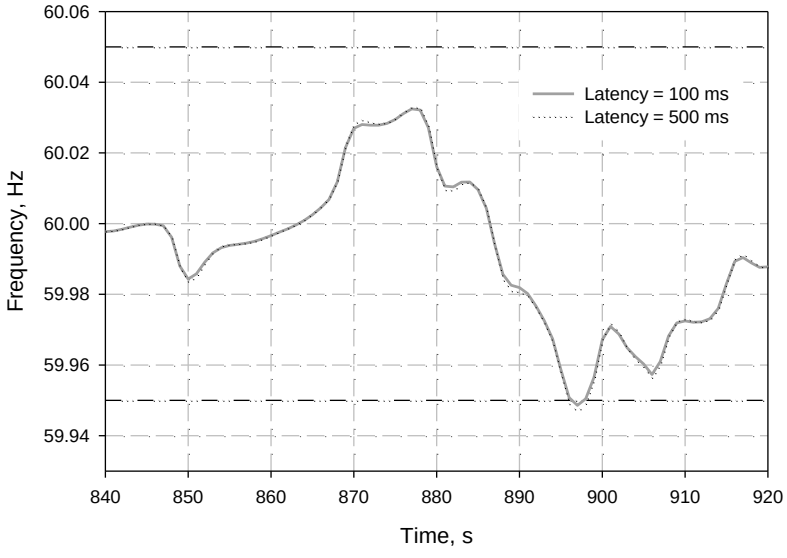


Figure 4.9. System frequency response with variable responsive load with 25% of PV penetration.

Figure 4.10 shows the impact of 100 msec and 500 msec DR latency on the system frequency, where 15% of responsive loads is considered for DR. There is no discernible difference between the system frequency responses with latencies of 100 msec and 500 msec and therefore the two curves are laid on top of each other. Figure 4.10 (b) is a zoomed-in view of a portion of Figure 4.10 (a).



(a)



(b)

Figure 4.10. (a) System frequency response with 25% PV penetration, (b) zoomed-in view.

Table 4.1 shows the minimum and maximum frequency, and standard deviation, and RMSE of frequency (compared to 60 Hz) for governor droop control, AGC and 15% and 25% DR. It is again clear that in all cases, DR outperforms the other methods, and 25% DR is better than 15% DR. The values are calculated using the results obtained between 1000 sec and 9000 sec. The values before 1000 sec were excluded from the statistical analysis because the system had yet to reach steady state from its initial value.

Conclusion

In this chapter, DR has been utilized to stabilize the system frequency with high penetrations of variable PV generation. Different simulation results have revealed the effectiveness of the proposed DR strategy in comparison to AGC. It also has been observed that the system frequency improved as the amount of available responsive load increased. It was also noticed that long communication delays in load controls could negatively impact the system frequency. However, the system performance was acceptable for communication delays of up to 500 msec.

Acknowledgement

This work was in part supported by DOE Award DE-FG02-11ER46817 and by Montana State University.

References Cited

[4.1] S.A. Pourmousavi, A.S. Cifala, and M.H. Nehrir, "Impact of high penetration of PV generation on frequency and voltage in a distribution feeder," in *Proc*. North American Power Symposium (NAPS), Champaign, IL, 2012, pp. 1–8.

[4.2] K. Kawamura, et al., "Avoided cost of effects of voltage control by demand response in a distribution network with high integration of rooftop PV," in *Proc.* Innovative Smart Grid Tech. IEEE PES., Washington DC, 2013, pp. 1–6.

[4.3] S.A. Pourmousavi and M.H. Nehrir, "Demand response for smart microgrid: Initial results," in *Proc*. Innovative Smart Grid Tech. IEEE PES., Anaheim, CA, 2011, pp. 1–6.

[4.4] J.A. Taylor, et al., "Price and capacity competition in zero-mean storage and demand response markets," in *Proc.* 50th Annual Allerton Conference on Communication, Control, and Computing, , Monticello, IL, 2012, pp. 1316–1323.

[4.5] N. Navid-Azarbaijani and M.H. Banakar, "Realizing load reduction functions by aperiodic switching of load groups," *IEEE Trans. Power Syst*., vol. 27, no. 1, pp. 721–727, May 1996.

[4.6] K.Y. Huang, H.C. Chin, Y.C. Huang, "A model reference adaptive control strategy for interruptible load management," *IEEE Trans. Power Syst*., vol. 19, no. 1, pp. 683–689, Feb. 2004.

[4.7] D. Westermann and A. John, "Demand matching wind power generation with wide-area measurement and demand-side management," *IEEE Trans. Energy Covers*., vol. 22, no. 1, pp. 145–149, March 2007.

[4.8] R. Jia, M.H. Nehrir, and D.A. Pierre, "Voltage control of aggregate electric water heater load for distribution system peak load shaving using field data," in *Proc.* 39th North American Power Symposium (NAPS '07), pp. 492–497.

[4.9] M.H. Nehrir, B.J. LaMeres, and V. Gerez, "A customer-interactive electric water heater demand-side management strategy using fuzzy logic," in *Proc*. IEEE PES Winter Meeting, vol. 1, New York, NY, 1999, pp. 433–436.

[4.10] S.N. Patrick, "Control of aggregate electric water heaters for load shifting and balancing intermittent renewable energy generation in a smart grid environment," M.S. Thesis, Department of Electrical and Computer Engineering, Montana State University, Bozeman, 2011.

[4.11] N. Lu and S. Katipamula, "Control strategies of thermostatically controlled appliances in a competitive electricity market," in *Proc.* 2005 IEEE PES General

Meeting, 2005, pp. 202–207.

[4.12] W. Xiao and W.G. Dunford, "A modified adaptive hill climbing MPPT method for photovoltaic power systems," in *Proc.* IEEE 35th Annual Power Electronics Specialists Conference, vol. 3, 2004, pp. 1957–1963.

[4.13] X. Yu and K. Tomsovic, "Application of linear matrix inequalities for load frequency control with communication delays," *IEEE Trans. Power Syst.*, vol. 19, no. 3, pp. 1508–1515, Aug. 2004.

[4.14] Y.G. Rebours, et al., "A survey of frequency and voltage control ancillary services-Part I: Technical features," *IEEE Trans. Power Syst.*, vol. 22, no. 1, pp. 350–357, Feb. 2007.

[4.15] A. Brooks, et al., "Demand dispatch: using real-time control of demand to help balance generation and load," *IEEE Power Energy Mag.*, vol. 8, no. 3, pp. 20–29, May/June 2010.

[4.16] C.M. Colson, "Toward real-time power management of microgrids for power system integration: A decentralized multi-agent based approach," Ph.D. Dissertation, Montana State University, 2012.

[4.17] C.M. Colson and M.H. Nehrir, "Comprehensive real-time microgrid power management and control with distributed agents," *IEEE Trans. Smart Grid*, vol. 4, no. 1, pp. 617–627, March 2013.

[4.18] S.A. Pourmousavi and M.H. Nehrir, "Real-time central demand response for primary frequency regulation in microgrids," *IEEE Trans. Smart Grid*, vol. 3, no. 4, pp. 1988-1996, Dec. 2012.

CHAPTER 5

REAL-TIME OPTIMAL DEMAND RESPONSE FOR FREQUENCY REGULATION IN SMART MICROGRID ENVIRONMENT

Contribution of Authors and Co-Authors

Manuscripts in Chapters 2 through 12

Author: S. A. Pourmousavi

Contributions: Developed PJM balancing reserve market for an islanded MG, designed objective function and technical constraint for optimization, coded the optimization problem in MATLAB®/m-file, designed different simulation setup, prepared all the simulation setup and results, manuscript and all figures.

Co-author: M. H. Nehrir

Contributions: Provided important insight and overview of the research, interpretation of the results, and aided in the preparation of the manuscript.

Manuscript Information Page

Seyyed Ali Pourmousavi Kani, M. Hashem Nehrir

International Conference on Power and Energy System (EuroPES), 2012

Status of the manuscript:
____ Prepared for submission to a peer-reviewed conference
____ Officially submitted to a peer-reviewed conference
____ Accepted by a peer-reviewed conference
_X_ Published in a peer-reviewed conference proceedings

Published by the International Association of Science and Technology for Development (IASTED)

REAL-TIME OPTIMAL DEMAND RESPONSE FOR FREQUENCY REGULATION IN SMART MICROGRID ENVIRONMENT

The following work was presented at IASTED EuroPES 2012 Conference and is published in the conference proceedings

S.A. Pourmousavi, and M.H. Nehrir

Department of Electrical and Computer Engineering, Montana State University, Bozeman, MT 59717

Abstract

Real-time DR in smart µgrid has been shown to be an effective tool for frequency regulation with increased penetration of renewable energy resources into the grid. Since DR is recognized as an incentive or direct payment to the participants, it is consequently desired to minimize the cost of DR for the utility. This chapter presents an optimal DR strategy for minimizing the cost of DR for the utility in smart grid era. The economic model developed by Pennsylvania/New Jersey/Maryland (PJM) utility in U.S. is used on an IEEE 13-bus standard system. Simulation results verify the effectiveness of the proposed approach to minimize the cost of DR for the utility. It is also shown that the DR, with or without optimization, decreases the overall cost of frequency regulation for the utility compared to the conventional spinning reserve, without sacrificing system stability.

Introduction

Traditionally, frequency and voltage regulation, known as ancillary services, are provided by operating reserves which are basically flexible capacity generators, available when needed, to maintain secure operation of power systems. From an economic

perspective, the above response services and reserve power are costly and any method which manages to reduce the magnitude of these services, without sacrificing system stability, is of significant importance [5.1] ,[5.2].

DR traditionally refers to the changes in electricity usage by end-use customers from their normal consumption through direct control or interruptible/curtailable programs during peak hours [5.3]. Recently, this understanding of DR has been reformed because of the rapid progress in communication protocols and technology, where two-way communication with individual loads has become a reality. As a result, DR is redefined as the capability to aggregate and precisely control individual loads on command at all times [5.4].

One technical aspect of DR is providing AS in a smart grid or MG with high penetration of renewable power generation. It has been shown that real-time DR is effective in providing voltage and frequency regulation in a MG in the absence of conventional voltage and frequency regulation services [5.5]-[5.13]. It is also well-known that there is a cost associated with DR. Utilities will need to provide an incentive or direct payment to encourage their customers to participate in their DR program. Thus, it is important for the utility to minimize this cost based on the available responsive loads and the different cost of DR. Since the AS (i.e., frequency regulation) perform in a fraction of a minute (usually on the order of a few seconds), any optimization technique used for minimizing the cost of the AS must be faster than the response time of the AS.

While many studies have been reported on the different aspects of DR (including analyzing the potential of DR for AS [5.3]-[5.13], planning and modeling [5.14]-[5.17],

and the economic costs/benefit analysis of DR for the utility and customers [5.18], [5.19]), there is no comprehensive study on real-time cost minimization of DR. This paper presents a comprehensive algorithm to minimize the cost of DR for the utility. A real-time DR algorithm developed in [5.12] and [5.13] (and in Chapter 3) and a DR model introduced by the Pennsylvania/New Jersey/Maryland (PJM) utility [5.16] are used. Because of the linearity of the objective function and the relatively small size of the problem, LP–simplex method– is used to solve the optimization problem. Results from the proposed algorithm are compared with those from the conventional AS (i.e., spinning reserve) and the DR without optimization for further evaluations. The results of this chapter verify the effectiveness of the proposed optimal DR strategy to provide frequency regulation with reduction in cost for the utility, without sacrificing system stability.

Economic Model of DR in PJM Electricity Market

Different economic models for DR have been proposed in the literature [5.14]-[5.18]. One of these models, which has been implemented in an actual power system, is introduced in [5.18]. PJM, as a regional transmission organization (RTO) and a part of the eastern U.S. interconnection grid with more than 51 million customers [5.20], established hourly markets for regulation and the contingency reserves including a real-time DR market. Two types of DR programs are offered by PJM: Emergency DR Program and Economic DR Program [5.18]. This section focuses on the latter, which is formalized as follows:

"PJM pays the Locational Marginal Price (LMP) to customers if the LMP in a given zone is above a trigger point (set by PJM at $75/MWh). When the LMP is less than

or equal to $75/MWh, PJM pays the customer the difference between the LMP and the generation and transmission (G&T) components of the customer's bill [5.18]. In PJM, LMP is defined as the cost to serve the next MW of load at a specific location, using the lowest production cost of all available generation, while observing all transmission limits. The cost of marginal losses is not currently included in the PJM implementation of LMP [5.20].''

PJM offers this economic DR program in both its day-ahead and real-time markets. Although the PJM real-time economic DR program deals with hourly market, this model is adopted in instantaneous DR market in this chapter. The incentives to the customers who participated in the DR market will be in the form of payment related to the LMP at the time of the demand curtailment [5.18]. The direct payment to the ith market participant curtailing 1 MW of demand (known as Cost of DR, CoDR) is given by [5.18]:

$$CoDR_{i,t} = \begin{cases} LMP_{i,t} & LMP_{i,t} \geq LMP^{*} \\ \left(LMP_{i,t} - GT_i\right) & GT_i < LMP_{i,t} < LMP^{*} \\ 0 & GT_i > LMP_{i,t} \end{cases} \tag{5.1}$$

where $CoDR_{i,t}$ is the cost of DR for the participants in zone i at time t, $LMP_{i,t}$ is the locational marginal price in zone i at time t, GT_i is the cost of generation and transmission for the participants in zone i, and LMP^{*} is the trigger locational marginal price.

Based on (5.1), if the $LMP_{i,t}$ price is greater than the trigger price, then the utility will pay the full price to the DR participants at that time. Considering the fact that the $LMP_{i,t}$ is basically the cost of the spinning reserve in zone i at time t, it seems as there is

no benefit for the utility in this situation for doing DR. The truth is, as it is shown in the results section, the utility will save money even in this case because of loss reduction due to DR. In addition, there are certain economic advantages for the utility in two other situations [the last two conditions given in (5.1)] due to the difference between the cost of spinning reserve and DR. Therefore, the utility will benefit through AS provided by DR.

Once the $LMP_{i,t}$ goes below the trigger price, the utility will not pay anything to the DR participants. Therefore, there is no motivation for the customers to participate in the real-time DR program. In this chapter, it is assumed that no individual loads participate in the real-time DR market when $LMP_{i,t}$ is less than the trigger price. Consequently, two possible scenarios can be derived based on the $LMP_{i,t}$ and LMP^{*}.

Proposed Optimal DR Strategy

In this chapter, the aforementioned PJM economic DR model is employed to develop the proposed optimal DR strategy. The goal is to minimize the cost of DR for the utility in the real-time market without sacrificing system stability. The schematic diagram of the proposed optimal DR strategy is depicted in Figure 5.1. This strategy can be applied to any distribution feeder configuration with the three following assumptions:

- ✓ Two-way communication is required to the individual customers' loads.
- ✓ The size of the system will determine the complexity of the optimization problem. Therefore, achieving optimal or near optimal solution should be feasible in a given time step.
- ✓ The system frequency is assumed to be the same at different locations along the grid, which is a reasonable assumption for small distribution feeders. Although,

the proposed method can be extended for larger distribution feeders with different frequency.

As shown in Figure 5.1, the single frequency measurement at the point of common coupling (PCC) is the input to the "DR Strategy Unit". This unit is in charge of determining the total amount of responsive load which has to be turned off to balance generation and demand and stabilize the system frequency regardless of its interruption cost. Two DR strategies have been developed for the real-time DR applications. One is based on AHC control [5.12] and the other, called Comprehensive Controller, is based on the combination of the AHC and a step-by-step (SBS) controller [5.13]. Both methods are explained in Chapter 3.

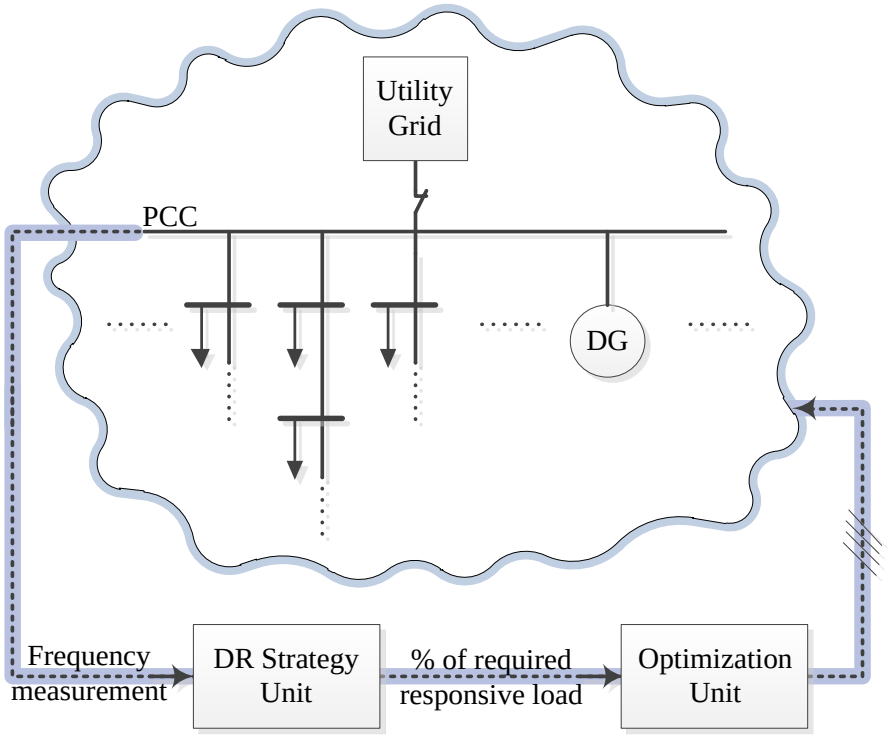


Figure 5.1. Schematic diagram of the proposed optimal DR strategy.

The comprehensive control strategy discussed in Chapter 3 is used in this chapter as well. In this control strategy, the AHC controller calculates the required amount of responsive load to be turned off depending on the frequency deviation from its normal value, and the SBS controller takes action once the AHC controller has brought the frequency deviation within ±0.05 Hz. The SBS controller is responsible for minimizing the amount of manipulated responsive load at steady-state and therefore provides improved quality of service (QoS) to the customers. As a result of improved customers' QoS, a larger amount of responsive load will be available for further frequency stabilization in case needed. This way, the cost of DR to the utility is reduced because fewer customer loads are manipulated.

Once the total amount of manipulated load has been determined by the "DR Strategy Unit", the "Optimization Unit" calculates the share of each individual load in the DR market based on the final cost for the utility. The objective function is set to minimize the cost of DR for the utility subject to some equality and inequality constraints. Different heuristic and gradient-based optimization techniques can be used to solve this problem based on two important factors: the time interval of optimization and the size of the problem. Usually, gradient-based methods have very slow convergence and high probability of being trapped in the local minima. However, they are more reliable for near optimal solutions in larger systems. In this chapter, as a first step, LP-simplex method is chosen for cost optimization because of the linear nature of the objective function and linear equality/inequality constraints. MATLAB®/Optimization Toolbox [5.21] has been used to evaluate the effectiveness of the method in real-time cost

optimization for DR.

Simplex Method

LP has a diverse range of real-life applications in economic analysis, planning, operations research, computer science, and engineering due to its simplicity [5.22]. It is well-known that the number of iterations in the simplex method is just a small multiple of the problem dimension [5.22], which consequently hold it as a promising candidate in this chapter. The general form of LP problem is stated as [5.22]:

$$\begin{aligned} &\boldsymbol{min}\ \ f(x) = C^T \boldsymbol{.} x \\ &Subject\ to\boldsymbol{:}\ \begin{cases} A\boldsymbol{.}x = b \\ x \geq 0 \end{cases} \end{aligned} \tag{5.2}$$

where *f(x)* is the objective function, *x* is the decision variable vector, *C* is the linear objective function coefficient vector, and *A* and *b* are the equality constraints. Further details on the LP-Simplex method can be found in standard optimization textbooks, e.g. [5.22].

According to (5.1), two different scenarios can be designed based on the $LMP_{i,t}$:

*Scenario I***:** When the trigger price (LMP^*) is assumed to be less than $LMP_{i,t}$. In this case, based on (5.1), the utility is responsible to pay the fixed $LMP_{i,t}$ price to the DR market participants. Therefore, the price for DR for all individual loads is the same as the cost of spinning reserve, and there is no need for optimization based on the final cost of DR for the utility. However, a loss minimization algorithm for DR will help to show a possible increase in the benefits of DR for the utility. This cost of DR (*CoDR*) for the utility can be calculated as follows:

$$CoDR_t = \sum_i (P_i.t) \times LMP_{i,t} \quad \text{for each period} \tag{5.3}$$

where P_i is the amount of manipulated power from responsive load i (MW), t is the time duration (hour), and i is the number of responsive loads participating in the DR market.

Scenario II: In this scenario, $GT_i<LMP_{i,t}<LMP^*$. In this case, according to (5.1), the DR participants will receive the difference between $LMP_{i,t}$ and GT_i cost in their zone. Since the price of generation and transmission for different individual loads is not the same, the cost of DR for the utility will be different for different customers. Therefore, it is beneficial to the utility to do DR based on the minimum cost, and based on (5.2), the LP problem for the proposed optimal DR can be defined as follows:

$$\textbf{min } CoDR_t = \sum_i (P_i.t) \times (LMP_{i,t} - GT_i)$$
$$Subject\ to: \begin{cases} \sum_i P_i = P_{total,t} \\ P_i < P_{i,max} \end{cases} \tag{5.4}$$

where $P_{total,t}$ is the total amount of responsive load which should be turned off, and $P_{i,max}$ is the maximum amount of responsive load i participating in the DR market. Remember that $P_{total,t}$ is already determined by the "DR Strategy Unit" at each time step.

System of Study

To verify the effectiveness of the proposed optimal DR strategy, it was implemented on the IEEE standard 13-bus distribution network, [5.23], [5.24], shown in Figure 5.2. In order to be able to observe the frequency behavior of the system as a MG, the utility source of the original model was replaced with a 15-MW diesel generator

(DiG). The torque of the DiG can be adjusted to set the DiG's operating point (e.g., to light or heavy loading). The dynamic model for the diesel engine with a speed governor and excitation controller and synchronous generator are extracted from MATLAB®/Simulink SimPowerSystems toolbox [5.25]. The parameters of the DiG are given in Table 5.1 [5.25].

Table 5.1. The DiG parameters.

Synchronous generator parameters	
Nominal power	15 MVA
Line-to-line voltage	69 kV
Nominal frequency	60 Hz
d-axis reactance (X_d, $X_{d'}$, $X_{d''}$)	1.305, 0.296, 0.252 p.u.
q-axis reactance (X_q, $X_{q'}$, $X_{q''}$)	0.474, 0.243, 0.18 p.u.
Inertia coefficient	2.2 sec
Governor and Diesel Engine parameters	
Regulator gain	40
Regulator time constants (T_1, T_2, T_3)	0.01, 0.02, 0.2 sec
Engine time delay	0.14 sec
Excitation controller parameters	
Regulator gain	200
Regulator time constants	0.02 sec
Damping filter gain and time constant	0.001, 0.1 sec

To observe the system frequency deviation, the maximum mechanical torque of the DiG is limited to a certain point in each case. A 0.6-MW load is also added at the PCC to increase the overall load so that the frequency deviation from 60 Hz can be noticeable.

The distribution system shown in Figure 5.2 includes five aggregated loads which are located in different zones of the feeder with different losses. 15% of the nominal capacity of each load is considered to be available for DR. Also, two-way communication

between the utility control center and each load is assumed to be available. The G&T cost for the different loads maybe different, depending on their location. The G&T costs used in this study are given in Table 5.2. The $LMP_{i,t}$ is assumed to be the same for all five zones, as LMP_t.

Table 5.2. G&T prices for different zones.

	Load 1 (*i=1*)	Load 2 (*i=2*)	Load 3 (*i=3*)	Load 4 (*i=4*)	Load 5 (*i=5*)
GT_i ($/MWh)	47	45	40	53	50

Simulation Studies

As mentioned earlier, two different scenarios are considered in this chapter for DR and conventional frequency regulation cost calculations. As discussed in section 5.6.1, Scenario I, the cost of DR for all individual loads is the same as the cost of spinning reserve. Therefore, no cost optimization is needed for this scenario. In this case, simulation studies have been carried out for conventional frequency regulation (Con-f-reg) and DR with no optimization (DR-no-opt). However, Scenario II includes three different studies: "Con-f-reg," "DR-no-opt," and Optimal DR (Opt-DR). In the case of "Con-f-reg," spinning reserve is considered as conventional AS which will be provided by the DiG. Therefore, the limitations on the DiG torque have been removed in this case. In other words, 100% of the load demand is accommodated by the DiG with the price of LMP_t. Furthermore, the cost/benefit analysis is only performed for a heavy loading condition, under which the frequency drops below 60 Hz and the utility needs to disconnect a part of the load if spinning reserve is not used.

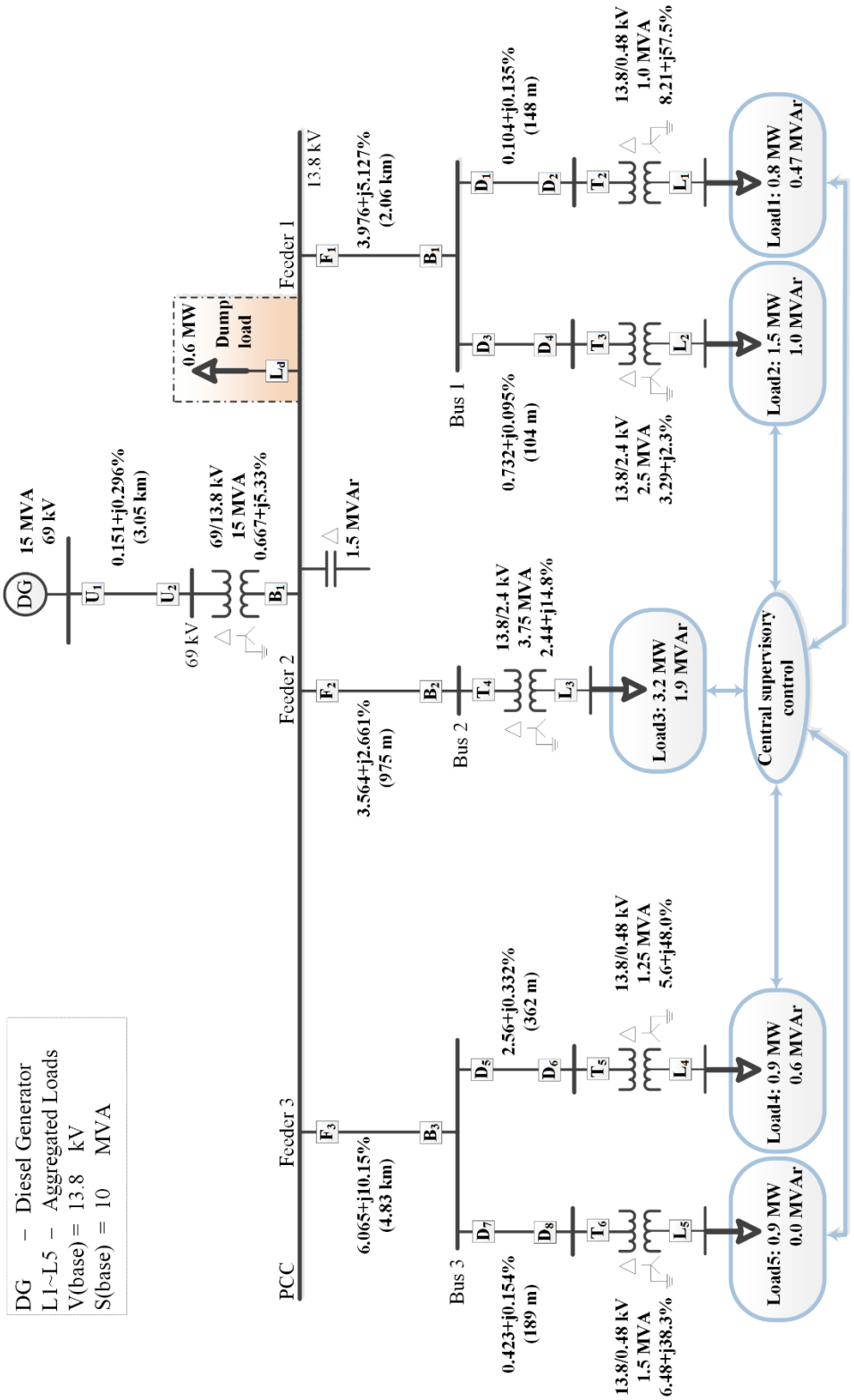


Figure 5.2. Modified IEEE 13-bus standard distribution system schematic diagram.

All calculations in this section have been done for 50 sec, the DR strategy is updated every 20 msec, and the average computation time of optimization is less than 1 msec. All simulations are done on a desktop with 2 Intel® Zeon® 2.13 GHz processors.

Scenario I

In this case, the 0.6-MW dump load is added to the MG at t=7 sec. The LMP_t and the trigger price (LMP^*) are assumed to be \$90/MWh and \$75/MWh, respectively. These are the prices used by PJM [5.18]. As a result, system frequency starts to deviate from 60 Hz. In the "Con-f-reg" case, the excess required power is provided by the DiG while in the "DR-no-opt" case the balance between generation and demand is achieved through DR. As a result, the "DR-no-opt" case shows 1.98% reduction in the cost of frequency regulation through DR for the utility compared to the "Con-f-reg" case through purchasing more power from spinning reserve. This percentage of improvement, especially when the cost of spinning reserve and DR are the same, is a consequence of less power loss in the MG as a result of DR. It is well-known that power loss reduction is one of the countless advantages of DR for the utility through disconnecting a portion of the responsive loads. The 1.98% savings proves this fact in this relatively small MG.

Figure 5.3 shows the system frequency for the two cases in Scenario I. It can be observed that the frequency is in the acceptable range (60±0.05 Hz) in both cases studied. But, as noted above, the "DR-no-opt" case achieves frequency stabilization with a reduced cost of frequency regulation for the utility. In Figure 5.4, the percent variation in responsive load is shown for the "DR-no-opt" case. During the transient period, more responsive loads are used to regulate the system frequency as fast as possible. However,

the overall responsive load variation was not jeopardized the system stability. The negative sign by the responsive load changes in Figure 5.4 shows a decrease in the amount of responsive load (i.e., the percentage of responsive loads that have been turned off at any given time). In the "Con-f-reg", no responsive load has been changed. In other words, frequency regulation has been provided by the DiG in the "Con-f-reg" case.

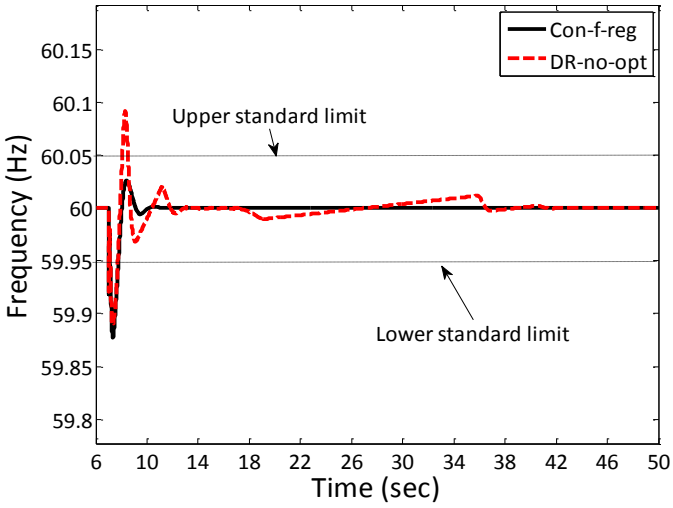


Figure 5.3. System frequency in Scenario I.

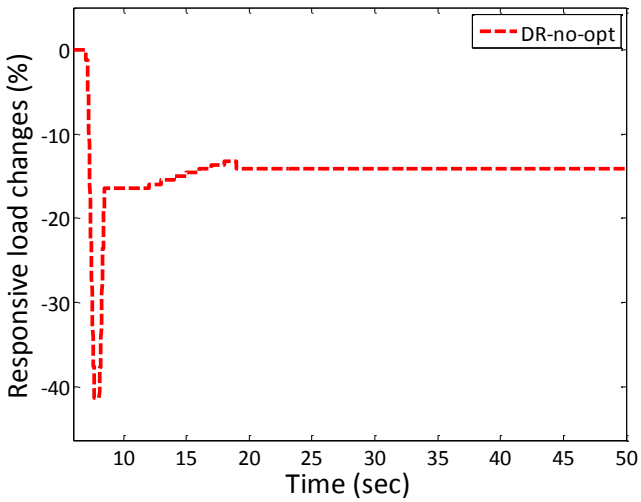


Figure 5.4. Total responsive load changes in Scenario I.

Scenario II

In this scenario, in addition to the "Con-f-reg" and the "DR-no-opt", the proposed optimal DR is also applied. The LMP_t and the trigger price (LMP^*) are assumed to be US$60/MWh and US$75/MWh, respectively. The same simulation studies, carried out in Scenario I, were also carried out for Scenario II for all three cases. Both the DR strategies show a significant reduction in the frequency regulation cost. The "DR-no-opt" case has 23.8% cost reduction and the "Opt-DR" has a cost savings of 28.8%. Therefore, the cost savings of the "Opt-DR" compared to the "DR-no-opt" is 5% in this case. The cost savings through "Opt-DR" will be more significant for larger grids and MGs.

Figure 5.5 shows the frequency response for the three cases discussed. It can be concluded that the DR strategy has no significant negative impact on the system frequency regulation compared to conventional ancillary services. The small spike in frequency during the transient period for the DR strategy has negligible effect on the system frequency response.

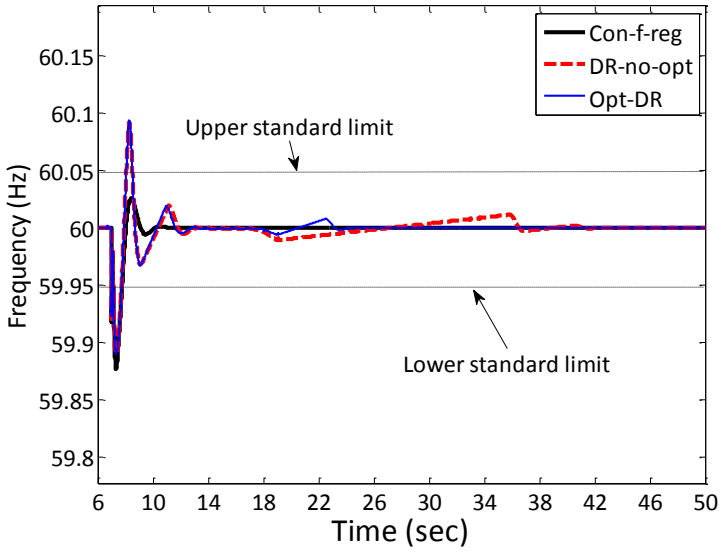


Figure 5.5. System frequency in Scenario II.

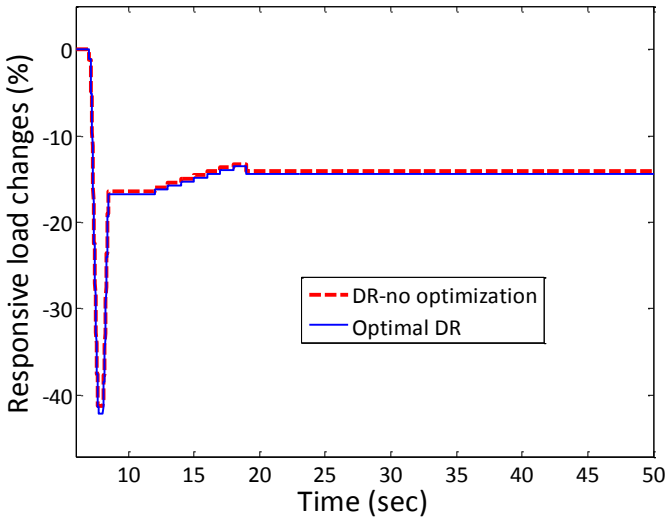


Figure 5.6. Total responsive load changes in Scenario II.

In Figure 5.6, the response of DR strategy for responsive load variation is shown for both the "DR-no-opt" and "Opt-DR". The amount of manipulated responsive load is essentially the same in both cases.

Conclusion

This chapter presents a general optimal DR strategy for frequency regulation in a MG. The proposed algorithm includes a comprehensive DR strategy, presented in Chapter 3 and in [5.13], along with the optimization technique (LP-simplex method). Simulation results show the effectiveness of the general DR strategy versus conventional AS through spinning reserve. More importantly, the proposed optimal DR strategy shows even more cost reduction for the utility while it shows no significant negative impact on the frequency response.

Acknowledgement

This work was in part supported by Pacific Northwest National Laboratory (PNNL), which is operated for the U.S. Department of Energy by Battelle under Contract DE-AC05-76RL01830, and by the DOE Award DE-FG02-11ER46817.

References Cited

[5.1] U.S. Dept. of Energy, "Benefits of demand response in electricity markets and recommendations for achieving them," a report to U.S. Congress, Feb. 2006. Available online: http://eetd.lbl.gov/ea/ems/reports/congress-1252d.pdf

[5.2] Federal Energy Regulatory Commission, "Assessment of demand response and advanced metering," A report to U.S. Congress, Dec. 2008. Available online: http://www.ferc.gov/legal/staff-reports/demand-response.pdf

[5.3] M.H. Albadi and E.F. El-Saadany, "A summary of demand response in electricity markets," *Electr. Pow. Syst. Res.*, vol. 78, no. 11, pp. 1989–1996, Nov. 2008.

[5.4] A. Brooks, et al., "Demand dispatch: using real-time control of demand to help balance generation and load," *IEEE Power Energy Mag.*, vol. 8, no. 3, pp. 20–29, May/June 2010.

[5.5] D. Trudnowski, M. Donnelly, and E. Lightner, "Power-system frequency and stability control using decentralized intelligent loads," in *Proc.* IEEE PES Transmission and Distribution Conf. and Exhibition, Dallas, TX, 2005, pp. 1453–1459.

[5.6] G.C. Heffner, C.A. Goldman, and M.M. Moezzi, "Innovative approaches to verifying demand response of water heater load control," *IEEE Trans. on Power Delivery*, vol. 21, no. 1, pp. 388–397, Jan. 2006.

[5.7] J.A. Short, D.G. Infield, and L.L. Freris, "Stabilization of grid frequency through dynamic demand control," *IEEE Trans. Power Syst.*, vol. 22, no. 3, 1284–1293, Aug. 2007.

[5.8] R. Jia, M.H, Nehrir, and D.A. Pierre, "Voltage control of aggregate electric water heater load for distribution system peak load shaving using field data," in *Proc.* 39th North American Power Symposium (NAPS '07), Las Cruces, NM, 2007, pp. 492–497.

[5.9] J. Kondoh, N. Lu, and D.J. Hammerstrom, "An evaluation of the water heater load potential for providing regulation service," *IEEE Trans. Power Syst.*, vol. 26, no. 3, pp. 1309–1316, Aug. 2011.

[5.10] A. Molina-Garcia, F. Bouffard, and D.S. Kirschen, "Decentralized demand-side contribution to primary frequency control," *IEEE Trans. Power Syst.*, vol. 26, no. 1, pp. 411–419, Feb. 2011.

[5.11] D. Angeli and P-A. Kountouriotis, "A stochastic approach to dynamic-demand refrigerator control," *IEEE Trans. Control Syst. Technol.*, vol. 20, no. 3, pp. 581–592, May 2012.

[5.12] S.A. Pourmousavi and M.H. Nehrir, "Demand response for smart microgrid: Initial results," in *Proc*. IEEE PES Innovative Smart Grid Technologies (ISGT), Anahiem, CA, 2011, pp. 1–6.

[5.13] S.A. Pourmousavi, M.H. Nehrir, and C. Sastry, "Providing ancillary services through demand response with minimum load manipulation," in *Proc*. North American Power Symposium (NAPS), Boston, MA, 2011, pp. 1–6.

[5.14] J. Medina, N. Muller, and C.I. Roytelman, "Demand response and distribution grid operations: opportunities and challenges," *IEEE Trans. Smart Grid*, vol. 1, no. 2, pp. 193–198, Sept. 2010.

[5.15] H. Saele and O.S. Grande, "Demand response from household customers: experiences from a pilot study in Norway," *IEEE Trans. Smart Grid*, vol. 2, no. 1, pp. 102–109, March 2011.

[5.16] A.J. Conejo, J.M. Morales, and L. Baringo, "Real-time demand response model," *IEEE Trans. Smart Grid*, vol. 1, no. 3, pp. 236–242, Dec. 2010.

[5.17] D.T. Nguyen, M. Negnevitsky, and M. de Groot, "Pool-based demand response exchange-concept and modeling," *IEEE Trans. Power Syst.*, vol. 26, no. 3, pp. 1677–1685, Aug. 2011.

[5.18] R. Walawalkar, at. Al., "An economic welfare analysis of demand response in the PJM electricity market," *Energ. Policy*, vol. 36, no. 10, pp. 3692–3702, Oct. 2008.

[5.19] M. Klobasa, "Analysis of demand response and wind integration in Germany's electricity market," *IET Renew. Pow. Gen.*, vol. 4, no. 1, pp. 55–63, Jan. 2010.

[5.20] PJM Electricity Utility, Available online: http://pjm.com/about-pjm.aspx

[5.21] MATLAB/ Optimization Toolbox, document, Available online: http://www.mathworks.com/help/pdf_doc/optim/optim_tb.pdf

[5.22] A. Antoniou and W.S. Lu, *Practical optimization algorithms and engineering applications*, Springer Science, NY, 2007.

[5.23] F. Katiraei, M.R, Iravani, and P.W. Lehn, "Micro-grid autonomous operation during and subsequent to islanding process," *IEEE Trans. Power Del.*, vol. 20, no. 1, pp. 248–257, Jan. 2005.

[5.24] V. Menon and M.H. Nehrir, "A hybrid islanding detection technique using voltage unbalance and frequency set point," *IEEE Trans. Power Syst.*, vol. 22, no. 1, pp. 442–448, Feb. 2007.

[5.25] MATLAB/Simulink SimPowerSystems document, Available online: http://www.mathworks.com/

CHAPTER 6

INTRODUCING DYNAMIC DEMAND RESPONSE IN THE LFC MODEL

Contribution of Authors and Co-Authors

Manuscripts in Chapters 2 through 12

Author: S. A. Pourmousavi

Contributions: Developed the idea of adding real-time DR control loop in the well-known LFC model, derived the state-space model of the proposed LFC-DR model, linearized the nonlinear component of the model (namely DR delay), derived steady-state, sensitivity, and stability formulations of the proposed LFC-DR model, designed different simulation studies, and prepared the manuscript, figures, tables, and interpretation of the results.

Co-author: M. H. Nehrir

Contributions: Provided important insight and overview of the research, interpretation of the results, and aided in the preparation of the manuscript.

Manuscript Information Page

Seyyed Ali Pourmousavi Kani, M. Hashem Nehrir

IEEE Transactions on Power Systems, 2014

Status of the manuscript:
____ Prepared for submission to a peer-reviewed journal
____ Officially submitted to a peer-reviewed journal
____ Accepted by a peer-reviewed journal
_X_ Published in a peer-reviewed journal

Published by the Institute of Electrical and Electronics Engineering (IEEE)

This article has been accepted for inclusion in a future issue of this journal. Content is final as presented, with the exception of pagination.

Introducing Dynamic Demand Response in the LFC Model

S. Ali Pourmousavi, *Student Member, IEEE*, and M. Hashem Nehrir, *Life Fellow, IEEE*

***Abstract*—Demand response (DR) has proved to be an inevitable part of the future grid. Much research works have been reported in the literature on the benefits and implementation of DR. However, little works have been reported on the impacts of DR on dynamic performance of power systems, specifically on the load frequency control (LFC) problem. This paper makes an attempt to fill this gap by introducing a DR control loop in the traditional LFC model (called LFC-DR) for a single-area power system. The model has the feature of optimal operation through optimal power sharing between DR and supplementary control. The effect of DR communication delay in the controller design is also considered. It is shown that the addition of the DR control loop increases the stability margin of the system and DR effectively improves the system dynamic performance. Simulation studies are carried out for single-area power systems to verify the effectiveness of the proposed method.**

***Index Terms*—Demand response (DR), linear quadratic regulator (LQR), sensitivity, single-area power system model, smart grid, stability, steady-state error.**

I. Introduction

TRADITIONALLY, frequency regulation in power system is achieved by balancing generation and demand through load following, i.e., spinning and non-spinning reserves [1]. The future power grid, on the other hand, is foreseen to have high penetration of renewable energy (RE) power generation, which can be highly variable. In such cases, energy storage and responsive loads show great promise for balancing generation and demand, as they will help to avoid the use of the traditional generation following schemes, which can be costly and/or environmentally unfriendly.

Given the limited availability, low efficiency, and high cost of large storage devices, real-time smart responsive load participation, known as demand response (DR), has been actively considered for power balancing. It can be achieved by active consumer participation in real-time to maintain balance between generation and demand with two-way communication [2]. It is well known that DR increases system reliability and flexibility to manage the variability and uncertainty of some RE resources, decreases the cost of operation, and enhances system efficiency. Furthermore, DR can be used to provide ancillary services (AS) for regulation reserve and to respond momentarily to the area control error (ACE). Although AS are called more frequently than traditional load shedding events, the annual total hours of curtailment is much less, and individual events are much shorter. Thus, AS programs may appeal to retail customers, as they will find more frequent and short on/off switching of some of their end-use loads more acceptable than infrequent and long curtailments [3]. Examples of customer end-use loads that have instantaneous response and are potential candidates for DR are electric water heaters (EWHs) and HVACs. For the above reasons considerable attention has been recently given to DR for different purposes, e.g., economic benefits of DR [4]–[8], offline planning and day-ahead scheduling [9]–[15], availability assessment of the DR resources for reserve capacity [16]–[18], and analysis of the effectiveness of DR in providing AS at the islanded distribution-level microgrids [19]–[21]. A number of studies have also addressed the effectiveness of decentralized dynamic demand control on stabilization of grid frequency, mainly at the transmission level [22]–[31]. However, the above studies present the following shortcomings:

- They do not present a general framework for the analysis of the impacts of DR on a general power system model and load [22]–[28], [30], [31].
- AGC model has not been considered in the analysis [22], [24]–[28], [30].
- Only specific loads (such as HVAC, EWHs and lighting) have been considered in [23], [24], [27] and specific power systems without generalization [22], [23], [25]–[28], [30].
- Communication delay in central DR, and measurement delay in decentralized DR have not been considered [22]–[26], [30], [31].
- Frequency regulation as AS have not been studied. Only under-frequency load shedding (UFLS) characterization has been analyzed [30], [31].
- Unreal assumptions for the availability of DR at all times have been made [29].
- Load-damping coefficient, which can improve frequency stabilization, has been ignored [27].
- Only sensitivity analysis of frequency-related load-damping coefficient characteristic without generalization and DR control is presented [31].

In the last five decades, traditional LFC models have been revised and modified to include the different types of power plants, including RE power generation with actual limitations, such as ramp-up/down limits, in the traditional and de-regulated power market [32], [33]. These models are useful in small disturbance studies such as small variations in load and generation,

Manuscript received February 01, 2013; revised March 01, 2013, June 05, 2013, August 13, 2013, and October 15, 2013; accepted December 11, 2013. This work was supported by the U.S. Department of Energy, Office of Science, Basic Energy Sciences , under Award # DE-FG02-11ER46817. Paper no. TPWRS-00140-2013.

The authors are with the Electrical and Computer Engineering Department, Montana State University, Bozeman, MT 59717 USA (e-mail: s.pourmousavikani@msu.montana.edu; hnehrir@ece.montana.edu).

Digital Object Identifier 10.1109/TPWRS.2013.2296696

0885-8950 © 2014 IEEE. Personal use is permitted, but republication/redistribution requires IEEE permission.
See http://www.ieee.org/publications_standards/publications/rights/index.html for more information.

This article has been accepted for inclusion in a future issue of this journal. Content is final as presented, with the exception of pagination.

and in controller design. However, so far in the literature, the concept of control in the LFC model has only focused on the generation side, and DR has not been included in these studies. In this paper we modify the general small-signal model of a power system used in LFC studies by introducing a DR control loop to the LFC model (called LFC-DR).

Other goals of the paper are to make the model as general as possible and to include communication latency associated with DR between the load aggregator companies (Lagcos) and the end-use customers' devices. This is an important parameter in the system dynamic performance of LFC-DR. We have assumed the communication delay between the balancing authority (BA) and the Lagcos to be the same as that between the BA and generation companies (Gencos). We have not considered these delays in our study since the focus of this paper is on the evaluation of the DR loop in the LFC model. The proposed LFC-DR also gives an opportunity to the system operator to choose the DR option or spinning/non-spinning reserve, or a combination of the two, based on the real-time market price. Furthermore, the LFC-DR model can be used to estimate the actual value of the required responsive load manipulation when the magnitude of the disturbance is unknown to the system operator.

Another motivation for this study is the importance of the dynamic performance of a power system with DR to provide AS. Several real cases of DR operation have revealed that extreme shedding of the responsive loads in emergency DR could lead to unexpected power oscillations, which complicate the sequential generation control [34], [35]. The LFC-DR model will help the operators to investigate the impact of DR on the dynamic performance of the system prior to its usage and during the automatic generation control (AGC) design process.

The idea of DR for AS used in this paper, has been fully explored in our previous work [21] and will not be repeated here. In such a model, the Lagcos will work with the customers and inform the utilities, e.g., independent system operators, of the amount of DR available. An example of such a model is the PJM electricity market [4].

The remainder of this paper is organized as follows: In Section II, the concept of LFC-DR model is developed for a single-area power system. The model is analytically evaluated in Section III. The controller design is presented in Section IV, and simulation results are given in Section V. Section VI includes a discussion of exceptional cases not explored in this paper and the future work. Finally, the paper is concluded in Section VII.

II. Problem Formulation for Single-Area Power System

The general low-order linearized power system model for the purpose of frequency control synthesis and analysis is given by the power balance equation in the frequency-domain [33], [36]:

$$\Delta P_T(s) - \Delta P_L(s) = 2H.s.\Delta f(s) + D.\Delta f(s) \qquad (1)$$

where

$\Delta P_T(s) - \Delta P_L(s)$	incremental power mismatch;
$\Delta f(s)$	frequency deviation;

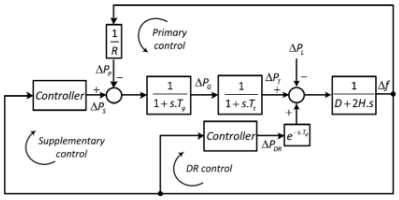


Fig. 1. Block-diagram representation of a single-area power system model.

$2H$	equivalent inertia constant;
D	equivalent load-damping coefficient;
s	Laplace transform operator.

Since DR for AS performs like spinning reserve in magnitude and power flow direction, i.e., once frequency deviation is negative (positive), it is required to turn OFF (ON) a portion of the responsive loads (i.e., DR), (1) can be simply modified as follows to include DR:

$$\Delta P_T(s) - \Delta P_L(s) + \Delta P_{DR}(s) = 2H.s.\Delta f(s) + D.\Delta f(s). \qquad (2)$$

In some earlier works such as [25], [26], and [31], the effect of DR has been included in the load-damping coefficient, D. We believe the effect of DR should be separated because D is an inherent parameter of the system and is not a controllable one, whereas DR is an intentional control signal. In addition, (2) will permit to have a separate control loop for DR, which is more realistic and gives a better structure for controller design. The block diagram for single-area power system with a simplified non-reheat steam turbine is shown in Fig. 1, where the feedback loop for DR is also shown. T_g and T_t are the equivalent speed-governor and turbine time constants, respectively, R is the equivalent droop value, and T_d is the equivalent DR delay. The parameters of the system can be the equivalent of all generation assets and load damping of the same area. This model is selected to convey the main idea of this paper. In our future work, this model will be extended to multi-area interconnected power systems with multiple Gencos and Lagcos.

Unlike the usual spinning reserve-provider power plants, there is no ramp up and down limitations on the DR resources. In other words, the power consumption status of controllable loads can be changed instantaneously by the command signal they receive. Therefore, the only obstacle for DR (disregarding the aggregation of small loads) is communication delay, known as latency, which could affect the system dynamic performance.

A. State-Space Dynamic Model for LFC-DR

State-space representation of the LFC model is a useful tool for the application of modern/robust control theory [33]. It can also be used for creating a general framework of LFC in dynamic frequency analysis which can be conveniently modified and applied to power system of any size. We therefore derive the dynamic model of the power system, including DR in the state-space representation, to study the effect of DR on LFC performance and controller design. Although the proposed LFC-DR model of Fig. 1 is based on a simplified power system model

This article has been accepted for inclusion in a future issue of this journal. Content is final as presented, with the exception of pagination.

with a non-reheat steam turbine, similar analysis and conclusions can be extended to other types of turbines, such as hydro or reheat-steam turbine.

The state-space realization of a single-area power system with DR (shown in Fig. 1) is given by

$$\dot{\mathbf{x}}(t) = \mathbf{A}.\mathbf{x}(t) + \mathbf{B}.\mathbf{u}(t) + \mathbf{\Gamma}.w(t)$$
$$y(t) = \mathbf{C}.\mathbf{x}(t) \tag{3}$$

where $\mathbf{A}$ is the system matrix, $\mathbf{B}$ is the control input matrix, $\mathbf{\Gamma}$ is the disturbance matrix, $\mathbf{x}$ is the state vector, $\mathbf{u}(t)$ is the input vector, $w(t)$ is the disturbance variable, $\mathbf{C}$ is the observation matrix, and $y(t)$ is the system output. In order to derive the linear state-space model of the system, it is required to have a linear model of the system under study. From Fig. 1, it can be seen that the system has only one nonlinear element which is the time delay in the DR control loop. Therefore, we need to linearize the time delay for derivation of the linear state-space model. *Padé* approximation, used for linearizing the DR time delay, is explained in the following subsection.

B. Padé Approximation

Padé approximation has been widely used to linearize systems with time delays in control engineering with very strong convergent results [37]. It basically approximates time delays by a quotient of polynomials. Specifically, the *Padé* function for $e^{-s.T_d} \approx R_{pq}(-s.T_d)$ is defined as follows [38]:

$$R_{pq}(e^{-s.T_d}) = D_{pq}(e^{-s.T_d})^{-1}.N_{pq}(e^{-s.T_d}) \tag{4}$$

where

$$N_{pq}(e^{-s.T_d}) = \sum_{k=0}^{p} \frac{(p+q-k)!p!}{(p+q)!k!(p-k)!}.(-s.T_d)^k \tag{5}$$

$$D_{pq}(e^{-s.T_d}) = \sum_{k=0}^{q} \frac{(p+q-k)!q!}{(p+q)!k!(q-k)!}.(s.T_d)^k. \tag{6}$$

N_{pq} and D_{pq} are polynomials of order p and q, respectively. It is usually common for the numerator and denominator of the approximation fractional functions to have the same order, and the order usually varies between 5 and 10 [37]. Fig. 2 shows the phase of the step response in frequency-domain of the *Padé* approximation with different orders in comparison to a pure time delay of 0.1 sec. Since the cut-off frequency of the low pass filters, i.e., speed-governor and turbine, in the model of the power system are usually less than 15 rad/sec, the 5th-order *Padé* approximation is acceptable and is used in this study. The magnitudes of all orders of *Padé* approximation in the frequency domain have also been compared to that of pure time delay. They are all at 0 dB and not shown here.

The signal flow graph for the state-space model of the power system shown in Fig. 1 with 5th-order *Padé* approximation is sketched in Fig. 3. The state variables are also shown in this figure for future reference. The gains of the feedback and feed-

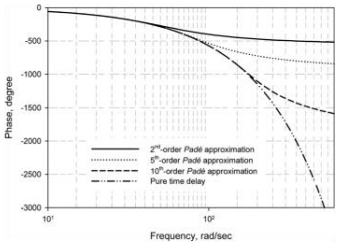


Fig. 2. Different order of *Padé* approximation for pure time delay, $T_d = 0.1$ sec.

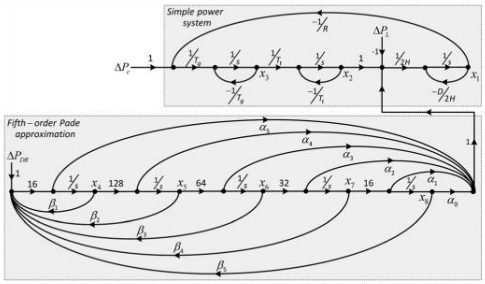


Fig. 3. Signal flow graph of the single-area power system model with 5th-order *Padé* approximation.

TABLE I
Padé APPROXIMATIONS FEED-FORWARD AND FEEDBACK VALUES FOR SIGNAL FLOW GRAPH

α_0	α_1	α_2	α_3	α_4	α_5
$945/2^{21}.T_d^5$	$-945/2^{22}.T_d^4$	$105/2^{17}.T_d^3$	$-105/2^{15}.T_d^2$	$15/2^9.T_d$	$-1/2^4$
	β_1	β_2	β_3	β_4	β_5
	$-15/2^3.T_d$	$-105/2^9.T_d^2$	$-105/2^{12}.T_d^3$	$-945/2^{18}.T_d^4$	$-945/2^{21}.T_d^5$

forward paths of the 5th-order *Padé* approximation are given in Table I. T_d is the DR communication latency.

With the above approximation of time delay nonlinearity, the state-space representation of the system (3) has the matrices given in (7)–(10) at the bottom of the next page, where T is the transpose operation of matrices. For more complicated power systems, the upper left partition of matrix A, and the left partitions of other matrices can be modified to represent the new power system model. The other partitions of the matrices should be properly resized based on the order of the new power system model.

III. ANALYTICAL EVALUATION OF THE MODEL

In this section, steady-state error evaluation, sensitivity analysis, and system stability of the LFC model with and without the DR control loop are presented.

This article has been accepted for inclusion in a future issue of this journal. Content is final as presented, with the exception of pagination.

A. Steady-State Error Evaluation

The primary control loop in Fig. 1, known as frequency droop control, is the fastest intentional control action in a power system but it is not enough to make the frequency deviation go to zero at steady-state. For this reason, the supplementary frequency control loop, as shown in Fig. 1, is required for further control. However, the DR control loop is also added to the problem in this study. Therefore, it is necessary to investigate the impact of the DR control loop on the steady-state error of the given power system in Fig. 1. Later in this subsection, a synthesis of controller design, based on optimal sharing between DR and supplementary control loops, will be derived from the steady-state error evaluation.

The conventional LFC steady-state equations are well-documented, e.g. [33], [36]. Adding the DR control loop to the conventional LFC model, the system frequency deviation can be expressed as follows:

$$\Delta f(s) = \frac{1}{2H.s + D}\left[\Delta P_T(s) - \Delta P_L(s) + G(s).\Delta P_{DR}(s)\right] \tag{11}$$

where

$$\Delta P_T(s) = H(s).\left[\Delta P_S(s) - \frac{1}{R}.\Delta f(s)\right], \tag{12}$$

$$H(s) = \frac{1}{(1+s.T_g)(1+s.T_t)}$$

$$G(s) = \frac{-s^5 + \frac{30}{T_d}.s^4 - \frac{420}{T_d^2}.s^3 + \frac{3360}{T_d^3}.s^2 - \frac{15120}{T_d^4}.s + \frac{30240}{T_d^5}}{s^5 + \frac{30}{T_d}.s^4 + \frac{420}{T_d^2}.s^3 + \frac{3360}{T_d^3}.s^2 + \frac{15120}{T_d^4}.s + \frac{30240}{T_d^5}}. \tag{13}$$

It can be seen that any type of power system model with equivalent turbine and governor can be represented by modifying $H(s)$. Substituting (12) into (11) yields

$$\Delta f(s) = \frac{1}{2H.s + D}\left[H(s).\left[\Delta P_S - \frac{1}{R}.\Delta f(s)\right] - \Delta P_L(s) + G(s).\Delta P_{DR}(s)\right]. \tag{14}$$

Solving (14) for $\Delta f(s)$ will result in the frequency deviation equation as follows:

$$\Delta f(s) = \frac{1}{\Psi(s)}.\left[H(s).\Delta P_S(s) + G(s).\Delta P_{DR}(s)\right] - \frac{1}{\Psi(s)}.\Delta P_L(s) \tag{15}$$

where

$$\Psi(s) = 2H.s + D + \frac{H(s)}{R}. \tag{16}$$

In the LFC analysis, it is common to use a step load disturbance for $\Delta P_L(s)$ as

$$\Delta P_L(s) = \frac{\Delta P_L}{s}. \tag{17}$$

Based on the final value theorem, and substituting (17) into (15), the steady-state value of the system frequency deviation can be obtained as follows:

$$\Delta f_{SS} = \lim_{s\to 0} s.\Delta f(s) = \frac{\Delta P_{S,SS} + \Delta P_{DR,SS} - \Delta P_L}{\Psi(0)} \tag{18}$$

where

$$\Delta P_{S,SS} = \lim_{s\to 0} s.H(s).\Delta P_S(s) \tag{19}$$

$$\Delta P_{DR,SS} = \lim_{s\to 0} s.G(s).\Delta P_{DR}(s) \tag{20}$$

$$\Psi(0) = D + \frac{H(0)}{R} = D + \frac{1}{R} \approx B. \tag{21}$$

Therefore, $\Psi(0)$ is equivalent to the system frequency response characteristics, B, and the steady-state frequency deviation can be written as follows:

$$\Delta f_{SS} = \frac{\Delta P_{S,SS} + \Delta P_{DR,SS} - \Delta P_L}{D + \frac{1}{R}}. \tag{22}$$

It can be seen from (22) that the frequency deviation will not be zero unless the supplementary and/or DR controls exist. Also, DR control loop gives an extra degree of freedom for

---

$$\mathbf{A} = \left[\begin{array}{ccc|ccccc} \frac{-D}{2H} & \frac{1}{2H} & 0 & \frac{30}{2H.T_d\times 2^3} & 0 & \frac{105}{2H.T_d^3\times 2^{11}} & 0 & \frac{945}{2H.T_d^5\times 2^{20}} \\ 0 & \frac{-1}{T_t} & \frac{1}{T_t} & 0 & 0 & 0 & 0 & 0 \\ \frac{-1}{R.T_g} & 0 & \frac{-1}{T_g} & 0 & 0 & 0 & 0 & 0 \\ \hline 0 & 0 & 0 & \frac{-30}{T_d} & \frac{-105}{T_d^2\times 2^5} & \frac{-105}{T_d^3\times 2^8} & \frac{-945}{T_d^4\times 2^{14}} & \frac{-945}{T_d^5\times 2^{17}} \\ 0 & 0 & 0 & 128 & 0 & 0 & 0 & 0 \\ 0 & 0 & 0 & 0 & 64 & 0 & 0 & 0 \\ 0 & 0 & 0 & 0 & 0 & 32 & 0 & 0 \\ 0 & 0 & 0 & 0 & 0 & 0 & 16 & 0 \end{array}\right] \tag{7}$$

$$\mathbf{B}^T = \left[\begin{array}{ccc|ccccc} 0 & 0 & \frac{1}{T_g} & 0 & 0 & 0 & 0 & 0 \\ \frac{-1}{2H} & 0 & 0 & 16 & 0 & 0 & 0 & 0 \end{array}\right] \tag{8}$$

$$\mathbf{\Gamma}^T = \left[\begin{array}{ccc|ccccc} \frac{-1}{2H} & 0 & 0 & 0 & 0 & 0 & 0 & 0 \end{array}\right] \tag{9}$$

$$\mathbf{C} = \left[\begin{array}{ccc|ccccc} 1 & 0 & 0 & 0 & 0 & 0 & 0 & 0 \end{array}\right],\ D = [0] \tag{10}$$

This article has been accepted for inclusion in a future issue of this journal. Content is final as presented, with the exception of pagination.

system frequency regulation. In addition, the following conclusions can be drawn from (22):

- The steady-state error is not dependent on the delay and the order of its approximation.
- With DR available in the LFC, a higher reliability of frequency regulation can be achieved, since the DR control loop can complement the supplementary control loop. In cases when the supplementary control is not available, the performance of the frequency regulation can be guaranteed by the DR loop, if enough DR resources are available.
- In order to have zero frequency deviation at steady-state, the required control effort can be split between the supplementary and DR control loops. In other words, an ISO/RTO will have the opportunity to perform the regulation services in a cost effective way and analyze the frequency response of the system quickly. This goal can be achieved only in the proposed formulation [(22)] with an added control loop for DR (Fig. 1).

Further discussion to the last conclusion is: consider a situation where there is no DR available. The frequency error will be zero at steady-state if $\Delta P_{S,SS} = \Delta P_L$. It means that the supplementary control should provide enough spinning and/or non-spinning reserve at the time of disturbance. With DR available in the LFC, the required control effort, called Ω in this study, can be split between the two control loops based on their cost at real-time electricity market as follows:

$$\begin{cases} \Delta P_S(s) = \alpha.\Omega \\ \Delta P_{DR}(s) = (1-\alpha).\Omega \end{cases} \tag{23}$$

where $0 < \alpha < 1$ is the share of traditional regulation services in the required control effort. $\alpha = 1$ means that the total required regulation will be provided by the traditional regulation services, i.e. spinning and non-spinning reserve, and $\alpha = 0$ is for the time when all the required control would be provided by DR. The decision on the value of α should be made by the ISO/RTO, based on the price of DR and the traditional regulation services in a real-time market, explored by the authors in [21]. Then, it is possible for the ISO/RTO to effectively and quickly assess the different scenarios of LFC to evaluate the system performance under various circumstances. Finally, the steady-state value of the two inputs should be

$$\begin{aligned} \Delta P_{S,SS} &= \alpha.\Delta P_L \\ \Delta P_{DR,SS} &= (1-\alpha).\Delta P_L. \end{aligned} \tag{24}$$

B. Sensitivity Analysis for the Feedback System With and Without DR

In this subsection, an analytical method is utilized to study the impact of the DR control loop on the overall sensitivity of the closed-loop system w.r.t. the open-loop system. It is also desired to measure the sensitivity of the closed-loop system w.r.t. the coefficient α. The first sensitivity analysis is quite important since it shows the robustness of the closed-loop system performance when the system parameters are subjected to any change or variation. The second sensitivity analysis is also necessary since α is an important parameter in the performance of the LFC-DR model.

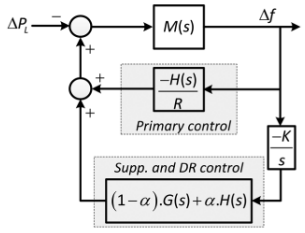


Fig. 4. Modified power system model with integral controller for DR and supplementary control loops.

The power system model shown in Fig. 1 is modified for this part with a single integral controller (with gain K) for both the supplementary and DR control loops, and also for the rest of this paper, as shown in Fig. 4. This modification will also allow us to split the required control effort between the DR and supplementary control loops, as was discussed in Section III-A.

For the power system shown in Fig. 4, the closed-loop transfer function relating the system frequency deviation to a step change in the load can be derived as follows:

$$\begin{aligned} &\left(\frac{\Delta f(s)}{\Delta P_L(s)}\right)_{DR} \\ &= \frac{-M(s)}{1+\frac{H(s).M(s)}{R}+\frac{K}{s}.\alpha.H(s).M(s)+\frac{K}{s}.(1-\alpha).G(s).M(s)} \\ &\left(\frac{\Delta f(s)}{\Delta P_L(s)}\right)_{S} \\ &= \frac{-M(s)}{1+\frac{H(s).M(s)}{R}+\frac{K}{s}.H(s).M(s)} \end{aligned} \tag{25}$$

where K is integral feedback gain of the system and $M(s)$ is

$$M(s) = \frac{1}{D+2H.s}. \tag{26}$$

In (25), the first expression is the closed-loop transfer function when both DR and supplementary control loops are available, whereas the second equation shows the closed-loop transfer function for conventional LFC (with no DR). The open-loop transfer function, where only the primary control exists, can be derived as follows:

$$T_{OL}(s) = \left(\frac{\Delta f(s)}{\Delta P_L(s)}\right)_{OL} = \frac{-M(s)}{1+\frac{H(s).M(s)}{R}}. \tag{27}$$

In order to derive the sensitivity function of the closed-loop system w.r.t. the open-loop system, (25) can be simplified and rearranged using (27) :

$$\begin{aligned} T_{DR} &= \left(\frac{\Delta f(s)}{\Delta P_L(s)}\right)_{DR} \\ &= \frac{1}{(T_{OL}(s))^{-1} - \frac{K}{s}.\alpha.H(s) - \frac{K}{s}.(1-\alpha).G(s)} \\ T_S &= \left(\frac{\Delta f(s)}{\Delta P_L(s)}\right)_{S} = \frac{1}{(T_{OL}(s))^{-1} - \frac{K}{s}.H(s)}. \end{aligned} \tag{28}$$

This article has been accepted for inclusion in a future issue of this journal. Content is final as presented, with the exception of pagination.

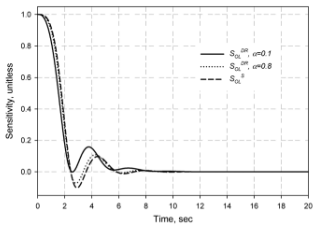


Fig. 5. Closed-loop system w.r.t. the open-loop system sensitivity values of a simulation study for LFC with and without DR.

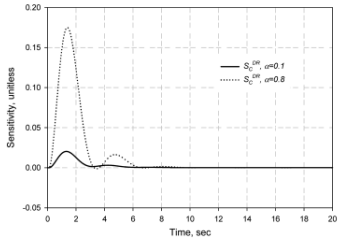


Fig. 6. Closed-loop system w.r.t. α sensitivity values for the LFC-DR model, $\alpha = 0.1$ and $\alpha = 0.8$.

TABLE II
POWER SYSTEM PARAMETERS FOR THE SIMULATION STUDY [33]

T_g	T_t	R	$2H$	D	T_d	ΔP_L	K
0.08 sec	0.4 sec	3.0 Hz/p.u.	0.1667 pu. sec	0.015 p.u./Hz	0.1 sec	0.01 p.u.	0.2

Therefore, the unitless sensitivity function of the closed-loop system w.r.t. the open-loop system, for systems with and without DR, can be written as follows:

$$\$_{OL}^{DR} = \frac{\frac{\partial T_{DR}}{\partial T_{OL}}}{\frac{T_{DR}}{T_{OL}}} = \frac{(T_{OL}(s))^{-1}}{(T_{OL}(s))^{-1} - \frac{K}{s}.\alpha.H(s) - \frac{K}{s}.(1-\alpha).G(s)}$$
$$\$_{OL}^{S} = \frac{\frac{\partial T_S}{\partial T_{OL}}}{\frac{T_S}{T_{OL}}} = \frac{(T_{OL}(s))^{-1}}{(T_{OL}(s))^{-1} - \frac{K}{s}.H(s)}. \quad (29)$$

It is noted from (29) that the closed-loop system is highly sensitive to the changes in the open-loop system, i.e., any change in the value of T_{OL} will have a large effect on $\$_{OL}^{DR}$ and $\$_{OL}^{S}$. From (29), the ratio of sensitivity functions can be expressed as

$$\frac{\$_{OL}^{DR}}{\$_{OL}^{S}} = \frac{(T_{OL}(s))^{-1} - \frac{K}{s}.H(s)}{(T_{OL}(s))^{-1} - \frac{K}{s}.\alpha.H(s) - \frac{K}{s}.(1-\alpha).G(s)}. \quad (30)$$

Equation (30) can be rearranged as follows:

$$\frac{\$_{OL}^{DR}}{\$_{OL}^{S}} = \frac{(T_{OL}(s))^{-1} - \frac{K}{s}.H(s) - \frac{K}{s}.\alpha.H(s) + \frac{K}{s}.\alpha.H(s)}{\underbrace{(T_{OL}(s))^{-1} - \frac{K}{s}.\alpha.H(s)}_{\Phi} \underbrace{- \frac{K}{s}.(1-\alpha)}_{\varphi}.G(s)}$$
$$= \frac{1 - \frac{\varphi}{\Phi}.H(s)}{1 - \frac{\varphi}{\Phi}.G(s)}. \quad (31)$$

Therefore, it can be observed from (31) that the closed-loop LFC-DR is slightly less sensitive than the system without DR only if $H(s) > G(s)$, assuming Φ and φ have the same sign. In order to compare the sensitivity functions, a simulation study was carried out for an arbitrary integral feedback gain. The sensitivity values for both closed-loop systems are shown in Fig. 5. The values of the different parameters for this simulation study are given in Table II.

Two different values for α are used in Fig. 5 to show that a higher DR share (smaller α) will result in less sensitivity of the closed-loop system w.r.t the open-loop system. That is, the closed-loop system becomes less sensitive to the variation of uncertain parameters of the open-loop system. When $\alpha = 0.8$ (i.e., 80% of the required regulation would be provided by the supplementary control and 20% is from DR), the sensitivity values for both the closed-loop systems, with and without DR, are almost similar. This is a good indication that the 5th-order *Padé* approximation, used for linearizing the time delay in the DR loop, doesn't have any negative impact on the system performance. A similar study has been carried out to investigate the sensitivity of the closed-loop system w.r.t. the integral feedback gain, and similar results have been obtained.

Since α is an important parameter in the performance of the closed-loop system with DR, it is useful to evaluate the sensitivity of the closed-loop system w.r.t. this coefficient. The sensitivity function can be written as follows:

$$\$_{\alpha}^{DR} = \frac{\frac{\partial T_{DR}}{\partial \alpha}}{\frac{T_{DR}}{\alpha}} = \frac{\alpha.\frac{K}{s}(H(s) - G(s))}{(T_{OL}(s))^{-1} - \frac{K}{s}.\alpha.H(s) - \frac{K}{s}.(1-\alpha).G(s)}. \quad (32)$$

The previous simulation setup was utilized for two different values of α. Sensitivity results are shown in Fig. 6.

It can be seen from Fig. 6 that the closed-loop system is less sensitive to α when the DR control loop takes a higher share in the frequency regulation, i.e., smaller α values.

C. Stability Analysis of the Closed-Loop Systems

A prerequisite for satisfactory control of a feedback control system is its stability, and gain and phase margins are two criteria commonly used for stability evaluation [37]. The gain and phase margins can be obtained from the Bode diagrams of the open-loop transfer function of the closed-loop system since the zeros of the characteristic equation are poles of the closed-loop system [37]. Using the load disturbance, $\Delta P_L(s)$ as the system input, the open-loop transfer functions are

$$\underbrace{1 + \frac{H(s).M(s)}{R} + \frac{K}{s}.\alpha.H(s).M(s) + \frac{K}{s}.(1-\alpha).G(s).M(s)}_{\vartheta^{DR}} = 0$$
$$\underbrace{1 + \frac{H(s).M(s)}{R} + \frac{K}{s}.H(s).M(s)}_{\vartheta^{S}} = 0 \quad (33)$$

where ϑ^{DR} and ϑ^{S} are the open-loop transfer function for the closed-loop systems with and without DR, respectively. Here, the control characteristics of the closed-loop systems ((33)) can

This article has been accepted for inclusion in a future issue of this journal. Content is final as presented, with the exception of pagination.

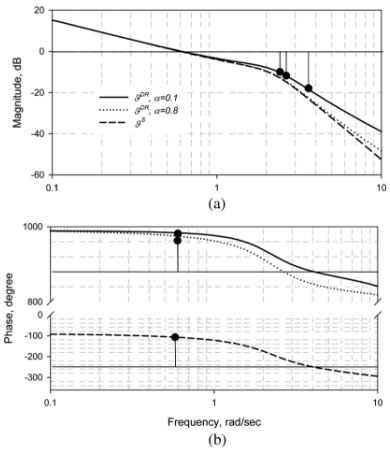


Fig. 7. Bode plot of the closed-loop systems for stability analysis, (a) magnitude, and (b) phase.

TABLE III
PHASE AND GAIN MARGINS FOR THE OPEN-LOOP TRANSFER FUNCTION ASSOCIATED WITH EACH CLOSED-LOOP SYSTEMS

	$\vartheta^{DR}, \alpha = 0.1$	$\vartheta^{DR}, \alpha = 0.8$	ϑ^{S}
Gain margin, *dB*	14.1	11.3	10.3
Phase margin, *degree*	83.5	74.8	72.2

be obtained by taking the feedback gain as a variable parameter. From (33), it is possible to calculate the new open-loop transfer functions, $\hat{\vartheta}^{DR}$ and $\hat{\vartheta}^{S}$. These transfer functions have the same root-locus properties as of ϑ^{DR} and ϑ^{S} as follows:

$$1 + \underbrace{K.\frac{R.[\alpha.H(s).M(s) + (1-\alpha).G(s).M(s)]}{s.[R + H(s).M(s)]}}_{\hat{\vartheta}^{DR}} = 0$$
$$1 + \underbrace{K.\frac{R.H(s).M(s)}{s.[R + H(s).M(s)]}}_{\hat{\vartheta}^{S}} = 0. \tag{34}$$

The Bode plots of the systems of (34) are shown in Fig. 7. The parameters of the case study are given in Table II. It can be seen from Fig. 7 that both systems (with and without DR) are relatively stable; however, larger gain and phase margins have been achieved when the DR control loop is added to the system. The phase and gain margins are given in Table III. It can be noticed from this table that a higher share of control effort for the DR control loop, i.e., smaller α, will provide a higher gain and phase margin, indicating a more stable system. In addition, the table shows that the 5th-order *Padé* approximation has no negative impacts on the stability of the system, as discussed in Section II-A.

IV. GENERAL APPROACH FOR CONTROLLER DESIGN FOR THE LFC-DR MODEL

Several different classical and modern control theories have been utilized for the LFC problem [32]. In this section, a general controller design approach for the LFC problem with the DR control loop is presented. Here, we use the widely used linear quadratic regulator (LQR) for controller design. We will examine other effective control design approaches, which will include parameter uncertainty and measurement noise, in our future work.

The simplified version of the LQR problem is to design the controller such that the performance index (35) is minimized for the system given in (3) [39]:

$$\Im = \int_0^\infty [\mathbf{x}^T.\mathbf{Q}.\mathbf{x} + \rho.\mathbf{u}^T.\mathbf{R}.\mathbf{u}].dt \tag{35}$$

where ρ is a weighting factor chosen by the designer, considering the trade-off between system transient performance and control effort. $\mathbf{Q}$ is an n-by-n semidefinite symmetric state cost matrix (n is the number of system states), $\mathbf{R}$ is an m-by-m positive definite symmetric control cost matrix (m is the number of control inputs), and $x^T = [x_1, \cdots, x_8]$ (where $x_1 = \Delta f$, $x_2 = \Delta P_g$, $x_3 = \Delta P$, and $x_4, \cdots, x_8$ are the states associated with the 5th-order *Padé* approximation).

Using (23), it can be shown that the control input to the supplementary controller $(u_1 = \Delta P_S)$ and to the DR controller $(u_2 = \Delta P_{DR})$ are related as follows:

$$u_1 = \frac{\alpha}{1-\alpha}.u_2 \qquad or \qquad u_2 = \frac{1-\alpha}{\alpha}.u_1. \tag{36}$$

For the system with unified control inputs, all the state-space matrices will remain unchanged, except the control input matrix $\mathbf{B}$, where (8) is modified to include $u_2 = F(u_1)$ as follows:

$$\hat{\mathbf{B}}^T = \left[\begin{array}{cc|c|cccc} \frac{\alpha-1}{2H.\alpha} & 0 & \frac{1}{T_g} & \frac{16(1-\alpha)}{\alpha} & 0 & 0 & 0 & 0 \end{array}\right]. \tag{37}$$

It is also possible to use $u_1 = F(u_2)$ in (8). However, as will be shown in the simulation results in Section V, the system performances in the two cases are nearly identical.

It is also noted that all the system states are non-zero except Δf, where the goal is to keep Δf as close to zero as possible. As a result, the full-state feedback controller cannot guarantee zero steady-state error for frequency deviation. Therefore, an integral controller is necessary to ensure zero steady-state error in the system frequency. In the early works on the application of optimal control to the LFC problems, e.g., [40]–[43], it was common to fix this problem with redefining the states in terms of their steady-state values, which essentially needs a prior knowledge of the disturbance. However, in most real-world cases the disturbance to the power system is an unknown parameter. Therefore, in this study, an *ad hoc* solution to the integral control problem is utilized by augmenting the state vector [39]. The design will also be robust against any changes in the

This article has been accepted for inclusion in a future issue of this journal. Content is final as presented, with the exception of pagination.

system parameters. Modifying the state-space model in (3) to include the integrator, the augmented state equations become

$$\begin{bmatrix}\dot{\mathbf{x}}\\ \dot{x}_I\end{bmatrix} = \begin{bmatrix}\mathbf{A} & 0\\ \mathbf{C} & 0\end{bmatrix}.\begin{bmatrix}\mathbf{x}\\ x_I\end{bmatrix} + \begin{bmatrix}\hat{\mathbf{B}}\\ 0\end{bmatrix}.\hat{u} + \begin{bmatrix}\mathbf{\Gamma}\\ 0\end{bmatrix}.w$$
$$y = [\mathbf{C} \quad 0].\begin{bmatrix}\mathbf{x}\\ x_I\end{bmatrix} \tag{38}$$

where $\hat{u} = u_2$. The augmented state-space equation can be written as follows:

$$\dot{\tilde{\mathbf{x}}} = \tilde{\mathbf{A}}.\tilde{\mathbf{x}} + \tilde{\mathbf{B}}.\hat{u} + \tilde{\mathbf{\Gamma}}.w$$
$$\tilde{y} = \tilde{\mathbf{C}}.\tilde{\mathbf{x}} \tag{39}$$

where the states are defined as $\mathbf{x}^T = [\Delta f, \Delta P_g, \Delta P_t, x_4, \cdots, x_8, \int \Delta f.dt]$. The matrices for the modified system are

$$\tilde{\mathbf{A}} = \left[\begin{array}{c|c}\mathbf{A} & \mathbf{0}_{8\times 1}\\ \hline [1 \quad 0_{1\times 7}] & 0\end{array}\right], \tilde{\mathbf{B}}^T = [\hat{\mathbf{B}} \mid 0],$$
$$\tilde{\mathbf{\Gamma}}^T = [\mathbf{\Gamma} \mid 0], \tilde{\mathbf{C}} = [\mathbf{C} \mid 0]. \tag{40}$$

If the augmented system matrix is controllable, then the control law and the state feedback can be defined as

$$\hat{u} = -[\mathbf{K} \quad K_I].\begin{bmatrix}\mathbf{x}\\ x_I\end{bmatrix} = -\tilde{\mathbf{K}}.\tilde{\mathbf{x}}. \tag{41}$$

To employ the LQR method, it is required to define the state and control weighting matrices, $\mathbf{Q}$ and R (scalar quantity), respectively. Before defining the weighting matrices, a set of frequency response requirements should be defined:

- The steady-state frequency deviation following a step-change in the load must be zero, i.e., $[\Delta f]^2$ [40].
- The time error represented by the integral of the frequency deviation should not exceed ± 3 seconds, i.e., $[\int \Delta f.dt]^2$ [40].

Eventually, the weighting matrices considering the above requirements will be as follows:

$$\mathbf{Q} = diag(1 \quad \mathbf{0}_{1\times 7} \quad 1),\ R = [1]. \tag{42}$$

In the next section, simulation results for the LFC-DR model of a single-area power system are presented to verify the effectiveness of the proposed model.

V. Simulation Results for Single-Area Power System

In order to show some important features of the proposed LFC-DR model, the results of several different simulation studies are reported in this section for a single-area power system. In order to make a fair comparison, similar LQR design procedure has been employed for controller design for both systems, with and without DR. The parameters used in the simulation studies are given in Table II. The LQR problem has been solved using MATLAB/Control System Toolbox.

In the first simulation study, a 0.01 pu load disturbance was applied to the single-area power system with conventional LFC and the proposed LFC-DR model. The system frequency deviation is shown in Fig. 8.

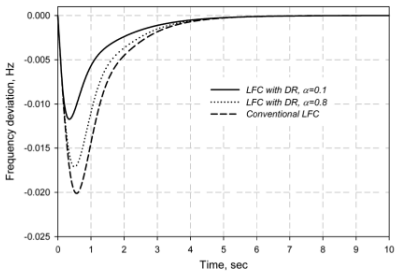


Fig. 8. Frequency deviation for conventional LFC and LFC-DR models.

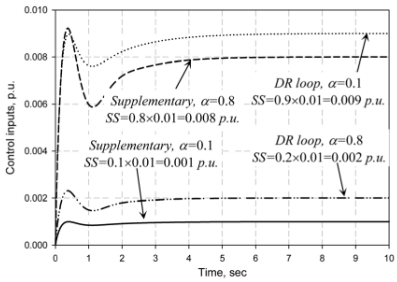


Fig. 9. Steady-state values of the control inputs for the LFC-DR model.

It can be seen that when $\alpha = 0.1$ (i.e., 10% of the required regulation is provided by the supplementary control and 90% from DR), the LFC-DR model has a superior performance over the conventional LFC during the transient period. Specifically, the overshoot in the system frequency deviation is decreased by about 42.5%. The results show improvement in the settling time as well. The same simulation was repeated for $\alpha = 0.8$. As expected, the lower DR control effort resulted in less improvement in the system dynamic performance. It can be observed that the dynamic performance of the system approaches that of conventional LFC for higher values of α.

The supplementary and DR control inputs are shown in Fig. 9, for the same simulation. As discussed in Section III-A, the steady-state values of the control inputs are based on the share between the DR and the supplementary control loops, i.e., the value of α, which is decided by the regional ISO/RTO based on the real-time electricity market. The steady-state value calculations are also shown in Fig. 9 which match with (24).

A simulation study was carried out to show the impact of the order of *Padé* approximation on the performance of the system, the results of which are shown in Fig. 10. 2nd- and 5th-order *Padé* approximations are considered in the proposed LFC-DR model and compared with the conventional LFC, for $\alpha = 0.1$. It can be seen from Fig. 10 that the results from the 2nd- and 5th-order *Padé* approximation are almost identical. It is mainly because the simplified governor and turbine models are low pass filters which restrict the system response to lower frequency ranges, where *Padé* approximation is exactly the same as pure time delay, as discussed in Section II. Therefore, for simplicity,

This article has been accepted for inclusion in a future issue of this journal. Content is final as presented, with the exception of pagination.

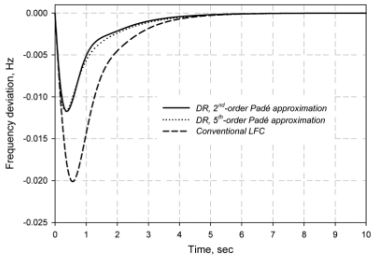


Fig. 10. Controller performance for different order of *Padé* approximation.

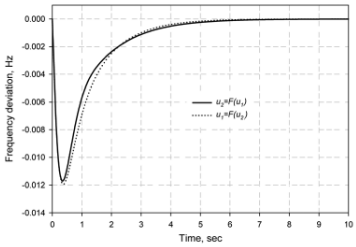


Fig. 11. Impact of different unified inputs on the performance of the LFC-DR model.

2nd-order *Padé* approximation can be employed for more complicated power systems without negative impacts on the final results.

As discussed in Section IV, the two control inputs are unified as a single input for the controller design as a function of α. The control input unification can be done in two ways: unifying $u_1(t)$ as a function of $u_2(t)$ or vice versa [$u_1 = (\alpha/(1-\alpha)).u_2$ or $u_2 = ((1-\alpha)/\alpha).u_1$]. To show the impact of unification, a simulation study was carried out to compare the performance of the system for both unification cases, and the results are shown in Fig. 11. It can be observed that the difference between the two unifying approaches is negligible. In other words, the unifying control input can be chosen arbitrarily without any negative impact on the performance of the LFC-DR model.

One significant feature of the proposed LFC-DR model is the possibility for the ISO/RTO to evaluate the impact of communication delay of the DR control loop on the system performance for frequency stabilization. In order to show the impact of latency, a simulation study was performed for different values of communication latency for $\alpha = 0.1$. Simulation results are shown in Fig. 12. The lowest communication delay (lowest T_d) is for a small power system with fast two-way communication link, such as wireless communication, between the Lagcos and individual loads. It can be seen that the LFC-DR model gives a better performance compared to the conventional LFC when $\mathrm{T_d} \leq 0.2$ sec. When the time delay exceeds 0.2 sec, it deteriorates the performance of the LFC-DR, and the response is even worse than that of conventional LFC for $\mathrm{T_d} = 0.4$ sec. This is not surprising since the single-area power system under study has a very fast dynamic response. In larger power systems with

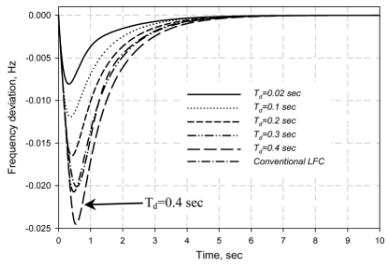


Fig. 12. Impact of latency on the performance of the LFC-DR model.

TABLE IV
POWER SYSTEM PARAMETERS FOR THE SIMULATION STUDY [44]

T_g	T_t	R	$2H$	D	ΔP_L
0.3 sec	0.8 sec	2.4 Hz/p.u.	3.0 pu. sec	0.0083 p.u./Hz	0.01 p.u.

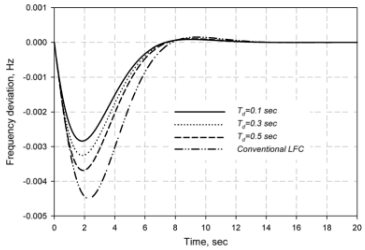


Fig. 13. Impact of DR latency on the performance of a slower single-area power system.

generation rate limiters and slow turbine-governor systems, a slower dynamic behavior would be expected from the supplementary control. But, the LFC-DR will keep its superior performance even for higher communication latencies (discussed below).

To show the impact of the DR latencies on a larger power system with high inertia and slower response, another simulation study was conducted with the parameters given in Table IV. It can be seen from Fig. 13 that for a larger and consequently slower power system, the performance of the LFC-DR model is superior to that of conventional LFC even for larger communication latencies. It has been shown in [6] that even with the current Internet infrastructure, a latency of 500 msec can be achieved easily. Therefore, it can be concluded that the DR with the largest available latency (500 msec) still can be effective for large power systems.

VI. DISCUSSION AND FUTURE WORK

Our proposed LFC-DR model responds to all frequency deviations as is the case in the traditional LFC model [33], [36]. However, if it is desired to prevent the LFC-DR model to respond to small frequency deviations, and also keep the linearity of the model, a deadband could be added to the input, ΔP_L.

This article has been accepted for inclusion in a future issue of this journal. Content is final as presented, with the exception of pagination.

ΔP_L could include the variation in any renewable generation that might be available in the power system as negative load. This is because of the fast dynamics of the common variable generation (wind, solar PV) compared to those of traditional power plants in the LFC model.

In this paper, we have explored the effectiveness of the LFC-DR model for frequency regulation at the transmission level in a single-area power system. However in general, large power systems are multi-area where different Gencos and Lagcos are available in each area. In our future work, we will report the application of LFC-DR in multi-area power systems.

VII. Conclusions

In this paper, a general framework is proposed to include DR into the LFC problem (LFC-DR). The proposed formulation can be expanded easily for any type of power system in size and characteristics. The framework adapts a real-time electricity market with existing load aggregators. It balances the power between generation and demand and stabilizes the system frequency by utilizing a percentage of available controllable loads and/or conventional supplementary control, based on the real-time market price. It also includes communication latencies in DR for controller design, using *Padé* approximation. It is shown through different analytical studies that the proposed LFC-DR framework will improve the stability margins in the conventional LFC model and is slightly less sensitive to the variation in the system parameters, such as changes in the open-loop transfer function. Similar results have also been obtained for the sensitivity of the closed-loop system w.r.t. the parameter α. Finally, the well-known LQR design is applied for full-state feedback controller design for a single-area power system. Simulation results show the effectiveness of the LFC-DR model in improving stabilization of the system frequency.

Acknowledgment

The authors would like to thank Dr. S. Shaw and Dr. R. Gunderson of Montana State University, and Dr. A. Gorji of the University of Toronto for the fruitful discussion of the feedback control theory.

References

[1] R. Doherty and M. O'Malley, "A new approach to quantify reserve demand in systems with significant installed wind capacity ," *IEEE Trans. Power Syst.*, vol. 20, no. 2, pp. 587–595, May 2005.

[2] U.S. Department of Energy, Smart Grid, Sep. 28, 2011 [Online]. Available: http://energy.gov/oe/technology-development/smart-grid

[3] C. Goldman, M. Reid, R. Levy, and A. Silverstein, Coordination of Energy Efficiency and Demand Response a Resource of the National Action Plan for Energy Efficiency, U.S. Environmental Protection Agency, U.S. Department of Energy , 2010, Tech. Rep.

[4] R. Walawalkar, S. Blumsack, J. Apt, and S. Fernands, "An economic welfare analysis of demand response in the PJM electricity market," *Energy Policy*, vol. 36, no. 10, pp. 3692–3702, Oct. 2008.

[5] M. Klobasa, "Analysis of demand response and wind integration in Germany's electricity market," *IET Renew. Power Gener.*, vol. 4, no. 1, pp. 55–63, Jan. 2010.

[6] A. Brooks, E. Lu, D. Reicher, C. Spirakis, and B. Weihl, "Demand dispatch: Using real-time control of demand to help balance generation and load ," *IEEE Power Energy Mag.*, vol. 8, no. 3, pp. 20–29, May/Jun. 2010.

[7] J. Medina, N. Muller, and I. Roytelman, "Demand response and distribution grid operations: Opportunities and challenges," *IEEE Trans. Smart Grid*, vol. 1, no. 2, pp. 193–198, Sep. 2010.

[8] H. Saele and O. S. Grande, "Demand response from household customers: Experiences from a pilot study in Norway," *IEEE Trans. Smart Grid*, vol. 2, no. 1, pp. 102–109, Mar. 2011.

[9] N. Ruiz, I. Cobelo, and J. Oyarzaabal, "A direct load control model for virtual power plant management," *IEEE Trans. Power Syst.*, vol. 24, no. 2, pp. 959–966, May 2009.

[10] A. J. Conejo, J. M. Morales, and L. Baringo, "Real-time demand response model," *IEEE Trans. Smart Grid*, vol. 1, no. 3, pp. 236–242, Dec. 2010.

[11] D. T. Nguyen, M. Negnevitsky, and M. de Groot, "Pool-based demand response exchange-concept and modeling," *IEEE Trans. Power Syst.*, vol. 26, no. 3, pp. 1677–1685, Aug. 2011.

[12] P. Faria, Z. Vale, J. Soares, and J. Ferreira, "Demand response management in power systems using a particle swarm optimization approach ," *IEEE Intell. Syst.*, to be published.

[13] M. Parvania and M. Fotuhi-Firuzabad, "Integrating load reduction into wholesale energy market with application to wind power integration ," *IEEE Syst. J.*, vol. 6, no. 1, pp. 35–45, Mar. 2012.

[14] K. Dietrich, J. M. Latorre, L. Olmos, and A. Ramos, "Demand response in an isolated system with high wind integration," *IEEE Trans. Power Syst.*, vol. 27, no. 1, pp. 20–29, Feb. 2012.

[15] M. Rastegar, M. Fotuhi-Firuzabad, and F. Aminifar, "Load commitment in a smart home," *J. Appl. Energy*, vol. 96, pp. 45–54, Aug. 2012.

[16] N. Navid-Azarbaijani and M. H. Banakar, "Realizing load reduction functions by aperiodic switching of load groups," *IEEE Trans. Power Syst.*, vol. 11, no. 2, pp. 721–727, May 1996.

[17] K. Y. Huang, H. C. Chin, and Y. C. Huang, "A model reference adaptive control strategy for interruptible load management," *IEEE Trans. Power Syst.*, vol. 19, no. 1, pp. 683–689, Feb. 2004.

[18] D. Westermann and A. John, "Demand matching wind power generation with wide-area measurement and demand-side management ," *IEEE Trans. Energy Convers.*, vol. 22, no. 1, pp. 145–149, Mar. 2007.

[19] S. A. Pourmousavi and M. H. Nehrir, "Demand response for smart microgrid: Initial results," in *Proc. 2nd IEEE PES Innov. Smart Grid Technol. (ISGT)*, Anaheim, CA, USA, 2011, pp. 1–6.

[20] S. A. Pourmousavi, M. H. Nehrir, and C. Sastry, "Providing ancillary services through demand response with minimum load manipulation ," in *Proc. 43rd North Amer. Power Symp. (NAPS)*, Boston, MA, USA, 2011, pp. 1–6.

[21] S. A. Pourmousavi and M. H. Nehrir, "Real-time central demand response for primary frequency regulation in microgrids," *IEEE Trans. Smart Grid*, vol. 3, no. 4, pp. 1988–1996, Dec. 2012.

[22] D. Trudnowski, M. Donnelly, and E. Lightner, "Power-system frequency and stability control using decentralized intelligent loads," in *Proc., IEEE PES Conf. Exhib. Transm. Distrib.*, Dallas, TX, USA, 2005, pp. 1453–1459.

[23] J. A. Short, D. G. Infield, and L. L. Freris, "Stabilization of grid frequency through dynamic demand control," *IEEE Trans. Power Syst.*, vol. 22, no. 3, pp. 1284–1293, Aug. 2007.

[24] A. Molina-García, F. Bouffard, and D. S. Kirschen, "Decentralized demand-side contribution to primary frequency control," *IEEE Trans. Power Syst.*, vol. 26, no. 1, pp. 411–419, Feb. 2011.

[25] D. Jay and K. S. Swarup, "Dynamic demand response and control in smart grid environment," in *Proc. Annual IEEE India Conf. (INDICON)*, Hyderabad, 2011, pp. 1–4.

[26] D. Jay and K. S. Swarup, "Frequency restoration using dynamic demand control under smart grid environment," in *Proc. IEEE PES Innovative Smart Grid Technologies—India (ISGT India)*, Kerala, 2011, pp. 311–315.

[27] K. Samarakoon, J. Ekanayake, and N. Jenkins, "Investigation of domestic load control to provide primary frequency response using smart meters ," *IEEE Trans. Smart Grid*, vol. 3, no. 1, pp. 282–292, Mar. 2012.

[28] D. Angeli and P.-A. Kountouriotis, "A stochastic approach to dynamic demand refrigerator control," *IEEE Trans. Control Syst. Technol.*, vol. 20, no. 3, pp. 581–592, May 2012.

[29] Z. Changhong, U. Topcu, and S. H. Low, "Frequency-based load control in power systems," in *Proc. American Control Conf. (ACC)*, Canada, 2012, pp. 4423–4430.

[30] L. R. Chang-Chien, L. N. An, T. W. Lin, and W. J. Lee, "Incorporating demand response with spinning reserve to realize an adaptive frequency restoration plan for system contingencies," *IEEE Trans. Smart Grid*, vol. 3, no. 3, pp. 1145–1153, Sep. 2012.

[31] H. Huang and F. Li, "Sensitivity analysis of load-damping characteristic in power system frequency regulation ," *IEEE Trans. Power Syst.*, vol. 28, no. 2, pp. 1324–1335, May 2013.

This article has been accepted for inclusion in a future issue of this journal. Content is final as presented, with the exception of pagination.

[32] Ibraheem, P. Kumar, and D. P. Kothari, "Recent philosophies of automatic generation control strategies in power systems," *IEEE Trans. Power Syst.*, vol. 20, no. 1, pp. 346–357, Feb. 2005.
[33] H. Bevrani, *Robust Power System Frequency Control*. New York, NY, USA: Springer, 2009, ch. 1–3.
[34] C.-C. Wu, W.-J. Lee, C.-L. Cheng, and H.-W. Lan, "Role and value of pumped storage units in an ancillary services market for isolated power system-simulation in the Taiwan power system," *IEEE Trans. Ind. Appl.*, vol. 44, no. 6, pp. 1924–1929, Nov./Dec. 2008.
[35] J. Mickey, "Using load resources to meet ancillary service requirements in the ERCOT market: A case study ," in *Proc. IEEE PES General Meeting*, Minneapolis, MN, USA, 2010, pp. 1–2.
[36] P. Kundur, *Power system Stability and Control*. New York, NY, USA: McGraw-Hill, 1994, ch. 11.
[37] R. C. Dorf and R. H. Bishop, *Modern Control Systems*, 7th ed. New York, NY, USA: Addison-Wesley, 1995, p. 807.
[38] G. H. Golub and C. F. Van Loan, *Matrix Computations*, 3rd ed. Baltimore, MD, USA: Johns Hopkins Univ. Press, 1996, pp. 572–574.
[39] G. F. Franklin, J. D. Powell, and A. Emami-Naeini, *Feedback Control of Dynamic Systems*, 3rd ed. New York, NY, USA: Addison-Wesley, 1994, p. 778.
[40] C. E. Fosha and O. I. Elgerd, "The megawatt-frequency control problem: A new approach via optimal control theory," *IEEE Trans. Power App. Syst.*, vol. PAS-98, no. 4, pp. 563–577, Apr. 1970.
[41] E. C. Tacker, C. C. Lee, T. W Reddoch, T. O. Tan, and P. M. Julich, "Optimal control of interconnected electric energy systems: A new formulation," *IEEE Proc. Lett.*, vol. 60, no. 10, pp. 1239–1241, Oct. 1972.
[42] G. Shirai, "Load frequency control using Lyapunov's second method: Bang-bang control of speed changer position ," *IEEE Proc. Lett.*, vol. 67, no. 10, pp. 1458–1459, Oct. 1979.
[43] S. C. Tripathy, T. S. Bhatti, C. S. Jha, O. P. Malik, and G. S. Hope, "Sampled data automatic generation control analysis with reheat steam turbines and governor dead-band effects," *IEEE Trans. Power App. Syst.*, vol. PAS-103, no. 5, pp. 1045–1051, May 1984.
[44] T. Hiyama, "Design of decentralized load-frequency regulators for interconnected power systems," *Proc. IEE Generation, Transmission, Distribution Conf.*, vol. 129, no. 1, pp. 17–23, 1982.



S. Ali Pourmousavi (S'07) received the B.S. degree with honors from the University of Mazandaran, Iran, in 2005 and the M.S. degree with honors from Amirkabir University of Technology (Tehran Polytechnic), Tehran, Iran, in 2008, all in electrical engineering. He is pursuing the Ph.D. degree in the Electrical and Computer Engineering (ECE) Department at Montana State University, Bozeman, MT, USA.

His research interests include energy management of hybrid power generation systems, load control and demand response, and wind speed and power forecasting.



M. Hashem Nehrir (S'68–M'71–SM'89–F'10–LF'13) received the B.S., M.S., and Ph.D. degrees from Oregon State University, Corvallis, OR, USA, in 1969, 1971, and 1978, respectively, all in electrical engineering.

He was with the Electrical Engineering Department, Shiraz University, Iran, from 1971 to 1986. Since 1987, he has been on the faculty of the Electrical and Computer Engineering Department, Montana State University, Bozeman, MT, USA, where he is a Professor. His research interests include modeling and control of power systems, alternative energy power generation systems, and application of intelligent controls to power systems. He is the author of three textbooks and an author or coauthor of numerous technical papers.

CHAPTER 7

LFC-DR MODEL EXPANSION TO MULTI-AREA POWER SYSTEMS

Contribution of Authors and Co-Authors

Manuscripts in Chapters 2 through 12

Author: S. A. Pourmousavi

Contributions: Expanded equations for the proposed LFC-DR model from chapter 6 to multi-area power system with multiple Gencos and Lagcos, developed sizable state-space model and actual implementation in MATLAB®/Simulink, designed different simulation setup including for multi-area power system, prepared all the figures and equations, and the first draft of the manuscript.

Co-author: M. H. Nehrir

Contributions: Provided important insight and overview of the research, interpretation of the results, and aided in the preparation of the manuscript.

Manuscript Information Page

Seyyed Ali Pourmousavi Kani, M. Hashem Nehrir

IEEE Transactions on Power System, 2014

Status of the manuscript:
_X_ Under Preparation for submission to a peer-reviewed journal
____ Officially submitted to a peer-reviewed journal
____ Accepted by a peer-reviewed journal
____ Published in a peer-reviewed journal

Published by the Institute of Electrical and Electronics Engineering (IEEE)

LFC-DR MODEL EXPANSION TO MULTI-AREA POWER SYSTEMS

The following work is under preparation to be submitted to the IEEE Transactions on Power Systems in 2014

S.A. Pourmousavi, and M.H. Nehrir

Department of Electrical and Computer Engineering, Montana State University, Bozeman, MT 59717

Abstract

Implementation of DR into the conventional LFC model for single-area power system, called LFC-DR, is explained in Chapter 6. Analytical analysis of the added control loop and simulation results for single-area power system are presented in Chapter 6. In this chapter, the idea is expanded to a general multi-area interconnected power system. Then, several simulation experiments are carried out to reveal the impacts of the new LFC on the dynamic performance of the different power systems. Simulation results show a superior performance of the LFC-DR model for different conditions and power system models.

Introduction

In the smart grid era, two-way communication will allow consumers' loads to participate in power system control as active agents. In this paradigm, Lagcos will be in charge of aggregating the available customers' responsive loads. Lagcos are the third party between consumers and the utilities and participate in the real-time electricity market with their offers. This type of DR program is actively pursued in some electricity markets, such as the PJM electricity market [7.1]. Although the effectiveness of DR has

been proved for the business side of the electrical power system operation, many technical aspects of DR are still unclear to the energy balancing authorities (BAs) and transmission system operators (TSOs).

One important technical aspect of power system operation is frequency regulation, known as AGC as a subset of AS, where the effectiveness and impact of DR are unknown. To evaluate the dynamic behavior and frequency regulation in a power system, a general linearized model of the power system at the transmission level, known as LFC model, has been developed in the past five decades [7.2]. However, these models do not include the effect of DR on the system dynamic behavior and controller design. In [7.3], a general formulation of the LFC with DR (LFC-DR model) and a robust control design (using the linear quadratic regulator (LQR) method) is presented for a single-area power system and its effectiveness is verified analytically.

In this chapter, the ideas presented in Chapter 6 are expanded and used for decentralized LFC model, as described in [7.2]. This reference has been widely used for controller design and small-signal stability analyses of multi-area interconnected power systems. The assumptions made here for system dynamic model and controller design are the same as given in Chapter 6. Therefore, the performance of the LFC-DR model for a large power system would essentially remain the same, as in Chapter 6, in terms of steady-state error, sensitivity and stability.

In this chapter, the Lagcos are introduced to the frequency regulation market in each area of the decentralized LFC model. As explained in Chapter 6, Lagcos are active players (agents) in the real-time electricity market with the price offers and the amount of

DR resources they can provide for frequency regulation in their geographical zone. The same concept holds for Gencos in each area. Therefore, the required AS for frequency regulation will be split between the several Gencos and Lagcos in each area based on their offer prices in the real-time electricity market. This decision should be made by the ISO/RTO every 4-10 seconds, which is the time period that the area control error (ACE) signal is generated by the BAs. This idea is included in the LFC-DR model.

Several simulation studies have been proposed in this chapter to reveal the effectiveness of the LFC-DR model. Each simulation study targets a specific feature of the proposed model in a multi-area power system. Simulation results verify that the proposed model properly integrates DR into the LFC model and improves system performance significantly.

Formulation Expansion to Multi-Area Power System with Multiple Gencos and Lagcos

Large power systems are normally divided into multiple areas connected by high voltage transmission lines or tie-lines, where each area may include generation units of different types. Therefore, it is necessary to consider the differences between Gencos in the LFC studies and controller design in each area. In the past two decades, a lot of attention has been focused on decentralized LFC model for controller design and analysis for interconnected power systems with multiple Gencos in each area [7.4]-[7.11]. It is shown that the LFC problem for a large power system can be effectively reduced to an equivalent LFC problem for each area. Then, each control area regulates the power interchange with the neighboring control areas, as well as its local frequency [7.2].

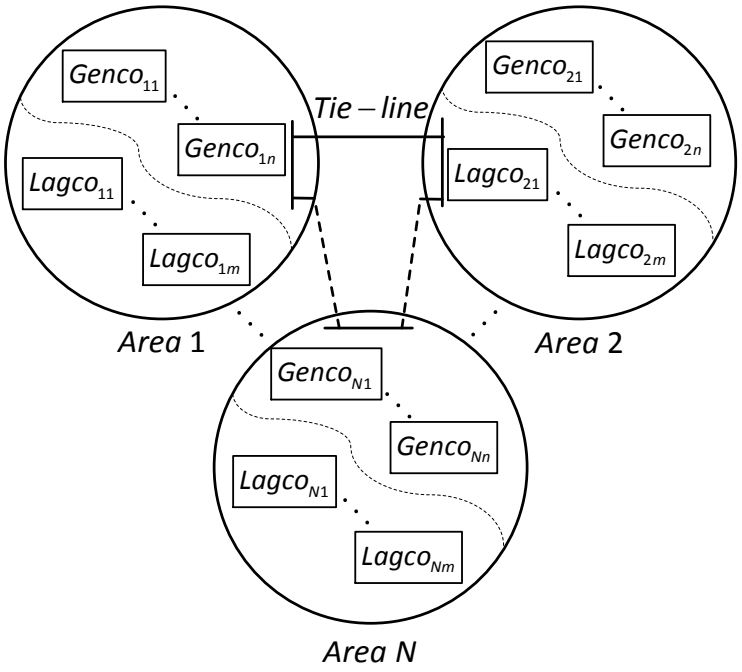


Figure 7.1. Multi-area power system with multiple Gencos and Lagcos.

The LFC model with multiple Gencos has already been developed, e.g., [7.2]. However to the best of our knowledge, the DR control concept has not been included in the LFC model. In this section, the proposed LFC-DR model (presented in Chapter 6) is expanded for a decentralized interconnected power system, where each interconnected area has multiple Gencos and Lagcos, as shown for a multi-area system in Figure 7.1.

Based on the principles explained in Chapter 6, the DR control loop can be added to each control area of the decentralized interconnected power system by multiple Lagcos. This idea is shown for area *i* of a multi-area power system in Figure 7.2. A simplified power system with non-reheat steam turbine is considered for each area, and it is assumed that all the states of the system are observable and measureable for the LQR design. The latter assumption may not be totally true in real-world applications.

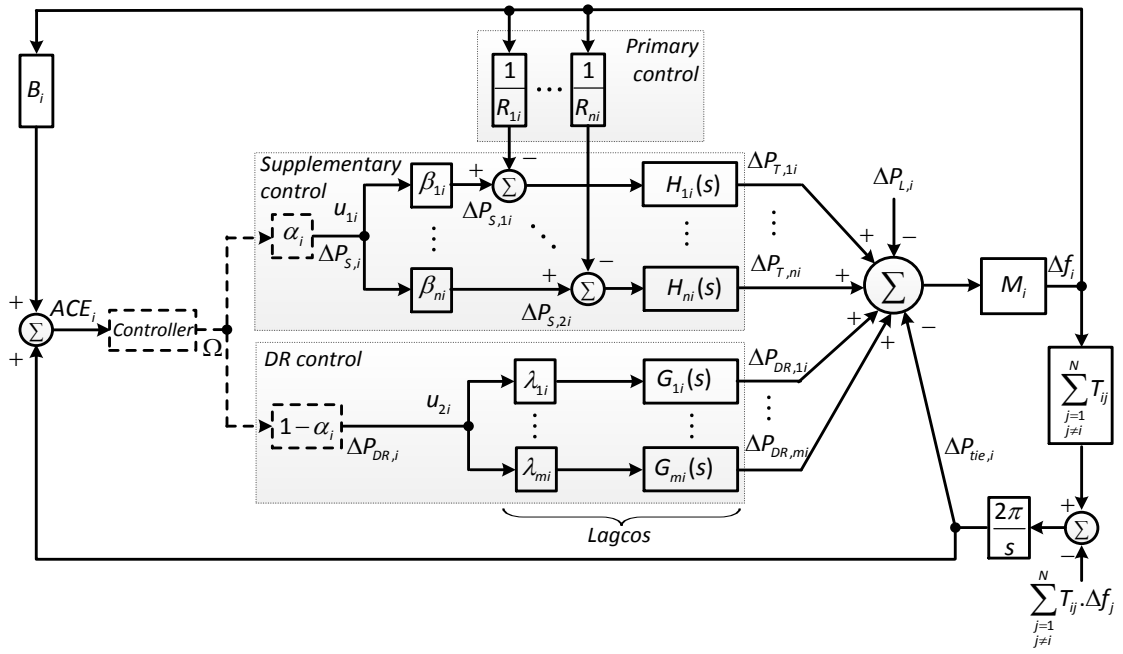


Figure 7.2. Block-diagram representation of area *i* of a general multi-area power system with multiple Gencos and Lagcos in each area.

However, it will not degrade the applicability of the full-state feedback design since the immeasurable states can be effectively estimated by the observers, as reported in [7.12]-[7.17]. Observer design is out of the scope of this dissertation.

The transfer functions shown in the figure are defined as follows:

$$M_i(s)=\frac{1}{2H_i.s+D_i},\ H_{ji}(s)=\frac{1}{(1+T_{g,ji})(1+T_{t,ji})}$$

$$G_{ji}(s)=\frac{-s^5+\frac{30}{T_{d,ji}}.s^4-\frac{420}{T_{d,ji}^2}.s^3+\frac{3360}{T_{d,ji}^3}.s^2-\frac{15120}{T_{d,ji}^4}.s+\frac{30240}{T_{d,ji}^5}}{s^5+\frac{30}{T_{d,ji}}.s^4+\frac{420}{T_{d,ji}^2}.s^3+\frac{3360}{T_{d,ji}^3}.s^2+\frac{15120}{T_{d,ji}^4}.s+\frac{30240}{T_{d,ji}^5}} \qquad (7.1)$$

where,

$2H_i$ is the equivalent inertia constant of area *i*,

D_i is the equivalent load-damping coefficient of area *i*,

$T_{g,ji}(s)$ is governor time constant of Genco *j* in area *i*,

$T_{t,ji}(s)$ is non-reheat turbine time constant of Genco *j* in area *i*,

$T_{d,ji}(s)$ is the communication latency of Lagco j in area i,

$\Delta f_i(s)$ is the frequency deviation,

s is the Laplace transform operator.

The unified control inputs ($u_{2i} = F(u_{1i})$) introduced in Chapter 6, are again used. α_i is the share of control effort between the supplementary control and the DR control loop for area *i*. The sharing rate, α_i, will be decided by the ISO/RTO based on the real-time electricity market. Then, the ACE signal for each area can be defined as follows:

$$ACE_i = \Delta P_{tie,i} + B_i.\Delta f_i \tag{7.2}$$

where B_i is the frequency bias constant for area *i*. As it can be seen from Figure 7.2, different Gencos will participate with different amount of power, based on their participation factor, , which will be assigned by the ISO/RTO. The different Gencos may decide to participate in the supplementary control action, or not, (based on their price offers, available generation, transmission lines congestions, etc.), where:

$$\sum_{k=1}^{n} \beta_{ki} = 1, \qquad 0 \le \beta_{ki} \le 1 \tag{7.3}$$

The same concept holds for the different Lagcos in each area participating in the frequency regulation, as shown in Figure 7.2. The Lagcos might have different dynamic characteristics, i.e. communication latency, and offer different prices in the electricity market and have different amount of aggregated load available for frequency regulation

services. As a result, the load aggregator participation factor, λ_{ki}, has been included in the proposed LFC-DR model. The Lagcos' participation factor has the following characteristic:

$$\sum_{k=1}^{m} \lambda_{ki} = 1, \qquad 0 \le \lambda_{ki} \le 1 \tag{7.4}$$

Different latencies in DR can be justified by the different communication infrastructure in different regions. Therefore, the ISO/RTO would be able to buy the required regulation services from different Lagcos, as well as Gencos.

Figure 7.2 is similar to Figure 1 of Chapter 6 from the dynamic components' point of view, except the ACE signal is used instead of frequency deviation as the parameter to be controlled. This change does not add any new dynamic to the system compared to the single-area power system. In addition, here an extra disturbance (namely the tie-line power deviation, $\sum_{j=1, j\neq i}^{N} T_{ij}.\Delta f_j$) is added to the LFC model of each area. Therefore, similar steady-state error, stability, and sensitivity analyses, as those presented in Chapter 6 for a single-area power system model, would apply to each control area of the multi-area system. But, the required control effort is increased since there are two disturbances imposed to each control area.

As for the single-area power system presented in Chapter 6, the time delay in DR control loop has been linearized using 5th-order *Padé* approximation, explained in Chapter 6. Therefore, the general state-space model of the power system with *N* interconnected areas, consisting of *n* Gencos and *m* Lagcos in each control area, as shown in Figure 7.2, can then be written as:

$$\begin{aligned} \dot{\mathbf{x}}_i &= \mathbf{A}_i.\mathbf{x}_i + \mathbf{B}_i.\mathbf{u}_i + \mathbf{\Gamma}_i.\mathbf{w}_i \\ y_i &= \mathbf{C}_i.\mathbf{x}_i + \mathbf{D}_i.\mathbf{u}_i \end{aligned} \tag{7.5}$$

where,

$$\begin{aligned} \mathbf{A}_i &= \begin{bmatrix} \mathbf{\Phi}_{11i} & \mathbf{\Phi}_{12i} & \mathbf{\Phi}_{13i} \\ \mathbf{\Phi}_{21i} & \mathbf{\Phi}_{22i} & \mathbf{\Phi}_{23i} \\ \mathbf{\Phi}_{31i} & \mathbf{\Phi}_{32i} & \mathbf{\Phi}_{33i} \end{bmatrix}, \mathbf{B}_i = \begin{bmatrix} \mathbf{\Lambda}_{11} & \mathbf{\Lambda}_{12} \\ \mathbf{\Lambda}_{21} & \mathbf{\Lambda}_{22} \\ \mathbf{\Lambda}_{31} & \mathbf{\Lambda}_{32} \end{bmatrix} \\ \mathbf{\Gamma}_i &= \begin{bmatrix} \mathbf{\Theta}_{11} \\ \mathbf{\Theta}_{21} \\ \mathbf{\Theta}_{31} \end{bmatrix}, \mathbf{C}_i = \begin{bmatrix} B_i & 1 & \mathbf{0}_{1\times 2n} & \mathbf{0}_{1\times 5m} \end{bmatrix}, \mathbf{D}_i = \begin{bmatrix} 0 & 0 \end{bmatrix} \end{aligned} \tag{7.6}$$

where $\mathbf{A}_i$ is the system matrix, $\mathbf{B}_i$ is the control input matrix, $\mathbf{\Gamma}_i$ is the disturbance matrix, $\mathbf{x}_i$ is the state vector, $\mathbf{u}_i$ is the input vector, $\mathbf{w}_i$ is the disturbance matrix, $\mathbf{C}_i$ is the observation matrix, and y_i is the system output vector. The sub-matrices ($\mathbf{\Phi}, \mathbf{\Lambda}, \mathbf{\Theta}$) for area *i* are given in Appendix B. Unifying the control inputs, as discussed in Chapter 6, enables the ISOs/RTOs to study the dynamic behavior of the system regarding the share of regulation services between the traditional supplementary control and DR. After the unification, all system matrices will remain the same except the input matrix, which is given as follows:

$$\widehat{\mathbf{B}}_i^T = \begin{bmatrix} \widehat{\mathbf{\Lambda}}_{11} & \widehat{\mathbf{\Lambda}}_{12} & \widehat{\mathbf{\Lambda}}_{13} \end{bmatrix} \tag{7.7}$$

The sub-matrices ($\widehat{\mathbf{\Lambda}}_{11}, \widehat{\mathbf{\Lambda}}_{12}, \widehat{\mathbf{\Lambda}}_{13}$) are given in Appendix B. In the above equation, the DR control input is unified based on the supplementary control input for area *i*, i.e. $u_{2i} = \left(1 - \alpha_i \middle/ \alpha_i\right).u_{1i}$. It has been shown in Chapter 6 that the unification (of u_{2i} in terms of u_{1i} or vice versa) yields nearly similar results. For multiple area interconnected power

system, the same LQR design procedure can be utilized for each area with unified inputs. For robust control, an integral controller ($\int ACE_i.dt$) is also introduced in this procedure to ensure zero steady-state error in the ACE signal in each area. The augmented system of area *i* is as follows:

$$\begin{aligned} \dot{\tilde{\mathbf{x}}}_i &= \tilde{\mathbf{A}}_i.\tilde{\mathbf{x}}_i + \tilde{\mathbf{B}}_i.\hat{u}_i + \tilde{\mathbf{\Gamma}}_i.\mathbf{w}_i \\ \tilde{y}_i &= \tilde{\mathbf{C}}_i.\tilde{\mathbf{x}}_i + \tilde{\mathbf{D}}_i.\hat{u}_i \end{aligned} \tag{7.8}$$

where the state vector for area *i* is:

$$\mathbf{x}_i^T = \left[\Delta f_i \;\; \Delta P_{tie,i} \;\; x_{GT,i} \;\; x_{DR,i} \;\; \int ACE_i \right] \tag{7.9}$$

where

$$x_{GT,i} = \left[\underbrace{\left[\Delta P_{G,1i} \;\; \Delta P_{T,1i} \right] \;\; \cdots \;\; \left[\Delta P_{G,1n} \;\; \Delta P_{T,1n} \right]}_{n \text{ units}} \right] \tag{7.10}$$

$$x_{DR,i} = \left[\underbrace{\left[X_{i,11} \;\; X_{i,12} \;\; X_{i,13} \;\; X_{i,14} \;\; X_{i,15} \right] \;\; \cdots \;\; \left[X_{i,m1} \;\; X_{i,m2} \;\; X_{i,m3} \;\; X_{i,m4} \;\; X_{i,m5} \right]}_{m \text{ load aggregator}} \right] \tag{7.11}$$

In order to use the LQR design, it is required to introduce the state and control weighting matrices; introduced in Chapter 6. Prior to that, it is necessary to define the system frequency requirements:

- ✓ The steady-state frequency deviation following a step change in load must be zero, i.e. $\left[\Delta f_i\right]^2$ [7.18].
- ✓ The steady-state change in tie-line power following a step-load change must be zero, i.e. $\left[\Delta P_{tie,i}\right]^2$ [7.18].
- ✓ The ACE at each area should be zero in steady-state. In addition, the time

error represented by the integral of the frequency deviation, should not exceed ±3 seconds, i.e. $\left[\int ACE_i.dt\right]^2$ [7.18].

As a result, the weighting matrices will be defined, based on the size of the system and the unified input matrices. This model and the proposed controller design can be applied for any size of power system with any number of Gencos and Lagcos in each area. In the following sections, the results of simulation studies designed to show the effectiveness of the proposed LFC-DR model for multi-area power systems are presented.

Simulation Results for Multi-Area Power System with Single Genco and Lagco

In this section, a simulation study is presented to evaluate the effectiveness of the proposed LFC-DR model for a multi-area power system. The system studied is a typical three-area interconnected power system, which could be realized from Figure 7.1, where each area is represented by a single Genco and Lagco. The parameters of the power system are given in Table 7.1.

The results are then compared to those from the conventional LFC model, as shown in Figure 7.3. In addition, the impact of communication latency on the performance of the system is investigated. For the sake of fair comparison, the same controller design and structure has been utilized for the system with and without DR. In the case of LFC-DR model, two different simulations have been performed for different shares (α_i) between supplementary control and DR to assess the impacts of large DR participation in the frequency regulation service.

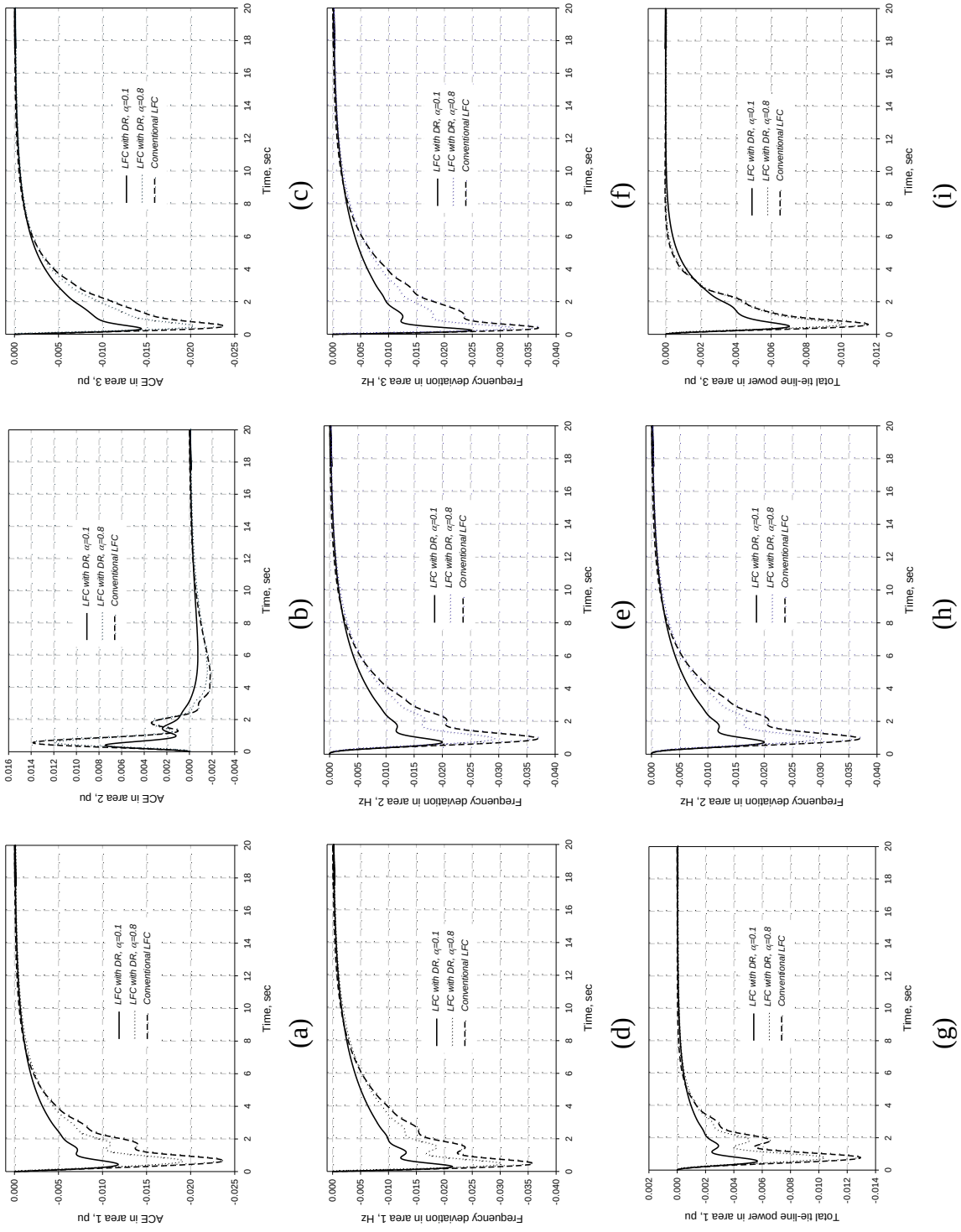


Figure 7.3. ACE, Frequency deviation, and total tie-line power in different areas for different α, multi-area power system with single Genco and Lagco.

Table 7.1. Three-area power system parameters for the simulation study [7.2].

Parameters	Area 1	Area 2	Area 3
D_i (pu/Hz)	0.015	0.016	0.015
$2H_i$ (pu.sec)	0.1667	0.2017	0.1247
R_i (Hz/pu)	3.00	2.73	2.82
T_{gi} (sec)	0.08	0.06	0.07
T_{ti} (sec)	0.40	0.44	0.30
B_i (pu/Hz)	0.3483	0.3827	0.3692
T_{ij} (pu/Hz)	T_{12} =0.20 T_{13} =0.25	T_{21} =0.2 T_{23} =0.12	T_{31} =0.25 T_{32} =0.12
T_{di} (sec)	0.1	0.1	0.1
α_i	[0.1, 0.8]	[0.1, 0.8]	[0.1, 0.8]
ΔP_{Li} (pu)	0.02	0.0	0.02

Deviation in ACE, Frequency, and Tie-Line Power

The system dynamic response to simultaneous step load disturbance of 0.02 pu in the areas 1 and 3 are shown in Figure 7.3. The DR latency is 100 msec for all Lagcos in the different areas. Two different sharing values (α_i) between conventional supplementary control and DR have been examined to show the effectiveness of the proposed LFC-DR model. In Figure 7.3 (a)-(c), variations in the ACE signal for the different areas are shown in response to simultaneous load disturbances in areas 1 and 3. When α_i =1, the system performance is identical to the conventional LFC. For α_i <1, the DR control loop is active, and in all three areas, the proposed LFC-DR model shows superior performance compared to the conventional LFC. Moreover, the performance is better for smaller values of α_i, i.e., higher DR share. The variations in frequency and tie-line power for the three areas are shown in Figure 7.3 (d)-(f) and Figure 7.3 (g)-(i), respectively, and again the system performance is improved when DR has a higher share, i.e., for smaller values of α_i.

In the above simulation experiments, the communication latency for all areas is considered to be the same; however it is possible to have different latencies for different areas based on (7.5) and (7.6) (expanded in Appendix B), as will be shown in the next section. This can technically happen when communication latency is different for different Lagcos, which might be based on the communication infrastructure of each area.

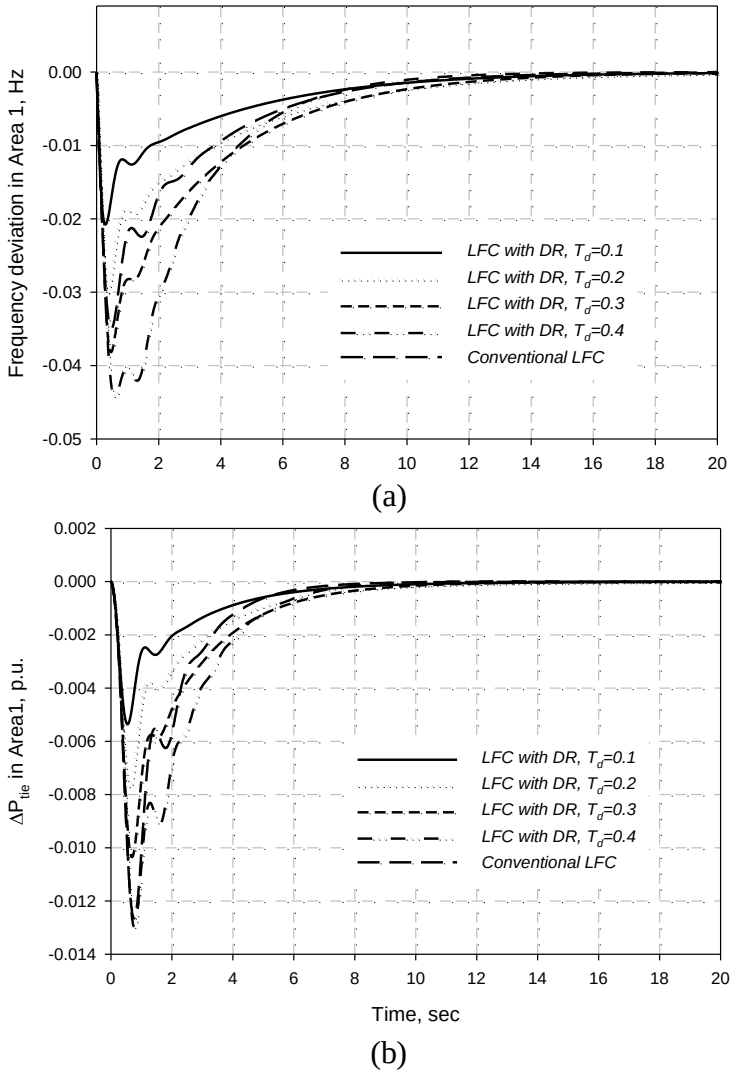


Figure 7.4. The impact of communication latency on, (a) frequency deviation, and (b) total tie-line power deviation in area 1.

The Impact of Latency on Dynamic Response

Since communication latency is an important parameter when DR is included in the LFC problem, it is always desired to evaluate its impact on the performance of the system. Therefore, a simulation has been carried out for different latencies while α_i =0.1.

Simulation results, given in Figure 7.4, show the impact of the DR communication latency on the performance of the system. The figure shows the frequency and tie-line power deviations for Area 1 only. The results are very similar for other areas. It is clear from Figure 7.4 that the dynamic behavior of the LFC-DR model is better than the one with the conventional LFC for communication delays smaller than 300 msec. However, the performance of the LFC-DR degrades when communication latency is greater than 300 msec. This impact is specific to the small power system under study. For large power systems with slower dynamics, the impact would be less.

Simulation Results for Multi-Area Power System with Multiple Gencos and Lagcos

In this section, the simulation results are presented to show the applicability of the proposed LFC-DR model to power system of any size. In addition, the effectiveness of the proposed DR control loop and the LQR design is evaluated and compared with the conventional LFC. The system studied is a large three-area power system with three Gencos and three Lagcos within each area, which could be realized from Figure 7.1. The areas are connected through stiff transmission lines; the system parameters, obtained from [7.21], are given in Table 7.2.

Table 7.2. Three-area power system with three Gencos and Lagcos for the simulation study [7.2].

MVA_{base} (1000 MW)	Gencos								
	Area 1			Area 2			Area 3		
	1	2	3	4	5	6	7	8	9
Capacity (MW)	1000	800	1000	1100	900	1200	850	1000	1020
D_i (pu/Hz)	0.015	0.014	0.015	0.016	0.014	0.014	0.015	0.016	0.015
$2H_i$ (pu.sec)	0.1667	0.12	0.2	0.2017	0.15	0.196	0.1247	0.1667	0.187
T_{tj} (sec)	0.4	0.36	0.42	0.44	0.32	0.4	0.3	0.4	0.41
T_{gj} (sec)	0.08	0.06	0.07	0.06	0.06	0.08	0.07	0.07	0.08
R_j (Hz/pu)	3.00	3.00	3.30	2.7273	2.6667	2.50	2.8235	3.00	2.9412
B_i (pu/Hz)	0.3483	0.3473	0.318	0.3827	0.3890	0.414	0.3692	0.3493	0.355
β_{ji}	0.4	0.4	0.2	0.6	0.0	0.4	0.0	0.5	0.5
	Lagcos								
λ_{ji}	0.3	0.5	0.2	0.4	0.2	0.4	0.1	0.2	0.7
$T_{d,ji}$ (sec)	0.15	0.1	0.1	0.2	0.1	0.05	0.1	0.15	0.1

Different communication latencies ($T_{d,ij}$), ranged from 50 to 200 msec, are considered for the Lagcos in the different areas, as shown in the last row of Table 7.2.

Step load increases of different magnitudes in the three areas are considered to evaluate the performance of the system with conventional LFC and two different values of α_i (α_i =0.1, 0.8) in the proposed LFC-DR model. The load disturbances for the three areas are $\Delta P_{L1} = 0.15$ pu, $\Delta P_{L2} = 0.12$ pu, and $\Delta P_{L3} = 0.1$ pu. The same LQR design is used for all cases.

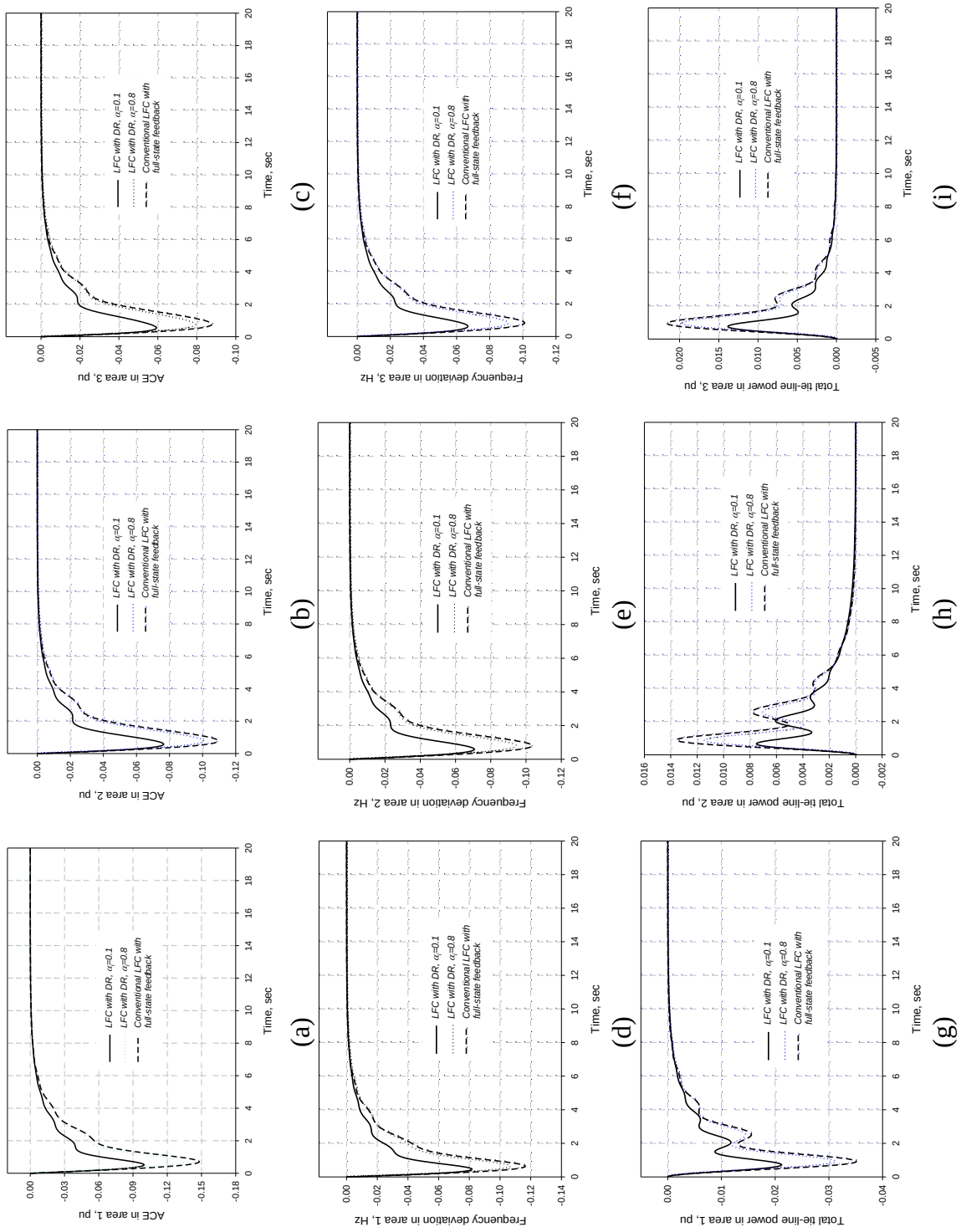


Figure 7.5. ACE, Frequency deviation, and total tie-line power in different areas for different α, multi-area power system with multiple Gencos and Lagcos.

Figure 7.5 shows the simulation results for the ACE (Figure 7.5 (a)-(c)), frequency deviation (Figure 7.5 (d)-(f)), and total tie-line power (Figure 7.5 (g)-(i)) for the LFC-DR model and for the conventional LFC, for the three areas. In general, in all cases the LFC-DR model when α_i =0.1 shows superior performance compared to the conventional LFC. In particular, the overshoot has decreased by nearly 30% in the LFC-DR (when α_i =0.1) compared to the conventional LFC. The settling time is also improved significantly for all areas when the LFC-DR with α_i =0.1 is applied. In all cases, the performance of the system with DR degrades as the value of α_i increases and trends toward the performance of the conventional LFC with full-state feedback design, as expected.

Conclusion

In this chapter, the proposed model and controller design (which were developed in Chapter 6 for a single-area power system) are expanded to a multi-area case with multiple Gencos and Lagcos. Then, simulation studies are designed and carried out for single-area power systems to show the most important features of the proposed LFC-DR model. It is shown that the proposed LFC-DR model can significantly improve the dynamic performance of the multi-area power system. In addition, the impact of communication latency on the performance of the system with the DR control loop is analyzed. Then, two simulations studies are presented for multi-area power systems with single and multiple Gencos and Lagcos. Simulation results show that in all cases, the proposed LFC-DR model has a superior performance compared to the performance of the conventional LFC. It has also been observed that the performance of the proposed LFC-

DR model is improved when a higher share (smaller values of α) has been devoted to the DR.

In general, it can also be concluded that the proposed LFC-DR model provides a general simulation framework for the researchers and ISOs/RTOs to study the different impacts of DR (technically and economically) on the system dynamic performance and frequency regulation at the transmission level.

Acknowledgement

This work was supported by the U.S. Department of Energy, Office of Science, Basic Energy Sciences, under Award # DE-FG02-11ER46817. The fruitful discussion of the feedback control theory with Dr. Steven Shaw, Dr. Robert Gunderson of Montana State University, and Dr. Ali Gorji of University of Toronto is acknowledged.

References Cited

[7.1] R. Walawalkar, et al., "An economic welfare analysis of demand response in the PJM electricity market," *Energ. Policy*, vol. 36, no. 10, pp. 3692–3702, Oct. 2008.

[7.2] H. Bevrani, *Robust Power System Frequency Control*, New York: Springer, 2009, ch. 1–3.

[7.3] S.A. Pourmousavi and M.H. Nehrir, "Introducing dynamic demand response in the LFC model," *IEEE Trans. Power Syst*., vol. 29, no. 4, pp. 1562–1572, July 2014.

[7.4] H. Kawabata and M. Kido, "A decentralized scheme of load frequency control power system," *Elect. Eng. Japan*, vol. 102, no. 4, pp. 100–106, Jul./Aug. 1982.

[7.5] Y.M. Park and K.Y. Lee, "Optimal decentralized load frequency control," *Elect. Power Syst. Res*., vol. 7, no. 4, pp. 279–288, Sept. 1984.

[7.6] M.S. Calovic, "Automatic generation control: Decentralized area-wise optimal solution," *Elect. Power Syst. Res*., vol. 7, no. 2, pp. 115–139, Apr. 1984.

[7.7] M. Aldeen and J.F. Marsh, "Observability, controllability and decentralized control of interconnected power systems," *Int. J. Comput. Elect. Eng*., vol. 16, no. 4, pp. 207–220, 1990.

[7.8] M. Aldeen, and J.F. Marsh, "Decentralized proportional-plus-integral control design method for interconnected power systems," in *Proc*. Inst. Elect. Eng., vol. 138, no. 4, pp. 263–274, Jul. 1991.

[7.9] M. Aldeen, "Interaction modeling approach to distributed control with application to power systems," *Int. J. Contr*., vol. 53, no. 5, pp. 1035–1054, 1991.

[7.10] T.C. Yang, H. Cimen, and Q.M. Zhu, "Decentralised load-frequency controller design based on structured singular values," in *Proc*. Inst. Elect. Eng. C, vol. 145, no. 1, pp. 7–14, Jan. 1998.

[7.11] T.C. Yang, Z.T. Ding, and H. Yu, "Decentralised power system load frequency control beyond the limit of diagonal dominance," *Int. J. Elect. Power Energy Syst*., vol. 24, no. 3, pp. 173–184, Mar. 2002.

[7.12] E.V. Bohn, and S.M. Miniesy, "Optimum load frequency sample data control with randomly varying system disturbances," *IEEE Trans. Power App. Syst*., vol. PAS-91, no. 5, pp. 1916–1923, Sept./Oct. 1972.

[7.13] K. Yamashita and T. Taniguchi, "Optimal observer design for load frequency

control," *Int. J. Elect. Power Energy Syst*., vol. 8, no. 2, pp. 93–100, Apr. 1986.

[7.14] A. Feliachi, "Load frequency control using reduced order models and local observers," *Int. J. Energy Syst*., vol. 7, no. 2, pp. 72–75, 1987.

[7.15] A. Rubaai and V. Udo, "An adaptive control scheme for LFC of multi-area power systems. Part I: Identification and functional design, Part-II: Implementation and test results by simulation," *Elect. Power Syst. Res*., vol. 24, no. 3, pp. 183–197, Sept. 1992.

[7.16] S. Velusami and K. Ramar, "Design of observer-based decentralized load-frequency controllers for interconnected power systems," *Int. J. Power Energy Syst*., vol. 17, no. 2, pp. 152–160, 1997.

[7.17] Y. Hain, R. Kulessky, and G. Nudelman, "Identification-based power unit model for load-frequency control purposes," *IEEE Trans. Power Syst*., vol. 15, no. 4, pp. 1313–1321, Nov. 2000.

[7.18] C.E. Fosha and O.I. Elgerd, "The megawatt-frequency control problem: A new approach via optimal control theory," *IEEE Trans. Power Ap. Syst*., vol. PAS-98, no. 4, pp. 563–577, April 1970.

[7.19] A. Brooks, et al., "Demand dispatch: Using real-time control of demand to help balance generation and load," *IEEE Power Energy Mag.*, vol. 8, no. 3, pp. 20–29, May/June 2010.

[7.20] T. Hiyama, "Design of decentralized load-frequency regulators for interconnected power systems," in *Proc*. IEE Generation, Transmission, and Distribution conf., vol. 129, no. 1, pp. 17–23, 1982.

[7.21] D. Rerkpreedapong, A. Hasanovic, and A. Feliachi, "Robust load frequency control using genetic algorithms and linear matrix inequalities," *IEEE Trans. Power Syst*., vol. 18, no. 2, pp. 855-861, May 2003.

CHAPTER 8

REAL-TIME DEMAND RESPONSE THROUGH AGGREGATE ELECTRIC WATER HEATERS FOR LOAD SHIFTING AND BALANCING INTERMITTENT WIND GENERATION

Contribution of Authors and Co-Authors

Manuscripts in Chapters 2 through 12

Author: S. A. Pourmousavi

Contributions: Proposed the original control approach for real-time DR, cooperated for coding in MATLAB®/m-file, interpreted the results, modified the simulation setup and redid all of them, prepared the manuscript, figures and tables.

Co-author: S. N. Patrick

Contributions: Developed EWH model and its aggregation, prepared actual hot water demand data and balancing reserve, developed economic analysis.

Co-author: M. H. Nehrir

Contributions: Provided important insight and overview of the research, interpretation of the results, and aided in the preparation of the manuscript.

Manuscript Information Page

Seyyed Ali Pourmousavi Kani, Stasha N. Patrick, M. Hashem Nehrir

IEEE Transactions on Smart Grid, 2014

Status of the manuscript:
____ Prepared for submission to a peer-reviewed journal
____ Officially submitted to a peer-reviewed journal
____ Accepted by a peer-reviewed journal
_X_ Published in a peer-reviewed journal

Published by the Institute of Electrical and Electronics Engineering (IEEE)

IEEE TRANSACTIONS ON SMART GRID, VOL. 5, NO. 2, MARCH 2014 769

Real-Time Demand Response Through Aggregate Electric Water Heaters for Load Shifting and Balancing Wind Generation

S. Ali Pourmousavi, *Student Member, IEEE*, Stasha N. Patrick, *Member, IEEE*, and M. Hashem Nehrir, *Life Fellow, IEEE*

***Abstract*—Demand response (DR) has shown to be a promising tool for balancing generation and demand in the future power grid, specifically with high penetration of variable renewable generation, such as wind. This paper evaluates thermostat set-point control of aggregate electric water heaters (EWHs) for load shifting, and providing desired balancing reserve for the utility. It also assesses the economic benefits of DR for the customers through time-of-use pricing. Simulation results reveal the achievement of the economic benefits to the customers while maintaining their comfort level and providing a large percentage of desired balancing reserve at the presence of wind generation.**

***Index Terms*—Aggregate electric water heaters (EWHs), balancing reserve, demand response, load shifting, smart grid, time-of-use (ToU) pricing, wind generation.**

I. Introduction

THE U.S. Department of Energy has established goals for a smart electric power grid, which facilitates customer participation and incorporation of clean, renewable generation sources, such as wind. "Enabling informed participation by customers" and "accommodating all generation and storage options" are two primary goals of smart grid identified by the U.S. DOE [1]. The first objective implies that in addition to allowing utility-based control of devices, the customers must also be given the opportunity to control their own power consumption and override any control signal from the utility to control/alter their power consumption in case needed. The second objective includes the incorporation of variable renewable energy sources (RES) on the electric power grid. However, the uncertain and variable nature of RES can create problems for power systems in providing balancing reserves when RES penetration is high, e.g., exceeding 20% [2]. As RES penetration increases, the conventional solution is to increase the amount of available reserve [3]. Since spinning reserves are mostly provided by fossil fuel-based power plants, their operation is costly and results in increased release of undesired emissions. While it is necessary to account for the variability of RES generation with balancing reserves, it is also desirable to have the ability to store any excess available power, e.g., any excess wind power, so that the excess power won't have to be curtailed [4].

One possible way to accomplish the above tasks is through demand response (DR). Specifically, residential electric water heaters (EWHs) and heat pumps are good candidates for this purpose, since electric energy can be stored as heat energy in their hot water tanks. Moreover, their control is both simple and fast. This paper is limited to control of EWHs only.

Residential EWHs account for approximately 20% of the U.S. residential daily energy demand and are the largest contributors to the morning and evening peaks in residential power demand [5]. It is therefore desired to shift a considerable percentage of EWHs power demand from hours of higher power demand to lower demand hours by heating the water during off-peak hours or when excess renewable energy is available. This procedure can also result in a large percentage of the balancing reserve necessary to integrate wind energy generation onto the grid. Therefore, it will be economically beneficial to the customers as well as utilities. However, considering that heat energy storage increases the heat losses of EWHs, the proposed DR algorithm should operate without significantly increasing the average daily energy demand and maximum power demand of the EWHs.

Thermostatically-controlled appliances (TCA) have been of interest in the last more than two decades to evaluate their benefits for load shifting and peak load shaving, e.g., [6]–[17]. Different control approaches from voltage control ([6], [7], [15]) to thermostat setpoint control, ([8], [10]–[12], [16], [17]) and ON/OFF control based on frequency deviation, ([9], [13], [14]) have been proposed for controllable residential loads to provide balancing reserve. The impacts of large-scale energy storage systems have also been investigated for balancing the variable renewable generation [18]. The following shortcomings relative to TCA control can be identified in the previous research, which have been addressed in this paper:

- Lack of economic benefit analyses to show the impact of direct load control (DLC) program on the cost of energy for the customers and utilities in [6]–[17],

Manuscript received March 20, 2013; revised April 29, 2013, June 25, 2013, August 21, 2013, and October 29, 2013; accepted November 02, 2013. Date of current version February 14, 2014. This work was in part supported by the DOE Award DE-FG02-11ER46817 and Pacific Northwest National Laboratory (PNNL), which is operated for the U.S. Department of Energy by Battelle under Contract DE-AC05-76RL01830. Paper no. TSG-00148-2013.

S. A. Pourmousavi and M. H. Nehrir are with the Electrical and Computer Engineering Department, Montana State University, Bozeman, MT 59717 USA (e-mail: s.pourmousavikani@msu.montana.edu; hnehrir@ece.montana.edu).

S. N. Patrick is with Rocky Mountain Power, Salt Lake City, UT 84111 USA (e-mail: stassja.noelle@gmail.com).

Color versions of one or more of the figures in this paper are available online at http://ieeexplore.ieee.org.

Digital Object Identifier 10.1109/TSG.2013.2290084

1949-3053 © 2014 IEEE. Personal use is permitted, but republication/redistribution requires IEEE permission.
See http://www.ieee.org/publications_standards/publications/rights/index.html for more information.

- Lack of accumulative energy analysis to show any increase/decrease in total energy consumption in [8]–[17],
- Violation of comfort level for some customers, reported in [16], [17]
- The need for additional expensive equipment (i.e., electronic switches and power electronic devices) for voltage control, proposed in [6], [7],
- Lack of investigation on load shifting together with a price signal response on a large number of controllable devices, [6]–[17],
- Short-term (i.e., few hours) simulation which doesn't reveal the pros and cons of the method proposed in the long-term (i.e., few days) considering weekdays and weekend days, [14],

In this paper, we evaluate the capability of aggregated EWHs as a DR tool to respond to control signals generated by the utility for load-shifting and balancing reserve. The thermostat setpoints of 1000 aggregated EWHs are controlled by the utility to respond to a time-of-use (ToU) pricing signal during the on-peak hours. As a result, some of the consumers electrical energy demand will be shifted from on-peak hours to off-peak periods. During the off-peak hours, the EWHs respond to a desired balancing reserve signal which also includes wind generation. However, the signal generated by the utility can be overridden by the customers if they choose to do so. We have not explored the consumers' override option in this paper.

The proposed model is compared to a no-control case, as well as to each of the above two control strategies (ToU pricing and balancing reserve). An important goal of the comparison is to assess the economic benefits of the proposed DR strategy for the customers, while maintaining safe water temperatures. It is desired to maintain this economic benefit without significantly increasing the total EWHs energy consumption and peak power demand. An actual desired balancing reserve signal is used in this study [19].

The rest of the paper is organized as follows. Section II covers the model formulation for both single and aggregated EWHs. The proposed thermostat setpoint control of aggregated EWHs is presented in Section III; simulation setup and configuration are covered in Section IV; and simulation results and discussions are given in Section V. Finally, the paper is concluded in Section VI.

II. Problem Formulation

Thermostat setpoint control of EWHs is one method to control their power consumption, which can be used: 1) to shift and flatten the demand profile and 2) to provide the balancing reserves needed in the presence of intermittent energy resources. An EWH has a thermostat setpoint ($T^i_{set}(t)$), and a deadband (D), where the temperature of the water inside the tank of each EWH (i) must be maintained within the range of the thermostat setpoint, i.e.:

$$T^i_{set}(t) - D \leq T_i(t) \leq T^i_{set}(t) \tag{1}$$

where $T_i(t)$ is the temperature of hot water inside of the tank of EWH i at time t. The tank of an EWH has a certain amount of thermal insulation (R value). This insulation is not 100% efficient, resulting in some heat loss. The heat loss through the tank increases when hot water with higher temperature is stored in the tank. A brief description of the modeling of an individual EWH and aggregated EWHs follows. More details on single residential EWH model are provided in [7], [20].

A. Individual EWH Model

The temperature of hot water inside of the EWH tank can be obtained as a function of time by (2) [20]:

$$T_h(t) = T_h(\tau).e^{-\left(\frac{1}{R'.C}\right)(t-\tau)} + \left\{G.R'.T_{out} + B(t).R'.T_{in} + Q.R'\right\}.\left[1 - e^{-\left(\frac{1}{R'.C}\right)(t-\tau)}\right] \tag{2}$$

where $T_h(t)$ is the water temperature inside EWH at time t (°F), τ is the previous sample ($t-1$, hours), C is the equivalent thermal mass (Btu/°F), G is the ratio of the surface area to thermal resistance of the tank, T_{out} is ambient environment temperature (°F). The parameters B and Q are piece-wise continuous terms whose expressions are given below ((4)) and defined in [7] and [20], and T_{in} is the incoming cold water temperature (°F). The parameters of (2) can be calculated as follows:

$$G = \frac{SA}{R}, \quad C = volume \times d_{water} \times C_p \tag{3}$$

where SA is the tank surface area (ft^2), R is the tank insulation thermal resistance (hour × ft^2 ×° F/BTU), *volume* is the capacity of the tank (gallons), d_{water} is the density of water (8.34 lbs/gallon), and C_p is the specific heat of water (1.0069 BTU/(lbs ×° F)). Other parameters in (2) are:

$$R' = \frac{1}{G + B(t)} \qquad B(t) = d_{water} \times F(t) \times C_p$$
$$Q = 3.4121 \times 10^{-8} \times (element\ kW\ rating) \tag{4}$$

It is shown in [21] that the average EWH daily power demand profile follows that of the average total daily residential demand for both weekday and weekend, as shown in Fig. 1. We therefore use the average residential electrical demand to shape the residential hot water demand curve by multiplying the average residential power demand by $K(t)$. This parameter is the amount of hot water produced by one kilowatt of electric power from T_{in} to $T_{set}(t)$ in one hour, neglecting convection losses. As shown in our previous work [7], the expression for $K(t)$ is as follows:

$$K(t) = \frac{1000\frac{\text{J}}{\text{s}} \times 3600\frac{\text{s}}{\text{hour}}}{1.0545 \times 10^3 \frac{\text{J}}{BTU_{ISO}} \times 1.00 \frac{BTU_{ISO}}{^\circ\text{F.lbs}}} \times \frac{1}{(T_{set}(t) - T_{in}) \times 8.34 \frac{\text{lbs}}{\text{gallon}}} \tag{5}$$

Note that in this paper, $K(\text{t})$ is a function of time, because it is a function of the thermostat setpoint, $T_{set}(t)$, which we are allowing to vary at each time step.

The value of hot water flow rate, $F(t)$, from each EWH tank is then equal to the consumer hot water demand rate at a given time, F_{demand}, as defined below:

$$F(t) = F_{demand}(t) = P_{avg}(t) \times K(t) \tag{6}$$

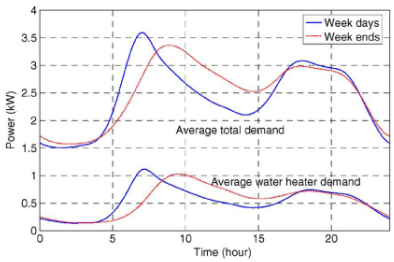


Fig. 1. Total power demand and EWH demand of an average house [7].

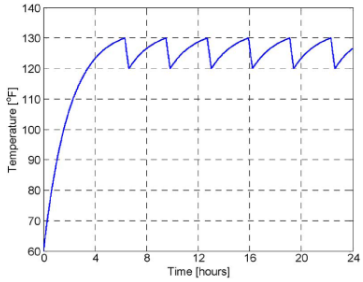


Fig. 2. Response of a single EWH with a 50-gallon hot water tank.

where $P_{avg}(t)$ is the average residential EWH power demand in kW.

Fig. 2 depicts the model response of an EWH with a 50-gallon hot water tank and consumption rate of 25 gal/hour, which is based on (2), where the EWH thermostat deadband is $D = 130 - 120 = 10°\text{F}$. The initial water temperature is assumed to be 60°F at the start of the simulation.

In this study, the EWHs thermostat setpoint is allowed to vary between 126°F and 160°F with a deadband of 10°F in some simulation cases reported in Table V (i.e., hot water temperature changes between 116°F–160°F). During peak power demand hours and/or when wind power is low, the thermostat setpoint of some EWHs are brought down to as low as 126°F in order to reduce energy consumption. Conversely, during off-peak hours and/or when excess wind power is available, the thermostat setpoint of some EWHs are set to as high as 160°F to absorb the available power.

Severe scalding can occur at water temperatures above 130°F, and as water temperature increases, the time for scalding to occur decreases logarithmically, to 5 seconds for water at 140°F and to just 0.5 seconds for water at 160°F [23]. To avoid scalding, the outflowing hot water will be mixed with the appropriate amount of cool water ($T_{in} = 60°\text{F}$) by a thermostatic mixing valve (TMV) prior to use. In such cases, not all of the water used by the customer is supplied by the EWH tank. It can be shown that the amount of hot water demand from the tank as a function of hot and cool water temperature and hot water consumed is [22]:

$$F(t) = F_{demand}(t).\frac{T_{mixed} - T_{in}}{T_h(t) - T_{in}} \tag{7}$$

TABLE I
PARAMETERS OF 1000 EWHS IN THE AGGREGATED MODEL [7], [22]

Parameters have a Random Normal Distribution for the 1000 EWH population.	
Parameter	**Value**
Tank volume (and tank surface area)	Mean 40 gallons, standard deviation 6.27, range approximately 20 to 65 gallons
Parameters have a Random Uniform Distribution for the 1000 EWH population.	
Parameter	**Value**
Thermal resistance of tank insulation, R	10 to 20 hour*ft^2*°F/BTU
Initial ON/OFF state	Approximately half ON, half OFF
Initial water temperature inside of the tank	120°F to 130°F

TABLE II
PARAMETERS THAT ARE THE SAME FOR ALL EWHS THROUGHOUT THE DURATION OF THE SIMULATION [22]

Parameter	Value
Temperature of cold water entering the tank, T_{in}	60 °F
Temperature of the ambient environment, T_{out}	70 °F
Deadband, D	10 °F
Heating element power in ON (OFF) state, P_{avg}	4.5 (0) kW

where T_{mixed} is the temperature of water after hot and cool water are mixed together. In this study $T_{mixed} = 116°\text{F}$.

B. Aggregated EWH Model

The aggregated EWH model comprises 1000 EWHs, whose parameters, given in (2), are set randomly within specific ranges [7]. Therefore, each EWH will respond slightly differently to thermostat setpoint control. This is due to the fact that each EWH has a different demand flow rate, tank insulation thermal resistance, tank surface area, and temperature during each time step. Table I shows the different parameter values used in the simulation, which are based on the actual EWHs data.

The parameters that are the same for all EWHs for the aggregated EWH model are given in Table II.

III. EWHs THERMOSTAT SETPOINT CONTROL

A. Control Based on Desired Balancing (INC/DEC) Reserve Signal

A desired balancing reserve signal, called INC/DEC (increase/decrease reserve), which is different from the ACE signal, is generated by the utilities every thirty seconds. Traditionally, when generation exceeds demand, utilities start decreasing the amount of reserve generation to balance total generation and load demand, i.e., a DEC signal is generated. However, in a grid with considerable penetration of RES, it is desirable to utilize all the excess renewable power when available.

Conventional power plants are not fast enough to match their output power with RES generation. Since the effect of increase in demand is the same as decrease in generation, an increase in demand can respond fast to the DEC signal. Likewise, when demand exceeds generation, an increase in reserve (or decrease

in demand) is required, and an INC signal is generated by the utility. The real set of INC/DEC signal used in our work is from a specific region served by the Bonneville Power Administration (BPA) and includes wind power generation [19]. There are approximately 1.36 million EWHs in this region for which the desired balancing reserve signal is obtained [22]. This data has been scaled for use with the 1000 EWHs in our study as given below.

$$\text{INC/DEC}_{scaled} = \frac{\text{INC/DEC}_{original}}{1.36 \times 10^6} \times 1000 \qquad (8)$$

The scaling approach used in (8) assumes that the power demand profile of the 1000 EWHs is as smooth as that of 1.36 million EWHs. In real cases, this may not be true because there is not as much diversity in the profile of 1000 EWHs as there is in the profile of 1.36 million EWHs. However, we were not able to get information about each individual EWH because of proprietary issues.

In this section, an algorithm is presented to adjust the thermostat setpoints of the 1000 EWHs in real-time according to the INC/DEC signal. In order to start the simulation, the following assumptions are made:

- Each EWH is assigned a random state at the beginning of the simulation—either ON or OFF—with even distribution.
- Each EWH is assigned a random initial thermostat setpoint, between the pre-defined range for the different cases studied. These cases will be discussed in Section IV. This setpoint determines the maximum and minimum temperatures that the EWH may reach. In the no control case (base case), the hot water temperature inside the EWHs' tanks varies between 120°F–130°F.
- Each EWH must maintain a temperature within the 10°F deadband below its setpoint. The size of this deadband is large enough so that the EWHs will not constantly switching ON and OFF.
- Smart grid environment is assumed where each EWH's thermostat setpoint may be adjusted by the utility at any time through two-way communication.

B. Calculation of Required Number of EWHs for DR Based on the INC/DEC Signal

In this study, the desired balancing reserve, INC/DEC, is the number of kilowatts of reserve or demand that needs to be created in order to balance generation with demand every 30 seconds. The proposed control algorithm runs every 5 seconds, by taking the difference between the actual balancing reserve desired and the balancing reserve that has been created since the beginning of the 30-second interval. Therefore, the needed balancing reserve is known every 5 seconds. Such communication is achievable through the current Internet as discussed in [24]. The major requirements for demand dispatch (from the communication point of view) are low-latency (about 500 ms, claimed to be available with the current Internet infrastructure) and quite small bandwidth. In [24], 3.2 million plug-in hybrid vehicles were considered in a simulation experiment with two-way communication, based on Internet protocols, to provide regulation service every 4 seconds through a central controller and load aggregators in the PJM market. Therefore, the communication requirement for our proposed control strategy could easily be achieved in the smart grid era.

In order to calculate the number of EWHs that need to be turned ON or OFF, it is important to calculate how many EWHs are about to turn OFF (i.e., $N_{turningOFF}(t)$) or ON (i.e., $N_{turningON}(t)$) in the next 30-second period by reaching their upper thermostat setpoint or falling to their lower water temperature. This is done to exclude these EWHs in the proposed algorithm because they are going to change state in the next 5 seconds. It is done by comparing the water temperature of each EWH in the ON state to its thermostat setpoint ($T^i_{set}(t)$), and that of each EWH in the OFF state to its lower temperature limit ($T^i_{set}(t) - D$). The temperature change for each EWH depends on the demanded hot water flow rate, current EWH water temperature, surface area of tank, and insulation thermal resistance of the EWH, as per (2). If the balancing reserve needed is less than half the power capacity of one EWH (less than 2.25 kW), then no EWHs will need to change state. This deadband prevents oscillations in the number of EWHs turning ON or OFF.

The balancing reserve created is calculated as follows:

$$P^{created}_{INC/DEC}(t) = -\left(P^{total}_{EWH}(t) - P^{total}_{EWH}\left(floor\left(\frac{t}{6}\right)\times 6\right)\right) \qquad (9)$$

where $P^{created}_{INC/DEC}(t)$ is the balancing reserve that has been created since the beginning of the 30-second period, $P^{total}_{EWH}(t)$ is the total power consumed by all EWHs at the present 5-second period which is calculated knowing the EWHs in the ON state and their nominal power consumption (Table II), $P^{total}_{EWH}(floor(t/6) \times 6)$ is the total power consumed by all EWHs at the beginning of the 30-second period, when the desired balancing reserve signal was first deployed, and $floor()$ is the MATLAB built-in function to round numbers to the lower whole number. The needed balancing reserve is calculated as follows:

$$P^{needed}_{INC/DEC}(t) = P^{desired}_{INC/DEC}(t) - P^{created}_{INC/DEC}(t) \qquad (10)$$

where $P^{needed}_{INC/DEC}(t)$ is the amount of balancing reserve that is still needed to be created in order to meet the desired balancing reserve, and $P^{desired}_{INC/DEC}(t)$ is the desired balancing reserve for the 30-second period. Finally, the number of EWHs to change at time t is calculated as follows:

$$N_{change}(t) = \left|round\left(\frac{P^{needed}_{INC/DEC}(t)}{P_{EWH}}\right)\right| \qquad (11)$$

where P_{EWH} is the power consumed by one EWH in the ON state (given in Table II), and $round()$ is the MATLAB built-in function to round numbers to the nearest whole number.

1) Desired Balancing Reserve Smaller (Greater) Than Zero: If the balancing reserve needed is smaller (greater) than zero, then more DEC (INC) is required, which means a decrease (increase) in reserve or an increase (decrease) in demand is needed. Therefore, the utility control must ensure that the

required number of EWHs, $N_{needed}(t)$, are turned ON (OFF) in each 5-second interval. This value is calculated as follows:

$$N_{needed}(t) = N_{change}(t) + [N_{turningON}(t) - N_{turningOFF}(t)] \times sign\left(P^{needed}_{INC/DEC}(t)\right) \quad (12)$$

where $N_{change}(t)$ is the calculated number of EWHs to be changed based on the balancing reserve signal for the next 5 seconds, $N_{turningON}(t)$ is the number of EWHs turning ON by the end of the present 5-second interval by falling to their lower temperature setpoint, $N_{turningOFF}(t)$ is the number of EWHs turning OFF by the end of the present 5-second interval by reaching their thermostat setpoint, $P^{needed}_{INC/DEC}(t)$ is the amount of balancing reserve that still needs to be created in order to meet the desired balancing reserve, and $sign()$ is the signum function in MATLAB to determine the sign of a number.

2) Desired Balancing Reserve Equal to Zero: If the balancing reserve needed is zero, then the net difference between the number of EWHs turning ON and OFF must be zero. If the net EWHs are turning ON (OFF), then an equal number of EWHs must be turned OFF (ON), so that no new balancing reserve is created, as defined by (13):

$$N_{needed}(t) = N_{turningON}(t) - N_{turningOFF}(t) \quad (13)$$

Using the $N_{needed}(t)$ calculated by the (13), there is a need for a mechanism to select the appropriate EWHs to be turned ON or OFF. If $N_{needed}(t)$ is smaller (greater) than zero, then some EWHs need to be turned OFF (ON) through thermostat setpoint control. The new setpoints are then chosen such that the thermostat setpoint of each chosen EWHs is lower (higher) than the present temperature. Once the water temperature of these EWHs is higher (lower) than their new thermostat setpoint, the EWHs will turn OFF (ON).

The proposed algorithm first makes an array, containing all of the temperatures of the EWHs in the ON (OFF) state, which are not going to turn OFF (ON) automatically in the next 5 seconds. Then, if the number of available EWHs in the ON (OFF) state is greater than or equal to $N_{needed}(t)$, then $N_{needed}(t)$ of these EWHs are chosen at random. If the number of available EWHs in the ON (OFF) state is less than $N_{needed}(t)$, then all of these EWHs are assigned new thermostat setpoints, which will cause them to turn OFF (ON). Equation (14) determines the new thermostat setpoint of each EWH to be turned OFF while (15) is used when EWHs are required to turn ON:

$$T_{new,set}(t) = T_{EWHtemp}(t) - \Delta T \quad (EWHs\ turning\ OFF) \quad (14)$$

$$T_{new,set}(t) = T_{EWHtemp}(t) + \Delta T + D \quad (EWHs\ turning\ ON) \quad (15)$$

where ΔT is a temperature deviation used to ensure that the new thermostat setpoint is lower (higher) than the present EWH temperature at the end of the 5-second period. In this study, ΔT is equal to 0.12°F, as this is the maximum temperature change that a water heater, with the parameters used in these experiments, can experience during a 5-second period. This value can be increased in real-world applications without affecting the proposed procedure.

TABLE III
BASE RATE FOR ELECTRIC ENERGY CONSUMED IN TOU PRICING SCHEME FOR PACIFIC POWER† [25]

Monthly usage [kWh]	Price [¢/kWh]
0-500	3.873
501-1000	4.590
1001_{+}	5.664

†Pacific Power is a utility in Portland, OR.

TABLE IV
TOU ELECTRICITY RATE ADJUSTMENTS IN RESIDENTIAL SECTOR (RATE SCHEDULE 4) FOR PACIFIC POWER [26]

	On-peak charge (06-10, 17-20 hours)	Off-peak credit (Rest of the day)
Winter	+$0.03316	-$0.01125

IV. SIMULATION SETUP AND CONFIGURATIONS

Five experimental models are designed to evaluate the effectiveness of the proposed thermostat control strategy. These cases (CASEs 0, 1, 2A, 2B, 3) are described below.

CASE0: No EWH Thermostat Setpoint Control: This case represents the operation of EWHs under no thermostat setpoint control. It is used as the base case for comparison with the other four cases studied, as given below. In this case, the hot water temperature varies between 120°F to 130°F.

CASE1: EWH Thermostat Setpoint Control Based Only on Balancing Reserve Desired by the Utility: In this case, the balancing reserve signal from the utility is used for EWH thermostat setpoint control for the whole day. In our study, the utility has full control over the thermostat setpoints of all EWHs. The hot water temperature varies between 116°F to 160°F in this case.

CASE2: EWH Thermostat Setpoint Control Based Only on ToU Pricing: ToU pricing is implemented by utilities, imposing higher prices during peak hours, and lower prices during off-peak hours. The goal is to encourage consumers to consume more power during off-peak hours and less during peak hours. In this study, it is assumed that all the customers participate in this DR program because of the economic benefit they gain. Oregon-based Pacific Power's electricity pricing rate structure for residential application is used in this study. It includes a constant charge depending on the amount of monthly electric energy consumption, as tabulated in Table III, and on-peak hours extra charge and off-peak hours credits, as given in Table IV.

In this study, the prices reported in Tables III and IV are used in all CASEs for the sake of comparison.

In this case, the thermostat setpoints of all EWHs are set to the minimum allowable temperature, 126°F (i.e., $T_{water} \geq$ 116°F) during on-peak hours. During off-peak hours, two different cases are defined. In CASE2A, the EWHs thermostat setpoints are set to 130°F during off-peak hours. However, this may not allow the EWHs to store enough thermal energy to make it through the on-peak hours without reaching the minimum temperature and thus turning ON. Therefore, another scenario, CASE2B, is introduced where the thermostat setpoints

TABLE V
BRIEF DESCRIPTION OF ALL FOUR DIFFERENT CASES

Case NO.	Description
CASE0	No control (hot water temperature: 120°F-130°F)
CASE1	Thermostat setpoint control - balancing reserves only (hot water temperature: 116°F-160°F)
CASE2A	Thermostat setpoint control –ToU pricing only (hot water temperature: 116°F-130°F)
CASE2B	Thermostat setpoint control – ToU pricing only (hot water temperature: 116°F-160°F)
CASE3	Thermostat setpoint control - balancing reserve and ToU pricing (hot water temperature: 116°F-160°F)

are set to 160°F during off-peak hours. In this case, when the on-peak period begins, the majority of EWHs have a temperature between 150°F and 160°F. The goal is for the EWHs to remain in the OFF state during the on-peak periods, i.e. not reaching the lower limit of water temperature (116°F) to cause the EWHs to turn back ON.

CASE3: EWH Thermostat Setpoint Control Based on ToU Pricing, and Balancing Reserve Desired: In CASE3, both the ToU pricing signal and balancing reserve signal are used. The ToU pricing signal has the highest priority of the two control signals due to the customer's desire for economic benefit. In this case, the EWHs operate based on ToU pricing signal during on-peak hours, and their setpoints are set to 126°F, the minimum allowable setpoint which ensures that the temperature of the water in the EWH tank never fall below 116°F. Thus, the EWHs consume less energy when the price for electricity is high. During off-peak hours, when the electricity price is low, all the EWHs opt into balancing reserve based setpoint control, and all setpoints are maintained between 126°F and 160°F. Table V summarizes the five cases discussed above.

The above experimental simulation cases are carried out focusing on six GOALs (areas of performance) discussed below.

GOAL1: Maintain Customer Comfort Level: The water within the EWH tank must always remain within safe temperature limits, as defined in Table V for each case. This is the highest priority goal, and is never allowed to be compromised.

GOAL2: Load Shifting From On-Peak to Off-Peak Hours: The ratio of total energy demand during on-peak hours to total energy demand during off-peak hours should be minimal, and lower in the control cases than in the no-control case.

GOAL3: Peak Load Equality or Reduction: The maximum aggregated EWH power demand in the control cases should be less than or equal to their maximum power demand in the no-control case. Significant increase in peak power demand is undesirable because this would necessitate the availability of large spinning reserves capacity which is not cost effective to the utility and customers and not environmentally friendly.

GOAL4: Total Energy Demand Equality or Reduction: The total energy consumed in the control cases should be less than or equal to the total energy demand in the no-control case. A large increase in total energy demand is undesirable to the customers. A small increase in energy demand can be compensated by the utility through direct payment or other methods as an incentive offered to the customers to participate in the program. In a better scenario, the economic benefits for the participating customers should compensate for the cost of the excess energy used.

TABLE VI
BRIEF DESCRIPTION OF ALL SIX DIFFERENT GOALS

GOAL NO.	Description
GOAL1	Maintain customer comfort level
GOAL2	Load shifting from on-peak to off-peak hours
GOAL3	Peak load equality or reduction
GOAL4	Total energy demand equality or reduction
GOAL5	Economic benefit to the customer
GOAL6	Provide desired balancing reserves

GOAL5: Economic Benefit to the Customer: The total cost to the customer in the control cases should be less than or equal to the total cost in the no-control case. It occurs when the customers shift their energy consumption from on-peak hours to off-peak periods, which will also result in flattening utility's power demand profile. Therefore, this strategy will benefit both the utility and customers.

GOAL6: Provide Desired Balancing Reserves: This is a high-priority goal, preceded in importance only by GOALs 1 and 2. The balancing reserves created in the control cases should match the balancing reserves desired by the utility with minimal error. In this study, minimal error is half of the power capacity of one 4.5 kW EWH (i.e., 2.25 kW). With this goal, some of the balancing reserves currently provided by fossil fuel based spinning reserve would be provided through EWHs DR. It can also allow high penetration of wind generation into the power grid. Table VI summarizes all six goals.

V. SIMULATION RESULTS AND DISCUSSION

In this section, two sets of simulation results showing the operation of the 1000 EWHs will be discussed. As it will be shown in Section V-A, among the different CASEs studied (Table V), CASE3 proves to be the best choice for the utility while it also has economic benefit for the customers. Therefore, simulation results for this case are given and discussed first in the below Section V-A. A comprehensive comparison between the results obtained for the different cases, based on the six goals discussed above, is presented in Section V-B.

A. Simulation Results for CASE3

In CASE3, the thermostat setpoints of all EWHs are set to 126°F during on-peak hours, in response to the ToU pricing scheme. During off-peak hours, the EWHs provide balancing reserves, allowing the thermostat setpoints to be adjusted between 126°F and 160°F. The performance of the EWHs is evaluated below, relative to the six GOALs given in Table VI.

GOAL1: Maintain Customer Comfort Level: Fig. 3 shows the outgoing water temperature of the 1000 EWHs during one week of simulation for CASE3. It is clear that the hot water supply is always maintained within reasonable and safe operating limits, (116°F–160°F).

The diversity of the parameters of the EWH population (Table I) as well as a large temperature range of the EWHs at any given time is of great importance for a successful DR program. In this regard, during off-peak hours the EWHs in CASE3 are evenly distributed between increasing and decreasing water temperature. However, during the on-peak hours all the EWHs respond to the ToU pricing signal, i.e. their thermostat setpoints

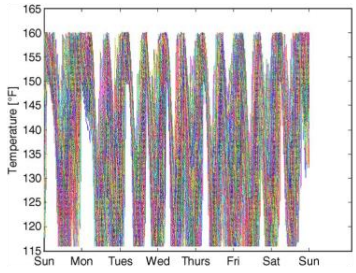


Fig. 3. Outgoing water temperature of 1000 EWHs, CASE3.

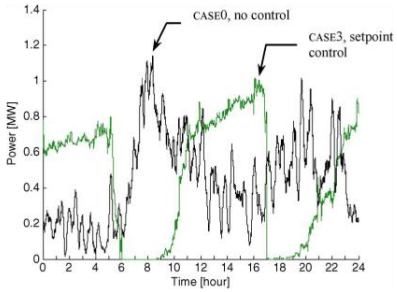


Fig. 4. Total power demand of 1000 EWHs, Wednesday, CASE3.

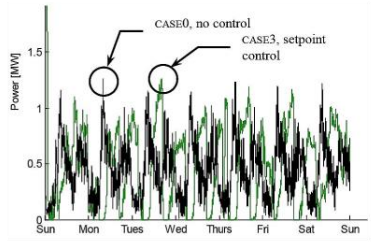


Fig. 5. Total EWHs demand for the one-week of simulation.

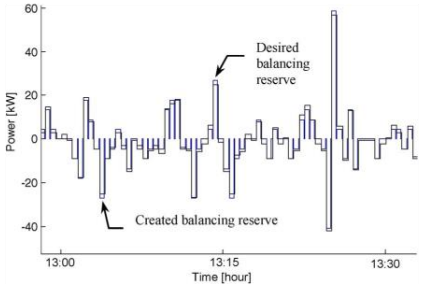


Fig. 6. Balancing reserve (INC/DEC signals) desired and created, Saturday, CASE3.

are lowered to 126°F so that they mostly stay off, and as a result, their water temperature decreases.

GOAL2: Load Shifting From On-Peak to Off-Peak Hours: Fig. 4 shows the total EWHs' power demand in response to CASE3 for a winter day. It is clear that, compared to the no-control case, the total EWHs power demand during on-peak hours has been reduced and shifted to off-peak hours. These are important steps toward flattening the distribution system load profile.

As shown in Fig. 4, it is clear that the EWHs' energy use in CASE3 (compared to CASE0) has been shifted from the on-peak hours to the off-peak periods due to ToU pricing. Considering that the EWH demand is only a portion of the total residential demand, the EWH load shifting helps in flattening the total residential demand profile.

GOAL3: Peak Load Equality or Reduction: The total EWHs' peak demand for the one-week simulation study remained approximately the same in CASE3 as in the no setpoint control, CASE0 as shown in Fig. 5. The peak demand is circled in the figure for both CASEs. The maximum EWHs power demand in both cases is 1.26 MW during a week.

GOAL4: Total Energy Demand Equality or Reduction: In CASE3, the total energy consumption of the 1000 EWHs increased by 4.7% compared to the no-control case (CASE0). In spite of this increase in energy use, there is still economic benefit for both the participating customers and the utility because of the benefit gained from ToU pricing, as discussed below (GOAL5), and the fact that the energy consumption of most of the EWHs is shifted to the off-peak hours (GOAL2). The cost of increase in the EWHs energy consumption due to heat loss can also be considered as a portion of the cost of the DR ancillary services.

GOAL5: Economic Benefit to the Customer: Under the ToU pricing scheme, the total weekly cost for the average EWH is $4.92 (as shown in Fig. 11), which is 45.01% less expensive than the $8.89 cost in CASE0. This is a great economic benefit for the customers even if they are not compensated by the utility for the small increase in the EWH energy consumption due to heat loss.

GOAL6: Provide Desired Balancing Reserves: Fig. 6 shows the desired and created balancing reserve (INC/DEC) signals for CASE3 for one half hour period during the off-peak hours, 13:00–13:30. These two curves are on top of each other most of the time. For the one-week simulation, the desired and created balancing reserve (INC/DEC) signals matched perfectly 75.92% of the time (i.e., the difference was less than 2.25 kW). This is a reasonable achievement given the fast variation of the actual balancing reserve signal.

Fig. 7 shows the Probability Distribution Function (PDF) for the absolute value of the absolute error between the balancing reserve desired by the utility and that created by the 1000 EWH population. There was a high probability of very small errors, and a very low probability of large errors.

B. Comparison of the Different Control Strategies

In this subsection, the performance of the control strategies (CASEs) are compared relative to the six GOALs discussed above.

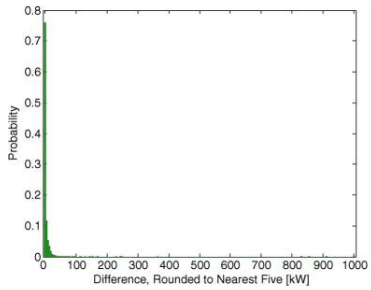


Fig. 7. PDF for absolute error between balancing reserve desired and created, CASE3.

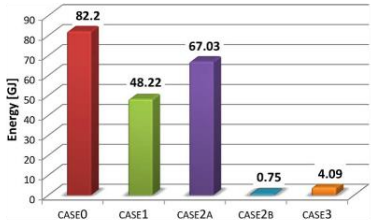


Fig. 8. Total demand during on-peak hours for different cases.

GOAL1: Maintain Customer Comfort Level: In all experimental cases, customer comfort level is maintained for the entire one-week simulation. The hot water supply is always maintained within the reasonable and safe operating limits, as defined (for each case) in Table V [22]. Only CASEs 1, 2B, and 3 allowed the water temperature to reach 160°F.

GOAL2: Load Shifting From On-Peak to Off-Peak Hours: Fig. 8 compares the total energy demand during on-peak hours (06–10, 17–20 hours) for all EWHs for the one-week of simulation for all cases.

In CASE2A, the maximum thermostat setpoint of 130°F during off-peak hours does not allow the EWHs to store enough energy to last through the peak periods. As a result, many of the EWHs reach their lower setpoints during the on-peak hours and turn ON. Therefore, in CASE2A, the EWHs use more energy during on-peak hours. However, in CASE1, the balancing reserve signal is used throughout the day which turns ON and OFF the EWHs during the on-peak hours. This is why the cost of energy is less in CASE2B compared to CASE1, which will be discussed in GOAL5. CASE2B is very successful compared to CASE2A because of the higher thermostat setpoint (160°F) during the off-peak hours, as opposed to 130°F in CASE2A. Therefore, in CASE2B, the EWHs have more thermal energy stored for use during the on-peak hours and their energy consumption during this period is very small.

CASEs 2B and 3 are by far the most successful in shifting the load from the on-peak periods to the off-peak hours. In both CASEs, the balancing reserve control allows the water temperature to increase to as high as 160°F during the off-peak hours. However, the average water temperature during the on-peak hours is higher in CASE2B than in CASE3, because in CASE3,

TABLE VII
THE ONE-WEEK ENERGY CONSUMPTION OF THE EWHS DURING OFF-PEAK AND ON-PEAK PERIODS FOR DIFFERENT CASES

CASE NO.	Off-peak hours energy [GJ]	On-peak hours energy [GJ]	% of the one-week on-peak power to total EWHs demand
CASE0	191.17	82.20	30.07%
CASE1	231.44	48.22	17.24%
CASE2A	206.08	67.03	24.54%
CASE2B	288.95	0.75	0.26%
CASE3	282.13	4.09	1.43%

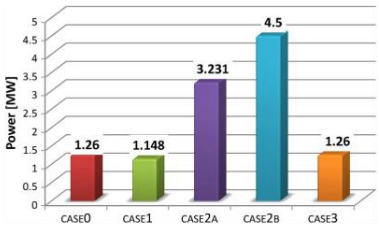


Fig. 9. Maximum total EWHs' power demand for different cases.

the EWHs are controlled during the off-peak hours with the balancing reserve signal which causes some EWHs not to reach to the maximum 160°F setpoint. Therefore, more energy is used during the on-peak hours in CASE3 than in CASE2B. Table VII shows the total EWHs' energy consumption during the off-peak and on-peak hours, and the percentage of EWHs' on-peak energy consumption to their total energy consumption for the one-week simulation study.

It is clear from Table VII that in CASE3 the EWHs use significantly less energy during the on-peak hours compared to the other cases without undesirable peak power demand increase, which will be discussed in GOAL3. This would greatly benefit the utilities and help to flatten their daily electric demand profile considering that the EWHs consume roughly 30% of the total electrical energy consumption in the residential sector during the peak-demand periods [7].

GOAL3: Peak Load Equality or Reduction: Fig. 9 compares the maximum power demand of the 1000 EWHs in each case. The maximum possible demand, if all EWHs were to be in the ON state at once, is 4.5 MW. CASE0 had a slightly higher peak power demand than CASE 1. This is because in CASE0, the ON/OFF cycling of the EWHs is only controlled by the hot water demand, while in CASE1 the desired balancing reserve signal also influences the operation of EWHs. As a result, fewer EWHs are turned ON at the same time in CASE1.

In CASEs 2A and 2B, the thermostat setpoints of all EWHs are set to their ceilings during off-peak hours (130°F in CASE2A and 160°F in CASE2B). This will cause all EWHs to act in the same way at the same time and decreases diversity. As a result, more EWHs stay in the ON mode at the same time during the off-peak hours, compared to CASEs 0, 1 and 3 and result in a higher peak power (Fig. 9). Moreover, the higher thermostat setpoint in CASE2B further increases the chance of having all EWHs in the ON mode at the same time. Therefore,

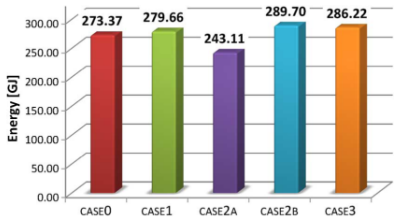


Fig. 10. Total weekly energy demand for different cases.

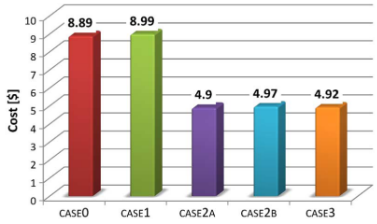


Fig. 11. Average weekly cost per EWH for different cases.

it can be concluded that CASEs 2A and 2B cannot be the options for the utility.

CASE3 has a slightly higher peak demand than CASE1. It is because the hot water temperature in most EWH tanks has reached close to the minimum value allowed (116°F) at the end of the on-peak period. Therefore these EWHs can only respond to DECs (i.e., increases in power demand.)

GOAL4: Total Energy Demand Equality or Reduction: Fig. 10 compares the total energy consumed by all EWHs in the one-week simulation period. The total one-week energy consumption of all EWHs is within 10% of each other in the different cases studied. Since the primary goals of these experiments are to provide balancing reserves and shift some of the demand from the on-peak hours to the off-peak periods, total energy consumption is less important as long as it is not increased greatly. CASE3, which was the most effective case of all for load shifting and providing balancing reserve (without increasing peak power demand) had about 4.7% increase in total energy consumption than the no-control case (CASE0). This small increase in energy consumption can be justified as the cost of ancillary services provided for the utility.

GOAL5: Economic Benefit to the Customer: In all CASEs, the price of the electricity is kept the same, as reported in Tables III and IV. But, the ToU pricing signal is only used as control signal in the CASEs 2A, 2B and 3. Fig. 11 compares the average cost of electricity for a single EWH in the one-week simulation period.

CASEs 0 and 1 are the most expensive ones, because electricity price doesn't affect power consumption through the ToU pricing signal. In CASEs 2A and 2B, the ToU pricing signal is the only signal used for thermostat setpoint control. These cases have a definite economic benefit for the consumers over CASEs 0 and 1. However, the large increases in the peak power in CASEs 2A and 2B (Fig. 9) have caused these cases to be ruled out as a possible method of control.

Although in both CASEs 2B and 3, the customers responded to the pricing signal by lowering the EWH thermostat setpoint to 126°F during the on-peak hours, the cost was 1.01% lower in CASE3 than in CASE2B. This is due to the fact that in CASE2B, the EWHs thermostat setpoints are always 160°F during the off-peak hours, thus causing the EWHs to consume more energy overall, as compared to CASE3, where the balancing reserve signal is used during off-peak hours.

GOAL6: Provide Desired Balancing Reserves: In CASEs 0 and 2 (2A and 2B), there were no balancing reserve control signals, and the balancing reserve matching could not be evaluated. CASE1, in which the only control signal was the desired balancing reserve, was able to provide the needed balancing reserves a higher percentage (93.17%) of the time compared to 75.92% for CASE3. This is because in CASE3, the pricing signal takes priority during on-peak hours, and balancing reserves are not provided during those periods.

Overall, CASE3 is considered the most effective amongst all the CASEs studied, as it provides economic benefit to the participating customers, as well as some load shifting and balancing reserve for the utility without considerable increase in energy consumption.

VI. Discussion and Conclusion

This study shows that thermostat setpoint control of aggregated EWHs can be beneficial to the utility as well as the participating customers. The proposed method considers load shifting and price signal response simultaneously, investigates the impacts of the method for a week as opposed to few hours, and includes economic benefit analysis for the customers to participate in the DR program.

Five control methods were explored considering six goals with the highest priority goals being customer comfort level and safety (i.e., maintaining the water temperature within safe limits) and load shifting from on-peak demand hours to off-peak hours. Simulation results show that among the five control methods studied, the method that combines utility control of EWHs thermostat setpoint control along with customers responding to the ToU price signal provided by the utility (CASE3) yields the best results. It provided hot water (between 116°F–160°F) all the time, resulted in a significant reduction of EWHs' demand during the on-peak hours and provided load shifting. It also provided balancing reserves for the utility in the presence of wind generation (75.92% of the time during off-peak hours). Moreover, this control method resulted in a large reduction (45.01%) in the cost of electricity for the customers compared to the no-control case (CASE0). Therefore, both the utility and customers can benefit from this control method.

In addition to wind power, solar power could also be partially or fully accommodated using the proposed method. Beyond the benefits to the utility and customers, such DR strategies will also have invaluable environmental benefits, i.e. reduction in undesired emissions, as a result of avoiding the use of fossil fuel-based spinning and non-spinning reserves.

REFERENCES

[1] U.S. Department of Energy, "Smart grid," Sep. 28, 2011 [Online]. Available: http://energy.gov/oe/technology-development/smart-grid

[2] H. Holttinen *et al.*, "Design and operation of power systems with large amounts of wind power," VTT Technical Research Centre of Finland, Helsinki, Finland, Rep. 2493, 2009.

[3] R. Doherty and M. O'Malley, "A new approach to quantify reserve demand in systems with significant installed wind capacity," *IEEE Trans. Power Syst.*, vol. 20, no. 2, pp. 587–595, May 2005.

[4] P. Denholm, E. Ela, B. Kirby, and M. Milligan, "The role of energy storage with renewable electricity generation," National Renewable Energy Laboratory, Tech. Rep. NREL/TP-6A2-47187, Jan. 2010.

[5] U.S. Energy Information Administration, "Residential energy consumption survey," Sep. 28, 2011 [Online]. Available: http://www.eia.gov/consumption/residential/reports/electronics.cfm

[6] M. H. Nehrir, B. J. LaMeres, and V. Gerez, "A customer-interactive electric water heater demand-side management strategy using fuzzy logic," in *Proc. IEEE Power Eng. Soc. Winter Meet.*, New York, 1999, pp. 433–436.

[7] M. H. Nehrir, R. Jia, D. A. Pierre, and D. J. Hammerstrom, "Power management of aggregate electric water heater loads by voltage control," in *Proc., IEEE Power Eng. Soc. Gen. Meet.*, Tampa, FL, USA, 2007, pp. 492–497.

[8] N. Lu and S. Katipamula, "Control strategies of thermostatically controlled appliances in a competitive electricity market," in *Proc., IEEE Power Eng. Soc. Gen. Meet.*, San Francisco, CA, USA, 2005, pp. 202–207.

[9] N. Lu and T. Nguyen, "Grid FriendlyTM appliances—Load-side solution for congestion management," in *Proc., 2005/2006 IEEE PES Transm. Distrib. Conf. Exhib.*, Dallas, TX, USA, 2006, pp. 1269–1273.

[10] D. S. Callaway, "Tapping the energy storage potential in electric loads to deliver load following and regulation, with application to wind energy," *Energy Convers. Manage.*, vol. 50, no. 9, pp. 1389–1400, 2009.

[11] S. Parkinson, D. Wang, C. Crawford, and N. Djilali, "Comfort-constrained distributed heat pump management," in *Proc. IEEE Intersoc. Electr. Electron. Eng. (ICSGCE 2011)*, Piscataway, NJ, USA, 2011.

[12] D. Wang, S. Parkinson, W. Miao, H. Jia, C. Crawford, and N. Djilali, "Online voltage security assessment considering comfort-constrained demand response control of distributed heat pump systems," *Appl. Energy*, 2012.

[13] N. Lu, D. J. Hammerstrom, and S. N. Patrick, "Grid friendly device model development and simulation," Pacific Northwest National Laboratory, Richland, WA, USA, Rep. 18998, 2009.

[14] J. A. Short *et al.*, "Stabilization of grid frequency through dynamic demand control," *IEEE Trans. Power Syst.*, vol. 22, no. 3, pp. 1284–1293, Aug. 2007.

[15] J. Kondoh, N. Lu, and D. J. Hammerstrom, "An evaluation of the water heater load potential for providing regulation service," *IEEE Trans. Power Syst.*, vol. 26, no. 3, pp. 1309–1316, Aug. 2011.

[16] N. Lu, "An evaluation of the HVAC load potential for providing load balancing service," *IEEE Trans. Smart Grid*, vol. 3, no. 3, pp. 1263–1270, Sep. 2012.

[17] N. Lu and Y. Zhang, "Design considerations of a centralized load controller using thermostatically controlled appliances for continuous regulation reserves," *IEEE Trans. Smart Grid*, vol. 4, no. 2, pp. 914–921, Jun. 2013.

[18] D. Shively *et al.*, "Energy storage methods for renewable energy integration and grid support," in *Proc., IEEE Energy 2030 Conf.*, Atlanta, GA, USA, 2008, pp. 1–6.

[19] Bonneville Power Administration, "Wind generation and total load in the BPA balancing authority" [Online]. Available: http://transmission.bpa.gov/Business/Operations/Wind/

[20] P. S. Dolan and M. H. Nehrir, "Development of a residential electric water heater model using energy flow analysis," in *Proc. 24th North Amer. Power Symp.*, Reno, NV, USA, Oct. 1992, pp. 272–277.

[21] "Descriptions of electric energy use in single family residences in the Pacific Northwest, 1986–1992," Office of Energy Resources Bonneville Power Administration. Portland, OR, USA, Dec. 1992.

[22] S. N. Patrick, "Control of aggregate EWHs for load shifting and balancing intermittent renewable energy generation in a smart grid environment," M.S thesis, Electrical Engineering, Montana State University-Bozeman, , 2011.

[23] M. L. Katcher, "Scald burns from hot tap water," *J. Amer. Med. Assoc.*, vol. 246, no. 11, pp. 1219–1292, Sep. 1981.

[24] A. Brooks, E. Lu, D. Reicher, C. Spirakis, and B. Weihl, "Demand dispatch: Using real-time control of demand to help balance generation and load," *IEEE Power Energy Mag.*, vol. 8, no. 3, pp. 20–29, May/Jun. 2010.

[25] Pacific Power, *Comparing Your Power Options,* May 31, 2011 [Online]. Available: http://www.pacificpower.net/content/dam/pacific_power/doc/Your_Account/Pay_Your_Bill/Highlights_August_10/2190-37_PP_LabelInsert_Residential-OR.pdf

[26] Pacific Power, *Oregon On-Peak & Off-Peak Hours,* May 31, 2011 [Online]. Available: http://www.pacificpower.net/ya/po/otou/ooh.html

S. Ali Pourmousavi (S'07) is a Ph.D. student in the Electrical and Computer Engineering (ECE) Department at Montana State University, Bozeman, MT, USA.

Stasha N. Patrick (S'07–M'13) received her B.S. and M.S. degrees from Montana State University, Bozeman, MT, USA, in 2008 and 2011 respectively, both in electrical engineering.

M. Hashem Nehrir (S'68–M'71–SM'89–F'10) is a Professor in the Electrical and Computer Engineering Department at Montana State University, Bozeman, MT, USA.

CHAPTER 9

OWNERSHIP COST CALCULATION FOR DISTRIBUTED ENERGY RESOURCES USING UNCERTAINTY AND RISK ANALYSES

Contribution of Authors and Co-Authors

Manuscripts in Chapters 2 through 12

Author: S. A. Pourmousavi

Contributions: Developed the simplified grid model (SGM) for the simulation with all of its components conceptually and in MATLAB®/Simulink, designed different simulation setups, including moving clouds, different types of SGM, and frequency/voltage figures.

Co-author: M. H. Nehrir

Contributions: Provided important insight and overview of the research, interpretation of the results, and aided in the preparation of the manuscript.

Co-author: R. K. Sharma

Contributions: Supervised the project, reviewed the final manuscript.

Manuscript Information Page

Seyyed Ali Pourmousavi Kani, M. Hashem Nehrir, Ratnesh K. Sharma

IEEE Transactions on Power Systems, 2014

Status of the manuscript:
____ Prepared for submission to a peer-reviewed journal
_X_ Officially submitted to a peer-reviewed journal
____ Accepted by a peer-reviewed journal
____ Published in a peer-reviewed journal

Published by the Institute of Electrical and Electronics Engineering (IEEE)

OWNERSHIP COST CALCULATIONS FOR DISTRIBUTED ENERGY RESOURCES USING UNCERTAINTY AND RISK ANALYSES

The following work is submitted for possible publication on the IEEE Transactions on Power Systems in 2014

S.A. Pourmousavi[1], M.H. Nehrir[1], R. K. Sharma[2]

[1] *Department of Electrical and Computer Engineering, Montana State University, Bozeman, MT 59717*

[2] *Energy Management Department, NEC Laboratory America Ltd., Cupertino, CA 95014*

Abstract

Ownership cost calculation plays an important role in optimal operation of DERs and MGs in the future power system, known as smart grid. In this chapter, a general framework for ownership cost calculation is proposed using uncertainty and risk analyses. Four ownership cost calculation approaches are introduced and compared based on their associated risk values. Finally, the best method is chosen based on a series of simulation results, performed for a typical diesel generator (DiG). Although simulation results are given for a DiG (as commonly used in MGs), the proposed approaches can be applied to other MG components, such as batteries, with slight modifications, as presented in this chapter. The analyses and proposed approaches can be useful in MG optimal design, optimal power flow, and market-based operation of the smart grid for accurate operational cost calculations.

Introduction

In the smart grid era, cost-based operation of DERs and MGs, including their

ownership costs, is inevitable. Strictly speaking, accurate operational cost calculation plays an important role for profitable operation of DERs for their owners, as one of the major goals projected for the smart grid [9.1]. In general, different uncertainty sources can be envisioned for different elements of the operational cost (such as depreciation and operating costs), which are the actual causes of inaccuracy in the cost calculations. Therefore, an accurate operational cost calculation model considering uncertainties with lower risk is essential for power/energy management and optimal sizing of MGs, as well as for optimal power flow, power scheduling, and market-based operation of power systems. This chapter proposes a general framework for DERs ownership cost calculation, which is an important part of the operational cost considering existing uncertainties and associated risks.

Power and energy management of islanded and grid-tied MGs is important for their optimal operation and to minimize their operational costs, e.g. [9.2]-[9.19]. However in these references, the ownership cost of the equipment is not investigated explicitly nor in some cases considered in the optimal MG operation. For example, only fuel cost is considered for a DiG, [9.2], [9.3], [9.5]-[9.9], [9.13], [9.15]; or in some other literature, e.g., [9.11], [9.12], [9.16], [9.17], the cost of DiG operation is considered as a price offered by the owner (similar to bids given by the participants in the electricity market). Also in [9.4] and [9.10], the battery cost is not included in the proposed management algorithm. In [9.14] and [9.19], the battery cost is explored based on the estimated battery lifetime, however the proposed approaches do not consider the uncertainties in the operation of the battery that could alter the true battery cost. As a

result, substantial fluctuations were observed in the estimated cost, particularly in the earliest days of operation, when a high level of uncertainty occurs. In [9.18], the battery ownership cost is incorporated in the MG operation objective function, however it will be shown in this chapter that it will not always give accurate results.

There is a great amount of literature in the area of optimal sizing of MG components, where cost of all equipment (such as DiG and battery) is considered. A comprehensive literature review on this topic is given in [9.20]. Nevertheless, the actual operational uncertainties and associated risks in the ownership cost calculations are not investigated. Similar deficiencies exist in several technical reports on the cost-benefit analysis of battery technologies, e.g. [9.21], [9.22]. All in all, there is no independent study on the ownership cost calculation, to the best of our knowledge.

This chapter lays out a general framework for DERs ownership cost calculation considering uncertainty and risk analyses. Initially, four different approaches are presented to calculate DERs ownership cost, where two of the approaches are proposed by the authors. Various uncertainty sources in the calculations are then introduced, where an appropriate discrete probability density function (DPDF) is specified for each in the simulation studies. In order to define the appropriate DPDFs for the uncertain parameters, an islanded MG has been designed using HOMER® [9.23] and the data obtained has been utilized. Then, a general basis for sensitivity and risk analyses based on the DPDFs is developed. Finally, the best model is chosen based on the uncertainty analysis along with risk calculation through simulation studies. To show the applicability and adaptability of the proposed framework to other DERs, the proposed model is also adapted for battery

ownership cost calculations.

Problem Statement

The operational cost calculation (known as machinery cost in industrial engineering and engineering economic analysis) is typically divided into two categories (as shown in Figure 9.1): 1) "*ownership costs*", which occur regardless of machine use (usually expressed per hour of operation), and 2) "*operating costs*", which vary directly with the amount of machine use [9.24], [9.25]. The true value of these costs cannot be known until the machine is sold or worn out. However, these costs can be estimated by making a few assumptions about machines' life, annual use, and fuel and labor costs. These assumptions should be treated as uncertainty sources in the calculations through uncertainty and risk analyses.

Ownership costs (also called fixed costs) include depreciation, interest (opportunity cost), taxes, insurance, and housing and maintenance facilities [9.24], [9.25]. In MGs, it is not common to insure the lifetime of a device. Therefore, insurance (insurance of equipment replacement in case of fire or other natural disaster) is neglected [9.26]. The housing cost (the cost of shelter or building to keep the equipment safe) is included in the capital investment of the equipment. However, property taxes which are commonly considered in farm machinery cost estimations [9.26], are ignored in our study, as they are usually less than 1% of the purchase cost altogether. Instead, we will focus on the most important parameters, such as machines' lifetime and their annual use. Therefore, the ownership cost calculation will be limited to the depreciation cost calculation and its components (i.e., salvage value and economic lifetime).

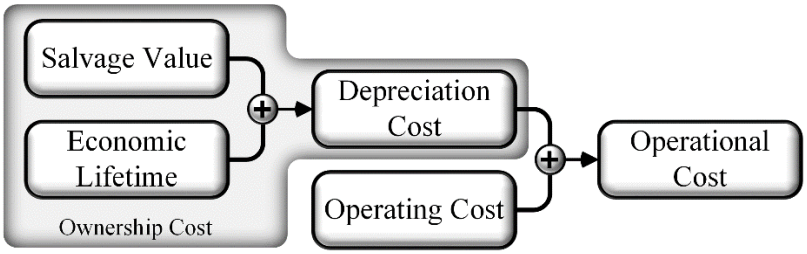


Figure 9.1. Overview of the operational cost calculation model adapted for this chapter.

The *operating cost* is the second and last part of the operational cost calculations. This cost can be so different from one DER to another; even from one manufacturer to another; and from one size to another. Therefore, it is complicated, if not impossible, to develop a general framework for operating cost calculation for different DERs. Furthermore, the operating cost is significantly less than the ownership cost for many DERs, such as battery, solar Photovoltaic (PV) panels, wind turbines, etc. As an example, the operating cost of solar PV panels is approximated as 0.005 $/kW in [9.4], which is negligible compared to the operating cost of DiG. For DiGs, the operating cost is an important factor since it includes fuel cost. This chapter only explores ownership cost calculations considering uncertainties.

The Proposed General Framework for Ownership Cost Calculation

Depreciation is a cost subsequent from wear, obsolescence, and age of a machine where age and accumulated hours of use are usually the most important factors in determining the remaining value of a machine [9.24]-[9.26]. Prior to annual depreciation cost calculations, economic life for the machine and the salvage value at the end of its economic lifetime are necessary to be specified.

Economic Life: There are two different economic lifetimes considered in this chapter: 1) The *economic life of an equipment*, defined as the number of years (for PVs), hours (for DiGs), or ampere-hours (A.h.) for battery, for which costs are to be approximated, and 2) The *project lifetime*, which can be expressed as the economic lifetime of a project based on the longest equipment lifetime in the system, or other considerations such as the user's expected lifetime of the whole project. As a result, some of the equipment with relatively shorter lifetime, compared to the project lifetime, will experience replacement(s) during the project lifetime. For instance, if a DiG lasts six years, and the project lifetime is expected to be 20 years, the DiG will have to be replaced three times throughout the project lifetime (i.e., at year six, 12 and 18 of the project).

Although the useful lifetime of different devices are expressed in different terms, similar principles can be employed for their ownership cost calculation with minor modifications.

Salvage Value: The salvage value is an estimate of the sale value of the equipment at the end of its economic lifetime [9.24]-[9.26]. As it is shown in Figure 9.1, a prior knowledge about this value is essential at the time of ownership cost calculation. Without loss of generality, this value is considered to be zero in this chapter because equipment such as DiGs and batteries will be used until they are totally worn out. As a result, they are assumed to have no value at the end of their lifetime.

Based on the definition and assumptions given above, four different approaches are introduced below for ownership cost calculation. Then, uncertainty sources are identified and a method for performing risk analysis is developed. Here, all equations are

developed for DiG without loss of generality. Simulation results and comparisons of the four approaches are given in the earlier section. Similar equations with slight modifications (as given for battery in the earlier section) can be utilized for other DERs.

Approach I (Base-case): No Replacement Cost

In this approach, the depreciation cost is calculated based on the equipment's economic lifetime and its salvage value. It is also assumed that the lifetime of the project is the same as the economic lifetime of the equipment. This is a standard approach in the ownership cost calculation [9.24] and will be considered as the base-case scenario for comparison with other approaches.

The depreciation cost (C_{dep}) can be expressed as:

$$C_{dep} = C_{pur} - C_{sal} \tag{9.1}$$

where C_{pur} and C_{sal} are the capital cost and salvage value of the equipment ($), respectively. Since no replacement of the equipment is considered throughout the project lifetime:

$$C_{pur} = C_{pur,0} \tag{9.2}$$

where $C_{pur,0}$ ($) is the current purchase (capital) price of the equipment, including installation fees and transportation. The combined costs of depreciation and interest can be calculated by using the *capital recovery factor*. This cost is called equivalent uniform annual cost (EUAC) [9.25]. Capital recovery is the dollar amount that would have to be set aside each year to repay the value lost due to depreciation, and pay the interest costs [9.25], as given below:

$$C_{EUAC} = C_{dep} \times CRF\left(i,n\right) \tag{9.3}$$

where $CRF\left(i,n\right)$ is:

$$CRF\left(i,n\right) = \frac{i \times \left(1+i\right)^{n}}{\left(1+i\right)^{n} - 1} \tag{9.4}$$

where *n* is the project lifetime, and *i* is the effective annual interest rate calculated in terms of the effective annual interest rate (i_{int}) and inflation (i_{inf}) as follows:

$$i = \frac{i_{\text{int}} - i_{\text{inf}}}{1 + i_{\text{inf}}} \tag{9.5}$$

where i_{int} can be considered as opportunity cost of investment if someone uses its own capital and i_{inf} is the annual inflation rate. This method of depreciation calculation is called *Straight-line depreciation* [9.25]. Effective interest rate is considered to be constant throughout the lifetime of the project since its variation does not significantly affect the calculations.

The ownership cost per hour for the DiG can be estimated by estimating the annual operation hours of the DiG, neglecting insurance, taxes and housing costs of the equipment, as follows [9.26]:

$$C_I^h = \frac{C_{EUAC}}{h_y} \tag{9.6}$$

where h_y is the estimated annual hours of operation for the DiG studied.

Approach II: No Replacement Cost
and Effective Annual Interest Rate

In this approach, which has been widely used in chapter, e.g., [9.18], the effective interest rate and equipment replacement are ignored. The hourly ownership cost of DiG (per A.h. in case of batteries) can be determined by (9.7):

$$C_{II}^{h} = \frac{C_{dep}}{h_y} \tag{9.7}$$

where C_{dep} is calculated by (9.1), and h_n is the estimated economic lifetime of the equipment (in terms of hours for DiGs and A.h. for batteries). It will be revealed in the simulation studies that Approach II yields erroneous results which could lead to a series of incorrect decisions, e.g., in the cost-based power/energy management algorithms or in the electricity market.

Approach III: Cost Calculations
Considering Replacement Cost

In this proposed approach, the purchase cost of the equipment, defined by (9.2), will be modified to include replacement(s) cost as follows:

$$C_{pur} = C_{pur,0} + C_{rep} \times NO_{rep} \tag{9.8}$$

where C_{rep} is the replacement cost of the equipment; and NO_{rep} is the number of replacements of the equipment throughout the project lifetime. Replacement cost is considered to be 70% of the present worth (i.e., the current purchase price), since some installation fees such as wiring or housing will not be paid again. Here, we propose two approaches (III.A and III.B explained below) to calculate the ownership cost using the

depreciation cost explained above and considering replacement cost.

Approach III.A-EUAC with Replacement. In this approach, a similar procedure to Approach I will be executed using (9.3)-(9.5), to calculate the EUAC. Finally, the ownership cost per hour for the DiG can be calculated using the estimated annual operation hours of the DiG (h_y) as follows:

$$C^h_{III.A} = \frac{C_{EUAC}}{h_y} \tag{9.9}$$

It can be seen from (9.9) that the annual operation hours of the equipment is utilized to normalize the ownership cost. As it can be noticed from the explanation given above, so far the difference between Approach I and Approach III.A is only the depreciation cost calculation considering replacement costs.

Approach III.B-Depreciation with Replacement. Similar to Approach III.A, depreciation cost of the equipment will be calculated using the replacement cost of the equipment throughout the lifetime of the project. However, the EUAC is not used and depreciation cost will be directly utilized for ownership cost calculation. Contrary to Approach III.A, in Approach III.B, the total depreciation cost is divided by the estimated economic lifetime of the equipment (expressed in terms of hours for DiG, and in A.h. for batteries) to calculate the cost per hour for DiG (or per A.h. for battery) as follows:

$$C^h_{III.B} = \frac{C_{dep}}{h_n.\left(NO_{rep}+1\right)} \times \left(1+i\right)^j \tag{9.10}$$

where C_{dep} is calculated by (9.8); and j is the current year of operation.

From the equations developed for the different Approaches, different sources of uncertainty can be identified for the equipment ownership cost calculation. It basically implies that the ownership cost calculations may not be accurate unless the variations of these parameters are considered, further meaning that uncertainty and risk analyses are required for accurate calculations. In addition, risk analysis provides a basis to compare the effectiveness and accuracy of the given Approaches. The uncertainty sources and corresponding uncertainty and risk analyses are presented in the next sub-section.

Uncertainty and Risk Analysis

Several uncertainty sources can be identified as follows:

1) Equipment's number of replacement throughout the project lifetime (which depends on its economic lifetime and annual operation pattern),

2) Equipment's cost of replacement,

3) Inflation and interest rates.

Equipment's cost of replacement is highly unpredictable for new technologies since any breakthrough in a technology or unexpected market changes can influence the cost of the technology. For mature technologies such as DiGs, it is less likely to see any significant changes in the cost. Therefore, equipment's cost of replacement is not included as an uncertainty source for DiG. Also, inflation and interest rates are very stable in developed countries and do not present substantial variations. In this chapter, as the first attempt to consider uncertainty in the ownership cost calculation of MG components, attention is put on the first source of uncertainty, which can significantly affect the ownership cost, i.e. uncertainty source 1. The uncertainty sources 2 and 3 are

neglected in this study. However, these uncertainties can be included in the calculations if desired.

The number of replacement of an equipment (NO_{rep}) is primarily related to the usage pattern of the equipment and can be different from one year to another. It is also a function of the economic lifetime of the equipment which is not a certain parameter either, as discussed earlier. Although reasonable values can be assigned to the annual operation hours and economic lifetime of the equipment to obtain its number of replacement(s), they will be treated as uncertainty sources with appropriate DPDF for uncertainty and risk analyses in this chapter.

It is common in engineering economic analysis to use two to five outcomes with discrete probabilities to assess the uncertainty associated with the future events (such as equipment's annual operation hours and economic lifetime) [9.24], [9.25]. In most cases, the two to five outcomes represent the best trade-off between representing the range of possibilities and the amount of calculation required [9.25]. This is usually based on expert judgment or through prior experimental or simulation studies. Therefore, appropriate DPDF should be assigned to each uncertain parameter, given in the earlier section, prior to the risk analysis.

With the values estimated by the chosen DPDFs for the two sources of uncertainty (i.e., equipment's annual operation hours and useful lifetime), it is conceivable to calculate the hourly cost for each possible outcome. It essentially yields the sensitivity of the ownership cost with respect to the uncertain parameters. Although the impact of uncertain parameters on the ownership cost can be observed in the

sensitivity analysis, this analysis is not efficient for larger number of uncertainty sources and outcomes. Risk calculation can be very helpful in this context; it provides a legitimate basis to compare different approaches to find the most robust and reliable one.

As defined in [9.25], risk can be thought of as the chance of getting an outcome other than the expected value with an emphasis on something unpredictable. The common risk measure is the standard deviation, which measures the dispersion of outcomes about the expected value. Prior to risk calculation, it is required to calculate the expected values of each outcome for both uncertainty sources. It is therefore essential to calculate the joint probability distributions since there are two different uncertainties. It is assumed that the two uncertain parameters chosen are statistically independent, where the joint probability of a combined event is simply the product of the probabilities for the two events [9.25]. It is intuitive assumption that the annual operation hours of a DiG has no meaningful impact on its useful lifetime (i.e., the total operation hours) or vice versa. Therefore, the expected value of hourly cost for each approach can be drawn from (9.11) [9.25]:

$$EV_i\left[C_i^h\right]=\sum_{m=1}^{ELT}\sum_{n=1}^{AOH}\left\langle P_{\{X=m\}}^{ELT}.P_{\{X=n\}}^{AOH}.C_i^h\left(m,n\right)\right\rangle \tag{9.11}$$

where *ELT* is the number of events for the equipment's economic lifetime; *AOH* is the number of outcomes for annual operation hours; $P_{\{X=m\}}^{ELT}$ and $P_{\{X=n\}}^{AOH}$ are the probability of each event; and $C_i^h\left(m,n\right)$ is the hourly ownership cost for "*m*" hours of DiGs' useful lifetime and "*n*" hours of annual operation for the ith approach. From the expected value, it is possible to calculate the risk (standard deviation) for the four approaches discussed

as follows:

$$\sigma_i = \sqrt{\left\{ EV_i\left[X^2 \right] - \left[EV_i\left[X \right] \right]^2 \right\}} \tag{9.12}$$

Using (9.11), equation (9.12) can be rewritten as:

$$\sigma_i = \sqrt{\left\{ \sum_{m=1}^{ELT} \sum_{n=1}^{AOH} \left\langle P_{\{X=m\}}^{ELT} . P_{\{X=n\}}^{AOH} . \left\{ C_i^h\left(m,n\right) \right\}^2 \right\rangle - \left[EV\left[C_i^h \right] \right]^2 \right\}} \tag{9.13}$$

where σ_i shows the risk associated with the ith approach considering uncertainties. The best approach is the one with lower risk as long as its total payment throughout the project lifetime is not significantly different (less than 1% different) from the base-case (i.e., approach I.)

Simulation Studies and Results

In this section, comprehensive simulation results are presented for a specific DiG to assess the effectiveness of the proposed framework in its ownership cost calculation, and to find the best approach in comparison with the base-case approach. DiG is used as an example in this chapter since it is the most common device in MGs. Simulation results are divided into two sub-sections. In the first sub-section, the accuracy of Approaches II, III.A, and III.B is verified in comparison with the base-case through a set of simulation studies. In the second sub-section, sensitivity, uncertainty and risk analyses are given for the approaches that pass the verification test. As it was explained in the earlier section, the appropriate DPDFs will also be defined for each uncertain parameter prior to risk analysis.

Verification Study

Approach I is known as the standard machinery cost calculation method [9.24]-[9.26]. Therefore, other approaches should yield similar (or close) accumulative payment for the same outcomes. If accumulative payment throughout the project lifetime obtained from an approach is not close enough (within 1%) to the one obtained from the base-case, it will be rejected. For each approach, a simulation study is carried out where a DiG unit is considered to have 20000 hours of economic lifetime and 5000 annual operation hours for different project lifetime (4, 8, 12, 16, 20 years). The DiG selected for this study is a 10 kW diesel Genset [9.27]. Other required data for the simulation study is reported in Table 9.1.Simulation results for the different approaches are shown in Figure 9.2, where their corresponding error is compared to the base-case approach. Total accumulative payment for each approach for different length of project lifetime is depicted with bars. It is clear from Figure 9.2 that the accumulative payment in Approach II is not close to the base-case. Similar observation can be made by the error curves, where Approach II gives the highest error (about 4.8%). The error in Approach III.A is always less than 1%, while Approach III.B is more accurate for smaller length of project lifetime (with an error of near zero) and a maximum error of around 1.2% for 20 years of lifetime. Therefore, Approach II, which gave an error of near 5%, failed the verification test and should not be used for such studies because of large error. The error in Approaches III.A and III.B are within an acceptable range which means that they can be used in place of Approach I without jeopardizing the accuracy of the ownership cost calculations.

Table 9.1. Ownership cost calculation data.

DiG capital cost ($C_{pur,0}$), $	DiG replacement cost (C_{rep}), $	Inflation rate ($i_{\inf}$), %	Interest rate (i_{int}), %
6750	4725	1.5	3.5

Although the above simulation results give a perspective of the proposed Approaches, they do not represent a basis for comparison between different Approaches regarding uncertainty sources. Therefore, uncertainty and risk analyses are required for further evaluation of the proposed Approaches, given below.

Uncertainty and Risk Analyses

Prior to sensitivity and risk analyses, appropriate DPDFs are necessary to be assigned to each uncertainty source studied. Also, as mentioned earlier, two to five outcomes with discrete probabilities are required to be defined based on expert best judgment. These probabilities are obtained from the DPDFs.

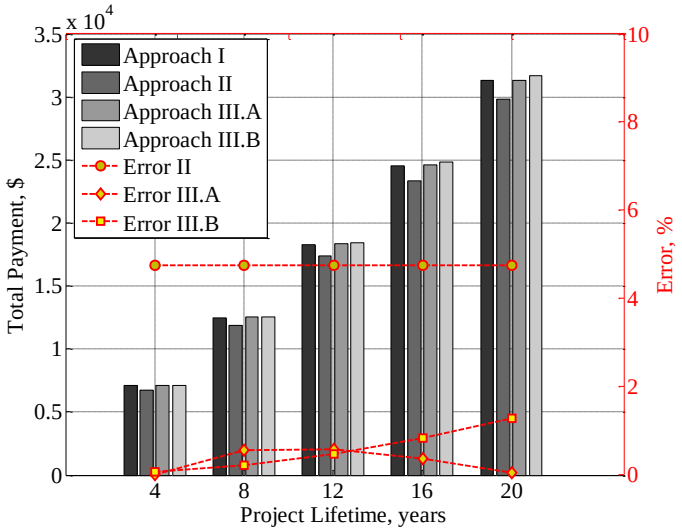


Figure 9.2. Accumulative payment of the DiG ownership cost for different approaches and their corresponding error in comparison with Approach I.

Appropriate DPDF for DiG Useful Lifetime. DiGs usually work 15000-25000 hours depending on their rated power, quality and interval of maintenance, quality of diesel fuel, and loading condition throughout their lifetime [9.28]. In general with regular overhaul (i.e., complete maintenance), the typical lifetime of a DiG could be up to 13 years. It is also well-known that the economic lifetime is usually less for smaller DiGs. The 10-kW DiG under study is more likely to have an economic lifetime in the 17000-hour range. The Hypergeometric distribution is used to generate the probability values for the DiG economic lifetime. Hypergeometric distributions are originally used to describe samples where the selections from a binary set of items are not replaced [9.29]. In this chapter, the shape of the distribution is found to be appropriate where the probability of the lower values (with the highest probability at 17000 hours) is higher than the larger values, as shown in Figure 9.3. The Hypergeometric PDF is given as follows [9.29]:

$$P_{\{X=k\}}^{ULT} = \frac{\binom{K}{k}\binom{N-K}{n-k}}{\binom{K}{n}} \tag{9.14}$$

where N is the total number of items (70 in this study); K is the total number of items with desired trait (14 in this study); n is the number of items in the sample (10 in this study); and k is the number of items with desired trait in the sample (15000 to 20000 hours). The generated probabilities are shown in Figure 9.3.

Table 9.2. MG design specifications obtained from HOMER®.

	DiG	PV	Battery
Rated capacity	10 kW	17 kW	24 kWh
Annual operation	7676 hour/year	3803 hour/year	801 kWh/year

Appropriate DPDF for DiG Annual Operation Hours. In this case, another DPDF is required since the annual operation hours is a different source of uncertainty with a different behavior. In order to have an estimate of the DiG annual operation hours, HOMER® software [9.23] has been used to design an islanded MG for a remote area with three residential units each of which has a power consumption profile of a typical U.S. resident [9.30]. The component sizes and annual operation obtained for the MG (including PV solar panels, a DiG, and a battery bank), for a typical residential load, are given in Table 9.2.

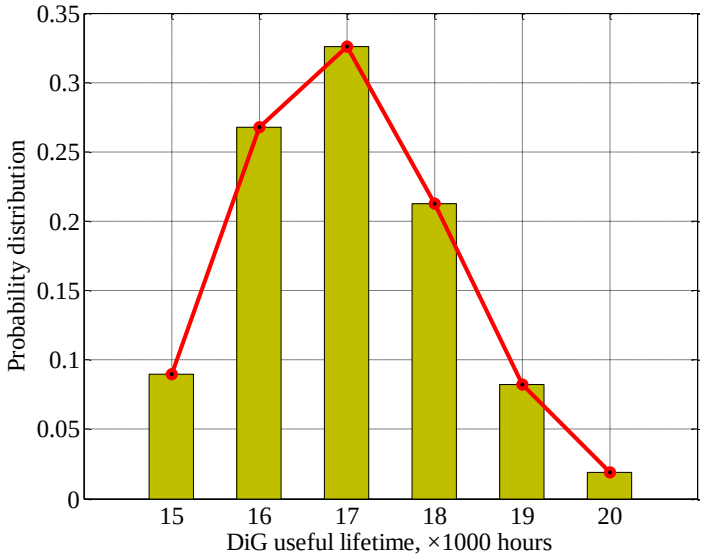


Figure 9.3. PDF for DiG useful lifetime created by Hypergeometric DPDF.

Based on the MG specification given in Table 9.2, it is estimated that the DiG will work around 7700 hours (out of the maximum 8760 hours) a year. However, it is possible that the DiG would operate more or less than 7700 hours per year, with a higher probability for larger annual operation hours. The reason for this can be two-fold: 1) HOMER software does not include the stochastic nature of renewable generation and load demand in the design procedure, and 2) the only renewable generation source in the designed MG is solar PV whose output power is unpredictable, which increases the required reserve that must be provided by the DiG. For this reason, the extreme value discrete distribution is selected as an appropriate DPDF for annual operation hours [9.31]:

$$P^{AOH}_{\{X|\mu,\sigma\}} = \sigma^{-1}\exp\left(\frac{X-\mu}{\sigma}\right).\exp\left(-\exp\left(\frac{X-\mu}{\sigma}\right)\right) \tag{9.15}$$

where it returns the PDF of type 1 extreme value distribution with location parameter μ (3 in this study) and scale parameter σ (1.5 in this study), evaluated for the values in X. Extreme value distributions are frequently used to model the smallest or largest value among a large set of independent random values representing measurements or observations [9.31]. This DPDF is chosen since it produces the expected probability distributions following the hypothesis derived above for the annual operation hours. The probability distribution of the annual operation hours for the DiG is shown in Figure 9.4.

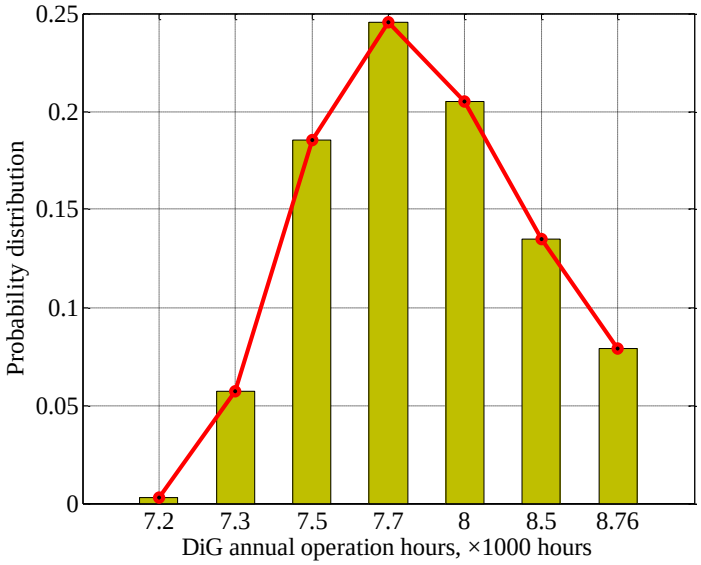
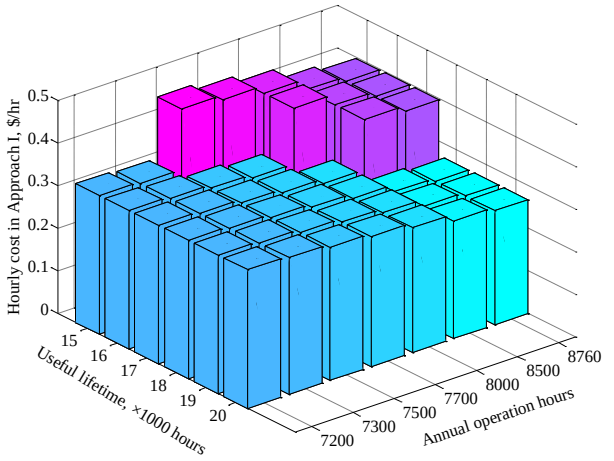


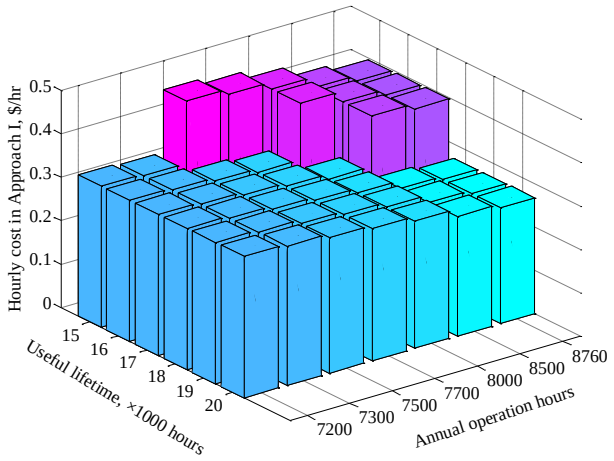
Figure 9.4. PDF for DiG annual operation hours created by Extreme Value DPDF.

Although the DPDFs of the uncertainty sources can be different for different studies, similar analyses can be performed. Therefore, the proposed framework can be employed for different components of MGs. In this chapter, similar DPDFs will be used for different Approaches for fair comparison.

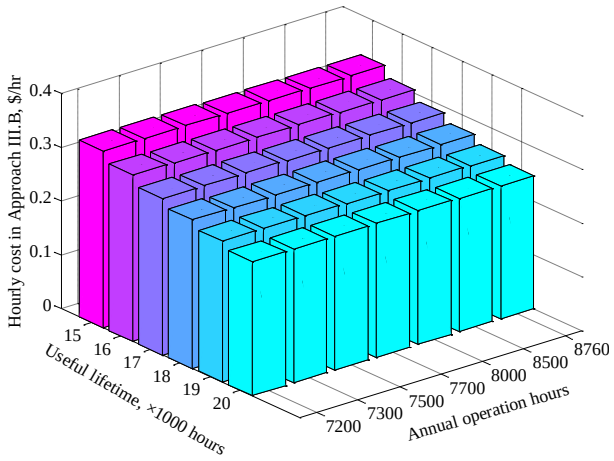
With different outcomes considered for the DiG annual operation hours and useful lifetime, it is possible to perform a sensitivity analysis by calculating hourly cost for each approach. The results from Approaches I, III.A and III.B are shown in Figure 9.5 (a), (b), and (c), respectively. The project lifetime is assumed to be 20 years in these simulations. The other parameters used in the simulation are given in Table 9.1.



(a)



(b)



(c)

Figure 9.5. Hourly cost for the DiG with different outcomes generated for the two uncertain parameters for (a) Approach I (base-case), (b) Approach III.A, and (c) Approach III.B.

It can be seen from Figure 9.5 (b) that Approach III.A is more sensitive to the uncertain parameters (compared to the base-case in Figure 9.5 (a)); however its variations are smaller. Furthermore, Figure 9.5 (c) reveals that the variations in the annual operation hours have negligible impact on the ownership cost (less than 1%) in Approach III.B. This is a significant improvement in the uncertainty analysis.

Table 9.3. Ownership cost calculation fata for the DiG.

Terms of analysis	Approach I	Approach III.A	Approach III.B
Expected Cost ($/hour)	0.3042	0.3377	0.2644
Risk Value ($/hour)	0.1113	0.1111	0.0869

The expected ownership cost and risk value (i.e., standard deviation) for Approaches I, III.A, and III.B are calculated for the DiG using (9.11)-(9.13). The results are given in Table 9.3. Although the expected ownership cost is not meaningful in terms of uncertainty and risk analyses, it provides the hourly ownership cost which has to be included in the operational cost of the DiG. Alternatively, looking at the risk value associated with each Approach shows that Approach III.B has the lowest risk in the calculation in the presence of uncertainty. In other words, it basically shows that Approach III.B is significantly less risky (about 22% compared to Approach I), considering possible variations in the uncertain parameters, when calculating ownership cost. Therefore, it can be concluded that Approach III.B is the best method (among the four approaches) to calculate the ownership cost with high accuracy and lower risk associated with the two uncertainty sources.

In the next section, the formulation of ownership cost for storage battery as

another DER in a MG setting is presented.

Ownership Cost Formulation for Batteries

Generally speaking, the proposed framework for ownership cost calculation can be applicable to other MG components, however sometimes slight modifications may be required to make the framework fit a specific DER. Specifically, one special modification is required when the useful lifetime of the device is expressed in something other than hours. For instance, battery useful lifetime is expressed as battery nominal charge life (A.h.). Therefore, it is essential to modify the equations to adapt them to batteries. This section covers such modifications needed to calculate the ownership cost of batteries.

As it was discussed in the earlier sections, the useful lifetime of battery and its salvage value are required for depreciation cost calculation. The economic life of battery banks is the number of years (in terms of battery A.h.) for which costs are to be estimated. This is important, particularly for Approaches III.A and III.B, where the economic life of the battery bank with the required number of replacement(s) throughout the project lifetime should be considered. A battery has a finite lifespan which is quantified by summing together the entire A.h. discharged during each of its cycles to determine a cumulative A.h. capacity for the battery's life. The total charge life of a battery is calculated from manufacturer's specifications as follows [9.14], [9.18]:

$$\Gamma_r = L_r.D_r.C_r \tag{9.16}$$

where Γ_r is the charge life of a battery (A.h.); L_r is its cycle lifetime at rated depth of discharge (DoD) and discharge current; D_r is the rated DoD; and C_r is the A.h. capacity

at rated discharge current. In reality, a battery is not always operated at its rated values, and it is well-known that the total A.h. through a battery during its effective lifetime is directly dependent upon the DoD during each cycle [9.14], [9.18]. Therefore, a relationship can be established between the cycle-to-cycle DoD and battery effective lifetime. The unified effects of DoD and discharge rate on battery lifespan can be expressed as follows [9.18]:

$$d_{eff}(i) = d_{act}(i).\left(\frac{C_r}{C_{act}(i)}\right).\left(\frac{DoD_{act}(i)}{DoD_r}\right)^{u_0}.e^{u_1\left(\frac{DoD_{act}(i)}{DoD_r}-1\right)} \tag{9.17}$$

where $d_{eff}(i)$ is the effective A.h. discharge of the battery at discharge event *i*; $d_{act}(i)$ is the actual discharged energy of the battery (A.h.); C_r is the battery A.h. capacity at rated discharge current; C_{act} is the actual battery capacity at each time interval; $DoD_{act}(i)$ is the actual DoD at discharge event *i* (%); DoD_r is the rated DoD (%) in event *i*; and u_0 and u_1 are curve-fitting coefficients. All the equations for calculating the depreciation cost in each Approach are valid here as well. For example, to obtain the battery ownership cost using Approach III.B, (9.10) is modified to calculate the ownership cost per effective A.h. by estimating the annual accumulative discharged A.h. as follows:

$$C_{III.B}^{A.h} = \frac{C_{dep}}{\sum_{each\ year} d_{eff}(i)\times\left(NO_{rep}+1\right)}\times(1+i)^j \tag{9.18}$$

The uncertainty and risk analyses for this situation can be achieved by following the steps given in the earlier sections. Note that appropriate DPDFs for a battery might be different from those given for DiG and are based on the annual usage and useful lifetime of the battery.

Simulation studies have been carried out for battery and yield similar results as for DiG, where Approach III.B was found to be the best model.

Conclusion

Cost-based operation of DERs and MGs, including their ownership costs, is inevitable in the smart grid era. This chapter proposes a general framework for ownership cost calculation considering uncertainty and risk associated with the calculations. Two new ownership cost calculation approaches are proposed and compared with two approaches from the literature. It is shown through a series of simulation studies that the new Approaches III.A and III.B yield very accurate results in comparison with the base-case (Approach I), which is commonly used in the literature. In addition, a risk analysis of the proposed approaches shows that the proposed Approach III.B is 22% less risky compared to Approach I. It is also shown through sensitivity analysis that Approach III.B is more robust against the annual operation hour variations, unlike the other Approaches discussed.

In general, the proposed ownership cost calculation framework can be utilized (with minor modifications) for different components of MGs. As an example, in addition to DiG, the proposed framework is modified and given for batteries. Simulation results for battery (not given in this chapter) also reached the same conclusion that Approach III.B is the most robust one.

Acknowledgement

This work was supported by NEC Labs America, and the U.S. Department of

Energy, Office of Science, Basic Energy Sciences, under Award # DE-FG02-11ER46817.

References Cited

[9.1] U.S. DOE, office of electric transmission and distribution, “Grid 2030: A national vision for electricity’s second 100 years,” July 2003.

[9.2] N. Hatziargyriou, et al., “Energy management and control of island power systems with increased penetration from renewable sources,” in *Proc*. IEEE PES Winter Meeting, vol. 1, New York, USA 2002, pp. 335–339.

[9.3] M. Korpås and A. T. Holen, “Operation planning of hydrogen storage connected to wind power operating in a power market,” *IEEE Trans. Energy Convers*., vol. 21, no. 3, pp. 742–749, Sept. 2006.

[9.4] S. Chakraborty and M.G. Simoes, “PV-microgrid operational cost minimization by neural forecasting and heuristic optimization,” in *Proc*. IEEE Industry Applications Society Annual Meeting, Edmonton, Canada 2008, pp. 1–8.

[9.5] S.A. Pourmousavi, et al., "Real-time energy management of a stand-alone hybrid wind-microturbine energy system using particle swarm optimization," *IEEE Trans. Sustain. Energy*, vol. 1, no 3, pp. 193–201, Oct. 2010.

[9.6] F.A. Mohamed and H.N. Kovio, “Power management strategy for solving power dispatch problems in microgrid for residential applications,” in *Proc*. IEEE International Energy Conference and Exhibition, Manama, Bahrain 2010, pp. 746–751.

[9.7] R. Noroozian and H. Vahedi, “Optimal management of microgrid using bacterial foraging algorithm,” in *Proc*. 18th Iranian Conference on Electrical Engineering, Isfahan, Iran 2010, pp. 895–900.

[9.8] B. Asato, et al., “Optimal operation of smart grid in isolated island,” in *Proc*. International Power Engineering Conference, Singapore 2010, pp. 1100–1105.

[9.9] M. Ross, et al., “Analysis of energy storage sizing and technologies,” in *Proc*. IEEE Electric Power and Energy Conference, Halifax, Canada 2010, pp. 1–6.

[9.10] H. Kanchev, et al., “Energy management and operational planning of a microgrid with a PV-based active generator for smart grid applications,” *IEEE Trans. Ind. Electron*., vol. 58, no. 10, pp. 4583–4592, Feb. 2011.

[9.11] D. E. Olivares, C. A. Canizares, and M. Kazerani, “A centralized optimal energy management system for microgrids,” in *Proc*. IEEE PES GM, San Diego, USA 2011, pp. 1–6.

[9.12] T. Logenthiran, et al., “Multiagent system for real-time operation of a microgrid in

real-time digital simulator," *IEEE Trans. Smart Grid*, vol. 3, no. 2, pp. 925–933, Apr. 2012.

[9.13] S. Conti, et al., "Optimal dispatching of distributed generators and storage systems for MV islanded microgrids," *IEEE Trans. Power Del.*, vol. 27, no. 3, pp. 1243–1251, May 2012.

[9.14] S.A. Pourmousavi, R.K. Sharma, and B. Asghari, "A framework for real-time power management of a grid-tied microgrid to extend battery lifetime and reduce cost of energy," in *Proc*. IEEE PES Innovative Smart Grid Technologies, Washington D.C., USA 2012, pp. 1–8.

[9.15] A. Sobu and G. Wu, "Dynamic optimal schedule management method for microgrid system considering forecast errors of renewable power generations," in *Proc*. IEEE International Conference on Power system Technology, Auckland, USA 2012, pp. 1–6.

[9.16] C.M. Colson and M.H. Nehrir, "Comprehensive real-time microgrid power management and control with distributed agents," *IEEE Trans. Smart Grid*, vol. 4, no. 1, pp. 617–627, Jan. 2013.

[9.17] J. Quanyuan, X. Meidong, and G. Guangchao, "Energy management of microgrid in grid-connected and stand-alone modes," *IEEE Trans. Power Syst*., vol. 28, no. 3, pp. 3380–3389, Aug. 2013.

[9.18] C.M. Colson, et al., "Improving sustainability of hybrid energy systems Part I: Incorporating battery round-trip efficiency and operational cost factors," *IEEE Trans. Sustain. Energy*, vol. 5, no. 5, pp. 37–45, Jan. 2014.

[9.19] A. Hooshmand, B. Asghari, and R. Sharma, "A novel cost-aware multi-objective energy management method for microgrids,", in *Proc*. 2013 IEEE PES Innovative Smart Grid Technologies, Washington, DC, USA, pp. 1–6.

[9.20] R. Luna-Rubio, et al., "Optimal sizing of renewable hybrids energy systems: A review of methodologies," *Solar Energy*, vol. 86, no. 4, pp. 1077–1088, Apr. 2012.

[9.21] S.M. Schoenung, "Characteristics and technologies for long- vs. short-term energy storage: A study by the DOE energy storage systems program," Sandia National Laboratory, SAND2001-0765, Mar. 2001.

[9.22] D. Rastler, "Electricity energy storage technology options: A white paper primer on applications, costs and benefits," Electric Power Research Institute (EPRI), NO. 1020676, Dec. 2010.

[9.23] HOMER ENERGY: Energy Modeling Software for Hybrid Renewable Energy Systems, Available online: http://homerenergy.com/

[9.24] L.E. Bussey, *The Economic Analysis of Industrial Projects*, Prentice-Hall Inc.: New Jersey, 1978, ch. 4 and 11.

[9.25] D.G. Newnan, J.P. Lavelle, and T.G. Eschenback, *Engineering Economic Analysis*, 10th edition, Oxford University Press, 2009, ch. 10.

[9.26] W. Edwards, "Estimating farm machinery costs," Ag. Decision Maker, Iowa State University, NO. A3-29, Nov. 2009. Available online: http://www.extension.iastate.edu/publications/pm710.pdf

[9.27] CumminsOnan Commercial SD 10000, Available online: http://www.cumminsonan.com/cm/products/diesel/compare?gensetId=20&detail=true

[9.28] M. Pipattanasomporn, M.Willingham, and S. Rahman, "Implications of on-site distributed generation for commercial/industrial facilities," *IEEE Trans. Power Syst*., vol. 20, no. 1, pp. 206–212, Jan. 2005.

[9.29] MATLAB Documentation, Available online: http://www.mathworks.com/help/stats/hypergeometric-distribution.html

[9.30] "Descriptions of electric energy use in single family residences in the pacific northwest, 1986-1992," Office of Energy Resources, Bonneville Power Administration, Portland, OR, December 1992.

[9.31] MATLAB Documentation, Available online: http://www.mathworks.com/help/stats/negative-binomial-distribution.html

CHAPTER 10

A FRAMEWORK FOR REAL-TIME POWER MANAGEMENT OF A GRID-TIED MICROGRID TO EXTEND BATTERY LIFETIME AND REDUCE COST OF ENERGY

Contribution of Authors and Co-Authors

Manuscripts in Chapters 2 through 12

Author: S. A. Pourmousavi

Contributions: Developed a dynamic model of a grid-tied MG for power management study in MATLAB®/Simulink, proposed a methodology to calculate battery cost of operation in real-time, developed a real-time power management for cost minimization and battery life expansion, developed simulation studies, prepared manuscript, interpretation of results and figures.

Co-author: Ratnesh K. Sharma

Contributions: Provided important insight and overview of the research, interpretation of the results, and aided in the preparation of the manuscript.

Co-author: Babak Asghari

Contributions: Provided important insight and overview of the research, interpretation of the results, and aided in the preparation of the manuscript.

Manuscript Information Page

Seyyed Ali Pourmousavi Kani, Ratnesh K. Sharma, Babak Asghari

IEEE Innovative Smart Grid Technologies (ISGT), 2012

Status of the manuscript:
____ Prepared for submission to a peer-reviewed conference
____ Officially submitted to a peer-reviewed conference
____ Accepted by a peer-reviewed conference
_X_ Published in a peer-reviewed conference proceedings

Published by the Institute of Electrical and Electronics Engineering (IEEE)

A FRAMEWORK FOR REAL-TIME POWER MANAGEMENT OF A GRID-TIED MICROGRID TO EXTEND BATTERY LIFETIME AND REDUCE COST OF ENERGY

The following work is presented in ISGT 2012 Conference and is published in the conference proceedings

S.A. Pourmousavi[1], R. K. Sharma[2], and Babak Asghari[2]

[1] *Department of Electrical and Computer Engineering, Montana State University, Bozeman, MT 59717*

[2] *Energy Management Department, NEC Laboratory America Ltd., Cupertino, CA 95014*

Abstract

Because of different technical and economic concerns, battery has become an inevitable part of a MG as well as the most expensive component. This further necessitates a real-time power management system to guarantee the healthy operation and maximum battery lifetime based on the net cost of energy. Therefore, this chapter attempts to present a real-time management framework for a grid-tied MG based on the lifetime and cost estimation of battery. In order to verify the effectiveness of the proposed framework, a grid-tied commercial MG, which includes wind turbine, solar PV panels and Li-Ion battery, is optimally sized by HOMER®. Then, dynamic model of different components have been developed in MATLAB/Simulink® for real-time power management study. Finally, simulation studies have been carried out for a year with actual load demand, wind speed, ambient temperature, solar radiation, and time-based electricity tariff. Simulation results show that the proposed framework effectively extends the battery lifetime while slightly decreases the cost of energy for customer.

Nomenclature

L_R	Battery cycle life at rated DoD and discharge current.
D_R	DoD for which rated cycle life was determined.
C_R	Rated ampere-hour capacity at rated discharge.
u_0, u_1, and u_2	Coefficients of the DoD fitting function.
D	Actual DoD.
C_A	Actual capacity at discharge current.
d_{act}	Ampere-hour of the discharge event.
T	System operation time, day.
AC	Annualized Cost, $/year.
RBC	Rated Battery Capacity, kW.
CC	Capital Cost, $/kW.
RC	Replacement Cost, $/kW.
SFF	Sinking Fund Factor.
CRF	Capital Recovery Factor.
O&MC	Annual Operation and Maintenance Cost, $/kAh/year.
f	Inflation rate, %.
i	Actual interest rate.
i_{nom}	Nominal interest rate, %.
NO. rep	Number of Replacement of the battery, round (Y_{proj} / Y_{rep}).

Y_{proj}	Useful lifetime of the project, year.
Y_{rep}	Useful lifetime of the battery calculated by BLE, year.
P_W	Wind power, kW.
P_{PV}	PV solar power, kW.
P_{grid}	Scheduled power from the grid, kW.
P_{load}	Load demand, kW.
SoC	State of Charge of the battery, %.

Introduction

MG is an emerging technology which promises to achieve many simultaneous goals for power system stakeholders, from generator to consumer [10.1]. Its framework offers a mean to capitalize on diverse energy sources in a decentralized way, while reducing the burden on the grid by generating power close to the consumer. Since MG with distributed generation (DG) systems fall within city load centers (<69 kVA) at electric utility substations, near feeders, within neighborhoods, and at industrial, commercial, and residential customer locations [10.2], storage devices such as battery are necessary to:

- ✓ Manage electric grid peak demand,
- ✓ Improve reliability and outage mitigation, compensate for intermittent power generation from DGs,
- ✓ Provide AS especially in islanded mode of operation,
- ✓ Increase electric grid load factor and utilization via the smart grid.

As a result, storage devices are the necessary components of MGs as a mean to

achieve high penetration of intermittent RES into the grid. According to [10.2], the desired size of the energy storage device for distributed energy storage systems (DESS) application is 25-200 kW for single-phase and 25-75 kW for three-phase systems, and its duration and desired lifetime are 2-4 hours and 10-15 years, respectively. The desired values in the case of commercial and industrial (C&I) energy management are 50-1000 kW in size, 3-4 hours duration, and 15 years lifetime [10.2]. This way, different battery technologies, such as Lithium-Ion batteries, can be sought as promising candidates.

The available power from RES, particularly wind turbine, is highly variable and somewhat random. Consequently, batteries in hybrid power systems, whether in DESS or C&I energy management applications, experience a very irregular pattern of charge and discharge cycles. On the other hand, it is well-known that battery useful lifetime depends on its discharge pattern. Therefore, managing discharge pattern is a promising approach for battery life maximization. Since one can say that maximum battery lifetime can be achieved when battery kept idle (i.e., the nominal lifetime), there should be a rational definition for maximum lifetime of the battery. In this chapter, this term is defined as the maximum battery lifetime by taking the cost of energy into consideration at each management interval. In other words, the maximizing battery lifetime is beneficial as long as the cost of the energy provided to the customer is minimum at the time of management.

While most research has been focused on optimal sizing and unit commitment of such systems, few studies have dealt with real-time management of a hybrid energy system [10.3]. To the best of our knowledge, maximizing battery lifetime considering

minimum cost of energy has not been addressed in the literature. This chapter attempts to introduce a management framework to achieve maximum battery lifetime based on battery life estimation and the price of energy. The proposed procedure is developed for the grid-tied MGs which include wind turbine and solar PV panels as generation assets and Li-Ion battery as storage device. The system is optimally designed using HOMER® with actual wind speed, solar irradiation, grid electricity price, and load demand data. Since unit commitment problem is beyond the scope of this chapter, the scheduled grid power in real-time simulation is assumed to be equal to the grid power calculated by HOMER®. Then, dynamic model of each component for the system studied is developed in MATLAB/Simulink®. Different power management strategies are then implemented on the dynamic model of the MG with actual data for a year. Eventually, results from different management approaches are compared.

The Proposed Real-Time Power Management Framework

Batteries are usually equipped with a battery management system (BMS) which can be an electronic device that manages a rechargeable battery (cell or battery pack), by monitoring its state, calculating secondary data, reporting that data, protecting it, controlling its environment, and/or balancing it. However, there is no real-time supervisory power management system at the top level of MG to regulate battery discharge in order to maximize its lifetime. While battery is usually the most expensive part of such systems at the time of installation, and needs frequent replacement, a real-time power management can be extremely helpful to guarantee the appropriate use of battery. Generally, real-time management strategy performs at a smaller time interval,

e.g., every few seconds or minutes. The results of such systems are the power sharing between the different generation and storage assets in a MG.

It is well-known that PV and wind generation is almost free after installation because of no fuel cost. Thus, it is beneficial to use available power from wind and PV as much as possible. Therefore, the real-time power management problem will be limited to power sharing between battery and grid. Grid power is available at time-of-use rates, and is limited to a maximum of 40kW in this study. Possible explanations might be a weak distribution system, lack of enough generation, and/or low capacity of different equipment such as overhead lines and/or transformers. As it was mentioned earlier, the purchased power from the grid is scheduled a day ahead as unit commitment problem. In this chapter, we are not dealing with the unit commitment problem. Therefore, the scheduled power from the grid is considered as a known input parameter in the management system. It is also assumed that the battery will be charged only when excess wind and/or PV power is available. In other words, battery will not be charged by the power purchased from the grid. Replacement cost is the most effective factor in the CEB calculation. Based on the discharge pattern, batteries need to be replaced periodically to maintain system performance. Therefore, CEB is directly related to the battery aging which depends on its discharge pattern. As a result, the power management algorithm should decide upon the battery discharge pattern, associated lifetime, and cost. Since maximum battery lifetime occurs when battery is kept idle (which is not rational), a competing objective is required in the power management algorithm. In this study, final cost of energy is considered as the competing objective.

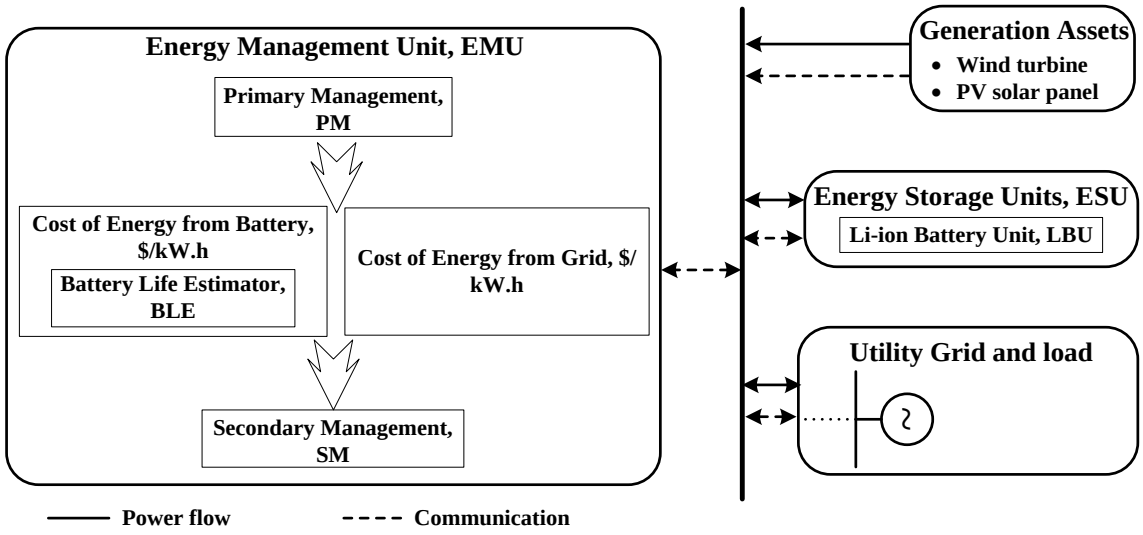


Figure 10.1. Block-diagram of the proposed management framework.

A schematic block-diagram of the energy management unit (EMU) with different components of the system studied is shown in Figure 10.1. In order to calculate the cost of energy from the battery, it is required to calculate the number of its replacements during the lifetime of the project. As a result, it is required to estimate the battery lifetime based on its discharge pattern in the past. Therefore, the management strategy starts with the battery lifetime estimation, which is shown as Battery Life Estimator (BLE) unit in Figure 10.1. Then, the CEB will be estimated, in $/kWh. Finally, the decisions will be made based on the secondary management (SM) strategy between battery and grid. Different strategies can be developed in the SM procedure, such as the one defined in this chapter.

Since the overall management system is responsible for both charging and discharging of the battery, the proposed framework is broken into two hierarchical steps as follows:

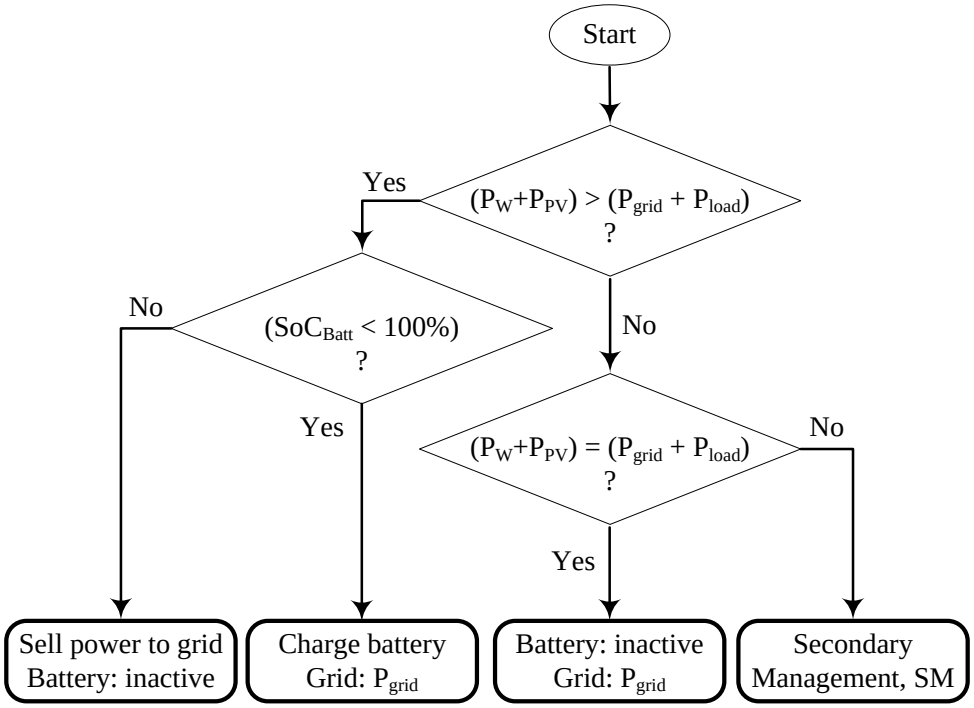


Figure 10.2. Schematic diagram for the proposed PM strategy.

- ✓ *Primary Management (PM):* In this step, primary decisions about power flow between generation resources and the energy storage unit will be made based the available information from different generation assets, battery state of charge (SOC) and availability of the grid. This part of the management is shown in Figure 10.2.
- ✓ • *Secondary Management (SM):* Whenever battery discharging or purchasing excess power from the grid is required, the decision will be made by the proposed strategy in the SM unit. The goal is to extend the battery lifetime based on the final price of energy for the customers.

Battery Lifetime Estimator, BLE

In this section, the proposed BLE technique is described in details. Different techniques in literatures are developed for battery life estimation; however they fall within at least one of the shortcomings listed below for the purpose of this study:

- ✓ Complicated and slow, e.g., [10.4], [10.7],
- ✓ Need detailed information on the battery performance which usually is not available in battery datasheets, e.g., [10.5], [10.6], [10.8]-[10.11],
- ✓ Only appropriate for long estimation intervals (in the order of days or week) with significant error, e.g., [10.7], [10.10]
- ✓ Valid only for certain type of batteries, e.g., [10.5], [10.6].

In this study, battery life estimation technique introduced in [10.12] and [10.13] is utilized. This technique is developed based on three premises which have been discussed in [10.14]. In this technique, depths of discharge and rates of discharge are considered as major indicators for battery life estimation. Assuming the presence of temperature and humidity controls, the impact of battery temperature on its aging can be ignored. A significant feature of this technique is the fact that it works based on the battery performance and cycle life data provided by the manufacturer, and supplemented by a limited amount of empirical test data. This technique also eliminates the need for an electrochemical model of the battery [10.12]. The three premises are as follows:

Premise 1: Each cell has a finite life [10.12]. It will reach the end of its useful life when the cumulative effective ampere-hours of individual effective ampere-hours corresponding to a series of discharge events equal the rated charge life of the cell. The

rated charge life is given as [10.12]:

$$\Gamma_R = L_R.D_R.C_R \tag{10.1}$$

Premise 2: The actual charge life of the cell is a function of the DoD. Therefore, the effective ampere-hour discharge in a given discharge event may be more or less than the actual discharge based on the actual DoD. In order to determine this functional relationship, the following function has been used to perform the best fit to the cell cycle life data vs. DoD [10.12]:

$$L = u_2\left(\frac{D_R}{D}\right)^{u_0} .\boldsymbol{exp}\left(u_1\left(1-\frac{D}{D_R}\right)\right) \tag{10.2}$$

Different methods can be applied to perform the curve fitting. Two different methods have been used in this chapter including PSO [10.3] and non-linear least square (NLLS) method from MATLAB® curve fitting toolbox. It is shown in [10.3] that PSO, as a heuristic optimization technique, is able to achieve optimal solution in a small fraction of a second. Also, NLLS is a popular regression method which has been used in [10.12] and [10.13]. The results of curve fitting are shown and compared in simulation results.

Premise 3: The charge life of the cell, Γ, drops whenever the cell is discharged at a rate faster (higher discharge current) than the nominal rate. Furthermore, the reduction in life will have a close functional relationship to the observed reduction in ampere-hour capacity with increasing discharge rate [10.12]. This effect can be expressed fairly accurately by the following two-parameter function:

$$d_{eff} = \left(\frac{C_R}{C_A}\right)^{v_0} .\boldsymbol{exp}\left(v_1\left(1-\frac{C_R}{C_A}\right)\right).d_{act} \tag{10.3}$$

Since battery manufacturers typically conduct battery life testing at a single discharge rate, usually the rate for which the cell's rated capacity is given, enough data is not available to determine the parameters v_0 and v_1. Therefore, the effect of discharge rate will be estimated using a simplified form of Eq. (3) where v_0 is set equal to 1 and v_1 is set to 0:

$$d_{eff} = \left(\frac{C_R}{C_A}\right).d_{act} \tag{10.4}$$

In order to calculate C_A related to each discharge event, 1-D cubic spline interpolation has been applied in this study. Using (10.2) and (10.4), the effects of DoD and discharge rate are combined simply by multiplying the factors as follows [10.12]:

$$d_{eff} = \left(\frac{D_A}{D_R}\right)^{u_0} .\boldsymbol{exp}\left(u_1\left(1-\frac{D_A}{D_R}\right)\right).\left(\frac{C_R}{C_A}\right).d_{act} \tag{10.5}$$

Equation (10.5) gives the effective discharge for a single discharge event. In order to estimate the lifetime of a battery which has been exposed to a series of discharge patterns, accumulative effective discharge is required. Finally, lifetime of the battery can be calculated as follows [10.12]:

$$L_{time} = \frac{L_R.D_R.C_R}{\sum_{i=1}^{n} d_{eff,i}}.T \tag{10.6}$$

The procedure of battery life estimation is shown in Figure 10.3.

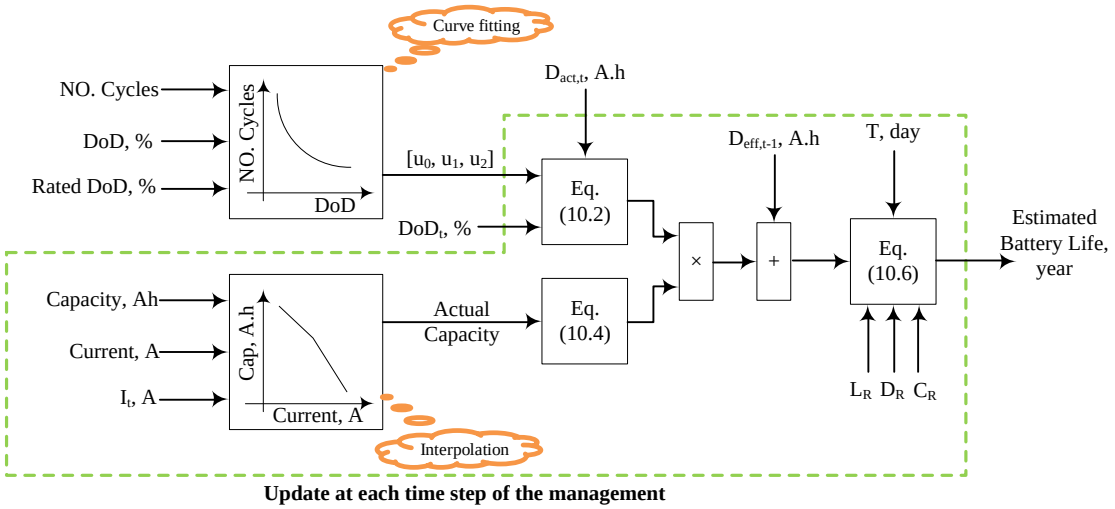


Figure 10.3. BLE model represented in a block-diagram.

Calculation of Cost of Energy from Battery (CEB)

The number of battery replacements over the lifetime of the project can be approximated from the battery life estimation. In this study, the following cost model is used to calculate the CEB [10.15], [10.16]. Note that the battery charging cost is set to zero since it will only be charged when excess PV and wind power is available.

$$AC = RBC \times \left\{ \left[CC + RC \times SFF\left(i, Y_{rep}\right) \right] \times CRF\left(i, Y_{proj}\right) \right\} + RBC \times O\&MC \times \left(1+f\right)^{n} \tag{10.7}$$

where,

$$SFF\left(i, Y_{rep}\right) = \sum_{n=1}^{NO.rep} \frac{1}{\left(1+i\right)^{n \times Y_{rep}}} \tag{10.8}$$

$$CRF\left(i, Y_{proj}\right) = \frac{i \times \left(1+i\right)^{Y_{proj}}}{\left(1+i\right)^{Y_{proj}} - 1} \tag{10.9}$$

$$i = \frac{(i_{nom} - f)}{(1 + f)} \tag{10.10}$$

The capital cost and O&MC of the battery are derived from [10.2] and [10.16], respectively. The capital cost of the battery varies based on its application [10.2]. For commercial building in the range of 25-50 kWh, capital cost of the battery is estimated at $4240/kW in average (the actual price varies from $2800 to $5600/kW) [10.2]. Since the capital cost includes cost of battery, power electronics, cost of installation, step-up transformer, smart-grid communication and controls, and grid interconnection to utility, the replacement cost is considered to be 60% of the capital cost [10.2]. For O&MC, the capital cost approximately is $50/kAh/year [10.16]. In this chapter, the nominal annual interest and inflation rates are assumed to be 3.5% and 1.5%, respectively. For ease of comparison, the cost of electricity from battery is calculated in $/kWh instead of $/year, as follows:

$$CEB = \frac{AC}{8760 \times RBC} \quad [\$/\text{kWh}] \tag{10.11}$$

A graphical user interface (GUI) was developed to interactively examine the impacts of different parameters on the battery life estimation and its cost of operation, which is shown in Figure C.1. Different scenarios can be designed and compared on the same figures.

Simulation Results

In this section, simulation results for different parts of the proposed management framework are presented and discussed.

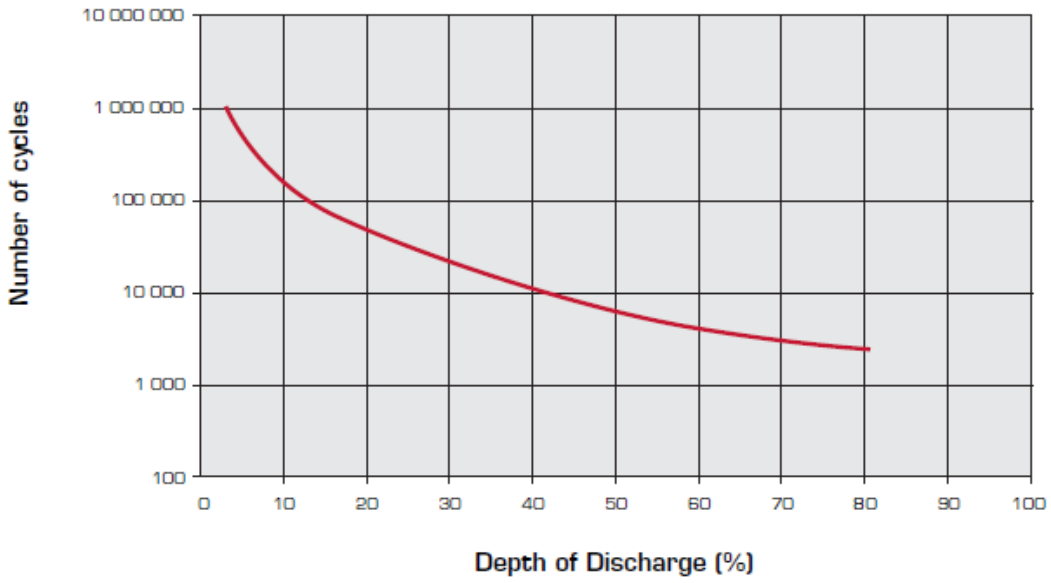


Figure 10.4. Cycle life vs. DoD for Intensium Flex High Energy Li-Ion battery, SAFT Company.

Results of Curve Fitting and Interpolation

In this study, the Intensium Flex High Energy Lithium-Ion battery pack from SAFT company is considered [10.17]. The experimental life cycle data of the battery for different DoD is shown in Figure 10.4, measured by the company.

Actual capacity of the battery in different discharge current can be determined by using the experimental data commonly given in battery specification. Table 10.1 shows the actual discharge current for different discharge time duration for the battery used in this study.

Table 10.1. Amperes on Discharge table for Intensium Flex High Energy Li-Ion battery, SAFT Company.

	Duration (min)					
Rated Capacity	1	10	30	60	180	300
45 A.h	197.92	131.25	75	40.62	14.17	9

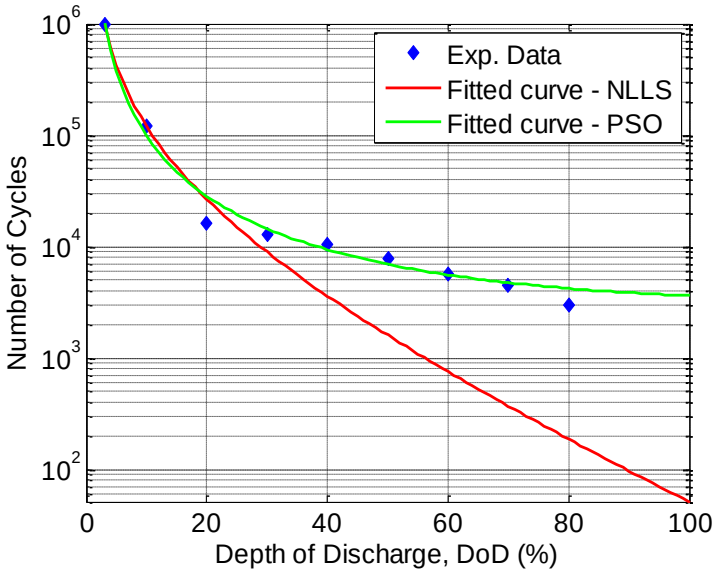


Figure 10.5. Curve fitting results for two different methods.

As mentioned in the earlier sections, curve fitting on the data provided in Figure 10.4 is required to determine the coefficients of the function in (10.2). Figure 10.5 shows the curve fitting results using PSO and NLLS.

The root mean square error (RMSE) of the curve fitting results is calculated for both methods as follows:

$$RMSE = \sqrt{\frac{x_1^2 + x_2^2 + \cdots + x_n^2}{n}} \tag{10.12}$$

where x_n is the error between data sample n and the value obtained by fitted curve. The RMSE was 0.124 and 3.509 for PSO and NLLS methods, respectively. It can be concluded from Figure 10.5 and the RMSE that the results from PSO are significantly accurate compared to those from NLLS method. As a result, the accuracy of the battery lifetime estimation will be improved which consequently enhances the cost of battery calculations.

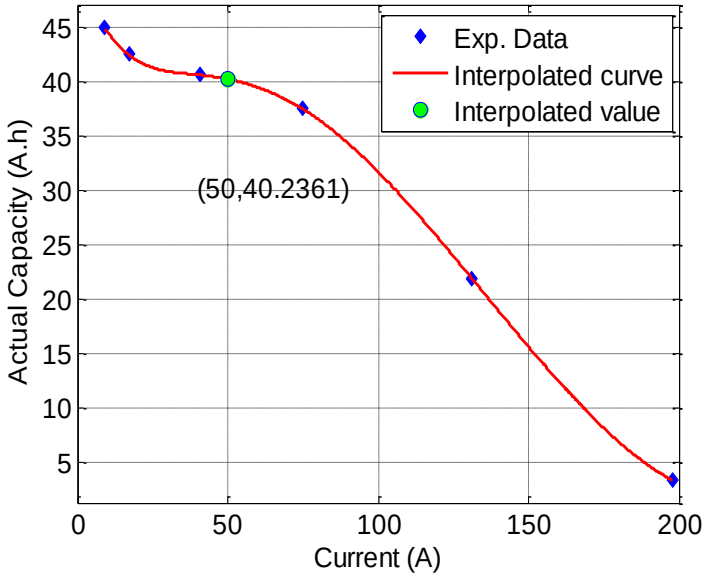


Figure 10.6. Actual capacity of the battery at different discharge rates.

As it was mentioned earlier, the actual discharge current has significant impact on the battery aging, where (10.4) is given to account for this impact. Equation (10.4) requires data interpolation at each specific discharge current using the experimental data given in the manufacturer datasheet (see Table 10.1). Interpolation results for the data given in Table 10.1 and a sample interpolated discharge current are shown in Figure 10.6. As expected, the actual capacity of the battery reduces when the discharge rates increases. Based on the theory explained in the earlier section, this effect exponentially increases for higher discharge rates, shown in Figure 10.6.

BLE and CEB Test

Unfortunately, there was no experimental data available for the battery discharge profile (discharge current magnitude and duration) to test the proposed BLE algorithm. Therefore, an arbitrary discharge profile is created with different discharge current

magnitude and duration for a day, given in Table 10.2. Then, similar discharge pattern is repeated for 100 days for the simulation study. The goal of this simulation is to show the impact of curve fitting algorithm on the battery life estimation and the resulting cost. In this simulation study, it is assumed that the primary management fully charges the battery after each discharge. Therefore, enough power is always available in the battery for discharge. Total discharge time of the battery is considered to be 165 minutes during a day, i.e., less than 3 hours. Different high power and energy pulses are included in the created discharge pattern. Also, the discharge current is always maintained below the critical value given in Table 10.2.

The BLE algorithm has been simulated for different ratios of current magnitude and its time duration, given in Table 10.2, for both NLLS and PSO methods. In Figure 10.7, results obtained from both NLLS and PSO are shown when the discharge current magnitude is scaled from 90% to 130% of the original values in Table 10.2, while the time duration is kept constant. It can be seen from Figure 10.7 that the estimated values from NLLS and PSO follow the same trend; however the estimated values are significantly different at each point. In other words, error in the BLE unit using NLLS approach can result in significant error in the CEB calculation.

Table 10.2. The arbitrary discharge pattern created for a day.

Time, min	1	1	1	2	2	3	4	4	5
Current, A	100	150	130	120	110	30	40	40	50
Time, min	5	5	10	11	11	20	20	30	30
Current, A	90	80	60	20	50	60	70	50	65

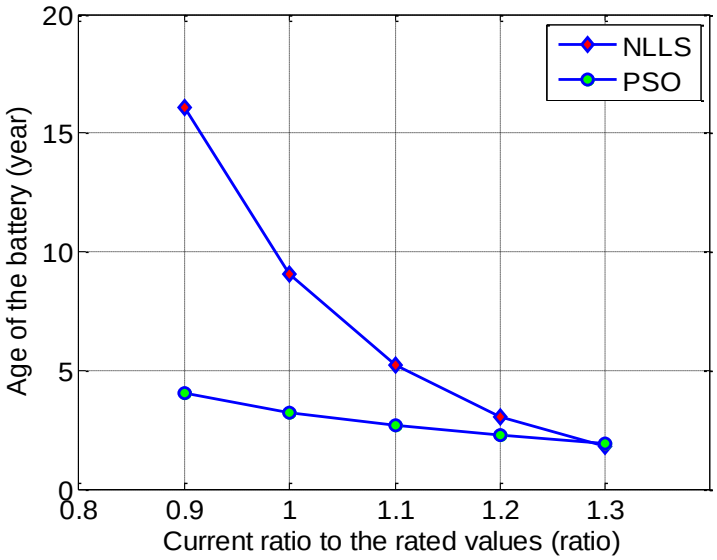


Figure 10.7. The BLE calculations for different current magnitudes, obtained from the curve fitting using NLLS and PSO methods.

For the discharge pattern given in Table 10.2, the corresponding CEB is calculated for both curve fitting methods used in this chapter, i.e., NLLS and PSO. The useful lifetime of the project is assumed to be 20 years in the simulation studies. The battery cell has rated capacity of 45 Ah at 48 V as the nominal voltage. The rated DoD is 80% based on the information provided by the company [10.17].

Figure 10.8 shows the CEB for different ratio of discharge current magnitudes. It can be seen that the CEB values obtained using PSO curve fitting method are significantly bigger than those obtained by NLLS method because of the difference in the estimated BLE in the two methods, shown in Figure 10.7.

Also, another simulation study has been performed on the proposed BLE model. In this case, the current magnitude is remained constant and the time duration of each discharge event has been changed from 80% to 120%. Both NLLS and PSO curve fitting methods have been employed in separate simulation study.

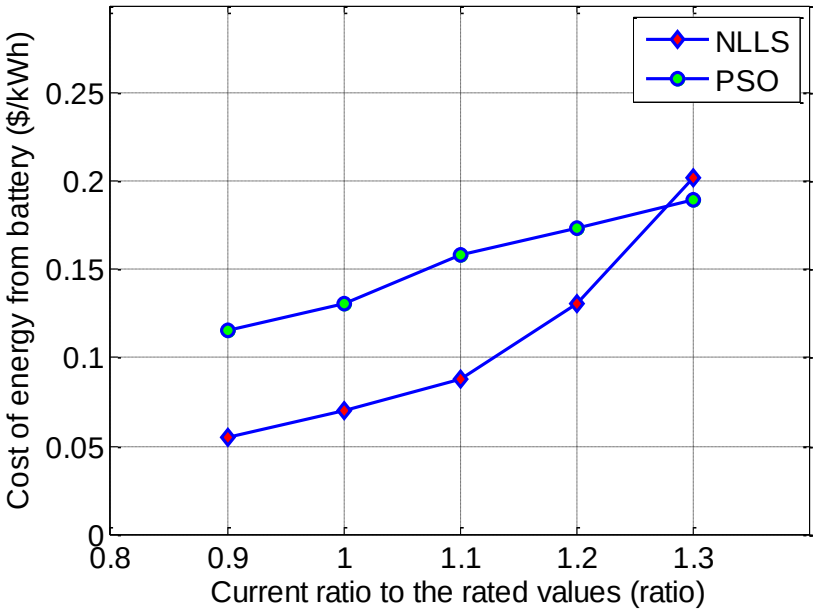


Figure 10.8. The CEB for different discharge current magnitudes, obtained from the curve fitting results using NLLS and PSO methods.

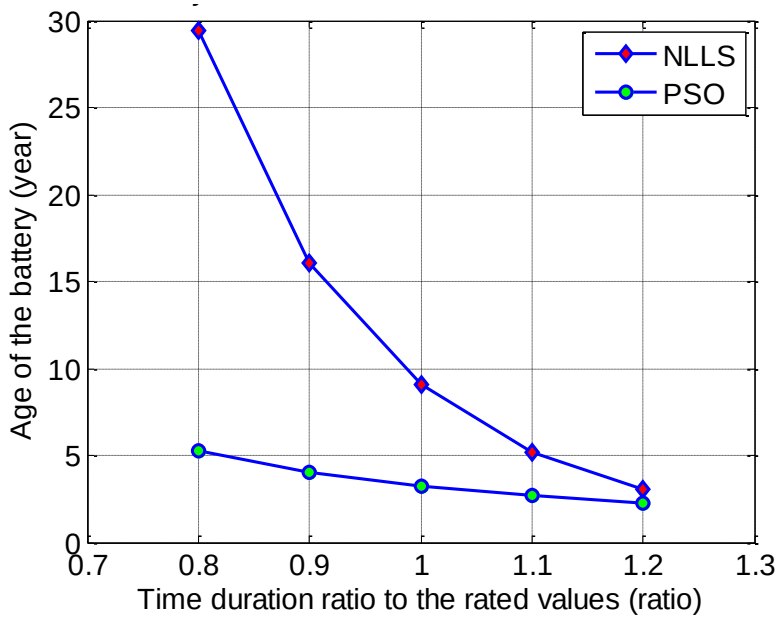


Figure 10.9. The BLE values for different time duration studies, obtained using NLLS and PSO curve fitting methods.

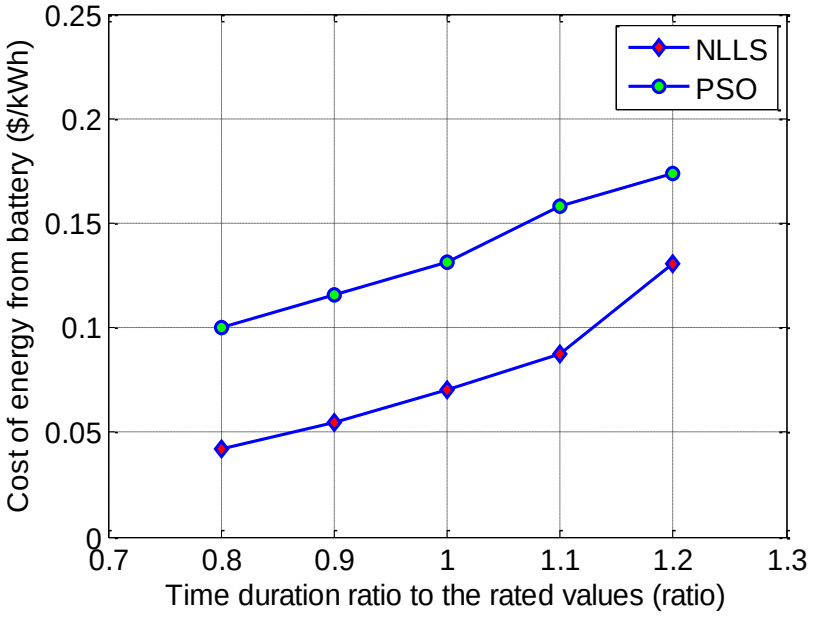


Figure 10.10. The calculated CEB for different discharging time durations obtained using NLLS and PSO curve fitting methods.

Simulation results are shown in Figure 10.9. Similar pattern to the CEB calculations can be observed in this case as well. Again, significant difference between the two methods in Figure 10.9 can be described using the significant error in the quality of NLLS method for curve fitting, i.e., Figure 10.5.

In Figure 10.10, the CEB is shown when discharging current magnitude is assumed to be constant and the time duration of the discharge pattern varies. Again, the estimated CEB using PSO curve fitting method is higher than the ones from NLLS.

The Proposed Management Framework

In order to evaluate the effectiveness of the proposed management framework, a grid-tied MG including wind turbine and PV solar panels as generation resources and Lithium-Ion battery pack as storage device is considered in this section. The MG has

been optimally sized with HOMER® considering the fact that the battery is not allowed to be charged by the grid. Also, the values for the power purchased from the grid in the output of the HOMER® design are used as scheduled hourly power from grid in the dynamic simulations. In real-world applications, the day-ahead economic dispatch problem should be solved to obtain the scheduled hourly power from the grid. Since the day-ahead economic dispatch only works in hourly basis with predicted load demand and renewable power generation, generation and demand mismatch might occur in real-time operation. Here, the real-time power management is the only solution to avoid power mismatch and to maintain the system stability. The size of the MG component is calculated as follows:

- ✓ Wind turbine: 20 kW
- ✓ PV solar panels: 40 kW
- ✓ Lithium-Ion battery: 38.8 kWh

The grid-tied islanded MG configuration is shown in Figure 10.1. The battery specification is also given in Table 10.3. Actual minute-by-minute wind speed, solar irradiation, ambient temperature, and load demand data are used in this study. The load demand data is measured in a commercial building. The average load demand during a year, the peak load and load factor are 34.7 kW, 63.8 kW, and 0.546, respectively. In order to perform real-time power management, dynamic model of the MG component has been developed in MATLAB/Simulink. The time-based electricity tariffs are used in this study, which are given in Table 10.4.

Table 10.3. Intensium Flex High Energy Lithium-Ion battery specification.

Nominal voltage of each pack, V	48
Capacity (C/3), Ah	45
Lifetime at +20 ^{o}C perm, year	20
Lifetime at +40 ^{o}C, year	>10
Cycle life (80% DoD, 20 ^{o}C)	3000
NO. of pack in series, and parallel	6, and 1

Table 10.4. Cost of electricity from the grid.

Peak Summer[1]	$0.16489 /kWh
Part-Peak Summer[2]	$0.06595 /kWh
Off-Peak Summer[3]	$0.03298 /kWh
Part-Peak Winter[4]	$0.05334 /kWh
Off-Peak Winter[5]	$0.03556 /kWh

[1] 12:00 noon to 6:00 p.m. Monday through Friday (except holidays)
[2] (8:30 a.m. to 12:00 noon) AND (6:00 p.m. to 9:30 p.m.) Monday through Friday (except holidays)
[3] 9:30 p.m. to 8:30 a.m. Monday through Friday AND All day Saturday, Sunday, and holidays
[4] 8:30 a.m. to 9:30 p.m. Monday through Friday (except holidays)
[5] 9:30 p.m. to 8:30 a.m. Monday through Friday (except holidays) AND All day Saturday, Sunday, and holidays

According to the SM strategy in the proposed framework, three different cases can be recognized. In all cases, the decisions made by the management framework are updated every minute to determine the share of power between battery and the grid. The simulation has been carried out for a year for each scenario.

CASE I. If the battery SoC is greater than 20% (since the rated DoD of the battery is 80% [10.17]), the battery should provide the required power. Otherwise, the grid will provide the required power.

CASE II. If the battery SoC is greater than 20% and the CEB is less than the cost of energy from the grid, the battery should meet the demand. Otherwise, the grid will provide the required power.

CASE III. In this case, it is assumed that the battery cannot be discharged.

Therefore, required power will be purchased from the grid regardless of its cost.

Different scenarios from those developed in this study can be defined within the SM block such as heuristic optimization-based methodologies. However, this is out of scope of this chapter. Note that in CASE III, the battery has not been used. Therefore, the CEB and its lifetime are not shown in results.

In Figure 10.11, the battery life estimation for CASEs I and II is shown. In CASE I, the battery ages faster due to the more frequent usage. Therefore, it is expected to see a higher CEB in CASE I compared to CASE II, as shown in Figure 10.12. At the beginning of the estimation, fast fluctuations can be observed due to the lack of enough discharge information. However, the accuracy of the estimation improves gradually when time succeeds. There are several fluctuations in the battery after 50 days for CASE II because of replacement cost. More specifically, whenever the battery life estimation drops below 20 years, replacement cost for at least one battery will be added to the energy cost.

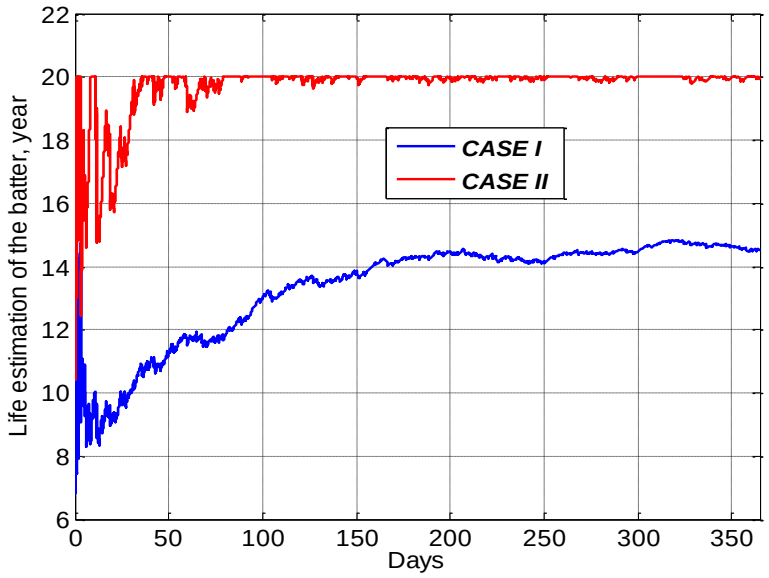


Figure 10.11. Battery life estimation for CASES I and II for a year of simulation.

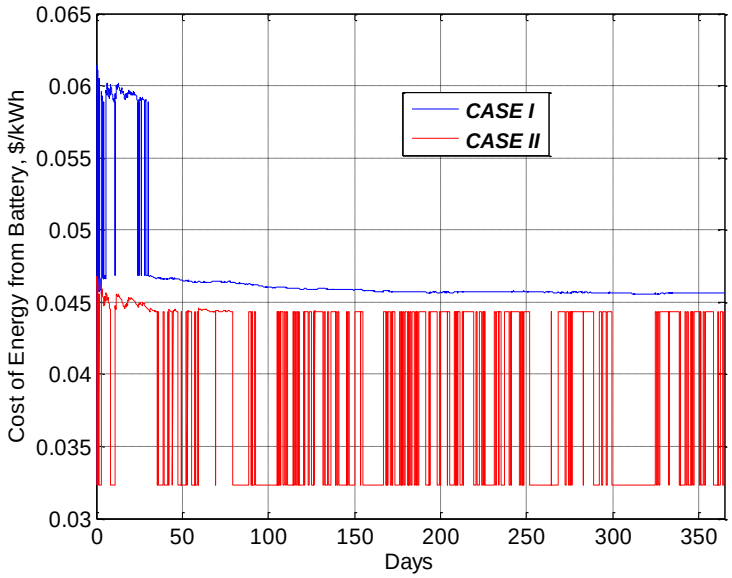


Figure 10.12. The CEB per kWh in both CASEs for a year of simulation.

The accumulative CEB based on the utilization of the battery for CASEs I and II are shown in Figure 10.13. The cost of energy is reduced in CASE II because of increase in the battery lifetime estimation, which eventually results in a lower cost for the consumers.

Note that in both CASEs, total load demand has been met either by the power from battery or the grid. However, the aggregated payment by the end of the year in CASE I is almost twice as the one in CASE II. These results show the effectiveness of the proposed management framework in extending the battery lifetime and reducing the cost of energy for the consumer simultaneously.

Table 10.5. Controlled power cost in each case and percentage of savings.

	Battery payment, $	% of money saving
CASE I	588	9.26
CASE II	527	18.67
CASE III	648	--

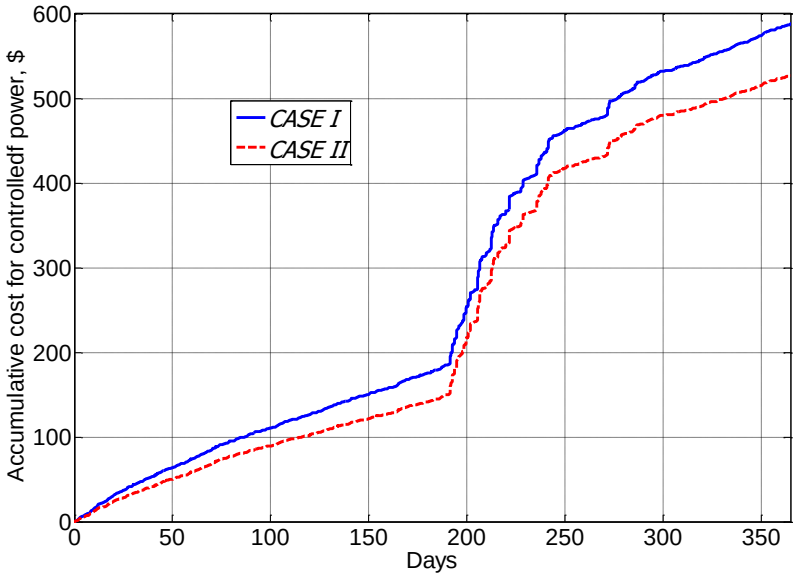


Figure 10.13. Accumulative cost of energy extracted from battery for both CASEs for a year of simulation.

The total electricity cost for the controlled power at the end of the year for different CASEs are presented in Table 10.5. It can be seen that the total cost of electricity is slightly reduced in CASEs I and II compared to CASE III. In other words, the proposed management framework can reduce the total cost in CASEs I and II at the end of the year. Also, the total cost of electricity (for controlled and uncontrolled power) at the end of the year of simulation has been decreased by 0.42% and 0.85% in CASEs I and CASE II, respectively, compared to CASE III. The saving in both CASEs I and II is marginal because of relatively small size of the battery compared to other component in the MG. This way, only a small amount of load can be met by the battery, and the grid has the biggest share in providing power to the MG. Therefore, the impact of the battery operation on the total cost of the MG operation is not significant.

Conclusion

Storage devices are an inevitable part of any MG, where they are usually the most expensive component of MGs. In this chapter, a power management framework is proposed for a grid-tied MG with battery as storage device. The goal is to extend the battery life as well as to reduce the cost of the energy for the consumer. Simulation results show that both goals have been achieved through the proposed power management framework.

References Cited

[10.1] C.M. Colson, M.H. Nehrir, and S.A. Pourmousavi, "Towards real-time microgrid power management using computational intelligence methods," in *Proc.* IEEE PES General Meeting, Minneapolis, USA, July 2010, pp. 1–8.

[10.2] EPRI, "Electricity energy storage technology options: A white paper primer on applications, costs and benefits," Dec. 2010. Available online: http://www.electricitystorage.org/images/uploads/docs/EPRI_StorageReport_5_11.pdf

[10.3] S.A. Pourmousavi, et al., "Real-time energy management of a stand-alone hybrid wind-microturbine energy system using particle swarm optimization," *IEEE Trans. Sustain. Energy*, vol. 1, no. 3, pp. 193–201, Oct. 2010.

[10.4] R. Hobbs, et al., "Development of predictive techniques for determination of remaining life for lead-acid batteries under fast charge," in *Proc.* Battery Conference on Applications and Advances, 1999, pp. 177–188.

[10.5] K. Takei, et al., "Cycle life estimation of lithium secondary battery by extrapolation method and accelerated aging test," *J. Power Sources*, vol. 97-98, pp. 697–701, July 2001.

[10.6] A. Yamashita, et al., "Capacity estimation and lifetime expectancy of large-scale nickel metal hydride backup batteries," in *Proc.* Telecommunications Conference INTELEC, 2005, pp. 291–295.

[10.7] P.E. Pascoe and A.H. Anbuky, "Standby power system VRLA battery reserve life estimation scheme," *IEEE Trans. Energy Convers.*, vol. 20,no. 4, pp. 887–895, Dec. 2005.

[10.8] C.C. Hua, et al., "Design and implementation of a residual capacity estimator for lead-acid batteries," in *Proc.* Industrial Electronics and Applications, ICIEA, pp. 2018–2023, 2007.

[10.9] X. Wei, B. Zhu, and W. Xu, "Internal resistance identification in vehicle power lithium-ion battery and application in lifetime estimation," in *Proc.* International Conference on Measuring Technology and Mechatronics Automation, vol. 3, pp. 388–392, 2009.

[10.10]W.L. Burgess, "Valve regulated lead acid battery float service life estimation using a Kalman filter," *J. Power Sources*, vol. 191, no. 1, pp. 16–21, June 2009.
[10.11]D. Haifeng, W. Xuezhe, and S. Zechang, "A new SOH prediction concept for the power lithium-ion battery used on HEVs," in *Proc.* IEEE Conference on Vehicle Power and Propulsion, VPPCEE, 2009, pp. 1649–1653.

[10.12]S. Drouilhet and B.L. Johnson, "A battery life prediction method for hybrid power applications," AIAA Aerospace Sciences Meeting and Exhibit, 1997.

[10.13]J.F. Manwell, et al., "Improvements to the hybrid2 battery model," Windpower Conference, 2005.

[10.14]P. Symons, "Life estimation of lead-acid battery cells for utility energy storage," in *Proc.* 5th Conference on Batteries for Utility Storage, San Juan, Puerto Rico, July 1995.

[10.15]A. Kashefi Kaviani, G.H. Riahy, and SH.M. Kouhsari, "Optimal design of a reliable hydrogen-based stand-alone wind/PV generating system considering component outages," *Renew. Energ.*, vol. 34, no. 11, pp. 2380–2390, Nov. 2009.

[10.16]H. Yang, et al., "Optimal sizing method for stand-alone hybrid solar/wind system with LPSP technology by using genetic algorithm," *Solar Energy*, vol. 82, no. 4, pp. 354–367, April 2008.

[10.17]SAFT Batteries, Available online: http://www.saftbatteries.com/doc/Documents/stationary/Cube782/IntFLEX_0708.ce3d756b-b571-4cf3-a952-ad069f830ed1.pdf

CHAPTER 11

REAL-TIME ENERGY MANAGEMENT OF A STAND-ALONE HYBRID WIND-MICROTURBINE ENERGY SYSTEM USING PARTICLE SWARM OPTIMIZATION

Contribution of Authors and Co-Authors

Manuscripts in Chapters 2 through 12

Author: S. A. Pourmousavi

Contributions: Developed real-time power management framework considering PSO technique, implemented MG model with management algorithm in MATLAB®/Simulink, designed all the simulation studies, prepared manuscript, figures and tables.

Co-author: M. H. Nehrir

Contributions: Provided important insight and overview of the research, interpretation of the results, and aided in the preparation of the manuscript.

Co-author: C. M. Colson

Contributions: Provided insight about the microturbine model, and aided in the preparation of the manuscript.

Co-author: C. Wang

Contributions: Developed PV and wind turbine dynamic models in MATLAB®/Simulink, and provided useful insights on the interpretation of the results.

Manuscript Information Page

Seyyed Ali Pourmousavi Kani, M. Hashem Nehrir, Christopher M. Colson, Caisheng Wang

IEEE Transactions on Sustainable Energy, 2010

Status of the manuscript:
____ Prepared for submission to a peer-reviewed journal
____ Officially submitted to a peer-reviewed journal
____ Accepted by a peer-reviewed journal
_X_ Published in a peer-reviewed journal

Published by the Institute of Electrical and Electronics Engineering (IEEE)

IEEE TRANSACTIONS ON SUSTAINABLE ENERGY, VOL. 1, NO. 3, OCTOBER 2010 193

Real-Time Energy Management of a Stand-Alone Hybrid Wind-Microturbine Energy System Using Particle Swarm Optimization

S. Ali Pourmousavi, *Student Member, IEEE*, M. Hashem Nehrir, *Fellow, IEEE*, Christopher M. Colson, *Student Member, IEEE*, and Caisheng Wang, *Senior Member, IEEE*

***Abstract*—Energy sustainability of hybrid energy systems is essentially a multiobjective, multiconstraint problem, where the energy system requires the capability to make rapid and robust decisions regarding the dispatch of electrical power produced by generation assets. This process of control for energy system components is known as energy management. In this paper, the application of particle swarm optimization (PSO), which is a biologically inspired direct search method, to find real-time optimal energy management solutions for a stand-alone hybrid wind-microturbine (MT) energy system, is presented. Results demonstrate that the proposed PSO-based energy management algorithm can solve an extensive solution space while incorporating many objectives such as: minimizing the cost of generated electricity, maximizing MT operational efficiency, and reducing environmental emissions. Actual wind and end-use load data were used for simulation studies and the well-established sequential quadratic programming optimization technique was used to validate the results obtained from PSO. Promising simulation results indicate the suitability of PSO for real-time energy management of hybrid energy systems.**

***Index Terms*—Battery bank, microturbine (MT), optimization methods, real-time energy management, wind power generation.**

I. Introduction

INCREASINGLY, forces such as cost, environmental concerns, and technological availability are exerting influence on power system design and implementation. Localized frameworks that combine diverse generation and storage components in a microgrid architecture, known as energy systems, are emerging to offer electrical consumers the opportunity to tailor their installed assets to meet local requirements. Renewable energy power generation sources such as wind and solar photovoltaic (PV), and emerging low- or zero-emission power generation devices, such as microturbine (MT) and fuel cells (FCs), fall in this category. These energy sources can complement each other to overcome the variable nature of the renewable energy sources, and together with energy storage (ES), improve system reliability and energy sustainability to the maximum extent possible. Such systems can be used stand-alone as independent microgrids for electrifying remote areas far from the grid, e.g., [1]–[4], or to serve a collection of loads in the urban areas, in grid-connected or island mode, e.g., [5] and [6]. In either case, proper unit sizing of the available energy sources is necessary to ensure that proper generation capacity is available for a particular application. Extensive work has been done in this area, e.g., [7]–[12]; many dependable computer-based programs are also available for this purpose, e.g., [13]–[15].

Effective energy management of hybrid energy systems is necessary to ensure optimal energy utilization and energy sustainability to the maximum extent. Furthermore, given the intermittent nature of the renewable energy resources involved and the multiple objectives that need to be satisfied (some of which may be conflicting), the energy management system (EMS) is complex and needs to find solutions quickly and continuously, e.g., every minute or few minutes. In general, conventional optimization techniques are too slow to be used for real-time optimization of the subject multiobjective, multiconstraint energy management problem. As a result, recently, research in this area has been focused on the application of intelligent control for unit sizing and energy utilization of hybrid energy systems, e.g., [16]–[20]. However, most of the reported work is on off-line applications such as generation unit sizing and optimal power dispatch, and little work has been reported on real-time management of energy systems using multiobjective optimization [5], [21].

This paper targets the real-time application of a heuristic multiobjective optimization technique, particle swarm optimization (PSO) [22], [23], for energy management of a hybrid energy system, which is achieved in a small fraction of a second. A hybrid stand-alone wind-MT-ES system is considered to supply the equivalent load requirements of a 120-home residential neighborhood, shown in Fig. 1. The primary components of the system are a wind energy conversion system (WECS) that utilizes a self-excited induction generator (SEIG) [1], [4], a single-shaft microturbine generator (MTG) that incorporates an SEIG as well [1], and a battery bank. The ratings of these components used in this study are given in the Fig. 1. However,

Manuscript received March 30, 2010; revised May 11, 2010; accepted July 19, 2010. Date of publication July 29, 2010; date of current version September 22, 2010. This work was supported in part by Pacific Northwest National Laboratory, which is operated for the U.S. Department of Energy by Battelle under Contract DE-AC05-76RL01830, in part by the National Science Foundation (NSF) under Grant ECS-0823865, and in part by the Visiting Scholar Project administrated through the State Key Laboratory of Power Transmission Equipment and System Security and New Technology at Chongqing University in China.

S. A. Pourmousavi, M. H. Nehrir, and C. M. Colson are with the Electrical and Computer Engineering Department, Montana State University, Bozeman, MT 59717 USA (e-mail: s.pourmousavikani@msu.montana.edu; christopher.colson@msu.montana.edu; hnehrir@ece.montana.edu).

C. Wang is with the Division of Engineering Technology and the Department of Electrical and Computer Engineering, Wayne State University, Detroit, MI 48202 USA (e-mail: cwang@wayne.edu).

Color versions of one or more of the figures in this paper are available online at http://ieeexplore.ieee.org.

Digital Object Identifier 10.1109/TSTE.2010.2061881

1949-3029/$26.00 © 2010 IEEE

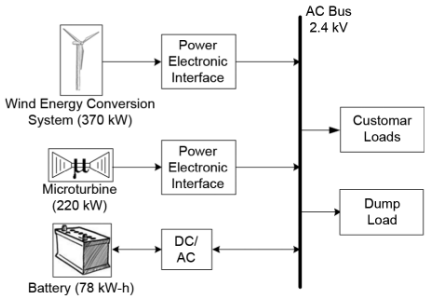


Fig. 1. Configuration of the proposed system.

the proposed intelligent EMS described in the paper can be applied to other WECS and MT configurations, such as a WECS or a MT which utilize a permanent magnet synchronous generator, and to other hybrid systems.

The study reported in this paper is the continuation of a previous work by the authors [1], where the design of an EMS for a hybrid wind-MT energy system is reported; however, no optimization was used in that reference. In the current paper, a real-time PSO-based EMS for the hybrid wind-MT-ES system is proposed. In addition, the well-established analytical optimization technique, sequential quadratic programming (SQP) [25], was also used to validate the results obtained using PSO. Actual wind and end-use load data were used in the simulation studies, conducted in the MATLAB/Simulink environment.

The objective function for both optimization algorithms (PSO and SQP) used is updated every 3 min, during which load and generation are considered constant. The choice to update the optimization at a smaller interval is possible, but at the expense of longer simulation time. The storage battery bank was used to ensure long-term energy sustainability and to supply the power needed during each interval to cover short-duration transients caused by sudden changes in load or wind speed. The extremely fast convergence speed of PSO [33] and the promising simulation results obtained show the potential of this multiobjective optimization technique for real-time energy management of multisource energy systems. It should be noted that the focus of the reported work is on energy management, where 24-hour simulation studies were conducted. Unit sizing and system voltage and frequency characteristics and stabilization are not discussed in this paper and will be reported in a future work.

This paper is organized as follows. Formulation of the optimization problem is discussed in Section II. Section III gives a description of the proposed EMS. In Section IV, PSO is briefly discussed and, PSO-based energy management is presented. Simulation results are given in Section V. A discussion is presented in Section VI and concluding remarks are given in Section VII.

II. Formulation of the Optimization Problem

The objective function developed for the EMS for the hybrid system presented here takes into account a number of factors including the cost of energy produced by the WECS and MT, as well as the technical constraints of the optimization procedure. In this section, the cost functions for the MT and WECS and the required constraints are developed.

A. MT Cost Function and Constraints

The MT cost function can be expressed as follows [5]:

$$F_{t,\mathrm{MT}} = C_{\mathrm{MT}}.F_{\mathrm{MT}}.P_{t,\mathrm{MT}}.\Delta T + \mathrm{OM}_{t,\mathrm{MT}} + \mathrm{SC}_{t,\mathrm{MT}} \quad (1)$$

where

$F_{t,\mathrm{MT}}$	total operating cost of the MT (\$);
C_{MT}	fuel cost of the MT unit ($\$/\mathrm{m}^3$). Natural gas was used as fuel at a cost of 0.3571 $\$/\mathrm{m}^3$ [26];
F_{MT}	fuel consumption rate (m^3/kWh). $F_{\mathrm{MT}} = 0.85$ m^3/kWh was used in this study [21];
$P_{t,\mathrm{MT}}$	decision variable representing the real power output from the MT unit (kW);
ΔT	energy management time step which is set at 3 min in this study (h), i.e., the optimization is updated every 3 min;
$\mathrm{OM}_{t,\mathrm{MT}}$	operation and maintenance (O & M) cost of the MT unit (\$);
$\mathrm{SC}_{t,\mathrm{MT}}$	start-up cost of the MT unit (\$).

The O & M cost of the MT is assumed to be proportional with the produced energy [5], [27]

$$\begin{aligned}\mathrm{OM}_{t,\mathrm{MT}} &= K_{\mathrm{OC}}.P_{t,\mathrm{MT}}.\Delta T \\ &= 0.00587 \times P_{t,\mathrm{MT}}.\Delta T\end{aligned} \quad (2)$$

where the proportionality constant K_{OC} is taken as 0.00587 \$/kWh for MT [5]. The start-up cost of the MT depends on the length of time the unit has been turned OFF before starting up once again [5], [28]

$$\mathrm{SC}_{t,\mathrm{MT}} = \left(\sigma_{\mathrm{MT}} + \delta_{\mathrm{MT}}\left(1 - e^{-\tau_{\mathrm{off},\mathrm{MT}}/\tau_{\mathrm{MT}}}\right)\right) \cdot \left(1 - u_{(t-1),\mathrm{MT}}\right) \quad (3)$$

where σ_{MT} and δ_{MT} are the hot start-up and cold start-up costs for the MT, respectively. τ_{MT} is the MT cooling time constant, $\tau_{\mathrm{off},\mathrm{MT}}$ is the time the MT has been OFF, and $u_{(t-1),\mathrm{MT}}$ shows the status of the MT (being ON or OFF) at time step $t-1$. If cold start-up of the MT requires power to run the MT's auxiliary systems [29], then the WECS or battery is required to provide this cold start-up power. In this study, the MT's hot start-up time is 30 s, cold start-up time is 200 s, and its cooling time constant is 520 s [29]. In general, for optimization studies that include MT, hot and cold start-up costs should be included; however, in this particular case, the value of these parameters do not affect the optimization results, because the fuel cost of the MT [i.e., the first term on the right side of (1)] is always higher than the total cost of operating the WECS.

Emissions cost has not been considered in this work because of unavailability of data or function [29]; however, if such data or function is available, an expression for this cost can be added to the objective function (1).

The output power of the MT unit in stable operation is restricted by its lower and upper limits as follows:

$$P_{\mathrm{MT}}^{\min} \leq P_{t,\mathrm{MT}} \leq P_{\mathrm{MT}}^{\max}. \tag{4}$$

In our case, the maximum available power from the MT is 220 kW and the lower limit is zero, i.e., the MT can be turned OFF when the output power from the WECS is enough to meet the demanded power. Once the MT is switched ON ($u_{t,\mathrm{MT}} = 1$), it has to operate continuously for a certain length of time before being switched OFF ($u_{t,\mathrm{MT}} = 0$). Also, a certain OFF-time period has to be achieved, meaning that the MT must be OFF for a certain period before being restarted. Violation of such constraints can shorten the unit's life time. These constraints are formulated as continuous run/stop time constraints as follows:

1) Evaluate whether the MT may be shut OFF by comparing the ON-time of the MT in the previous steps of the energy management with the MT's minimum up-time ($\mathrm{MUT}_{\mathrm{MT}}$)

$$\text{if} \quad (T_{\mathrm{MT}}^{on} - \mathrm{MUT}_{\mathrm{MT}}) \geq 0, \quad \text{then} \quad T_{\mathrm{MT}}^{on} = 0, \quad u_{t,\mathrm{MT}} = 0 \tag{5}$$

2) Evaluate whether the MT may be started up by comparing the OFF-time of the MT in the previous time steps with the MT's minimum down-time ($\mathrm{MDT}_{\mathrm{MT}}$)

$$\text{if} \quad \left(T_{\mathrm{MT}}^{\mathrm{off}} - \mathrm{MDT}_{\mathrm{MT}}\right) \geq 0, \quad \text{then} \quad T_{\mathrm{MT}}^{\mathrm{off}} = 0, \quad u_{t,\mathrm{MT}} = 1 \tag{6}$$

where $T_{\mathrm{MT}}^{\mathrm{on}}$, $T_{\mathrm{MT}}^{\mathrm{off}}$ (s) are the time length the MT has been ON or OFF, respectively. In this study, $\mathrm{MUT}_{\mathrm{MT}} = 600$ s and $\mathrm{MDT}_{\mathrm{MT}} = 300$ s [29]. Also, the number of starts and stops should not exceed a certain maximum depending on the MT specifications [5]

$$\varepsilon_{\mathrm{start-stop}} \leq N_{\max} \tag{7}$$

where $\varepsilon_{\mathrm{start-stop}}$, is the number of start-stops during simulation, and $N_{\max}$ is the maximum number of start-stops. In this study, $N_{\max} = 30$, which is never reached.

B. WECS Cost Function and Constraints

The following cost function is used for the WECS [20]:

$$F_{t,\mathrm{WT}} = C_{\mathrm{WT}}.P_{t,\mathrm{WT}}.\Delta T \tag{8}$$

where $F_{t,\mathrm{WT}}$ is the cost of wind-generated energy, $P_{t,\mathrm{WT}}$ and C_{WT} are the WECS' wind power (kW) and its cost coefficient for the generated energy at each time step ($/kWh), respectively. In this study, $F_{t,\mathrm{WT}}$ is always less than $F_{t,\mathrm{MT}}$. The value of C_{WT} depends on the actual cost of the wind-generated energy, which, in this case, is taken as $0.1/kWh. Again, this factor will not affect the results since $F_{t,\mathrm{WT}} < F_{t,\mathrm{MT}}$.

The output power of the WECS is restricted based on its power curve and parameters. The following parameters are used in this study [1]:

1) Cut-in speed, $v_{\mathrm{cut-in}} = 3$ m/s;
2) Rated speed, $v_{\mathrm{rated}} = 14$ m/s;
3) Cut-out speed, $v_{\mathrm{cut-out}} = 25$ m/s.

The WECS does not generate any power for $v_{\mathrm{wind}} < v_{\mathrm{cut-in}}$. Pitch control is used to limit the output power of the WECS to its rated value (370 kW) when $v_{\mathrm{rated}} < v_{\mathrm{wind}} < v_{\mathrm{cut-out}}$, and the WECS output power is zero for $v_{\mathrm{wind}} > v_{\mathrm{cut-out}}$. The details of the WECS modeling are given in [30]. The WECS output power is calculated at each time step using the wind speed at that instant. The power balance (equality constraint) for the WECS and MT to meet the load demand is

$$P_{t,\mathrm{MT}} + P_{t,\mathrm{WT}} = P_{t,\mathrm{Load}} \tag{9}$$

$$0 \leq P_{t,\mathrm{WT}} \leq p_{t,\mathrm{WT}}^{\max} \tag{10}$$

where $P_{t,\mathrm{Load}}$ is the load demand at each time step. Proper optimization techniques can then be used to best share power amongst the generation sources of the hybrid system to minimize the cost of electricity while satisfying the equality and inequality constraints given above. According to the following objective function, total operational cost is minimized:

$$\text{Min. Objective Func.} = F_{t,\mathrm{MT}} + F_{t,\mathrm{WT}}. \tag{11}$$

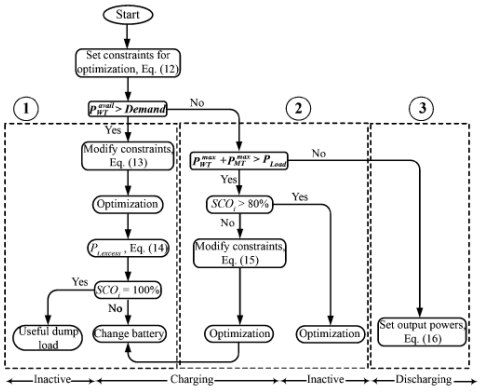


Fig. 2. Proposed energy management strategies for the WECS-MT-ES-EWH system.

III. Proposed Real-Time EMS

The flowchart for the proposed energy management, which accounts for multiple simultaneous objectives for the hybrid energy system, is annotated in Fig. 2. As shown in this figure, the battery has three states; charging, discharging, and inactive. The battery is in the inactive or charging mode in *scenarios* 1 and 2, and in discharging mode in *scenario* 3. The primary objectives of the EMS are as follows:

1) minimize the cost of energy generation;
2) maximize battery life by monitoring and controlling its state of charge (SOC) and charge/discharge process;
3) maximize the use of excess available wind power in a useful dump load when the battery is fully charged in an attempt to increase system utilization [34];
4) when the MT is in operation, adjust its operating point to near its rated power to increase its operation efficiency and reduce its environmental impact [29];
5) maximize the average available stored energy in the battery (i.e., higher battery SOC), hence improving system reliability.

At the start of the proposed energy management algorithm, the boundary equations for the energy sources involved and the equality constraints are defined as follows:

$$\begin{cases} P_{t,\mathrm{WT}}^{\max} = P_{t,\mathrm{WT}}^{\mathrm{avail}}, \quad P_{\mathrm{WT}}^{\min} = 0; \\ P_{\mathrm{MT}}^{\mathrm{rated}} = 220\ \mathrm{kW}, \quad P_{t,\mathrm{MT}}^{\min} = 0, \\ P_{t,\mathrm{supply}} = \mathrm{Demand}_t, \\ P_{t,\mathrm{supply}} = P_{t,\mathrm{WT}}^{\mathrm{optim}} + P_{t,\mathrm{MT}}^{\mathrm{optim}} \pm P_{t,\mathrm{batt}} \end{cases} \tag{12}$$

- where $P_{t,\mathrm{WT}}^{\max}$ and $P_{t,\mathrm{WT}}^{\min}$ are the maximum and minimum wind power limitations for the WECS, respectively;
- $P_{\mathrm{MT}}^{\mathrm{rated}}$ and $P_{t,\mathrm{WT}}^{\min}$ are the maximum (rated) and minimum power limitation for the MT;
- $P_{t,\mathrm{supply}}$ is the overall power demand of the hybrid system, including power supplied to the load, dump load, and to the battery;
- Demand_t is the power demanded by the load at time t;
- $P_{t,\mathrm{WT}}^{\mathrm{optim}}$ and $P_{t,\mathrm{MT}}^{\mathrm{optim}}$ are the optimized share of the WECS and the MT after optimization;
- $P_{t,\mathrm{batt}}$ is the amount of charge/discharge power to/from the battery.

Scenario 1: As shown in Fig. 2, if the maximum available power from the WECS is greater than demand, there is excess power available from the WECS which can be used to charge the battery, if needed. Otherwise, the excess power is supplied to a useful dump load, e.g., an auxiliary electric water heater (EWH) to preheat water, as proposed in [34]. Therefore, the actual demand is set to the available power from the WECS, i.e., the equality constraint (9) of the optimization will change to

$$P_{t,\mathrm{supply}} = P_{t,\mathrm{WT}}^{\mathrm{avail}}. \tag{13}$$

After performing optimization, the excess available power is the difference between the total generation and demand as follows:

$$P_{t,\mathrm{excess}} = P_{t,\mathrm{WT}}^{\mathrm{optim}} + P_{t,\mathrm{MT}}^{\mathrm{optim}} - \mathrm{Demand}_t. \tag{14}$$

As shown in Fig. 2, the excess power is used to charge the battery, if the battery is not fully charged. Otherwise, the battery will remain inactive and the excess power is directed to the useful dump load. In this operation mode, the mechanical stress on the wind turbine is reduced because the WECS output power is not limited by pitch control.

Scenario 2: In cases where power from the WECS is not enough to meet the demand, the MT will be turned ON. In this case, if the total power from the WECS and MT is greater than demand and the battery SOC is higher than 80%, the battery remains inactive and the optimization procedure will be performed to determine the generation dispatch of the WECS and MT. If the battery SOC is lower than 80%, the optimization constraints will be changed as follows:

$$\begin{cases} P_{t,\mathrm{batt}}^{\min} = 1\ \mathrm{kW} \\ P_{t,\mathrm{supply}} = P_{t,\mathrm{WT}}^{\max} + P_{t,\mathrm{MT}}^{\mathrm{rated}}. \end{cases} \tag{15}$$

This way, the excess power will be used to charge the battery bank, which can increase the reliability of the whole system, resulting in improved energy sustainability. According to [35], recharging lead-acid batteries immediately after discharging will extend battery life significantly. In order to avoid charging the battery at very low currents, which can reduce the battery lifespan, the lower limit of the battery charging power is arbitrarily set to 1 kW (about 3 A). Also, the upper battery charge power is limited to 62.4 kW (about 200 A) to keep the battery in safe condition. Note that this strategy is only applied when the MT is already turned ON to meet a part of the demand, because turning ON the MT only for charging the battery will add hot start-up cost to the energy production cost. Moreover, the number of starts and stops of the MTG can affect its life and efficiency. Cost analysis of MT operation is beyond the scope of this paper and has not been carried out.

Scenario 3: If the total power from the WECS and MTG is less than demand, the battery needs to be discharged to meet demand. In this condition, optimization is not necessary and the output power from the WT, MT, and battery is as follows:

$$\begin{cases} P_{\mathrm{WT}}^{\mathrm{optim}} = P_{\mathrm{WT}}^{\mathrm{avail}} \\ P_{\mathrm{MT}}^{\mathrm{optim}} = P_{\mathrm{MT}}^{\mathrm{rated}} = 220\ \mathrm{kW} \\ P_{\mathrm{batt}} = \mathrm{Demand} - P_{\mathrm{WT}}^{\mathrm{optim}} - P_{\mathrm{MT}}^{\mathrm{optim}}. \end{cases} \tag{16}$$

In this study, two optimization techniques are used: the evolutionary algorithm, PSO, and the conventional technique, SQP. PSO is the main optimization algorithm used; it is described in Section IV. The PSO-based EMS developed for this study, is described in Section IV-A. SQP-based EMS is used to verify the results of the PSO-based strategy.

IV. Particle Swarm Optimization

The PSO algorithm is performed at each time step (every 3 min) to determine the optimum balance of the WECS and MT to meet demand. Wind speed data, demand data, status of the MT, and the battery SOC are the input values to the optimization block. The battery model used and the method of calculating battery SOC are available in the MATLAB/Simulink SimPowerSystems toolbox [31]. Since the proposed optimization system operates in real-time, fast and accurate optimization methods should be employed. If any changes in demand or wind speed occur during the optimization intervals, the storage battery will respond to the power transients.

PSO is a population-based stochastic optimization technique developed by Kennedy and Eberhart [32], inspired by social behavior of bird flocking, fish schooling, and swarm theory. PSO shares many similarities with evolutionary computation techniques such as genetic algorithms (GAs). The system is initialized with a population of random solutions and searches for optima by updating generations. However, unlike GA, PSO has no evolution operators such as crossover and mutation. In PSO, the potential solutions, named as particles, "fly" through the problem space following the current optimum particles. Each particle is regarded as a point in a d-dimensional space that adjusts "flying" according to its own flying experience and flying experience of other particles.

PSO is simple in concept. It has few parameters to adjust and is easy to implement. In the past several years, PSO has been successfully applied in many research and application areas. In general, all the application areas that the other evolutionary application techniques are good at are the application areas for PSO. Reference [33] gives a comprehensive overview of PSO and its applications in power systems, and discusses its fast convergence speed and advantage over other stochastic methods.

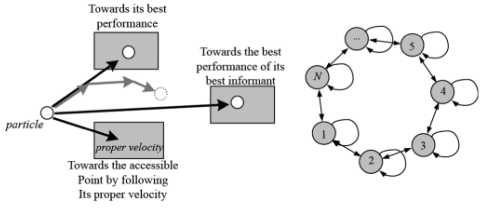


Fig. 3. (a) Three fundamental elements the particles position updating. (b) Graph of influence of a swarm of N particles in circular form with three informants for each particle [22].

The original PSO maintains a population of particles (x_1, x_2, . . ., x_p) which are initially distributed uniformly around the search space. Each particle represents a potential solution to the optimization problem. Let p be the size of the swarm. For each particle i, the position x_i is updated as follows [22], [32]:

$$x_{k+1}^i = x_k^i + v_{k+1}^i. \tag{17}$$

Each particle in PSO is associated with a pseudovelocity $v_{k+1}^i \left(-v_{\max}^i \le v_{k+1}^i \le v_{\max}^i\right)$, which represents the rate of the position change for the particle [22], [32]

$$v_{k+1}^i = \omega_k v_k^i + c_1 r_{1,k} \left(p_k^i - x_k^i\right) + c_2 r_{2,k} \left(p_k^{gi} - x_k^i\right). \tag{18}$$

Equation (18) is used to calculate each particle's new velocity v_{k+1}^i based on its previous velocity v_k^i and the distances of its current position x_k^i from its own best experience (position) and the best experienced position of its own informants, p_k^{gi}, according to Fig. 3(a). Here, subscripts k and i indicate a pseudotime increment and the number of particles, respectively; r_1 and r_2 represent uniform random numbers between 0 and 1, which will be regenerated at each iteration. c_1 and c_2 are two positive constants, called the cognitive and social parameter, respectively (in this study, they are chosen as $c_1 = 1.5$ and $c_2 = 1.5$) [22], [32].

Initially (at time step $t = 0$), the particles' velocities v_0^i are random numbers within the boundary $0 \le v_0^i \le v_{\max}^i$. The maximum velocity $v^{\max}$ allowed actually serves as a constraint that controls the maximum global exploration ability PSO can have. Then, each particle flies toward a new position according to (17) and (18). The inertia weight ω_k in (18) should be neither too large, which could result in premature convergence, nor too small, which can slow down convergence excessively (they are chosen as $\omega_{\min} = 0.6$ and $\omega_{\max} = 1.2$; ω holds the $\omega_{\min}$ value at the beginning of each simulation cycle and increases linearly to $\omega_{\max}$ at the end) [22]. Therefore, the particles have a tendency to fly towards better and better search areas over the course of the search process. As a result, the search can always reach an optimum or a solution very close to the optimum using fewer fitness evaluations [22].

The performance of each particle is measured according to a predefined fitness function, which is related to the problem to be solved. Each particle moves around the search space updating its velocity and position based on the best positions (P_{best}) thus far discovered by itself and by its informants. If all the particles are informed by each other, all the information acquired is disseminated immediately. This is a favorable scenario; however, it is highly risky to have a behavior that is too uniform, i.e., when all the particles will act uniformly [22]. Conversely, if each particle has too few informants, more diversified behaviors will be obtained. This scenario carries the risk that poor information can be transmitted.

In this study, the information links between the particles were defined once (and kept unchanged throughout the simulation), generally according to the "circular" diagram shown in Fig. 3(b) [22].

The N particles of the swarm are laid out virtually on a circle, and numbered sequentially from 1 by traversing the circle. Each particle has a set of informants of fixed size K.

The neighborhood of size K of a particle is obtained from the virtual circle by recruiting alternately on the right and left of its position, until a total of $K - 1$ neighbors are obtained. The particle itself is also included, i.e., $K = 3$. In this study, a swarm with five particles is used. Handling PSO by informant configuration, shown in Fig. 3(b), leads us to differentiate properly between the two functions provided by the particles: exploring the search space and memorizing the best position P_{best} found during this search. These two functions are carried by distinct particles [22].

A. PSO-Based Energy Management

To apply PSO to the WECS-MT energy management problem at hand, $P_{t,\text{WT}}$ is selected as a decision variable to be optimized by PSO. The variable $P_{t,\text{MT}}$ is then computed using the equality constraint given by (9). To optimize the problem in each step, initial swarms are defined as follows:

$$P_{t,\text{WT}} = \text{rand}() \times \left(P_{t,\text{WT}}^{\text{avail}} - P_{\text{WT}}^{\min}\right) + P_{\text{WT}}^{\min} \tag{19}$$

where $\text{rand}()$ represents uniform random numbers between 0 and 1, $P_{t,\text{WT}}^{\text{avail}}$ is the maximum available power from the WECS, which is calculated by the algorithm given in Fig. 2 using wind speed data. Then, the output power of the MT can be calculated as follows:

$$P_{t,\text{MT}} = P_{t,\text{Load}} - P_{t,\text{WT}}. \tag{20}$$

Given that the energy resource (wind) for the WECS is free and environmentally friendly, the overall objective of the WECS-MT system is to operate the WECS to the full capacity needed and operate the MT when the WECS cannot supply all the demanded power by itself. Two energy management scenarios are considered.

Case 1, no Optimization, WECS-MT-ES: In this case, the WECS power will supply the load and if excess power is available, it will be used to charge the storage battery if it is not fully charged ($\text{SOC} = 100\%$). Otherwise, the WECS output power is limited to that required by the load. The MT will be used when the combination of WECS and battery power is not sufficient to supply the load. Therefore, the WECS maximum power dispatch is governed by the following equation:

$$\begin{cases} \text{if } p_{t,\text{WT}}^{\text{avail}} > P_{t,\text{Load}} \& \text{SOC}_t = 100\% \Rightarrow P_{t,\text{WT}}^{\max} = P_{t,\text{Load}} \\ \text{else}: \quad p_{t,\text{WT}}^{\max} = P_{t,\text{WT}}^{\text{avail}}. \end{cases} \tag{21}$$

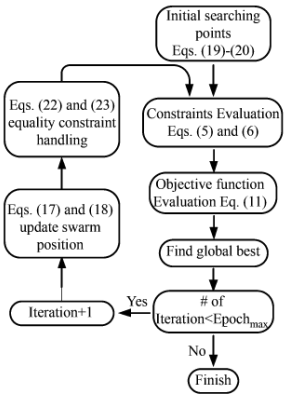


Fig. 4. Flowchart for the proposed PSO algorithm.

This case is similar to that presented in [1]. Its disadvantage is that when the available wind power is greater than demand and the battery is fully charged (i.e., when (21) is not satisfied), then the WECS power must be limited.

Case 2, Optimized, WECS-MT-ES-Dump Load: This is the preferred energy management strategy, where the maximum available power is extracted from the WECS at all times. If the available wind power is more than load demand and the storage battery is full, the excess available power of the WECS is supplied to a useful dump load. In a previous study by the second author, it has been shown that an auxiliary EWH can be used as a useful dump load [34]. Any excess available wind power will be supplied to the auxiliary EWH to preheat the water before entering the main residential EWH. It has been shown in [34] that the energy used by the main residential EWH can be reduced considerably by using an auxiliary EWH as a dump load. This scenario is adapted in the Case 2 study.

In the PSO algorithm, the values of initial guesses used for the objective functions are assigned by intuition (best guess). The best possible answer will then be selected and the swarms' positions will be updated, for each decision variable according to (17) and (18). The following equality constraints are applied at each iteration to modify the swarms' positions:

$$\text{if } P_{t,\mathrm{MT}} < 0 \rightarrow \begin{cases} P_{t,\mathrm{WT}} = P_{t,\mathrm{WT}} - |P_{t,\mathrm{MT}}| \\ P_{t,\mathrm{MT}} = 0 \end{cases} \tag{22}$$

$$\text{if } P_{t,\mathrm{WT}} > P_{t,\mathrm{WT}}^{\max} \rightarrow \begin{cases} P_{t,\mathrm{MT}} = P_{t,\mathrm{MT}} + \left(P_{t,\mathrm{WT}}^{\max} - P_{t,\mathrm{WT}}\right) \\ P_{t,\mathrm{WT}} = P_{t,\mathrm{WT}}^{\max}. \end{cases} \tag{23}$$

The above equality constraints ensure that improper selections for $P_{t,\mathrm{MT}}$ and $P_{t,\mathrm{WT}}$ values are adjusted into the space of appropriate dispatch assignments. The flowchart for the proposed PSO algorithm is illustrated in Fig. 4. For the initial searching points, 5 swarms and 50 iterations are used. These values are chosen by experience; caution must be taken to ensure that the solution converges within the maximum number of iterations. In this study, when the above values were used, the optimal solution was reached within 0.012 s.

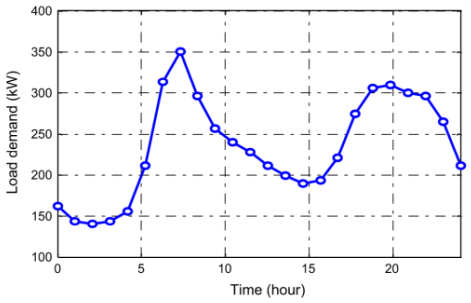


Fig. 5. Hourly average demand of 120 typical residences in the Pacific Northwest area [36].

As stated earlier, the well-established analytical optimization algorithm, SQP, which is available in MATLAB, is used to validate the results obtained using PSO. SQP is applied to show the accuracy and fast convergence time of PSO. SQP optimization is based on quadratic programming which uses a quasi-Newton method. Detailed description of SQP is beyond the scope of this paper; interested readers are referred to the comprehensive literature available on this optimization technique, e.g., [25].

V. Simulation Results

The stand-alone wind-MT-ES system in this study is designed to supply power to a residential neighborhood in the U.S. Pacific Northwest area consisting of 120 houses. The typical average residential daily load demand profile used is obtained from the Pacific Northwest regional information reported in [36]. The total aggregate hourly average load demand of the residential neighborhood is shown in Fig. 5.

Actual wind data is used in this case study, obtained from the online records of the weather station at Deer Lodge, Montana, affiliated with the Pacific Northwest Cooperative Agricultural Weather Network (AgriMet) [37]. The hourly average wind speed data, recorded on March 12, 2007 at a height of 2 m, was chosen for the 24-hour simulation study. This date was chosen because its 24-hour average wind speed closely matched the annual average wind speed for the area. The wind data on this date was also used in the study (by the authors) reported in [1], which would make the comparison of the results obtained using the proposed EMS with those reported in [1] easier. Data reported in [37] was corrected for the proposed wind turbine hub height of 40 m, shown in Fig. 6, using the following expression [38]:

$$v_{s1} = v_{s0} \cdot \left(\frac{H_1}{H_0}\right)^{\alpha} \tag{24}$$

where v_{s1}, v_{s0} (m/s) are wind speeds at the hub height H_1 and the height H_0 (m) at which the data was collected. α is the wind speed correction exponent; in this study, α sets to 0.13 [7], [38].

The energy management algorithm discussed in Section IV is used with PSO and SQP optimization techniques, and simulation results were compared with those reported in [1], where no optimization was used (i.e., case 1—no optimization—in this study).

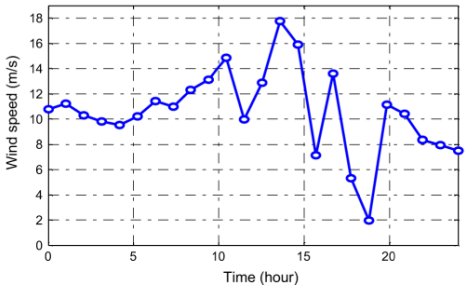


Fig. 6. Actual corrected wind speed data for Deer Lodge, MT on March 12, 2007 [37], corrected to hub height of 40 m.

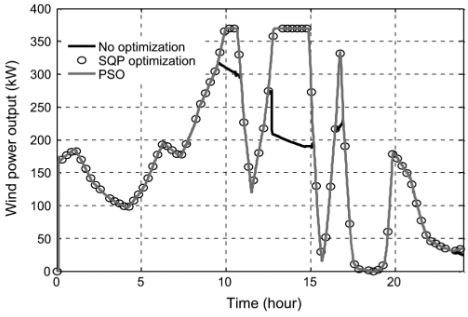


Fig. 7. Wind power output for different management algorithms and optimization methods.

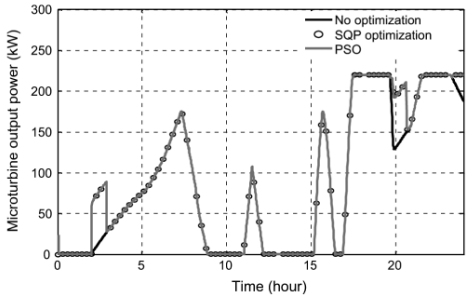


Fig. 8. MTG output power for different management algorithms and optimization methods.

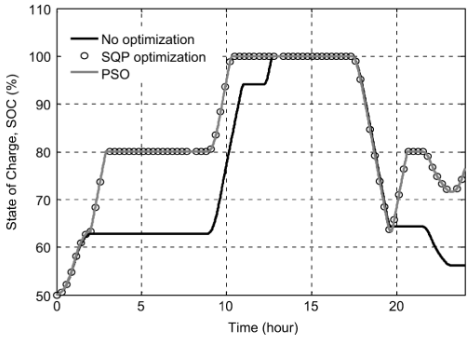


Fig. 9. SOC of battery for different algorithms and optimization methods.

Fig. 7 shows the output power of the WECS corresponding to the wind speed profile shown in Fig. 6. It is noted that the wind power profiles for the proposed EMS (PSO- and SQP-based EMS) are exactly the same (PSO-based is shown as a grey line; SQP-based is highlighted with circles), but the power profile is slightly different under no optimization (i.e., during the periods 9:30–10:30, 12:30–15:00, and 16:00–16:30), where the responses are shown with solid (dark) line. In the first high-wind period (9:30–10:30 h), the excess power from the WECS is higher than the battery charging limit. Therefore, the WECS power is limited (by pitch control) to the amount of demand plus maximum battery charging power. Similarly, in the next high-wind period (12:30–15:00 h and 16:00–16:30 h), the WECS output power is more than demand and the battery is fully charged. Therefore, in the no optimization scenario, the output power from the WECS is further limited by pitch controller as described in [30], whereas, in the case of the proposed EMS, the excess wind power available in the same periods is delivered to the useful dump load, as shown later in Fig. 11. During the periods 10:00–10:30 and 12:30–15:00, the available wind power is higher than the WECS rated power. Therefore, pitch control is applied to limit the WECS power to its rated value.

Fig. 8 shows the MTG output power profile for the three scenarios explored. In most cases, the MTG produces power when the available wind power is not sufficient to meet the demand. However, under the proposed EMS (using PSO or SQP), when the MT is operating and the battery SOC is below 80%, the MT will operate at rated power to take advantage of improved efficiency and reduced emission [29], and the excess available power is used to charge the battery (Fig. 8, 2:30–3:30, 19:30–21:00, and 23:30–24:00 h).

Fig. 9 shows the SOC of the battery for the three scenarios studied. The initial battery SOC is assumed to be 50% to better show its charge/discharge pattern. From the results shown, the superiority of the optimized energy management scenarios (in keeping the battery SOC higher) over when no optimization is used is clear. Because of its improved SOC profile, the battery is in a better state of health, and has a longer lifespan [35].

Fig. 10 shows the battery power profile for the three scenarios. In the no optimization scenario, the battery will charge when the WECS power is in excess of demand (0:00–2:00, 9:00–11:00, 12:00–12:30 h) and will discharge when the WECS plus MTG cannot meet the power demand (17:00–19:30, 22:00–23:30 h). In the remainder of the hours, the battery remains idle. Under the proposed EMS, in addition to the above charging periods, the battery is also charged when the WECS plus MTG power is in excess of demand (i.e., 2:00–3:00, 19:30–21:00, and 23:30–24:00 h). During these periods, the battery is further charged by the MTG since the MTG is operating near its rated

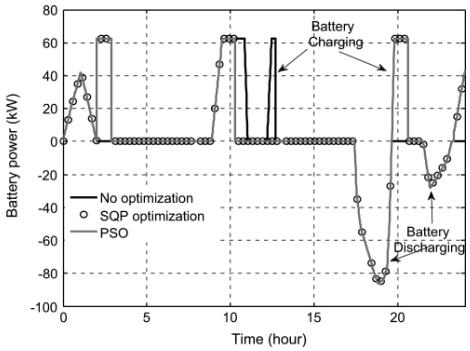


Fig. 10. Battery power for different power management algorithms in a day.

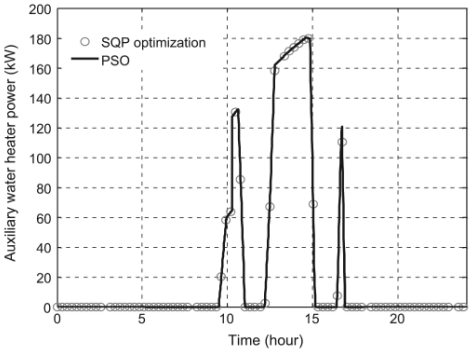


Fig. 11. Auxiliary water heater power for a day in the proposed energy management strategy.

power to further charge the battery when the battery SOC is below 80%. As shown in Fig. 10, the battery charging power is limited to 62.4 kW (about 200 A) for safety reasons.

Fig. 11 shows the periods when excess power is available from the WECS or MT. This excess power is delivered to a useful dump load (e.g., an auxiliary EWH) for the PSO and SQP optimization strategies. No useful dump load was considered under the "no optimization" case, reported in [1].

VI. Discussion

A stand-alone hybrid wind-MT-ES system has been used herein to explore the feasibility of a proposed PSO-based energy management algorithm for real-time applications. In this case, since priority is given to wind power production because of obvious advantages, the objective functions defined for the optimization problem are linear. As a result, the simulation results obtained when using the PSO and SQP algorithms are exactly the same. However, in more complex systems, where the objective functions are nonlinear, the random nature of the PSO-based EMS can improve the final results in comparison with the analytical-based optimization techniques [33]. It is our plan to apply the proposed PSO-based EMS to more complex multisource systems in future work.

TABLE I
Computation Time for Different Optimization Techniques

Optimization Algorithm	PSO	SQP Optimization
Time (seconds)	0.012	0.957

Because the objective here is to explore the feasibility of application of PSO for real-time EMS, the convergence time of the PSO algorithm is highly important. Table I shows a comparison of the computation time for the PSO- and SQP-based EMS for the wind-MT-ES system. As noted in the table, PSO convergence time is nearly 90 times faster than the analytical SQP optimization. This fast response of the PSO is critically important in its real-time application for energy management of multisource renewable energy-based systems.

VII. Conclusions

Real-time PSO-based energy management of a stand-alone hybrid wind-MT-ES system was presented in this paper. The developed EMS promotes energy sustainability in two ways: first, by ensuring an optimal balance between the attached generation sources based on the multiple constraints, and second, by incorporating desirable energy objectives into the EMS decision-making process. Specifically, the following factors are also considered:

1) the use of a useful dump load (an auxiliary EWH) to increase energy efficiency of the system;
2) keeping the operating point of the MT near its rated value when feasible to increase its operation efficiency and reduce its environmental impact;
3) maximizing the average available stored energy in the battery by striving to keep its SOC at 80% or higher, hence improving overall system reliability and increasing the battery life.

Simulation results show the suitability and potential benefits of the proposed PSO-based energy management strategy for the hybrid system.

In order to verify the validity of the proposed approach, simulation results were also obtained for the same system using the well-established SQP optimization and when no optimization was used. Simulation results compare well and show the benefits of the proposed EMS in increasing the overall system reliability and energy sustainability. In particular, the main advantage of the PSO-based energy management strategy is its extremely fast convergence time, which is critically important for real-time energy management applications.

Acknowledgment

The authors wish to acknowledge the valuable discussions they have had with Dr. D. Hammerstrom and Dr. R. Sastry of the Pacific Northwest National Laboratory and Dr. J. Sheppard from the Computer Science Department at Montana State University.

REFERENCES

[1] C. Wang, M. H. Nehrir, C. M. Colson, and J. Li, "Power management of a stand-alone hybrid wind-microturbine distributed generation system," in *Proc. Power Electronics and Machines in Wind Applications (PEMWA 2009)*, Jun. 24–26, 2009, pp. 1–7.

[2] R.-J. Wai, C.-Y. Lin, R.-Y. Duan, and Y.-R. Chang, "High-efficiency power conversion system for Kilowatt-level stand-alone generation unit with low input voltage," *IEEE Trans. Ind. Electron.*, vol. 55, no. 10, pp. 3702–3714, Oct. 2008.

[3] F. Valenciaga and P. F. Puleston, "Supervisor control for a stand-alone hybrid generation system using wind and photovoltaic energy," *IEEE Trans. Energy Convers.*, vol. 20, no. 2, pp. 398–405, Jun. 2005.

[4] C. Wang and M. H. Nehrir, "Power management of a stand-alone wind/photovoltaic/fuel cell energy system," *IEEE Trans. Energy Convers.*, vol. 23, no. 3, pp. 957–967, Sep. 2008.

[5] F. A. Mohamed and H. N. Koivo, "Microgrid online management and balancing using multiobjective optimization," in *Proc. IEEE Power Tech 2007*, Lausanne, Switzerland, Jul. 1–5, 2007, pp. 639–644.

[6] F. Katiraei and M. R. Iravani, "Power management strategies for a microgrid with multiple distributed generation units," *IEEE Trans. Power Syst.*, vol. 21, no. 4, pp. 1821–1831, Nov. 2006.

[7] W. D. Kellogg, M. H. Nehrir, G. Venkataraman, and V. Gerez, "Generation unit sizing and cost analysis for stand-alone wind, photovoltaic and hybrid wind/PV systems," *IEEE Trans. Energy Convers.*, vol. 13, no. 1, pp. 70–75, Mar. 1998.

[8] D. B. Nelson, M. H. Nehrir, and C. Wang, "Unit sizing and cost analysis of stand-alone hybrid wind-PV-fuel cell power generation system," *Renewable Energy*, vol. 31, pp. 1641–1656, 2006.

[9] E. Koutroulis, D. Kolokotsa, A. Potirakis, and K. Kalaitzakis, "Methodology for optimal sizing of stand-alone photovoltaic/wind-generator systems using genetic algorithms," *Solar Energy*, vol. 80, pp. 1072–1088, 2006.

[10] H. Yang, W. Zhou, L. Lu, and Z. Fang, "Optimal sizing method for stand-alone hybrid solar-wind system with LPSP technology by using genetic algorithm," *Solar Energy*, vol. 82, pp. 354–367, 2008.

[11] W. Lingfeng and C. Singh, "Multicriteria design of hybrid power generation systems based on a modified particle swarm optimization algorithm," *IEEE Trans. Energy Convers.*, vol. 24, no. 1, pp. 163–172, Mar. 2009.

[12] A. Kashefi, G. H. Riahy, and S. M. Kouhsari, "Optimal design of a reliable hydrogen-based stand-alone wind/PV generating system, considering component outages," *Renewable Energy*, vol. 34, no. 11, pp. 2380–2390, Nov. 2009.

[13] HOMER Energy LLC National Renewable Energy Laboratory (NREL) [Online]. Available: http://homerenergy.com/about.asp

[14] DER-CAM—Distributed Energy Resources Customer Adoption Model Lawrence Berkeley National Laboratory (LBNL) [Online]. Available: http://der.lbl.gov/dercam.html

[15] C. Marnay, G. Venkataramanan, M. Stadler, A. S. Siddiqui, R. Firestone, and B. Chandran, "Optimal technology selection and operation of commercial-building microgrids," *IEEE Trans. Power Syst.*, vol. 23, no. 3, pp. 975–982, Aug. 2008.

[16] V. Miranda and H. P. Sio, "Economic dispatch model with fuzzy wind constraints and attitudes of dispatchers," *IEEE Trans. Power Syst.*, vol. 20, no. 4, pp. 2143–2145, Nov. 2005.

[17] C. L. Chen, "Simulated annealing-based optimal wind-thermal coordination scheduling, generation," *Transmission & Distribution, IET*, vol. 1, no. 3, pp. 447–455, May 2007.

[18] B. C. Ummels, M. Gibescu, E. Pelgrum, W. L. Kling, and A. J. Brand, "Impacts of wind power on thermal generation unit commitment and dispatch," *IEEE Trans. Energy Convers.*, vol. 22, no. 1, pp. 44–51, Mar. 2007.

[19] C. Chun-Lung, "Optimal wind-thermal generating unit commitment," *IEEE Trans. Energy Convers.*, vol. 23, no. 1, pp. 273–280, Mar. 2008.

[20] J. Hetzer, D. C. Yu, and K. Bhattarai, "An economic dispatch model incorporating wind power," *IEEE Trans. Energy Convers.*, vol. 23, no. 2, pp. 603–611, Jun. 2008.

[21] C. A. Hernandez-Aramburo, T. C. Green, and N. Mugniot, "Fuel consumption minimization of a microgrid," *IEEE Trans. Ind. Appl.*, vol. 41, no. 3, pp. 673–681, May/Jun. 2005.

[22] M. Clerc, *Particle Swarm Optimization*. Hoboken, NJ: Wiley, 2008.

[23] K. Y. Lee and M. A. El-Sharkawi, *Modern Heuristic Optimization Techniques: Theory and Applications to Power Systems*. Piscataway, NJ: Wiley, IEEE Press, 2008.

[24] S. R. Guda, C. Wang, and M. H. Nehrir, "Modeling of microturbine power generation systems," *Elect. Power Compon. Syst.*, vol. 34, pp. 1027–1041, 2006.

[25] A. Antoniou and W. S. Lu, *Practical Optimization: Algorithms and Engineering Applications*. New York: Springer, 2007, ch. 15.

[26] Price of natural gas in the U.S. 2009 [Online]. Available: http://tonto.eia.doe.gov/oog/info/ngw/ngupdate.asp

[27] A. M. Azmy and I. Erlich, "Online optimal management of PEM fuel cells using neural networks," *IEEE Trans. Power Delivery*, vol. 29, no. 2, pp. 1051–1058, Apr. 2005.

[28] S. O. Orero and M. R. Irving, "Large scale unit commitment using a hybrid genetic algorithm," *Int. J. Elect. Power Energy Syst.*, vol. 19, no. 1, pp. 45–55, 1997.

[29] Summary of Results From Testing a 30-kW-Microturbine and Combined Heat and Power (CHP) System, DOE/EE-0316 U.S. Dept. of Energy, Office of Energy Efficiency and Renewable Energy, 2007.

[30] C. Wang, "Modeling and control of hybrid wind/photovoltaic/fuel cell distributed generation systems," Ph.D. dissertation, Montana State Univ., Bozeman, MT, 2006.

[31] MATLAB/Simulink SimPowerSystems Documentation [Online]. Available: http://www.mathworks.com/

[32] J. Kennedy and R. C. Eberhart, "Particle swarm optimization," in *Proc. IEEE Int. Conf. Neural Networks*, 1995, pp. 39–43.

[33] Y. Del Valle, G. K. Venayagamoorthy, S. Mohagheghi, J.-C. Hernandez, and R. G. Harley, "Particle swarm optimization: Basic concepts, variants and applications in power systems," *IEEE Trans. Evol. Comput.*, vol. 12, no. 2, pp. 171–195, Apr. 2008.

[34] M. H. Nehrir, B. J. LaMeres, G. Venkataramanan, V. Gerez, and L. A. Alvarado, "An approach to evaluate the general performance of stand-alone wind/photovoltaic generation systems," *IEEE Trans. Energy Convers.*, vol. 15, no. 4, pp. 433–439, Dec. 2000.

[35] V. Pop, H. J. Bergveld, D. Danilov, Regtien, P. L. Paul, Notten, and H. L. Peter, *Battery Management Systems: Accurate State-of-Charge Indication for Battery-Powered Applications*. New York: Springer, 2008, pp. 23–37.

[36] J. Cahill, K. Ritland, and W. Kelly, *Description of Electric Energy Use in Single Family Residences in the Pacific Northwest 1986–1992*. Portland, OR: Office of Energy Resources, Bonneville Power Administration, Dec. 1992.

[37] Pacific Northwest Cooperative Agricultural Weather Network, AgriMet Historical Dayfile Data Access, Deer Lodge, MT (DRLM) [Online]. Available: http://www.usbr.gov/pn/agrimet/webaghrread.html

[38] G. M. Masters, *Renewable and Efficient Electric Power Systems*. Hoboken, NJ: Wiley, 2004.

S. Ali Pourmousavi (S'07) is working toward the Ph.D. degree in the Electrical and Computer Engineering (ECE) Department, Montana State University, Bozeman.

M. Hashem Nehrir (M'88–SM'89–F'10) is a professor with the Electrical and Computer Engineering (ECE) Department, Montana State University, Bozeman.

Christopher M. Colson (S'06) is working toward the Ph.D. degree in the Electrical and Computer Engineering (ECE) Department, Montana State University, Bozeman.

Caisheng Wang (M'02–SM'08) is a faulty member with Electrical and Computer Engineering (ECE) Department and Division of Engineering Technology, Wayne State University, Detroit, MI.

CHAPTER 12

MULTI-TIMESCALE POWER MANAGEMENT FOR ISLANDED MICROGRIDS INCLUDING STORAGE AND DEMAND RESPONSE

Contribution of Authors and Co-Authors

Manuscripts in Chapters 2 through 12

Author: S. A. Pourmousavi

Contributions: Developed extensive modeling of the MG component in MATLAB®/m-file and GUIs, designed a comprehensive real-time rule-based power management algorithm and different simulation studies, prepared actual data for the MG design and simulations, and the manuscript, figures and tables.

Co-author: M. H. Nehrir

Contributions: Provided important insight and overview of the research, interpretation of the results, and aided in the preparation of the manuscript.

Co-author: R. K. Sharma

Contributions: Provided useful insight and financial support for the project.

Manuscript Information Page

Seyyed Ali Pourmousavi Kani, M. Hashem Nehrir, Ratnesh K. Sharma

IEEE Transactions on Smart Grid, 2014

Status of the manuscript:
____ Prepared for submission to a peer-reviewed conference
_X_ Officially submitted to a peer-reviewed conference
____ Accepted by a peer-reviewed conference
____ Published in a peer-reviewed conference proceedings

Published by the Institute of Electrical and Electronics Engineering (IEEE)

MULTI-TIMESCALE POWER MANAGEMENT FOR ISLANDED MICROGRIDS INCLUDING STORAGE AND DEMAND RESPONSE

The following work is officially submitted to the IEEE Transactions on Smart Grid for possible publication

S. A. Pourmousavi[1], M. H. Nehrir[1], and R. K. Sharma[2]

[1] *Department of Electrical and Computer Engineering, Montana State University, Bozeman, MT 59717*

[2] *Energy Management Department, NEC Laboratory America Ltd., Cupertino, CA 95014*

Abstract

Power management is an essential tool for MG safe and economic operation, particularly in the islanded mode. In this chapter, a multi-timescale cost-effective power management algorithm is proposed for islanded MG operation targeting generation, storage, and demand management. Comprehensive dynamic modeling, cost, and emission calculations of the MG components are developed in this chapter to facilitate high accuracy management. While the MG's overall power management and operation is carried out every several minutes to hours, depending on the availability of the required data, simulation for highly dynamic devices (such as batteries and EWHs used for DR) are performed every minute. This structure allows accurate, scalable, and practical power management taking into consideration the intra-interval dynamics of battery and EWHs. Two different ON/OFF strategies for EWH control are also proposed for DR application. Then, the power management algorithm is implemented using the two different DR strategies and the results are compared with the no-DR case. Actual solar irradiation, temperature, non-EWH load demand, and hot water consumption data are employed in the simulation studies. The simulation results for the MG studied show the effectiveness

of the proposed algorithm to reduce both MG's cost and emission

Introduction

According to the DOE's list of five fundamental technologies that will drive the smart grid [12.1], "advanced control methods to observe essential components for rapid diagnosis and precise solutions to events" is envisioned as one of the most critical apparatus for successful implementation of smart grid. Given the complexity of the smart grid implementation, MGs have emerged as a bridging technology to pave the way to the smart grid [12.2]. The key to wider recognition and employment of MGs is innovative power management strategy [12.3].

In general, real-time MG management is classified into energy and power management. The energy management algorithms deal with monitoring and operation of a complex system of electrical, thermal, and mechanical components with emphasis on desired and longer term outcomes. However, the objective of power management is to affect the instantaneous operational conditions towards certain desired parameters [12.4]-[12.11]. From a general perspective, both power and energy management refer to control actions that are based on particular objectives.

MG management algorithms can be divided into centralized [12.4]-[12.9] and decentralized architecture [12.10], [12.11]. Structurally, MGs can be operated in grid-tied [12.4], [12.7], [12.9]-[12.11], islanded [12.5], [12.6], or a combination of both modes, e.g., [12.8]; each of the above modes has certain requirements to be fulfilled. This chapter focuses on the design, modeling, and proposing a comprehensive cost-effective multi-timescale power management algorithm for an islanded MG that operates independently

in a remote area. In islanded MGs, AS is provided using storage and DR to compensate renewable generation and load demand variability. The MG components include a DiG, solar PV panels, and storage batteries, which are commonly available for residential applications.

Although the DR is foreseen to be an essential part of MGs' cost-effective operation, some literature on power management do not include the DR in their proposed algorithm, e.g. [12.6]-[12.8], and others consider generic load for DR, e.g. [12.5], [12.10], [12.11]. However, in this study, the DR is implemented with EWHs for which a dynamic model with actual hot water consumption data is used. Two different ON/OFF control algorithms (called DR.A and DR.B) are introduced and implemented to provide the required increase or decrease in load at the time needed.

Moreover, the multi-timescale structure of the proposed algorithm allows two different simulation intervals for MG components based on their dynamic behavior and the available data. This way, simulation interval of highly dynamic components (e.g., battery and EWHs) will be decoupled from those of the available load and generation data, which might be available with different intervals (e.g., 20 minutes or 1 hour). This way, the flexibility and accuracy of the algorithm will be increased, which can result in faster control.

Although a rule-based algorithm may not be ideal for grid-tied and plug-and-play operation on MGs, they are ideal in real-world applications, in particular for rural areas with minimum computational burden. The multi-timescale structure, the cost-effective operation, the DR application, and detailed dynamic modeling of MG components

(including emission production, cost of operation, and efficiency) are the major contributions of this study. MATLAB® GUIs were developed to easily scale and modify the proposed MG structure and simulation time interval as well as to observe the MG performance through a monitoring GUI during the simulation. The GUIs are given in Appendix D.

MG Design and Modeling

In the following sub-sections, MG design and dynamic modeling are presented for the MG's components, including solar PV, diesel generator (DiG), storage, and EWH loads.

MG Design

The proposed islanded MG (Figure 12.1) is designed for a residential neighborhood including 100 houses. The residential units are assumed to have EWHs, which are used as candidates for the DR (when needed) to provide AS for the MG. Optimal MG design (unit sizing) is carried out using HOMER® [12.12]. Actual minute-by-minute residential load data, recorded for a single house between 2006 to 2010, has been used [12.13]. The data has been scaled up to represent power consumption of 100 houses. Actual solar irradiation and ambient temperature have also been used [12.9]. It is assumed that all PV arrays experience similar solar irradiation and ambient temperature. The optimized component sizes for the application obtained from HOMER are: 570 kW of PV, 350 kW of DiG, and 840 kWh of battery.

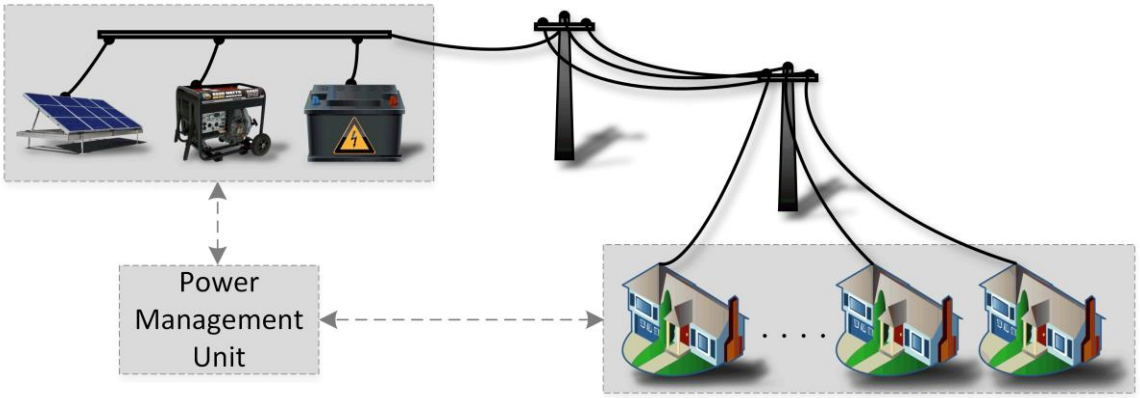


Figure 12.1. Schematic diagram of the MG configuration.

MG Dynamic Model

Dynamic modeling of the MG components is an essential part of this chapter for the proposed multi-timescale structure to perform accurate simulation and decisions making. In this sub-section, dynamic model of each component will be briefly explained in addition to the cost and emission calculations that were applied for each component.

PV Model. In this chapter, a dynamic mathematical model of PV, [12.14], is used where the PV operating point is calculated based on solar irradiation and ambient temperature. An actual grid wattage PV module from SunPower Corporation (SPR-200-BLK) which is suitable for residential applications was selected for modeling [12.15]. The maximum power point (MMP) of the PV module at different solar irradiation and ambient temperatures is obtained using the first derivative of the module instantaneous power with respect to the module's voltage. In order to avoid solving numerical nonlinear equation in each iteration, the MPP corresponding to different common solar irradiation levels and ambient temperature were calculated and stored in a 2-D lookup table for future use in the power management algorithms (PMA). This procedure simplifies the

implementation of the proposed PMA. A 100-W/m^2 solar irradiation interval and 3ºC temperature interval is used in the 2-D lookup table. These intervals are small enough for precise linear approximation between two neighboring sample points. This has been verified through sensitivity analyses for different solar irradiation values and ambient temperatures, which are not given in this chapter.

Since the PV system is connected to the MG through DC/DC and DC/AC converters, the efficiency of converters has also been modeled as a function of the normalized input power [12.7]. Since converters' efficiency drops rapidly for small loading, a deadband of 5% of the module nominal power (i.e., 200 W) was considered for PV operation.

In addition to the dynamic model of the MG components, their accurate operational cost calculation is also essential for an accurate PMA. The operational cost is commonly divided into ownership and operating costs [12.16]. In order to calculate the ownership cost of MG components, a general framework considering uncertainty and risk analyses was used, which has been proposed in Chapter 9. However, no ownership cost is considered for the PV system because PV modules usually last for 20-25 years, equal or more than the 20-year project lifetime assumed. Therefore, no replacement cost is required throughout the project lifetime. Also, PV operating cost (which only comprises maintenance cost) is very cheap, less than 0.005 $/kWh [12.18]. Therefore, it is reasonable to consider PV power as negative load to extract its maximum available power at any time.

DiG Model. Since DiGs are equipped with electronic speed governor and

automatic voltage regulator (AVR), their dynamic behavior is not a concern as long as the simulation interval does not go below one minute. The DiG selected for this study is rated at 350 kW (CumminsOnan Commercial DFEG-C350D6 diesel genset) with 1.5 and 2.1 seconds recovery time for voltage and frequency after 100% load changes, respectively [12.19]. In addition, DiGs have incredibly fast cold startup time (about 10 seconds for DiGs smaller than 1000 kW) [12.20]. Therefore, the DiG modeling for this study is limited to its cost and emission calculations. Fuel consumption data for the DiG studies are given in Table 12.1. It should be noted that DiGs are usually responsible to establish frequency in an islanded MG, which requires the DiG to operate in standby mode at all times. Therefore, the DiG will consume a minimum amount of fuel (15 L/hour) at no load.

Based on the approach reported in [12.17], the ownership cost for the DiG under consideration is calculated as $1.6018/hour. The DiG operating cost consists of fuel cost, cost of other regularly replaceable components, and overhaul costs. Fuel consumption data for a variety of DiGs ranging from 6 to 2260 kW are compiled and modeled in [12.10], and is utilized in HOMER® [12.12]. However, employing a similar linear model for the DiG studied does not show an acceptable fit to the data given in Table 12.1.

Table 12.1. Actual fuel consumption for the DiG studied [12.19].

Model C350D6	No load	25% load	50% load	75% load	100% load
Fuel Consumption (L/hour)	15	30.2	50.4	72	96

A quadratic polynomial curve fitting (12.1) is tried on the data using MATLAB/Curve Fitting toolbox [12.21], and it gives an excellent fit to the data:

$$F_{DiG}(i) = C_{fuel}.\left(0.0001773\,\mathrm{P}_{DiG}^{2}(i) + 0.1709\,\mathrm{P}_{DiG}(i) + 14.67\right) \qquad (12.1)$$

where $\mathrm{P}_{DG}(i)$ is the DiG operating power level (kW) at interval *i*; and C_{fuel} is the cost of diesel which is \$0.97/L in this study. Comparison of the two methods (i.e., linear vs. quadratic curves) yields substantial differences which can result in erroneous fuel and cost calculations which can result in a series of incorrect decisions for the MG operation.

Maintenance cost is another component of DiG's operating cost which has been ignored in some studies, e.g. [12.22]. Since the non-fuel operating cost data was not available for the specific DiG studied, the non-fuel operating cost data for 1-10 MW DiGs reported by EPRI, [12.23], is utilized. The total maintenance cost (i.e., operating cost less fuel cost) is approximated as \$75.44/kW-installed by looking at the 20-year net present value of costs [12.23]. Therefore, annual maintenance cost of the 350-kW DiG used in this study can be approximated as \$1320/year. This cost is for all maintenance levels and overhaul of the DiG used.

There is no emission data provided for this specific 350-kW DiG. However, a survey has been carried out for the smaller size (e.g., 10 kW) DiGs used in residential applications on military bases from the manufacturer of the DiG used in this study [12.24]. In this reference, several experiments are carried out on three different 10-kW DiGs from the same company, and CO_2, CO, Ethylene, NO_2, NO, and hydrocarbon (HC) production are reported. Since CO and CO_2 typically account for more than 99% of the carbon emitted in engine exhaust [12.24], the emission production (EM_{DG}) is categorized into CO_2 and non-CO_2 emissions, i.e., non-CO_2 emissions are combined to simplify the overall emission equation. A fifth-order polynomial is found to be a good fit

for the data as follows:

$$EM_{DiG}^{j}(i) = a_1^j.P_{DiG}^5(i) + a_2^j.P_{DiG}^4(i) + a_3^j.P_{DiG}^3(i) + a_4^j.P_{DiG}^2(i) + a_5^j.P_{DiG}(i) + a_6^j \quad (12.2)$$

where j is the type of emission at interval i. Coefficients for the emission types are given in Table 12.2. For the 350-kW DiG studied, all values are linearly scaled up by multiplying by 35.

The total cost of emission, which is a function of fuel consumption, can be calculated as follows:

$$C_{DiG}^{j}(i) = C^j.EM_{DiG}^{j}(i).F_{DiG}(i) \times \frac{0.832}{1000} \quad (12.3)$$

where C^j is the damage cost (externality cost) of pollutant j, and $\frac{0.832}{1000}$ is the conversion factor for $\frac{1kg\,of\ fuel}{liter} \times \frac{gr}{kg}$. The damage costs of CO_2 is estimated as \$0.014/kg in [12.25]. The cost for non-CO_2 pollutants is taken from [12.26], which is estimated at \$4.2/kg pollutant (total hydrocarbon) since they are the most dangerous pollutant for living organs health. The DiG efficiency can be calculated as follows [12.10]:

$$\eta_{DiG} = \frac{P_{out}}{P_{in}} = \frac{3600 \times P_{DiG}(i)}{F_{DiG}(i).E_c} \quad (12.4)$$

where E_c is the diesel energy density (35000 kJ/L). The efficiency values for the linear and quadratic fuel consumption functions are shown in Figure 12.2. The significant difference between the two curves can be due to the two different methods for fuel consumption calculation.

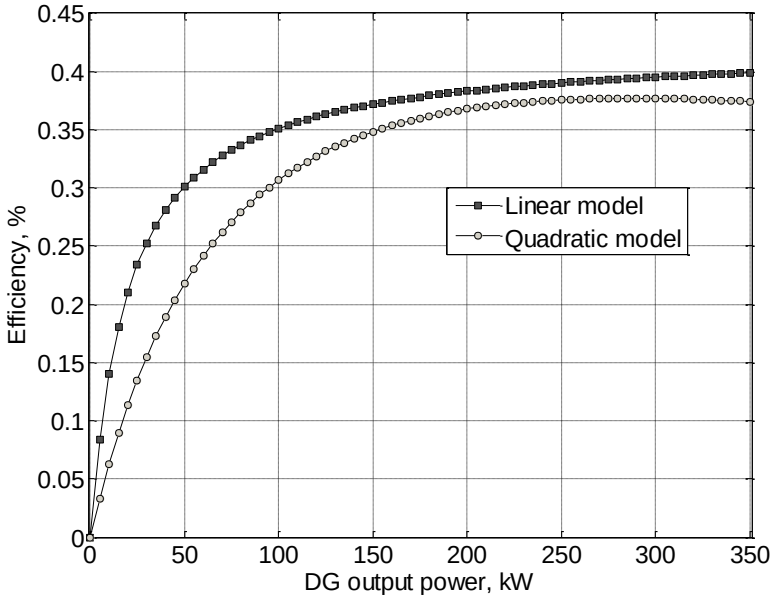


Figure 12.2. The overall efficiency of the DiG based on input and output energy.

Table 12.2. Curve-fitted coefficients of the functions for emission production.

Type	a_1^j	a_2^j	a_3^j	a_4^j	a_5^j	a_6^j
CO_2	1.511	-35.47	290.1	-1011	1519	1422
Non-CO_2	-0.01859	0.4579	-4.128	17.959	-43.776	105.9

Battery Model. In this chapter, a commonly used valve-regulated lead-acid (VRLA) battery dynamic model, described in [12.27], is used which later has also been adapted for power/energy management studies in [12.28]. The VRLA model is slightly modified for this chapter to work based on its output power instead of voltage. Instantaneous power, voltage, current, state of charge (SOC), internal temperature, and efficiency are important parameters of the battery which are monitored and calculated by the model developed in every one minute interval.

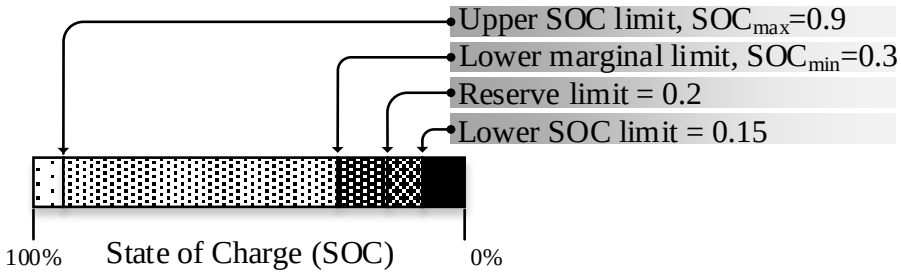


Figure 12.3. Classification and operational framework for battery SOC limits [12.30].

Battery operational cost, which consists of ownership and operating costs, is also considered in this study. The battery ownership cost ($1.1815/Ampere-hour in this study) is calculated based on uncertainty and risk analyses, reported in Chapter 9 and in [12.17]. Since the battery does not consume fuel and does not experience moving and mechanical parts, its operating cost is treated as a percentage of the total investment cost (1%-2.5%) [12.29].

Battery safe operation control is a complicated task in a MG and is essential for its optimal operation. A thorough study of the battery chemical reactions is given in [12.30], where, the general battery operation framework is given as in Figure 12.3. A similar principle is utilized for the battery operation in this study.

EWH Model. Residential EWHs are utilized as the DR medium in this study. The dynamic model of a single EWH used in this study is similar to the one in [12.31]. Similar EWH model were also used in [12.32], [12.33], where the water temperature is allowed to rise to 160 ºF. The thermostatic-controlled valve is utilized in the model to assure safe hot water temperature for the household to avoid scalding and burning. No cost is considered for DR since customers' hot water temperature will not go beyond a

pre-defined limit (i.e., customers' quality of service (QoS) is always considered as the highest priority and will not be violated). This procedure utilizes any excess available energy in the residential EWHs, when available.

Figure 12.4 shows a flowchart diagram of the simulation environment developed for this study in MATLAB®. At each management interval, the following information (as shown in Figure 12.4) are given as input to the simulation environment: hot water flow rate and water temperature of each EWH, ambient temperature and solar irradiation for PV system, nominal DiG capacity, non-EWH load demand, battery SOC, voltage, and temperature from the last interval, and power step value, ΔP . ΔP is used in each interval to calculate the maximum amount of power to charge the battery (or to discharge from the battery).

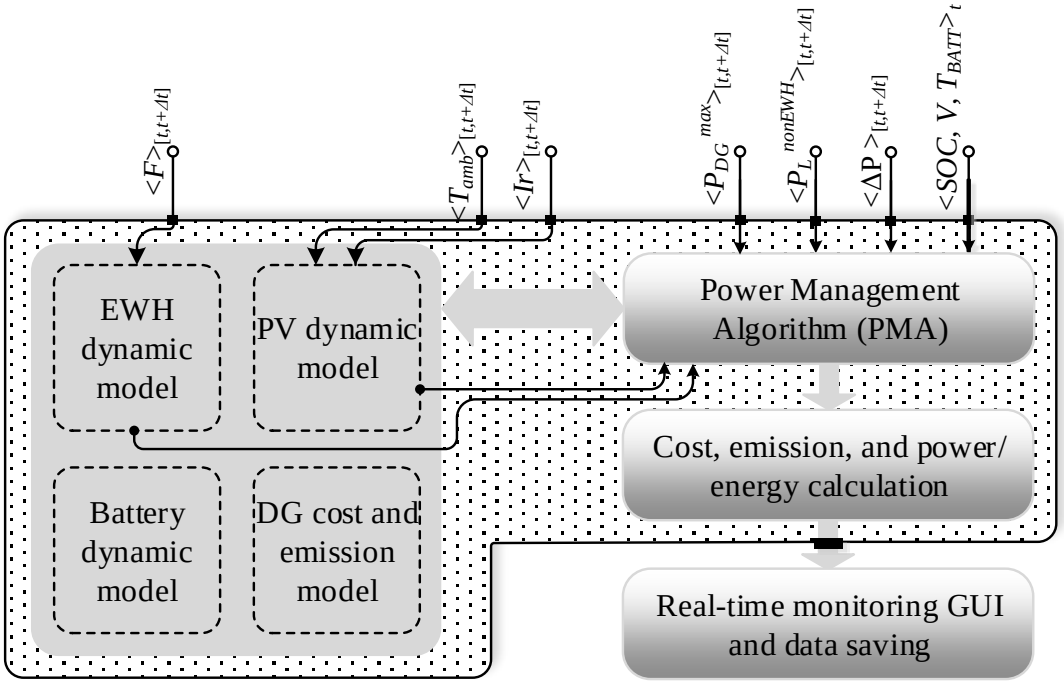


Figure 12.4. Flowchart diagram of the MG simulation environment developed for this study.

As shown in Figure 12.4, the data will be pre-processed or directly transmitted to the PMA to calculate the operating points of the MG components. Finally, power/energy, cost and emission will be calculated.

A MATLAB®-based graphical user interface (GUI) is developed to attain all the required data for the simulation (Figure D.1 in Appendix D). The GUI allows great flexibility and scalability of the MG for further investigation with different parameters and sizes. Finally, a second GUI is developed to show the real-time simulation results at each interval (Figure D.2 in Appendix D). At the end of the simulation, a summary of the final results appears. This GUI also makes the plotting of the different system parameters very easy.

The Proposed Power Management Algorithm

MGs often comprise fixed and variable generation, storage, and load within a restricted geographical area. Therefore, it is essential to have a real-time management system to assign appropriate setpoints to different components, to protect them from operating outside their safe region, and to manage generation, storage and demand. Numerous objectives have been proposed for MG real-time power management [12.34]. However, desired objectives may be different from one MG to another, system operators/owners choose the objectives that best fit their MG topology (grid-tied or islanded) to meet their need. In this section, the design of the multi-timescale rule-based power management algorithm for cost-effective operation of the designed MG is explained.

Multi-timescale power management based on pre-defined rules can be an

effective tool for MG operation as long as the number and size of the available components and their dynamic behavior are known to the operator. One major advantage of the rule-based PMA is that they are incredibly fast and computationally efficient compared to the power management algorithms with optimization techniques, particularly in real-time applications. It is because the fact that the decision-making process is already designed based on all possible scenarios using prior knowledge about the system. Additionally, rule-based PMAs are easy to implement in real-world applications, particularly for islanded MGs in remote areas. In addition, the multi-timescale simulation and management structure, proposed in this study, helps to increase the simulation speed with higher accuracy by choosing different simulation intervals based on the components' requirements. Moreover, the proposed rule-based algorithm targets least cost of the MG operation using least expensive components when possible. Rule-based algorithms become less applicable and effective in MGs with many devices and objectives or MG with features such as plug-and-play operation.

The proposed PMA shown in Figure 12.4 is expanded in Figure 12.5. As shown in the figure, the battery and EWHs simulations are carried out in one-minute intervals (i.e., heavy gray area), while the rest of the simulation (light gray area) is performed in a pre-defined interval, which can be minutes to hours. A description of the input parameters to the PMA is given in Appendix E.1.

For the non-EWH load demand data, which is available every minute in this chapter, the average power is calculated and utilized for the length of the management interval. Using all the input parameters shown in Figure 12.5, the PMA unit computes the

operating point of each MG component. Here, three different rules can be identified in Figure 12.5 which are clarified as follows:

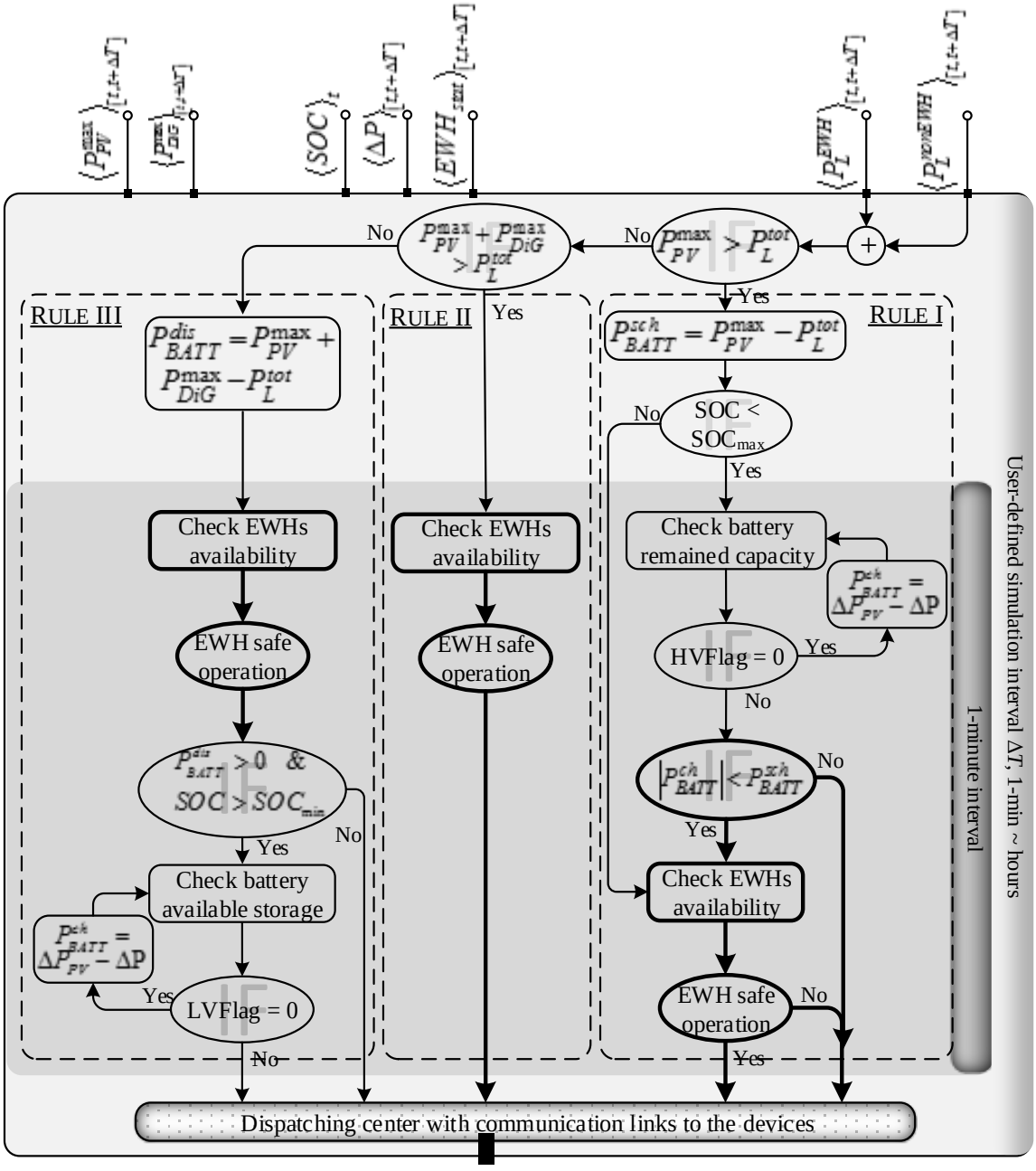


Figure 12.5. Schematic diagram for the proposed multi timescale rule-based power management algorithm.

RULE I (Right Column in Figure 12.5)

In this rule, the total load demand is less than the available PV power in the interval ahead, i.e., $P_L^{tot} < P_{PV}^{\max}$, where $P_L^{tot} = P_L^{EWH} + P_L^{nonEWH}$. Therefore, the excess power, i.e. $P_{BATT}^{sch} = P_L^{tot} - P_{PV}^{\max}$, can be stored in the battery if the battery SOC is less than the pre-defined maximum value. The proposed strategy is given in **Algorithm 1** of Appendix E.2. Note that battery simulation is performed every minute, regardless of the length of the management interval, to increase the accuracy and better observation of the battery performance. The one-minute simulation interval helps to accurately calculate maximum charging power in the battery considering the minute-by-minute battery dynamic and its nonlinear behavior. The *HVFlag* is a variable in the battery model that shows the battery overvoltage or equivalently battery maximum SOC violation, or battery maximum charging power. In RULE I, the battery will be utilized before the DR because a higher battery SOC results in a higher battery lifetime. If the battery is not able to store all the excess PV power, the maximum possible power will be calculated based on the first inner loop shown in the right column in Figure 12.5. Based on the convention used in this chapter, battery is in charging mode when the power is negative ($P_{BATT}^{sch} < 0$), and it is in discharging mode when power is positive ($P_{BATT}^{sch} > 0$). The battery charging algorithm is given in Appendix E.2. Finally, the operating point of the battery for the interval ahead can be obtained, given as $\langle P_{BATT} \rangle_{[t,t+\Delta T]}$. Since the battery will be charged only by excess PV generation, no cost is assigned to the battery operation in the charging mode.

If excess PV power is still available (i.e., $\langle P_{PV}^{excess} \rangle_{[t,t+\Delta T]} > 0$), the status of EWHs

(as DR resource) will be examined to store the excess power in the form of heat energy. Similar to the battery, this part of the simulation will also be carried out every minute regardless of the management interval. The DR strategies are designed to fulfill two important conditions: 1) the increase in EWHs power should not exceed the excess PV power available at each interval, 2) no more than the pre-specified number of EWHs are allowed to be on simultaneously to control peak power. These conditions assure that the EWHs accurately participate in the DR implementation. The proposed DR strategy is given in **Algorithm 2** of Appendix E.3. Based on the same principles mentioned in **Algorithm 2**, two different ON/OFF control strategies (explained below) are proposed, where in both cases the customers' quality of service (QoS) has the highest priority:

DR.A: In this case, upper and lower hot water temperature setpoint remain between 120-160 ºF throughout the day.

DR.B: In this case, a dynamic structure for the upper setpoint for hot water temperature is considered. While the lower setpoint remains at 120 ºF throughout the day for all EWHs, the upper setpoint remains at 130 ºF unless there is excess PV power. In that case, the hot water temperature upper setpoint will be elevated to 160 ºF. In DR.A and DR.B when the water temperature goes above 130 ºF, the outflowing hot water will be mixed with an appropriate amount of cool water by a thermostatic mixing valve (TMV) prior to use to avoid scalding. Details of the calculations are explained in [12.32] and [12.33]. The difference between the two cases (i.e., DR.A and DR.B) is significant, as will be shown in the simulation results.

In the rare cases when there is excess PV power and the battery and EWHs are

fully charged, the excess energy needs to be curtailed using PEIs in the PV system, or dissipates in a dump load.

RULE II (Middle Column in Figure 12.5)

In this rule, the total load demand is less than the available PV power plus the DiG nominal power in the interval ahead, i.e., $P_L^{tot} < \left(P_{PV}^{\max} + P_{DiG}^{\max}\right)$. As shown in Figure 12.5, the battery is idle. However in order to guarantee the cost-effective operation in the proposed PMA, the DR strategy is used to decrease the required power from the DiG, as much as possible. Then, the remaining load demand will be provided by the DiG as much as needed, i.e., $\left\langle P_L^{tot} = P_{PV}^{\max} + P_{EWH}^{ctrl} + P_{DiG} \right\rangle_{[t,t+\Delta T]}$, where P_{EWH}^{ctrl} is the amount of power provided by the DR strategy. In this study, the DiG is operated in the standby mode, where it consumes some fuel even at no load. As a result, the total operational cost will be cheaper if the DiG is utilized before the battery. This way, the cost-effective operation of the MG will be achieved, and the MG cost of operation will be equal to the DiG operational cost. As a result of the DiG operation, its emissions and damage costs will also be calculated in this rule.

RULE III (Left Column in Figure 12.5)

In this rule, the total load demand is higher than the total of available PV power and the nominal power of the DiG in the interval ahead; i.e., $P_L^{tot} > \left(P_{PV}^{\max} + P_{DiG}^{\max}\right)$. Therefore, the battery and DR should be utilized to meet the remaining load demand. Since there is no cost associated with DR in the MG, it is beneficial to perform the DR strategy before the battery. Therefore, the DR procedure will be executed to provide load

reduction as much as possible in order to avoid large and random load interruption in the MG. The DR procedure in this rule is similar to the one explained in **Algorithm 2** (Appendix E.3) except that the EWHs will be sorted in ascending order based on their hot water temperatures. The two limiting conditions given for the DR in RULE I are also valid in this rule. It should be noted that the ON/OFF commands for the EWHs will be overridden in both of the DR algorithms if the hot water temperature goes beyond the pre-defined upper and lower limits. One-minute simulations will always be carried out for the EWHs in this rule.

If there is still undelivered load demand after the DR procedure completed, the battery will be discharged to meet the remaining load demand. In this case, if the battery SOC is higher than the minimum ($SOC_{\min}$), the maximum derivable energy from the battery will be calculated for the interval ahead using the inner loop in the left column in Figure 12.5. For this purpose, a similar procedure to the one in **Algorithm 1** (Appendix E.2) is developed in **Algorithm 3** (Appendix E.4) for the battery discharging, except that the discharged power is positive based on the power flow convention defined in this study. In addition, *LVFlag* is used instead of the *HVFlag*, which is introduced in the battery model to show the low-voltage status of the battery, or equivalently to show if the battery SOC goes below the pre-defined minimum value, or if the pre-defined discharging power limit is violated. High accuracy in the battery model is guaranteed by the one-minute simulation to capture the inherited nonlinearity in the battery model. In rare cases that the battery and the DR cannot meet the shortage in generation, the partial undelivered load in the MG will be realized, which has to be shed. In this rule, MG

operational cost will be computed as the sum of DiG cost and the battery cost in the discharging mode.

Simulation Results and Discussion

In order to show the effectiveness and applicability of the proposed multi-timescale rule-based power management algorithm, simulation studies using actual data are carried out for the MG presented in Figure 12.1. Based on the availability and the type of DR mechanism, three different management algorithms (namely no-DR, DR.A, and DR.B) are simulated and their results are compared. The precision of the calculations is chosen to be 1 W; i.e., all the calculations and actual data are rounded towards 1 W, which is a reasonable assumption for real-world applications.

Since the actual one-minute load data used in this study was measured for only one house, the load demand data for 100 houses is generated by normal random distribution with average of 0.1 kW and standard deviation of 0.2, as shown in Figure 12.6. The different characteristics of the load demand data (e.g., peak hours and annual energy consumption) match the numbers given in [12.35]. For simulation intervals larger than one minute, the average load demand data is used. In addition to the non-EWH load data, hot water flow-rate for each customer is also required for the EWHs model. These data are calculated from the real set of average residential EWH daily demand available in [12.36] with the method explained in [12.33]. Since there was only average hot water demand available in [12.36], a normal distribution with an average temperature of 125 ºF and standard deviation of 5 ºF are employed to generate the data for 100 customers; the results are shown in Figure 12.7 for all houses.

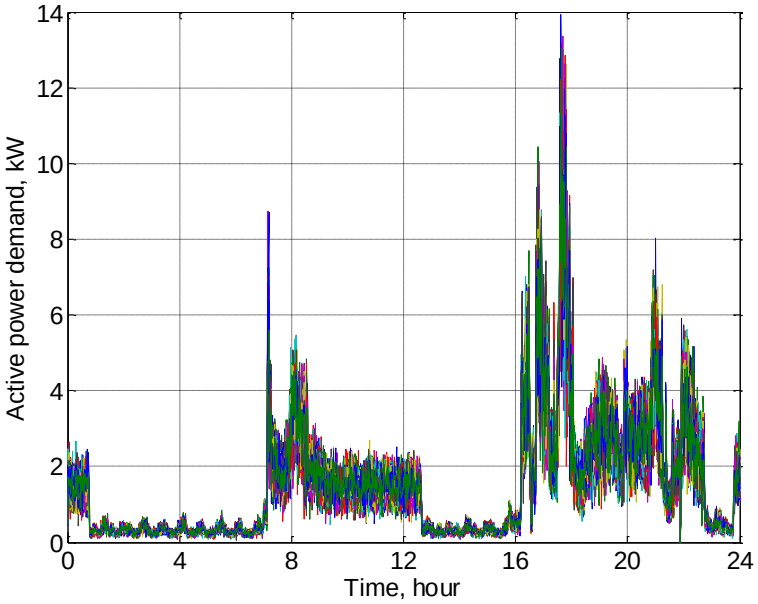


Figure 12.6. Minute-by-minute active non-EWH load demand (winter weekday) for 100 houses [12.13].

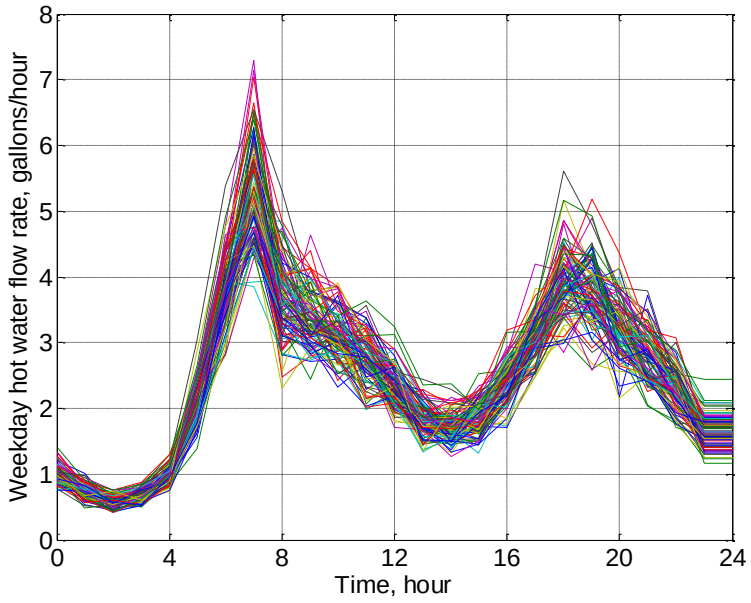


Figure 12.7. Hot water consumption for 100 houses in the MG, winter weekday.

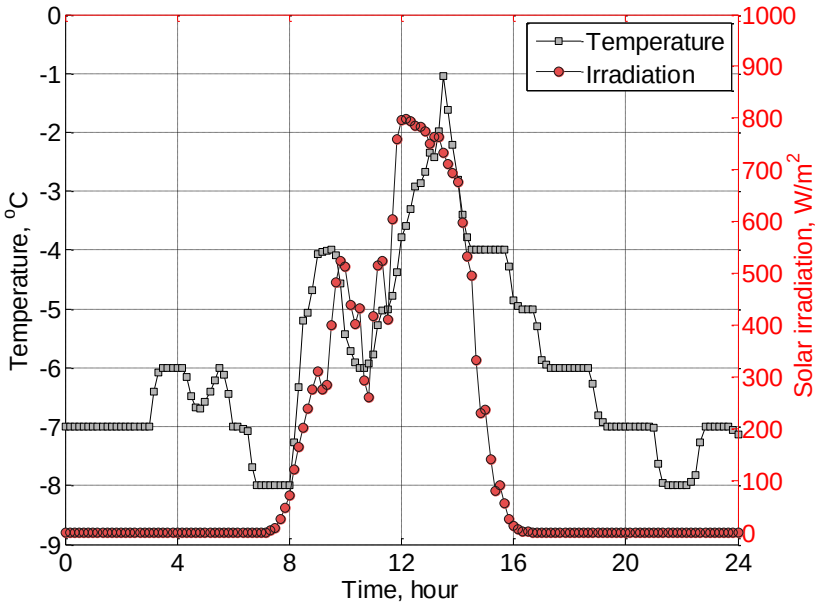


Figure 12.8. Temperature and solar irradiation for a non-cloudy weekday in the winter [12.9].

The actual temperature and solar irradiation data, employed in this study, are shown in Figure 12.8 for a weekday in the winter. It is assumed that all PV modules experience similar ambient temperature and solar irradiation level.

Three different simulations are performed with DR.A, DR.B, and without DR (No-DR) to show the effectiveness of the proposed PMAs with DR. For all simulation studies, the power management is updated every 20 minutes, and the simulation is performed for 24 hours. Additionally, the DiG is operated in standby mode for the three cases. The simulation results are reported in Table 12.3 for the MG presented in Figure 12.1.

In the remainder of this section, the effect of PMAs with DR.A and DR.B on the performance of the MG and its component is compared with the No-DR PMA, based on the results given in Table 12.3.

Table 12.3. Simulation results of the MG operation for the three PMAs for 24 hours.

PMAs	*No-DR*	*DR.A*	*DR.B*
PV			
Total generation, kWh	1325.171	1631.8417	1749.3663
Unused energy, kWh	508.4457	201.775	84.2503
Average efficiency, %	89.0605	89.7931	89.855
DiG			
Total generation, kWh	3187.408	2981.8243	2876.8337
Fuel Consumption, L	1044.8309	996.173	971.1315
Average efficiency, %	23.0945	22.0459	22.0328
Battery			
Discharge, kWh	242.645	179.2043	203.1227
Charge, kWh	445.2683	440.8677	480.9853
Average efficiency, %	92.4503	92.9302	91.1408
MG Emission			
Total CO_2, kg	1661.7	1632.4	1603.7
Total Non-CO_2, kg	53.4	51.0	49.9
Total damage cost, $	38.2105	37.1239	36.4132
Total load, kWh	4309.9557	4352.0027	4348.3373
Total undelivered load, kWh	20.7687	7.1467	8.112
Total MG operation cost, $	1339.3116	1245.8123	1238.1705

Solar PV Panel

It can be seen from Table 12.3 that the PV power utilization is increased by 23.1% and 32.0% in the DR.A and DR.B algorithms, respectively, compared to the *No-DR*. This is because of employing the DR in the management algorithm. When the EWHs' upper thermostat setpoint is increased to 160 ºF, a large amount of heat storage capacity is provided by the EWHs hot water tanks. The percentage of increase is less in the *DR.A* algorithm compared to the *DR.B* algorithm because the upper thermostat setpoint in the *DR.A* is set to 160 ºF for the whole day. This way, less free capacity in the hot water tanks will be available when excess PV generation is available in the middle of the day. The increase in power extraction from the PV also resulted in slightly higher

efficiency of the PV unit due to higher efficiency of the converters.

DiG

According to Table 12.3, in the PMAs with *DR.A* and *DR.B*, the total generated energy by the DiG is decreased by 6.45% and 9.74% and the total fuel consumption decreased by 4.66% and 7.05%, respectively. Since the DiG fuel consumption is a nonlinear function of its output power, the percent reduction in the total generated power by the DiG is not equal to its corresponding total fuel consumption for the two PMAs. Storing the excess PV generation as hot water using the DR strategies (which results in less power consumption by the EWHs in the hours ahead) as well as reducing EWHs power consumption during power shortage are the two major reasons for the reduction in the DiG generation. However, the average efficiency of the DiG is slightly decreased in the *DR.A* and *DR.B* algorithms compared to the *No-DR* algorithm. This is because the utilization of the DR decreases the need for the DiG power and as a result, the DiG operates in the lower range of its rated power where its efficiency is lower, as shown in Figure 12.2.

Battery

The battery discharging is decreased by 26.14% and 16.29% in *DR.A* and *DR.B*, respectively, compared to the *No-DR* case. This is because using any excess PV generation to preheat water in EWHs decreases the energy required by the EWHs during high demand hours. Therefore, less energy from the battery is required to meet the load demand. In general, any reduction in the battery discharging reduces the MG operational

cost, increases battery lifetime, and provides more storage for unexpected loss of PV power and load variations. The battery SOC for the three simulation cases is shown for one day in Figure 12.9. The battery discharging starts around 7:30 AM in the *DR.B* algorithm. Since the upper thermostat setpoint in the *DR.B* algorithm is set to 130 ºF during normal condition (i.e., during the time of no excess PV generation availability), and because the DR is employed more often, as given in RULE II, more EWHs will turn on early in the morning during first peak period (approximately 7:30-9:00 AM), as shown in Figure 12.7. This way, the PV and the DiG cannot meet the total load demand, so the battery is discharged to provide the remaining load demand. The hot water temperature for all households is shown in Figure 12.10 (a) and (b) for the *DR.A* and *DR.B* PMAs. It can be seen that at around 7:30 AM, hot water temperatures for most of EWHs reach to about 143 ºF in the PMA with *DR.A*, and the EWHs stay off during the morning peak hours. However during this peak demand period, the hot water temperature in the majority of the EWHs go below 125 ºF in the *DR.B* PMA, where some of the EWHs turn on resulting in more demand from the EWHs during the morning peak hours.

In addition, it can be seen from Figure 12.9 that the battery discharging occurs approximately during 17:00 to18:30 and 21:00 to 22:30 for the *No-DR* case, while the battery is idle for the other two PMAs. This is because the EWHs could not store hot water during off-peak hours because of the 130 ºF upper thermostat setpoint. Therefore, some of the EWHs will be turned on during the second daily peak hours which increase the need for power. This way, the battery will be discharged to compensate the shortage in generation.

Due to the early battery discharge in the *DR.B* PMA, the accumulative battery charging energy at the end of the day is more than the other PMAs. As shown in Figure 12.10 (b), the EWHs hot water temperature increase toward 160 ºF during the excess PV generation hours (approximately during 12:00-15:00 hours.) This causes all the EWHs to be off during the second daily peak hours (approximately 16:30-21:00), which is the main reason for lower battery discharging in *DR.A* and *DR.B* compared to the *No-DR* case, shown in Figure 12.9. Although the average efficiency of the battery is decreased when the DR is used, the average battery SOC for a day of simulation did not change significantly for the three PMAs. The average battery SOC is 63.8%, 64.0%, and 63.3% for *No-DR*, *DR.A*, and *DR.B*, respectively.

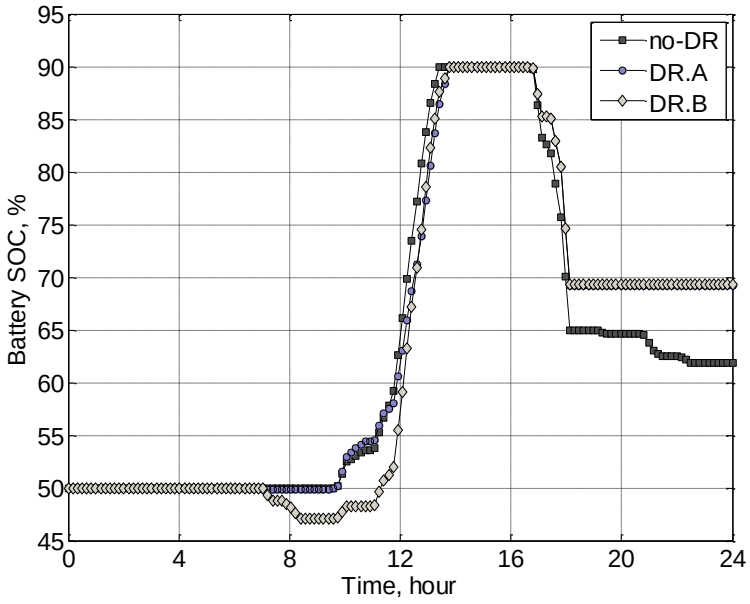
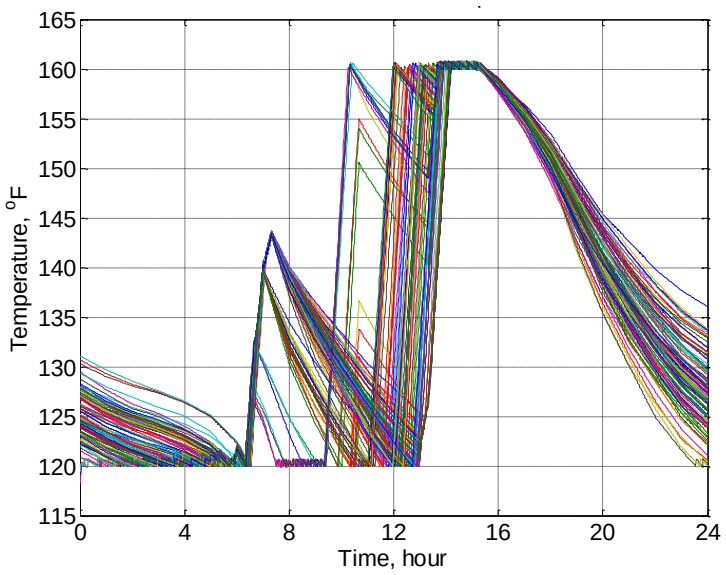
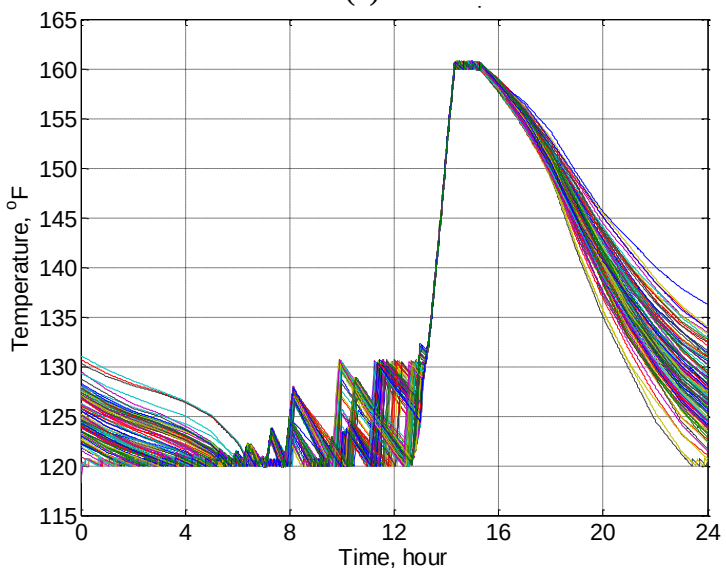


Figure 12.9. Battery SOC for the proposed management systems, with and without DR.



(a)



(b)

Figure 12.10. The hot water temperature for all household in (a) DR.A, and (b) DR.B PMAs.

MG Emission

As expected, the total MG emission is reduced because of the DiG generation reduction when the DR strategies are used. The reduction in CO_2 and non-CO_2 emissions for the *DR.A* and the *DR.B* compared to the *No-DR* PMA are tabulated in Table 12.4.

1.8% and 3.5% reduction for CO_2 emission as well as 4.5% and 6.6% reduction in non-CO_2 emissions are observed for the *DR.A* and *DR.B*, respectively, compared to the *No-DR* case. This results in 2.8% and 4.7% reduction in total damage cost for *DR.A* and *DR.B*, respectively, compared to the *No-DR* case.

Table 12.4. Reduction in CO_2 and non-CO_2 emissions in the *DR.A* and *DR.B* PMAs.

PMAs	DR.A	DR.B
Decrease in CO_2 emissions	1.8%	3.5%
Decrease in non-CO_2 emissions	4.5%	6.6%

Total Undelivered Load

Although for the size of the MG studied, the total undelivered power for the *No-DR* PMA is negligible (less than 0.5% compared to the total load demand), this value is reduced by 65.6% and 60.9% for the *DR.A* and *DR.B* PMAs, respectively. Undelivered power occurs when the total reduction in generation, storage, and EWHs' power is less than the sum of the non-EWH load demand and the power demand of the EWHs that are forced to be on. For the *DR.A* and *DR.B* PMAs, undelivered load demand occurred during 16:40-17:00 (1.659 kW and 1.329 kW for *DR.A* and *DR.B*, respectively) and during 17:40-18:00 (19.781 kW and 22.998 kW for *DR.A* and *DR.B*, respectively). According to Figure 12.10, during these periods all EWHs are off, and the DR cannot be used to avoid undelivered load demand.

Total MG Operational Cost

As given in Table 12.3, the total MG operational cost is reduced by 6.98% and 7.55% for the *DR.A* and *DR.B* PMAs, respectively, compared to the *No-DR* PMA. It is

because of the fact that when the DR strategies are employed, the DiG output energy and the battery discharge decrease. These reductions in energy demand have resulted in noticeable cost reduction in the MG operation.

Conclusion

In this chapter, a rule-based multi-timescale cost-effective power management algorithm, is proposed to effectively include generation, storage, and the DR within the same management framework. The MG design and dynamic modeling are briefly discussed, and the power management algorithm is presented. Two different EWH DR strategies (*DR.A* and *DR.B*) are proposed and compared with the *No-DR* case. Simulation results showed that incorporating the DR in the management algorithm increased the PV power utilization; decreased the DiG total generation, its fuel consumption and emissions; increased the battery average SOC; and decreased the total undelivered load in the MG. As a result, the MG operational costs are decreased remarkably when the DR is employed in the PMA.

Each of the DR strategies has certain advantages over the other; the choice of which one to use depends on the specific circumstances and is to be made by the owner/operator of the MG. *DR.A* is a better approach when the average efficiency of the DiG and battery, and the undelivered load demand are important. On the other hand, *DR.B* is better in terms of the MG operational cost, PV power utilization, and the total MG emissions. It should be noted that the proposed PMAs need to be modified to accommodate other variable generation sources (such as wind) according to their variable nature, as was done in this chapter for solar PV.

Acknowledgement

This work was supported by NEC Labs America, and the U.S. Department of Energy, Office of Science, Basic Energy Sciences, under Award # DE-FG02-11ER46817.

References Cited

[12.1] U.S. DOE, office of electric transmission and distribution, "GRID 2030: A national vision for electricity's second 100 years," July 2003.

[12.2] F. Katiraei, et al., "Microgrids management: Controls and operation aspects of microgrids," *IEEE Power Energy Mag*., vol. 6, no. 3, pp. 54–65, May/June 2008.

[12.3] C.M. Colson, M.H. Nehrir, and S.A. Pourmousavi, "Towards real-time microgrid power management using computational intelligence methods," in *Proc*. PES GM, Minneapolis, USA 2010, pp. 1–8.

[12.4] A.G. Tsikalakis and N.D. Hatziargyriou, "Centralized control for optimizing microgrids operation," *IEEE Trans. Energy Convers*., vol. 23, no. 1, pp. 241–248, Feb. 2008.

[12.5] S.A. Pourmousavi, et al., "Real-time energy management of a stand-alone hybrid wind-microturbine energy system using particle swarm optimization," *IEEE Trans. Sustain. Energy*, vol. 1, no 3, pp. 193–201, Oct. 2010.

[12.6] F.A. Mohamed and H.N. Kovio, "Power management strategy for solving power dispatch problems in Microgrid for residential applications," in *Proc*. IEEE International Energy Conference and Exhibition, Manama, Bahrain 2010, pp. 746–751.

[12.7] Y. Riffonneau, et al., "Optimal power flow management for grid connected PV systems with batteries," *IEEE Trans. Sustain. Energy*, vol. 2, no. 3, pp. 309–320, Feb. 2011.

[12.8] B. Belvedere, et al., "A microcontroller-based power management system for standalone microgrids with hybrid power supply," *IEEE Trans. Smart Grid*, vol. 3, no. 3, pp. 422–431, May 2012.

[12.9] S.A. Pourmousavi, R.K. Sharma, and B. Asghari, "A framework for real-time power management of a grid-tied microgrid to extend battery lifetime and reduce cost of energy," in *Proc*. IEEE PES Innovative Smart Grid Technologies, Washington D.C., USA 2012, pp. 1–8.

[12.10]C.M. Colson and M.H. Nehrir, "Comprehensive real-time microgrid power management and control with distributed agents," *IEEE Trans. Smart Grid*, vol. 4, no. 1, pp. 617–627, Jan. 2013.

[12.11]C.M. Colson, M. H. Nehrir, R. K. Sharma, and B. Asghari, "Improving sustainability of hybrid energy systems Part II: Managing multiple objectives with a multiagent system," *IEEE Trans. Sustain. Energy*, vol. 5, no. 1, pp. 46–54, Jan. 2014.

[12.12]HOMER ENERGY: Energy Modeling Software for Hybrid Renewable Energy Systems, Available online: http://homerenergy.com/

[12.13]"Individual household electric power consumption Data Set," Machine Learning Repository, University of California-Irvine, Available online: http://archive.ics.uci.edu/ml/datasets/Individual+household+electric+power+consumption#

[12.14]E. Lorenzo, et. Al, *Solar Electricity Engineering of Photovoltaic Systems*, Earthscan Publications Ltd., pp. 316, Jan. 1994.

[12.15]SunPower Corp., "SPR-200-BLK, residential PV Module," specification sheet Available online: http://www.energyplus.com.sg/products/32.pdf

[12.16]L.E. Bussey, *The Economic Analysis of Industrial Projects*, Prentic-Hall Inc.: New Jersey, 1978, ch. 4 and 11.

[12.17]S.A. Pourmousavi, M.H. Nehrir, and R.K. Sharma, "Ownership cost calculations for distributed energy resources using uncertainty and risk analysis," Submitted to the *IEEE Trans. Pow. Syst.* for possible publication, March 2014.

[12.18]S. Chakraborty and M.G. Simoes, "PV-microgrid operational cost minimization by neural forecasting and heuristic optimization," in *Proc*. IEEE Industry Applications Society Annual Meeting, Edmonton, Canada 2008, pp. 1–8.

[12.19]CumminsOnan Commercial SD 10000, Available online: https://powersuite.cummins.com/PSWEB/login.action

[12.20]M. Pipattanasomporn, M. Willingham, and S. Rahman, "Implications of on-site distributed generation for commercial/industrial facilities," *IEEE Trans. Power Syst*., vol. 20, no. 1, pp. 206–212, Feb 2005.

[12.21]MATLAB Curve Fitting Toolbox, MathWorks Inc., Available online: http://www.mathworks.com/products/curvefitting/

[12.22]A. Sobu and G. Wu, "Dynamic optimal schedule management method for microgrid system considering forecast errors of renewable power generations," in *Proc*. IEEE International Conference on Power system Technology, Auckland, USA 2012, pp. 1–6.

[12.23]D. Thimsen, "Cost of utility distributed generators, 1-10 MW," EPRI, Rep. no. 1007760, March 2003.

[12.24]D. Zhu, et al., "In-plume emission test stand 2: Emission factors for 10- to 100-

kW U.S. Military Generators," *JAPCA J. Air Waste Ma*., vol. 59, no. 12, pp. 1446–1457, Dec. 2009.

[12.25]R.S.J. Tol, "The marginal damage costs of carbon dioxide emissions: An assessment of the uncertainties," *Energ. Policy*, vol. 33, no. 16, pp. 2064–2074, Nov. 2005.

[12.26]D. Burtraw and S.J. Szambelan, "U.S. emissions trading markets for SO2 and NOx," Discussion Paper, Resources for the future company, RFF DP 09-40, Oct. 2009.

[12.27]M. Ceraolo, "New dynamical models of lead-acid batteries," *IEEE Trans. Power Syst.*, vol. 15, no. 4, pp. 1184–1190, Nov. 2000.

[12.28]C.M. Colson, et al., "Improving sustainability of hybrid energy systems Part I: Incorporating battery round-trip efficiency and operational cost factors," *IEEE Trans. Sustain. Energy*, vol. 5, no. 1, pp. 37–45, Jan. 2014.

[12.29]EPRI, "Electricity energy storage technology options: A white paper primer on applications, costs and benefits," Dec, 2010. Available online: http://www.electricitystorage.org/images/uploads/static_content/technology/resources/ESA_TR_5_11_EPRIStorageReport_Rastler.pdf

[12.30]R. Lassseter and M. Erikson, "Integration of battery-based energy storage element in the CERTS microgrid," Final Report Task 4, prepared for U.S. DOE., Oct. 2009, ch. 6.

[12.31]P.S. Dolan, M.H. Nehrir, and V. Gerez, "Development of a Monte Carlo based aggregate model for residential electric water heater loads," *Electr. Pow. Syst. Res*., vol. 36, no. 1, pp. 29–35, Jan. 1996.

[12.32]S.N. Patrick, "Control of aggregate electric water heaters for load shifting and balancing intermittent renewable energy generation in a smart grid environment," M.S thesis in Electrical Engineering, Montana State University-Bozeman, 2011.

[12.33]S.A. Pourmousavi, S.N. Patrick, and M.H. Nehrir, "Real-time demand response through aggregate electric water heaters for load shifting and balancing intermittent wind generation," *IEEE Trans. Smart Grid*, vol. 5, no. 2, pp. 769–778, March 2014.

[12.34]C.M. Colson and M.H. Nehrir, "A review of challenges to real-time power management of microgrids," in *Proc*. IEEE PES GM, Calgary, Canada 2009, pp. 1–8.

[12.35]C.M. Colson and M.H. Nehrir, "An alternative method to load modeling for obtaining end-use load profiles," in *Proc*. IEEE NAPS, Starkville, USA 2009, pp. 1–5.

[12.36]"Descriptions of electric energy use in single family residences in the pacific

northwest, 1986- 1992," Office of Energy Resources, Bonneville Power Administration, Portland, OR, December 1992.

CHAPTER 13

CONCLUSIONS

This dissertation made an attempt to address the necessity and complexity of regulation services in the smart grid and MGs in the presence of variable RES generation using real-time DR. Different studies and models are developed to first show the impacts of variable RES on the frequency and voltage of the power grid in the transmission and distribution systems. Then, different heuristic and optimal real-time DR approaches are proposed to remedy this impact. Additionally, real-time power management of grid-tied and islanded MGs are investigated, considering simultaneous generation, storage, and DR management. Extensive dynamic models of different generation, storage, and load are developed in MATLAB®/Simulink and m-files for different part of the dissertation. The following conclusions can be drawn from the work reported in the dissertation:

1. As it is presented in Chapter 1, MGs are promising technology to achieve the smart grid goals. However, effective and wide application of MGs relies on appropriate control methodologies, especially for cost-effective management of assets and regulation services.

2. High penetration of variable RES generation can have negative impact on the frequency and voltage behavior of the power grid which results in severe stability issues, as shown in Chapters 2 to 4. This impact is more visible and severe in the islanded MGs. Distributing the RES generation in a large geographical area, if possible, may be helpful but cannot be an effective solution for this problem.

3. In order to effectively evaluate the application of real-time DR for regulation

services, and to compare their effectiveness against traditional methods (such as AGC), a simulation framework is required. This framework is developed in Chapters 2 and 4 to integrate a simple model of the grid along with traditional regulation services, i.e., SGM. The proposed simulation framework can easily be extended to power system of any size and utilized in similar studies.

4. At the transmission level, where large wind farms are expected to be implemented, real-time DR seems to be inevitable. However, there is not a single comprehensive tool to include DR for evaluation and controller design. In order to fill this gap, the well-known LFC model is enhanced in Chapters 6 and 7 with a real-time DR control loop considering DR communication delay. To make the proposed model more effective and real, an electricity market structure is adapted and the model is extended to multi-area power system with multiple Gencos and Lagcos in each area. This model is an effective tool for DR performance evaluation and controller design at the transmission level.

5. In order to compensate inherent variations of RES generation, it is shown that real-time DR can be very effective to maintain balance between generation and demand in Chapters 2 to 8 for distribution and transmission systems. Despite the delay existing in the communication with DR resources, these approaches are still a better solution to the frequency and voltage issues, particularly in the islanded MGs. An innovative real-time DR algorithm is proposed for islanded MG applications which not only provide regulation services to the MG, but also guarantees the minimum load manipulation, which is an important criterion for successful implementation of DR programs. Based on

our best knowledge, this algorithm was the first of its own at the time. Simulation results show that the proposed control algorithm can also be effective for up to 300 msec of DR communication delay. The proposed control algorithm will significantly impact the application of real-time DR in the islanded MGs, and will motivate smart grid developers to implement MGs.

6. Customer participation and utilities investment on the required infrastructure play important roles in successful DR programs implementation. Therefore, cost-effective operation of the DR programs can considerably be useful to this end. As a result, an optimal real-time DR approach is developed in Chapter 5 by adapting the PJM regulation market in this dissertation. Simulation results show that not only the frequency and voltage regulation is significantly improved using the proposed technique compared to the traditional spinning and non-spinning reserves, but also proved that DR can provide more cost-effective regulation services for the utilities. Additionally, it is shown that the utilization of DR for regulation services can decrease system power losses. Both of the above results can be effective in reducing the price of electricity for customers. This significant achievement can broaden the acceptance of the DR amongst customers and utilities at the same time.

7. Application of real-time DR is not only limited to islanded MGs. Aggregated responsive load can participate in the regulation services at the transmission level as well. To show this, a controller is developed in Chapter 8 using aggregated EWHs model to provide regulation services in a transmission system with large penetration of wind generation. The proposed method not only provide more than 75% of the required

balancing reserve, but also decrease operational cost for both the utilities and customers simultaneously without affecting customers' QoS. It can also be effective in shifting load from on-peak hours to the off-peak periods. This method can motivate customers to participate in the DR programs, and utilities to develop effective DR programs and to implement the required infrastructure for DR.

8. Despite the communication delay existing in the DR, it is shown in Chapters 3 to 7 that the DR resources can provide faster regulation services (i.e., faster up and down ramping regulation) compared to the traditional spinning and non-spinning reserves. It results in faster frequency regulation in islanded MGs equipped with real-time DR compared to the AGC method. This is another motivation, besides economic, for the utilities to develop effective DR programs and to implement the required infrastructure.

9. As mentioned earlier, cost-effective operation of islanded MGs is very important to broaden MGs acceptance and utilization in the power system. Therefore, effective approach for cost calculation finds a central role in this regard. To the best of our knowledge, there is no comprehensive model for ownership cost calculation (as one of the two costs associated with the MG component cost calculations) considering the uncertainties and risk in the calculation. An attempt is made to bridge this gap with the proposed ownership cost calculation method, presented in Chapter 9, to determine this cost for DERs in uncertain conditions. The proposed general approach can be utilized for different types of DERs and storage units. The effectiveness of the proposed methods is shown through different simulation studies.

10. Real-time power management is a vital tool for any grid-tied and islanded

MG. While centralized and decentralized algorithms have their own advantages and shortcomings, different central rule-based and optimal power management algorithms for different MGs are developed in Chapters 10 to 12. Different generation, storage, and load dynamic modeling has been done in these chapters to provide appropriate simulation environment for different simulation studies. Also, different objectives are considered in the proposed algorithms. The innovation of the proposed algorithms can be summarized as simultaneous generation, storage, and DR management, suitability of specific loads for DR management, guaranteed optimality of the solutions for both rule-based and optimal algorithms, battery lifetime maximization, and finding the solutions in real-time. Simulation results show the effectiveness of the proposed algorithms in reducing MG operational cost, extending battery lifetime, and the effectiveness of real-time DR applications.

This dissertation tried to address a significant challenge of smart grid and MG to employ large penetration of variable RES. It is shown that the impact of large penetration of variable RES can be smoothed using appropriate real-time DR algorithms. Additionally, it is shown that the proposed real-time algorithms can be beneficial for both customers and utilities at the transmission and distribution levels and can be effective in real-time power management algorithms developed to guarantee optimal operation of the MGs.

REFERENCES CITED

[1.1] Edison Tech. Center, "The history of alternating current: AC power history and timeline," Available online: http://edisontechcenter.org/AC-PowerHistory.html#early

[1.2] Office of Electric Transmission and Distribution, "Grid 2030: A national vision for electricity's second 100 years," U.S. Department of Energy (U.S. DOE), July 2030.

[1.3] North American Electric Reliability Corporation (NERC) Interconnections, Available online: http://www.nerc.com/AboutNERC/keyplayers/Pages/default.aspx

[1.4] U.S. Department of Energy, "The smart grid: An introduction. How a smarter grid works as an enabling engine for our economy, our environment and our future." Available online: http://energy.gov/oe/downloads/smart-grid-introduction-0

[1.5] J. Moura, "Assessment of the North American bulk power system: A reliability perspective on future needs and challenges," NERC Reliability Assessment Electricity Security Plan (ESAP) Workshop, Oct. 2013.

[1.6] M. Amin, "North American electricity infrastructure: system security, quality, reliability, availability, and efficiency challenges and their societal impacts," National Science Foundation (NSF) report on Continuing crises in national transmission infrastructure: impacts and options for modernization, Ch. 2, June 2004.

[1.7] K. Vu, M.M. Begouic, D. Novosel, "Grids get smart protection and control," *IEEE Comput. Appl. Power*, vol. 10, no. 4, pp. 40–44, Oct. 1997.

[1.8] Independent Statistics & Analysis, "International energy statistics," U.S. Energy Information Administration, Available online: http://www.eia.gov/cfapps/ipdbproject/iedindex3.cfm?tid=2&pid=2&aid=7&cid=US,&syid=1985&eyid=2011&unit=MK

[1.9] Independent Statistics & Analysis, "Annual energy review 2011," U.S. Energy Information Administration, Report NO: DOE/EIA-0384(2011), Sept. 2012.

[1.10] *Smart Grid Coordination Group – Sustainable Processes*, European Committee for Electrotechnical Standardization, pp. 84, Nov. 2012.

[1.11] Federal Incentives/Policies for Renewable Energy, "Residential renewable energy tax credit," Available online: http://www.dsireusa.org/library/includes/incentive2.cfm?Incentive_Code=US37F&State=federal&currentpageid=1&ee=0&re=1

[1.12] California Incentives/Policies for Renewable & Efficiency, "Burbank water & power – green building incentive program," Available online: http://www.dsireusa.org/incentives/incentive.cfm?Incentive_Code=CA86F&re=0&ee=0

[1.13] Solar Energy Industries Association (SEIA), "Solar Industry Data in Q3 2013," Available online: http://www.seia.org/research-resources/solar-industry-data

[1.14] Renewable Portfolio Standard Policies, Database of State Incentives for Renewables & Efficiency, U.S. Department of Energy, March 2013, Available online: http://www.dsireusa.org/documents/summarymaps/RPS_map.pdf

[1.15] U.S. Energy Information Association (EIA), "Electricity market trends," Available online: http://www.eia.gov/forecasts/aeo/MT_electric.cfm

[1.16] Independent Statistics & Analysis, "Annual energy outlook 2013," U.S. energy information administration, Dec. 2013, Available online: http://www.eia.gov/forecasts/aeo/MT_electric.cfm

[1.17] Edison Electric Institute (EEI), "Transmission investment: Adequate returns and regulatory certainty are key," June 2013.

[1.18] National Energy Policy Act of 1992, Available online: http://www.ferc.gov/legal/maj-ord-reg/epa.pdf

[1.19] North American Electric Reliability Corporation (NERC), "2013 long-term reliability assessment," Dec. 2013.

[1.20] The Electricity Technology Roadmap: Meeting the Critical Challenges of the 21st Century, 2003 Summary and Synthesis, EPRI, product no: 1010929, Available online: http://mydocs.epri.com/docs/CorporateDocuments/StrategicVision/Roadmap2003.pdf

[1.21] Independent Statistics & Analysis, "Electricity reliability data by NERC regions," U.S. Energy Information Administration, Available online: http://www.eia.gov/electricity/data/eia411/

[1.22] Renewables 2012 Global Status Report, Renewable Energy Policy Network for the 21st Century, Available online: http://www.ren21.net/Resources/Publications/REN21Publications/Renewables2012GlobalStatusReport.aspx

[1.23] EPRI 2001, *Electricity Infrastructure Security Assessment*, Vol. I-II, EPRI, Palo Alto, CA, Nov. and Dec. 2001.

[1.24] "OPEC Oil Embargo 1973–1974". U.S. Department of State, Office of the Historian, Available online: http://history.state.gov/milestones/1969-1976/oil-embargo

[1.25] J.H. Kim and A. Shcherbakova, "Common failures of demand response," *Energy*, vol. 36, no. 2, pp. 873–880, Feb. 2011.

[1.26] Independent Statistics & Analysis, "Electricity purchases, sales for resale, import/exports, reliability," U.S. Energy Information Administration, Dec. 2013, Available online: http://www.eia.gov/electricity/data/eia411/

[1.27] ABB Group. America, "Energy efficiency in the power grid," Published in 2007.

[1.28] Energy Efficiency & Renewable Energy, "2011 renewable energy data book," U.S. Department of Energy.

[1.29] U.S. Energy Information Administration, "State electricity profiles 2010," Report No DOE/EIA-0348(01)/2, Jan. 2012.

[1.30] Independent Statistics & Analysis, "Electric power monthly with data for December 2013," U.S. Energy Information Administration, Feb. 2014.

[1.31] Energy Laboratory, Massachusetts Institute of Technology, "Assessment of transmission congestion for major electricity market in the U.S.," Report NO: MIT EL 01-009 WP, Feb. 2001.

[1.32] S. Chakraborty and M.G. Simoes, "PV-microgrid operational cost minimization by neural forecasting and heuristic optimization," in *Proc*. IEEE Industry Applications Society Annual Meeting, Edmonton, Canada 2008, pp. 1–8.

[1.33] Annual Energy Outlook 2013, "Summary: generating capacity," U.S. Energy Information Administration, Dec. 2013, Available online: http://www.eia.gov/totalenergy/data/annual/showtext.cfm?t=ptb0811a

[1.34] Annual Energy Outlook 2013, "Summary: Emissions from energy consumption for electricity generation," U.S. Energy Information Administration, Dec. 2013, Available online: http://www.eia.gov/totalenergy/data/annual/showtext.cfm?t=ptb1105a

[1.35] Independent Statistics and Analysis, "AEO2014 early release overview," U.S. Energy Information Administration, Dec. 2013, Available online: http://www.eia.gov/forecasts/aeo/er/early_elecgen.cfm?src=Renewable-b2

[1.36] N. Jenkins, et al., *Embedded Generation*, The Institution of Electrical Engineers, London, 2000.

[1.37] R.C. Dugan, et al., *Electric Power Systems Quality*, 2nd Ed., McGraw-Hill, 2003.

[1.38] T. Ackermann (editor), *Wind Power in Power Systems*, Wiley, 2005.

[1.39] B. Fox, et al., *Wind Power Integration - Connection and System Operational Aspects*, The Institution of Engineering and Technology, London, 2007.

[1.40] M.H.J. Bollen and F. Hassan, I*ntegration of Distributed Generation in Power Systems*, Wiley – IEEE Press, 2011.

[1.41] M.H.J. Bollen, *The Smart Grid: Adapting the Power System to New Challenges*, Morgan & Claopool Publishers, 2011.

[1.42] C.L. Wadhwa, *Electrical Power Systems*, New Age International Publishers, 2006, ch. 13.

[1.43] A. Lopez, et al., "U.S. renewable energy technical potentials: A GIS-based analysis," National Renewable Energy Laboratory, NREL/TP-6A20-51946, July 2012.

[1.44] Energy Efficiency & Renewable Energy, "2012 renewable energy data book," U.S. DOE, Available online: http://www.nrel.gov/news/press/2013/5302.html

[1.45] Office of Energy Efficiency & Renewable Energy, "Advantages and challenges of wind energy," U.S. DOE, Available online: http://energy.gov/eere/wind/advantages-and-challenges-wind-energy

[1.46] D.J.C. MacKay, *Sustainable Energy Without Hot Air*, UIT Cambridge Ltd., 1st Ed., 2009, ch. 26.

[1.47] C.L. Archer and M.Z. Jacobson, "Supplying baseload power and reducing transmission requirements by interconnecting wind farms," *Journal of Applied Meteorology and Climatology* (American Meteorological Society), vol. 46, no. 11, pp. 1701–1717, Nov. 2007.

[1.48] Y.H. Wan, "Long-term wind power variability," National Renewable Energy Laboratory, NREL/TP-5500-53637, Jan. 2012.

[1.49] University of Oregon, Solar Radiation Monitoring Laboratory website. Available online: http://solardat.uoregon.edu/

[1.50] M. McDermott, "Denmark inaugurates world's largest offshore wind farm - 209 MW Horns Rev 2," Sept. 2009, Available online: http://www.treehugger.com/renewable-energy/denmark-inaugurates-worlds-largest-offshore-wind-farm-209-mw-horns-rev-2.html

[1.51] Energy Numbers, "Capacity factors at Danish offshore wind farms," March 2014, Available online: http://energynumbers.info/capacity-factors-at-danish-offshore-wind-farms

[1.52] Independent Statistics & Analysis, "What is a capacity factor?" U.S. Energy Information Administration, Available online:

http://www.eia.gov/tools/faqs/faq.cfm?id=187&t=3

[1.53] D. Van Zandt, et al., "Ontario wind integration study: Final report to OPA, IESO, and CanWEA," GE Energy, Oct. 2006.

[1.54] M.R. Milligan, "Modeling utility-scale wind power plants Part 2: Capacity credit," National Renewable Energy Laboratory, Technical Report NREL/TP-500-29701, March 2002.

[1.55] G.J.W. Van Bussel and M.B. Zaaijer, "Reliability, availability and maintenance aspects of large-scale offshore wind farms," in *Proc.* 2001 European wind energy conference, Copenhagen, Denmark; 2011, pp. 557–560.

[1.56] J. Ribrant and L.M. Bertling, "Survey of failures in wind power systems with focus on Swedish wind power plants during 1997–2005," *IEEE Trans. Energy Convers.*, vol. 22, no. 1, pp. 167–173, March 2007.

[1.57] P.J. Tavner, et al., "Influence of wind speed on wind turbine reliability," *Wind Engineering*, vol. 30, no. 1, pp. 55–72, Jan. 2006.

[1.58] G. Sinden, "Characteristics of the UK wind resource: Long-term patterns and relationship to electricity demand," *Energ. Policy*, vol. 35, no. 1, pp. 112–127, Jan. 2007.

[1.59] P. Brown, "U.S. renewable electricity: How does wind generation impact competitive power markets," CRS Report for U.S. Congress R42818, Congressional Research Service, Nov. 2012.

[1.60] D. Corbus, et al., "Up with wind - studying the integration and transmission of higher levels of wind power," *IEEE Power Energy Mag.*, vol. 7, no. 6, pp: 36–46, Nov/Dec. 2009.

[1.61] A.A. Edris, et al., "Proposed terms and definitions for flexible AC transmission system (FACTS)", *IEEE Trans. Power Del.*, vol. 12, no. 4, pp. 1848–1853, Oct. 1997.

[1.62] N. Etherden and M.H.J. Bollen, "Increasing the hosting capacity of distribution networks by curtailment of renewable energy resources", in *Proc.* IEEE Trondheim Power Tech, June 2011, pp. 1–7.

[1.63] A.K. Kazerooni, et al., "Dynamic thermal rating applications to facilitate wind energy integration", in *Proc.* IEEE Trondheim Power Tech, June 2011 pp. 1–7.

[1.64] D. Rastler, "Electricity energy storage technology options: A white paper primer on applications, costs, and benefits," EPRI 1020676, Dec. 2010.

[1.65] U. Eberle, B. Muller, and R. von Helmolt, "Fuel cell electric vehicles and hydrogen infrastructure: Status 2012," *Energy & Environment Science*, vol. 5, no. 10, pp. 8780–8798, July 2012.

[1.66] P. Hoffmann, *Tomorrow's Energy: Hydrogen, Fuel Cells, and the Prospects for a Cleaner Planet*, MIT Press, 2002.

[1.67] C. Wang and M.H. Nehrir, "Fuel cells and load transients," *IEEE Power Energy Mag.*, vol. 5, no. 1, pp. 58–63, Jan/Feb 2007.

[1.68] Florida Solar Energy Center, "Hydrogen basics: Storage," Available online: http://www.fsec.ucf.edu/en/consumer/hydrogen/basics/storage.htm

[1.69] Hydrogen and Fuel Cells Program, "Hydrogen storage," U.S. Department of Energy, Available online: http://www.hydrogen.energy.gov/storage.html

[1.70] J.S. Thorp, et al., "Feasibility of adaptive protection and control", *IEEE Trans. Power Del.*, vol. 8, no. 3, pp. 975–983, July 1993.

[1.71] W.S. Tan, et al., "Optimal distributed renewable generation planning: A review of different approaches," *Renew. Sust. Energ. Rev.*, vol. 18, pp. 626–645, Feb. 2013.

[1.72] T. Xu and P.C. Taylor, "Voltage control techniques for electrical distribution networks including distributed generation," in *Proc.* 17th World Congress of the International Federation of Automatic Control, Seoul, South Korea, July 2008, pp. 11967–11971.

[1.73] T.J.T. Hashim, A. Mohamed, and H. Shareef, "A review on voltage control methods for active distribution networks," *PRZEGLĄD ELEKTROTECHNICZNY* (*Electrical Review*), vol. 88, no. 6, pp. 304–312, 2012.

[1.74] N. Hatziargyriou, "Microgrids - The key to unlock distributed energy resources?" *IEEE Power Energy Mag.*, vol. 6, no. 3, pp. 26–29, May/June 2008.

[1.75] J. Driesen and F. Katiraei, "Design for distributed energy resources", *IEEE Power Energy Mag.*, vol. 6, no. 3, pp. 30–39, May/June 2008.

[1.76] N. Martensen, P. Lund, and N. Mathew, "The cell controller pilot project: From surviving system black-out to market support," in *Proc.* 21st International Conference on Electricity Distribution (CIRED), Frankfurt, June 2011.

[1.77] *CERTS Microgrid Test Bed*, Dolan Technology Center, Available online: http://certs.aeptechlab.com/

[1.78] P. Asmus, “Why microgrids are moving into the mainstream: Improving the efficiency of the larger power grid,” *IEEE Electrific. Mag.*, vol. 2, no. 1, pp. 12–19, March 2014.

[1.79] A. Khamis, et al., “A review of islanding detection techniques for renewable distributed generation systems,” *Renew. Sust. Energ. Rev.*, vol. 28, pp. 483–493, Dec. 2013.

[1.80] Z. Zeng, et al., “Topologies and control strategies of multi-functional grid-connected inverters for power quality enhancement: A comprehensive review,” *Renew. Sust. Energ. Rev.*, vol. 24, pp. 223–270, Aug. 2013.

[1.81] C. Natesan, et al., “Survey on microgrid: Power quality improvement techniques,” *ISRN Renewable Energy*, Hindawi Publishing Corporation, 2014, pp. 1–7.

[1.82] K. LaCommare and C. Marnay, “Microgrids and heterogeneous power quality and reliability,” *International Journal of Distributed Energy Recourses*, vol. 4, no. 4, pp. 1–11, Oct. 2008.

[1.83] R. O’Neill, “Smart grids sound transmission investments,” *IEEE Power Energy Mag.*, vol. 5, no. 5, pp. 104–102, Sep–Oct. 2007.

[1.84] C.M. Colson and M.H. Nehrir, “A review of challenges to real-time power management of microgrids,” in *Proc*. IEEE PES General Meeting, Calgary, Canada, July 2009, pp. 1–8.

[1.85] X. Guan, Z. Xu, and Q-S. Jia, “Energy-efficient buildings facilitated by microgrid,” *IEEE Trans. Smart Grid*, vol. 1, no. 3, pp. 243–252, Dec. 2010.

[1.86] R. Cowart, et al., “Efficient reliability: The critical role of demand-side resources in power systems and markets,” The Regulatory Assistance Project prepared for The National Association of Regulatory Utility Commission, June 2001.

[1.87] S.A. Pourmousavi and M.H. Nehrir, "Real-time optimal demand response for frequency regulation in smart microgrid environment," in *Proc*. 11th IASTED International conference on Power and Energy Systems (EuroPES2012), Naples, Italy, June. 2012, pp. 194–200.

[1.88] J.D. Kueck, R.M. Staunton, and B.J. Kirby, “Microgrids and demand response,” *Public Utility Fortnightly*, May 2003, pp. 55–58.

[1.89] M. Amin and B.F. Wollenberg, “Toward a smart grid: Power delivery for the 21st century”, *IEEE Power Energy Mag.*, vol. 3, no. 5, pg. 34–41, Sept/Oct 2005.

[1.90] M. Amin, "The self-healing grid: A concept two decades in the making," IEEE Smart Grid Technical Community, Available online: http://smartgrid.ieee.org/march-2013/813-the-self-healing-grid-a-concept-two-decades-in-the-making

[1.91] C.M. Colson, "Towards real-time power management of microgrids for power system integration: A decentralized multi-agent based approach," PhD Dissertation, Montana State University, Nov. 2012.

[1.92] C. Marnay, et al., "Policymaking for microgrids: Economic and regulatory issues of microgrid implementation," *IEEE Power Energy Mag.*, vol. 6, no. 3, pp. 66–77, May/June 2008.

[1.93] M.S. Mahmoud, S.A. Hussain, and M.A. Abido, "Modeling and control of microgrid: An overview," *Journal of Franklin Institute*, vol. 351, no. 5, pp. 2822–2859, May 2014.

[1.94] C.M. Colson and M.H. Nehrir, "A review of challenges to real-time power management of microgrids," in *Proc*. IEEE PES General Meeting, Calgary, Canada, July 2009, pp. 1–8.

[1.95] F. Katiraei, et al., "Microgrids management: Controls and operation aspects of microgrids," *IEEE Power Energy Mag.*, vol. 6, no. 3, pp. 54–65, May/June 2008.

[1.96] H. Holttinen, et al., "Design and operation of power systems with large amounts of wind power," *VTT Technical Research Centre of Finland*, Helsinki, Finland, Rep. 2493, 2009.

[1.97] R. Doherty and M. O'Malley, "A new approach to quantify reserve demand in systems with significant installed wind capacity," *IEEE Trans. Power Syst*., vol. 20, no. 2, pp. 587–595, May 2005.

[1.98] I. Gyuk, et al., "The United State of storage: Federal and state collaboration on electric energy storage," *IEEE Power Energy Mag.*, vol. 3, no. 2, pp. 31–39, March/April 2005.

[1.99] D. Westermann and A. John, "Demand matching wind power generation with wide-area measurement and demand-side management," *IEEE Trans. Energy Convers.*, vol. 22, no. 1, pp. 145–149, March 2007.

[1.100]A. Faruqui, S. Sergici, and A. Sharif, "The impact of informational feedback on energy consumption – A survey of the experimental evidence," *Energy*, vol. 35, no. 4, pp. 1598–1608, Apr. 2010.

[1.101]J.W. Zarnikau, "Demand participation in the restructured electric reliability

council of Texas market," *Energy*, vol. 35, no. 4, pp. 1535–1543, Apr. 2010.

[1.102]K. Herter and S. Wayland, "Residential response to critical-peak pricing of electricity: California evidence," *Energy*, vol. 35, no. 4, pp. 1561–1567, Apr. 2010.

[1.103]J. Torriti, M.G. Hassan, and M. Leach, "Demand response experience in Europe: Policies, programs and implementation," *Energy*, vol. 35, no. 4, pp. 1575–1583, Apr. 2010.

[1.104]J. Wang, et al., "Demand response in China," *Energy*, vol. 35, no 4, pp. 1592–1597, Apr. 2010.

[1.105]M.H. Albadi and E.F. El-Saadany, "A summary of demand response in electricity markets," *Electr. Pow. Syst. Res.*, vol. 78, no. 11, pp. 1989–1996, Nov. 2008.

[1.106]R. Walawalkar, et al., "An economic welfare analysis of demand response in the PJM electricity market," *Energ. Policy*, vol. 36, no. 10, pp. 3692–3702, Oct. 2008.

[1.107]T.J. Park and S.H. Hong, "Experimental case study of a BACnet-based lighting control system," *IEEE Trans. Autom. Sci. Eng.*, vol. 6, no. 2, pp. 322–333, Apr. 2009.

[1.108]M. Klobasa, "Analysis of demand response and wind integration in Germany's electricity market," *IET Renew. Pow. Gen.*, vol. 4, no. 1, pp.55–63, Jan. 2010.

[1.109]H. Saele and O.S. Grande, "Demand response from household customers-Experiences from a pilot study in Norway", *IEEE Trans. Smart Grid*, vol. 2, no. 1, pp. 102–109, Mar. 2011.

[1.110]A. Brooks, et al., "Demand dispatch: Using real-time control of demand to help balance generation and load," *IEEE Power Energy Mag.*, vol. 8, no. 3, pp. 20–29, May/June 2010.

[1.111]J. Medina, N. Muller, and I. Roytelman, "Demand response and distribution grid operations: Opportunities and challenges," *IEEE Trans. Smart Grid*, vol. 1, no. 2, pp. 193–198, Sept. 2010.

[1.112]A.J. Conejo, J.M. Morales, and L. Baringo, "Real-time demand response model," *IEEE Trans. Smart Grid*, vol. 1, no. 3, pp. 236–242, Dec. 2010.

[1.113]D. Trudnowski, M. Donnelly, and E. Lightner, "Power-system frequency and stability control using decentralized intelligent loads," in *Proc.* IEEE PES Conf. and Exhibition Transmission and Distribution, Dallas, TX, 2005, pp. 1453–1459.

[1.114]G.C. Heffner, C.A. Goldman, and M.M. Moezzi, "Innovative approaches to

verifying demand response of water heater load control," *IEEE Trans. Power Del.*, vol. 21, no. 1, pp. 388–397, Jan. 2006.

[1.115]J.A. Short, D.G. Infield, and L.L. Freris, "Stabilization of grid frequency through dynamic demand control," *IEEE Trans. Power Syst.*, vol. 22, no. 3, pp. 1284–1293, Aug. 2007.

[1.116]R. Jia, M.H, Nehrir, and D.A. Pierre, "Voltage control of aggregate electric water heater load for distribution system peak load shaving using field data," in *Proc.* 39th North American Power Symposium (NAPS '07), Las Cruces, NM, 2007, pp. 492–497.

[1.117]J. Kondoh, N. Lu, and D.J. Hammerstrom, "An evaluation of the water heater load potential for providing regulation service," *IEEE Trans. Power Syst.*, vol. 26, no. 3, pp. 1309–1316, Aug. 2011.

[1.118]A. Molina-Garcia, F. Bouffard, and D.S. Kirschen, "Decentralized demand-side contribution to primary frequency control," *IEEE Trans. Power Syst.*, vol. 26, no. 1, pp. 411–419, Feb. 2011.

[1.119]D. Angeli and P.A. Kountouriotis, "A stochastic approach to dynamic-demand refrigerator control," *IEEE Trans. Control Syst. Technol.*, vol. 20, no. 3, pp. 581–592, May 2012.

[1.120]S.A. Pourmousavi and M.H. Nehrir, "Demand response for smart microgrid: Initial results," in *Proc.* IEEE PES Innovative Smart Grid Technologies (ISGT), Anahiem, CA, 2011, pp. 1–6.

[1.121]S.A. Pourmousavi, M.H. Nehrir, and C. Sastry, "Providing ancillary services through demand response with minimum load manipulation," in *Proc.* North American Power Symposium (NAPS), Boston, MA, 2011, pp. 1–6.

[1.122]K.Y. Huang, H.C. Chin, and Y.C. Huang, "A model reference adaptive control strategy for interruptible load management," *IEEE Trans. Power Syst.*, vol. 19, no. 1, pp. 683–689, Feb. 2004.

[1.123]F. De Ridder, M. Hommelberg, and E. Peeters, "Four potential business cases for demand side integration," in *Proc.* 6th International Conference on the European Energy Market, 2009, pp. 1–6.

[1.124]N. Ruiz, I. Cobelo, and J. Oyarzabal, "A direct load control model for virtual power plant management," *IEEE Trans. Power Syst.*, vol. 24, no. 2, pp. 959–966, May 2009.

[1.125]C.M. Colson, M.H. Nehrir, and S.A. Pourmousavi, "Towards real-time microgrid

power management using computational intelligence methods," in *Proc*. IEEE PES GM, Minneapolis, USA, July 2010, pp. 1–8.

[1.126]A.G. Tsikalakis and N.D. Hatziargyriou, "Centralized control for optimizing microgrids operation," *IEEE Trans. Energy Convers*., vol. 23, no. 1, pp. 241–248, Feb. 2008.

[1.127]S.A. Pourmousavi, et al., "Real-time energy management of a stand-alone hybrid wind-microturbine energy system using particle swarm optimization," *IEEE Trans. Sustain. Energy*, vol. 1, no 3, pp. 193–201, Oct. 2010.

[1.128]F.A. Mohamed and H.N. Kovio, "Power management strategy for solving power dispatch problems in microGrid for residential applications," in *Proc.* IEEE International Energy Conference and Exhibition, Manama, Bahrain 2010, pp. 746–751.

[1.129]Y. Riffonneau, et al., "Optimal power flow management for grid connected PV systems with batteries," *IEEE Trans. Sustain. Energy*, vol. 2, no. 3, pp. 309–320, Feb. 2011.

[1.130]B. Belvedere, et al., "A microcontroller-based power management system for standalone microgrids with hybrid power supply," *IEEE Trans. Smart Grid*, vol. 3, no. 3, pp. 422–431, May 2012.

[1.131]S.A. Pourmousavi, R.K. Sharma, and B. Asghari, "A framework for real-time power management of a grid-tied microgrid to extend battery lifetime and reduce cost of energy," in *Proc*. IEEE PES Innovative Smart Grid Technologies, Washington D.C., USA 2012, pp. 1–8.

[1.132]C.M. Colson and M.H. Nehrir, "Comprehensive real-time microgrid power management and control with distributed agents," *IEEE Trans. Smart Grid*, vol. 4, no. 1, pp. 617–627, Jan. 2013.

[1.133]C. Colson, et al., "Improving sustainability of hybrid energy systems Part II: Managing multiple objectives with a multi-agent system," *IEEE Trans. Sustain. Energy*, vol. 5, no. 1, pp. 46–54, Jan. 2014.

[1.134]A. Dewan, et al., "Alternative power sources for remote sensors: A review," *J. Power Sources*, vol. 245, pp. 129-143, Jan. 2014.

[1.135]M. Peng, L. Liu, and C. Jiang, "A review on the economic dispatch and risk management of the large-scale plug-in electric vehicles (PHEVs)-penetrated power systems," *Renew. Sust. Energ. Rev*., vol. 16, no. 3, pp. 1508–1515, Apr. 2012.

[1.136]Y.W. Li and C. Kao, "An accurate power control strategy for power-electronics

interfaced distributed generation units operating in a low-voltage multi-bus microgrid", *IEEE Trans. Power Electron*., vol. 24, no. 12, pp. 2977–2988, Dec. 2009.

[1.137]E. Serban and H. Serban, "A control strategy for a distributed power generation microgrid application with voltage- and current-controlled source converter", *IEEE Trans. Power Electron*., vol. 25, no. 12, pp. 2981–2992, May 2010.

[1.138]K. Jong-Yul, et al., "Cooperative control strategy of energy storage system and microsources for stabilizing the microgrid during islanded operation", *IEEE Trans. Power Electron*., vol. 25, no. 12, pp. 3037–3048, Sept. 2010.

[1.139]T.L. Vandoorn, et al., "A control strategy for islanded microgrids with DC-link voltage control", *IEEE Trans. Power Del*., vol. 26, no. 2, pp. 703–713, Jan. 2011.

[1.140]C. Cho, et al., "Active synchronizing control of a microgrid", *IEEE Trans. Power Electron*., vol. 26, no. 12, pp. 3707–3719, July 2011.

[1.141]S. Conti, et al., "Optimal dispatching of distributed generators and storage systems for MV islanded microgrids," *IEEE Trans. Power Del*., vol. 27, no. 3, pp. 1243–1251, May 2012.

[1.142]C.M. Fonseca and P.J. Fleming, "Multi-objective optimization and multiple constraint handling with evolutionary algorithms-Part I: a unified formulation," *IEEE Trans. on Systems, Man., and Cybernetics Part A: Systems and Humans*, vol. 28, no. 1, pp. 26–37, Jan. 1998.

[2.1] Solar Energy Industries Association, U.S. Solar Market Insight (TM): 2010 Year in Review (Executive Summary), 2010, Solar Energy Industries Association.

[2.2] T.S. Basso, "High-penetration, grid-connected Photovoltaic technology codes and standards," in *Proc.* 33rd IEEE Photovoltaic Specialists Conference, San Diego, USA, May 2008, pp. 1–6.

[2.3] IEEE STD 1547, *Standard for Interconnecting Distributed Resources with Electric Power Systems*, June 2003.

[2.4] P. Piagi and R.H. Lasseter, "Autonomous control of microgrids," in *Proc*. IEEE PES General Meeting, Montreal, CA, Jun. 2006, pp. 18–22.

[2.5] N. Hatziargyriou, "MICROGRIDS: Large scale integration of micro-generation to low voltage grids," EU Project No. ENK5-CT-2002-00610, Available online: http://www.microgrids.eu/micro2000/presentations/19.pdf

[2.6] P. Denholm and M. Hand, "Grid flexibility and storage required to achieve very

high penetration of variable renewable electricity," *Energ. Policy*, vol. 39, no. 3, pp. 1817–1830, March 2011.

[2.7] MATLAB® SimPowerSystems Toolbox: Users' Guide, Available online: http://www.mathworks.com/help/releases/R13sp2/pdf_doc/physmod/powersys/powersys.pdf

[2.8] C. Wang, "Modeling and control of hybrid wind/Photovoltaic/fuel cell distributed generation systems," Ph.D. Dissertation, Montana State University, Bozeman, 2006.

[2.9] National Renewable Energy Laboratory (NREL), "NREL: MIDC/Oahu irradiance grid," Available online: http://www.nrel.gov/midc/oahu_archive/

[2.10] California Energy Commission's Intermittency Analysis Project Study, "Appendix B - Impact of intermittent generation on operation of California power grid," Available online: http://www.uwig.org/CEC-500-2007-081-apb.pdf

[2.11] P. Kundur, *Power System Stability and Control*, McGraw-Hill Inc., 1994, ch. 11.

[2.12] D. Trudnowski, M. Donnelly, and E. Lightner, "Power-system frequency and stability control using decentralized intelligent loads," in *Proc.* IEEE PES Conference and Exhibition Transmission and Distribution, Dallas, USA, May 2005, pp. 1453–1459.

[2.13] J.A. Short, D.G. Infield, and L.L. Freris, "Stabilization of grid frequency through dynamic demand control," *IEEE Trans. on Power Syst.*, vol. 22, no. 3, pp. 1284–1293, Aug. 2007.

[2.14] D. Das, "A fuzzy multiobjective approach for network reconfiguration of distribution systems," *IEEE Trans. Power Del.*, vol. 21, no. 1, pp. 202–209, Jan. 2006.

[2.15] Y.G. Rebours, et al., "A survey of frequency and voltage control ancillary services—Part I: Technical features" , *IEEE Trans. Power Syst.*, vol. 22, no. 1, pp. 350–357, Feb. 2007.

[2.16] S.A. Pourmousavi and M.H. Nehrir, "Demand response for smart microgrid: Initial results," in *Proc.* 2nd IEEE PES Innovative Smart Grid Technologies Conference, Anaheim, USA, Jan. 2011, pp. 1–6.

[2.17] S.A. Pourmousavi, M.H. Nehrir, and C. Sastry, "Providing ancillary services through demand response with minimum load manipulation," in *Proc.* North American Power Symposium, Boston, USA, Aug. 2011, pp. 1–6.

[2.18] J.D. Glover, M.S. Sarma, and T.J. Overbye, *Power System Analysis and Design*, Stamford, CT, Cengage Learning, 2008, ch. 11.

[2.19] B.L. Schenkman, D.G. Wilson, and R.D. Robinett III, "Photovoltaic distributed generation for Lanai power grid real-time simulation and control integration scenario," in *Proc.* International Symposium on Power Electronics, Electrical Drives, Automation and Motion, Pisa, Italy, 2010, pp. 154–157.

[3.1] U.S. Dept. of Energy, "Benefits of demand response in electricity markets and recommendations for achieving them," A report to U.S. Congress, Feb. 2006. Available online: http://eetd.lbl.gov/ea/ems/reports/congress-1252d.pdf

[3.2] Federal Energy Regulatory Commission, "Assessment of demand response and advanced metering," A report to U.S. Congress, Dec. 2008. Available online: http://www.ferc.gov/legal/staff-reports/demand-response.pdf

[3.3] G.C. Heffner, C.A. Goldman, and M.M. Moezzi, "Innovative approaches to verifying demand response of water heater load control," *IEEE Trans. Power Del.*, vol. 21, no. 1, pp. 388–397, Jan. 2006.

[3.4] R. Jia, M.H, Nehrir, and D.A. Pierre, "Voltage control of aggregate electric water heater load for distribution system peak load shaving using field data," in *Proc.* 39th North American Power Symposium (NAPS '07), 2007, pp. 492–497.

[3.5] J. Kondoh, N. Lu, and D.J. Hammerstrom, "An evaluation of the water heater load potential for providing regulation service," *IEEE Trans. Power Syst.*, vol. 26, no. 3, pp. 1309–1316, Aug. 2011.

[3.6] N. Lu and S. Katipamula, "Control strategies of thermostatically controlled appliances in a competitive electricity market," in *Proc.* Power Engineering Society General Meeting, vol. 1, pp. 202–207, 2005.

[3.7] R. Walawalkar, et al., "An economic welfare analysis of demand response in the PJM electricity market," *Energ. Policy*, vol. 36, no. 10, pp. 3692–3702, Oct. 2008.

[3.8] M. Klobasa, "Analysis of demand response and wind integration in Germany's electricity market," *IET Renew. Pow. Gen.*, vol. 4, no. 1, pp. 55–63, Jan. 2010.

[3.9] A. Brooks, et al., "Demand dispatch: using real-time control of demand to help balance generation and load," *IEEE Power Energy Mag.*, vol. 8, no. 3, pp. 20–29, May/June 2010.

[3.10] J. Medina, N. Muller, and I. Roytelman, "Demand response and distribution grid operations: opportunities and challenges," *IEEE Trans. Smart Grid*, vol. 1, no. 2, pp. 193–198, Sept. 2010.

[3.11] H. Saele and O.S. Grande, "Demand response from household customers: experiences from a pilot study in Norway," *IEEE Trans. Smart Grid*, vol. 2, no. 1, pp. 102–109, 2011.

[3.12] A.J. Conejo, J.M. Morales, and L. Baringo, "Real-time demand response model," *IEEE Trans. Smart Grid*, vol. 1, no. 3, pp. 236–242, Dec. 2010.

[3.13] D.T. Nguyen, M. Negnevitsky, and M. de Groot, "Pool-based demand response exchange—concept and modeling," *IEEE Trans. Power Syst.*, vol. 26, no. 3, pp. 1677–1685, Aug. 2011.

[3.14] P. Faria, et al., "Demand response management in power systems using a particle swarm optimization approach," *IEEE Intell. Syst.*, vol. 28, no. 4, pp. 43–51, July 2013.

[3.15] M. Parvania and M. Fotuhi-Firuzabad, "Integrating load reduction into wholesale energy market with application to wind power integration," *IEEE Syst. J.*, vol. 6, no. 1, pp. 35–45, March 2012.

[3.16] K. Dietrich, et al., "Demand response in an isolated system with high wind integration," *IEEE Trans. Power Syst.*, vol. 27, no. 1, pp. 20–29, Feb. 2012.

[3.17] D. Trudnowski, M. Donnelly, and E. Lightner, "Power-system frequency and stability control using decentralized intelligent loads," in *Proc.* IEEE PES Conference and Exhibition Transmission and Distribution, pp. 1453–1459, 2005.

[3.18] J.A. Short, D.G. Infield, and L.L. Freris, "Stabilization of grid frequency through dynamic demand control," *IEEE Trans. Power Syst.*, vol. 22, no. 3, pp. 1284–1293, Aug. 2007.

[3.19] A. Molina-García, F. Bouffard, and D.S. Kirschen, "Decentralized demand-side contribution to primary frequency control," *IEEE Trans. Power Syst.*, vol. 26, no. 1, pp. 411–419, Feb. 2011.

[3.20] D. Angeli and P-A. Kountouriotis, "A stochastic approach to dynamic-demand refrigerator control," *IEEE Trans. Control Syst. Technol.*, vol. 20, no. 3, pp. 581–592, May 2012.

[3.21] S.A. Pourmousavi and M.H. Nehrir, "Demand response for smart microgrid: Initial results," in *Proc.* IEEE PES Innovative Smart Grid Technologies (ISGT), pp. 1–6, 2011.

[3.22] S.A. Pourmousavi, M.H. Nehrir, and C. Sastry, "Providing ancillary services through demand response with minimum load manipulation," in *Proc.* North American Power Symposium (NAPS), pp. 1–6, 2011.

[3.23] North American Electric Reliability Corporation, "Standard BAL-004-0 - Time Error Correction," Apr. 2005. Available online: http://www.nerc.com/files/BAL-004-0.pdf

[3.24] F. Katiraei, M.R, Iravani, and P.W. Lehn, "Micro-grid autonomous operation during and subsequent to islanding process," *IEEE Trans. Power Del.*, vol. 20, no. 1, pp. 248–257, Jan. 2005.

[3.25] V. Menon and M.H. Nehrir, "A hybrid islanding detection technique using voltage unbalance and frequency set point," *IEEE Trans. Power Syst.*, vol. 22, no. 1, pp. 442–448, Feb. 2007.

[3.26] MATLAB/Simulink SimPowerSystems Documentation, Available online: http://www.mathworks.com/

[3.27] IEEE Std 421.5-2005 (Revision of IEEE Std 421.5-1992), "IEEE recommended practice for excitation system models for power system stability studies," pp. 1–85, 2006.

[3.28] A. Yazdani and R. Iravani, *Voltage-Sourced Converters in Power Systems: Modeling, Control, and Applications*, Wiley-IEEE Press, John & Sons, 2010.

[4.1] S.A. Pourmousavi, A.S. Cifala, and M.H. Nehrir, "Impact of high penetration of PV generation on frequency and voltage in a distribution feeder," in *Proc*. North American Power Symposium (NAPS), Champaign, IL, 2012, pp. 1–8.

[4.2] K. Kawamura, et al., "Avoided cost of effects of voltage control by demand response in a distribution network with high integration of rooftop PV," in *Proc.* Innovative Smart Grid Tech. IEEE PES., Washington DC, 2013, pp. 1–6.

[4.3] S.A. Pourmousavi and M.H. Nehrir, "Demand response for smart microgrid: Initial results," in *Proc*. Innovative Smart Grid Tech. IEEE PES., Anaheim, CA, 2011, pp. 1–6.

[4.4] J.A. Taylor, et al., "Price and capacity competition in zero-mean storage and demand response markets," in *Proc.* 50th Annual Allerton Conference on Communication, Control, and Computing, , Monticello, IL, 2012, pp. 1316–1323.

[4.5] N. Navid-Azarbaijani and M.H. Banakar, "Realizing load reduction functions by aperiodic switching of load groups," *IEEE Trans. Power Syst*., vol. 27, no. 1, pp. 721–727, May 1996.

[4.6] K.Y. Huang, H.C. Chin, and Y.C. Huang, "A model reference adaptive control strategy for interruptible load management," *IEEE Trans. Power Syst*., vol. 19, no. 1, pp. 683–689, Feb. 2004.

[4.7] D. Westermann and A. John, “Demand matching wind power generation with wide-area measurement and demand-side management,” *IEEE Trans. Energy Covers*., vol. 22, no. 1, pp. 145–149, March 2007.

[4.8] R. Jia, M.H. Nehrir, and D.A. Pierre, "Voltage control of aggregate electric water heater load for distribution system peak load shaving using field data," in *Proc.* 39th North American Power Symposium (NAPS ’07), pp. 492–497.

[4.9] M.H. Nehrir, B.J. LaMeres, and V. Gerez, "A customer-interactive electric water heater demand-side management strategy using fuzzy logic," in *Proc*. IEEE PES Winter Meeting, vol. 1, New York, NY, 1999, pp. 433–436.

[4.10] S.N. Patrick, “Control of aggregate electric water heaters for load shifting and balancing intermittent renewable energy generation in a smart grid environment,” M.S. Thesis, Department of Electrical and Computer Engineering, Montana State University, Bozeman, 2011.

[4.11] N. Lu and S. Katipamula, "Control strategies of thermostatically controlled appliances in a competitive electricity market," in *Proc.* 2005 IEEE PES General Meeting, 2005, pp. 202–207.

[4.12] W. Xiao and W.G. Dunford, “A modified adaptive hill climbing MPPT method for photovoltaic power systems,” in *Proc.* IEEE 35th Annual Power Electronics Specialists Conference, vol. 3, 2004, pp. 1957–1963.

[4.13] X. Yu and K. Tomsovic, “Application of linear matrix inequalities for load frequency control with communication delays,” *IEEE Trans. Power Syst*., vol. 19, no. 3, pp. 1508–1515, Aug. 2004.

[4.14] Y.G. Rebours, et al., “A survey of frequency and voltage control ancillary services-Part I: Technical features,” *IEEE Trans. Power Syst*., vol. 22, no. 1, pp. 350–357, Feb. 2007.

[4.15] A. Brooks, et al., “Demand dispatch: using real-time control of demand to help balance generation and load,” *IEEE Power Energy Mag.*, vol. 8, no. 3, pp. 20–29, May/June 2010.

[4.16] C.M. Colson, “Toward real-time power management of microgrids for power system integration: A decentralized multi-agent based approach,” Ph.D. Dissertation, Montana State University, 2012.

[4.17] C.M. Colson and M.H. Nehrir, “Comprehensive real-time microgrid power management and control with distributed agents,” *IEEE Trans. Smart Grid*, vol. 4, no. 1, pp. 617–627, March 2013.

[4.18] S.A. Pourmousavi and M.H. Nehrir, "Real-time central demand response for primary frequency regulation in microgrids," *IEEE Trans. Smart Grid*, vol. 3, no. 4, pp. 1988-1996, Dec. 2012.

[5.1] U.S. Dept. of Energy, "Benefits of demand response in electricity markets and recommendations for achieving them," a report to U.S. Congress, Feb. 2006. Available online: http://eetd.lbl.gov/ea/ems/reports/congress-1252d.pdf

[5.2] Federal Energy Regulatory Commission, "Assessment of demand response and advanced metering," A report to U.S. Congress, Dec. 2008. Available online: http://www.ferc.gov/legal/staff-reports/demand-response.pdf

[5.3] M.H. Albadi and E.F. El-Saadany, "A summary of demand response in electricity markets," *Electr. Pow. Syst. Res.*, vol. 78, no. 11, pp. 1989–1996, Nov. 2008.

[5.4] A. Brooks, et al., "Demand dispatch: using real-time control of demand to help balance generation and load," *IEEE Power Energy Mag.*, vol. 8, no. 3, pp. 20–29, May/June 2010.

[5.5] D. Trudnowski, M. Donnelly, and E. Lightner, "Power-system frequency and stability control using decentralized intelligent loads," in *Proc.* IEEE PES Transmission and Distribution Conf. and Exhibition, Dallas, TX, 2005, pp. 1453–1459.

[5.6] G.C. Heffner, C.A. Goldman, and M.M. Moezzi, "Innovative approaches to verifying demand response of water heater load control," *IEEE Trans. Power Del.*, vol. 21, no. 1, pp. 388–397, Jan. 2006.

[5.7] J.A. Short, D.G. Infield, and L.L. Freris, "Stabilization of grid frequency through dynamic demand control," *IEEE Trans. Power Syst.*, vol. 22, no. 3, 1284–1293, Aug. 2007.

[5.8] R. Jia, M.H. Nehrir, and D.A. Pierre, "Voltage control of aggregate electric water heater load for distribution system peak load shaving using field data," in *Proc.* 39th North American Power Symposium (NAPS '07), Las Cruces, NM, 2007, pp. 492–497.

[5.9] J. Kondoh, N. Lu, and D.J. Hammerstrom, "An evaluation of the water heater load potential for providing regulation service," *IEEE Trans. Power Syst.*, vol. 26, no. 3, pp. 1309–1316, Aug. 2011.

[5.10] A. Molina-Garcia, F. Bouffard, and D.S. Kirschen, "Decentralized demand-side contribution to primary frequency control," *IEEE Trans. Power Syst.*, vol. 26, no. 1, pp. 411–419, Feb. 2011.

[5.11] D. Angeli and P-A. Kountouriotis, "A stochastic approach to dynamic-demand

refrigerator control," *IEEE Trans. Control Syst. Technol.*, vol. 20, no. 3, pp. 581–592, May 2012.

[5.12] S.A. Pourmousavi and M.H. Nehrir, "Demand response for smart microgrid: Initial results," in *Proc*. IEEE PES Innovative Smart Grid Technologies (ISGT), Anahiem, CA, 2011, pp. 1–6.

[5.13] S.A. Pourmousavi, M.H. Nehrir, and C. Sastry, "Providing ancillary services through demand response with minimum load manipulation," in *Proc*. North American Power Symposium (NAPS), Boston, MA, 2011, pp. 1–6.

[5.14] J. Medina, N. Muller, and C.I. Roytelman, "Demand response and distribution grid operations: opportunities and challenges," *IEEE Trans. Smart Grid*, vol. 1, no. 2, pp. 193–198, Sept. 2010.

[5.15] H. Saele and O.S. Grande, "Demand response from household customers: experiences from a pilot study in Norway," *IEEE Trans. Smart Grid*, vol. 2, no. 1, pp. 102–109, March 2011.

[5.16] A.J. Conejo, J.M. Morales, and L. Baringo, "Real-time demand response model," *IEEE Trans. Smart Grid*, vol. 1, no. 3, pp. 236–242, Dec. 2010.

[5.17] D.T. Nguyen, M. Negnevitsky, and M. de Groot, "Pool-based demand response exchange-concept and modeling," *IEEE Trans. Power Syst.*, vol. 26, no. 3, pp. 1677–1685, Aug. 2011.

[5.18] R. Walawalkar, at al., "An economic welfare analysis of demand response in the PJM electricity market," *Energ. Policy*, vol. 36, no. 10, pp. 3692–3702, Oct. 2008.

[5.19] M. Klobasa, "Analysis of demand response and wind integration in Germany's electricity market," *IET Renew. Pow. Gen.*, vol. 4, no. 1, pp. 55–63, Jan. 2010.

[5.20] PJM Electricity Utility, Available online: http://pjm.com/about-pjm.aspx

[5.21] MATLAB/ Optimization Toolbox, document, Available online: http://www.mathworks.com/help/pdf_doc/optim/optim_tb.pdf

[5.22] A. Antoniou and W.S. Lu, *Practical optimization algorithms and engineering applications*, Springer Science, NY, 2007.

[5.23] F. Katiraei, M.R, Iravani, and P.W. Lehn, "Micro-grid autonomous operation during and subsequent to islanding process," *IEEE Trans. Power Del.*, vol. 20, no. 1, pp. 248–257, Jan. 2005.

[5.24] V. Menon and M.H. Nehrir, "A hybrid islanding detection technique using voltage unbalance and frequency set point," *IEEE Trans. Power Syst.*, vol. 22, no. 1, pp. 442–448, Feb. 2007.

[5.25] MATLAB/Simulink SimPowerSystems document, Available online: http://www.mathworks.com/

[6.1] R. Doherty and M. O'Malley, "A new approach to quantify reserve demand in systems with significant installed wind capacity," *IEEE Trans. Power Syst*., vol. 20, no. 2, pp. 587–595, May 2005.

[6.2] U.S. Department of Energy. (2011, September 28). Smart Grid, Available online: http://energy.gov/oe/technology-development/smart-grid.

[6.3] C. Goldman, et al., "Coordination of energy efficiency and demand response a resource of the National Action Plan for Energy Efficiency," U.S Environmental Protection Agency and U.S. Department of Energy, Tech. Rep., 2010.

[6.4] R. Walawalkar, et al., "An economic welfare analysis of demand response in the PJM electricity market," *Energ. Policy*, vol. 36, no. 10, pp. 3692–3702, Oct. 2008.

[6.5] M. Klobasa, "Analysis of demand response and wind integration in Germany's electricity market," *IET Renew. Power Gener*., vol. 4, no. 1, pp. 55–63, Jan. 2010.

[6.6] A. Brooks, et al., "Demand dispatch: Using real-time control of demand to help balance generation and load," *IEEE Power Energy Mag*., vol. 8, no. 3, pp. 20–29, May/June 2010.

[6.7] J. Medina, N. Muller, and I. Roytelman, "Demand response and distribution grid operations: Opportunities and challenges," *IEEE Trans. Smart Grid*, vol. 1, no. 2, pp. 193–198, Sept. 2010.

[6.8] H. Saele and O.S. Grande, "Demand response from household customers: Experiences from a pilot study in Norway," *IEEE Trans. Smart Grid*, vol. 2, no. 1, pp. 102–109, March 2011.

[6.9] N. Ruiz, I. Cobelo, and J. Oyarzaabal, "A direct load control model for virtual power plant management," *IEEE Trans. Power Syst*., vol. 24, no. 2, pp. 959–966, May 2009.

[6.10] A.J. Conejo, J.M. Morales, and L. Baringo, "Real-time demand response model," *IEEE Trans. Smart Grid*, vol. 1, no. 3, pp. 236–242, Dec. 2010.

[6.11] D.T. Nguyen, M. Negnevitsky, and M. de Groot, "Pool-based demand response exchange-concept and modeling," *IEEE Trans. Power Syst*., vol. 26, no. 3, pp. 1677–1685, Aug. 2011.

[6.12] P. Faria, et al., "Demand response management in power systems using a particle swarm optimization approach," *IEEE Intell. Syst*., vol. 28, no. 4, pp. 43–51, July/Aug. 2013.

[6.13] M. Parvania and M. Fotuhi-Firuzabad, "Integrating load reduction into wholesale energy market with application to wind power integration," *IEEE Syst. J*., vol. 6, no. 1, pp. 35–45, March 2012.

[6.14] K. Dietrich, et al., "Demand response in an isolated system with high wind integration," *IEEE Trans. Power Syst*., vol. 27, no. 1, pp. 20–29, Feb. 2012.

[6.15] M. Rastegar, M. Fotuhi-Firuzabad, and F. Aminifar, "Load commitment in a smart home," *J. Appl. Energy*, vol. 96, pp. 45–54, Aug. 2012.

[6.16] N. Navid-Azarbaijani and M.H. Banakar, "Realizing load reduction functions by aperiodic switching of load groups," *IEEE Trans. Power Syst*., vol. 11, no. 2, pp. 721–727, May. 1996.

[6.17] K.Y. Huang, et al., "A model reference adaptive control strategy for interruptible load management," *IEEE Trans. Power Syst*., vol. 19, no. 1, pp. 683–689, Feb. 2004.

[6.18] D. Westermann and A. John, "Demand matching wind power generation with wide-area measurement and demand-side management," *IEEE Trans. Energy Convers*., vol. 22, no. 1, pp. 145–149, March 2007.

[6.19] S.A. Pourmousavi and M.H. Nehrir, "Demand response for smart microgrid: initial results," in *Proc*. 2nd IEEE PES Innov. Smart Grid Technol. (ISGT), California, 2011, pp. 1–6.

[6.20] S.A. Pourmousavi, M.H. Nehrir, and C. Sastry, "Providing ancillary services through demand response with minimum load manipulation," in *Proc*. 43rd North Amer. Power Symp. (NAPS), Massachusett, 2011, pp. 1–6.

[6.21] S.A. Pourmousavi and M.H. Nehrir, "Real-time central demand response for primary frequency regulation in microgrids," *IEEE Trans. Smart Grid*, vol. 3, no. 4, pp. 1988-1996, Dec. 2012.

[6.22] D. Trudnowski, M. Donnelly, and E. Lightner, "Power-system frequency and stability control using decentralized intelligent loads," in *Proc*. IEEE PES Conf. Exhib. Transm. Distrib., Texas, 2005, pp. 1453–1459.

[6.23] J.A. Short, D.G. Infield, and L.L. Freris, "Stabilization of grid frequency through dynamic demand control," *IEEE Trans. Power Syst*., vol. 22, no. 3, pp. 1284–1293, Aug. 2007.

[6.24] A. Molina-García, F. Bouffard, and D.S. Kirschen, "Decentralized demand-side contribution to primary frequency control," *IEEE Trans. Power Syst*., vol. 26, no. 1, pp. 411–419, Feb. 2011.

[6.25] D. Jay and K.S. Swarup, "Dynamic demand response and control in smart grid environment," In *Proc*. Annual IEEE India Conference (INDICON), Hyderabad, 2011, pp. 1–4.

[6.26] D. Jay and K.S. Swarup, "Frequency restoration using dynamic demand control under smart grid environment," In *Proc*. IEEE PES Innovative Smart Grid Technologies – India (ISGT India), Kerala, 2011, pp. 311–315.

[6.27] K. Samarakoon, J. Ekanayake, and N. Jenkins, "Investigation of domestic load control to provide primary frequency response using smart meters," *IEEE Trans. Smart Grid*, vol. 3, no.1, pp. 282–292, March 2012.

[6.28] D. Angeli and P.A. Kountouriotis, "A stochastic approach to dynamic demand refrigerator control," *IEEE Trans. Control Syst. Technol*., vol. 20, no. 3, pp. 581–592, May 2012.

[6.29] Z. Changhong, U. Topcu, and S.H. Low, "Frequency-based load control in power systems," In *Proc*. American Control Conference (ACC), Canada, 2012, pp. 4423–4430.

[6.30] L.R. Chang-Chien, et al., "Incorporating demand response with spinning reserve to realize an adaptive frequency restoration plan for system contingencies," *IEEE Trans. Smart Grid*, vol. 3, no. 3, pp. 1145–1153, Sept. 2012.

[6.31] H. Huang and F. Li, "Sensitivity analysis of load-damping characteristic in power system frequency regulation," *IEEE Trans. Power Syst*., vol. 28, no. 2, pp. 1324–1335, May 2013.

[6.32] I. Ibraheem, P. Kumar, and D.P. Kothari, "Recent philosophies of automatic generation control strategies in power systems," *IEEE Trans. Power Syst*., vol. 20, no. 1, pp. 346–357, Feb. 2005.

[6.33] H. Bevrani, *Robust Power System Frequency Control*, New York: Springer, 2009, ch. 1–3.

[6.34] C.C. Wu, et al., "Role and value of pumped storage units in an ancillary services market for isolated power system-simulation in the Taiwan power system," *IEEE Trans. Ind. Appl.*, vol. 44, no. 6, pp. 1924–1929, Nov/Dec 2008.

[6.35] J.Mickey, "Using load resources to meet ancillary service requirements in the ERCOT market: A case study," in *Proc*. IEEE PES Gen. Meet., Minnesota, 2010, pp. 1-2.

[6.36] P. Kundur, *Power system Stability and Control*. New York: McGraw-Hill, 1994, ch. 11.

[6.37] R.C. Dorf and R.H. Bishop, *Modern Control Systems*: 7th ed., New York: Addison-Wesley Publishing Company, 1995, p. 807.

[6.38] G.H. Golub and C.F. Van Loan, *Matrix Computations*: 3rd ed., Baltimore: The Johns Hopkins University Press, 1996, pp. 572-574.

[6.39] G.F. Franklin, J.D. Powell, and A. Emami-Naeini, *Feedback Control of Dynamic Systems*: 3rd ed., New York: Addison-Wesley Publishing Company, 1994, p. 778.

[6.40] C.E. Fosha and O.I. Elgerd, "The megawatt-frequency control problem: A new approach via optimal control theory," *IEEE Trans. Power Ap. Syst*., vol. PAS-98, no. 4, pp. 563–577, April 1970.

[6.41] E.C. Tacker, et al., "Optimal control of interconnected electric energy systems: a new formulation," *IEEE Proc. letters*, vol. 60, no. 10, pp. 1239–1241, Oct. 1972.

[6.42] G. Shirai, "Load frequency control using Lyapunov's second method: Bang-bang control of speed changer position," *IEEE Proc. letters*, vol. 67, no. 10, pp. 1458–1459, Oct. 1979.

[6.43] S.C. Tripathy, et al., "Sampled data automatic generation control analysis with reheat steam turbines and governor dead-band effects," *IEEE Trans. Power Ap. Syst*., vol. PAS-103, no. 5, pp. 1045–1051, May 1984.

[6.44] T. Hiyama, "Design of decentralized load-frequency regulators for interconnected power systems," in *Proc*. IEE Generation, Transmission, and Distribution conf., vol. 129, no. 1, 1982, pp. 17–23.

[7.1] R. Walawalkar, et al., "An economic welfare analysis of demand response in the PJM electricity market," *Energ. Policy*, vol. 36, no. 10, pp. 3692–3702, Oct. 2008.

[7.2] H. Bevrani, *Robust Power System Frequency Control*, New York: Springer, 2009, ch. 1–3.

[7.3] S.A. Pourmousavi and M.H. Nehrir, "Introducing dynamic demand response in the LFC model," *IEEE Trans. Power Syst*., vol. 29, no. 4, pp. 1562–1572, July 2014.

[7.4] H. Kawabata and M. Kido, "A decentralized scheme of load frequency control power system," *Elect. Eng. Japan*, vol. 102, no. 4, pp. 100–106, Jul./Aug. 1982.

[7.5] Y.M. Park and K.Y. Lee, "Optimal decentralized load frequency control," *Elect. Power Syst. Res*., vol. 7, no. 4, pp. 279–288, Sept. 1984.

[7.6] M.S. Calovic, "Automatic generation control: Decentralized area-wise optimal solution," *Elect. Power Syst. Res*., vol. 7, no. 2, pp. 115–139, Apr. 1984.

[7.7] M. Aldeen and J.F. Marsh, "Observability, controllability and decentralized control of interconnected power systems," *Int. J. Comput. Elect. Eng*., vol. 16, no. 4, pp. 207–220, 1990.

[7.8] M. Aldeen and J.F. Marsh, "Decentralized proportional-plus-integral control design method for interconnected power systems," in *Proc*. Inst. Elect. Eng., vol. 138, no. 4, pp. 263–274, Jul. 1991.

[7.9] M. Aldeen, "Interaction modeling approach to distributed control with application to power systems," *Int. J. Contr*., vol. 53, no. 5, pp. 1035–1054, 1991.

[7.10] T.C. Yang, H. Cimen, and Q.M. Zhu, "Decentralised load-frequency controller design based on structured singular values," in *Proc*. Inst. Elect. Eng. C, vol. 145, no. 1, pp. 7–14, Jan. 1998.

[7.11] T.C. Yang, Z.T. Ding, and H. Yu, "Decentralised power system load frequency control beyond the limit of diagonal dominance," *Int. J. Elect. Power Energy Syst*., vol. 24, no. 3, pp. 173–184, Mar. 2002.

[7.12] E.V. Bohn and S.M. Miniesy, "Optimum load frequency sample data control with randomly varying system disturbances," *IEEE Trans. Power App. Syst*., vol. PAS-91, no. 5, pp. 1916–1923, Sept./Oct. 1972.

[7.13] K. Yamashita and T. Taniguchi, "Optimal observer design for load frequency control," *Int. J. Elect. Power Energy Syst*., vol. 8, no. 2, pp. 93–100, Apr. 1986.

[7.14] A. Feliachi, "Load frequency control using reduced order models and local observers," *Int. J. Energy Syst*., vol. 7, no. 2, pp. 72–75, 1987.

[7.15] A. Rubaai and V. Udo, "An adaptive control scheme for LFC of multi-area power systems. Part I: Identification and functional design, Part-II: Implementation and test results by simulation," *Elect. Power Syst. Res*., vol. 24, no. 3, pp. 183–197, Sept. 1992.

[7.16] S. Velusami and K. Ramar, "Design of observer-based decentralized load-frequency controllers for interconnected power systems," *Int. J. Power Energy Syst*., vol. 17, no. 2, pp. 152–160, 1997.

[7.17] Y. Hain, R. Kulessky, and G. Nudelman, "Identification-based power unit model for load-frequency control purposes," *IEEE Trans. Power Syst*., vol. 15, no. 4, pp. 1313–1321, Nov. 2000.

[7.18] C.E. Fosha and O.I. Elgerd, "The megawatt-frequency control problem: A new approach via optimal control theory," *IEEE Trans. Power Ap. Syst*., vol. PAS-98, no. 4, pp. 563–577, April 1970.

[7.19] A. Brooks, et al., "Demand dispatch: Using real-time control of demand to help balance generation and load," *IEEE Power Energy Mag.*, vol. 8, no. 3, pp. 20–29, May/June 2010.

[7.20] T. Hiyama, "Design of decentralized load-frequency regulators for interconnected power systems," in *Proc*. IEE Generation, Transmission, and Distribution conf., vol. 129, no. 1, pp. 17–23, 1982.

[7.21] D. Rerkpreedapong, A. Hasanovic, and A. Feliachi, "Robust load frequency control using genetic algorithms and linear matrix inequalities," *IEEE Trans. Power Syst*., vol. 18, no. 2, pp. 855–861, May 2003.

[8.1] U.S. Department of Energy. (2011, September 28). Smart Grid. Available online: http://energy.gov/oe/technology-development/smart-grid.

[8.2] H. Holttinen, et al., "Design and operation of power systems with large amounts of wind power", VTT Technical Research Centre of Finland, Helsinki, Finland, Rep. 2493, 2009.

[8.3] R. Doherty and M. O'Malley, "A new approach to quantify reserve demand in systems with significant installed wind capacity", *IEEE Trans. Power Syst*., vol. 20, no. 2, pp. 587–595, May 2005.

[8.4] P. Denholm, et al., "The role of energy storage with renewable electricity generation," National Renewable Energy Laboratory, Technical Report NREL/TP-6A2-47187, Jan. 2010.

[8.5] U.S. Energy Information Administration. (2011, September 28). Residential Energy Consumption Survey. Available online: http://www.eia.gov/consumption/residential/reports/electronics.cfm.

[8.6] M.H. Nehrir, B.J. LaMeres, and V. Gerez, "A customer-interactive electric water

heater demand-side management strategy using fuzzy logic," in *Proc.* IEEE Power Engineering Society Winter Meeting, New York City, NY, 1999, pp. 433–436.

[8.7] M.H. Nehrir, et al., "Power management of aggregate electric water heater loads by voltage control," in *Proc.* IEEE Power Engineering Society General Meeting, Tampa, FL, 2007, pp. 492–497.

[8.8] N. Lu and S. Katipamula, "Control strategies of thermostatically controlled appliances in a competitive electricity market," in *Proc.* IEEE Power Engineering Society General Meeting, San Francisco, CA, 2005, pp. 202–207.

[8.9] N. Lu and T. Nguyen, "Grid Friendly™ Appliances – load-side solution for congestion management", in *Proc.* Transmission and Distribution Conf. and Exhibition, 2005/2006 IEEE PES, Dallas, TX, 2006, pp. 1269–1273.

[8.10] D.S. Callaway, "Tapping the energy storage potential in electric loads to deliver load following and regulation, with application to wind energy," *Energ. Convers. Manag*., vol. 50, no. 9, pp. 1389–1400, May 2009.

[8.11] S. Parkinson, et al., "Comfort-constrained distributed heat pump management," in *Proc*. IEEE Intersoc. Electr. Electron. Eng. (ICSGCE 2011), Piscataway, NJ, 2011.

[8.12] D. Wang, et al., "Online voltage security assessment considering comfort-constrained demand response control of distributed heat pump systems," *Appl. Energy*, vol. 96, no. 3, pp. 104–114, Aug. 2012.

[8.13] N. Lu, D.J. Hammerstrom, and S.N. Patrick, "Grid Friendly™ Device model development and simulation," Pacific Northwest National Laboratory, Richland, WA, Rep. 18998, 2009.

[8.14] J.A. Short, et al, "Stabilization of grid frequency through dynamic demand control", *IEEE Trans. Power Syst*., vol. 22, no. 3, pp. 1284–1293, Aug. 2007.

[8.15] J. Kondoh, N. Lu, and D.J. Hammerstrom, "An evaluation of the water heater load potential for providing regulation service," *IEEE Trans. Power Syst*., vol. 26, no. 3, pp. 1309–1316, Aug. 2011.

[8.16] N. Lu, "An evaluation of the HVAC load potential for providing load balancing service," *IEEE Trans. Smart Grid*, vol. 3, no. 3, pp. 1263–1270, Sept. 2012.

[8.17] N. Lu and Y. Zhang, "Design considerations of a centralized load controller using thermostatically controlled appliances for regulation reserves," *IEEE Trans. Smart Grid*, vol. 4, no. 2, pp. 914–921, Dec. 2012.

[8.18] D. Shively, et al, "Energy storage methods for renewable energy integration and grid support", in *Proc.* IEEE Energy 2030 Conf., Atlanta, GA, 2008, pp. 1–6.

[8.19] Bonneville Power Administration, "Wind generation and total load in the BPA balancing authority," Available online: http://transmission.bpa.gov/Business/Operations/Wind/

[8.20] P.S. Dolan and M.H. Nehrir, "Development of a residential electric water heater model using energy flow analysis," in *Proc.* 24th North American Power Symposium conference, Nevada, USA, Oct 1992, pp. 272–277.

[8.21] "Descriptions of electric energy use in single family residences in the pacific northwest, 1986-1992," Office of Energy Resources, Bonneville Power Administration, Portland, OR, Dec. 1992.

[8.22] S.N. Patrick, "Control of aggregate EWHs for load shifting and balancing intermittent renewable energy generation in a smart grid environment," M.S thesis in Electrical Engineering, Montana State University-Bozeman, 2011.

[8.23] M.L. Katcher, "Scald burns from hot tap water", *J. Amer. Medical Assoc.*, vol. 246, no. 11, pp. 1219–1292, Sept. 1981.

[8.24] A. Brooks, et al., "Demand dispatch: Using real-time control of demand to help balance generation and load," *IEEE Power Energy Mag*., vol. 8, no. 3, pp. 20–29, May/June 2010.

[8.25] Pacific Power. (2011, May 31). Comparing Your Power Options. Available online: http://www.pacificpower.net/content/dam/pacific_power/doc/Your_Account/Pay_Your_Bill/Highlights_August_10/2190-37_PP_LabelInsert_Residential-OR.pdf.

[8.26] Pacific Power. (2011, May 31). Oregon On-Peak & Off-Peak Hours. Available online: http://www.pacificpower.net/ya/po/otou/ooh.html.

[9.1] U.S. DOE, office of electric transmission and distribution, "Grid 2030: A national vision for electricity's second 100 years," July 2003.

[9.2] N. Hatziargyriou, et al., "Energy management and control of island power systems with increased penetration from renewable sources," in *Proc*. IEEE PES Winter Meeting, vol. 1, New York, USA 2002, pp. 335–339.

[9.3] M. Korpås and A.T. Holen, "Operation planning of hydrogen storage connected to wind power operating in a power market," *IEEE Trans. Energy Convers*., vol. 21, no. 3, pp. 742–749, Sept. 2006.

[9.4] S. Chakraborty and M.G. Simoes, “PV-microgrid operational cost minimization by neural forecasting and heuristic optimization,” in *Proc*. IEEE Industry Applications Society Annual Meeting, Edmonton, Canada 2008, pp. 1–8.

[9.5] S.A. Pourmousavi, et al., "Real-time energy management of a stand-alone hybrid wind-microturbine energy system using particle swarm optimization," *IEEE Trans. Sustain. Energy*, vol. 1, no 3, pp. 193–201, Oct. 2010.

[9.6] F.A. Mohamed and H.N. Kovio, “Power management strategy for solving power dispatch problems in microgrid for residential applications,” in *Proc*. IEEE International Energy Conference and Exhibition, Manama, Bahrain 2010, pp. 746–751.

[9.7] R. Noroozian and H. Vahedi, “Optimal management of microgrid using bacterial foraging algorithm,” in *Proc*. 18th Iranian Conference on Electrical Engineering, Isfahan, Iran 2010, pp. 895–900.

[9.8] B. Asato, et al., “Optimal operation of smart grid in isolated island,” in *Proc*. International Power Engineering Conference, Singapore 2010, pp. 1100–1105.

[9.9] M. Ross, et al., “Analysis of energy storage sizing and technologies,” in *Proc*. IEEE Electric Power and Energy Conference, Halifax, Canada 2010, pp. 1–6.

[9.10] H. Kanchev, et al., “Energy management and operational planning of a microgrid with a PV-based active generator for smart grid applications,” *IEEE Trans. Ind. Electron*., vol. 58, no. 10, pp. 4583–4592, Feb. 2011.

[9.11] D.E. Olivares, C.A. Canizares, and M. Kazerani, “A centralized optimal energy management system for microgrids,” in *Proc*. IEEE PES GM, San Diego, USA 2011, pp. 1–6.

[9.12] T. Logenthiran, et al., “Multiagent system for real-time operation of a microgrid in real-time digital simulator,” *IEEE Trans. Smart Grid*, vol. 3, no. 2, pp. 925–933, Apr. 2012.

[9.13] S. Conti, et al., “Optimal dispatching of distributed generators and storage systems for MV islanded microgrids,” *IEEE Trans. Power Del*., vol. 27, no. 3, pp. 1243–1251, May 2012.

[9.14] S.A. Pourmousavi, R.K. Sharma, and B. Asghari, "A framework for real-time power management of a grid-tied microgrid to extend battery lifetime and reduce cost of energy," in *Proc*. IEEE PES Innovative Smart Grid Technologies, Washington D.C., USA 2012, pp. 1–8.

[9.15] A. Sobu and G. Wu, “Dynamic optimal schedule management method for

microgrid system considering forecast errors of renewable power generations," in *Proc*. IEEE International Conference on Power system Technology, Auckland, USA 2012, pp. 1–6.

[9.16] C.M. Colson and M.H. Nehrir, "Comprehensive real-time microgrid power management and control with distributed agents," *IEEE Trans. Smart Grid*, vol. 4, no. 1, pp. 617–627, Jan. 2013.

[9.17] J. Quanyuan, X. Meidong, and G. Guangchao, "Energy management of microgrid in grid-connected and stand-alone modes," *IEEE Trans. Power Syst*., vol. 28, no. 3, pp. 3380–3389, Aug. 2013.

[9.18] C.M. Colson, et al., "Improving sustainability of hybrid energy systems Part I: Incorporating battery round-trip efficiency and operational cost factors," *IEEE Trans. Sustain. Energy*, vol. 5, no. 5, pp. 37–45, Jan. 2014.

[9.19] A. Hooshmand, B. Asghari, and R. Sharma, "A novel cost-aware multi-objective energy management method for microgrids,", in *Proc*. 2013 IEEE PES Innovative Smart Grid Technologies, Washington, DC, USA, pp. 1–6.

[9.20] R. Luna-Rubio, et al., "Optimal sizing of renewable hybrids energy systems: A review of methodologies," *Solar Energy*, vol. 86, no. 4, pp. 1077–1088, Apr. 2012.

[9.21] S.M. Schoenung, "Characteristics and technologies for long- vs. short-term energy storage: A study by the DOE energy storage systems program," Sandia National Laboratory, SAND2001-0765, Mar. 2001.

[9.22] D. Rastler, "Electricity energy storage technology options: A white paper primer on applications, costs and benefits," Electric Power Research Institute (EPRI), NO. 1020676, Dec. 2010.

[9.23] HOMER ENERGY: Energy Modeling Software for Hybrid Renewable Energy Systems, Available online: http://homerenergy.com/

[9.24] L.E. Bussey, *The Economic Analysis of Industrial Projects*, Prentice-Hall Inc.: New Jersey, 1978, ch. 4 and 11.

[9.25] D.G. Newnan, J.P. Lavelle, and T.G. Eschenback, *Engineering Economic Analysis*, 10th edition, Oxford University Press, 2009, ch. 10.

[9.26] W. Edwards, "Estimating farm machinery costs," Ag. Decision Maker, Iowa State University, NO. A3-29, Nov. 2009. Available online: http://www.extension.iastate.edu/publications/pm710.pdf

[9.27] CumminsOnan Commercial SD 10000, Available online: http://www.cumminsonan.com/cm/products/diesel/compare?gensetId=20&detail=true

[9.28] M. Pipattanasomporn, M.Willingham, and S. Rahman, "Implications of on-site distributed generation for commercial/industrial facilities," *IEEE Trans. Power Syst*., vol. 20, no. 1, pp. 206–212, Jan. 2005.

[9.29] MATLAB Documentation, Available online: http://www.mathworks.com/help/stats/hypergeometric-distribution.html

[9.30] "Descriptions of electric energy use in single family residences in the pacific northwest, 1986-1992," Office of Energy Resources, Bonneville Power Administration, Portland, OR, December 1992.

[9.31] MATLAB Documentation, Available online: http://www.mathworks.com/help/stats/negative-binomial-distribution.html

[10.1] C.M. Colson, M.H. Nehrir, and S.A. Pourmousavi, "Towards real-time microgrid power management using computational intelligence methods," in *Proc.* IEEE PES General Meeting, Minneapolis, USA, July 2010, pp. 1–8.

[10.2] EPRI, "Electricity energy storage technology options: A white paper primer on applications, costs and benefits," Dec. 2010. Available online: http://www.electricitystorage.org/images/uploads/docs/EPRI_StorageReport_5_11.pdf

[10.3] S.A. Pourmousavi, et al., "Real-time energy management of a stand-alone hybrid wind-microturbine energy system using particle swarm optimization," *IEEE Trans. Sustain. Energy*, vol. 1, no. 3, pp. 193–201, Oct. 2010.

[10.4] R. Hobbs, et al., "Development of predictive techniques for determination of remaining life for lead-acid batteries under fast charge," in *Proc.* Battery Conference on Applications and Advances, 1999, pp. 177–188.
[10.5] K. Takei, et al., "Cycle life estimation of lithium secondary battery by extrapolation method and accelerated aging test," *J. Power Sources*, vol. 97-98, pp. 697–701, July 2001.

[10.6] A. Yamashita, et al., "Capacity estimation and lifetime expectancy of large-scale nickel metal hydride backup batteries," in *Proc.* Telecommunications Conference INTELEC, 2005, pp. 291–295.

[10.7] P.E. Pascoe and A.H. Anbuky, "Standby power system VRLA battery reserve life estimation scheme," *IEEE Trans. Energy Convers.*, vol. 20,no. 4, pp. 887–895, Dec. 2005.

[10.8] C.C. Hua, et al., "Design and implementation of a residual capacity estimator for lead-acid batteries," in *Proc.* Industrial Electronics and Applications, ICIEA, pp. 2018–2023, 2007.

[10.9] X. Wei, B. Zhu, and W. Xu, "Internal resistance identification in vehicle power lithium-ion battery and application in lifetime estimation," in *Proc.* International Conference on Measuring Technology and Mechatronics Automation, vol. 3, pp. 388–392, 2009.

[10.10] W.L. Burgess, "Valve regulated lead acid battery float service life estimation using a Kalman filter," *J. Power Sources*, vol. 191, no. 1, pp. 16–21, June 2009.

[10.11] D. Haifeng, W. Xuezhe, and S. Zechang, "A new SOH prediction concept for the power lithium-ion battery used on HEVs," in *Proc.* IEEE Conference on Vehicle Power and Propulsion, VPPCEE, 2009, pp. 1649–1653.

[10.12] S. Drouilhet and B.L. Johnson, "A battery life prediction method for hybrid power applications," AIAA Aerospace Sciences Meeting and Exhibit, 1997.

[10.13] J.F. Manwell, et al., "Improvements to the hybrid2 battery model," Windpower Conference, 2005.

[10.14] P. Symons, "Life estimation of lead-acid battery cells for utility energy storage," in *Proc.* 5th Conference on Batteries for Utility Storage, San Juan, Puerto Rico, July 1995.

[10.15] A. Kashefi Kaviani, G.H. Riahy, and SH.M. Kouhsari, "Optimal design of a reliable hydrogen-based stand-alone wind/PV generating system considering component outages," *Renew. Energ.*, vol. 34, no. 11, pp. 2380–2390, Nov. 2009.

[10.16] H. Yang, et al., "Optimal sizing method for stand-alone hybrid solar/wind system with LPSP technology by using genetic algorithm," *Solar Energy*, vol. 82, no. 4, pp. 354–367, Apr. 2008.

[10.17] SAFT Batteries, Available online: http://www.saftbatteries.com/doc/Documents/stationary/Cube782/IntFLEX_0708.ce3d756b-b571-4cf3-a952-ad069f830ed1.pdf

[11.1] C. Wang, et al., "Power management of a stand-alone hybrid wind-microturbine distributed generation system," in *Proc.* Power Electronics and Machines in Wind Applications (PEMWA 2009), 24-26 June 2009, pp. 1–7.

[11.2] R.J. Wai, et al., "High-efficiency power conversion system for kilowatt-level stand-alone generation unit with low input voltage," *IEEE Trans. Industrial Electronics*, vol. 55, no. 10, pp. 3702–3714, Oct. 2008.

[11.3] F. Valenciaga and P.F. Puleston, "Supervisor control for a stand-alone hybrid generation system using wind and photovoltaic energy," *IEEE Trans. Energy Convers.*, vol. 20, no. 2, pp. 398–405, Sept. 2005.

[11.4] C. Wang and M.H. Nehrir, "Power management of a stand-alone wind/-photovoltaic/fuel cell energy system," *IEEE Trans. Energy Convers.*, vol. 23, no. 3, pp. 957–967, Sept. 2008.

[11.5] F.A. Mohamed and H.N. Koivo, "MicroGrid online management and balancing using multiobjective optimization," in *Proc.* Power Tech 2007, IEEE Lausanne, Switzerland, 1-5 July 2007, pp. 639–644.

[11.6] F. Katiraei and M.R. Iravani, "Power management strategies for a microgrid with multiple distributed generation units," *IEEE Trans. Power Syst.*, vol. 21, no. 4, pp. 1821–1831, Nov. 2006.

[11.7] W.D. Kellogg, et al., "Generation unit sizing and cost analysis for stand-alone wind, photovoltaic and hybrid wind/PV systems," *IEEE Trans. Energy Convers.*, vol. 13, no. 1, pp.70–75, March 1998.

[11.8] D.B. Nelson, M.H. Nehrir, and C. Wang, "Unit sizing and cost analysis of stand-alone hybrid wind-PV-fuel cell power generation system," *Renew. Energ.*, vol. 31, no. 10, pp. 1641–1656, Aug. 2006.

[11.9] E. Koutroulis, et al., "Methodology for optimal sizing of stand-alone photovoltaic/wind-generator systems using genetic algorithms," *Solar Energy*, vol. 80, no. 9, pp. 1072–1088, Sept. 2006.

[11.10] H. Yang, et al., "Optimal sizing method for stand-alone hybrid solar–wind system with LPSP technology by using genetic algorithm," *Solar Energy*, vol. 82, no. 4, pp. 354–367, April 2008.

[11.11] W. Lingfeng and C. Singh, "Multicriteria design of hybrid power generation systems based on a modified swarm optimization algorithm," *IEEE Trans. Energy Convers.*, vol. 24, no. 1, pp. 163–172, March 2009.

[11.12] A. Kashefi, G.H. Riahy, and S.M. Kouhsari, "Optimal design of a reliable hydrogen-based stand-alone wind/PV generating system, considering component outages," *Renew. Energ.*, vol. 34, no. 11, pp. 2380–2390, Nov. 2009.

[11.13] HOMER Energy LLC, National Renewable Energy Laboratory (NREL), Available online: http://homerenergy.com/about.asp

[11.14] DER-CAM - Distributed Energy Resources Customer Adoption Model, software

developed by Lawrence Berkeley National Laboratory (LBNL), Available online: http://der.lbl.gov/dercam.html

[11.15]C. Marnay, et al., "Optimal technology selection and operation of commercial-building microgrids," *IEEE Trans. Power Syst.*, vol. 23, no. 3, pp. 975–982, Aug. 2008.

[11.16]V. Miranda and H. Pun Sio, "Economic dispatch model with fuzzy wind constraints and attitudes of dispatchers," *IEEE Trans. Power Syst.*, vol. 20, no. 4, pp. 2143–2145, Nov. 2005.

[11.17]C.L. Chen, "Simulated annealing-based optimal wind-thermal coordination scheduling, Generation," *IET Gener. Transm. Distrib.*, vol. 1, no. 3, pp. 447–455, May 2007.

[11.18]B.C. Ummels, et al., "Impacts of wind power on thermal generation unit commitment and dispatch," *IEEE Trans. Energy Convers.*, vol. 22, no. 1, pp. 44–51, March 2007.

[11.19]C. Chun-Lung, "Optimal wind–thermal generating unit commitment," *IEEE Trans. Energy Convers.*, vol. 23, no. 1, pp. 273–280, March 2008.

[11.20]J. Hetzer, D.C. Yu, and K. Bhattarai, "An economic dispatch model incorporating wind power," *IEEE Trans. Energy Convers.*, vol. 23, no. 2, pp. 603–611, June 2008.

[11.21]C.A. Hernandez-Aramburo, T.C. Green, and N. Mugniot, "Fuel consumption minimization of a microgrid," *IEEE Trans. Ind. Appl.*, vol. 41, no. 3, pp. 673–681, May/June 2005.

[11.22]M. Clerc, *Particle Swarm Optimization*. Wiley, John & Sons, 2008.

[11.23]K.Y. Lee and M.A. El-Sharkawi, *Modern Heuristic Optimization Techniques: Theory and Applications to Power Systems*, John Wiley & Sons, IEEE press, Piscataway, NJ, 2008.

[11.24]S.R. Guda, C. Wang, and M.H. Nehrir "Modeling of microturbine power generation systems," *Electr. Pow. Compo. Sys.*, vol. 34, pp. 1027–1041, Aug. 2006.

[11.25]A. Antoniou and W.S. Lu, *Practical Optimization: Algorithms and Engineering Applications*. Springer Science & Business Media B.V., 2007, ch. 15.

[11.26]Natural Gas Production, Energy Information Administration (EIA), Available online: http://tonto.eia.doe.gov/oog/info/ngw/ngupdate.asp

[11.27]A.M. Amy and I. Erlich, "Online optimal management of PEM fuel cells using

neural networks," *IEEE Trans. Power Del.*, vol. 29, no. 2, pp. 1051–1058, Apr. 2005.

[11.28]S.O. Orero and M.R. Irving, "Large scale unit commitment using a hybrid genetic algorithm," *Int. J. Elec. Power.*, vol. 19, no. 1, pp. 45–55, Jan. 1997.

[11.29]U.S. Dept. of Energy (U.S. DOE), Office of Energy Efficiency and Renewable Energy, "Summary of results from testing a 30-kW-microturbine and combined heat and power (CHP) system", DOE/EE-0316, 2007.

[11.30]C. Wang, "Modeling and control of hybrid wind/photovoltaic/fuel cell distributed generation systems," Ph.D. Dissertation, Montana State University, Bozeman, MT, 2006.

[11.31]MATLAB/Simulink SimPowerSystems Documentation, Available online: http://www.mathworks.com/

[11.32]J. Kennedy and R.C. Eberhart, "Particle swarm optimization", in *Proc.* IEEE international conference on neural networks, 1995, pp. 39–43.

[11.33]Y. Del Valle, et al., "Particle swarm optimization: basic concepts, variants and applications in power systems", *IEEE Trans. Evol. Comput.*, vol. 12, no. 2, pp. 171–195, Apr. 2008.

[11.34]M.H. Nehrir, et al., "An approach to evaluate the general performance of stand-alone wind/photovoltaic generation systems", *IEEE Trans. Energy Convers.*, vol. 15, no. 4, pp. 433–439, Dec. 2000.

[11.35]V. Pop, et al., *Battery Management Systems: Accurate State-of-Charge Indication for Battery-Powered Applications*. Springer Science & Business Media B.V., 2008, page: 23.37.

[11.36]J. Cahill, K. Ritland, and W. Kelly, "Description of electric energy use in single family residences in the Pacific Northwest 1986-1992," Office of Energy Resources, Bonneville Power Administration, December 1992, Portland, OR.

[11.37]Pacific Northwest Cooperative Agricultural Weather Network, AgriMet Historical Dayfile Data Access, Deer Lodge, MT (DRLM), Available online: http://www.usbr.gov/pn/agrimet/webaghrread.html.

[11.38]G.M. Masters, *Renewable and Efficient Electric Power Systems*, Wiley, 2004.

[12.1] U.S. DOE, office of electric transmission and distribution, "GRID 2030: A national vision for electricity's second 100 years," July 2003.

[12.2] F. Katiraei, et al., "Microgrids management: Controls and operation aspects of

microgrids," *IEEE Power Energy Mag*., vol. 6, no. 3, pp. 54–65, May/June 2008.

[12.3] C.M. Colson, M.H. Nehrir, and S.A. Pourmousavi, "Towards real-time microgrid power management using computational intelligence methods," in *Proc*. PES GM, Minneapolis, USA 2010, pp. 1–8.

[12.4] A.G. Tsikalakis and N.D. Hatziargyriou, "Centralized control for optimizing microgrids operation," *IEEE Trans. Energy Convers*., vol. 23, no. 1, pp. 241–248, Feb. 2008.

[12.5] S.A. Pourmousavi, et al., "Real-time energy management of a stand-alone hybrid wind-microturbine energy system using particle swarm optimization," *IEEE Trans. Sustain. Energy*, vol. 1, no. 3, pp. 193–201, Oct. 2010.

[12.6] F.A. Mohamed and H.N. Kovio, "Power management strategy for solving power dispatch problems in Microgrid for residential applications," in *Proc*. IEEE International Energy Conference and Exhibition, Manama, Bahrain 2010, pp. 746–751.

[12.7] Y. Riffonneau, et al., "Optimal power flow management for grid connected PV systems with batteries," *IEEE Trans. Sustain. Energy*, vol. 2, no. 3, pp. 309–320, Feb. 2011.

[12.8] B. Belvedere, et al., "A microcontroller-based power management system for standalone microgrids with hybrid power supply," *IEEE Trans. Smart Grid*, vol. 3, no. 3, pp. 422–431, May 2012.

[12.9] S.A. Pourmousavi, R.K. Sharma, and B. Asghari, "A framework for real-time power management of a grid-tied microgrid to extend battery lifetime and reduce cost of energy," in *Proc*. IEEE PES Innovative Smart Grid Technologies, Washington D.C., USA 2012, pp. 1–8.

[12.10] C.M. Colson and M.H. Nehrir, "Comprehensive real-time microgrid power management and control with distributed agents," *IEEE Trans. Smart Grid*, vol. 4, no. 1, pp. 617–627, Jan. 2013.

[12.11] C.M. Colson, et al., "Improving sustainability of hybrid energy systems Part II: Managing multiple objectives with a multi-agent system," *IEEE Trans. Sustain. Energy*, vol. 5, no. 1, pp. 46–54, Jan. 2014.

[12.12] HOMER ENERGY: Energy Modeling Software for Hybrid Renewable Energy Systems, Available online: http://homerenergy.com/

[12.13] "Individual household electric power consumption Data Set," Machine Learning Repository, University of California-Irvine, Available online: http://archive.ics.uci.edu/ml/datasets/Individual+household+electric+power+consumption

#

[12.14]E. Lorenzo, et. Al, *Solar Electricity Engineering of Photovoltaic Systems*, Earthscan Publications Ltd., pp. 316, Jan. 1994.

[12.15]SunPower Corp., "SPR-200-BLK, residential PV Module," specification sheet Available online: http://www.energyplus.com.sg/products/32.pdf

[12.16]L.E. Bussey, *The Economic Analysis of Industrial Projects*, Prentic-Hall Inc.: New Jersey, 1978, ch. 4 and 11.

[12.17]S.A. Pourmousavi, M.H. Nehrir, and R.K. Sharma, "Ownership cost calculations for distributed energy resources using uncertainty and risk analysis," Submitted to the *IEEE Trans. Power Syst*. for possible publication, March 2014.

[12.18]S. Chakraborty and M.G. Simoes, "PV-microgrid operational cost minimization by neural forecasting and heuristic optimization," in *Proc*. IEEE Industry Applications Society Annual Meeting, Edmonton, Canada 2008, pp. 1–8.

[12.19]CumminsOnan Commercial SD 10000, Available online: https://powersuite.cummins.com/PSWEB/login.action

[12.20]M. Pipattanasomporn, M. Willingham, and S. Rahman, "Implications of on-site distributed generation for commercial/industrial facilities," *IEEE Trans. Power Syst*., vol. 20, no. 1, pp. 206–212, Feb 2005.

[12.21]MATLAB Curve Fitting Toolbox, MathWorks Inc., Available online: http://www.mathworks.com/products/curvefitting/

[12.22]A. Sobu and G. Wu, "Dynamic optimal schedule management method for microgrid system considering forecast errors of renewable power generations," in *Proc*. IEEE International Conference on Power system Technology, Auckland, USA 2012, pp. 1–6.

[12.23]D. Thimsen, "Cost of utility distributed generators, 1-10 MW," EPRI, Rep. no. 1007760, March 2003.

[12.24]D. Zhu, et al., "In-plume emission test stand 2: Emission factors for 10- to 100-kW U.S. Military Generators," *JAPCA J. Air Waste Ma*., vol. 59, no. 12, pp. 1446–1457, Dec. 2009.

[12.25]R.S.J. Tol, "The marginal damage costs of carbon dioxide emissions: An assessment of the uncertainties," *Energ. Policy*, vol. 33, no. 16, pp. 2064–2074, Nov. 2005.

[12.26]D. Burtraw and S.J. Szambelan, “U.S. emissions trading markets for SO2 and NOx,” Discussion Paper, Resources for the future company, RFF DP 09-40, Oct. 2009.

[12.27]M. Ceraolo, “New dynamical models of lead-acid batteries,” *IEEE Trans. Power Syst.*, vol. 15, no. 4, pp. 1184–1190, Nov. 2000.

[12.28]C.M. Colson, et al., “Improving sustainability of hybrid energy systems Part I: Incorporating battery round-trip efficiency and operational cost factors,” *IEEE Trans. Sustain. Energy*, vol. 5, no. 1, pp. 37–45, Jan. 2014.

[12.29]EPRI, "Electricity energy storage technology options: A white paper primer on applications, costs and benefits," Dec, 2010. Available online: http://www.electricitystorage.org/images/uploads/static_content/technology/resources/ESA_TR_5_11_EPRIStorageReport_Rastler.pdf

[12.30]R. Lassseter and M. Erikson, “Integration of battery-based energy storage element in the CERTS microgrid,” Final Report Task 4, prepared for U.S. DOE., Oct. 2009, ch. 6.

[12.31]P.S. Dolan, M.H. Nehrir, and V. Gerez, “Development of a Monte Carlo based aggregate model for residential electric water heater loads,” *Electr. Pow. Syst. Res.*, vol. 36, no. 1, pp. 29–35, Jan. 1996.

[12.32]S.N. Patrick, “Control of aggregate electric water heaters for load shifting and balancing intermittent renewable energy generation in a smart grid environment,” M.S thesis in Electrical Engineering, Montana State University-Bozeman, 2011.

[12.33]S.A. Pourmousavi, S.N. Patrick, and M.H. Nehrir, "Real-time demand response through aggregate electric water heaters for load shifting and balancing intermittent wind generation," *IEEE Trans. Smart Grid*, vol. 5, no. 2, pp. 769–778, March 2014.

[12.34]C.M. Colson and M.H. Nehrir, “A review of challenges to real-time power management of microgrids,” in *Proc*. IEEE PES GM, Calgary, Canada 2009, pp. 1–8.

[12.35]C.M. Colson and M.H. Nehrir, “An alternative method to load modeling for obtaining end-use load profiles,” in *Proc*. IEEE NAPS, Starkville, USA 2009, pp. 1–5.

[12.36]“Descriptions of electric energy use in single family residences in the pacific northwest, 1986- 1992,” Office of Energy Resources, Bonneville Power Administration, Portland, OR, December 1992.

APPENDICES

APPENDIX A

SIMULATION DIAGRAMS OF THE FEEDER-CONFIGURED MG

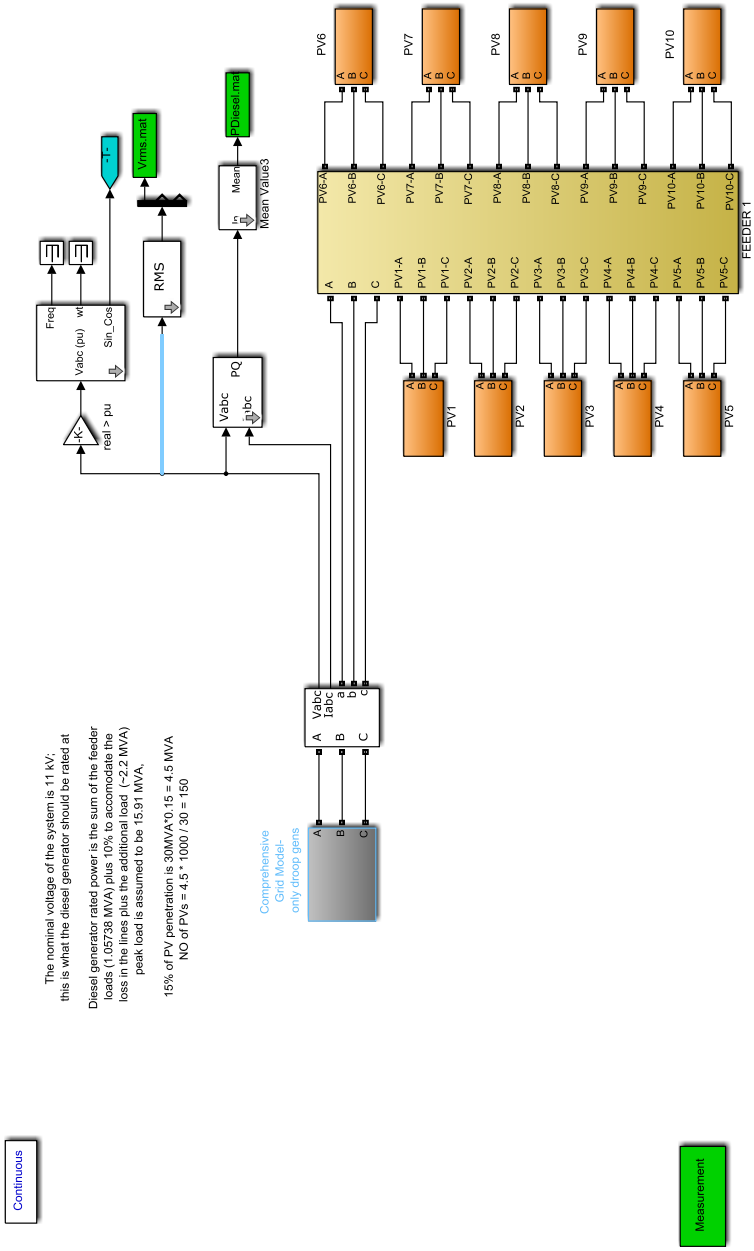


Figure A.1: Simulation diagram of feeder-configured MG for distributed PV study.

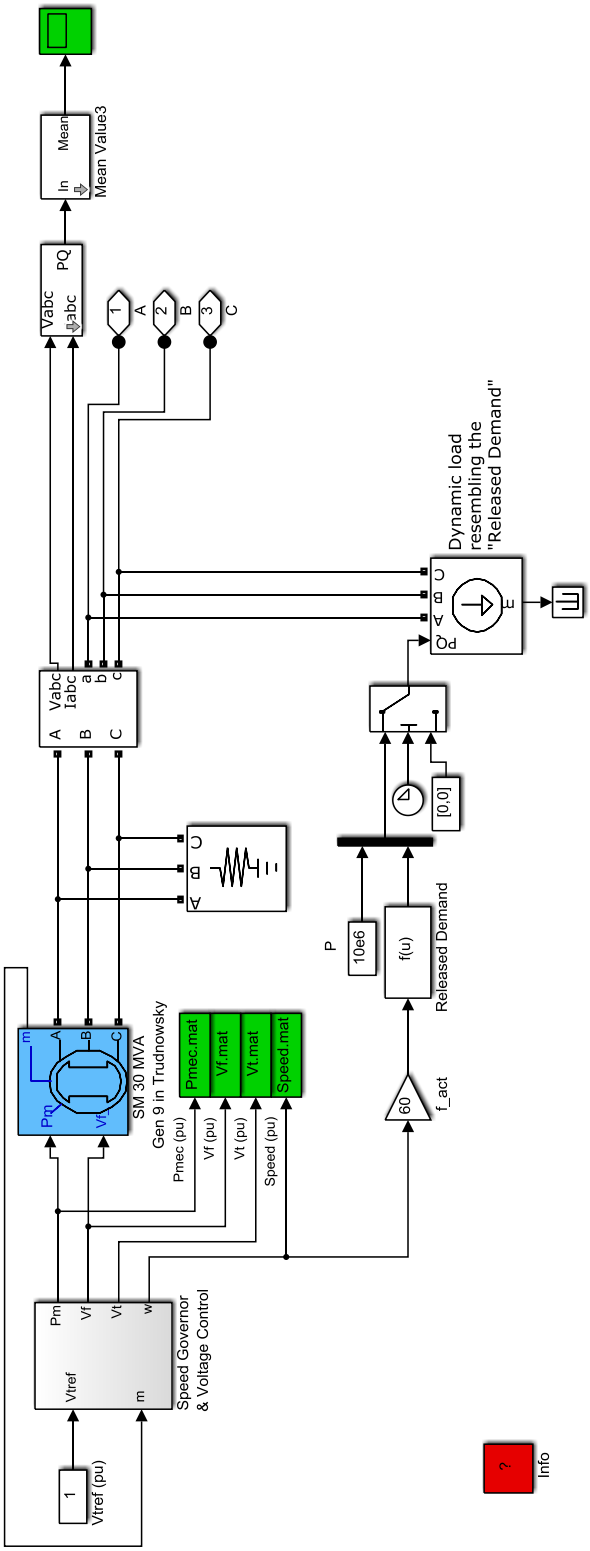


Figure A.2: The SGM model with frequency and voltage controller and dynamic load.

APPENDIX B

SUS-MATRICES FOR THE LFC-DR MODEL DEVELOPED FOR MULTI-AREA POWER SYSTEM WITH MULTIPLE GENCOS AND LAGCOS

Sub-matrices for the system matrix (i.e., matrix $\mathbf{A}_i$ in (7.5) and (7.6)) can be calculated for any multi-area power system with multiple Gencos and Lagcos as below:

$$\boldsymbol{\Phi}_{11i}=\begin{bmatrix} \dfrac{-D_i}{2H_i} & \dfrac{-1}{2H_i} \\ 2\pi\sum\limits_{\substack{j=1\\ j\neq i}}^{N} T_{ij} & 0 \end{bmatrix},\quad \boldsymbol{\Phi}_{12i}=\begin{bmatrix} \underbrace{\begin{bmatrix} 0 & \dfrac{1}{2H_i} \\ 0 & 0 \end{bmatrix} \cdots \begin{bmatrix} 0 & \dfrac{1}{2H_i} \\ 0 & 0 \end{bmatrix}}_{n \text{ generation units}} \end{bmatrix},\ \boldsymbol{\Phi}_{21i}=\begin{bmatrix} \begin{bmatrix} \dfrac{-1}{T_{g,1i}.R_{1i}} & 0 \\ 0 & 0 \end{bmatrix} \\ \vdots \\ \begin{bmatrix} \dfrac{-1}{T_{g,ni}.R_{ni}} & 0 \\ 0 & 0 \end{bmatrix} \end{bmatrix},$$

$$\boldsymbol{\Phi}_{22i}=\begin{bmatrix} \begin{bmatrix} \dfrac{-1}{T_{g,1i}} & 0 \\ \dfrac{1}{T_{t,1i}} & \dfrac{-1}{T_{t,1i}} \end{bmatrix} & & \mathbf{0}_{2n-2\times 2n-2} \\ & \ddots & \\ \mathbf{0}_{2n-2\times 2n-2} & & \begin{bmatrix} \dfrac{-1}{T_{g,ni}} & 0 \\ \dfrac{1}{T_{t,ni}} & \dfrac{-1}{T_{t,ni}} \end{bmatrix} \end{bmatrix}$$

$$\boldsymbol{\Phi}_{13}=\begin{bmatrix} \underbrace{\begin{bmatrix} \dfrac{30}{2H_i.T_{d,1i}\times 2^3} & 0 & \dfrac{105}{2H_i.T_{d,1i}^3\times 2^{11}} & 0 & \dfrac{945}{2H_i.T_{d,1i}^5\times 2^{20}} \\ 0 & 0 & 0 & 0 & 0 \end{bmatrix} \cdots \begin{bmatrix} \dfrac{30}{2H_i.T_{d,mi}\times 2^3} & 0 & \dfrac{105}{2H_i.T_{d,mi}^3\times 2^{11}} & 0 & \dfrac{945}{2H_i.T_{d,mi}^5\times 2^{20}} \\ 0 & 0 & 0 & 0 & 0 \end{bmatrix}}_{m \text{ load aggregators}} \end{bmatrix}$$

$$\boldsymbol{\Phi}_{23i}=\left[\mathbf{0}_{2n\times 5m}\right],\boldsymbol{\Phi}_{31i}=\left[\mathbf{0}_{5m\times 2}\right],\boldsymbol{\Phi}_{32i}=\left[\mathbf{0}_{5m\times 2n}\right]$$

$$\boldsymbol{\Phi}_{33i}=\begin{bmatrix}\begin{bmatrix}\frac{-30}{T_{d,1i}} & \frac{-105}{T_{d,1i}^2\times 2^5} & \frac{-105}{T_{d,1i}^3\times 2^8} & \frac{-945}{T_{d,1i}^4\times 2^{14}} & \frac{-945}{T_{d,1i}^5\times 2^{17}}\\ 128 & 0 & 0 & 0 & 0\\ 0 & 64 & 0 & 0 & 0\\ 0 & 0 & 32 & 0 & 0\\ 0 & 0 & 0 & 16 & 0\end{bmatrix} & & \mathbf{0}_{5m-5\times 5m-5}\\ & \ddots & \\ \mathbf{0}_{5m-5\times 5m-5} & & \begin{bmatrix}\frac{-30}{T_{d,mi}} & \frac{-105}{T_{d,mi}^2\times 2^5} & \frac{-105}{T_{d,mi}^3\times 2^8} & \frac{-945}{T_{d,mi}^4\times 2^{14}} & \frac{-945}{T_{d,mi}^5\times 2^{17}}\\ 128 & 0 & 0 & 0 & 0\\ 0 & 64 & 0 & 0 & 0\\ 0 & 0 & 32 & 0 & 0\\ 0 & 0 & 0 & 16 & 0\end{bmatrix}\end{bmatrix}$$

Also, the sub-matrices required to calculate the control input matrix (i.e., matrix $\mathbf{B}_i$ in (7.5) and (7.6)) are as follows:

$$\boldsymbol{\Lambda}_{11}=\left[\mathbf{0}_{2\times 1}\right],\boldsymbol{\Lambda}_{12}=\begin{bmatrix}\frac{-1}{2H_i}\\ 0\end{bmatrix},\boldsymbol{\Lambda}_{21}^T=\begin{bmatrix}\underbrace{\begin{bmatrix}\frac{\beta_{1i}}{T_{g,1i}} & 0\end{bmatrix}\ \cdots\ \begin{bmatrix}\frac{\beta_{ni}}{T_{g,ni}} & 0\end{bmatrix}}_{n\text{ generation units}}\end{bmatrix},\boldsymbol{\Lambda}_{22}=\left[\mathbf{0}_{2n\times 1}\right],\boldsymbol{\Lambda}_{31}=\left[\mathbf{0}_{5m\times 1}\right],$$

$$\mathbf{\Lambda}_{32}^{T}=\left[\underbrace{\begin{bmatrix}16\lambda_{1i} & 0 & 0 & 0 & 0\end{bmatrix}\ \cdots\ \begin{bmatrix}16\lambda_{mi} & 0 & 0 & 0 & 0\end{bmatrix}}_{m\ load\ aggregator}\right]$$

The disturbance matrix (i.e., matrix $\mathbf{\Gamma}_i$ in(7.5) and (7.6)) can be computed for any multi-area power system as follows:

$$\mathbf{\Theta}_{11}=\begin{bmatrix}\dfrac{-1}{2H_i} & 0\\ 0 & -2\pi\end{bmatrix},\mathbf{\Theta}_{21}=\begin{bmatrix}\mathbf{0}_{2n\times 2}\end{bmatrix},\mathbf{\Theta}_{31}=\begin{bmatrix}\mathbf{0}_{5m\times 2}\end{bmatrix}$$

Finally, the modified input matrix (i.e., matrix $\widehat{\mathbf{B}}_i^T$ in (7.7)) can be determined using the following sub-matrices:

$$\widehat{\mathbf{\Lambda}}_{11}=\begin{bmatrix}\dfrac{\alpha_i-1}{2H_i.\alpha_i}\\ 0\end{bmatrix},\widehat{\mathbf{\Lambda}}_{12}^{T}=\left[\underbrace{\begin{bmatrix}\dfrac{\beta_{1i}}{T_{g,1i}} & 0\end{bmatrix}\ \cdots\ \begin{bmatrix}\dfrac{\beta_{ni}}{T_{g,ni}} & 0\end{bmatrix}}_{n\ generation\ units}\right]$$

$$\widehat{\mathbf{\Lambda}}_{13}^{T}=\left[\underbrace{\begin{bmatrix}\dfrac{16\lambda_{1i}.(1-\alpha_i)}{\alpha_i} & 0 & 0 & 0 & 0\end{bmatrix}\ \cdots\ \begin{bmatrix}\dfrac{16\lambda_{mi}.(1-\alpha_i)}{\alpha_i} & 0 & 0 & 0 & 0\end{bmatrix}}_{m\ load\ aggregator}\right]$$

APPENDIX C

BATTERY LIFE ESTIMATION AND OPERATIONAL COST CALCULATION GUI

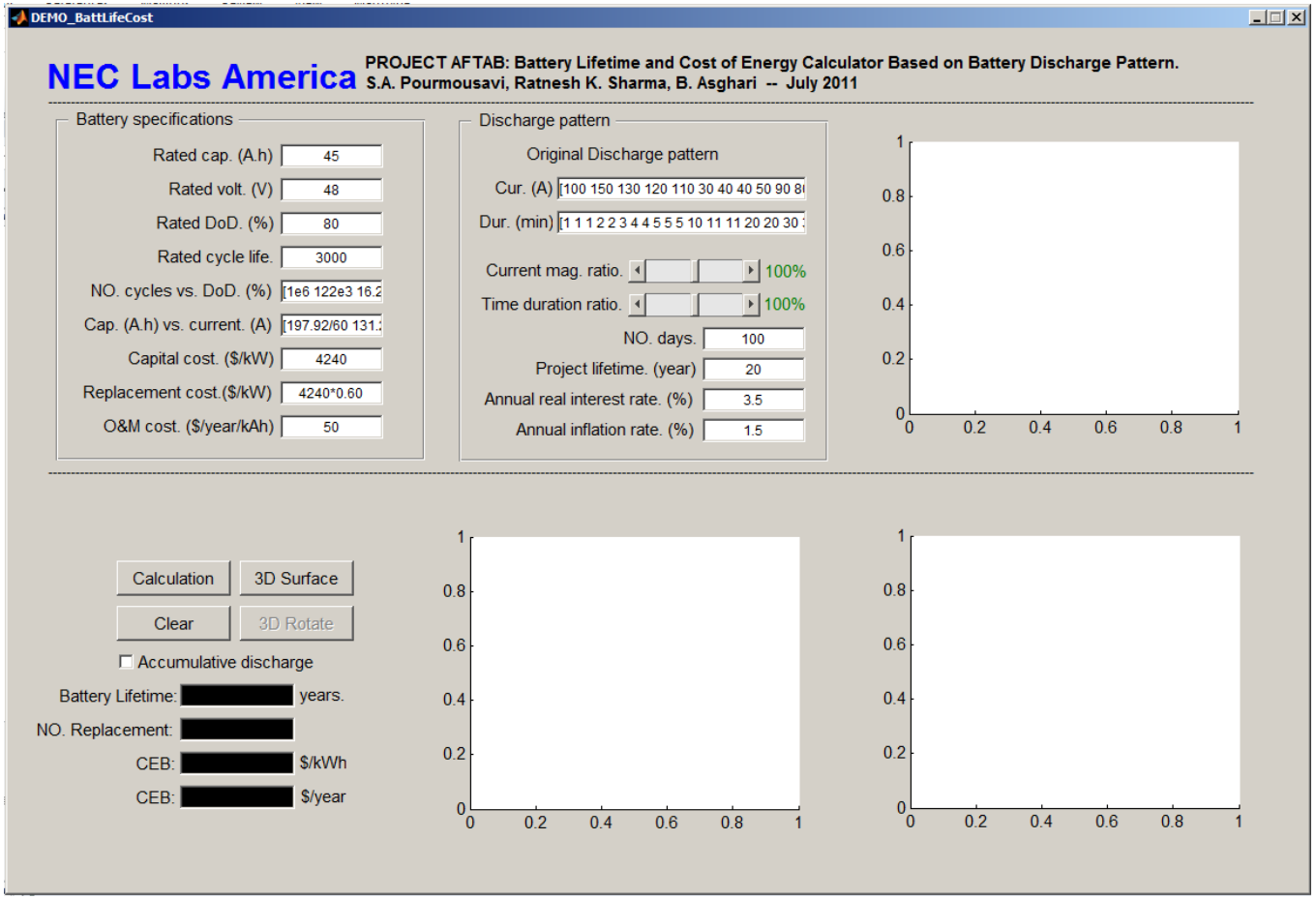


Figure C.1: battery life estimation and operational cost calculation and comparison

APPENDIX D

MULTI-TIMESCALE POWER MANAGEMENT GUIs

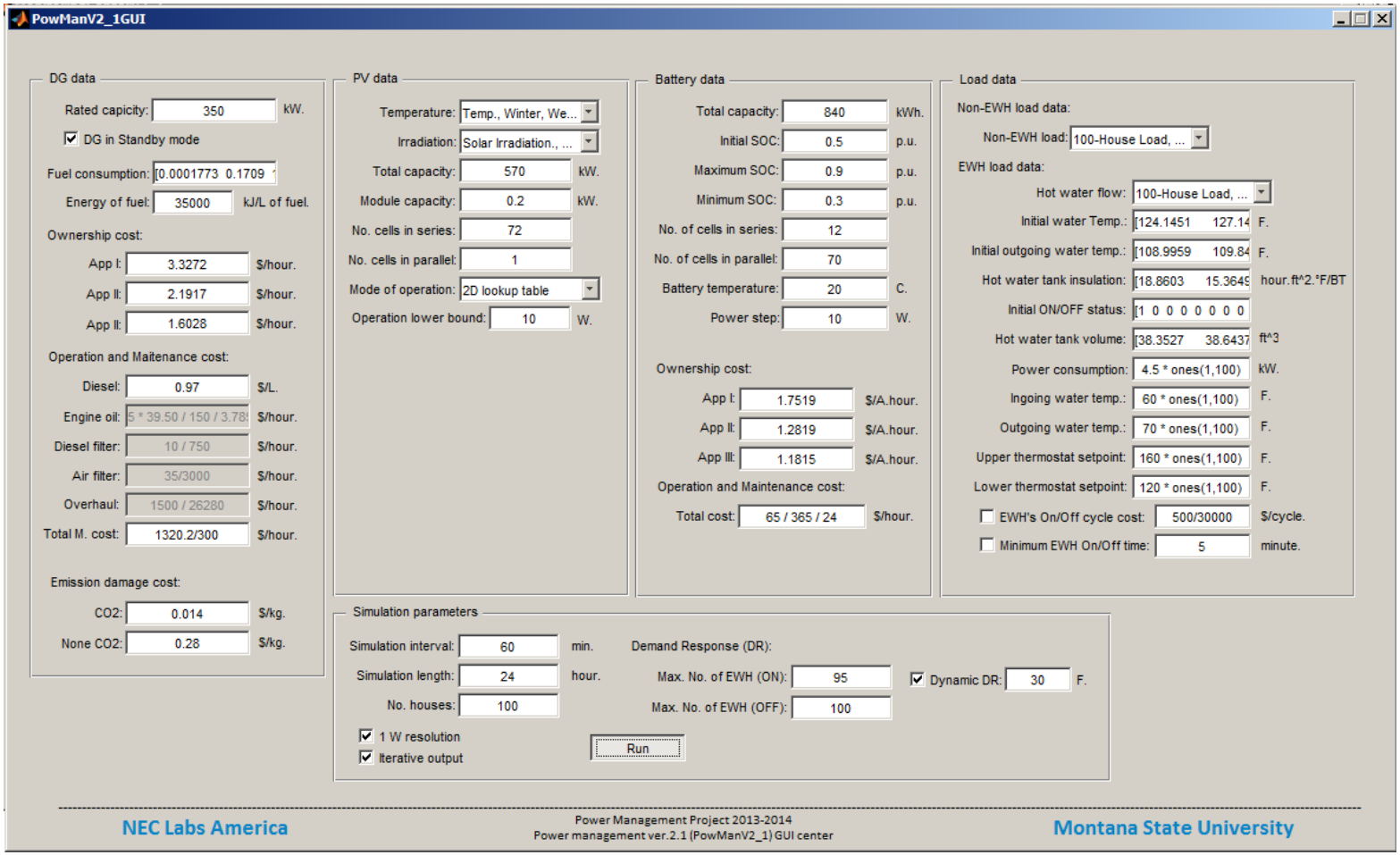


Figure D.1: GUI developed to attain required data for multi-timescale power management.

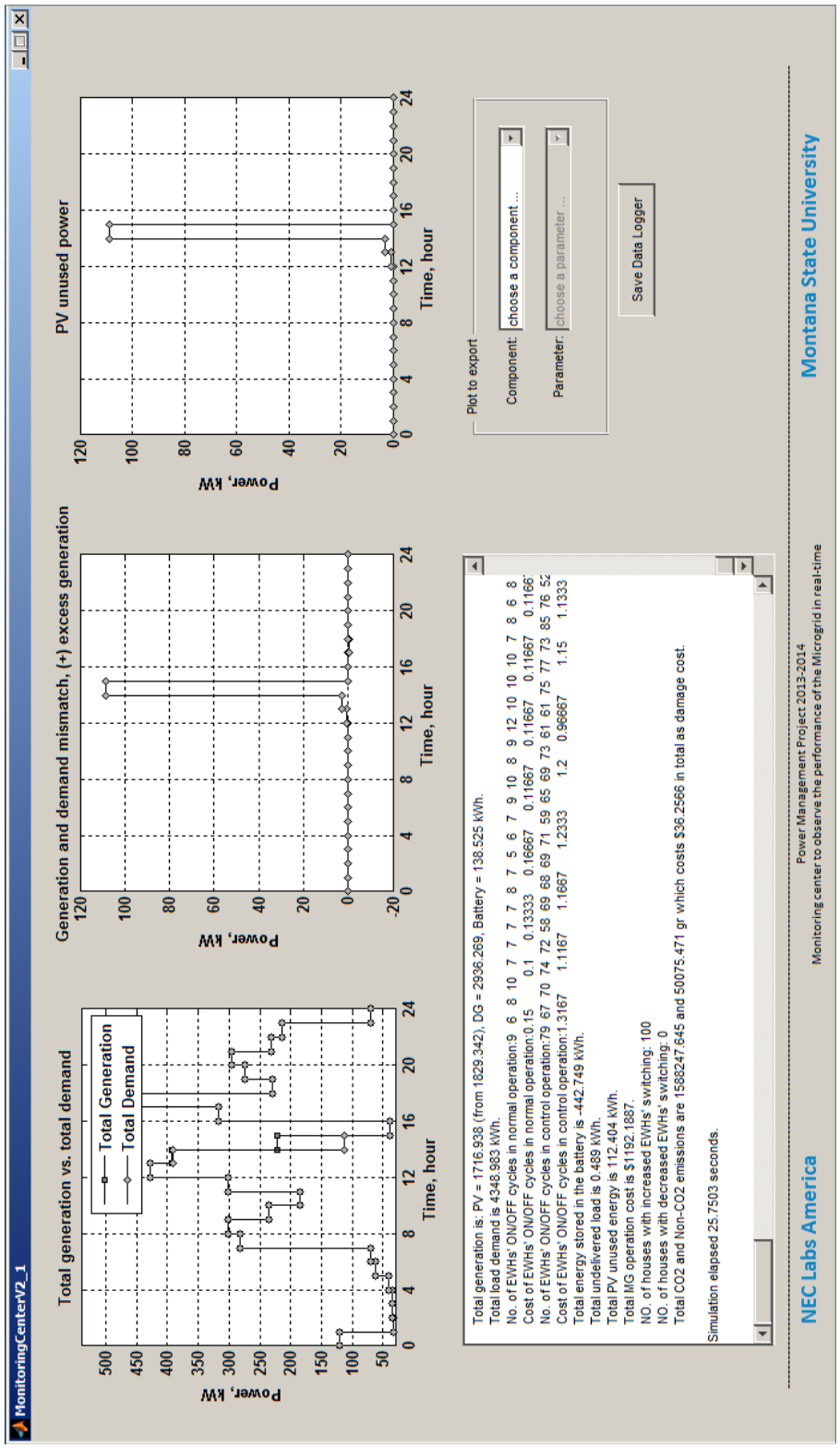


Figure D.2: GUI developed to show the results of power management and summary of the operation.

APPENDIX E

INPUT DESCRIPTION, ALGORITHMS, AND PSEUDO-CODES

APPENDIX E.1

Different input parameters to the PMA are defined as follows:

$\langle P_{PV}^{\max} \rangle_{[t,t+\Delta T]}$: Maximum PV available power for the interval ahead (i.e., t to $t+\Delta T$), calculated by "PV dynamic model" module, shown in Figure 12.4.

$\langle P_{DiG}^{\max} \rangle_{[t,t+\Delta T]}$: Nominal capacity of the DiG unit. P_{DiG} is a constant throughout Chapter 12, but it can change in different time intervals.

$\langle SOC \rangle_t$: The latest value of the battery SOC.

$\langle \Delta P \rangle_{[t,t+\Delta T]}$: is used in each interval to calculate the maximum amount of power to charge the battery (or to discharge from the battery).

$\langle EWH_{stat} \rangle_{[t,t+\Delta T]}$: EWHs' primary ON/OFF status calculated by "EWH dynamic model" module, shown in Figure 12.4, based on the actual hot water flow rate at the beginning of the simulation for each interval.

$\langle P_L^{EWH} \rangle_{[t,t+\Delta T]}$: Load demand from the EWHs for t to $t+\Delta T$ interval, calculated by "EWH dynamic model" module.

$\langle P_L^{nonEWH} \rangle_{[t,t+\Delta T]}$: Non-EWH load demand for t to $t+\Delta T$ interval.

APPENDIX E.2

Battery charging algorithm (**Algorithm 1**) developed in Chapter 12 is given in pseudo-code style as follows. Required input parameters are also introduced.

Algorithm 1. BATTERY CHARGING

Required: Battery SOC, internal voltage and temperature at the end of the last interval, step power change (ΔP), battery scheduled power (P_{BATT}^{sch}), and simulation interval (ΔT).

1: $P_{BATT}^{ch} \leftarrow P_{BATT}^{sch}$

2: *HVFlag* = ***BattModel***† ($P_{BATT}^{ch}, \langle SOC, V, T \rangle_t, \Delta T$)

3: **While (***HVFlag* = 0**)** & **(** $P_{BATT}^{ch} < 0$ **) do**

4: $P_{BATT}^{ch} = P_{BATT}^{ch} + \Delta P$

5: *HVFlag* = ***BattModel***($P_{BATT}^{ch}, \langle SOC, V, T \rangle_t, \Delta T$)

6: **End While**

7: **If (***HVFlag* = 1**)** & **(** $P_{BATT}^{ch} < 0$ **) then**

8: $\langle P_{BATT} \rangle_{[t,t+\Delta T]} = P_{BATT}^{ch}$; $\langle P_{PV}^{excess} \rangle_{[t,t+\Delta T]} = P_{BATT}^{sch} - P_{BATT}^{ch}$;

9: **Else**

10: $\langle P_{BATT} \rangle_{[t,t+\Delta T]} = 0$; $\langle P_{PV}^{excess} \rangle_{[t,t+\Delta T]} = P_{BATT}^{sch}$;

11: **End If**

† "BattModel" is the dynamic model of the battery developed in MATLAB® m-file.

APPENDIX E.3

EWHs ON/OFF algorithm (**Algorithm 2**) developed in Chapter 12 is given in pseudo-code style as follows. Required input parameters are also introduced.

Algorithm 2. EWHS ON/OFF CONTROL ALGORITHM*

Required: PV excess power (P_{PV}^{excess}), EWHs consumption and status ($S_i^{t+\Delta T}$) for the interval ahead and at the end of the last interval, number of EWHs (NO_{EWH}), and simulation interval (ΔT).

1: $P_{DR}^{on} \leftarrow P_{PV}^{excess}$, $t \leftarrow 1$
2: **For** (t < ΔT) **do**
3: *Ind*=***sort***†($\langle T_i \rangle_t$; $i = 1,...,NO_{EWH}$,'*descending*')
4: calculate $P_{EWH}^{total,orig}(t)$,
5: **While** (i < NO_{EWH}) **do**
6: **If** ($\langle T_i \rangle_{t-1} > T_i^{\max}$) **then** $S_i(t) \leftarrow 0$
7: **Else If** ($\langle T_i \rangle_{t-1} < T_i^{\min}$) **then** $S_i(t) \leftarrow 1$
8: **Else**
9: **If** ($S_i(t) = 0$), **then** $S_i(t) = 1$
10: temp = sum($S_i(t)$; $i = 1,...,NO_{EWH}$)
11: calculate $P_{EWH}^{total,\text{new}}(t)$
11: **If** (temp > Max_{on}) ||
(($P_{EWH}^{total,\text{new}}(t) - P_{EWH}^{total,orig}(t)$) > P_{DR}^{on}), **then**
12: $S_i(t) = 0$; break;
13: **End If**
14: **End If**
15: **End If**
16: Data=***EWHModel***¶($\langle S_i, T_i, F_i \rangle_t$)
17: $i \leftarrow i + 1$
18: **End While**
19: $t \leftarrow t + 1$
20: **End For**
21: $\left\langle P_{PV}^{excess} = P_{PV}^{excess} - \left(P_{EWH}^{total,\text{new}}(t) - P_{EWH}^{total,orig}(t) \right) \right\rangle_{[t,t+\Delta T]}$

† "sort" is the sorting algorithm in MATLAB®.

¶ "EWHModel" is the dynamic model of the single EWH developed in MATLAB® m-file.

* Required modifications for **Algorithm 2** in RULE III for reduction in the EWHs consumption:

1: $P_{DR}^{off} \leftarrow P_{Load}^{undelivered}$, $t \leftarrow 1$

3: Ind=***sort***†$(\langle T_i \rangle_t ; i = 1,...,NO_{EWH}$, '*ascending*')

9: **If** ($S_i(t) = 1$), **then** $S_i(t) = 0$

11: **If** (temp > Max_{off}) ||
(($P_{EWH}^{total,\text{new}}(t)$ - $P_{EWH}^{total,orig}(t)$) > P_{DR}^{off}), **then**

12: $S_i(t) = 1$; break;

21: $\left\langle P_{Load}^{undelivered} = P_{Load}^{undelivered} - \left(P_{EWH}^{total,\text{new}}(t) - P_{EWH}^{total,orig}(t) \right) \right\rangle_{[t,t+\Delta T]}$

APPENDIX E.4

Battery discharging algorithm (**Algorithm 3**) developed in Chapter 12 is given in pseudo-code style as follows. Required input parameters are also introduced.

Algorithm 3. BATTERY DISCHARGING

Required: Battery SOC, internal voltage and temperature at the end of the last interval, step power change (ΔP), battery scheduled power (P_{BATT}^{sch}), and simulation interval (ΔT).

1: $P_{BATT}^{dis} \leftarrow P_{BATT}^{sch}$

2: *LVFlag* = ***BattModel***† ($P_{BATT}^{dis}, \langle SOC, V, T \rangle_t, \Delta T$)

3: **While (***LVFlag* = 0**)** & **(** $P_{BATT}^{dis} > 0$ **) do**

4: $P_{BATT}^{dis} = P_{BATT}^{dis} - \Delta P$

5: *LVFlag* = ***BattModel***($P_{BATT}^{dis}, \langle SOC, V, T \rangle_t, \Delta T$)

6: **End While**

7: **If (***LVFlag* = 1**)** & **(** $P_{BATT}^{dis} > 0$ **) then**

8: $\langle P_{BATT} \rangle_{[t,t+\Delta T]} = P_{BATT}^{dis}$; $\langle P_{Load}^{undelivered} \rangle_{[t,t+\Delta T]} = P_{BATT}^{sch} - P_{BATT}^{dis}$;

9: **Else**

10: $\langle P_{BATT} \rangle_{[t,t+\Delta T]} = 0$; $\langle P_{Load}^{undelivered} \rangle_{[t,t+\Delta T]} = P_{BATT}^{sch}$;

11: **End If**

† "BattModel" is the dynamic model of the battery developed in MATLAB® m-file.

APPENDIX F

AUTHOR PEER-REVIEWED PUBLICATIONS

Journal publications

S.A. Pourmousavi, M.H. Nehrir, "LFC-DR Model Expansion to Multi-Area Power System," Under Preparation, 2014.

S.A. Pourmousavi, M.H. Nehrir, R.K. Sharma, "A Novel Optimal Power Management for an Islanded Microgrid Including Generation, Storage, and Demand Response," Under Preparation, 2014.

S.A. Pourmousavi, M.H. Nehrir, R.K. Sharma, "Multi-Timescale Power Management for Islanded Microgrids Including Storage and Demand Response," Submitted for possible publication in the *IEEE Trans. Smart Grid*, April. 04, 2014.

S.A. Pourmousavi, M.H. Nehrir, R.K. Sharma, "Ownership Cost Calculations for Distributed Energy Resources using Uncertainty and Risk Analyses," Submitted for possible publication in the *IEEE Transactions on Power Systems*, March. 07, 2014.

S.A. Pourmousavi, M.H. Nehrir, "Introducing Dynamic Demand Response in the LFC Model," *IEEE Transactions on Power Systems*, vol. 29, no. 4, pp. 1562–1572, July 2014.

S.A. Pourmousavi, S.N. Patrick, M.H. Nehrir, "Real-Time Demand Response through Aggregate Electric Water Heaters for Load Shifting and Balancing Intermittent Wind Generation," *IEEE Trans. Smart Grid*, Vol. 5, Issue. 2, March 2014, pp. 769–778.

S.A. Pourmousavi, M.H. Nehrir, "Real-Time Central Demand Response for Primary Frequency Regulation in Microgrids", *IEEE Trans. Smart Grid*, Vol. 3, Issue 4, 2012, pp.1988–1996. (Presented Paper to IEEE PES GM 2013)

S.A. Pourmousavi, M.H. Nehrir, C.M. Colson, and C. Wang, "Real-Time Energy Management of a Stand-Alone Hybrid Wind-Microturbine Energy System Using Particle Swarm Optimization", *IEEE Transactions on Sustainable Energy*, Vol. 1, Issue 3, 2010, pp. 193 – 201. (Presented Paper to IEEE PES GM 2010)

Conference publications

R. Ahmadi, **S. A. Pourmousavi**, J. R. Pillai, H. M. Hasanien, B. Bak-Jensen, and M. Hashem Nehrir, "Optimal Sizing and Allocation of Residential Photovoltaic Panels in a Distribution Network for Ancillary Services Application," to be *In Proc.* the *International Conference on Optimization of Electrical and Electronic Equipment* (*OPTIM 2014*), Romania, Feb. 2014.

K. Marchese, **S. A. Pourmousavi**, M. H. Nehrir, "The Application of Demand Response for Frequency Regulation in an Islanded Microgrid with High Penetration of Renewable Generation," in *Proceedings* of the 2013 North American Power Symposium, Kansas city, USA, 2013, pp. 1-6.

S.A. Pourmousavi, A.S. Cifala, and M.H. Nehrir, “Impact of High Penetration of PV Generation on Frequency and Voltage in a Distribution Feeder," in *Proceedings* of the 2012 North American Power Symposium, Urbana-Champaign, USA, 2012, pp. 1-8.

A.J. Litchy, C. Young, **S.A. Pourmousavi**, and M.H. Nehrir, “Technology Selection and Unit Sizing for a Combined Heat and Power Microgrid: Comparison of DER-CAM and HOMER Application Programs," in *Proceedings* of the 2012 North American Power Symposium, Urbana-Champaign, USA, 2012, pp. 1-6.

S.A. Pourmousavi, M.H. Nehrir, "Real-Time Optimal Demand Response for Frequency Regulation in Smart Microgrid Environment," in *Proceedings* of the 11th IASTED PES (EuroPES2012), Naples, Italy, 2012.

S.A. Pourmousavi, Ratnesh K. Sharma, Babak Asghari, “A Framework for Real-Time Power Management of a Grid-Tied Microgrid to Extend Battery Lifetime and Reduce Cost of Energy,” in *Proceedings* of the 3rd IEEE PES Conference on Innovative Smart Grid Technologies (ISGT 2012), Washington D.C., 2012, pp. 1-8.

S.A. Pourmousavi, M.H. Nehrir, C. Sastry, “Providing Ancillary Services through Demand Response with Minimum Load Manipulation”, in *Proceedings* of the IEEE 43th North American Power Symposium (NAPS 2011), Boston, MA, 2011, pp. 1-6.

S.A. Pourmousavi, M.H. Nehrir, “Demand Response for Smart Microgrid: Initial Results”, in *Proceedings* of the IEEE PES Conference on Innovative Smart Grid Technologies (ISGT 2011), Anaheim, CA, 2011, pp. 1-6.

C.M. Colson, M.H. Nehrir, **S. A. Pourmousavi**, “Towards Real-time Microgrid Power Management using Computational Intelligence Methods”, in *Proceedings* of IEEE PES General Meeting, Minneapolis, MN, 2010, pp. 1-8.